LEABHARLANN CHOLÁISTE NA TRÍONÓIDE, BAILE ÁTHA CLIATH | TRINITY COLLEGE LIBRARY DUBLIN
Ollscoil Átha Cliath | The University of Dublin

Terms and Conditions of Use of Digitised Theses from Trinity College Library Dublin

Copyright statement

All material supplied by Trinity College Library is protected by copyright (under the Copyright and Related Rights Act, 2000 as amended) and other relevant Intellectual Property Rights. By accessing and using a Digitised Thesis from Trinity College Library you acknowledge that all Intellectual Property Rights in any Works supplied are the sole and exclusive property of the copyright and/or other IPR holder. Specific copyright holders may not be explicitly identified. Use of materials from other sources within a thesis should not be construed as a claim over them.

A non-exclusive, non-transferable licence is hereby granted to those using or reproducing, in whole or in part, the material for valid purposes, providing the copyright owners are acknowledged using the normal conventions. Where specific permission to use material is required, this is identified and such permission must be sought from the copyright holder or agency cited.

Liability statement

By using a Digitised Thesis, I accept that Trinity College Dublin bears no legal responsibility for the accuracy, legality or comprehensiveness of materials contained within the thesis, and that Trinity College Dublin accepts no liability for indirect, consequential, or incidental, damages or losses arising from use of the thesis for whatever reason. Information located in a thesis may be subject to specific use constraints, details of which may not be explicitly described. It is the responsibility of potential and actual users to be aware of such constraints and to abide by them. By making use of material from a digitised thesis, you accept these copyright and disclaimer provisions. Where it is brought to the attention of Trinity College Library that there may be a breach of copyright or other restraint, it is the policy to withdraw or take down access to a thesis while the issue is being resolved.

Access Agreement

By using a Digitised Thesis from Trinity College Library you are bound by the following Terms & Conditions. Please read them carefully.

I have read and I understand the following statement: All material supplied via a Digitised Thesis from Trinity College Library is protected by copyright and other intellectual property rights, and duplication or sale of all or part of any of a thesis is not permitted, except that material may be duplicated by you for your research use or for educational purposes in electronic or print form providing the copyright owners are acknowledged using the normal conventions. You must obtain permission for any other use. Electronic or print copies may not be offered, whether for sale or otherwise to anyone. This copy has been supplied on the understanding that it is copyright material and that no quotation from the thesis may be published without proper acknowledgement.

POTENTIAL PHARMACEUTICAL APPLICATIONS OF SEPIOLITE

Presented by

Alecia Rowena Barry, B.Sc. (Pharm.), M.P.S.I.

under the direction and supervision of

Professor Patrick B. Deasy, B.Sc. (Pharm.), M.A., Ph.D., F.T.C.D., F.P.S.I.

for a

DOCTOR OF PHILOSOPHY DEGREE

at the

University of Dublin, Trinity College

Research for which was performed in

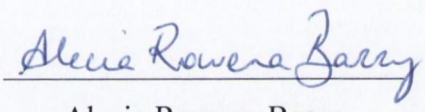
Pharmaceutics and Pharmaceutical Technology,
THE SCHOOL OF PHARMACY

November 2007

TRINITY COLLEGE
0 8 APR 2008
LIBRARY DUBLIN
THESIS
8334

DECLARATION

This thesis has not been submitted as an exercise for a degree at any other university. It is entirely the work of the undersigned author, except where duly acknowledged. The author agrees that the Library may lend or copy this thesis upon request.



Alecia Rowena Barry

To Mum and Dad

SUMMARY

The focus of the research presented in this thesis was on the potential pharmaceutical applications of sepiolite from the Vallecas-Vicálvaro region in Spain. Initial studies involved extensive characterisation of sepiolite from this deposit, with a particular emphasis on those properties which would influence its pharmaceutical acceptability and functionality. FT-IR and pXRD indicated that the sample was of high mineralogical purity and intermediate crystallinity. SEM revealed the fibrous morphology of the sample and confirmed the absence of potentially carcinogenic long fibers. EDXA indicated that the principal elements were silicon, magnesium and oxygen, consistent with the chemical formula of sepiolite. Lower but appreciable amounts of calcium, aluminium, potassium and iron were also present. ICP-MS indicated the presence of trace levels of a number of other metals. The specific surface area of sepiolite, as determined using N_2 adsorption data, was extremely high (285 m^2/ g). 60% of the total surface area resided within micropores.

Sepiolite was evaluated for use as a tabletting aid. Preliminary compressibility studies were indicative of a high degree of plastic deformation, compressibility and compactibility. Furthermore, DSC and TGA confirmed compatibility of sepiolite with a number of commonly used tabletting excipients. However, untreated sepiolite exhibited poor flowability and an extremely low bulk density. Mercury intrusion porosimetry indicated that ~ 57% bulk volume of sepiolite was accounted for by void spaces due to poor fiber packing. Spray drying of sepiolite improved fiber packing efficiency and increased bulk density and flowability. Another novel sepiolite grade (SepKoll) was prepared by spray drying sepiolite in combination with the binder Kollidon® VA 64. Characterisation of these novel spray dried bases confirmed that spray drying did not alter the degree of crystallinity or average fiber length. These novel spray dried grades were used to tablet poorly compressible paracetamol. One-way ANOVA confirmed that the novel spray dried bases produced tablets of similar hardness to Avicel® PH101 and significantly harder tablets than a Ludipress®/Kollidon® VA 64 (9:1) blend ($p<0.001$). Tablets prepared using SepKoll exhibited significantly lower friability than those prepared using spray dried sepiolite, Avicel® PH101 or Ludipress®/Kollidon® VA 64. All sepiolite-based tablets disintegrated more quickly than those prepared using Avicel® PH101 or Ludipress®/Kollidon® VA 64 ($p<0.001$). *In vitro* testing confirmed that the drug release rate from spray dried sepiolite and SepKoll tablets was comparable to that from Avicel® PH101 or Ludipress®/Kollidon® VA 64 tablets, with > 90% drug release occurring during the first hour. Surface profiling

indicated that the sepiolite-based compacts exhibited low surface rugosity, thus facilitating their coating with release-modifying and taste-masking polymers. Sepiolite was evaluated as an "all-in-one" filler-binder-disintegrant in the tabletting of paracetamol by wet granulation. Comparison of sepiolite with Avicel® PH101 indicated that the use of sepiolite led to improved intragranular binding efficiency, reduced granule friability, increased compactibility, comparable tablet surface topography and more rapid *in vitro* disintegration and drug release relative to Avicel® PH101. The compressibility and compactibility of Avicel® PH101 were reduced following wet granulation as was its ability to act as a disintegrant. Although the compressibility of sepiolite was likewise reduced (presumably due to improved fiber packing), compactibility and disintegrant properties were retained.

The use of sepiolite as a rheological modifier was investigated. Data from continuous shear rheology of aqueous sepiolite suspensions were fitted to a number of rheological models. At low sepiolite concentrations, low-yield systems of approximate plastic behaviour resulted. Higher concentrations produced systems with higher yields and pseudoplastic character. Brownian motion-induced collisions were demonstrated to be critical in the development of an interfibrous network and consequently of a yield stress. The effect of temperature on the rheological behaviour of sepiolite suspensions was dependent on two confounding variables, namely the relative rotational diffusion coefficient and the suspending medium viscosity. The response of sepiolite dispersions to changes in pH could be predicted by consideration of the DLVO theory and the change in zeta potential as a function of pH. Observed flow behaviour at pH 5.8 was not in keeping with that predicted using the DLVO theory. This anomaly suggested that certain fiber-fiber associations (i.e. edge-to-edge, edge-to-face, face-to-face) were favoured over others at different pH values and thus supported the existence of a heterogeneous edge-face surface charge. Electrolytes capable of specific adsorption to the fiber surface could cause both agglomeration and deflocculation of sepiolite suspensions depending on their concentration and the nature of their charge.

Sepiolite and a novel co-spray dried sepiolite/NaCMC grade were evaluated as suspending agents using calamine lotion BP as a model system. The sepiolite-based lotion exhibited rheological and sedimentation behaviour comparable to the BP formulation. The performance of the novel co-spray dried sepiolite/ NaCMC grade was comparable to Avicel® CL-611.

ACKNOWLEDGEMENTS

First and foremost, I would like to offer my sincerest gratitude to my supervisor, Professor Patrick Deasy, who has supported me throughout my thesis with his patience and knowledge whilst allowing me the space to work in my own way. The door to his office was always open and I am very much indebted to him for the guidance he has provided throughout the course of this work. I gratefully acknowledge the financial assistance provided by the Irish Research Council for Science, Engineering and Technology (IRCSET) throughout my studies.

I extend my sincere thanks to Neal Leddy and Sean Kelly of the Centre for Microscopy and Analysis for their help with SEM, EDXA, BET surface area analysis and ICP-MS. I would also like to thank the academic, administrative and technical staff of Pharmaceutics and Pharmaceutical Technology, and in particular Dr. Anne Marie Healy, Dr. Lidia Tajber, Liesa Eckhardt, Derek Coss, Brian O'Reilly, Conan Murphy and Pat Quinlan, for their assistance during the course of my research. My thanks are extended to Mrs. Ingrid Hook for use of the WinSEEDLE v5.1a software (Regent Instruments, Inc., Canada) and to Lene Visdal-Johnsen for training me in. I also wish to thank Dr. Abina Crean of the School of Pharmacy, University College Cork, for putting their zeta-sizing facilities at my disposal.

I would like to thank my fellow post-graduates for their friendship and support over the years (in alphabetical order): Adam Byrne, Rob Byrne, Ciaran Carolan, Miriam Carr, Jenny Coppins, Dave Coughlan, Deirdre D'Arcy, Cinmoy Dey, Gerry Dillon, Shadeed Gad, Tom Greene, Jason Horan, Gillian Hudson, Niall Keely, Emma Lawless, Juan Marquez, Aonghus McHugh, Xue Li, Cora Nestor, Fiona Ní Chearúil, Orla Ní Ógain, Lorraine Nolan, Katie Ryan, Anne Salter, Álmath Spooner, Lidia Tajber, Lene Visdal-Johnsen, Martina White and Tao Zhang. The friendship of Álmath, Jenny, Katie, Lorraine, Martina, Miriam and Orla is especially appreciated. I must offer my sincerest gratitude to Katie, Lorraine, Martina, Orla and Rob for dropping everything at a moment's notice to perform the unenviable task of proofreading my thesis; it is undoubtedly better for their contribution. I would also like to thank Lorraine, Orla and Jenny for running around collecting stationery, library books and corrected proofs, and generally keeping me organised while juggling a new job with writing my thesis (not something I'd recommend!). Special thanks to Katie, not only for her amazing insight on all things

pharmaceutical, but for her unfaltering friendship, wise words, encouragement through those dark times and generally for making Lab 1/04 a very special place.

I would also like to thank my friends outside of College for their friendship, willingness to go out and endless ability to put bad lab results into perspective! Lorraine Fenton, Therese Byrne and Carla Buckley deserve a special mention for putting up with my borderline bipolar mood swings while writing up and for negotiating (without a single complaint) the ever increasing number of paper mountains that have cropped up in the sitting room, hallway and kitchen. (I promise that they will be moved soon…).

Finally, special thanks go to my parents, my sister, Natalie, and my brothers, Darryl and Conrad, for their constant support and patience throughout my studies. My Mum deserves a special mention for bearing the brunt of my frustration and stress during writing up, for the endless supply of her legendary sticky toffee pudding and bacon-cheese rolls (a cure for all ills!) and for her unflagging patience and encouragement.

"Undertake something that is difficult; it will do you good. Unless you try to do something beyond what you have already mastered, you will never grow."

-Ronald E. Osborn

TABLE OF CONTENTS

Title page		i
Declaration		iii
Dedication		v
Summary		vii
Acknowledgements		ix
Table of Contents		xi
Presentations associated with this thesis		xxii
Symbols and Abbreviations		xxiii

Introduction

Chapter 1. Introduction 1

1.1	Origin and scope		1
1.2	Sepiolite		4
	1.2.1	An introduction to clays, clay minerals and sepiolite	4
	1.2.2	Worldwide sources of sepiolite	5
	1.2.3	Formation of sepiolite	6
	1.2.4	Structure of sepiolite	7
	1.2.5	Molecular access to the intracrystalline channels	11
1.3	Applications of sepiolite		12
	1.3.1	Introduction	12
	1.3.2	Sorption capacity	12
		1.3.2.1 Introduction	12
		1.3.2.2 Applications based on sorptive properties	13
	1.3.3	Rheological properties	16
		1.3.3.1 Introduction	16
		1.3.3.2 Applications based in rheological properties	17
	1.3.4	Applications of sepiolite of particular relevance to pharmaceutics	18
		1.3.4.1 Animal feedstuffs	18
		1.3.4.2 Evaluation as a biomaterial	19
		1.3.4.3 Evaluation as a wound dressing material	20
		1.3.4.4 Antidiarrhoeal preparations	21

1.3.5 Sepiolite and magnesium trisilicate 21
1.4 Tabletting 24
1.4.1 Introduction 24
1.4.2 Pharmaceutical powder compaction 24
1.4.2.1 Particle deformation 24
1.4.2.2 Mechanisms of interparticulate bonding 26
1.4.3 Tabletting by wet granulation 26
1.4.4 Tabletting by direct compression 29
1.4.5 Direct compression bases (DCBs) 32
1.4.5.1 Introduction 32
1.4.5.2 Preparation of DCBs 34
1.4.5.2.1 Spray drying 34
1.4.5.2.2 Co-processing 37
1.4.5.3 Microcrystalline cellulose (Avicel® PH) – a DCB prepared by spray drying 39
1.4.5.4 Ludipress® – a DCB produced by co-processing 44
1.5 Colloidal systems 45
1.5.1 Introduction 45
1.5.2 Aqueous clay dispersions – hydrophobic colloidal systems 46
1.5.2.1 DLVO theory of stabilization of hydrophobic colloids 46
1.5.2.1.1 Introduction 46
1.5.2.1.2 The electrical double layer 46
1.5.2.1.3 Interparticle double layer repulsion 48
1.5.2.1.4 Interparticle van der Waals attraction 48
1.5.2.1.5 Total energy of interaction 49
1.5.2.1.6 Stabilization of hydrophobic colloids 50
1.6 Rheology 52
1.6.1 Introduction 52
1.6.2 Newtonian and non-Newtonian flow behaviour 52
1.6.3 Thixotropy 54
1.7 Pharmaceutical suspensions 56
1.7.1 Introduction 56
1.7.2 Stability issues – sedimentation and caking 56
1.7.3 Formulation of stable suspensions 57
1.7.3.1 Modification of particle size of suspended drug 57

1.7.3.2 Use of structured vehicles 58
1.7.3.3 Preparation of flocculated/ deflocculated systems 59
1.8 Paracetamol 61
1.8.1 Introduction 61
1.8.2 Molecular structure 61
1.8.3 Physicochemical properties 62
1.8.4 Stability 63
1.8.5 Pharmacology of paracetamol 64
1.9 Calamine lotion 65

Experimental

Chapter 2. Materials 67

Chapter 3. Methodology 71

3.1 Physico-chemical characterisation of sepiolite powder (Pangel®-S9) 71
3.1.1 Powder X-ray Diffraction (pXRD) 71
3.1.2 Fourier Transform Infra-red Spectroscopy (FT-IR) 72
3.1.3 Energy Dispersive X-ray Analysis (EDXA) 72
3.1.4 Inductively Coupled Plasma Mass Spectroscopy (ICP-MS) 73
3.1.5 Thermogravimetric Analysis (TGA) 73
3.1.6 Differential Scanning Calorimetry (DSC) 73
3.1.7 Karl Fischer (KF) Analysis 73
3.1.8 Scanning Electron Microscopy (SEM) 74
3.1.9 N_2 gas adsorption 74
3.1.9.1 BET surface area determination 74
3.1.9.2 Determination of micropore volume and surface area using the t-plot method 76
3.1.10 Mercury Intrusion Porosimetry (MIP) 78
3.1.11 Helium Pycnometry 78
3.2 Physical processing of sepiolite 79
3.2.1 Preparation of milled samples 79
3.2.2 Preparation of heat treated sepiolite samples 79
3.3 Preparation of spray dried (SD) sepiolite, SepKoll and SepCMC 79

3.4 Characterisation of novel spray dried excipients 81
3.4.1 Preparation of physical mixes 81
3.4.2 Techniques used in the characterisation of the spray dried excipients 81
3.5 Tabletting studies 81
3.5.1 Evaluation of the compression properties of sepiolite 81
3.5.2 Paracetamol solubility study 82
3.5.3 Preparation of the blends for tabletting by direct compression 82
3.5.4 Preparation of granules using a wet granulation method 83
3.5.5 Characterisation of the Direct Compression Bases (DCBs) and granulates prepared by wet granulation 84
3.5.5.1 Density and flowability analysis 84
3.5.5.1.1 Tapped and bulk density determination 84
3.5.5.1.2 Angle of repose 85
3.5.5.1.3 Critical orifice diameter 86
3.5.5.2 Particle sizing – powder-in-air analysis 87
3.5.5.3 Granule friability determination 87
3.5.6 Tablet production 88
3.5.6.1 Uniformity of content 88
3.5.6.2 Preparation of tablets 88
3.5.7 Characterisation of tablets 89
3.5.7.1 Tablet porosity determination 89
3.5.7.2 Heckel Compression Analysis 89
3.5.7.3 Kawakita Compression Analysis 90
3.5.7.4 Tablet hardness testing 90
3.5.7.5 Tablet tensile strength determination 91
3.5.7.6 Tablet friability testing 91
3.5.7.7 Disintegration testing 91
3.5.7.8 *In vitro* drug release study 92
3.5.7.9 Surface profiling using non-contact optical profilometry 92
3.6 Sepiolite-excipient and sepiolite-drug interaction study 93

3.7 Suspension studies 94
3.7.1 Determination of the zeta potential of sepiolite 94
3.7.2 Preparation of sepiolite dispersions to be studied by SEM 94
3.7.3 Particle sizing - powder-in-liquid analysis 95
3.7.4 Rheology 95
3.7.4.1 Introduction 95
3.7.4.2 Influence of dispersion speed and time on the rheology of sepiolite suspensions 97
3.7.4.3 Influence of concentration on the rheology of sepiolite suspensions 97
3.7.4.4 Influence of pH on the rheology of sepiolite suspensions 98
3.7.5 Assessment of the sedimentation behaviour of sepiolite suspensions 99
3.7.5.1 Determination of sedimentation rate as a function of storage temperature 99
3.7.5.2 Susceptibility to vibrational stress 99
3.7.5.3 Ease of redispersion 99
3.7.6 Influence of electrolytes and dispersing agents on the sedimentation and rheological behaviour of sepiolite suspensions 100
3.7.6.1 Sodium chloride and calcium chloride 100
3.7.6.2 Cetrimide, sodium citrate and sodium polyphosphate 101
3.8 Evaluation of sepiolite and SepCMC as suspending agents in Calamine Lotion 101
3.8.1 Formulation 101
3.8.2 Rheological evaluation of modified lotions 103
3.8.3 Sedimentation behaviour and redispersibility of modified lotions 103
3.9 Statistical Methods 104
3.9.1 Two sample t-tests 104
3.9.2 Paired t-tests 104
3.9.3 Analysis of Variance (ANOVA) 105
3.9.4 Factorial Experimental Design 105
3.9.5 Regression Analysis 106

Chapter 4. Physico-chemical characterisation of sepiolite (Pangel®-S9) 107

4.1 Introduction 107
4.2 Confirmation of identity and identification of impurities 108
4.2.1 Powder X-ray Diffraction (pXRD) 108
4.2.1.1 Introduction 108
4.2.1.2 X-ray diffractograms of Pangel®-S9 112
4.2.2 Fourier Transform Infra-red Analysis (FT-IR) 115
4.2.3 Energy Dispersive X-ray Analysis (EDXA) 118
4.2.4 Inductively Coupled Plasma Mass Spectroscopy (ICP-MS) 119
4.3 Thermogravimetric Analysis (TGA) 121
4.4 Macroscopic and microscopic appearance of sepiolite (Pangel®-S9) 123
4.4.1 Introduction 123
4.4.2 SEM of sepiolite (Pangel®-S9) 123
4.4.3 The effects of dry grinding on the microscopic appearance of sepiolite 125
4.4.4 The effects of thermal treatment on the microscopic appearance of sepiolite 127
4.5 Textural analysis 129
4.5.1 Introduction 129
4.5.2 Specific surface area determination 129
4.5.2.1 Establishing ideal degassing conditions 129
4.5.2.2 Nitrogen adsorption isotherms 130
4.5.2.3 BET surface area determination 132
4.5.2.4 Determination of the external surface area, micropore surface area and micropore volume 133
4.5.3 Helium Pycnometry and Mercury Intrusion Porosimetry (MIP) 135
4.5.3.1 Introduction 135
4.5.3.2 Results 136
4.5.4 Correlation of surface area results from N_2 adsorption and MIP 139
4.6 Conclusions 139

Chapter 5. Preparation and evaluation of modified grades of sepiolite as multipurpose excipients in tabletting by direct compression 143

5.1 Introduction 143
5.2 Preliminary assessment of the compression properties of sepiolite 143
5.3 Direct compression – requirements for excipients and the search for new excipients 147
5.3.1 Introduction 147
5.3.2 Preparation of modified sepiolite grades for use as DCBs 148
5.3.2.1 Introduction 148
5.3.2.2 Rationale for incorporation of Kollidon® VA 64 in a co-spray dried product 148
5.3.2.3 Establishing optimum spray drying conditions for the preparation of novel sepiolite grades 149
5.4 Characterisation of the novel spray dried excipients 151
5.4.1 Introduction 151
5.4.2 Assessment of powder properties relevant to tabletting 152
5.4.2.1 Flowability 152
5.4.2.2 Particle morphology and size distribution 156
5.4.2.3 Powder X-ray Diffraction (pXRD) studies 160
5.4.2.4 FT-IR analysis 161
5.4.2.5 Thermal analysis (TGA, DSC) and KF analysis 163
5.4.2.6 BET surface area and porosity 165
5.5 Comparison of the tabletting performance of novel sepiolite grades with other DCBs using paracetamol as an active ingredient 169
5.5.1 Rationale for choice of paracetamol as model drug 169
5.5.2 Uniformity of mixing 169
5.5.3 Compression Modelling 171
5.5.3.1 Heckel Compression Analysis 172
5.5.3.1.1 Introduction 172
5.5.3.1.2 Results of Heckel Analysis 173

5.5.3.2 Kawakita Compression Analysis 178
5.5.3.2.1 Introduction 178
5.5.3.2.2 Results of Kawakita Analysis 179
5.5.3.3 Correlation of results from Heckel and Kawakita Analysis 181
5.5.4 Tensile strength profiles 182
5.5.5 Tablet hardness and friability testing 185
5.5.6 Disintegration testing of tablets 187
5.5.7 *In vitro* drug release study 189
5.5.8 Surface profiling using non-contact optical profilometry 190
5.5.8.1 Introduction 190
5.5.8.2 Results of surface profiling 191
5.6 Excipient compatibility 197
5.7 Conclusions 198

Chapter 6. Evaluation of sepiolite as a multipurpose excipient in tabletting by wet granulation 203

6.1 Introduction 203
6.2 Preliminary studies – development of formulations and the determination of optimum production parameters 204
6.2.1 Development of suitable wet granulation formulations 204
6.2.2 Establishing suitable production parameters 207
6.3 Characterisation of granulates 211
6.3.1 Uniformity of drug content 211
6.3.2 Granulate flowability 211
6.3.3 Microscopic structure of granules 214
6.3.4 Granule sizing 215
6.3.5 Granule friability 219
6.4 Characterisation of the tablets produced by granulate compression 221
6.4.1 Compression Modelling 221
6.4.1.1 Heckel Compression Analysis 221
6.4.1.2 Kawakita Compression Analysis 225
6.4.1.3 Correlation of results from Heckel and Kawakita Analysis 226

6.4.2 Tensile strength profiles 228
6.4.3 Influence of wet granulation on compressibility and compactibility of MCC and sepiolite 230
6.4.4 Tablet hardness and friability testing 232
6.4.5 Disintegration testing of tablets 233
6.4.6 *In vitro* drug release profiles 235
6.4.7 Surface profiling using non-contact optical profilometry and SEM 236
6.5 Conclusions 240

Chapter 7. The effect of pH, temperature and electrolytes on the rheology and stability of aqueous sepiolite suspensions 243

7.1 Introduction 243
7.2 Gelling mechanism of bentonite 243
7.3 Gelling mechanism of sepiolite 247
7.3.1 Introduction 247
7.3.2 Ease of sepiolite gel formation – the influence of mixing speed and time on the resultant rheological properties 248
7.4 The relationship between sepiolite concentration, rheological behaviour and suspension stability 253
7.4.1 Introduction 253
7.4.2 Rheological behaviour of sepiolite suspensions of different concentration 254
7.4.3 Relationship between concentration and thixotropy 259
7.4.4 Relationship between sedimentation behaviour and concentration 266
7.5 The influence of pH on the rheological behaviour of sepiolite 268
7.5.1 Introduction 268
7.5.2 Zeta potential as a function of pH 269
7.5.3 Rheological behaviour of sepiolite suspensions as a function of pH 272
7.5.4 SEM of sepiolite suspensions at different pH values 277
7.5.5 Antithixotropy, thixotropy and pH 279

7.6 The influence of temperature on the rheology and stability of sepiolite suspensions 281
7.6.1 Introduction 281
7.6.2 Rheological behaviour of sepiolite suspensions at different temperatures 281
7.6.3 The influence of temperature on the sedimentation behaviour of sepiolite suspensions of different concentration 287
7.7 The influence of ageing on sepiolite suspensions 291
7.8 The influence of electrolytes and deflocculating agents on the rheological and sedimentation behaviour of sepiolite suspensions 295
7.8.1 Introduction 295
7.8.2 Sodium chloride 297
7.8.3 Calcium chloride 300
7.8.4 Cetrimide 304
7.8.5 Sodium citrate 312
7.8.6 Sodium polyphosphate (NaPP) 318
7.9 Conclusions 324

Chapter 8. Evaluation of the performance of different grades of sepiolite as suspending agents in a model pharmaceutical suspension 329

8.1 Preparation of a novel rheological grade of sepiolite 329
8.1.1 Introduction 329
8.1.2 Establishing optimum spray drying conditions for the preparation of SepCMC 330
8.2 Characterisation of SepCMC 331
8.2.1 Introduction 331
8.2.2 SEM 331
8.2.3 Particle sizing 332
8.2.4 pXRD 333
8.2.5 FT-IR 334
8.3 Preliminary rheological investigations 335
8.4 Evaluation of the performance of sepiolite and SepCMC as suspending agents using calamine lotion as a model system 341
8.4.1 Introduction 341

8.4.2 Development of suitable formulations 341
8.4.3 Evaluation of the rheological behaviour of the modified calamine lotion formulations 343
8.4.4 Sedimentation behaviour of modified calamine lotion formulations 351
8.5 Conclusions 355

General Discussion **357**

References **373**

Appendices **421**

Appendix 1: UV calibration curves used to determine the concentration of paracetamol in solution 421
Appendix 2: Saturation solubility results 422
Appendix 3: FT-IR reference spectrum for sepiolite 423
Appendix 4: BET transform plots 424
Appendix 5: DSC/ TGA traces used to establish sepiolite-excipient compatibility 425
Appendix 6: Rheological parameters for sepiolite suspensions treated with electrolytes 433
Appendix 7: Rheological parameters for Calamine lotion derivatives 438
Appendix 8: Summary of sphericity results for sepiolite pellets prepared by extrusion-spheronisation using water as a granulating agent 439

PRESENTATIONS ASSOCIATED WITH THIS THESIS

Oral Presentations

Barry, A.R., Deasy, P.B., 2004. Pharmaceutical Applications of Sepiolite, *Socrates Intensive Programme: Innovative Therapeutics: from molecules to medicines,* Faculty of Pharmacy, University of Parma, Italy, July 2004.

Poster Presentations

Barry, A.R., Deasy, P.B., 2004. The design of novel drug delivery systems using microporous particles. Irish Research Council for Science, Engineering and Technology (IRCSET) National Symposium, Kilmainham, Dublin, November 2004.

Barry, A.R., Deasy, P.B., 2004. Pharmaceutical applications of sepiolite. 26th Joint Research Seminar, Queen's University Belfast, March 2004.

Barry, A.R., Deasy, P.B., 2005. Tabletting applications of a novel microporous material. Irish Research Council for Science, Engineering and Technology (IRCSET) National Symposium, Croke Park conference centre, Dublin, November 2005.

Barry, A.R., Deasy, P.B., 2006. Comparative evaluation of the tabletting properties of sepiolite and microcrystalline cellulose. 28th Joint Research Seminar, Queen's University Belfast, April 2006.

ABBREVIATIONS AND SYMBOLS

α	alpha
β	beta
ε	permittivity of solution
λ	lambda (wavelength)
ρ	density
θ	theta
ζ	zeta (potential)
η_p	plastic viscosity
η	medium viscosity
σ_B	Bingham yield value
σ_{HB}	Herschel-Bulkley yield value
Φ_V	solid volume fraction (%)
Σ	sigma (sum of)
µeq	microequivalents
µg	micrograms
µL	microlitres
µm	micrometres
µM	micromolar
°	degrees
°C	degrees celsius
±	plus or minus
≥	greater than or equal to
≈	approximately equal to
∝	proportional to
a	Kawakita compressibility parameter
Å	Angströms
A	amperes
Ag	silver
Al	aluminium
amu	atomic mass units
ANOVA	analysis of variance
Ar	argon
As	arsenic

AUHC	area under Heckel curve, a measure of compressibility
AUTSC	area under tensile strength versus compression pressure, a measure of compactibility
Ba	barium
Be	beryllium
C	carbon (or concentration in chapter 7)
Ca	calcium
Cl	chlorine
Cd	cadmium
CEC	cationic exchange capacity
Co	cobalt
cm	centimetres
cps	centipoises
Cr	chromium
Cs	caesium
Cu	copper
d10	particle size below which 10% by volume of a sample lies
d50	median of particle size distribution by volume (mass median diameter)
d90	particle size below which 90% by volume of a sample lies
D	translational diffusion coefficient of Brownian motion in section 7.6
D_{rel}	relative translational diffusion coefficient of Brownian motion
D_R	rotational diffusion coefficient of Brownian motion
D_{Rrel}	relative rotational diffusion coefficient of Brownian motion
DCB	direct compression base
df	degrees of freedom
EDXA	energy dispersive x-ray analysis
EE	edge-to-edge
EF	edge-to-face
FF	face-to-face
E_v	activation energy
F	Faraday constant
FT-IR	Fourier Transform Infra Red spectroscopy

f_2	similarity factor
Fe	iron
g	grams (or acceleration due to gravity in Equation. 7.6h)
Ga	gallium
H	hydrogen
h	hour/hours
HB	Herschel-Bulkley
Hg	mercury
IARC	International Agency for Research on Cancer
ICH	International Conference for Harmonisation of Technical Requirements for Registration of Pharmaceuticals for Human Use
ICP-MS	Inductively Coupled Plasma Mass Spectroscopy
i.e.p.	isoelectric point, i.e. pH at which $\zeta = 0$ mV
J	joules
K	potassium (or Kelvin temperature unit)
$1/\kappa$	effective electrical double layer thickness, Debye length
k_B	Boltzmann constant
kg	kilograms
kV	kilovolts
L	litres
Li	lithium
ln	natural logarithm
log	logarithm to the base 10
m	metres
M	molar
mbar	millibars
MCC	microcrystalline cellulose (Avicel® PH101)
Mg	magnesium
meq	milliequivalents
mg	milligrams
min	minute/minutes
MIP	mercury intrusion porosimetry
mL	millilitres
mm	millimetres
mM	millimolar

mmol	millimoles
mN	milli Newtons
Mn	manganese
Mo	molybdenum
MPa	megapascals
mtor	millitorr
mV	millivolts
N	(1) Avogadro's number (6.023×10^{23} $mole^{-1}$), (2) normality in the case of solutions or (3) Newtons in the case of tablet hardness
n	number of replicates (or in a rheological context, the flow behaviour index)
N_2	nitrogen
Na	sodium
NaCMC	sodium carboxymethylcellulose
NaPP	sodium polyphosphate
Ni	nickel
nm	nanometres
O	oxygen
Pa	Pascals
Pb	lead
pF	picofarads
pH	minus log of hydrogen ion concentration
pK_a	dissociation constant for a weak acid
ppm	parts per million (mg /kg)
p.s.i.	pounds per square inch
Pt	platinum
PVP	polyvinylpyrrolidone
pXRD	powder X-ray diffraction
P_y	mean deformation pressure
r	radius
r^2	correlation coefficient
R	absolute gas constant (8.3143 J K^{-1} $mole^{-1}$)
R_a	average surface rugosity
Rb	rubidium

Rh	rhodium
RH	relative humidity
Rq	root mean square roughness
R_q/R_a	index of surface variability
R_t	maximum peak to valley height on a surface profile
rpm	revolutions per minute
RMS	root mean square
s	second/seconds
Sb	antimony
SD	spray dried
Se	selenium
SEM	scanning electron microscopy/micrograph
Si	silicon
Sr	strontium
SS	total sum of squares
STP	standard temperature and pressure (273.15 K and 760 mmHg)
t	time
T	absolute temperature
Te	tellurium
Ti	titanium
Tl	thallium
U	uranium
UCM	ultracentrifugal mill
UV	ultraviolet spectroscopy
V	vanadium
V_A	interparticle van der Waals attraction potential
V_0	original volume of a suspension before settling occurs
V_R	interparticle electrical double layer repulsion potential
V_u	volume occupied by the sediment in a suspension
v/v	volume per volume
w/v	weight per volume
w/w	weight per weight
XRD	X-ray diffraction

Y	yield strength
Z	ion valency
Zn	zinc
Zr	zirconium

Chapter 1

INTRODUCTION

1.1 ORIGIN AND SCOPE

Drugs are rarely administered as the pure substance alone but instead are given as formulated preparations, the quality of which depends not only on the active ingredients and the production processes used but also on the quality and performance of the excipients (Pifferi *et al.*, 1999; Levis, 2000; Byrne, 2004). Excipients are introduced into pharmaceutical formulations for numerous reasons; some excipients are used to improve the organoleptic properties such as taste, smell and colour, others are used to ensure stability during storage and use, others still facilitate preparation of tabletted forms of a drug or promote disintegration of orally administered solid dosage forms *in vivo*. The British Pharmacopoeia (BP) (2007) notes that excipients for pharmaceutical use include both organic and inorganic substances obtained from natural sources, by fermentation or by synthesis.

Clay minerals have been used for medicinal purposes since prehistoric times (Carretero, 2002). These minerals can act as active principles (gastrointestinal protectors, antidiarrhoeals, dermatological protectors) or excipients. Clays minerals used as excipients in pharmaceutical preparations to date are smectites, palygorskite (attapulgite), kaolinite and talc (Viseras and López-Galindo, 1999; Carretero, 2002). These minerals are used as: (a) lubricants in tablet manufacture (talc), (b) disintegration agents in tablets (smectites and palygorskite), (c) inert bases for cosmetics (palygorskite, kaolinite, smectites and talc) and (d) emulsion and suspension stabilizers on account of their thickening action (palygorskite and smectites). Their use in pharmaceutical preparations relates to the following properties: high sorptive capacity, large specific surface area, non-Newtonian rheological properties, chemical inertness and low or null toxicity to the patient (Carretero, 2002). There have been some preliminary investigations into the possible use of the fibrous clay mineral sepiolite in pharmaceutical preparations (del Hoyo *et al.*, 1996b; Ohta *et al.*, 1999;

Viseras and López-Galindo, 1999) but at the commencement of this PhD there were no commercial medicines for human use which include sepiolite in their formulation (Carretero, 2002). Exploitation of sepiolite in other related fields (e.g. in the preparation of animal feedstuffs, paints and fertilizers) prompted a comprehensive evaluation of its potential applications in a pharmaceutical context. Somewhat ironically and furthermore, unintentionally it appears, sepiolite is the subject of a monograph in both the BP (2007) and European Pharmacopoeia (PhEur) (2007) given that it is a naturally occurring form of the compound magnesium trisilicate (Anonymous, 1998).

Reports of an improvement in the quality and durability of pellets used in animal feeds following incorporation of sepiolite (Angulo *et al.*, 1995) were suggestive of binding properties that could be exploited in the preparation of solid oral dosage forms including both pellets and tablets. Cerezo *et al.* (2001) reported that sepiolite rapidly sorbs considerable volumes of water, a property that would suggest potential disintegrant activity. Consequently, the merits of sepiolite as an 'all-in-one' tablet diluent, binder and disintegrant were investigated (as were modified grades produced by spray drying) using both wet granulation and direct compression tabletting methods.

The rheological properties of sepiolite suspensions have been the focus of many publications. Suspensions are reported to be both pseudoplastic and thixotropic (Santarén, 1993, Santarén, 1996; Tolsa product brochure, 1999; Viseras *et al.*, 1999; Viseras and López-Galindo, 1999). To date all exploitation of, and research relating to these properties lies in the field of drilling muds and paint manufacture (Alvárez, 1984; Santarén, 1993). This is in spite of the fact that such rheological systems find widespread applicability in pharmaceutical suspensions, lotions and semi-solids. Sepiolite suspensions are also purported to be more robust than those of non-fibrous clays, resisting challenges to stability posed by high electrolyte concentrations and wide variations in pH (Santarén, 1993, Santarén, 1996; Tolsa product brochure, 1999; Viseras *et al.*, 1999; Viseras and López-Galindo, 1999). Although Nash (1996) has listed sepiolite amongst pharmaceutically useful suspending agents, no reports of its use, or even evaluation of its use, as such in a pharmaceutical system are evident in the literature. Consequently, a comprehensive evaluation of the rheological properties of sepiolite, guided by the properties and requirements of pharmaceutical systems, was undertaken. The change in rheological behaviour as a function of pH within a physiologically relevant range, as a

function of concentration of salts commonly used in pharmaceuticals (including sodium chloride, sodium citrate, calcium chloride) and as a function of temperature within that range used for storage of pharmaceuticals (4 – 40 °C) was examined. Novel sepiolite-based rheological additives were prepared and assessed using calamine lotion as a model pharmaceutical suspension.

1.2 SEPIOLITE

1.2.1 An introduction to clays, clay minerals and sepiolite

The word "clay" is used frequently in the literature. It is a broad term, encompassing, in addition to the clay minerals, natural materials composed of very fine-grained minerals, which exhibit some plasticity when mixed with water and harden on drying. The term is, therefore, applicable to all small-sized particles, normally < 2 μm, found in soils, sediments or as alteration products of rocks, including, apart from the clay minerals, lesser quantities of other minerals and/or organic products such as quartz, feldspars, carbonates, sulphates, iron and/or aluminium oxides, humus etc. (López-Galindo *et al.*, 2006). Clay minerals are a subgroup of clays belonging to the phyllosilicate mineralogical family (van Olphen, 1977). They are hydrated magnesium or aluminium silicates containing considerable amounts of K, Ca, Na, Fe and, occasionally, less common ions such as Ti, Mn and Li (López-Galindo *et al.*, 2006). The basic building blocks of the clay minerals are two-dimensional arrays of silicon-oxygen tetrahedra (silica sheets) and two-dimensional arrays of aluminium- and magnesium-oxygen-hydroxyl octahedra (gibbsite and brucite sheets respectively) (van Olphen, 1977). The analogous symmetry and the almost identical dimensions of the tetrahedral silica and the octahedral magnesia/ alumina sheets allow the sharing of oxygen atoms between these sheets. This sharing may occur between one silica sheet and one alumina sheet, as is the case in so-called 1:1 layer minerals. In the 2:1 layer minerals, one alumina or magnesia sheet shares oxygen atoms with two silica sheets, one on each side. The combination of an octahedral sheet and one or two tetrahedral sheets is called a layer. Within each layer, a certain unit repeats itself in a lateral direction and is termed the unit cell. Consequently, despite their varied chemical composition, these layer silicates can be classified into just a few major groups - smectites, illites, kaolinites, chlorites, fibrous and mixed-layer - based on layer type (1:1 or 2:1), layer charge and type of interlayer (van Olphen, 1977; Brindley and Brown, 1980).

Sepiolite is a 2:1 layer hydrated magnesium silicate belonging to the fibrous phyllosilicate group, the only other member of which is palygorskite (van Olphen, 1977). Sepiolite has been described as early as the eighteenth century when it was referred to as "meerschaum" due to the tendency of the porous form to float on the surface of the sea forming a layer of "sea foam". The name "sepiolite" was first used by Glocker in 1847 (Santarén, 1996). He

derived this term from the Greek word for cuttlefish because of the resemblance of its light and porous internal shell to sepiolite.

Sepiolite may occur in two forms (Fersman, 1913; cited in Alvárez, 1984): α sepiolite, which occurs as large bundles of crystalline fibers, and β sepiolite, which is a poorly crystallized spheroidal morphotype, formed as environmental conditions became less and less favourable in the deposit (Gehring *et al.*, 1994). The α-form is that of interest here. The felting in one, two or three dimensions of the extremely thin crystal fibers of sepiolite leads to their aggregation into a variety of different macroscopic forms, ranging from a structure of fibrous masses, as in the case of sepiolite found in Ampandrandava, Madagascar, to lumps as in sepiolite from Eskişehir, Turkey, to matted plates, commonly called "mountain leather" as in sepiolite from British Columbia, Canada, and finally in compacted form as in sepiolite from Vallecas-Vicálvaro, Spain (Preisinger, 1963; Frost *et al.*, 1998).

1.2.2 Worldwide sources of sepiolite

Deposits of sepiolite of commercial significance are located in Madrid and Toledo (Spain), Las Vegas (USA), Eskişehir (Turkey) and the Hunan Province (China). Occurrences of this mineral of no or minimal commercial interest are situated in Madagascar, the Amboseli basin (Kenya and Tanzania), El Bur (Somalia), Korea, France and Japan (Alvárez, 1984; Santarén, 1996; Singer *et al.*, 1998). Supply of sepiolite for the global market is almost exclusively from Spain, apart from some small scale production in the USA, Turkey and recently in China (Santarén, 1996). The world's largest producer of sepiolite is Tolsa with deposits in Vallecas-Vicálvaro (Madrid) and Yunclillos (Toledo). The deposit at Vallecas-Vicálvaro is sedimentary in origin and is the world's largest in terms of purity and reserve volume (Galan, 1996; Santarén, 1996; Tolsa, 1999). The annual production of sepiolite in Spain is close to 800,000 tonnes (O'Driscoll, 1992). Spanish production of sepiolite has shown a significant increase in recent years with a growth of approximately 10% per annum. This increase is largely due to the development of new applications for sepiolite, especially in the animal feed sector and in high added value products for different industrial applications (e.g. drilling muds, fillers in special rubber applications) (Santarén, 1996).

Sepiolite for use in this study was sourced from the Vallecas-Vicálvaro deposit for two reasons. The first of these is related to the high purity and size of the deposit (it accounts for more than 90% of the world's known reserves) and the second to the dimensions, and consequent health-related effects, of the sepiolite fibers. Sepiolites of non-sedimentary origin (e.g. those from China, Finland and Ampandrandava) have a higher degree of crystallinity and consequently longer fibers than those of sedimentary origin (Galan, 1996). Long fibers (> 5 μm) have been reported to have carcinogenic potential (Galan, 1996). The intrinsic biological activity of fibers appears to be related to their *in vivo* persistence with shorter fibers being more readily inactivated by phagocytosis than longer fibers (Stanton *et al.*, 1981; Bellmann *et al.*, 1997). No significant increase in tumor incidence in rats was found following an inhalation study using sepiolite from Vallecas-Vicálvaro (International Agency for Research on Cancer (IARC), 1997). Furthermore, Santarén and Alvárez (1994) reported epidemiological results for animal experiments involving administration of sepiolite from Vallecas-Vicálvaro by intrapleural injection and intraperitoneal inoculation. These results were consistently negative; indicating that sepiolite from Vallecas-Vicálvaro has low intrinsic biological activity and carcinogenic potential. Their findings were further corroborated by those of Bellmann *et al.* (1997).

1.2.3 Formation of sepiolite

Sepiolite shows diverse modes of mineral genesis. A variety of processes such as direct precipitation, alteration of volcanic ash, detrital transport and transformation from other minerals e.g. smectites, dolomite and magnesite have been suggested as formation mechanisms (Birsoy, 2002). Deposits of these minerals have been found in marine, transitional marine and continental-lacustrine environments, in continental solids and in association with igneous rocks. The deposits in Vallecas-Vicálvaro were formed during the Miocène period in lacustrine zones by chemical precipitation under semi-arid or arid climatic conditions (Santarén, 1996). The Vallecas-Vicálvaro deposit is situated to the north-east of Madrid and occupies 6.6 km^2. Figure 1.2a shows a log at this deposit (Galan and Castillo, 1984).

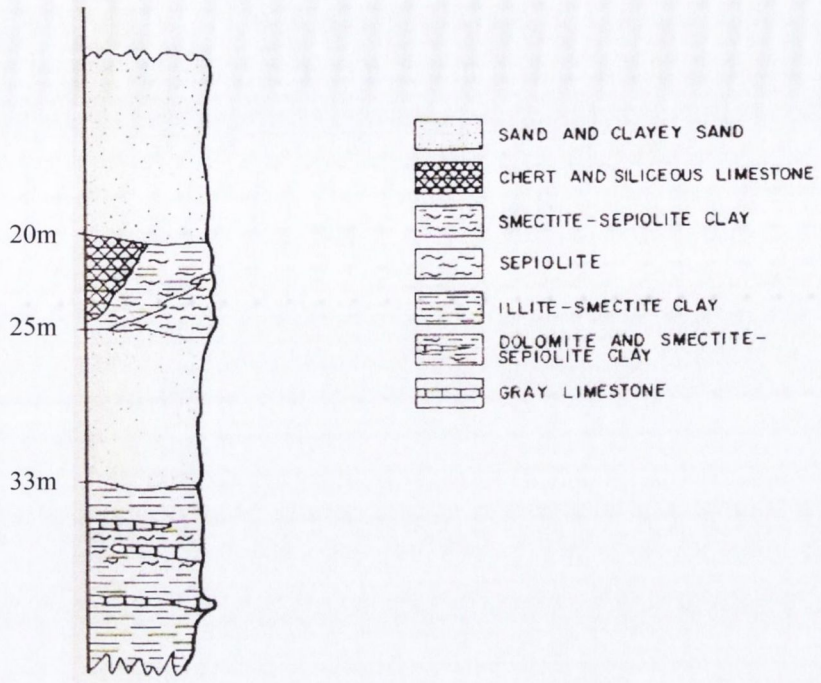


Figure 1.2a. Log at Vallecas-Vicálvaro, Madrid (Galan and Castillo, 1984).

Two exploitable layers of sepiolite are present. The upper layer changes laterally to dark chert, and the lower changes laterally to smectites at the north-west. Toward the south-east, the lower smectite clays change to saponitic bentonites of irregular distribution and quality. The sepiolite is typically between 65% and 97% pure, being accompanied by quartz, illite, feldspars and carbonates (Galan and Castillo, 1984).

1.2.4 Structure of sepiolite

The first attempt to elucidate the structure of sepiolite was made by Longchambon in 1937 (Alvárez, 1984). His work did establish that sepiolite was a distinct mineral, however, the study was not sufficiently comprehensive to account for all X-ray reflections (Brindley, 1959). The structure of sepiolite was studied further by Nagy and Bradley (1954, 1955), Martin-Vivaldi and Cano (1956), Brauner and Preisinger (1956), Preisinger (1959), Brindley (1959) and Brindley and Brown (1980). Nagy and Bradley (1955) were the first to present a structural model. They used the *hk*0 reflections from an X-ray fiber photograph to propose that the mineral consists of mica-like units extending parallel to the long fiber axis (*c*-axis). Brauner and Preisinger (1956) subsequently presented a slightly different model to that of Nagy and Bradley, which has become the currently accepted structure (Brindley and Brown, 1980). The chemical formula of the half unit cell, without substitutions, is $Si_{12}O_{30}Mg_8(OH)_4(OH_2)_4.8H_2O$ (Brauner and Preisinger, 1956). Figure 1.2b

illustrates the crystalline structure of sepiolite as deduced by Brauner and Preisinger (1956). The space group is orthorhombic with the unit cell parameters a = 13.4 Å, b = 26.8 Å and c = 5.28 Å.

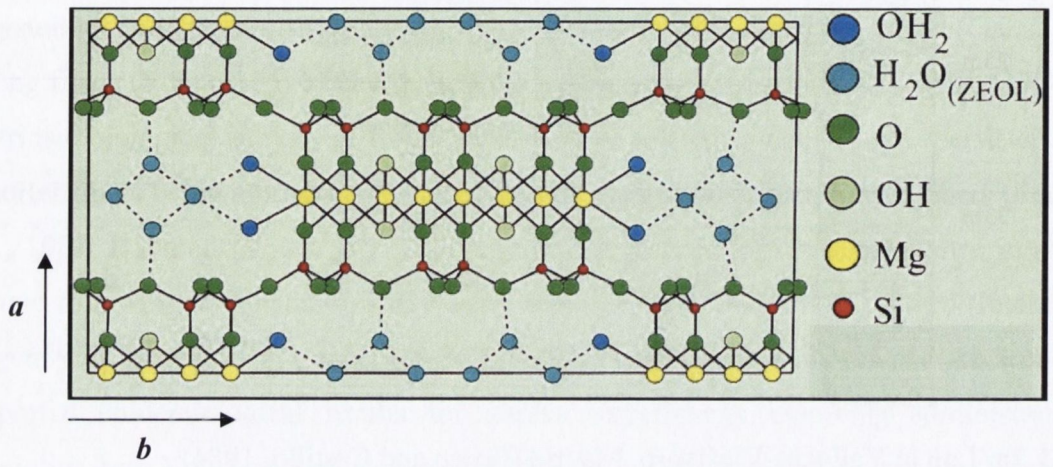


Figure 1.2b. Crystallographic structure of sepiolite showing the octahedral magnesia layers sandwiched between tetrahedral silica layers and the zeolithic channels (after Brauner and Preisinger 1956) (Adapted from Poppe *et al.*, 2001).

Sepiolite, like other phyllosilicates, is composed of two planar sheets: a tetrahedral silica sheet and an octahedral brucite sheet. Sepiolite is a 2:1 layer silicate as one magnesia sheet shares oxygen atoms with two silica sheets, one on either side (Figure 1.2b). Sepiolite differs from other layer silicates (apart from palygorskite) in that the octahedral sheet is discontinuous. This unusual superposition of the octahedral and tetrahedral sheets produces ribbons of a 2:1 talc-like phyllosilicate structure, each ribbon being linked to the next by inversion of every sixth SiO_4 tetrahedra along a set of Si–O–Si bonds (Alvárez, 1984; Galan, 1996). This structure of chain phyllosilicate results in a fibrous habit with rectangular intracrystalline channels of approximate dimensions 3.6 x 10.6 Å running parallel to the long axis of the fiber between opposing 2:1 ribbons (Alvárez, 1984; Galan, 1996; Santarén, 1996). These intracrystalline channels are also referred to as zeolithic channels. The structure of palygorskite (also termed attapulgite) is similar (Figure 1.2c), however inversion occurs at every fourth SiO_4 tetrahedra along a set of Si–O–Si bonds such that its ideal formula is given by Si_8O_{20} $(Mg,Al,Fe)_5(OH)_2(OH_2)_4.4H_2O$ and the intracrystalline channel cross-section is 3.6 x 6.4 Å (Brindley and Brown, 1980; Galan, 1996; Cerezo *et al.*, 2001).

The oxygen atoms at the edges of the discontinuous octahedral sheets are co-ordinated to magnesium cations on the ribbon side only, and co-ordination and charge balance are completed along the channel by protons, co-ordinated water and a small number of exchangeable cations (Galan, 1996). A variable amount of zeolithic water is also contained in the channels. It is bonded by hydrogen bonds (H-bonds) to the water co-ordinated to the magnesium ions (Alvárez, 1984; Ruiz-Hitzky, 2001). Removal of zeolithic water is easily achieved by exposure to thermal treatment at about 100 °C, whereas co-ordination water requires more drastic conditions (> 300 °C) (Alvárez, 1984). Removal of these co-ordinated water molecules results in folding of the structure and the loss of the zeolithic channels in agreement with both X-ray diffraction patterns and IR spectroscopic results (Ahlrichs *et al.*, 1975).

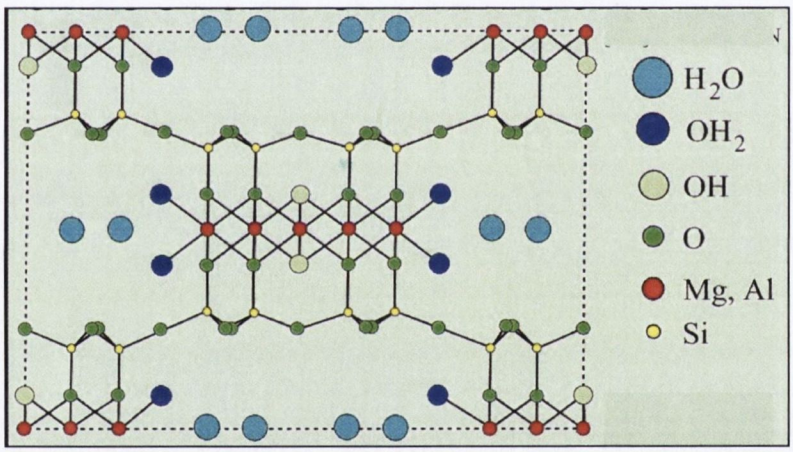


Figure 1.2c. Crystallographic structure of palygorskite (Adapted from Poppe *et al.*, 2001).

Fiber sizes vary widely depending on the site and mode of genesis. Fibers up to several centimetres in length and 100 nm in thickness have been reported in sepiolite samples from Ampandandrava but dimensions typically range from ~ 200-2000 nm in length, 10-30 nm in width and 5-10 nm in thickness for sepiolite from Vallecas-Vicálvaro (Alvárez, 1984; Galan, 1996; Santarén, 1996; Bellmann *et al.*, 1997). The parallel fibers are grouped together along the *c*-axis to form bundles of approximate diameter 100-300 nm (Knapp *et al.*, 1997). These bundles are arranged into loosely packed and porous aggregates with an extensive capillary network thereby accounting for the high porosity of sepiolite and its low bulk density.

As a consequence of the extensively corrugated external surface of the fibers and the internal surface area of the channels, sepiolite has the highest specific surface area of all

clays, approximately 300 m^2 /g (N_2 BET surface area; Santarén, 1996). The microporous channels account for 60 to 70% of the total surface area (Alvárez, 1984). The surface of sepiolite is very hydrophilic due to the high density of silanol (-SiOH) groups which occur approximately every 5 Å at the edges of the open channels on the external surface of the particle (Figure 1.2d) (Ahlrichs *et al.*, 1975; Santarén, 1996).

Substitution of Al or Fe^{3+} for Si in tetrahedral sites is usually low (range 0.2 - 1.3 atoms per 12 sites). The octahedral cations are primarily magnesium, but aluminian, ferrian and nickeloan varieties are known (Brindley and Brown, 1980) and are termed paramontmorillonite, xylotile and falcondoite respectively (Brindley and Brown, 1980; Alvárez, 1984). A Na-rich variety of sepiolite has also been described and is termed loughlinite (Preisinger, 1963). The cation-exchange capacity (CEC) can be defined as the sum of the exchangeable cations that a mineral can adsorb at a specific pH and consequently is a measure of the negative charges carried by a mineral (Bain and Smith, 1994). These negative charges are derived from (1) substitution of Si, and less commonly Mg, by atoms of lower valence, (2) broken bonds at edges and external surfaces and (3) the dissociation of accessible hydroxyl groups. The CEC of sepiolite is typically low and of the order of 10-15 mEq / 100 g (Santarén, 1996; Tolsa, 1999).

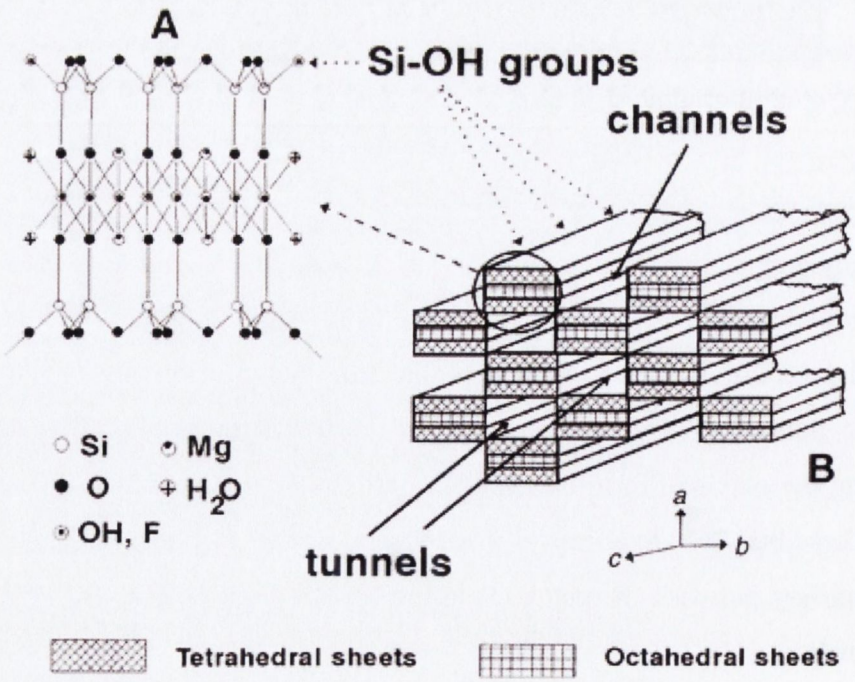


Figure 1.2d. Schematic model representing sepiolite structure (Reproduced from Ruiz-Hitzky, 2001).

1.2.5 Molecular access to the intracrystalline channels

Molecular access to the intracrystalline channels of sepiolite is an old and controversial topic (Ruiz-Hitzky, 2001). The difference in the surface area values when determined using different sorbates (e.g. 275 m^2/ g using pyridine, 470 m^2/ g using ethylene glycol, 276 m^2/ g using N_2) was attributed to the differing ability of different sorbates to penetrate the channels (Alvárez, 1984). Alvárez (1984) reported that the co-ordination and zeolithic water molecules can be substituted by small molecules of high polarity e.g. short chain primary alcohols, ammonia, acetone and ethylene glycol. Alcohols of longer chain length can also substitute the zeolithic and co-ordination water molecules, but only in the open channels of the external fiber surface. Hexane and hexene have been demonstrated to undergo intracrystalline sorption (Serna and Fernández, 1974). Barrer *et al.* (1954) reported the selective adsorption of linear hydrocarbons versus branched hydrocarbons and suggested that this preference may be attributed to the ability of linear molecules to penetrate the channels, which are likely to be inaccessible to the more sterically hindered branch-chained molecules. The tunnels are available to several gases (e.g. nitrogen, argon, carbon dioxide) following elimination of the zeolithic water (Dandy, 1968; Ruiz-Hitzky, 2001). Barrer and Mackenzie (1954) reported that the channels were not equally available to N_2, O_2 and CO_2 and hence concluded that polarity rather than molecular dimensions governed the effect. Molina-Sabio *et al.* (2001) have since disputed the existence of channels with preferential access to a given adsorbate by illustrating that the micropore volumes deduced from the adsorption of different molecules, all of a compatible geometry (N_2, CO_2, NH_3 and H_2O), on sepiolite led to an almost common value. Furthermore, this result provided proof for the mechanism of adsorption on sepiolite being typical of a microporous solid, the adsorbate filling the micropores in a liquid-like fashion. They concluded that the different values of surface area obtained when different sorbates were used related to the value of *a* used for the adsorbate (i.e. the effective cross-sectional area for one adsorbate molecule). The value of *a* is a function not only of the size of the molecule but is very much influenced by the crystal lattice of the adsorbent where specific adsorbent-adsorbate interactions occur (Molino-Sabio *et al.*, 2001). Consequently, use of inappropriate values of *a* will lead to discrepancies in the calculated non-microporous surface area. Inagaki *et al.* (1990) and Ruiz-Hitzky (2001) have demonstrated the intracrystalline sorption of atoms (argon), neutral organic molecules (benzene and pyridine) and charged organic species (methylene blue). 2,6-dimethylpyridine, a more

voluminous molecule than pyridine, did not migrate into the tunnels. Current findings therefore suggest that the penetration capacity is primarily dictated by molecular dimensions, polarity being of secondary importance.

1.3 APPLICATIONS OF SEPIOLITE

1.3.1 Introduction

Sepiolite is presently used in a wide variety of fields which take advantage of its sorption capacity and rheological behaviour (Alvárez, 1984). Applications of sepiolite are described here based on the underlying property which they exploit.

1.3.2 Sorption capacity

1.3.2.1 Introduction

The sorptive properties of sepiolite originate from the high surface area and porosity of the mineral. The sorptive capacity of sepiolite is greater than that of any other clay mineral; it is able to sorb more than 100% of its own weight of water and other liquids (Galan, 1996; Santarén, 1996). Three types of active sorption sites are recognized in sepiolite (Alvárez, 1984; Galan, 1996). They are (1) oxygen ions on the tetrahedral sheet of the ribbons; (2) water molecules co-ordinated to Mg ions at the edges of structural ribbons; and (3) silanol groups along the fiber *c*-axis. Owing to the low substitution of Si by ions of lower valence, the oxygen atoms are weak donors in electrons and their interaction with the sorbed-species will therefore be weak. Co-ordinated water molecules can form H-bonds with sorbed species while silanol groups can interact with adsorbed molecules on the external surface of sepiolite (Alvárez, 1984). Absorption may take place, in addition to adsorption, via capillary action and will be dictated by liquid density, viscosity and surface tension, all of which will influence the magnitude of capillary suction (Galan, 1996). Sepiolite preferentially sorbs polar liquids due to the hydrophilic nature of its surface and, in general, the sorption capacity varies in the following order: water > alcohols > acids > aldehydes > ketones > n-olefins > aromatics > paraffins (Santarén, 1996). The sorptive properties of sepiolite can be increased by heating between 200 and 300 °C, which removes surface-adsorbed and zeolithic water (Alvárez, 1984).

1.3.2.2 Applications based on sorptive properties

Adsorbent and absorbent applications of sepiolite are listed in Table 1.3a. Sepiolite has been used for absorbent properties since the 1930s. Use expanded significantly during World War II when it was used in granular form to absorb grease, oil, water, chemicals and other undesirable substances spilled on the floor of factories, stations and aircraft hangars (Galan, 1996). The pores in sepiolite are large enough to permit rapid saturation and, at the same time, are small enough to hold the liquid tenaciously by capillary action. The lack of inflammability is a further reason for the use of sepiolite in this application (Haden, 1961).

Pet litter accounts for ~70% of the total volume of sepiolite produced (Wilson, 2004). The popularity of sepiolite-based litters, which account for the highest proportion of mineral-based cat litters in Europe, is due to their low weight, chemical inertness, high liquid sorption, odour control characteristics and tendency to adsorb bacteria thus reducing their proliferation. Sugiura *et al.* (1991a, 1991b) demonstrated the ability of sepiolite to reduce the environmental concentration of gaseous NH_3 from 100 ppm to 18 ppm.

Table 1.3a. Adsorbent and absorbent applications of sepiolite (Adapted from Santarén, 1996).

Industrial absorbent	Façade cleaning
Moisture adsorption (humidity regulator)	Solvent cleaning
Pet litter	Bleaching earths
Pesticide carriers	Filler for rubber
Cigarette filter	Wastewater remediation
Catalyst carrier	

The absorbent properties which make sepiolite useful as a floor absorbent also find extensive use in converting pesticides and herbicides to free-flowing granules or powders. Many of these chemicals are liquids or sticky pastes which would be difficult or impossible to use as produced. Impregnated and absorbed within particles of sepiolite, the chemicals may be readily applied in the field (Haden, 1961). In addition, clay carriers have been shown to reduce volatilization and/ or leaching from the soils into surface and ground waters (Casal *et al.*, 2001). One such sepiolite-containing product is Mocap® 10G (Rhone-Poulenc), which contains Ethoprophos, an organophosphorous compound used as an

insecticide and nematicide. In an extension of this application, sepiolite has been demonstrated to facilitate the photostabilization of pesticides (Casal *et al.*, 2001). The photolability of many herbicides is a serious drawback for field applications since both the frequency of application and the amounts used must be increased in order to ensure effectiveness as a herbicide. Moreover, the sensitivity to photodecomposition determines the method of application, the persistence of the applied herbicide and the spectrum of weeds controlled (Margulies *et al.*, 1992). In order to achieve photostabilization, sepiolite must first be treated with a photoacceptor such as the organic cationic dye, thioflavin-T, which is able to participate in charge transfer processes with the pesticide. The pesticide is then adsorbed onto the treated sepiolite (Casal *et al.*, 2001). In the resultant organic-inorganic complexes, the protective cationic dye is linked to the clay surface through strong Coloumbic forces and H-bonds, whereas the pesticide molecules are retained by weaker bonds and can be more easily detached from the clay, as required for their biological activity (Margulies *et al.*, 1985; Margulies *et al.*, 1992).

Sepiolite has been used in cigarette filters, where the mineral preferentially adsorbs nitriles, ketones and other dangerous polar gaseous hydrocarbons over less polar compounds such as the aromatic hydrocarbons methylfuran and limonene, which enhance tobacco flavour (Alvárez, 1984; Galan, 1996). Fukumoto (1999) developed a honeycomb deodorizing filter composed of sepiolite together with silica gel and activated carbon. Its performance was superior to that of conventional filters. González *et al.* (2001) have developed humidity-controlling pellets composed of sepiolite together with either activated carbon or calcium chloride.

The majority of catalysts used in industry are impregnated on a support with good mechanical and thermal stability and a large surface area (Alvárez, 1984). Sepiolite, in granular form, meets these specifications. Watanabe *et al.* (2000) used calcined sepiolite-supported Pt/ Fe catalysts to achieve the catalytic complete oxidation of hydrocarbon and volatile organic compound emissions that result from combustion of a fossil fuel. Sepiolite is used to improve the mechanical properties of titanium dioxide, a support used in the catalytic oxidation of *o*-xylene to phthalic anhydride, the production of hydrocarbons from carbon monoxide and hydrogen and the selective catalytic reduction of nitrogen oxides (Knapp *et al.*, 1997). More recently, mixtures of sepiolite and zirconium oxide were used as a support for silver catalysts used in soot combustion (Güngör *et al.*, 2006). Mg^{2+} ions in

the sepiolite structure can be exchanged for catalytically active species such as Ni^{2+}, Pt^{n+}, Pd^{n+}, Zn^{2+} and Cu^{2+} (Galan, 1996) and hence modified sepiolite can act not only as a catalyst support but also as an active catalytic component. Santarén (1996) reported that sepiolite can trap vanadium and nickel, which can inactivate the costly zeolite catalysts during the fluid catalytic cracking of oil, thus prolonging the lifespan of these catalysts.

As a consequence of its adsorptive properties, sepiolite may be used in the remediation of wastewater. Brigatti *et al.* (1996, 1999) demonstrated the ability of sepiolite to remove heavy-metal ions from simulated inorganic polluted industrial wastewater. Affinity for heavy metal cations decreased in the order: $Cu^{2+} > Zn^{2+} > Cd^{2+} > Pb^{2+} \approx Co^{2+}$. Sepiolite pretreated with cationic surfactants has been used to sorb non-ionic organic compounds and anions such as chromate, nitrate and sulphate from industrial wastewaters (Boyd *et al.*, 1988; Smith and Jaffe, 1994; Li and Bowman, 1997; Li *et al.*, 2003). Sepiolite has also been used as a specific carrier for methanogenic bacteria used to produce methane from wastewater (Pérez-Rodríguez *et al.*, 1989; Pereira *et al.*, 2000). In addition to increasing the population of methanogenic bacteria, it also antagonizes the proliferation of sulphate-reducing bacteria, which produce hydrogen sulphide and thus reduce the quality of the gas (Santarén, 1996).

An interesting application that takes advantage of the sorptive properties of sepiolite is its use in the restoration and cleaning of stonework and marble (Hempel, 1969; Larney, 1971; Santarén, 1996). An aqueous sepiolite paste, when applied to the surface to be cleaned, will draw out the stains caused by the absorption of foodstuffs, beverages, soluble salts, corrosion products and environmental pollutants (Larney, 1971; Santarén, 1996).

Micronised grades of sepiolite (e.g. Pansil®) are used as fillers in special rubber applications where, due to its fibrous morphology, sepiolite provides a reticular system of high mechanical strength in extruded products, reducing the swelling in dies after extrusion and increasing the green strength (Santarén, 1996; Galan, 1996). Another use is as an additive in cement, where because of its elongate shape and absorbency, it strengthens the resulting concrete (Murray, 2002).

1.3.3 Rheological properties

1.3.3.1 Introduction

Colloidal grades of sepiolite give stable suspensions of high viscosity at relatively low concentrations following dispersion under high shear (Alvárez, 1984; Simonton *et al.*, 1988). The high shear dispersion conditions result in separation of individual fibers from the bundles such that an intricate intermeshed network of fibers results when at rest. Pangel® products are rheological sepiolite additives produced by Tolsa using a patented wet micronisation process, which disentangles bundles without breaking the needle-like particles, thereby increasing ease of dispersion in water (Figure 1.3a). Once adequately dispersed, most water is immobilized between particles and adsorbed on the external and internal particle surfaces (Santarén, 1993). A system of high viscosity thus results at rest. When suspensions are sheared at high rates, the network yields and the fibers are orientated in the direction of flow; a reduction in apparent viscosity is thus seen (Santarén, 1993). Re-establishment of the structure occurs on standing. Hence suspensions may be described as both pseudoplastic and thixotropic (Viseras *et al.*, 1999). Alvárez (1984), Santarén (1993, 1996) and Tolsa (1999) have reported that sepiolite suspensions are stable over a wide pH range, at high temperatures and high electrolyte concentrations.

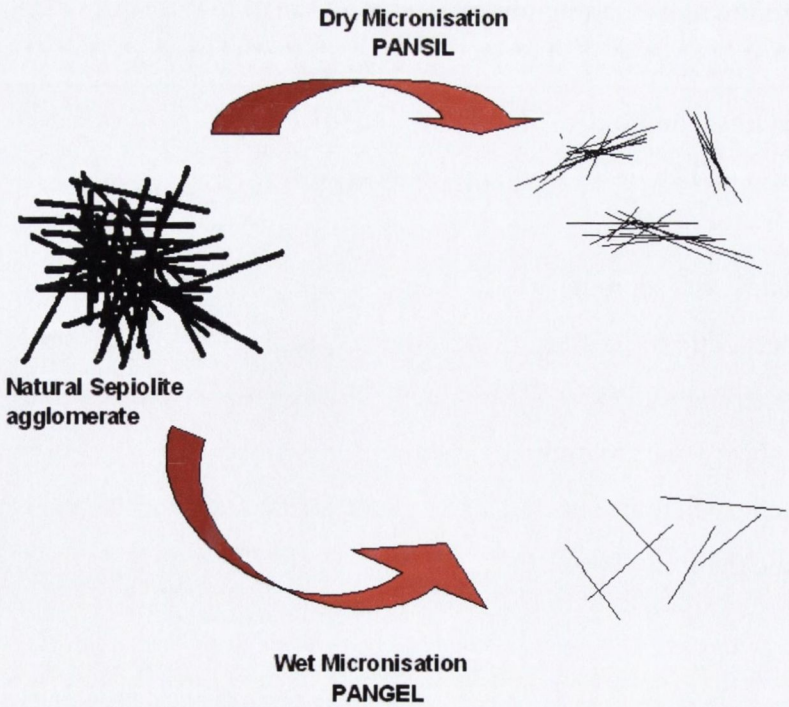


Figure 1.3a. Preparation of Pansil® and Pangel® from sepiolite agglomerate (Tolsa, 1999).

1.3.3.2 Applications based on rheological properties

Amongst the newer applications for sepiolite is its use as a drilling mud (Santarén, 1996). Drilling muds circulated through an oil well suspend the drill cuttings, thereby facilitating their removal from the well. In addition, they cool and lubricate the drill bit and form an impervious filter cake on the walls of the well, thus preventing loss of the fluid to porous formations (Haden, 1961; Santarén, 1996). The drilling mud must have certain rheological properties (Alvárez, 1984). It must be thixotropic with a certain gel strength when the mud is not in motion in order to avoid settling of the drill cuttings when pumping of the drill fluid ceases temporarily. It must be easily pumpable, be stable under the high temperatures occurring during deep drillings and should be little affected by large variations in the concentration of electrolytes encountered in the drilling process. Sepiolite muds fulfill all of these requirements. Sepiolite muds are used in preference to bentonite muds when drilling in areas where salt water brines are encountered or where soluble salts are present as they are less sensitive to salt (Santarén, 1996; Murray, 2000). They are also preferable to palygorskite muds as the fibrous palygorskite particles break across their crystal structure and lose viscosity with continued use (Galan, 1996). Specifications for sepiolite used in drilling are set by the American Petroleum Industry and include references to viscosity in salt saturated water, particle sizing by wet screening and moisture content (Santarén, 1996).

The colloidal properties of sepiolite are also exploited in the preparation of liquid suspension fertilizers, where the pseudoplastic behaviour conferred by sepiolite prevents settling of the insoluble particles when at rest while facilitating easy application through a spray nozzle due to the low apparent viscosity of the suspension when under high shear (Alvárez, 1984; Santarén, 1993; Santarén, 1996; Murray, 2000). In an analogous manner, sepiolite has been used to stabilize paint dispersions. The high viscosity at low shear prevents pigment settling during storage and provides good sag resistance yielding a drip-free paint. Conversely, the low viscosity at high shear provides good flow and leveling during application (Santarén, 1993). In addition, the dried coat exhibits good scrub resistance facilitating easy stain removal (Alvárez, 1984).

1.3.4 Applications of sepiolite of particular relevance to pharmaceutics

1.3.4.1 Animal feedstuffs

More recently, sepiolite has been used in the production of pelleted animal feedstuffs where inclusion of 2% w/w sepiolite has been found to improve binding within the mix, reducing the percentages of broken pellets and fines and the associated dust generation (Angulo *et al.*, 1995; Angulo *et al.*, 1996). Sepiolite was designated an approved EU feed additive (E-562) in 1990 and is licensed for use as a binder and anticaking agent at 2% w/w in feeds for all animal species (Santarén, 1996). It is sold under the tradename Exal®.

Beside its technological properties as a pellet binder, sepiolite shows interesting properties from a nutritional and environmental point of view, particularly with regard to pigs and other non-ruminants (Sardi *et al.*, 2004). Several authors (Castaing, 1994; Castaing and Noblet, 1997; Parisini *et al.*, 1999) demonstrated that the inclusion of a 2% w/w sepiolite additive in a basal pig grower diet improved nutrient utilization and resulted in a higher yield of lean meat without any adverse effect on animal performance. Ouhida (2000a, 2000b, 2000c) reported that the inclusion of 2% w/w sepiolite (Exal®) improved bodyweight gain in broiler chickens by improving organic matter digestibility through an alteration of jejunal digesta viscosity. The magnitude of the effect was comparable to the inclusion of crude enzyme extracts (β-glucanase and arabinoxylanase) in the feed. Associated with its large surface area and sorptive properties, sepiolite helps to reduce the number of dirty eggs by preventing production of liquid faeces, which would otherwise stain egg shells (Santarén, 1996). Sepiolite has been shown to be useful in the treatment of diarrhoea, especially in young animals (Santarén, 1996; Sardi *et al.*, 2004). Furthermore, owing to its sorptive properties, sepiolite can adsorb NH_4^+ molecules produced during the deamination of proteins or hydrolysis of urea along the alimentary tract of pigs and, afterwards, from excreta during storage (Bueno *et al.*, 1984). Moreover, sepiolite can effectively reduce the detrimental effects of mycotoxin-contaminated diets (Schnell *et al.*, 1993; Ramos *et al.*, 1996).

Sepiolite has recently been used as an inert carrier together with wheat flour in Aivlosin® (Schering-Plough Healthcare), a veterinary product containing the macrolide antibiotic acetylisovaleryltylosin. It is a dry mix, intended for mixing with foodstuff prior to administration to pigs for the treatment and prevention of Swine Enzootic Pneumonia

caused by susceptible strains of *Mycoplasma hyopneumoniae*, the treatment of Porcine Proliferative Enteropathy and of clinical outbreaks of Swine Dysentery (Schering-Plough product information).

1.3.4.2 Evaluation as a biomaterial

Interestingly, sepiolite has been demonstrated to interact with type I collagen to form a stable collagen-clay complex (Olmo *et al.*, 1985). The interaction of the protein with the clay surface provokes an exceptional arrangement of collagen in the same direction as the sepiolite fibers (Ruiz-Hitzky *et al.*, 2005). This complex has been evaluated as a biomaterial. It has been proposed that the complex, given its high mechanical strength and porous nature, could be used as a scaffold for the formation of new bone tissue (Olmo *et al.*, 1996). Several *in vitro* studies using human skin fibroblasts have demonstrated the biocompatibility of this complex; cell morphology, proliferation and collagen biosynthesis were unaltered and normal cell adhesion, attachment and spreading occurred on complex surfaces (Lizarbe *et al.*, 1987a; Olmo *et al.*, 1987; Olmo *et al.*, 1988). Furthermore, outgrowth of fibroblasts on a sepiolite-collagen complex was demonstrated to be normal (Lizarbe *et al.*, 1987b). The binding of collagen to the clay hindered its degradation by collagenase (Olmo *et al.*, 1987). Treatment of the protein-clay complex with glutaraldehyde caused cross-linking of the collagen and increased resistance to *in vivo* biological degradation without the loss of biocompatibility (Herrera *et al.*, 1995). Studies of *in vivo* implantation of these complexes in rat soft tissue (subcutaneous and intramuscular) revealed a focally intense foreign-body reaction with abundant giant cells, typical of resorbable biomaterials (Olmo *et al.*, 1992). The implants formed a continuous three-dimensional matrix, showing a fibrous and rough surface topography. Implants were resorbed within three months, while those treated with glutaraldehyde remained unaltered for the entire duration of the 4 month study. Collagen-sepiolite implants were well tolerated following subcutaneous administration; the immunological response was low as indicated by low serum levels of anti-bovine collagen antibody (Olmo *et al.*, 1992). The response of osseous tissue to the implantation of sepiolite-collagen complexes has also been considered (Herrera *et al.*, 1995). The complexes exhibited excellent biocompatibility; they supported mineral formation and allowed bone activity but did not enhance osseous regeneration. Resorption dynamics were similar to those in the soft tissue implants, although slower. Osseous regeneration followed resorption of the complexes thus

allowing healing of bone defects (Herrera *et al.*, 1995). Olmo *et al.* (1996) have thus proposed that these complexes be used as osseous implantation materials. Materials with such filling properties showing the ability to support mineral formation are of interest in orthopaedic surgery, where they facilitate bone repair, and in periodontology.

1.3.4.3 Evaluation as a wound dressing material

The sorptive properties of sepiolite were exploited in the preparation of dressings designed to adsorb odours from wounds. Wound odour is commonly produced by chronic leg or decubitus ulcers and fungating tumors. Short chain organic acids, together with amines and diamines such as cadaverine and putrescine, are responsible for the odour. These compounds are generated from degradation of tissue proteins and lipids by several microorganisms such as *Bacteroides, Clostridium*, *Klebsiella* and *Pseudomonas* (Thomas *et al.*, 1998). Furthermore, production of exudates from leg ulcers can be of the order of 4-12 g/ 10 cm^2 / 24 h (Thomas *et al.*, 1988). Ohta and co-workers (1999) developed a novel product in which the antibacterial povidone-iodine was infiltrated into the sepiolite structure. They demonstrated that this combination preparation adsorbs odours from malodorous wounds while preserving the antibacterial properties of povidone-iodine as confirmed by the absence of a change in the minimum inhibitory concentration. Furthermore, the authors did not observe any irritant reactions to the preparation when applied to a rabbit auricle, rabbit ophthalmic mucosa and human skin. The role of sepiolite as a wound-odour-controlling agent has been further developed by Köse *et al.* (2005). Köse and co-workers prepared a sepiolite-based wound dressing consisting of 2-5 g sepiolite powder (size range 297-720 μm) enclosed in a synthetic cellulosic fabric and sterilised using steam at high pressure. They demonstrated increased adsorption of odour and of simulated wound exudate relative to an activated charcoal dressing (Actisorb® Plus). Köse and co-workers (2005) noted that as sepiolite forms a gelatinous structure following absorption of exudate, loss of sepiolite particles through the fabric would be hindered. To date, this system has only been tested *in vitro*. The authors acknowledge that the effect of sepiolite on odour absorption, exudate absorption and wound pH in acute or chronic wounds in an *in vivo* situation, where effects may be altered by more complex physiological and biochemical interactions, has yet to be investigated.

1.3.4.4 Antidiarrhoeal preparations

Cerezo *et al.* (2001) and Carretero (2002) have reported that fibrous clays, namely palygorskite and sepiolite, are usefully applied in the symptomatic treatment of acute diarrhoea, on the basis of their capacity to sorb and retain water. Alvárez (1984) ascribes these clays a further role in the treatment of diarrhoea, given that they may adsorb the causative bacteria and toxins thus rendering them inactive. Antidiarrhoeal preparations containing palygorskite as the sole active agent for human use (e.g. Pharmasorb®, Actapulgite®) are commercially available in Europe and the US, as are products in which it is combined with other pharmacologically active agents (e.g. Kaopectate® Advanced formula, Diasorb®) (Cerezo *et al.*, 2001). Products available take the form of traditional tablets, chewable tablets and oral suspensions. The usual dose of palygorskite for the relief of diarrhoea is of the order of 1.2 g following each loose bowel movement, up to a maximum of 8.4 g daily. Despite its potential, no commercial antidiarrhoeal product containing sepiolite is currently available (Viseras and López-Galindo, 1999). This property has been exploited in farm animals, where it is a secondary benefit associated with the "food replacing value" of sepiolite. Its choice as a carrier for the antibiotic, acetylisovaleryltylosin, used in the treatment of dysentery in pigs may provide an additional benefit over other inert carriers given its antidiarrhoeal properties, although it must be stated that this is purely supposition.

1.3.5 Sepiolite and magnesium trisilicate

Magnesium trisilicate is a compound of variable composition corresponding to the approximate formula, $Mg_2Si_3O_8.xH_2O$, containing not less than 29% of magnesium oxide and not less than the equivalent of 65% of silicon dioxide, both calculated with reference to the ignited substance (BP, 2007; PhEur, 2007). Magnesium silicate is prepared by the reaction of sodium silicate and magnesium sulphate (Rowe *et al.*, 2003). Some authors (Anonymous, 1998; Rowe *et al.*, 2003) have indicated that sepiolite is a naturally occurring form of magnesium trisilicate, as it complies with the BP and PhEur definitions. Magnesium trisilicate has been widely used as an antacid at quantities of up to 2 g daily (Rowe *et al.*, 2003). It neutralizes stomach acid, producing magnesium chloride and silicon dioxide (Rowe *et al.*, 2003). Alvárez (1984) has noted previously that sepiolite can be used in combination with magnesium oxide and aluminium hydroxide in the treatment of

transient gastric hyperacidity. Many commercial antacid products contain "synthetic" magnesium trisilicate prepared by reaction of sodium silicate with magnesium sulphate (Alenic® Alka) (Shahjahan and Islam, 1998; Rowe *et al.*, 2003). Pharmacopoeial preparations include compound magnesium trisilicate oral powder BP, magnesium trisilicate mixture BP and compound magnesium trisilicate tablets BP. To date, the author is unaware of any commercial preparation containing magnesium trisilicate as sepiolite, nor indeed of any studies assessing the consequences for stability and efficacy when such a substitution is undertaken. Given that "synthetic" magnesium trisilicate does not display the characteristic rheological behaviour of sepiolite, it is likely that the effects of such a change in formulation could be quite profound and therefore, the proposed equivalence of magnesium trisilicate BP and sepiolite is questionable.

Magnesium trisilicate BP has been reported to reduce the bioavailability of certain drugs including nitrofurantoin (Naggar and Khalil, 1979), trimethoprim (Babhair and Tariq, 1983), chloroquine (McElnay *et al.*, 1982b) and mebeverine (Al-Gohary, 1990) and decrease the dissolution rate of others (e.g. paracetamol; Iwuagwu and Aloko, 1992). Reports regarding its effect on propranolol absorption are conflicting (McElnay *et al.*, 1982; Al-Gohary *et al.*, 1987). Magnesium trisilicate has been reported to adsorb *p*-hydroxybenzoic acid although this adsorption is not associated with a reduction in preservative activity (Allwood, 1982; van Doorne and Leijen, 1994). The major mechanism involved in the alteration of bioavailability appears to involve physical adsorption of the drug to the surface of magnesium trisilicate BP via van der Waals' interactions (Al-Gohary *et al.*, 1987). Adsorption of propranolol and other water-soluble beta blockers on magnesium trisilicate was reduced in the presence of competing cations (e.g. Mg^{2+}, Na^{+}) and at low pH (Al-Gohary *et al.*, 1987; Al-Gohary *et al.*, 1988). Reduction in the absorption of tetracyclines, amoxicillin, ampicillin and clindamycin have similarly been reported following oral administration with kaolin and likewise attributed to adsorption on the clay surface (Rowe *et al.*, 2003). Although there are no reports in the literature which refer directly to sepiolite causing a reduction in bioavailability of drugs, it is a distinct possibility that sepiolite could also cause a reduction in bioavailability when administered or formulated with certain drugs as has been reported for kaolin. Clearly the nature of the bonding involved in any adsorption to the clay surface will dictate its rate and extent of desorption. Hermosin *et al.* (1981) did note that hydrocortisone was adsorbed onto the surface of sepiolite by H-bonding interactions with surface silanol groups but was

readily desorbed by rinsing with water. Adsorption may also occur via a cationic exchange process, although given the lower CEC of sepiolite relative to that of kaolin (10 to 100 meq/ 100g; van Olphen, 1977; Deer *et al.*, 1992), halloysite (90 to 95 meq/ 100g) and bentonite (80 to 150 meq/ 100g; La Grega *et al.*, 1994), this adsorption mechanism may not play as significant a role as in the case of the other clays. Furthermore, given that a substantial proportion of the exchangeable cations in sepiolite lie within the zeolithic channels, the drug molecules must be able to access these channels in order to participate in ion exchange processes.

Levis (2000) recognized that these clay-drug interactions could be biopharmaceutically beneficial in that they could be used to modify/ sustain drug release. He attempted to exploit the high binding capacity and hollow tubular morphology of halloysite (approximate dimensions 0.25-0.4 μm in diameter, ~2 μm in length) in the production of a sustained release formulation of diltiazem hydrochloride. A substantial burst release was reported during *in vitro* testing of diltiazem hydrochloride-loaded halloysite. Less than 10% of the loaded drug exhibited delayed release and even in this instance, release reached 100% within 3 hours. Efforts were more successful with propranolol hydrochloride. Byrne (2004) demonstrated conclusively that it was the microtubular structure of halloysite, with its associated tortuosity, that was responsible for the extended release rather than some other factor. Furthermore, he reported that the negative surface charge of porous ceramics was dramatically reduced and in some cases, eradicated, at low pH values corresponding to those encountered in the stomach, thus reducing the ability of these ceramics to bind cationic drugs. Consequently, compatibility between clays and drugs needs to be evaluated on a case-by-case basis. It must be determined empirically due to the large number of interacting variables related to the physicochemical properties of the clay in question (e.g. CEC, identity of exchangeable cations, surface area, presence and dimensions of channels, hydrophilic/ hydrophobic nature of clay, presence of an interlayer space), in addition to those of the drug (Lagaly, 2001). A failure to modify drug bioavailability permits use of the clay as an inert carrier, whilst clay-drug interactions may be exploited in the development of sustained release formulations (Lin *et al.*, 2002; Byrne, 2004).

1.4 TABLETTING

1.4.1 Introduction

The tablet is the dominating pharmaceutical dosage form accounting for over 80% of dosage forms administered today (Rubinstein, 1987). This is the case for many reasons; not least because the tablet offers a convenient and safe way for the patient to administer a drug. The manufacturing procedure facilitates accurate dosing of the drug and tablets can be mass-produced with robust production procedures at relatively low manufacturing costs (Alderborn, 2002). Furthermore, pharmaceutical actives are generally more stable when formulated as solid dosage forms such as tablets rather than as liquid preparations (Berggren, 2003). The form is distinctive and identifiable as tablets come in a variety of shapes and colours and readily accept debossing techniques (Shiromani, 2006). In addition, they are less prone to tampering than other dosage forms and are convenient for packing and shipping (Shiromani, 2006). Drug release from tablets can be modified to meet biopharmaceutical and pharmacological requirements. However, the dosage form is not without its disadvantages, the greatest of which is that tablets may fail to deliver the whole of their drug content to the body or unintentionally delay the release of the drug (Cole, 1998). Formulators can choose from a wide range of tablet manufacturing methods – including direct compression, wet granulation and dry granulation.

1.4.2 Pharmaceutical powder compaction

1.4.2.1 Particle deformation

The behaviour of powders during tablet compression is often very complicated because air can exist both between and within particles. The physical nature of a powder column is different from that of a solid body, as powder can flow and therefore have the rheological properties of liquids (Paronen and Ilkka, 1996). On the other hand, phenomena typical of solid bodies, namely permanent deformation (plastic flow), reversible deformation (elasticity) and brittle fracturing, can also occur in powders. Tablets are usually prepared by uniaxial compression using eccentric presses or rotary tabletting machines. When a particle bed is subjected to an external load, the volume is reduced through a reduction in the inter- and intraparticulate pore space. The process of volume reduction is presented in

Figure 1.4a and involves an initial rearrangement of the particles, followed by particle deformation via elastic changes or plastic flow or particle failure by brittle fracture (Paronen and Ilkka, 1996; Berggren, 2003). The dominating volume reduction mechanism during the compression event depends on the properties of the consolidating material. Some materials are brittle and consolidate by brittle fracture or fragmentation, some are ductile and consolidate by plastic deformation, while others consolidate by both fragmentation and plastic flow. Plastic deformation usually occurs in powders in which the shear strength is less than the tensile strength, whereas fragmentation becomes dominant with hard, brittle materials in which the shear strength is greater than the tensile strength (Çelik and Driscoll, 1993). The mechanism of compaction will also be influenced by particle size (Paronen and Ilkka, 1996), moisture content (Bolhuis and Chowhan, 1996) and experimental conditions e.g. applied pressure, dwell time, velocity of compaction (Roberts and Rowe, 1985; Wells, 1988).

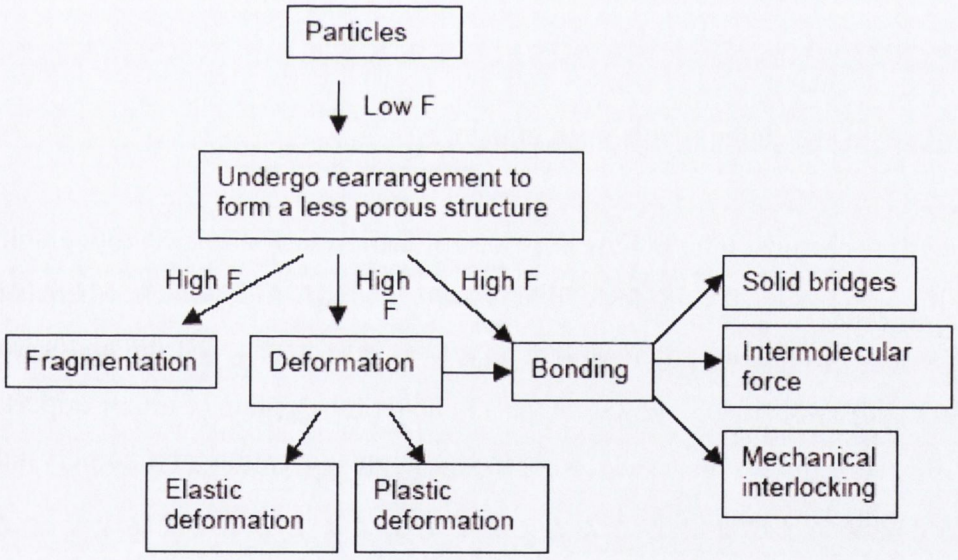


Figure 1.4a. The deformation mechanisms of powder particles upon compression (F = compression force) (Reproduced from Guo, 2002).

There is no pharmaceutical powder in existence that exhibits just one of the deformation mechanisms mentioned above (Guo, 2002). There is, however, a spectrum ranging from highly elastically deforming to highly plastically deforming to highly brittle materials. Even where materials are known to be brittle, smaller particles of these materials may deform plastically (Çelik and Driscoll, 1993).

1.4.2.2 Mechanisms of interparticulate bonding

During compression, the particles will be brought together into such close proximity that interparticulate bonds can be created, thus resulting in the production of a tablet of a certain strength. It has been suggested that the mechanical strength is governed by the interparticulate bonding mechanism and the area over which these bonds interact. Three types of interparticulate bond applicable to tablets include solid bridges, intermolecular forces and mechanical interlocking (Nyström and Karehill, 1996). Çelik and Driscoll (1993) reported that these bonds never act independently.

Solid bridges can be defined as areas of real contact, i.e. contact at an atomic level between adjacent surfaces in the compact. Different types of solid bridges have been proposed in the literature and include bridges formed by self-diffusion of atoms between surfaces, melting followed by resolidification, and recrystallization of soluble materials in the compacts (Nyström and Karehill, 1996).

The term "intermolecular forces" includes van der Waals forces, electrostatic forces and hydrogen bonding, of which the first is the dominant type.

The incidence of mechanical interlocking depends on the shape and surface topography of the particles. Smooth spherical particles will have little tendency to interlock, whereas long needle-like fibers and irregular particles might be expected to do so (Nyström and Karehill, 1996). Bonding with mechanical interlocking is a bonding mechanism of minor importance for most of the investigated materials with the possible exception of microcrystalline cellulose (Guo, 2002).

1.4.3 Tabletting by wet granulation

Wet granulation is a process of dry mixing, wet mixing and particle size enlargement (Propst, 2002). It is the oldest and most conventional way of making tablets (Bandelin, 1989). The main rationales for granulation prior to tabletting are: (1) to increase the bulk density of the powder mixture and thus ensure that the required volume of powder can be filled into the die; (2) to improve the flowability of the powder; (3) to facilitate volume dispensing; (4) to improve mixing homogeneity and reduce the risk of segregation; (5) to

improve the compactibility of the powder by adding a solution binder, which is effectively distributed on the particle surfaces; (6) to reduce dust generation in the tabletting mixture and (7) to control the rate of drug release (Bandelin, 1989; Alderborn, 2002).

An overview of the sequence of unit operations used in the production of tablets by wet granulation is presented in Figure 1.4b. Each step requires qualification, cleaning and cleaning validation. The greatest disadvantage associated with wet granulation lies in its cost (Propst, 2002), which is reflective of the space, labour, time, equipment and energy consumption involved. It is the most expensive of all available tabletting methods (Bandelin, 1989). In addition, there is the possibility of material loss during processing due to the transfer of material from one unit operation to another, which can increase the risk of cross-contamination of the products. Use of moisture and heat will lead to increased risk of drug degradation in the case of those drugs which are moisture sensitive and/or thermolabile (Alderborn, 2002; Propst, 2002; Shiromani, 2006). Ibrahim and Olurinola (1991) compared the levels of microbial contamination in wet granulation and direct compression methods of tablet production. They concluded that the direct compression method resulted in a product of higher microbial quality. The wet granulation stage proved to be most liable to microbial contamination owing to the use of both moisture and heat. Fasihi and Parker (1987) noted that the compression process reduced the microbial count in an extent related to the product of compression force and compaction speed, but Ibrahim and Olurinola (1991) noted that this inimical effect was more pronounced in the case of direct compression.

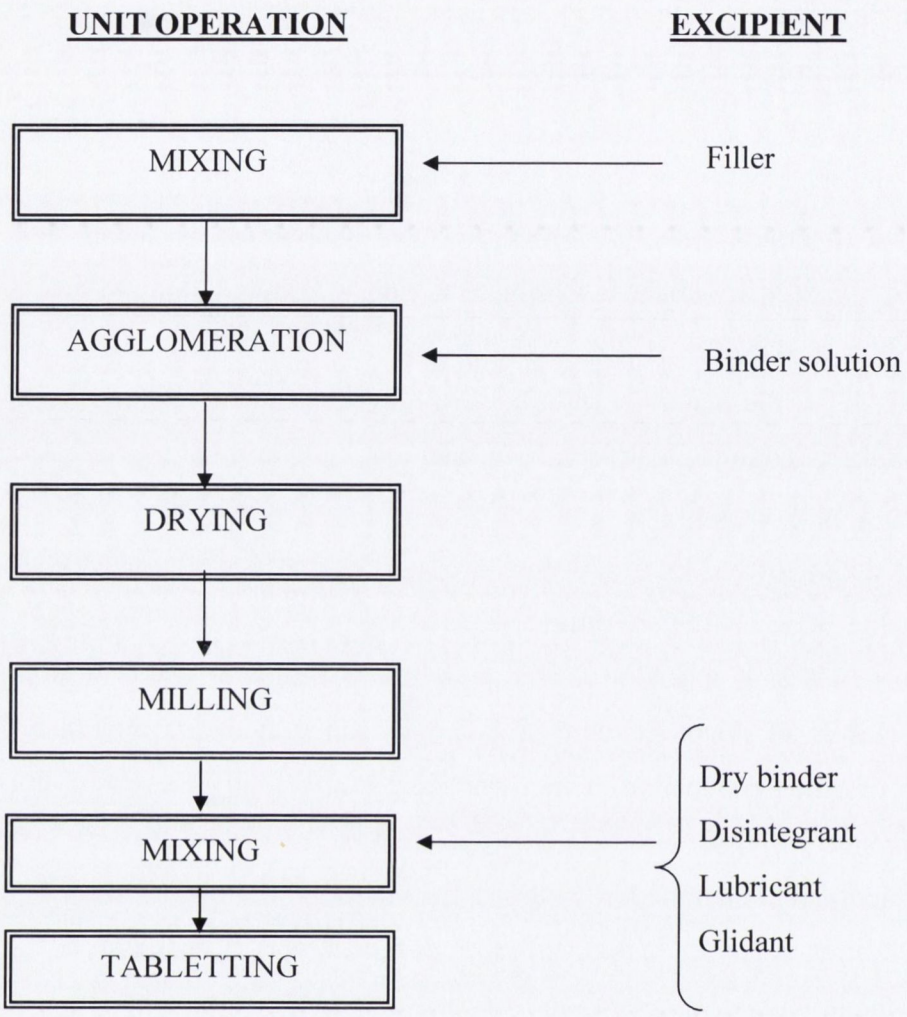


Figure 1.4b. Overview of the sequence of unit operations involved in the production of tablets via wet granulation (Adapted from Alderborn, 2002).

Despite these shortcomings, it continues to find widespread application for a number of reasons. Firstly, as it is the oldest method of tablet production, there is an extensive series of well established products where considerable data on product stability, safety, efficacy and bioavailability has been accumulated. In these cases, there is considerable reluctance to switch to an alternative tabletting method such as direct compression, which would require a change in the excipients and a re-evaluation of all such product properties in accordance with regulatory requirements (Bandelin, 1989). Secondly, wet granulation affords the production of a more uniform mixture with a reduced tendency to segregate relative to direct compression. When dealing with small amounts of a potent active or colour additive, wet granulation is consequently the method of choice (Alderborn, 2002). Finally, granulation is the only method suitable for the compression of high dose drugs of poor

tablettability as the inclusion of a sufficient amount of direct compression base (DCB) to render the mixture suitable for direct compression becomes unfeasible due to the resulting increase in tablet size (Bandelin, 1989).

1.4.4 Tabletting by direct compression

Direct compression is extremely popular amongst generic manufacturers, with 43% citing it as their method of choice. In comparison, just 27% of innovator companies rate direct compression as their first choice (Shiromani, 2006). Tablet production by direct compression involves just two unit processes in sequence; namely powder mixing and tabletting (Figure 1.4c). This in turn translates into reduced equipment and space requirements, lower labour costs, reduced processing time and lower energy costs (Bolhuis and Chowhan, 1996). Due to fewer unit operations, the validation and documentation requirements are also reduced (Gohel, 2005). Cost of validation can account for up to 20% of the total installed cost of any project (Cole, 1998). In addition, the removal of moisture and heat from the process reduces the risk of drug or excipient degradation and microbial contamination (Ibrahim and Olurinola, 1991). Furthermore, tablets produced by direct compression generally disintegrate into primary particles rather than granules, increasing the surface area exposed to the dissolution medium and consequently increasing the rate of drug dissolution (Alderborn, 2002). Although simple in terms of the unit processes involved, the direct compression process is highly influenced by powder characteristics such as flowability, compressibility and dilution potential. Approximately 70 to 80% of formulations contain excipients at higher concentrations than the active drug (York, 1992). As a consequence the processability of the formulation is largely dictated by the nature of the excipients. The fundamental requirement for successful direct compression is the production of a uniform mix, with little tendency to segregate during the transfer to hoppers, intermediary bulk containers and so forth. In order to limit segregation, the density and particle size distribution of the active must be matched to that of the excipient (Shiromani, 2006). Realistically, this can be very difficult to accomplish as many poorly soluble drugs are micronised to hasten dissolution rates (Alderborn, 2002). It seems that innovator companies favour the wet granulation process because of uncertainty over drug properties during scale-up while generic companies favour direct compression as it is the cheapest and by the time patents have expired, the physical properties of the drug substance are more clearly defined (Shangraw, 1989).

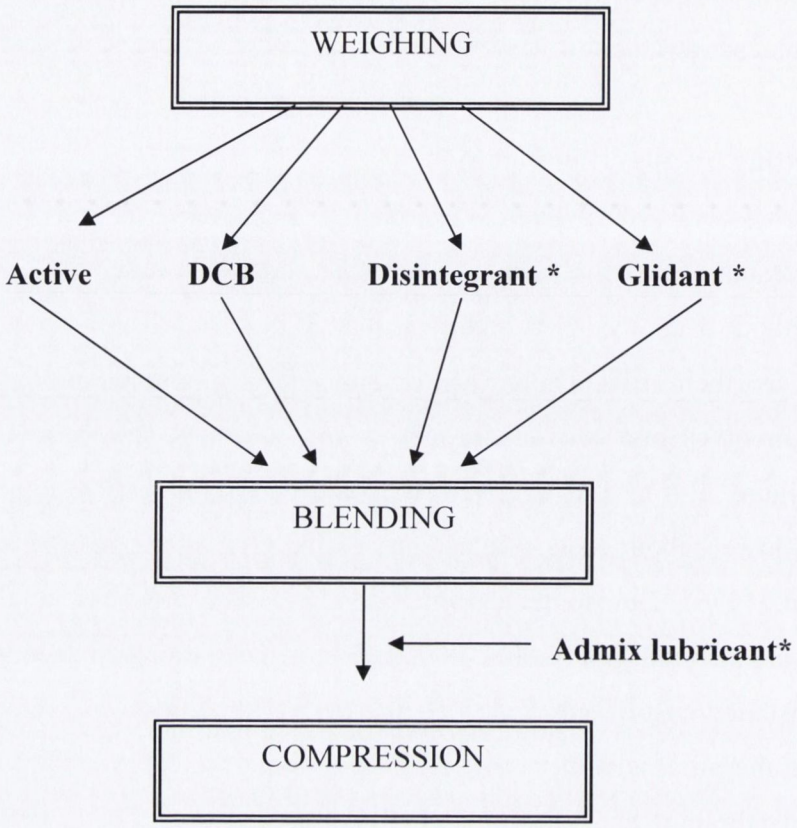


Figure 1.4c. Overview of the unit processes involved in direct compression (* some or all of the functions of a disintegrant, glidant and lubricant may be performed by the DCB in which case it is referred to as a multipurpose excipient (MPE)).

A comprehensive comparison of wet granulation and direct compression tabletting methods is presented in Table 1.4a.

Table 1.4a. Comparison of tabletting by wet granulation and direct compression (Adapted from Shangraw, 1989).

	Wet granulation	Direct compression
Compressibility	Harder tablets for poorly compressible substances	Potential problem for high-dose drugs and those with extremely low bulk density
Fluidity	Excellent in most cases	Many formulations may require a glidant Cannot micronise high-dose drugs
Content uniformity	Massing and drying induced	Segregation may occur in mass transport, hopper and feed frame
Lubricant	Less sensitive to lubricant softening and overblending	Minimal blending of magnesium stearate with plastically deforming DCBs due to high lubricant sensitivity
Disintegration	Often problems with granules	Lower levels of disintegrant usually necessary
Dissolution	1. Drug wetted during processing 2. Drug release from granules may be retarded if granules slow to disintegrate 3. Generally slower than direct compression	1. No wetting during processing, may need surface active agent 2. Dissolution may be slower if larger size drug crystals used 3. Generally faster than wet granulation
Costs	Increase in equipment, labor, time, process validation, energy, space requirements	Increase in the cost of raw materials and their quality control
Flexibility of formulation	Granulation covers raw material flaws	Properties of raw materials must be carefully defined
Stability	1. Problems with heat and/or moisture 2. Dissolution rate may decrease with time	1. No heat or moisture added 2. Dissolution rate rarely changes
Tabletting speed	May be faster	May require slower speeds
Dust	Less dusty	More dusty

1.4.5 Direct compression bases (DCBs)

1.4.5.1 Introduction

Very few excipients and even fewer drugs possess the properties necessary to permit direct compression into tablets. Physical processing is generally required to engineer powders with optimum functional properties and technical performance during tabletting (Bolhuis and Chowhan, 1996). Particle engineering is a broad-based concept that involves the manipulation of particle parameters, such as shape, size, size distribution, and of the simultaneous minor changes that occur at the molecular level, such as polymorphic changes (Nachaegari and Bansal, 2004). All of these parameters are translated into changes in the bulk-level properties such as flowability, compressibility and moisture sensitivity (Figure 1.4d).

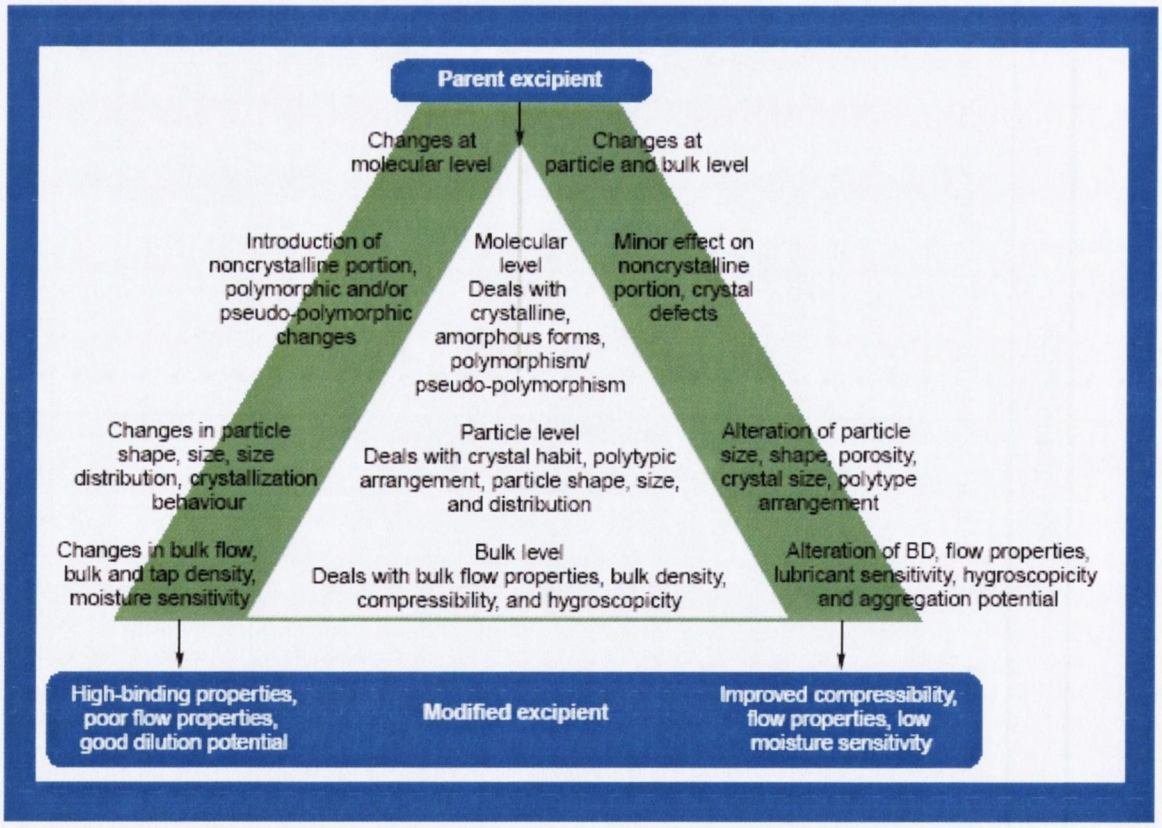


Figure 1.4d. Particle engineering by modification at the molecular, particle and bulk level. (BD = bulk density; Reproduced from Nachaegari and Bansal, 2004).

During recent years, significant progress has been made in producing filler-binders with enhanced physico-mechanical properties designed for direct compression into tablets.

These improvements were accomplished using different techniques, the most important of which are the following: grinding and/or sieving, crystallization techniques, granulation, dehydration and spray drying (Bolhuis and Chowhan, 1996). A combination of these particle engineering methods is often used (van der Voort Maarschalk and Bolhuis, 1998).

Indeed, the advent of direct compression as it is known today was made possible in the late 1950s with the commercial availability of spray dried lactose (Foremost Foods Co., San Francisco), the first tablet filler possessing the fluidity and compressibility necessary to form compacts in high-speed tablet presses i.e. the first direct compression base (DCB) (Shangraw *et al.*, 1981). A major drawback of the direct compression method is the very high cost of the direct compression bases (DCBs) owing firstly to the physical processing which the bases must undergo to render them directly compressible and secondly to the relatively small number in existence, which are in turn produced by an even smaller number of manufacturers (Bolhuis and Chowhan, 1996; Nachaegari and Bansal, 2004). Furthermore, it is not possible to change sources of supply or grades of raw materials without validating effects on fluidity, compressibility and solubility. This cost is typically more than offset by the economies described earlier (Shangraw, 1989).

Bolhuis and Chowhan (1996) list the most important requirements for a DCB as

1. high compactibility
2. good flowability
3. good blending properties
4. low lubricant sensitivity
5. good stability
6. chemical inertness
7. compatibility with other tabletting excipients (i.e. lubricants, glidants, colourants etc.)
8. capability of being reworked without loss of flow or compressibility characteristics and
9. batch to batch reproducibility.

Powder flowability is typically determined by powder properties such as particle size, size distribution and particle shape. These parameters can be relatively easily controlled by techniques such as milling, classification and agglomeration. This is in sharp contrast to

compactibility, which is predominantly dictated by material properties such as surface energy and deformation. Alteration of these parameters is generally extremely difficult, if not impossible, and they generally have an optimum value (van der Voort Maarschalk and Bolhuis, 1998).

1.4.5.2 Preparation of DCBs

1.4.5.2.1 Spray drying

Spray drying is a particle preparation technique that is widely used within the food, chemical, biochemical and pharmaceutical industries for different applications (Berggren, 2003). During spray drying, a solution or suspension is atomized and converted to solid particles by rapid evaporation in a one-step process. Spray drying encompasses four consecutive stages: (1) atomization of the feed dispersion into a spray; (2) spray-air contact; (3) convective drying of the spray; and (4) separation of the dried product from the drying gas (Broadhead *et al.*, 1992).

There are many different types of spray dryer (Aulton, 2002), but all generally contain the following features: a feed delivery system, an atomizer, a heated air supply, a drying chamber, a solid-gas separator and a product collection system (Masters, 1991). For normal industrial spray drying, there are three main atomizer designs: rotary, pressure nozzle and two-fluid nozzle (Oakley, 1997). In a rotary atomizer, the liquid to be atomized is fed onto a rapidly rotating vaned wheel or disk (Figure 1.4e(i)). The liquid is accelerated outward by centrifugal forces and ejected as a thin sheet of liquid, which is subsequently broken into droplets. These atomizers are virtually non-clogging and adjustments for the effect of feed rate on drop size can be easily made by varying the rotational speed. A major drawback however, is that they necessitate the use of very wide drying chambers as the droplets exit the atomizer at a high horizontal velocity (Lukasiewicz, 1989; Oakley, 1997). At large droplet sizes, the size of the drying chamber required can become unfeasibly large. In the pressure nozzle (Figure 1.4e(ii)) liquid is swirled either by a tangential inlet or slotted inserts. This swirl is sufficient to force the liquid outward as a thin film at the outlet orifice, which is subsequently ejected as a hollow cone of liquid and broken up into droplets. The sprays produced by these nozzles have a cone angle of approximately 60° and consequently require a narrower chamber than rotary atomizers. Pressure nozzles

therefore are preferred for the production of medium to large particles (Oakley, 1997). They are more susceptible to blockage and require the use of very high feed pressures, which may cause a high rate of abrasion and necessitate regular replacement of certain parts (Lukasiewicz, 1989). Two-fluid nozzle atomizers are frequently used for pilot-scale or small-scale production work (e.g. Büchi Mini Spray Dryer B-191). Their operating costs are generally prohibitively high at medium and large production scales. In the two-fluid nozzle atomizer, a high-velocity air stream atomizes the feed. Average droplet size is proportional to the viscosity and surface tension of the feed and inversely proportional to the mass ratio of atomizing air to feed material (Lukasiewicz, 1989).

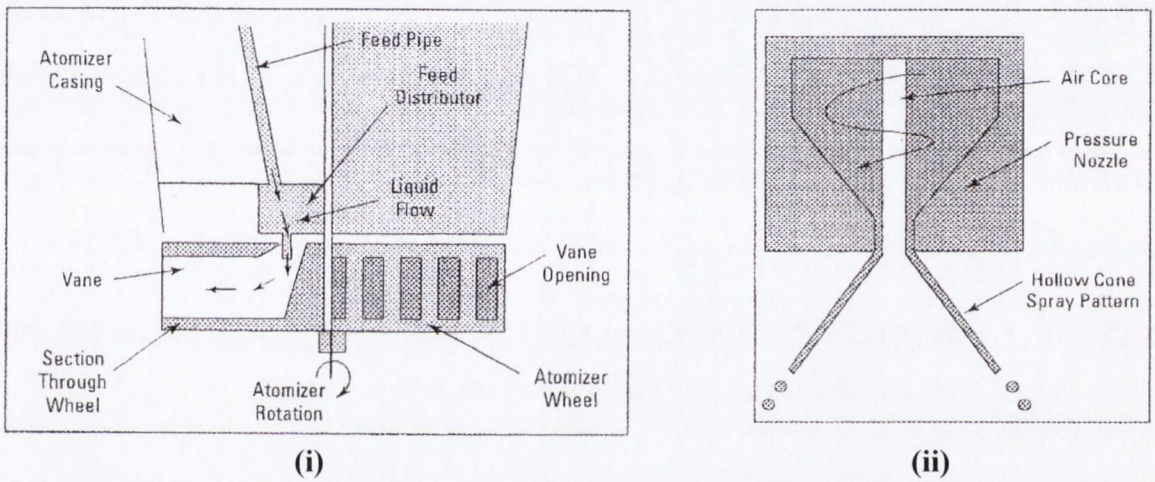
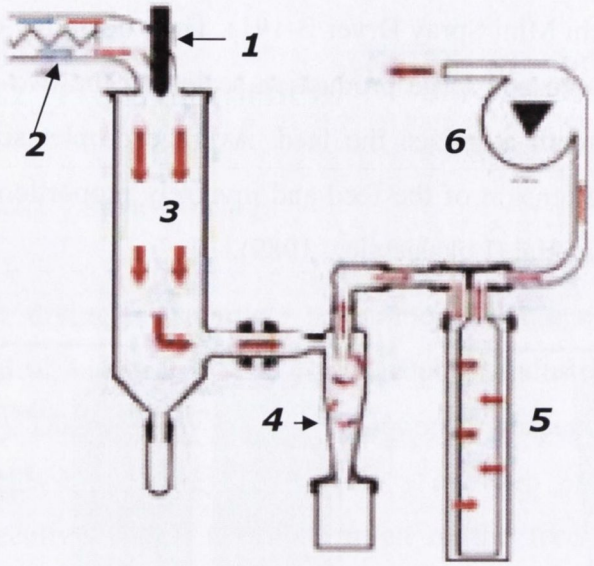


Figure 1.4e. Schematic of (i) a rotary atomizer and (ii) a pressure nozzle atomizer (Reproduced from Oakley, 1997).

The atomizing process produces an extremely large surface area for heat and mass transfer, which promotes rapid drying. The actual drying time will depend on the droplet size and how tightly bound the solvent is (Oakley, 1997). The droplets do not attain a high temperature owing in part to the rapid nature of the drying process and also to the fact that most of the heat is used as latent heat of vaporization (Aulton, 2002). Hence the process is suitable for heat-sensitive materials.

Although the geometry of the drying chamber may vary, the cylinder-on-cone design is by far the most common shape (Figure 1.4f). Cocurrent, countercurrent and mixed flow spray chambers may be used. In cocurrent chambers, the spray and hot drying gas are introduced at the top of the chamber and travel in the same direction through the dryer (Figure 1.4f). Countercurrent conditions are produced by locating the drying air inlet at the opposite end

of the chamber with respect to the atomizer. As a result, the dried particles come into contact with the hottest drying gas rendering this arrangement unsuitable for thermolabile compounds (Lukasiewicz, 1989; Oakley, 1997).



1. *Two-fluid nozzle, operated by compressed air to disperse the solution into fine droplets*
2. *Electric heating of the drying medium*
3. *Spray cylinder for drying the droplets to solid particles*
4. *Separation of the particles in the cyclone*
5. *Outlet filter to remove fine particles*
6. *Aspirator*

Figure 1.4f. Schematic of the Büchi Mini Spray Dryer B-191 illustrating cocurrent flow (Reproduced from Büchi spray drying training papers).

By changing the spray drying conditions (e.g. feed rate, atomizing air flow rate, inlet temperature), it is possible to alter and control properties such as particle shape, particle size distribution, bulk and particle density, flowability, moisture content and solid-state properties (Broadhead *et al.*, 1992; Corrigan, 1995; Oakley, 1997; Berggren, 2003). For crystalline materials, rapid cooling can produce porous solids with imperfect crystal structures containing amorphous material. Lattice defects imply a high deformability, in other words, an increased plasticity (van der Voort Maarschalk and Bolhuis, 1998). This increased compactibility coupled with the improvement in flowability usually associated with the production of spherical particles is the basis for its use as a technique to improve properties for direct compression. Examples of DCBs produced by spray drying are Avicel® PH101 (microcrystalline cellulose (MCC)), TRI-CAFOS S® (tricalcium phosphate) and Karion Instant® (sorbitol).

1.4.5.2.2 Co-processing

In recent years, a number of excipient mixtures were introduced utilising particle engineering in the design of combination products for direct compression. These co-processed excipients are single-bodied excipient combinations at a subparticle level as distinct from simple physical mixtures (Nachaegari and Bansal, 2004; Figure 1.4g). It has been demonstrated that the use of such co-processed products has, in a number of cases (e.g. Cellactose®, Ludipress® and Pharmatose®), resulted in a product which retains the functionality of both excipients while masking undesirable properties (Bolhuis and Chowhan, 1996). Such products avoid the rigorous and costly safety testing associated with a new chemical entity, given that both components have typically been in widespread use (Gohel, 2005). Co-processing two or more excipients provides a much broader platform for the manipulation of excipient functionality. The availability of a large number of excipients for co-processing ensures numerous possibilities to produce tailor-made "designer excipients" to address specific functionality requirements (Nachaegari and Bansal, 2004). Co-processing has typically been used to address problems associated with flowability, compressibility and disintegration behaviour.

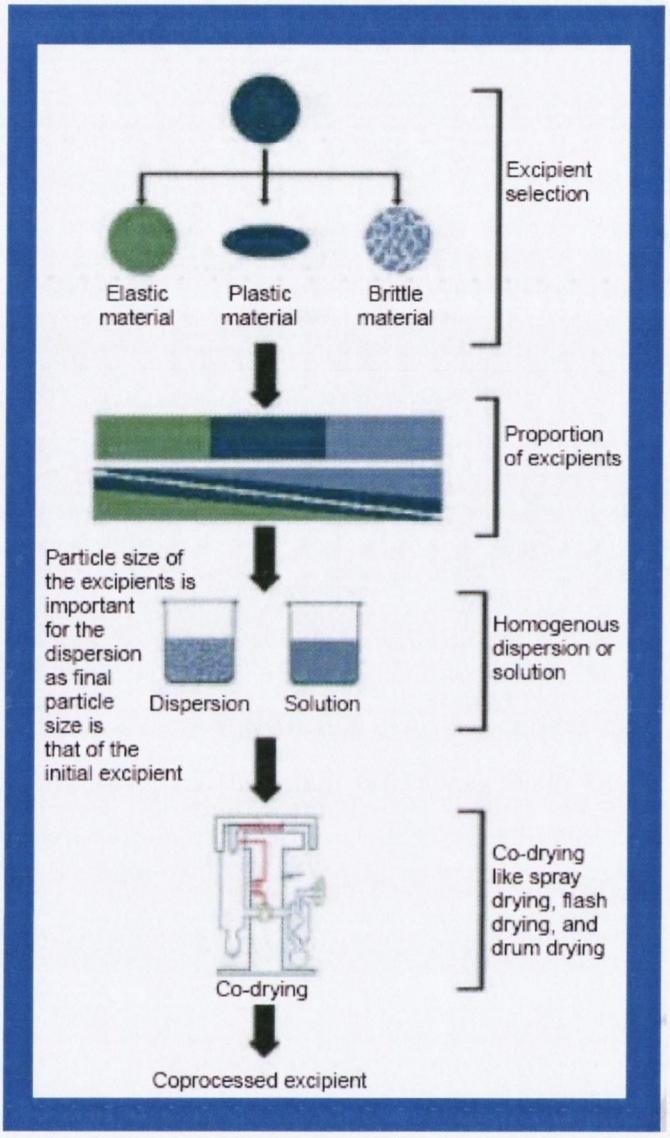


Figure 1.4g. Schematic representation of the co-processing method (Reproduced from Nachaegari and Bansal, 2004).

Co-processing began in the 1980s with the introduction of co-processed MCC and calcium carbonate and was soon followed by Cellactose® (Meggle Corporation, Germany). Silicified MCC (Prosolv®), a product produced by co-processing of colloidal silicon dioxide and MCC, is the most widely used co-processed excipient (Bolhuis and Chowhan, 1996). Filler-binder combinations were those most commonly investigated (Nachaegari and Bansal, 2004). Commonly used co-processed directly compressible excipients are listed in Table 1.4b.

Table 1.4b. Co-processed directly compressible excipients (Adapted from Gohel, 2005).

Brand name	Adjuvants	Manufacturer
Cellactose®	MCC, α-lactose monohydrate	Meggle Corp., Germany
Ludipress®	α-lactose monohydrate, Kollidon® 30, Kollidon® CL	BASF Pharma, Germany
Starlac®	Lactose monohydrate, maize starch	Roquette, France
Pharmatose® DCL 40	Anhydrous β-lactose, lactitol	DMV, Holland
Avicel® CE 15	MCC, guar gum	FMC Corp., USA
Prosolv®	MCC, colloidal silica	Penwest Pharmaceuticals, USA
Di-pac®	Sucrose, dextrin	American Sugar, USA
Advantose® FS 95	Fructose, starch	SPI Polyols, France
Emdex®	Maltose, dextrose	Edward Mendell, USA

1.4.5.3 Microcrystalline Cellulose (Avicel® PH) – a DCB prepared by spray drying

In a survey conducted by Shangraw and Dermarest (1993), filler-binders were rated based on their compactibility, solubility, supply, compatibility, ease of handling and physiological inertness. On the basis of these criteria, microcrystalline cellulose was rated as the number one filler-binder. MCC is described in the USP-NF (2006) as a purified, partially depolymerised cellulose prepared by treating α-cellulose, obtained as a pulp from fibrous plant material with mineral acids (Figure 1.4h). The cellulose fibers in the starting material are composed of millions of microfibers. In these microfibers, two different regions can be distinguished: a paracrystalline region, which is an amorphous and flexible mass of cellulose chains, and a crystalline region, which is composed of tight bundles of cellulose chains in a rigid linear arrangement (Bolhuis and Chowhan, 1996). The acid only penetrates the paracrystalline region, reducing them to sugars or soluble short chain fragments, which are thus removed, yielding aggregates of the more crystalline regions of the fibers (Sisson, 1966).

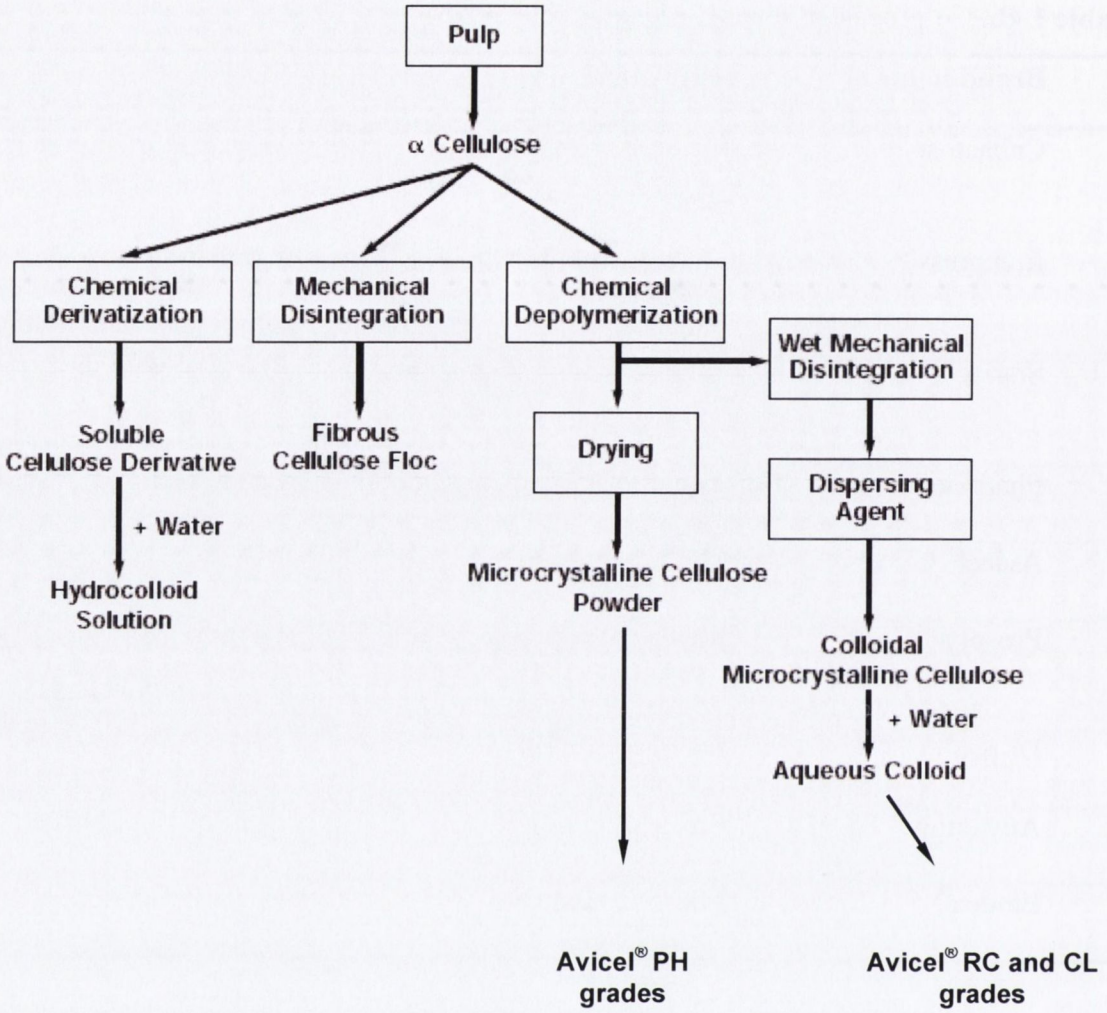


Figure 1.4h. The Avicel® manufacturing process (Adapted from Reier, 2000).

These cellulose microcrystals are of diameter 10 to 30 nm and can randomly aggregate together through hydrogen bonding to form aggregates (Figure 1.4i) (Yu and Atalla, 1998). After purification by filtration and spray drying, dry porous microcrystals are obtained. Pores may range in size from several nanometers to 10 nm or more. The manufacturing process may be thought of as breaking the cellulose fibrous material down to a microcrystalline form and then agglomerating these crystallites into aggregates or particles.

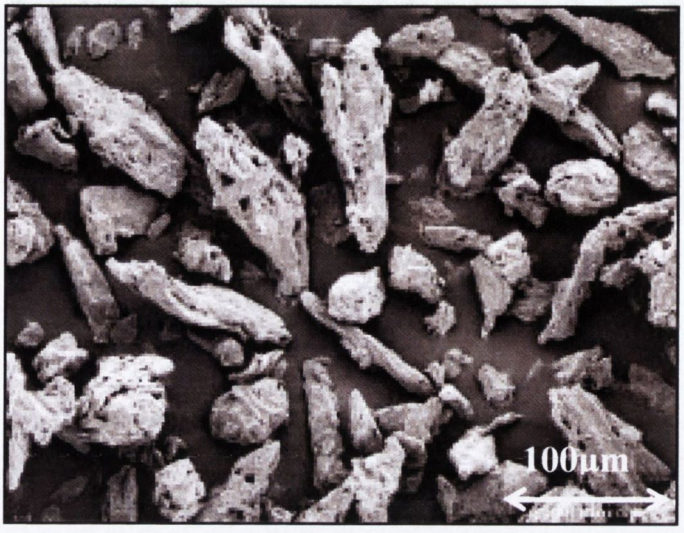


Figure 1.4i. SEM of Avicel® PH101 (Reproduced from Reier, 2000).

By controlling the atomization and drying conditions, particle size distribution and residual moisture content can be varied (Table 1.4c; Reier, 2000). MCC was marketed first by FMC under the trade name Avicel® PH. Ten different grades of Avicel® PH are currently available (Table 1.4c).

MCC is the most compressible of all DCBs and has the highest dilution potential. It has an extremely low coefficient of friction and therefore has no lubricant requirements itself. Lubrication is necessary when more than 20% drug or other excipient is added (Shangraw, 1989). Hydrogen bonding between the cellulose microcrystals and mechanical interlocking of these irregular elongated particles are responsible for the excellent binding properties of MCC (Bolhuis and Lerk, 1973). When compressed, the MCC particles are deformed plastically due to the presence of slip planes and dislocations (resulting from acid hydrolysis) on a microscale and the deformation of the spray dried agglomerates on a macroscale (Shangraw, 1989). MCC also acts as a disintegrant, although the disintegrating properties are not very consistent and depend very much on the formulation (Doelker, 1993).

Table 1.4c. Different grades of Avicel® PH available commercially (from FMC Corporation literature). Note: DC = direct compression.

Grade	Mean particle size (µm)	Moisture content (% w/w)	Applications
PH101	50	3-5	DCB, wet granulation, extrusion-spheronization.
PH102	100	3-5	As for PH101, larger particle size improves flow of fine powders.
PH102SCG	150	3-5	Special coarse grade used to improve flow.
PH103	50	<3	As for PH101 where moisture sensitive actives are concerned.
PH105	20	<5	Most compressible of the PH products but poorly flowable, used in the DC of coarse, granular or crystalline materials.
PH112	100	<1.5	As for PH102 where very moisture sensitive actives are concerned.
PH113	50	<2	As for PH101 where very moisture sensitive actives are concerned.
PH200	180	<5	Improved flowability; used to reduce weight variation and improve content uniformity in DC.
PH301	50	3-5	High density grade resulting in improved flowability, mixability, greater tablet weight uniformity and permits production of a larger batch size. Also used as a capsule-filling excipient.
PH302	100	3-5	As for PH301, larger particle size improves flowability further.

MCC has been extensively used in the wet granulation process of tablet making for a number of reasons:

1. It permits rapid, even wetting as the wicking action thoroughly distributes the granulating liquid throughout the powder bed.
2. The large surface area and adsorptive capacity renders it less sensitive to variations in water content and hence less susceptible to overwetting.
3. Less screen blocking occurs due to the good wet mass consistency.
4. It promotes rapid and uniform drying, thereby ensuring uniform final moisture content throughout the batch and reducing drying times and costs.
5. It acts as an auxiliary binder, producing larger granules with a reduced proportion of fines.
6. It also acts as a disintegrant, lubricant and glidant. However, in cases where the drug content exceeds 20%, a lubricant will be required (Bandelin, 1989; Propst, 2002).

MCC does however have a number of drawbacks. Firstly, the matchstick-like morphology and small particle size results in extremely poor flowability (Bolhuis and Chowhan, 1996). Poor flow in a DC operation can lead to excessive tablet weight variation and lack of content uniformity. Due to its plastic nature, it exhibits a high lubricant sensitivity. The compactibility of MCC is highly influenced by its moisture content. At an equilibrium moisture content of 5% w/w, most of the water will be within the porous structure of MCC and a large proportion of this bound moisture is thought to be hydrogen-bonded to small fragments of cellulose within the particle. During plastic deformation, this moisture will act as an internal lubricant, facilitating flow. Low moisture levels can result in capping (Bolhuis and Chowhan, 1996). It has been suggested that the presence of an optimum amount of water will prevent elastic recovery by lowering the yield point and facilitating the formation of bonds through hydrogen bond bridges (Khan *et al.*, 1981). MCC tablets are hygroscopic and softening accompanies this uptake of water. Furthermore, there is huge variability in the physical properties of MCC derived from different suppliers (Shangraw, 1989; Landin *et al.*, 1993) and consequently, given that the source cannot be changed without significant consequence for the properties of the finished product, negotiating power with suppliers is limited and thus MCC is expensive relative to other DCBs. Moreover, a dramatic reduction in compactibility of MCC has been reported following wet granulation (Staniforth *et al.*, 1988).

Different grades (Table 1.4c) with improved density and increased particle size were produced to address, at least in part, these shortcomings (Bolhuis and Chowhan, 1996). However, improved flow through particle size enlargement is achieved at the cost of reduced compactibility and increased lubricant sensitivity, presumably due to the inevitable reduction in surface area (Tobyn *et al.*, 1998). The functionality of MCC has been modified by blending with starch, lactose, dicalcium phosphate or codrying with starch and calcium sulphate (Wu *et al.*, 2001). However, all of these modifications offer direct compression tabletting performance that falls short of that of MCC alone. Silicified MCC (Prosolv®) was specifically designed to address the loss of compactibility that occurs following wet granulation of MCC and has proved the most successful strategy in terms of overcoming the limitations of MCC while retaining all of its advantages (Tobyn *et al.*, 1998; Rowe *et al.*, 2003).

1.4.5.4 Ludipress® - a DCB produced by co-processing

Ludipress® is a free-flowing granular product (Figure 1.4j) composed of the filler, α-lactose monohydrate (93% w/w); the binder, Kollidon® 30 (3.5% w/w); and the disintegrant, Kollidon® CL (3.5% w/w). The co-processing step involves granulation, which results in the coating of the lactose particles with povidone and crospovidone (Bolhuis and Chowhan, 1996; Gohel, 2005). From Figure 1.4j it is evident that the roughly spherical particles are made up of a large number of small crystals with smooth surfaces (Bolhuis and Chowhan, 1996). The compactibility of Ludipress®, both lubricated with 1% w/w magnesium stearate and unlubricated, was found to be much better than the corresponding physical mixture (Figure 1.4k; Baykara *et al.*, 1991; Schmidt and Rubensdörfer, 1994a, 1994b). It exhibits a high dilution potential, excellent flowability and low lubricant sensitivity, while retaining the non-hygroscopic nature of lactose (BASF product literature). Although it contains a disintegrant, the disintegration of Ludipress® tablets takes longer than tablets containing α-lactose monohydrate. The reduced rate of disintegration is attributed to the presence of povidone.

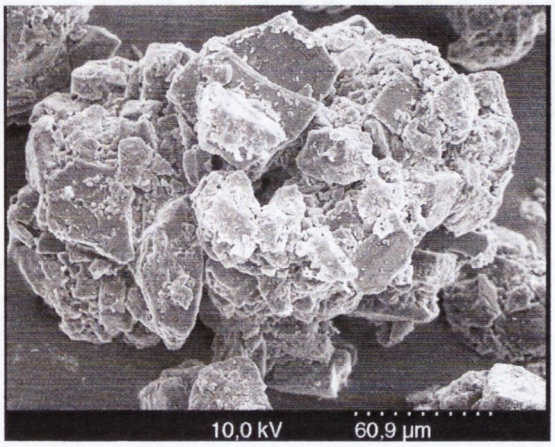


Figure 1.4j. Particle structure of Ludipress® grade (Bühler, 2004).

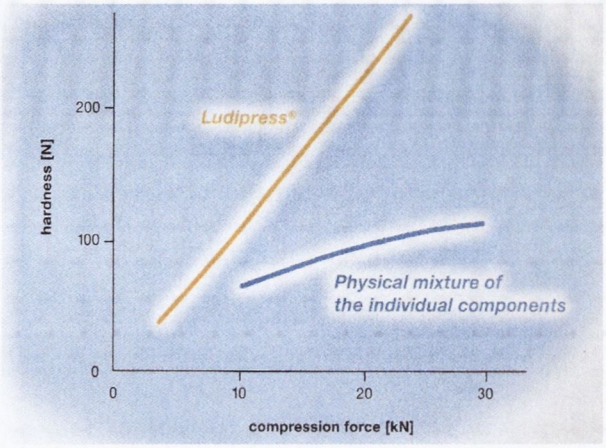


Figure 1.4k. Compression force/ tablet hardness curves for Ludipress® and its corresponding physical mixture (BASF product literature).

1.5 COLLOIDAL SYSTEMS

1.5.1 Introduction

Dispersed systems consist of particulate matter distributed throughout a continuous medium. The dispersed material may range in size from particles of atomic and molecular dimensions to particles of dimensions in the millimetre range. Dispersed systems have thus been classified into three groups based on the mean diameter of the dispersed particles, namely molecular dispersions (diameter < 1.0 nm), colloidal dispersions (diameter in range 1-500 nm) and coarse dispersions (diameter > 500 nm) (Martin, 1993). van Olphen (1977) reported that any particle having a linear dimension in the range 10^{-3} to 1 µm can be defined as a colloidal particle. The size limits are somewhat arbitrary, there being no distinct transition between either molecular dispersion and colloids or colloids and coarse dispersions. The overall physicochemical properties of the colloidal dispersion are determined by (a) the chemical and physical nature of the dispersed phase; (b) the chemical and physical properties of the dispersion medium; and (c) the nature of the interaction at the interfaces between air and the dispersion medium, and the dispersed phase and the dispersion medium (Vanderhoff, 1996). Colloidal systems can be classified as lyophobic and lyophilic in accordance with the relationship between the colloidal particle and dispersion medium. Lyophilic dispersions are those in which the dispersed material displays an affinity for the dispersion medium (van Olphen, 1977). Lyophobic colloids are

those in which the dispersed material has little, if any, affinity for the dispersion medium (Martin, 1993). Lyophobic colloidal particles form a two-phase system with the medium, and a phase boundary (of very large surface area) exists between the particles and dispersion medium (Martin, 1993). In lyophobic colloids, the interactions between particles, and between particles and the medium, are governed by the nature of the particle surface, in particular the surface charge density, and the manner in which it responds to changes in salt concentrations, organic materials and pH (Lagaly, 2005).

1.5.2 Aqueous clay dispersions – hydrophobic colloidal systems

Dispersions of small clay particles in water behave like hydrophobic colloids (van Olphen, 1977). Hydrophobic sols are never stable in the thermodynamic sense and consequently several changes occur in such systems over time. Firstly, where particles are more dense than the dispersion medium, they may settle slowly disturbing the homogeneity of the system. Such an occurrence is counteracted with varying success by diffusion forces and in some cases by interparticulate forces. Secondly, flocculation, or the agglomeration of particles, occurs when salt is added to a stable sol (van Olphen, 1977).

1.5.2.1 DLVO theory of stabilization of hydrophobic colloids

1.5.2.1.1 Introduction

The electrostatic stabilization of hydrophobic colloids was described independently by Derjaguin and Landau (1941) and Verwey and Overbeek (1948). The resultant theory is known as the DLVO (Derjaguin-Landau-Verwey-Overbeek) theory (van Olphen, 1977). According to the DLVO theory, a colloidal dispersion is stable when the potential energy of repulsion arising from the approach of charged particles exceeds the inherent attractive energy between the particles over a given distance of separation (Vanderhoff, 1996).

1.5.2.1.2 The electrical double layer

The basic principle behind the electrostatic stabilization of a colloidal dispersion is the accumulation of charge at the surface of the particles. This charge can originate via a number of mechanisms including dissociation of surface groups, ion deficiencies in the

crystal lattice and adsorption of ions from solution. The development of surface charge in the context of clay minerals is more complex and the surface charge is typically heterogeneous. This issue is discussed in further detail in Chapter 7. Irrespective of its origin, the presence of surface charge results in the accumulation of ions of opposite charge (counter-ions) in the medium near the particle surface due to electrostatic attraction. These ions have a tendency to diffuse from the surface to the bulk solution where the concentration is lower. Therefore, the concentration of counter-ions near the particle surface is high and decreases with increasing distance from the particle surface. The diffuse layer not only consists of an excess of ions of opposite sign; there is usually a deficiency of ions of the same charge near the surface, as these co-ions are electrostatically repelled by the surface. The diffuse counter-ion atmosphere and surface charge together constitute an "electrical double layer" (Figure 1.5a).

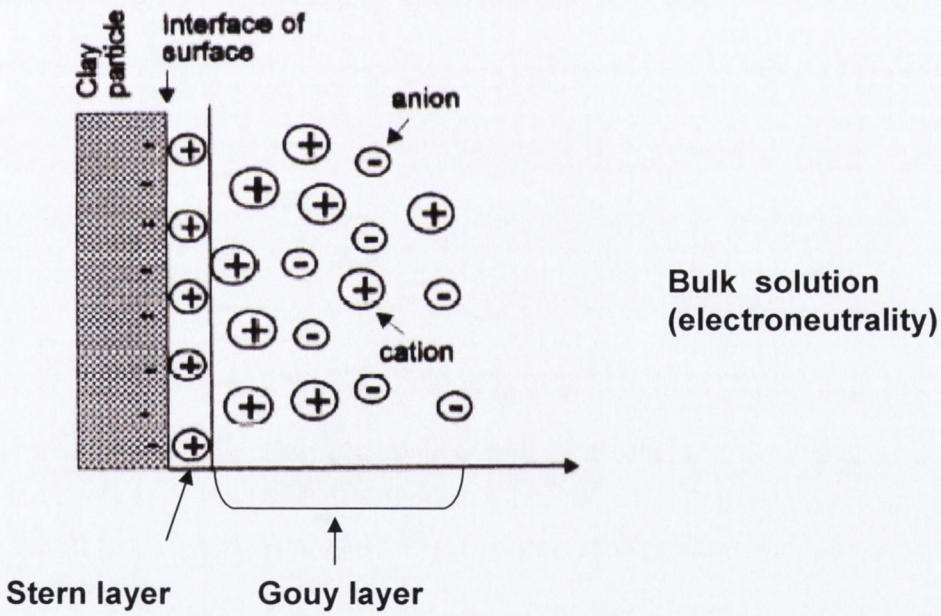


Figure 1.5a. The structure of the electrical double layer at the surface of a clay particle (Reproduced from Luckham and Rossi, 1999).

Counter-ions and co-ions in immediate contact with the surface are said to be located in the Stern layer. Ions further away from the surface form the diffuse or Gouy layer (International Union of Pure and Applied Chemistry (IUPAC), 1972). The charge at the particle surface gives rise to two electrostatic potentials relative to a point in the bulk solution: the surface potential, (ψ_0), which exists at the surface, and the Stern potential, (ψ_δ), which occurs at the inner boundary of the Gouy layer. When the particle moves

relative to the dispersion medium, part of the double layer moves with the particle, thus generating a shear plane. The potential at this plane is called the zeta potential (ζ) and it reflects the fall off in potential over the mobile part of the double layer. In practice it is assumed that it is equal to the Stern potential (Vanderhoff, 1996; Luckham and Rossi, 1999).

1.5.2.1.3 Interparticle double layer repulsion

As two particles approach each other in suspension due to Brownian motion, their diffuse double layers begin to interfere. Consequently, there is a change in the distribution of ions surrounding both particles leading to an increase in the free energy of the system (Luckham and Rossi, 1999). The amount of work required to carry out these changes and to bring the particles from infinite separation to a given distance is the repulsive energy or repulsive potential, V_R, and, for surface potentials less than 50 mV, is given by:

$$V_R = \left(\frac{Da\psi_0}{\kappa^2}\right)\ln\left[1+\exp\left(-\frac{S}{1/\kappa}\right)\right] \qquad \textbf{Equation 1.5a}$$

where D is the dielectric constant of the dispersion medium, a is the particle radius, $(1/\kappa)$ is the double layer thickness and S is the distance of separation between the two particles (Vanderhoff, 1996).

At higher surface potentials, the repulsive potential may also be described as a function of $[exp\ (-S/(1/\kappa))]$ (Luckham and Rossi, 1999). The repulsive potential therefore decreases exponentially with increasing particle separation (Luckham and Rossi, 1999).

1.5.2.1.4 Interparticle van der Waals attraction

These dispersion forces arise from the charge fluctuations in an atom associated with the motion of electrons, which produces a time-dependent dipole moment. A phase difference in the fluctuating dipoles leads to mutual attraction (Vanderhoff, 1996). The attractive energy between two particles of radius a at a distance of separation S, for $a >> S$, is:

$$V_A = \frac{aA^*}{12S} \qquad \textbf{Equation 1.5b}$$

where A^* is the effective Hamaker constant describing the attraction between the particles and the dispersion medium.

1.5.2.1.5 Total energy of interaction

The DLVO theory states that the total energy of interaction between colloidal particles, V_T, is given by the sum of the attraction and repulsion energies:

$$V_T = V_A + V_R \qquad \textbf{Equation 1.5c}$$

Figure 1.5b shows the variation of the total energy of interaction, V_T, between two colloidal particles with interparticle distance, S.

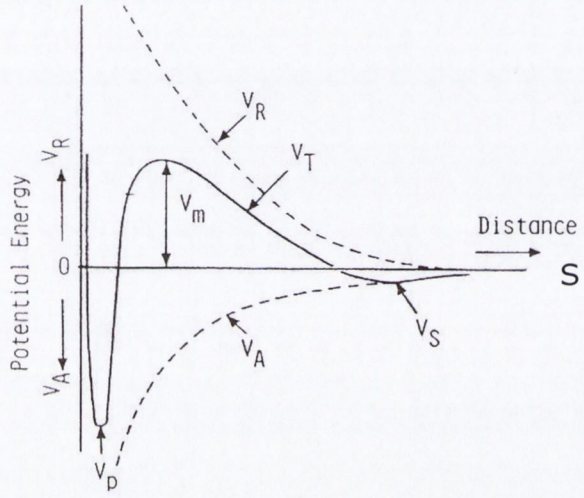


Figure 1.5b. Variation of attraction and repulsion energies and the net interaction energy as a function of particle separation (Adapted from Luckham and Rossi, 1999).

At small distances, the van der Waals attraction predominates, and the net interaction is attraction in the deep potential energy minimum, V_p, also termed the primary attractive minimum. Association of particles in the primary minimum results in irreversible coagulation of the particles (Vanderhoff, 1996). At greater distances, the electrostatic repulsion energy falls off more rapidly with increasing separation distance than the attraction energy and the net interaction is attraction in the shallow secondary minimum, V_s. Association of particles in the secondary minimum produces a flocculated state. Of significant importance is the occurrence of a maximum energy (V_m) at intermediate distances, which is considered as an energy barrier that the particles must overcome if they are to approach each other in the primary minimum of irreversible coagulation (Luckham and Rossi, 1999). The height of V_m, which is dependent on the magnitude of the zeta potential, determines the relative stability of the system. When V_m is greater than 10 to 20 kT, where k is the Boltzmann constant, collisions of the two particles produced by

Brownian motion will not overcome the barrier and agglomeration will not occur. This value of V_m typically corresponds to a zeta potential of 25 mV (Bhargava *et al.*, 1996).

In the case of plate-like clay particles like bentonite, both the surface charge and the associated double layer at the faces differ from that at the edges due to the differing ratios of silica and alumina groups present at these sites (van Olphen, 1977). When a suspension of bentonite flocculates, three different modes of particle association may occur: face-to-face (FF), edge-to-face (EF) and edge-to-edge (EE) (Figure 1.5c). The electrical interaction energy for the three types of association is governed by three different combinations of the two double layers (Luckham and Rossi, 1999).

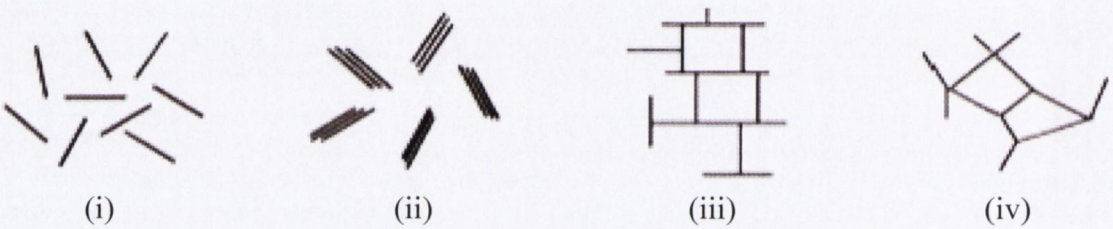


Figure 1.5c. Modes of particle association in clay suspensions: (i) dispersed; (ii) face-to-face (FF); (iii) edge-to-face (EF); and (iv) edge-to-edge (EE).

FF association best describes agglomeration resulting in thicker and larger flakes as the electrical double layers collapse. The reverse of agglomeration is known as dispersion. Flocculation of clay suspensions has been reported to be a consequence of EF and EE association (van Olphen, 1977; Luckham and Rossi, 1999). The effect of electrolytes, pH and temperature on the stability of colloidal clay systems is discussed in greater detail in Chapter 7.

1.5.2.1.6 Stabilization of hydrophobic colloids

Two general modes are currently recognized for the stabilization of lyophobic dispersions: electrostatic and polymeric stabilization. Electrostatic stabilization relies upon the adsorption of co-ions to the particle surface, thus increasing the zeta potential and the barrier to particle association in the primary minimum. Steric stabilization relates to the stabilization afforded by the adsorption of polymers to the particle surface (as in Figure

1.5d). The resulting steric hindrance and entropy repulsion prevents agglomeration of adjacent suspended particles (Nash, 1996). One of the main advantages of steric stabilization over electrostatic stabilization is its relative insensitivity to the presence of electrolytes (Vanderhoff, 1996; Luckham and Rossi, 1999). Furthermore, strongly hydrated hydrophilic polymers exert a further "protective" effect as their adsorption on the suspended particles results in the formation of a protective hydration layer around each suspended particle and a consequent significant lowering of the Hamaker constant, thus weakening the interparticle attraction. Displacement of specifically adsorbed counterions by the adsorbed polymer and orientated water molecules will further increase the magnitude of the V_R term in the DLVO theory (Luckham and Rossi, 1999). Steric stabilization can be combined with electrostatic stabilization (i.e. by the use of a polyelectrolyte), which is termed electrosteric stabilization (Luckham and Rossi, 1999).

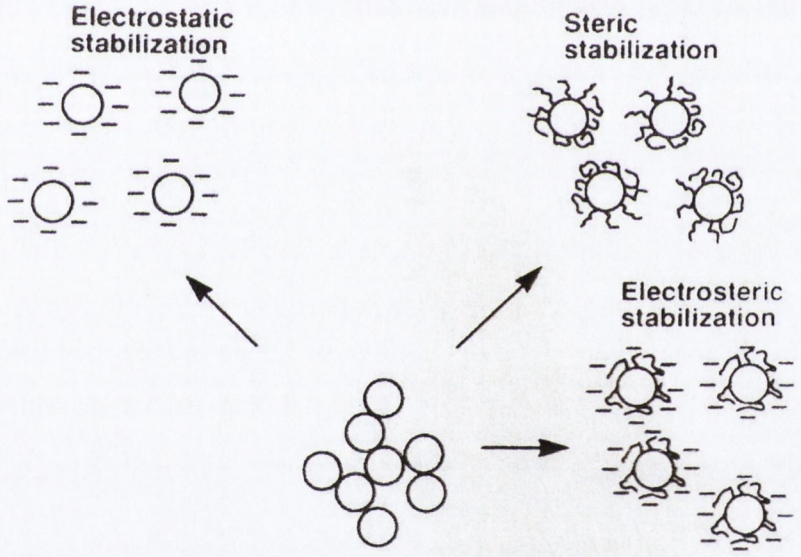


Figure 1.5d. Schematic representation of the mechanisms of electrostatic, steric and electrosteric stabilization (Reproduced from Rezwan, 1996).

1.6 RHEOLOGY

1.6.1 Introduction

Rheology is the study of flow and the deformation of matter (Radebaugh, 1996). The flow behaviour of any system is commonly described in terms of the relationship between the shear stress, σ, and the shear rate, γ. The shear rate is defined as the change of shear strain per unit time, and the shear stress as the tangential force applied per unit area (Luckham and Rossi, 1999). The ratio of the shear stress to the shear rate is called the viscosity, η, and is a measure of the resistance of a fluid to flow (van Olphen, 1977):

$$\eta = \frac{\sigma}{\dot{\gamma}} \qquad \textbf{Equation 1.6a}$$

1.6.2 Newtonian and non-Newtonian flow behaviour

A plot of the shear stress as a function of the shear rate is called a consistency curve. Four different types of flow may be distinguished: Newtonian, pseudoplastic, Bingham plastic, and dilatant, as illustrated in Figure 1.6a (Luckham and Rossi, 1999). When the shear stress is directly proportional to the shear rate, as in Equation 1.6a, the fluid is Newtonian and exhibits a constant viscosity. Newtonian flow is exhibited by liquids and solutions and in very dilute suspensions where the suspended particles do not interact with one another (Salter, 2003). In the other types of flow behaviour, the viscosity varies with the shear rate and these are called non-Newtonian fluids (Martin, 1993).

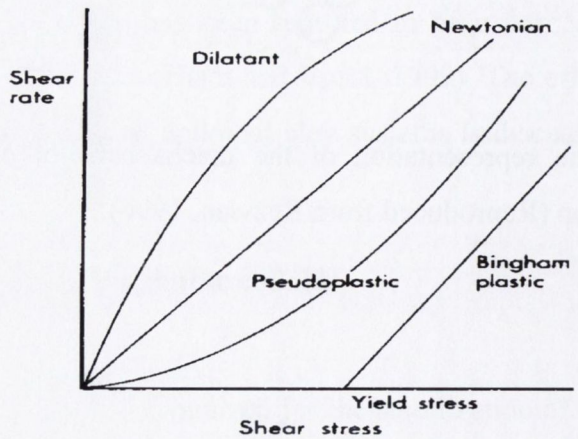


Figure 1.6a. Consistency curves depicting Newtonian, pseudoplastic, Bingham plastic and dilatant flow behaviour (Luckham and Rossi, 1999).

Many colloidal dispersions exhibit Bingham flow, which may be described by the following equation:

$$\sigma = \sigma_B + \eta_p \cdot \dot{\gamma} \qquad \textbf{Equation 1.6b}$$

where σ is the shear stress, σ_B is the Bingham yield point, $\dot{\gamma}$ is the shear rate and η_p is the plastic viscosity, defined as the slope of the curve (Radebaugh, 1996).

The Bingham model postulates that a finite stress must be applied to initiate flow and at greater stresses, flow will be Newtonian. The resistance of the suspension to flow can therefore be considered as consisting of two parts: a Newtonian part in which the shear rate is proportional to the shear stress and a non-Newtonian part in which the shear rate is zero irrespective of the magnitude of the applied shear stress (Luckham and Rossi, 1999).

If viscosity is a function of the rate of shear, a reduction of the viscosity with increasing rate of shear is called shear-thinning or pseudoplastic flow behaviour (van Olphen, 1977). Very dilute clay suspensions behave as pseudoplastic fluids, which may be described by the power-law equation:

$$\sigma = K \cdot \dot{\gamma}^n \qquad \textbf{Equation 1.6c}$$

where K is a measure of the consistency of the fluid; and n the flow-behaviour index, which is a measure of the decrease of apparent viscosity with shear rate (Luckham and Rossi, 1999).

Various rheological models have been proposed which describe the rheological behavior of clay suspensions. The models of Bingham plastic and of power law are the most popular because the flow equations are easy to use and describe the rheological data with sufficient accuracy (Kelessidis and Maglione, 2006). Many times though, rheological behavior of bentonite suspensions cannot be described with these simple models because of the non-linear behavior, not covered by the Bingham plastic model, and because they exhibit a yield stress, which is not modelled in the power law model. It is for this reason that other non-linear models have been suggested incorporating at the same time a yield stress. Examples of these models include the two parameter model of Casson and the three parameter models of Herschel–Bulkley. Many other models have also been suggested, containing four and even five parameters, which, however, have not found extensive use because of the complexity of the resulting flow equations (Kelessidis and Maglione, 2006).

The Herschel–Bulkley model is a three parameter model given by (Luckham and Rossi, 1999; Matijaŝić and Glasnović, 2002):

$$\sigma = \sigma_{HB} + K \cdot \dot{\gamma}^{n} \qquad \textbf{Equation 1.6d}$$

where σ is the shear stress, σ_{HB} is the Herschel-Bulkley yield point, K is the consistency index and n is the flow behaviour index, used to characterise behaviour at supra-yield stresses.

It incorporates the Newtonian model ($\sigma_{HB} = 0$, $K = \eta$, $n = 1$), the Bingham plastic model ($n = 1$) and the power law model ($\sigma_{HB} = 0$) (Kelessidis and Maglione, 2006). This model is often used to describe the flow behaviour of clay suspensions, in particular those of drilling muds (Luckham and Rossi, 1999; Matijaŝić and Glasnović, 2002).

If $n > 1$, then the fluid may be regarded as dilatant; where $n < 1$, the fluid is said to be pseudoplastic. A suspension with flow conforming to the Herschel-Bulkley model therefore behaves like a Bingham material at low shear rates: that is, it possesses a yield point, but after yielding, it exhibits pseudoplastic or shear-thickening behaviour (Radebaugh, 1996; Luckham and Rossi, 1999). In cases where the flow behaviour index is 1, the Herschel-Bulkley equation reduces to the Bingham model (Radebaugh, 1996).

The parameters of the above equations may be divided into two groups. The first group, the Bingham yield stress and Herschel-Bulkley yield stress relate to behaviour at low shear rates. The second group, namely the plastic viscosity and flow-behaviour index reflect the high shear rate behaviour of the fluid (Luckham and Rossi, 1999).

The Casson model is an empirical model, originally proposed to describe the rheological behavior of printing inks, but use is also made for drilling fluids, which are primarily clay suspensions (Kelessidis and Maglione, 2006). This model is given by:

$$\sigma^{1/2} = \sigma_0^{1/2} + \eta_p^{1/2} \cdot \dot{\gamma}^{1/2} \qquad \textbf{Equation 1.6e}$$

where σ is the shear stress, σ_0 is the yield point, $\dot{\gamma}$ is the shear rate and η_p is the viscosity.

1.6.3 Thixotropy

Clay suspensions often display thixotropic behaviour (van Olphen, 1977). Thixotropy is defined as a reversible, time-dependent, isothermal gel-sol-gel transformation (Nash, 1996). After mixing the suspension, the yield stress and apparent viscosity decrease (Curve 1 *versus* Curve 2, Figure 1.6b) but will recover with time if left to stand. If the shear rate is ramped-up and then immediately ramped-down, the stresses recorded for each rate of shear will be lower on the downward curve than on the upward curve and a 'hysteresis' loop is obtained (Curve 3, Figure 1.6b). This occurs because the fragments of the network, which are broken under shear, need time to re-establish a three-dimensional network. In addition, when a clay system is subjected to a constant rate of shear, the viscosity decreases with time as the gel structure is broken down until an equilibrium viscosity is reached (Luckham and Rossi, 1999).

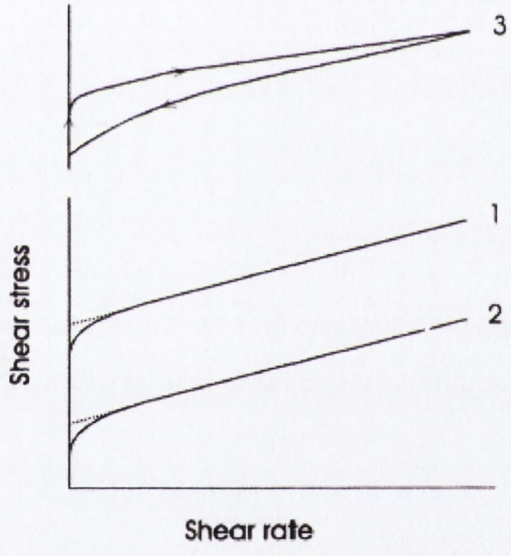


Figure 1.6b. Typical flow curves for concentrated thixotropic clay suspensions. (1) initial flow curve; (2) flow curve after mixing; and (3) thixotropic loop. (Reproduced from Luckham and Rossi, 1999).

1.7 PHARMACEUTICAL SUSPENSIONS

1.7.1 Introduction

Pharmaceutical suspensions are stable dispersions of a finely divided solid in a liquid vehicle, which is usually water-based (Ofner and Schnaare, 2001). Suspensions are used to prepare liquid preparations of drugs which are not adequately soluble and cannot be solubilised by the use of cosolvents or surfactants to permit formulation as a solution. As a dosage form they offer several advantages: (1) easy to swallow and hence preferred for geriatric and paediatric patients who can have difficulty in swallowing solid oral dosage forms such as tablets and capsules; (2) disagreeable tastes can often be overcome by purposefully limiting the amount of drug in solution and by flavouring the liquid vehicle; (3) improved chemical stability compared to solutions; (4) bioavailability is high and generally viewed in the following order for various dosage forms: solutions > suspensions > capsules > tablets (Ofner and Schnaare, 2001).

Martin (1993) listed three general classes of pharmaceutical suspension: orally administered suspensions, externally applied suspensions (topical lotions) and injectable (parenteral) suspensions. The following discussion pertains to the former two types. Oral suspensions are defined as "oral liquids containing one or more active ingredients suspended in a suitable vehicle. Suspended solids may slowly separate on standing but are easily redispersed" (BP, 2007). Those suspensions for cutaneous application are preparations of "one or more active ingredients….suspended in a suitable vehicle intended for the local or transdermal delivery of active ingredients".

1.7.2 Stability issues – sedimentation and caking

In most pharmaceutical suspensions, the particles are too large to permit their permanent suspension in water by Brownian motion. These suspensions will therefore sediment and the rate of sedimentation is related to the particle radius, the density of both the particle and the liquid, and the viscosity of the medium in accordance with Stokes' Law (Zatz *et al.*, 1996):

$$V = \frac{2r^2(\rho_s - \rho_L)g}{9\eta_s}$$ **Equation 1.7a**

where V is the sedimentation rate, r is the particle radius, ρ_s is the density of the suspended particle, ρ_L is the density of the liquid, g is the gravitational constant and η_s is the viscosity of the continuous phase.

Following sedimentation, the settled particles can become compacted at the bottom of the container to form a cake. Caking is one of the most difficult problems encountered in the formulation of a suspension (Bhargava *et al.*, 1996). Once a cake is formed, it is very difficult, if not impossible, to redisperse. Thus, the main objective in suspension formulation is to ensure that the dispersed particles do not settle on standing, or if the particles do settle, they should be easily redispersed on shaking and should produce a uniform dose on administration (Dell and Colliopoulos, 2001). Diffusible solids, such as light kaolin and magnesium trisilicate, sediment sufficiently slowly to enable a dose to be satisfactorily removed after redispersion. Indiffusible solids, such as chalk and sulphadimidine, sediment too rapidly and require the addition of other materials to reduce the sedimentation rate to an acceptable level (Pharmaceutical Codex, 1994). Thus control of sedimentation and caking is of primary importance in maintaining the integrity of a disperse system. Several approaches may be adopted, either separately or in tandem, to achieve suitable sedimentation and sediment characteristics. These strategies include particle size reduction, the use of structured vehicles and the preparation of flocculated/ deflocculated systems.

1.7.3 Formulation of stable suspensions

1.7.3.1 Modification of particle size of suspended drug

Particle size of a suspended drug is a critical parameter in a suspension formulation. The particle size of the insoluble drug plays a significant part in determining formulation elegance, rate of settling, absence of caking, rate of drug release and final stability of the product (Dell and Colliopoulos, 2001). According to Stokes' Law (Equation 1.7a), the rate of settling of the insoluble drug is proportional to the square of the particle radius. Therefore, smaller particles will settle more slowly than larger particles. The majority of pharmaceutical suspensions have drug particles in the range of 1-50 μm in diameter. If particles are less than ~3 μm, and their density does not differ by more than 20% from that

of the dispersion medium, the particles will remain suspended due to Brownian motion (Dell and Colliopoulos, 2001). Therefore, reduction of particle size has a beneficial effect on the physical stability of a suspension. In practice however, there is a limit to extent of size reduction that is feasible. Once a certain small particle size is attained, further size reduction tends to become disproportionately more difficult and expensive. Moreover, collisions of small particles due to Brownian motion can result in particle aggregation, followed by aggregate settling and caking. Once caking has occurred redispersion of the drug is often impossible (Dell and Colliopoulos, 2001).

1.7.3.2 Use of structured vehicles

The most practical method of controlling sedimentation is through the use of viscosity-building agents (Dell and Colliopoulos, 2001). Various substances, such as sugars and polyols, have been used over the years to build viscosity in aqueous drug systems and thereby retard sedimentation. However, they are usually Newtonian in nature and need to be used in large amounts to achieve the required viscosity (Zatz *et al.*, 1996). The concept of a "structured vehicle" relates to the use of certain clays and polymers which, in addition to developing viscosity in the system, also confer non-Newtonian flow characteristics on the system. Pseudoplasticity, the existence of a yield value and some degree of thixotropy are useful properties for a suspending agent and are more relevant to suspensions than Newtonian rheology (Zatz *et al.*, 1996; Dell and Colliopoulos, 2001).

Pseudoplastic flow behaviour is advantageous for suspensions as during sedimentation the settling particle generates a low shear rate, the corresponding viscosity is high, and sedimentation is inhibited. Conversely, when the suspension is shaken vigorously, a high shear rate is generated, the viscosity is decreased, and the suspension flows easily (Ofner and Schnaare, 2001). From a practical point of view, the suspension vehicle must be "thick" enough to suspend the particles and "thin" enough to pour easily. The balancing of these two requirements is difficult (Chong, 1962).

Dell and Colliopoulos (2001) have stressed the importance of a yield value in suspension stability and have noted that suspending agents which increase viscosity but do not establish a yield value do not always prevent sedimentation. In the case of systems which

have a yield value, particles may be infinitely suspended if the shearing stress generated by the settling particle is less than the yield stress of the system (Ofner and Schnaare, 2001).

Pseudoplastic suspensions are stable, but can be problematic for bottled suspensions if the pouring viscosity is significantly higher than the shaking viscosity, as rethickening on cessation of shaking the bottle is instantaneous (Dell and Colliopoulos, 2001). Thixotropic character is of paramount importance in bottled suspension formulations so that the suspension may be poured readily following agitation. Carbomer, clays and Avicel® RC and CL grades display such flow properties; hence their widespread use as suspending agents (Ofner and Schnaare, 2001; Vanderbilt Report no. 920, 2004).

1.7.3.3 Preparation of flocculated/ deflocculated systems

Although particle size reduction and/or the incorporation of a suspending agent can be used to retard the sedimentation rate, these strategies are frequently less successful in terms of preventing caking of settled particles. In fact, these measures can sometimes aggravate the problem of caking (Dell and Colliopoulos, 2001). The best approach to this problem is to achieve a controlled flocculation of the particles.

Suspensions can exist in essentially two states, deflocculated or flocculated, depending on how the suspension particles interact. The deflocculated state is defined as the condition where each suspension particle exists independently due to the high magnitude of interparticle repulsion (Ofner and Schnaare, 1996; Ofner and Schnaare, 2001). The rate of sedimentation in a deflocculated suspension is typically low, however settled particles form a dense, hard cake over time, which may be difficult or impossible to redisperse. Flocculation is the state where suspension particles attract each other and form loosely bound aggregates or flocs through weak van der Waals forces. These flocs behave as a unit but are easily broken down with shear (Ofner and Schnaare, 2001). Flocs settle rapidly, usually to a high sediment volume, and may be readily redispersed, even after standing for prolonged periods of storage (Nash, 1996). The chief advantage of a flocculated suspension is in its redispersibility (Figure 1.7a). Good pharmaceutical suspensions, according to Martin (1993), are best achieved through the formation of a stable floc, which resists the tendency toward either deflocculation or agglomeration. The level of flocculation is controlled in order to maintain reasonably sized aggregates or flocs. In this

way, redispersibility and sedimentation rate are kept in balance (Martin, 1993; Dell and Colliopoulos, 2001).

Flocculation may be achieved and controlled through the addition of electrolytes which tend to 'screen' the repulsive electrostatic interparticle forces and allow the approach of particles such that attractive forces predominate (Figure 1.5b). Alternatively, flocculation may be achieved through the use of polymers, which can link particles together into a floc.

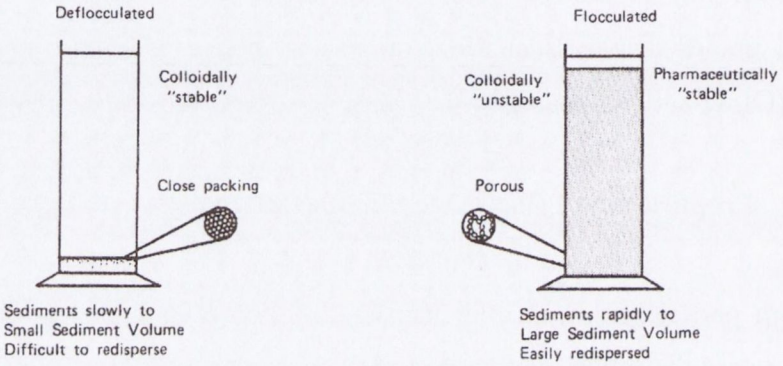


Figure 1.7a. Characteristics of flocculated and deflocculated systems (Nash, 1996).

Structured vehicles and controlled flocculation strategies may be used alone (Figure 1.7b, scheme A and B, respectively) or may be used in conjunction with one another (Figure 1.7b, scheme C).

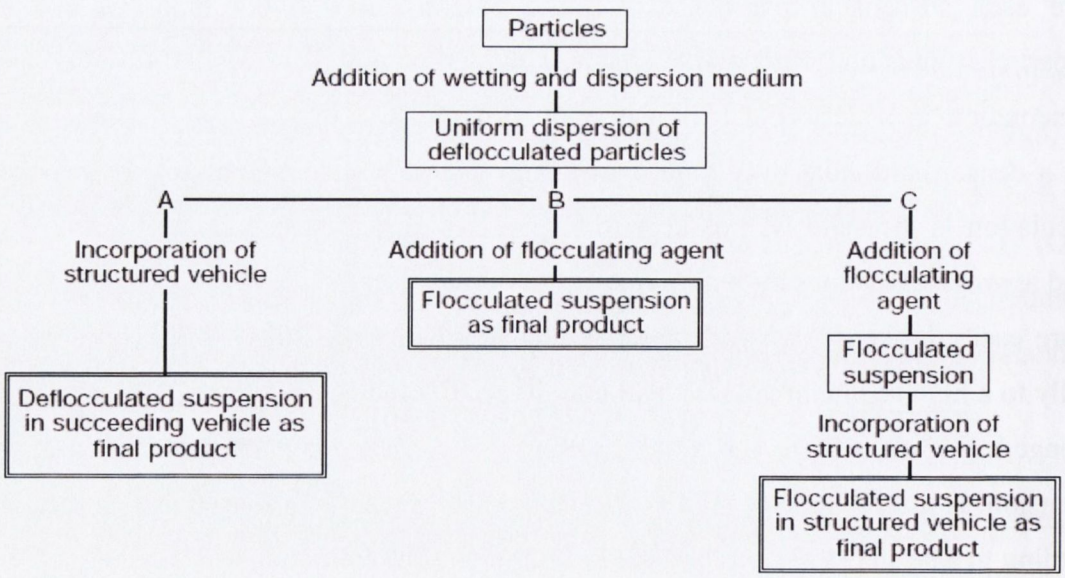


Figure 1.7b. Approaches to the formulation of stable suspensions (Ofner and Schnaare, 2001).

1.8 PARACETAMOL

1.8.1 Introduction

Paracetamol is an acylated aromatic amide, which was first introduced into medicine as an antipyretic/ analgesic by Von Mering in 1893. It had only limited use until 1949, when it was identified as the active metabolite of two older antipyretic drugs; acetanilide and phenacetin (Botting, 2000). Its popularity as an analgesic and antipyretic gradually increased and it is now the most widely used antipyretic and analgesic in the world (Beyer *et al.*, 2001). It is a major ingredient in numerous cold and flu medications and many prescription analgesics. In the Nordic countries, usage increased five-fold between 1978 and 1988, and in 1994/95 the rates in some developed countries were > 20 g/person/year. In the UK, consumption was reported to have increased from 1500 million 500 mg tablets per year in 1967/68 to 4000 million such tablets in 1993/94.

1.8.2 Molecular structure

Paracetamol is also known as acetaminophen, *N*-acetyl-*p*-aminophenol, 4-acetamidophenol and *p*-hydroxyacetanilide (El-Obeid and Al-Badr, 1985). The accepted chemical name of paracetamol is *N*-(4-Hydroxyphenyl)acetamide. Its molecular formula is $C_8H_9NO_2$ and its molecular weight is 151.2 amu (BP, 2007). The chemical structure of paracetamol is given in Figure 1.8a.

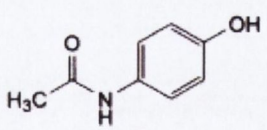


Figure 1.8a. Chemical structure of paracetamol (British Pharmacopoeia, 2007).

1.8.3 Physicochemical properties

For paracetamol, two polymorphs are fully described in the literature; the monoclinic form (also termed form I) and the orthorhombic form (also termed form II). A third polymorph has been reported but has not yet been isolated due to its instability (Nichols and Frampton, 1998; Al-Zoubi *et al*, 2002; Albertini *et al.*, 2004). The monoclinic form is thermodynamically stable and is used commercially, but it lacks slip planes and therefore it is not suitable for direct compression into tablets. Orthorhombic paracetamol is characterised by well-developed slip planes in its crystal structure and undergoes plastic deformation making it suitable for tabletting by direct compression (Nichols and Frampton, 1998). Furthermore, it has been reported that it is more soluble that the monoclinic form (Nichols and Frampton, 1998). For these reasons, it has been postulated that the orthorhombic form of paracetamol may have distinct processing advantages over the monoclinic form. Nichols and Frampton (1998) observed that form II does not readily convert to form I on storage for several months, or when mechanically stressed. Beyer *et al.* (2001) noted that a transition from form II to form I in tablets during storage should be without consequence for the bioavailability. To date, the only method reported for the reproducible production of polymorphically pure orthorhombic paracetamol powder involves crystallisation from melted monoclinic paracetamol in a non-oxidising atmosphere (Di Martino *et al.*, 1997). Form II has not been produced on the scale necessary for its commercial exploitation and consequently, the only commercially available form is monoclinic paracetamol, the thermodynamically most stable modification (Kalantzi *et al.*, 2006). Unless otherwise stated, all further references here pertain to the monoclinic form.

Paracetamol is a white odourless crystalline powder with a bitter taste (El-Obeid and Al-Badr, 1985). The melting point of paracetamol is 168-172 °C (United States Pharmacopeia (USP), 2006; BP, 2007). The solubility of paracetamol in various solvents is given in Table 1.8a. Etman and Naggar (1990) reported an aqueous solubility of 23.7 mg/ mL at 37 °C. The pH of a saturated aqueous solution of paracetamol in water is ~6 (El-Obeid and Al-Badr, 1985). The pK_a of paracetamol is 9.5 at 25 °C (Shaw *et al.*, 2005).

Table 1.8a. Solubility of paracetamol in various solvents at 25 °C (El-Obeid and Al-Badr, 1985). The solubility is indicated in terms of the BP (2007) definitions.

Solvent	Solubility
Water	Sparingly soluble
Ethanol	Freely soluble
Acetone	Soluble
Chloroform	Sparingly soluble
Glycerol	Sparingly soluble
Methanol	Freely soluble
Propylene glycol	Freely soluble
Ether	Insoluble
Methylene chloride	Very slightly soluble

Paracetamol exhibits poor compression ability, low flowability and its tablets show a tendency to cap (Garr and Rubinstein, 1992; Nichols and Frampton, 1998; Garekani *et al.*, 2000a; Garekani *et al.*, 2000b; Beyer *et al.*, 2001; Albertini *et al.*, 2004; Kaerger *et al.*, 2004). Due to these characteristics, the production of paracetamol tablets is almost exclusively by wet granulation (Martinello *et al.*, 2006). Attempts have been made to improve the compaction properties of paracetamol. Approaches have included spherical crystallization, which transforms crystalline drugs into agglomerated forms, crystallization from different solvents to produce different crystal habits and incorporation of additives by co-precipitation (Garekani *et al.*, 2000b).

1.8.4 Stability

Paracetamol is very stable in aqueous solution. The optimum pH range for stability is 5-7 (Koshy and Lach, 1961). The half-life in a solution buffered at pH 6 has been estimated as 21.8 years. Degradation is catalysed by acids and bases and the half-life is 0.73 years and 2.28 years at pH 2 and 9 respectively. The degradation products are acetic acid and *p*-aminophenol (Koshy and Lach, 1961). Paracetamol is light sensitive and the BP (2007) and USP (2006) require that all solid and liquid paracetamol formulations be protected from light.

1.8.5 Pharmacology of paracetamol

Paracetamol is widely used as an antipyretic and analgesic. In spite of its wide use, the mechanism of action of paracetamol has not been fully elucidated. It has been assumed that paracetamol has a similar mechanism of action to aspirin, on account of their similar chemical structure. That is, it has been assumed that paracetamol acts by reducing production of prostaglandins, which are involved in the pain and fever processes by inhibiting the cyclooxygenase (COX) enzyme. There are, however, a number of important differences between the effects of paracetamol and aspirin. Prostaglandins participate in the inflammatory response which is why aspirin has been known to trigger symptoms in asthmatics, but paracetamol has no appreciable anti-inflammatory action and hence does not have this side-effect (Paracetamol Information Centre). Consequently, paracetamol is not a member of the non-steroidal anti-inflammatory drugs (NSAIDs). Furthermore, the COX enzyme also produces thromboxanes, which are involved in blood clotting. This action of COX is unaffected by paracetamol but is inhibited by aspirin. Moreover, aspirin and the other NSAIDs commonly have detrimental effects on the stomach lining, where prostaglandins serve a protective role, but paracetamol, in normal doses, does not cause gastric irritation (Bosch *et al.*, 2006). Aspirin acts as an irreversible inhibitor of COX by directly blocking the enzyme's active site while paracetamol indirectly blocks COX, and this blockade is ineffective in the presence of peroxides (Boutaud *et al.*, 2002). This may explain why paracetamol is effective in the central nervous system and in endothelial cells but not in platelets and immune cells, which have high levels of peroxides. Although it exhibits reasonably potent analgesic properties, paracetamol is a weak inhibitor of both COX-1 and COX-2. It was thus proposed that it inhibits another variant of COX, which is only expressed in the brain and spinal cord, termed COX-3 (Botting, 2000; Swierkosz *et al.*, 2002; Botting and Ayoub, 2005).

Paracetamol is commonly administered in tablet, liquid suspension, suppository, intravenous or intramuscular form. The common adult dose is 500 mg to 1000 mg (BNF, 2006). The recommended maximum daily dose for adults is 4 g. When taken at recommended doses, it has an excellent safety profile, notably lacking the gastrointestinal side effects of aspirin and ibuprofen. Like NSAIDs (non-steroidal anti-inflammatory drugs) and unlike opioid analgesics, paracetamol has not been found to cause euphoria or alter mood in any way. It does not bear any risk of addiction, dependence, tolerance and

withdrawal (Bosch *et al.*, 2006). However, acute overdosage with paracetamol is relatively common and can be extremely serious. Paracetamol now has the somewhat inauspicious title of the substance most commonly used in deliberate self-poisoning in the UK (Sheen *et al.*, 2002). Ingestion of 10-15 g of paracetamol by adults may cause severe hepatocellular necrosis and doses of 20-25 g are potentially fatal (Sheen *et al.*, 2002; Drummer, 2004).

1.9 CALAMINE LOTION

Calamine lotion has been traditionally used for the relief of itch associated with skin rashes, sunburn, chicken pox, poison ivy, insect bites and stings. The active ingredient in calamine lotion is calamine. Calamine is a basic zinc oxide containing a small amount (~0.5% w/w) iron(III) oxide (USP, 2006). It is an amorphous, impalpable, pink or reddish brown powder; the colour depending on the variety and amount of iron(III) oxide present and the process by which it is incorporated (BP, 2007). The ferric oxide acts as a colouring agent and is not an active ingredient. Calamine inhibits itch through its cooling and protectant actions. The lotion will form a layer on the skin as it dries, and this works to absorb fluids from weeping lesions (DeSimone and Triplett, 1997). It can be applied topically to the affected area as needed. It acts as a mild antiseptic and can be used to prevent infections arising from scratching of the affected area. Bivings (1946) reported its effective use in acute infectious urticaria. Other sources have since reported that calamine lotion is often ineffective and is of little value in the symptomatic relief of insect bites and stings (BNF, 2006).

MATERIALS

In general, except where otherwise stated, reagent grade chemicals (termed General Purpose Reagent (GPR) or Analar Grade by BDH Chemicals (UK)) were used. The qualities or grades of materials listed here are those quoted by the manufacturer.

Description	Lot/Batch Number	Supplier
Aerosil® 200	Batch no.: BN1224	Degussa, Germany
Avicel® CL-611	Lot no.: E417N	FMC Corp., Belgium
Avicel® PH101 (microcrystalline cellulose)	Lot no.: 6712C	FMC Corp., Ireland
Avicel® RC-591	Lot no.: D245N	FMC Corp., Belgium
Bentonite BP	Lot no.: 104K0084	Sigma-Aldrich Chemicals, USA
Calamine BP	Lot no.: 49280	JM Loveridge plc, UK
Calamine lotion BP	Batch no.: BN J417B	Ovelle Pharmaceuticals, Ireland
Calcium chloride dihydrate	Lot no.: 195626/41705P01	Fluka Chemie, Czech Republic
Cetrimide (Hexadecyltrimethylammonium bromide)	Lot no.: 10026425	Lancaster Chemicals, England
Citric acid monohydrate	Lot no.: K91561538 223	BDH Laboratory Supplies, UK
Disodium hydrogen phosphate dodecahydrate	Lot no.: A484279 344	Merck KGaA, Germany
Emcompress®	Lot no.: A20EK	Penwest Chemicals, England

Description	Lot/Batch Number	Supplier
Ethanol		Cooley Distillery
Ethylene glycol	Lot no.: D017574D0	Aldrich Chemicals, USA
Eudragit® E PO	Batch no.: G041131159	Degussa, Germany
Explotab® (sodium starch glycolate)	Lot no.: 0508076827	Clonmel Healthcare Ltd., Ireland
Glycerol	Spectrophotometric grade, ≥99%, Lot no.: 035K0059	Sigma-Aldrich Chemicals, Malaysia
Hydranal®-Composite 5	Lot no.:6285B	Riedel-de Haën, Germany
Hydranal®-Standard 5.00	Lot no.:6186C	Riedel-de Haën, Germany
Hydrochloric acid (37% v/v)	Lot no.: 521599-114	Sigma-Aldrich Chemie, Germany
Kollidon® 25	Lot no.: 49364275L0	BASF Pharma, Germany
Kollidon® 30	Lot no.: 80127388Q0	BASF Pharma, Germany
Kollidon® 90F	Lot no.: 56401036W0	BASF Pharma, Germany
Kollidon® VA 64	Lot no.: 39148875L0	BASF Pharma, Germany
Liquefied phenol (50% w/w in water)	Lot no.: 0851750L	BDH Laboratory Supplies, UK
Ludipress®	Lot no.: 29051375L0	BASF Pharma, Germany
Magnesium stearate dihydrate	Lot no.: K29414743 138	BDH Laboratory Supplies, UK
Methanol	Lot no.: 2207A	Riedel-de Haën, Germany
Paracetamol BP powder grade (monoclinic, form I)		Sigma-Aldrich Chemicals, USA
Potassium bromide	Lot no.: S34447-116	Sigma-Aldrich Chemicals, USA
Sepiolite (Pangel®-S9)		Tolsa S.A., Spain
Sodium carboxymethylcellulose	Medium viscosity, Lot no.: 035K0033	Sigma-Aldrich Chemicals, USA
Sodium chloride	Lot no.: K9405432 127	BDH Laboratory Supplies, UK

Description	**Lot/Batch Number**	**Supplier**
Sodium citrate dehydrate	Lot no.: 073K0082	Sigma-Aldrich Chemicals, Japan
Sodium dihydrogen phosphate dihydrate	Lot no.: K91221445 402	Merck KGaA, Germany
Sodium hydroxide pellets	Lot no.: 13260	Riedel-de Haën, Germany
Sodium polyphosphate	Lot no.: JR01112ER	Sigma-Aldrich Chemicals, UK
Water	Deionised	
Zeta potential standard	Batch no.: 170601/S	Malvern Instruments, UK
Zinc oxide	Lot no.: K30995408 233	BDH Laboratory Supplies, UK

METHODOLOGY

3.1 PHYSICO-CHEMICAL CHARACTERISATION OF SEPIOLITE POWDER (PANGEL®-S9)

3.1.1 Powder X-ray Diffraction (pXRD)

X-ray diffraction patterns were obtained using a Siemens D500 X-ray powder diffractometer with associated DiffractPlus® software. A 1.00° dispersion slit, a 1.00° antiscatter slit and a 0.15° receiving slit were used. The Cu anode X-ray was operated at 40 kV and 30 mA in combination with a Ni filter to give monochromatic Cu $K_{\alpha 1}$ X-rays of wavelength 1.5418 Å.

Oriented aggregate mounts of untreated sepiolite and heat treated sepiolite (Section 3.2.2) were prepared using the filter-membrane peel technique (Drever, 1973; U.S. Geological Survey Open File Report 01-041). A 1% w/v suspension of sepiolite in deionised water was prepared using a high shear mixer (Ultra Turrax® T25, IKA Instruments, Germany) and filtered under vacuum using a 0.45 μm membrane filter (Supor®-450, 47 mm, Gelman Sciences). The moist filter was removed and wrapped around the exterior of a clean glass beaker with the clay film uppermost. The filter was retained in place using the thumb and forefinger. The clay film was then lightly rolled across a glass microscope slide to transfer the clay film to the slide. The film was allowed to air-dry at room temperature for 30 min. The oriented films were then subjected to ethylene glycol vapour treatment. Ethylene glycol was poured into the base of a desiccator to a depth of ~1 cm. The air-dried oriented aggregate mounts were placed on the desiccator shelf. The lid was fitted and the sealed desiccator was placed in an oven (Memmert Type UL40, Germany) at 70 °C overnight and removed just prior to analysis.

Randomly oriented powder samples were prepared by placing an excess of the powder in the cavity (depth 0.5 mm, diameter 9 mm) of a low background silica mount (Bruker AXS,

UK). The random orientation ensures that the incident X-rays have an equal chance of diffracting off any given crystal lattice face of the minerals in the sample (U.S. Geological Survey Open File Report 01-041).

All samples were scanned from 4 to 75° 2θ using a step size of 0.02° per second. The empty cavity mount and glass microscopic slide were X-rayed to correct for any background reading.

3.1.2 Fourier Transform Infra-red Spectroscopy (FT-IR)

FT-IR analysis was carried out using a Nicolet Magna-IR 560 E.S.P. spectrometer with associated Omnic software version 4.1 (Thermo Scientific, USA). Sample discs were prepared as follows. The sample to be analysed was dispersed at a concentration of 0.25% w/w in oven-dried spectroscopic grade KBr using a mortar and pestle (Madejová and Komadel, 2001). 0.2 g mixture was compressed into a disc using a 13 mm flat-faced punch and die set (Apollo Scientific, UK) in an IR press operating at 8000 kg pressure for 2 min. The IR spectrum (400 - 4000 cm^{-1}) of a KBr disc of the sample was determined based on averaging 64 sample and 64 background scans. The FT-IR instrument operated at a scan speed of 0.1 $cm^{-1}.s^{-1}$ and a resolution of 2 cm^{-1}. FT-IR spectra were compared to a reference spectrum of sepiolite from the FDM Reference Library using Essential FTIR™ software (Operant, LLC., USA).

3.1.3 Energy Dispersive X-ray Analysis (EDXA)

Semi-quantitative EDX analysis was carried out using a variable pressure scanning electron microscope (Hitachi S-3500N, Japan) and an X-ray detector (Princeton Gamma-Tech Instruments, USA). Prior to analysis 0.2 g powder samples were compressed into discs of diameter 13 mm using a flat-faced punch and die set in an IR press at a pressure of 2000 kg. The powder discs were mounted on aluminium stubs using adhesive carbon tape. The elemental content was determined at each of three randomly selected locations on the surface of the powder disc. A 20 keV electron beam was used with a take-off angle of 35°.

3.1.4 Inductively Coupled Plasma Mass Spectroscopy (ICP-MS)

Sepiolite powder was digested with concentrated HCl and H_2O_2 with heat prior to analysis. The digested material was diluted with deionised water to a known final volume. A dilution of this digest was analysed using an Agilent 7500a ICP-MS (USA) in quantitative mode.

3.1.5 Thermogravimetric Analysis (TGA)

TGA was performed using a Mettler Toledo TC15 thermoanalyzer (Switzerland) coupled to a microbalance (Mettler Toledo MT5, Switzerland). The system was controlled using Mettler Toledo STAR^e software (version 6.0). Samples were run over the temperature range 25 – 250 °C or 25 – 800 °C under N_2 purge at a heating rate of 10 °C /min. Aluminium and alumina crucibles were used for low and high temperature runs respectively.

3.1.6 Differential Scanning Calorimetry (DSC)

DSC was performed using a Mettler Toledo DSC 821^e (Switzerland) with associated STAR^e software (version 6.0). Hermetically sealed aluminium pans with three vent holes were used throughout the study. The samples were heated from 25 - 250 °C at a heating rate of 10 °C /min using N_2 as the purge gas.

3.1.7 Karl-Fischer (KF) Analysis

The moisture content of powders and granules was determined using a Karl Fischer apparatus 701 KF Titrino with a 6.0338.100 Pt electrode (Metrohm, Switzerland). The dispersion medium, methanol, was conditioned prior to use using Hydranal®-Composite 5 reagent. Hydranal®-Standard 5.00 was used for standardization of the reagent. 0.1 g samples of the material to be tested were introduced into the conditioned titration vessel. The water content (% w/w) was determined in duplicate.

3.1.8 Scanning Electron Microscopy (SEM)

Samples of powder were mounted on aluminium stubs using double-sided sticky tape. The powder layer was coated with a thin film of gold using a Polaron SC500 sputter coater (UK). Tablets, granules and sediments were prepared for SEM in an analogous fashion. The coated samples were examined using a field emission scanning electron microscope (Hitachi S4300, Japan). The morphology of the particles and the manner in which they associated with one another was examined. The effect of physical processing (e.g. milling and heating), as described in Sections 3.2.1 and 3.2.2 respectively, on the appearance and size of the fibers was studied.

3.1.9 N_2 gas adsorption

3.1.9.1 BET surface area determination

BET surface area and micropore measurements of the samples were performed using a Gemini II 2370 Surface Area Analyser (Micromeritics, USA) equipped with a vacuum pump (DirectTorr V 8905, Welch Vacuum Technology, USA). Nitrogen gas was used as the adsorbate; analyses were carried at -196 °C (77 K) and in duplicate. The instrumental settings during analysis are detailed in Table 3.1a. The saturation pressure of nitrogen was determined daily.

Prior to analysis samples were degassed by heating under N_2 flow using a Micromeritics Flow Prep 060 Degasser. Samples were cooled to room temperature under N_2 flow immediately before determination. Degassing conditions for sepiolite-based samples reported in the literature varied hugely. Consequently to establish ideal degassing time, the temperature was set at 150 °C, (which would facilitate the removal of the most commonly adsorbed molecule, water), and the time varied (0.5, 3, 5, 24 and 48 h). The resultant surface areas were recorded as a function of degassing time and subjected to statistical analysis. No significant increase ($p < 0.05$) in surface area was seen on increasing the degassing time above 3 h. Consequently ideal degassing conditions for sepiolite samples were established as heating at 150 °C under N_2 flow for 3 h. Samples other than sepiolite (e.g. Kollidon® VA 64-based samples) were degassed at 50 °C under N_2 flow. Following analysis, these samples were reweighed. Differences between the weight prior to and after

analysis were indicative of incomplete degassing. Where this was the case, the sample was run repeatedly until the weight after analysis was constant.

Filler rods were used to improve precision. Free space correction was carried out in the case of samples where the reported specific surface area was less than 25 m^2/ g (Gemini II 2370 Instruction Manual) through the addition of a suitable volume of an inert material having a negligible surface area (solid glass beads of diameter 3 mm) to the balance tube. Free space was determined using helium and correction was deemed to be achieved when the measured free space was in the range -0.5 to +0.5 cm^3.

Table 3.1a. Instrumental settings during BET surface area analysis.

Evacuation rate:	500 mm Hg/ min
Evacuation time:	1.0 min
Free space:	"None"*
First relative pressure:	0.01 P/ P_0
Last relative pressure:	0.90 P/ P_0
Number of points:	27
Analysis mode:	"Equilibrate"
Equilibration time:	10 s

*Free space determination was carried out in the case of samples where the quoted surface area was less than 25 m^2/ g.

The data were treated according to the BET adsorption isotherm equation:

$$\frac{P}{V_a(P_o - P)} = \frac{1}{V_m C} + \frac{C-1}{V_m C}\left(\frac{P}{P_o}\right) \qquad \textbf{Equation 3.1a}$$

where P, in mm Hg, is the relative vapour pressure of nitrogen gas in equilibrium with the surface at 77 K, P_o, in mm Hg, is the saturated pressure of the adsorbate gas, V_a, in mL, is the volume of *gas* adsorbed at STP, V_m, in mL, is the volume of *gas* adsorbed at STP to produce an apparent monolayer on the sample surface and C is a dimensionless constant related to the enthalpy of adsorption of the adsorbate gas on the powder sample.

The BET value, $\frac{P}{V_a(P_o - P)}$, was plotted against P/P_o in accordance with the BET equation (Equation 3.1a). Those data points yielding a straight line ($r^2 \geq 0.995$) were used in the determination of V_m in accordance with the USP Section <846> (2006).

The specific surface area, S, in m^2/ g, was calculated using the following equation:

$$S = \frac{V_m N \cdot a}{22{,}400 \cdot m} \qquad \textbf{Equation 3.1b}$$

where N is the Avogadro constant (6.023×10^{23} $mole^{-1}$), a is the effective cross-sectional area for one adsorbate molecule (0.162×10^{-18} m^2 for nitrogen), m is the mass, in g, of the test powder and 22,400 is the volume, in mL, occupied by 1 mole of adsorbate gas at STP.

3.1.9.2 Determination of micropore volume and surface area using the t-plot method

The t-plot method, which was first proposed by de Boer *et al.* (1966), was used to establish the micropore volume and surface area. For the purpose of this thesis, pores of width less than 20 Å are termed micropores, in accordance with the IUPAC convention (1972). The t-method is based on the determination of a t value in accordance with the following equation (Harkins and Jura, 1943):

$$t(\text{Å}) = \left(\frac{13.99}{\log P / P_o + 0.034} \right)^{\frac{1}{2}} \qquad \textbf{Equation 3.1c}$$

The t value is the statistical thickness of the adsorbed film at a given relative pressure (P/P_o) and assumes that the nitrogen molecules exhibit hexagonal close packing such that the thickness of a single molecular layer of nitrogen is 3.54 Å (Lowell and Shields, 1991). A t-plot is constructed by plotting the volume adsorbed, V, against the statistical thickness of the adsorbed layer, t, at the corresponding relative pressure, P/P_o. The shape of this plot can be used to determine the presence of micropores. In the case of non-porous samples, the absence of pores results in a linear increase in the adsorbed layer thickness with an increase in the volume adsorbed. Hence the t-plot will be a straight line passing through the origin, the slope of which will be directly proportional to the surface area (Lowell and Shields, 1991) in accordance with Equation 3.1d below:

$$S_t = \frac{V_{liq}}{t} \times 10^4 \qquad \textbf{Equation 3.1d}$$

where S_t is the total surface area (in m^2/ g) and V_{liq} is the adsorbed *liquid* layer volume (mL/ g) and t is the statistical layer thickness (in Å).

The adsorbed liquid volume (V_{liq}, mL/ g) may be determined from the volume of gas adsorbed (V_m, mL/ g at STP) using the equation:

$$V_{liq} = 0.00154468 V_m \qquad \textbf{Equation 3.1e}$$

where 0.00154468 represents a density conversion factor (Micromeritics Application Note n° 78, 1991).

In the case of a material possessing micropores, increased adsorption of gas will be seen at low relative pressures as adsorption will occur initially in the micropores in order to satisfy their excess potential energy originating from overlapping energy fields associated with the walls of the pores. As a consequence the t-plot, when extrapolated to the Y-axis, will show a positive intercept equal to the micropore volume when the density conversion factor is applied (Webb and Orr, 1997). The slope (Y) of this extrapolated line is proportional to the external surface area as all of the micropores have already been filled by capillary condensation and consequently any increase in the adsorbed volume is related solely to adsorption on the external surface area (Lowell and Shields, 1991). The external surface area, S_{ext} (in m^2 /g), can be calculated from the following equation:

$$S_{ext} = 0.00154468 Y \times 10^4 \qquad \textbf{Equation 3.1f}$$

where Y is the slope of the linear region of the t-plot (Lowell and Shields, 1991). The t-plots were typically linear over the statistical thickness range 3.5 to 7 Å.

The micropore surface area (S_{micro}) can be determined as the difference between the BET surface area (S_{BET}) and the external surface area:

$$S_{micro} = S_{BET} - S_{ext} \qquad \textbf{Equation 3.1g}$$

3.1.10 Mercury Intrusion Porosimetry (MIP)

MIP was carried out by MCA Services (UK) using an AutoPore IV 9500 (Micromeritics, USA). Intrusion pressures in the range 0 to 30,000 p.s.i., corresponding to pore diameters between 799 μm and 0.007 μm, were used. The assumed mercury density, surface tension and contact angle were 13.5335 g/ mL, 485 dynes/ cm and 140°, respectively. Samples were dried to constant weight in a vacuum oven prior to analysis. The characteristics of the 5 cm^3 "solid sample" type penetrometer used are given in Table 3.1b.

Table 3.1b. Characteristics of the 5 cm^3 "solid sample" penetrometer used in MIP.

Penetrometer constant (μL/ pF)	21.630
Penetrometer weight (g)	54.6223
Maximum head pressure (p.s.i.)	4.6800
Stem volume (mL)	1.1900
Penetrometer volume (mL)	4.0336

3.1.11 Helium Pycnometry

Helium pycnometry was performed using an AccuPyc 1330 (Micromeritics, USA). The pycnometer was calibrated before use. The true (skeletal) density measurements were performed on powdered sepiolite samples using a 1 cm^3 cup. Prior to analysis the samples were dried to a constant weight in a vacuum oven (Gallenkamp, UK) at 50 °C and -400 mbar to avoid the distorting effect of water vapour on volume measurement. All manipulations and transfers were conducted in such a manner as to minimise the exposure of the dried sample to atmospheric moisture. Samples were weighed on an MT5 microbalance (Mettler Toledo, Switzerland). As large a quantity of sample as could be accommodated within the 1 cm^3 cup was used to improve accuracy. After completion of each analytical run, the sample was reweighed. Where this mass differed from that prior to the run, this final mass was used in the determination of skeletal density. Analyses were performed at least in duplicate. The running parameters used are outlined in Table 3.1c.

Table 3.1c. Run parameters used in helium pycnometry.

Volume of sample cup (cm^3)	1
Volume of calibration standard (cm^3)	0.718463
Number of purges	10
Purge pressure (p.s.i.)	19.5
Number of runs	50
Run fill pressure (p.s.i.)	19.5
Equilibration rate (p.s.i. /min)	0.005

3.2 PHYSICAL PROCESSING OF SEPIOLITE

3.2.1 Preparation of milled samples

Milled samples of sepiolite (Pangel-S9®) were prepared using a ball mill, an ultracentrifugal mill (UCM) and a mortar and pestle. 20 g samples of sepiolite were introduced into the Retsch® ball mill and rotated at 28 rpm for either 5 or 10 min. 20 g samples of sepiolite were milled in an UCM (Retsch ZM100, Germany) fitted with an 8-tooth rotor and a 0.5 mm sieve ring at speeds of either of 14,000 rpm or 18,000 rpm. 20 g samples of sepiolite were ground by hand using a mortar and pestle for 5 or 10 min.

3.2.2 Preparation of heated treated sepiolite samples

Samples of sepiolite were heated to 400 °C and 550 °C respectively in a furnace (Nabertherm Program Controller S27, Germany) at a rate of 5 °C /min and held at the final temperatures of 400 °C and 550 °C for 1 h.

3.3 PREPARATION OF SPRAY DRIED (SD) SEPIOLITE, SepKoll AND SepCMC

During preliminary runs, 2% w/v sepiolite aqueous dispersions, prepared using a high shear mixer (Ultra Turrax® T25, IKA Instruments, Germany) operating at 24,000 rpm for 30 min, were spray dried with a Büchi B-191 Mini Spray Dryer (Büchi Laboratoriums-Technik AG, Switzerland) using the parameters cited in Table 3.3a. This spray drier uses a twin-fluid atomiser with a cocurrent flow arrangement. The ensuing yield was very low

and subsequently, spray drying was performed using ethanol/ water (60:40 v/v) as a dispersion medium for the clay. Suspensions for spray drying were prepared according to the formulations in Table 3.3b, using the mixing speed and time stated previously. In the case of SepCMC, sodium carboxymethylcellulose (NaCMC) was dispersed initially in the aqueous component of the dispersion medium and sepiolite in the ethanolic component. The ethanol phase was then added gradually while stirring to the aqueous phase. Dispersions were prepared immediately prior to spray drying. Spray drying conditions for the hydroethanolic dispersions are listed in Table 3.3a. As yields in all cases were relatively low, the yield resulting from a number of spray drying runs was combined for each product to form a composite sample upon which all further characterisation and functionality testing was performed.

Table 3.3a. Spray drying conditions.

Parameters	**Preliminary conditions**	**Final conditions**
Dispersion medium	Water	Ethanol/ water (60:40)
Inlet temperature (°C)	175	95
Outlet temperature (°C)	113	80/ 76/ 74[§]
Feed rate (%)	8	10
Aspirator (%)	100	100
Atomising air flow rate (L /min)	600	600

[§]outlet temperatures for SD sepiolite, SepKoll and SepCMC were 80 °C, 76 °C and 74 °C respectively.

Table 3.3b. Formulation of hydroethanolic-based dispersions for spray drying.

Product	**Dispersion Formulation (% w/v in ethanol/ water (60:40))**
SD Sepiolite	2% w/v sepiolite
SepKoll	2% w/v sepiolite + 0.222% w/v Kollidon® VA 64
SepCMC	2% w/v sepiolite + 0.354% w/v NaCMC (medium viscosity grade)

3.4 CHARACTERISATION OF NOVEL SPRAY DRIED EXCIPIENTS

3.4.1 Preparation of physical mixes

A physical mixture of spray dried sepiolite and Kollidon® VA 64 in the ratio 90:10 w/w was prepared in a Turbula mixer (Glen Creston Ltd., UK) operating at 42 rpm for 30 min. The characteristics of this physical mix were compared to the co-spray dried product. Similarly, a physical mixture containing spray dried sepiolite and NaCMC in the ratio 84.95:15.05 w/w was prepared using the conditions described previously.

3.4.2 Techniques used in the characterisation of the spray dried excipients

The novel spray dried excipients, and their corresponding physical mixtures, were characterised using pXRD, FT-IR, KF analysis, SEM and N_2 adsorption as described in Section 3.1. In addition, TGA was used in combination with DSC to identify any interaction/ incompatibility between sepiolite and the two polymers.

3.5 TABLETTING STUDIES

3.5.1 Evaluation of the compression properties of sepiolite

A method modified from that of Wells (1988) was used to establish the compression properties of sepiolite. Four aliquots of sepiolite (500 mg) and magnesium stearate (5 mg) were weighed out. Two samples were blended for 5 min (A and B), a third was blended for 30 min (C) and a fourth for 2.5 min (D) in a Turbula mixer (Glen Creston Ltd., UK) at 42 rpm. Samples A, C and D were loaded into a 13 mm punch and die set and compressed using an IR press at 1,000 kg; this compression pressure was held for 1 s and then released. The process was repeated for sample B but the load was held at 1,000 kg for 30 s before release. Following overnight storage (to allow any elastic recoil or work hardening to take place) the compacts were crushed diametrically using a tablet crushing device (Schleuniger 6D tablet hardness tester, Dr. Schleuniger Pharmatron, Switzerland) and the tablet hardness recorded in each case. All analyses were repeated a total of five times.

3.5.2 Paracetamol solubility study

The aqueous solubility of paracetamol was quoted as 1g /30-100 mL (Sweetman, 2004). Solubility studies were carried out in order to establish the exact aqueous solubility of the grade used, given that the solubility would have implications for the reproducibility of the wet granulation process. 0.4 g paracetamol was weighed out and placed in a 20 mL ampoule. 10 mL deionised water was added. The ampoule was flame sealed and placed in a shaker water bath (Model 25, Precision Scientific, USA) at 25 °C and shaken at 100 cycles per min for 24 h. Thereafter, the ampoule was allowed to stand in the water bath briefly to allow any undissolved drug to sediment. An aliquot of the supernatant was removed and filtered through a 0.45 μm membrane filter (Millex HV Durapore® PVDF membrane, Millipore, USA). Following appropriate dilution using deionised water, the absorbance of this solution was determined by UV spectroscopy (Spectronic Genesys 5, Thermo Scientific, USA) at λ = 257 nm. The concentration of paracetamol present was determined by reference to a calibration curve. A calibration curve was constructed by plotting the absorbance (λ = 257 nm) of standard paracetamol solutions against concentration. The calibration curve for paracetamol in water is given in Appendix 1. The experiment was repeated and the incubation time increased from 24 h to 48 h. There was no significant change in the value obtained following the longer incubation time (Appendix 2). The experiment was repeated twice.

3.5.3 Preparation of the blends for tabletting by direct compression

The direct compression bases were dry mixed in a Turbula mixer at 42 rpm for 30 min with paracetamol, magnesium stearate and Aerosil® 200 according to the formulations in Table 3.5a.

Table 3.5a. Formulations for direct compression tabletting studies (Quantities expressed as mg per tablet).

Excipient	Function	TABDC1 (mg)	TABDC2 (mg)	TABDC3 (mg)	TABDC4 (mg)	TABDC5 (mg)	TABDC6 (mg)
Paracetamol	Drug	250	250	250	250	250	250
Avicel® PH101	Filler/binder/ disintegrant	0	0	0	250	0	0
Ludipress®	Filler/binder/ disintegrant	0	0	0	0	225	0
SD sepiolite	Filler/binder/ disintegrant	250	0	225	0	0	0
SepKoll	Filler/binder/ disintegrant	0	250	0	0	0	0
Kollidon® VA 64	Binder	0	0	25	0	25	250
Mg Stearate	Lubricant	2.5	2.5	2.5	2.5	2.5	2.5
Aerosil® 200	Glidant	2.5	2.5	2.5	2.5	2.5	2.5

3.5.4 Preparation of granules using a wet granulation method

Formulations for wet granulation are presented in Table 3.5b. 50 g batches of each formulation were dry mixed in a planetary mixer (Kenwood Chef excel, UK) for 15 min and then moistened with deionised water (~55 mL). In the case of the TABF8 formulation, only half of the total quantity of Explotab® was added at this stage. Massing was continued for a further 5 min after which the wet mass was granulated by forcing it through a sieve of aperture size 1.2 mm. The granulates were dried at room temperature; drying was concluded when a final moisture content of 4 – 5% w/w was reached, as determined using KF analysis. The granules were then sized through a sieve of aperture size 710 μm. The resulting granules were screened on a 355 μm sieve and excess fines (> 10% by weight) were excluded.

The provisional compression weight of each batch (i.e. that weight of dry granulate containing 250 mg paracetamol) was calculated from the paracetamol content and moisture content of the dry powder blend prior to granulation and the residual moisture content following granulation. The remaining Explotab® was added to the TABF8 formulation. Magnesium stearate (0.5% w/w with reference to dried granulate) and Aerosil® 200

(0.5% w/w with reference to dried granulate) were added to the dry granulate for lubrication and glidant purposes respectively. The provisional compression weights were adjusted to take account of these additions. Three batches of each formulation were produced.

Table 3.5b. Wet granulation formulations (Quantities are expressed as a % of the total mass of the dry powder mix prior to wetting).

Excipient	Function	TABF4 (% w/w)	TABF5 (% w/w)	TABF6 (% w/w)	TABF7 (% w/w)	TABF8 (% w/w)	TABF9 (% w/w)
Paracetamol	Model drug	50	50	50	50	50	50
Sepiolite	Filler/ binder/ disintegrant	45	45	45	50	47.6	0
Avicel® PH101	Filler/ binder/ disintegrant	0	0	0	0	0	50
Kollidon® 25	Binder	5	0	0	0	0	0
Kollidon® 30	Binder	0	5	0	0	0	0
Kollidon® 90F	Binder	0	0	5	0	0	0
Explotab®	Disintegrant	0	0	0	0	2.4	0

3.5.5 Characterisation of the Direct Compression Bases (DCBs) and granulates prepared by wet granulation

3.5.5.1 Density and flowability analysis

3.5.5.1.1 Tapped and bulk density determination

The bulk density and tapped density of all DCBs and granulates was determined using a tapped density tester (Model SVM 12, Copley, UK). The 250 mL graduated cylinder of the machine was replaced by a 100 mL measuring cylinder given that a large volume of the spray dried excipients was not available. The graduated cylinder was filled with the test material to 50 mL and the mass of the material noted. With minimal disturbance to the

measuring cylinder, it was transferred to the tap density apparatus. The volume of the weighed sample was recorded at time zero (V_0), after 500 taps (V_{500}) and after 1250 taps (V_{1250}). Where the difference between V_{1250} and V_{500} was greater than 1 mL, the powder was subjected to a further 1250 taps. This final volume reading (V_{2500}) was noted and used in the determination of the tapped density. The bulk and tapped densities, Hausner ratios and Carr's Indices were calculated using the equations below; where M refers to the mass (in g) of the powder sample taken. Results are the average of at least two determinations.

$$\text{Bulk density (g/ mL)} = \frac{M}{V_0} \qquad \textbf{Equation 3.5a}$$

$$\text{Tapped density (g/ mL)} = \frac{M}{V_{1250}} \text{ or } \frac{M}{V_{2500}} \qquad \textbf{Equation 3.5b}$$

$$\text{Hausner ratio} = \frac{\text{Tapped density}}{\text{Bulk density}} \qquad \textbf{Equation 3.5c}$$

$$\text{Carr's Index} = \frac{(\text{Tapped} - \text{Bulk density}) \times 100}{\text{Tapped density}} \qquad \textbf{Equation 3.5d}$$

3.5.5.1.2 Angle of repose

The angle of repose was determined by measuring the height and diameter of the base of the cone obtained by allowing a sample to fall through a fixed distance from a defined funnel onto a horizontal surface (Muñoz-Ruiz *et al.*, 1994; Al-Achi *et al.*, 2003; Reddy *et al.*, 2003). The glass stemmed funnel, of dimensions outlined in Figure 3.5a, was clamped such that the tip was 2 cm from the horizontal bench top. The powder was poured through the funnel, until the mound formed touched the tip of the funnel. The diameter (d) of the mound formed was measured using a ruler. The angle of repose was calculated using the following equation:

$$\text{Angle of Repose (radians)} = \tan^{-1}(2h / d) \qquad \textbf{Equation 3.5e}$$

where h and d are the height and diameter of the powder cone formed. The angle of repose was converted to degrees using the radian-degree conversion tool on a scientific calculator. The quoted angle of repose is the average of three readings.

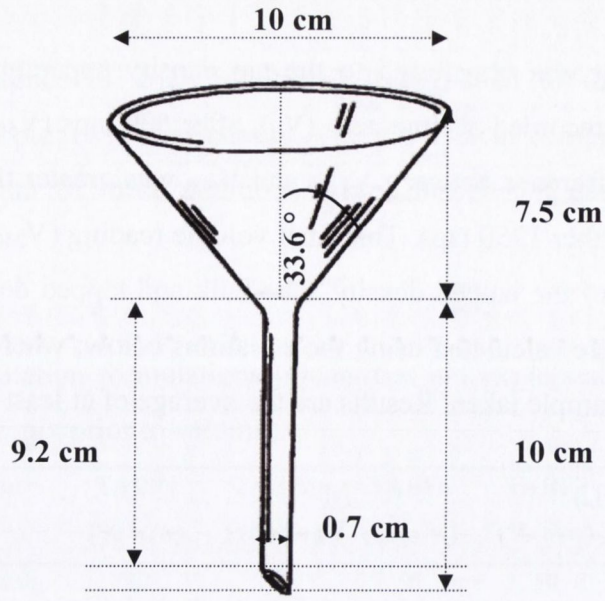


Figure 3.5a. Dimensions of glass funnel used for angle of repose determination.

3.5.5.1.3 Critical orifice diameter

The critical orifice diameter is a dynamic method of powder flow measurement which is more readily reconciled with flow from intermediary bulk containers and through hoppers. Gioia (1980) has investigated the use of this technique as a simple test to predict powder flowability in a capsule-filling operation.

The measurement device, referred to as a Flotest® (Copley Scientific, UK), used a cylinder of approximate volume 150 mL with a series of interchangeable base plate discs that had orifices of different diameter (range: 4 – 36 mm). The critical diameter is the size of the smallest orifice in the base plate disc through which powder in a cylinder will discharge on three successive attempts. During the powder filling stage, a shutter that could be removed without transferring vibration to the powder bed covered the orifice. The base plate disc with the 16 mm aperture was used first. Once the base plate was in position and the shutter closed, approximately 50 - 100 mL sample (depending on quantity available) was loaded into the cylinder through a funnel. The powder bed was allowed to settle for 30 s before opening the shutter.

The result was designated positive if the powder flowed through the orifice leaving behind powder in the form of an upside-down truncated cone. A powder that flocculates in bulk will on the other hand fall abruptly forming a cylindrical cavity ('ratholing'). In this instance, the test result was adjudged to be negative. Absence of any powder flow was also classed as a negative result. Where the test result was positive, the test was repeated using

base plates with smaller orifices until the result was negative. Where the result was negative, the size of the orifice was increased until the test was positive.

3.5.5.2 Particle sizing - Powder-in-air analysis

Measurement of the particle size distribution was obtained using a laser diffraction particle size analyzer (Mastersizer® 2000, Malvern Instruments, UK). Particles were dispersed using a Scirocco® dry powder feeder accessory with 2 – 2.5 bar pressure unless stated otherwise. Higher dispersive air pressures were required for the sizing of zinc oxide and calamine, while lower pressures (0.5 bar) were used for sizing of granulates. In the case of granulates, sizing was performed prior to excess fines removal and the addition of extragranular Explotab®, magnesium stearate and Aerosil® 200. An obscuration rate of 1.5 – 5% was obtained using a vibration feed rate of 50 - 60%. Data was processed according to the Mie theory using a refractive index appropriate to the material under investigation (Instruction manual of Mastersizer® 2000). The results quoted are the average of three determinations.

3.5.5.3 Granule friability determination

Granule friability was assessed using a method based on that of Ingelbrecht *et al.* (1997). 10 g granules were placed in a friabilator (Erweka Copley, TA 20, Germany) together with 200 glass beads of diameter 3 mm. The friabilator was run for 10 min at 25 rpm. After 10 min, the glass beads were removed. The abraded sample was placed on a sieve of aperture size 355 μm and shaken on a sieve shaker (Endecott 1 MK11, UK) for 5 min at an amplitude of 2 mm. The material remaining on the sieve was then weighed. The friability was calculated as follows:

$$\text{Granule friability (\%)} = 100 - \frac{(\text{Mass remaining on sieve} \times 100)}{9^{\#}} \qquad \textbf{Equation 3.5f}$$

[#] During production, the granulate was screened on a 355 μm sieve. Material passing through this sieve was classed as fines. Fines corresponding to 10% by weight of the granulate were included in the final product and so 10% by weight of the 10 g weighed out for friability testing (i.e. 1 g) would have passed through the sieve prior to the run in the friabilator and hence cannot be included in a measure of friability.

3.5.6 Tablet Production

3.5.6.1 Uniformity of mixing

Prior to tabletting, the direct compression blends and wet granulation batches were assayed for uniformity of paracetamol content. Samples of known weight were taken at random and made up to 100 mL with deionised water. Granulates were crushed using a mortar and pestle prior to assay. The mixtures were stirred for 8 h, after which time a 5 mL sample was withdrawn and filtered through a 0.45 μm membrane filter (Millex HV Durapore® PVDF membrane, Millipore, USA). The paracetamol concentration was determined by UV spectroscopy as described previously. The paracetamol content of the sample was expressed as a fraction of the theoretical content, which assumes a completely uniform mixture. Analyses were repeated for each batch and the average determined. Samples containing 100 ± 5% of the stated paracetamol content were deemed to be sufficiently uniform for tabletting.

3.5.6.2 Preparation of tablets

Aliquots equal to the calculated compression weight were compressed initially using a Manesty single punch, hand-operated tablet press (Model 1B 179, UK) fitted with 12.5 mm flat-faced tooling. The compression force was adjusted to produce tablets with an average breaking strain of 100 N. The die cavity depth and compression force were kept constant during the compression of the powder batches. Formulation development necessitates that the maximum load or compression force applied to the tablet be accurately known. The Manesty press was not fitted with a force gauge and so, following some preliminary studies, compression was subsequently performed in an IR press using a 13 mm flat-faced punch and die set. The compression pressure was 2000 kg and the dwell time 30 s unless otherwise stated (after Kumar *et al.*, 2001). For compression modeling and tensile strength analysis, compression forces of 1000 kg, 3000 kg, 4000 kg and 5000 kg were also used.

3.5.7 Characterisation of tablets

3.5.7.1 Tablet porosity determination

The volume of the compact at a given pressure was determined according to the equation:

$$V = \pi r^2 h \qquad \textbf{Equation 3.5g}$$

where V is the volume in g /cm^3, r is the compact radius in cm and h is the thickness of the compact in cm. The dimensions were measured using the callipers function on a Schleuniger 6D tablet hardness tester (Dr. Schleuniger Pharmatron, Switzerland). As these dimensions were measured after ejection from the press, the method is termed the 'out-of-die' method.

The apparent density (ρ_{app}) of the compact was calculated from the ratio of the tablet mass to the volume of compact. The porosity of the compact, ε, was then determined using the relationship:

$$\varepsilon = 1 - \left(\frac{\rho_{app}}{\rho_{true}} \right) = 1 - D \qquad \textbf{Equation 3.5h}$$

where ρ_{app} is the apparent density of the compact, ρ_{true} is the true density of the blends determined by helium pycnometry and D is the relative density of the powder compact (Zhang *et al.*, 2003).

3.5.7.2 Heckel Compression Analysis

Heckel plots (Heckel, 1961a) were constructed by plotting the natural log of the inverse of the compact porosity against the respective compression pressure. Regression analysis was performed on the linear portion of the curve. The slope of the resultant trendline, *k*, was converted to a mean deformation pressure (P_y) using the relationship:

$$P_y = 1/k \qquad \textbf{Equation 3.5i}$$

where P_y is the pressure at which plastic or visco-elastic behaviour becomes dominant (Hersey and Rees, 1971).

The yield strength, Y, was determined using the following equation (Heckel, 1961b):

$$Y = \left(\frac{1}{3k}\right) \qquad \textbf{Equation 3.5j}$$

The area under the Heckel curve (AUHC) was calculated using the trapezoidal method (Origin® software, version 7.5, Aston Scientific Ltd., UK) and used as a measure of the extent of volume reduction that the material had undergone over the entire compression pressure range (i.e. compressibility) (Kumar *et al.*, 2001).

3.5.7.3 Kawakita Compression Analysis

The Kawakita equation (Equation 3.5k) may be used to describe volume reduction of a powder bed upon application of pressure.

$$\frac{P}{C} = \frac{P}{a} + \frac{1}{ab} \qquad \textbf{Equation 3.5k}$$

where P is the compression pressure, a and b are Kawakita compression constants and C may is defined as follows:

$$C = 1 - \left(\frac{\rho_0}{\rho_P}\right) \qquad \textbf{Equation 3.5l}$$

where ρ_0 is the bulk density of the powder and ρ_P is the apparent compact density at pressure P.

Kawakita plots were constructed by plotting P/C against P. Regression analysis was performed on the linear region of the plot. The Kawakita compression parameter denoted by a in the equation was determined from the reciprocal of the slope of the linear portion of the plot. It is a measure of the decrease in powder volume at infinite applied pressure.

3.5.7.4 Tablet hardness testing

The mechanical strength (hardness) of the tablets was assessed by determining the tablet breaking force using a tablet hardness tester (Schleuniger 6D tablet hardness tester, Dr. Schleuniger Pharmatron, Switzerland). Measurements were conducted 24 h after compression to allow any work hardening or elastic recoil to take place. Prior to

assessment of the breaking force, the tablet diameter and thickness were determined using the callipers function on the hardness tester. The test was performed on ten tablets and the average hardness calculated.

3.5.7.5 Tablet tensile strength determination

The tensile strength of the compacts, σ, was calculated in accordance with the method of Fell and Newton (1968):

$$\sigma = \left(\frac{2H}{\pi DE} \right) \qquad \textbf{Equation 3.5m}$$

where σ is the tensile strength (N /cm^2), H is the tablet hardness (N), D is the tablet diameter (cm) and E is the tablet thickness (cm).

Tensile strength values quoted represent the average of three determinations. Tensile strength profiles were constructed by plotting tablet tensile strength against compression pressure over the pressure range 1,000 to 5,000 kg. The area under the curve (AUTSC) was determined using the trapezoidal method (Origin® software, version 7.5, Aston Scientific Ltd., UK).

3.5.7.6 Tablet friability testing

Twenty tablets were dedusted with the aid of a soft brush. The tablet sample was accurately weighed and placed in the drum of an Erweka Copley Friabilator TA 20 (Germany). The drum was rotated at 25 rpm for 4 min. Loose dust was removed from the tablet surfaces as before and any cracked, split or broken tablets were removed. The remaining intact tablets were weighed to the nearest milligram. The mass lost was expressed as a percentage of the initial mass.

3.5.7.7 Disintegration testing

The disintegration time of tablets in water at 37 °C was determined using a disintegration tester (Erweka Copley Disintegration Tester ZT 44, Germany) complying with BP specifications. The disintegration time quoted represents the average of six determinations.

3.5.7.8 *In vitro* drug release study

The release profile of paracetamol from the tablets was studied using a paddle dissolution apparatus (Erweka Copley Dissolution Tester, DT 6) complying with BP specifications. The paddles were centred to ensure that the shaft was equidistant from the vessel wall at all times during rotation. The height of the paddles was adjusted so that the base of the paddle was 25 ± 2 mm above the base of the vessel. The release rate was determined in 900 mL phosphate buffer pH 6.8 (containing 11.9 g/ L disodium hydrogen phosphate dodecahydrate and 5.2 g/ L sodium dihydrogen phosphate dihydrate; Pharmaceutical Handbook, 1980). The dissolution medium was degassed as per USP Section <711> (2006) and equilibrated at 37 °C ± 0.5 °C. Paddles were rotated at 50 rpm in accordance with BP specifications. 5 mL samples were withdrawn at 2.5, 5, 7.5, 10, 15, 30 min, 1, 2, 3, 4, 5, 6, 7, 8 and 24 h. The sample was taken from a zone midway between the surface of the dissolution medium and the top of the paddle. This zone was not less than 1 cm from the vessel wall (BP, 2007). 5 mL fresh dissolution medium was used to replace the volume withdrawn. The repeated removal of dissolution medium was accounted for in subsequent calculations. Samples were filtered using a 0.45 µm membrane filter (Millex HV Durapore® PVDF membrane, Millipore, USA) and analysed for paracetamol content by UV analysis at 257 nm, following appropriate dilution with phosphate buffer where necessary.

3.5.7.9 Surface profiling using non-contact optical profilometry

The profilometer (UBM Messtechnik GmbH, Germany) used in this work had a light spot diameter of 1 µm and a measurement range of ± 500 µm. Area scans of the top and bottom surfaces of tablets produced using the different formulations and compacted at different pressures were performed. The traverse lengths were 1 mm in the X-direction and 1 mm in the Y-direction (Seitavuopio *et al.*, 2003), with a resolution of 250 points per mm in the X-direction and 20 points per mm in the Y-direction. The resulting three dimensional surface profile was subjected to a 3rd order polynomial levelling process to remove any underlying slope on the X and Y-axes which would obscure the roughness parameters associated with the tablet surface. After levelling, the R_a and R_q parameters were determined by the UBSOFT® software (version 2.8 DOS, UBM Messtechnik GmbH) associated with the profiler.

The R_a value (also termed rugosity) represents the arithmetic mean of absolute values of all profile ordinates within the overall measurement area after digitally filtering out shape deviations and coarser waviness components, that is:

$$R_a = \frac{1}{nm} \sum_{i,j=1}^{n,m} |z_{ij}| \qquad \textbf{Equation 3.5n}$$

where n is the number of measurement points, z_{ij} is the i^{th} point in the j^{th} row where the number of rows is m.

The R_q value is the root-mean-square (RMS) average roughness of deviations from the mean plane (i.e. RMS of R_a), or the standard deviation of profile heights (Healy *et al.*, 1995; Narayan and Hancock, 2003), i.e.:

$$R_q = \sqrt{\frac{1}{nm} \sum_{i=1}^{n} \sum_{j=1}^{m} z_{ij}^2} \qquad \textbf{Equation 3.5o}$$

where n, m, z_{ij}, i and j have the meanings as described above.

The influence of different compression pressures on the tablet surface characteristics were investigated in the case of sepiolite formulations. In addition, the surfaces of the tablets evaluated were examined using SEM as described in Section 3.1.8.

3.6 SEPIOLITE-EXCIPIENT AND SEPIOLITE-DRUG INTERACTION STUDY

1:1 w/w physical mixtures of sepiolite and other tabletting excipients (magnesium stearate, Explotab®, Kollidon® 25, Kollidon® 30, Kollidon® 90F, Kollidon® VA 64 and Aerosil® 200) were prepared in a Turbula mixer at 42 rpm for 30 min. DSC and TG thermograms of all physical mixtures and all individual excipients were measured as previously described. Physical mixtures of paracetamol and sepiolite were likewise prepared and analysed.

3.7 SUSPENSION STUDIES

3.7.1 Determination of the zeta potential of sepiolite

Deionised water filtered through a 0.2 μm filter (Millex HV Durapore® PVDF membrane, Millipore, USA) was used in the preparation of all suspensions and solutions required for zeta potential measurements. A 0.2 % w/v aqueous suspension of sepiolite was prepared. The pH was measured using an Orion 420A pH meter (Orion Research Inc., USA) calibrated with standards of pH 4.01, 7.00 and 10.01. Using aliquots of this suspension, a series of suspensions of pH in the range 1-13 was prepared. The pH was adjusted by dropwise addition of 0.1 M hydrochloric acid or 0.1 M sodium hydroxide solutions. The suspensions were shaken overnight using a flask shaker. The pH was measured again prior to zeta sizing. The suspensions were allowed to stand for 15 min to allow the larger particles to settle. An aliquot from the supernatant was used to determine the zeta potential as a function of the final pH. The electrophoretic mobility of the sepiolite particles at 25 °C was determined using a Zetasizer Nano *ZS* (Malvern Instruments, UK) with associated Dispersion Technology Software version 4.20. Disposable DTS1060 folded capillary cells (Malvern Instruments, UK) were used. Prior to use, the zetasizer was calibrated using a standard solution (zeta potential = -50 ± 5 mV) supplied by the instrument manufacturer. Samples were replicated five times. The applied voltage varied between 50 and 151 V depending on the conductivity of the sample. The zeta potential was calculated from the measured electrophoretic mobilities using Smoluchowski's equation:

$$\zeta = \frac{4\pi\eta_s}{D} EM \qquad \textbf{Equation 3.7a}$$

where EM is the electrophoretic mobility, η_s is the viscosity of the suspending liquid, D is the dielectric constant and ζ is the zeta potential.

3.7.2 Preparation of sepiolite dispersions to be studied by SEM

Several millilitres of the suspension/ sediment of interest were placed on filter paper (Whatman 1 Qualitative, 185 mm diameter) to allow the excess water to be removed quickly and minimise the risk of interfering with any three-dimensional structure present in the suspension. The resulting filtrate was allowed to dry at room temperature and yielded a

thin film which was mounted on aluminium stubs and gold coated as described in Section 3.1.8 prior to visualisation using SEM.

3.7.3 Particle sizing - powder-in-liquid analysis

Measurements of the particle size distribution of aqueous sepiolite suspensions were obtained using a laser diffraction particle size analyzer Mastersizer® 2000 (Malvern Instruments, UK) with a Hydro® μP sample dispersion unit. Deionised water was used as the liquid dispersant. Prior to use, the deionised water was sonicated (Bran Sonic 220, USA) and filtered under vacuum using a 0.2 μm membrane filter (Gelman Sciences) to remove dissolved gases and any particulate matter. The machine was operated in manual mode. Anaerobic filling of the sample chamber was performed. Sufficient sample was then added to obtain an obscuration rate of 5-10% at a pump speed of 1750 rpm and ultrasound setting of 10% of the maximum. The results quoted are the average of three determinations.

3.7.4 Rheology

3.7.4.1 Introduction

The rheological properties of sepiolite suspensions were assessed using a Carri-Med rheometer CSL^2500 (TA Instruments, UK) with associated operating software (Rheology Solutions Software CSL^2 module version v1.2.2). It is a controlled stress/ controlled rate rheometer. It possesses an air bearing which permits virtually friction-free application of torque. The compressed air supply (37.5 bar) is passed through a desiccant-filter assembly to remove water and particulate matter. The peltier plate is temperature controlled via a constant water supply and permits rapid and accurate heating and cooling of samples. All experiments used a cone and plate test geometry. The cone angle was 4° and the gap size between the truncated cone and the plate was 52 μm.

The Rheology Solutions Data Module (version v.1.2.2) facilitated fitting of the data obtained from continuous shear rheology to a number of rheological models, including the Newtonian, Bingham, power law, Herschel-Bulkley (HB) and Casson models (Equations 3.7b - 3.7f respectively):

$$\sigma = \eta \cdot \dot{\gamma} \qquad \textbf{Equation 3.7b}$$

$$\sigma = \sigma_B + \eta_p \cdot \dot{\gamma} \qquad \textbf{Equation 3.7c}$$

$$\sigma = K \cdot \dot{\gamma}^n \qquad \textbf{Equation 3.7d}$$

$$\sigma = \sigma_{HB} + K \cdot \dot{\gamma}^n \qquad \textbf{Equation 3.7e}$$

$$\sigma^{1/2} = \sigma_0^{1/2} + \eta_c^{1/2} \cdot \dot{\gamma}^{1/2} \qquad \textbf{Equation 3.7f}$$

where σ is the shear stress, η is the Newtonian viscosity, γ is the shear rate, σ_B is the Bingham yield stress, η_p is the Bingham fluid plastic viscosity, σ_{HB} is the Herschel-Bulkley yield stress, K is the consistency index and n is the flow behaviour index, σ_0 is the Casson yield stress and η_c is the Casson fluid plastic viscosity (Kelessidis and Maglione, 2006). In cases where the flow behaviour index is 1, the Herschel-Bulkley equation reduces to the Bingham model; n values less than 1 indicate shear thinning behaviour while n values greater than 1 are indicative of shear thickening behaviour. In cases where the Herschel-Bulkley yield stress is zero, the Herschel-Bulkley equation reduces to the power law equation (Equation 3.7d).

Data from all flow curves obtained were sequentially fitted to each of these models and the best fit chosen on the basis of the standard error (TA Instruments, personal communication, 2007). The standard error was determined by the Rheology Solutions Data Module using the following equation:

$$std_error = \left(\frac{\sqrt{\frac{errorSum}{n-2}}}{|yMax - yMin|} .1000 \right) \qquad \textbf{Equation 3.7g}$$

where n is the number of data points; errorSum is the sum of ((yModel[i] – y[i])* (yModel[i] – y[i])), where i=1,….,n; yMax and yMin are the maximum and minimum attained values of y respectively (TA Instruments, personal communication, 2007). The smaller the standard error value, the more appropriate the model to describe the rheological behaviour of the fluid.

Unless otherwise indicated, all experiments were conducted at 20 ± 0.1 °C, using an equilibration time of 3 min. The influence of increasing the equilibration time above 3 min

on the rheological parameters of samples in the concentration range 0.25 – 4% w/v sepiolite was not found to be significant. Results represent the average of at least three determinations.

3.7.4.2 Influence of dispersion speed and time on the rheology of sepiolite suspensions

The effect of the preliminary dispersion conditions (namely mixing time and mixing speed) on the rheological parameters of the resultant sepiolite suspensions was investigated using a factorial design study (Table 3.7a). The two factors were investigated at each of two levels, thereby generating a 2^2 factorial design study with four design points.

Table 3.7a. 2^2 factorial experimental design used to assess the effect of mixing speed and time on the rheology of the resulting dispersion.

Variable	Level	
	1	2
Mixing speed (rpm)	13,500	24,000
Mixing time (min)	30	60

1% w/v sepiolite suspensions were prepared and dispersed by means of a high shear Ultra Turrax® T25 mixer (IKA Instruments, Germany) at each combination of mixing speed and mixing time. 100 mL volumes were prepared in all cases. The suspensions were allowed to stand for 24 h to allow for shear recovery after which time the rheology was studied using the Carri-Med rheometer CSL^{2}500. An equilibration time of 3 min was allowed following sample loading onto the peltier plate. Samples were subjected to a controlled continuous shear stress increasing from 0.4059 to 4.5 Pa over 3 min. Samples were run in triplicate, with fresh sample loaded for each run. The data from the flow curves were fitted to the rheological models described above and the best fit model, as adjudged using the standard error value was used to permit calculation of the corresponding yield value.

3.7.4.3 Influence of concentration on the rheology of sepiolite suspensions

0.25%, 0.5%, 1%, 2% and 4% w/v sepiolite suspensions were prepared in deionised water using the Ultra Turrax® T25 at 24,000 rpm for 30 min. Samples were loaded onto the

peltier plate of the rheometer as before and allowed to equilibrate for 3 min before commencing shear analysis. To establish a suitable range of shear stresses over which to run the samples, a number of preliminary experiments were conducted where the shear stress was increased manually and the resulting displacement and sample angular velocity noted. The stress at which sample displacement began to increase slowly and consistently was taken as the starting stress and that at which the angular velocity was exceeded was the upper stress limit (Practical Techniques I, Applied Rheology Symposium 2002). The stress range over which each concentration was run is presented in Table 3.7b below. The stresses were increased over a 3 min time period and decreased over a further 3 min period. Rheological modelling was carried out as described previously.

Table 3.7b. Shear stress range for sepiolite suspensions of different concentration.

Concentration (% w/v)	Lower stress limit (Pa)	Upper stress limit (Pa)
0.25	0.0597	4.4000
0.50	0.4059	4.4000
1.00	0.4059	4.5000
2.00	2.1000	14.000
4.00	7.0000	40.000

3.7.4.4 Influence of pH on the rheology of sepiolite suspensions

A 1% w/v sepiolite suspension was prepared as described in Section 3.7.4.3. Aliquots of this suspension were taken and the pH adjusted to 1.2, 5.8 and 13.1 by dropwise addition of 1 M HCl or 1 M NaOH. Ionic strength was kept constant at 0.121 moles.L^{-1} by addition of an appropriate quantity of NaCl. An unadjusted suspension (pH 8.2) was also included in the study for comparative purposes. The ionic strength of this dispersion was likewise adjusted using NaCl, such that a difference in ionic strength would not be an additional variable. Samples were run over a shear stress range of 0.4059 to 4.5 Pa (as described in Section 3.7.4.3) at 37 ± 0.1 °C. The rheological properties of the suspensions were evaluated 24 h after pH adjustment.

3.7.5 Assessment of the sedimentation behaviour of sepiolite suspensions

3.7.5.1 Determination of sedimentation rate as a function of storage temperature

To study the sedimentation behaviour of sepiolite suspensions, the relative sediment volume was determined as a function of time. The relative sediment volume, F, is defined as the ratio of the final volume of the sediment, V_u, to the original volume of the suspension before settling, V_0, as expressed in the following equation (Martin, 1993):

$$F = \frac{V_u}{V_0} \qquad \textbf{Equation 3.7h}$$

100 mL suspensions containing different concentrations of sepiolite were prepared as described previously and decanted into 100 mL stoppered graduated cylinders of uniform diameter. The value of F at room temperature was determined at various time intervals, namely: 1 h, 1 day, 7 days, 14 days, 21 days and 28 days after preparation. The experiment was repeated once. Further sets of sepiolite suspensions were prepared and stored at 4 °C in a fridge and at 40 °C in an oven (Gallenkamp, UK). The rate of sedimentation at these storage temperatures was determined in an analogous manner.

3.7.5.2 Susceptibility to vibrational stress

To examine the susceptibility of the structured vehicle to vibrational stress, graduated cylinders containing sepiolite suspensions of different concentration were placed on a Copley SVM 12 powder density tester (UK) and subjected to 10,000 taps over 40 min. The sedimentation rate was measured as described above.

3.7.5.3 Ease of redispersion

Redispersion studies were carried out on those suspensions in which sedimentation was observed following one month of standing. The ease of redispersion was deduced from the number of times each cylinder had to be rotated by hand through 360 ° at a rate of 20 rpm, to redisperse any sediment (Matthews and Rhodes, 1968). The end point was taken when the base of the graduated cylinder was free of sediment. It is an indirect indicator of flocculation (Ofner and Schnaare, 2000).

3.7.6 Influence of electrolytes and dispersing agents on the sedimentation and rheological behaviour of sepiolite suspensions

3.7.6.1 Sodium chloride and calcium chloride

A 2% w/v sepiolite suspension was prepared as described in Section 3.7.4.3. 3 M, 2 M and 1 M solutions of NaCl were prepared in deionised water. A series of 1 in 10 dilutions of the 1 M solution was performed to produce solutions of NaCl of concentration 10 μM – 0.1 M. 5 mL of the sepiolite suspension was placed in each of eight test tubes together with 5 mL of NaCl solution (Table 3.7c). The final concentration of sepiolite in all cases was 1% w/v. The tubes were shaken vigorously before being stoppered and allowed to stand at room temperature. Two replicates were prepared. A control was prepared by adding 5 ml sepiolite suspension to 5 ml deionised water. The appearance of the test tubes was noted at 0 h, 1 h, 1 day, 7 days and 28 days after preparation.

Table 3.7c. Scheme for evaluation of the effect of NaCl on the physical stability of sepiolite suspensions.

Test tube number	Concentration of NaCl solution added	Final concentration of NaCl in test tube[§]
1	3 M	1.5 M
2	2 M	1 M
3	1 M	0.5 M
4	100 mM	50 mM
5	10 M	5 mM
6	1 mM	0.5 mM
7	100 μM	50 μM
8	10 μM	5 μM

[§] Following addition of an equal volume of 2% w/v sepiolite suspension.

The rheological properties of the resulting suspensions were evaluated 24 h after preparation as described in Section 3.7.4.3. In order to clarify the mechanism of particle stabilization/ destabilization, the pH of the samples was monitored over time. Samples prepared as described in Section 3.7.2 were subjected to SEM analysis. The process was repeated for calcium chloride.

3.7.6.2 Cetrimide, sodium citrate and sodium polyphosphate

The effect of cetrimide, sodium citrate and sodium polyphosphate on the sedimentation and rheological behaviour of sepiolite suspensions was evaluated as in Section 3.7.6.1. A lower concentration range was however evaluated, following consideration of the work of Salter (2003) on the deflocculation of halloysite (Table 3.7d).

Table 3.7d. Scheme for evaluation of the effect of cetrimide, sodium citrate and sodium polyphosphate on the physical stability of sepiolite suspensions.

Test tube number	Concentration of dispersing agent* solution added	Final concentration of dispersing agent* in test tube§§
1	400 mM	200 mM
2	200 mM	100 mM
3	20 mM	10 mM
4	2 mM	1 mM
5	200 μM	100 μM
6	20 μM	10 μM
7	2 μM	1 μM
8	0.2 μM	0.1 μM

*The term 'dispersing agent' refers to cetrimide, sodium citrate or sodium polyphosphate.

§§ Following addition of an equal volume of 2% w/v sepiolite suspension.

3.8 EVALUATION OF SEPIOLITE AND SepCMC AS SUSPENDING AGENTS IN CALAMINE LOTION

3.8.1 Formulation

The formulation for calamine lotion BP is presented in Table 3.8a. The BP (2007) directions for preparation are as follows: triturate the calamine, zinc oxide and bentonite with a solution of sodium citrate in about 70 mL of purified water and add the liquefied phenol, glycerol and sufficient purified water to produce 100 mL. Modified calamine lotion formulations (Table 3.8b) were prepared to assess the effect of replacing bentonite with an alternative suspending agent on the rheological and sedimentation characteristics

of the lotion. The levels of sodium citrate were also adjusted in the case of preparations containing sepiolite as a suspending agent given its influence on the rheological properties of sepiolite.

Table 3.8a. Formulation for calamine lotion BP.

Excipient	Quantity (per 100 mL)
Calamine	15 g
Zinc oxide	5 g
Bentonite	3 g
Sodium citrate	0.5 g
Liquefied phenol	0.5 mL
Glycerol	5 mL
Purified water, freshly boiled and cooled	Sufficient to produce 100 mL

Three 100 mL batches of each product were prepared. In the manufacture of the modified calamine lotion formulations, the suspending agent was dispersed in 50 mL deionised water using an Ultra-Turrax® T25 mixer (IKA Instruments, Germany) at 24,000 rpm for 30 min. Where relevant, sodium citrate was then added and shearing continued for a further 5 min before the addition of calamine, zinc oxide, glycerol, liquefied phenol and remaining water. Following the addition of all excipients, shearing was continued for a further 5 min. Samples were allowed to stand for 24 hr before rheological evaluations were carried out.

Table 3.8b. Modified calamine lotion formulations, differing from the BP formulation only in terms of the suspending agent used and the quantity of sodium citrate present in the formulation.

Product	Suspending agent	Sodium citrate concentration	
		(M)	(% w/v)
1	No suspending agent	BP[1]	BP[1]
2	3% w/v bentonite (Calamine lotion BP - Ovelle®)	BP[1]	BP[1]
3	2% w/v Avicel® RC-591	BP[1]	BP[1]
4	2% w/v Avicel® CL-611	BP[1]	BP[1]
5	2% w/v sepiolite	0	0
6	2% w/v sepiolite	0.010	0.2941
7	2% w/v sepiolite	0.025	0.7353
8	2% w/v sepiolite	0.050	1.4705
9	2% w/v sepiolite	0.100	2.9410
10	2% w/v SepCMC	0	0
11	1.7% w/v spray dried sepiolite + 0.3% w/v NaCMC	0	0
12	1.7% w/v sepiolite + 0.3% w/v NaCMC	0	0
13	0.3% w/v NaCMC	0	0

[1]BP: as per BP formulation.

3.8.2 Rheological evaluation of modified lotions

The samples were loaded onto the peltier plate of the Carri-Med rheometer CSL[2]500 and allowed to equilibrate for 3 min. The shear rate was increased from 0 to 1000 s^{-1} over 1 min and then returned to zero over the same time period. Samples were run in triplicate, with fresh sample loaded for each run. Rheological modelling was carried out as before.

3.8.3 Sedimentation behaviour and redispersibility of modified lotions

The sedimentation behaviour of the modified calamine lotion formulations was assessed as described in Section 3.7.5. Following 50 days of standing, the number of standard 'shakes'

(Section 3.7.5.3) required to not only redisperse any sediment formed but also to generate a readily pourable liquid was determined.

3.9 STATISTICAL METHODS

Statistical analyses were carried out using:

- Minitab™ statistical software, release 13.32, Minitab Inc., USA
- Origin® Software, version 7.5, Aston Scientific Ltd., UK and
- Microsoft® Excel, Office Package, version 10.6501.6714, SP3.

3.9.1 Two sample t-tests

Two sample t-tests were used to compare the means of two independent samples. The test procedure involved defining a null and an alternative hypothesis. The null hypothesis was that the sample means were equal, while the alternative hypothesis was that they were not equal. A t-ratio was calculated using Equation 3.9a below. This t-ratio was compared with a critical value obtained from a student's t-distribution with (n -1) degrees of freedom at a significance level of 0.05, where n is equal to the sample number for each sample group. The null hypothesis was rejected when the t-ratio exceeded the critical value. The t-ratio for two sample means is given by:

$$t = \frac{(\bar{y}_2 - \bar{y}_1)}{\sqrt{\frac{2s^2}{n}}} \qquad \textbf{Equation 3.9a}$$

where t is the t-ratio, $\bar{y}_1$ is the mean of sample 1, $\bar{y}_2$ is the mean of sample 2 and s is the the standard deviation calculated using a pooled estimate of the average sample standard deviation (Mullins, 2003).

3.9.2 Paired t-tests

Paired t-tests were used to analyze the differences between dependent observations. The null hypothesis in this instance is that the mean difference between pairs of dependent

observations is zero; the alternative hypothesis is that the difference is not zero. The paired t-statistic, t, is given by:

$$t = \frac{\bar{d} - 0}{\left(\frac{s}{\sqrt{n}}\right)} \qquad \textbf{Equation 3.9b}$$

where $\bar{d}$ is the mean difference between pairs of observations, s is the standard deviation associated with the mean difference and n is the number of pairs of observations.

3.9.3 Analysis of Variance (ANOVA)

The statistical technique Analysis of Variance (ANOVA) was used to perform comparisons between the means of more than two independent samples. The null hypothesis was that all means are equal and the alternative was that they were not. The statistical assumptions underlying ANOVA were validated prior to analysis using residual and Normal-probability plots. One-way ANOVA is the simplest form of ANOVA and was used to assess the significance of changing the level of a single factor. ANOVA generates an F-statistic, analogous to the t-statistic for two sample t-tests. Minitab™ produces a p-value associated with the F-value. Values of p less than 0.05 were indicative of non-random variation (i.e. variation of statistical significance). Tukey's 'Honestly Significant Difference' (HSD) was used to determine the minimum difference between means that is necessary for statistical significance. A family significance level of 0.05 was used for HSD analysis.

3.9.4 Factorial Experimental Design

Full factorial experiments were designed using Minitab™ and are designated by the following nomenclature:

$$N = L^K \qquad \textbf{Equation 3.9c}$$

where K is the number of factors, L is the number of levels of each factor and N is the number of experiment runs.

Used in conjunction with ANOVA, these experimental designs allowed the determination of the existence and nature of statistically significant interactions between factors and the main effects of non-interacting factors.

3.9.5 Regression Analysis

Linear regression analysis was used to determine whether a linear relationship existed between two variables. This linear relationship may be represented by the following equation:

$$y = mx + c \qquad \textbf{Equation 3.9d}$$

where x is the independent variable, y is the dependent variable, m is the slope of the line and c is the intercept on the y-axis. The equation of the line was fitted to the data using the method of least squares. The adequacy of the data fit was determined using the correlation coefficient, r^2. A trendline is most reliable when $r^2 \approx 1$.

Power regression analysis was also performed to assess whether the relationship between two variables (x and y) may be described by an equation of the form:

$$y = cx^b \qquad \textbf{Equation 3.9e}$$

where c and b are constants.

Again, the methods of least squares was used to estimate values for the trendline and the r^2 value reveals how closely the estimated values for the trendline correspond to the actual data.

Regression analysis was conducted using Microsoft® Excel (version 10.6501.6714, SP3).

PHYSICO-CHEMICAL CHARACTERISATION OF SEPIOLITE (PANGEL®-S9)

4.1 INTRODUCTION

The use of a clay mineral for any specific application depends on both its chemical composition and its structure (platy/ fibrous etc.) (López-Galindo *et al.*, 2006). Sepiolite, as discussed in Chapter 1, is a fibrous 2:1 layer phyllosilicate of ideal chemical formula $Si_{12}O_{30}Mg_8(OH)_4(OH_2)_4.8H_2O$ (Brauner and Preisinger, 1956; Cerezo *et al.*, 2001). Although sepiolite deposits may be up to 97% pure, sepiolite is often found associated with other clays, namely smectites, illite and kaolinite, and non-clay minerals including phosphates, carbonates (in particular dolomite), quartz, mica and feldspar (Martin-Vivaldi and Cano-Ruiz, 1956; Galan, 1996; Viseras and López-Galindo, 1999; Karakaya *et al.*, 2004; Yalçin and Bozkaya, 2004; López-Galindo *et al.*, 2006). Some of these impurities (quartz, feldspars, Al-smectites, illite, kaolinite, chlorite) are detrital in origin, while others (carbonates, gypsum, Mg-smectites) are formed paragenetically with the fibrous clay minerals (Galan, 1996).

The chemical composition of sepiolite itself can also vary significantly depending on geological setting and the genesis of the deposit in question (Torres-Ruiz *et al.*, 1994; Viseras and López-Galindo, 1999). Substitution of other cations for Mg and Si in the octahedral and tetrahedral sheets respectively results in different net charge deficits; ultimately giving rise to very varied rheological behaviour (Simonton *et al.*, 1988; López-Galindo *et al.*, 2006). Furthermore, the dimensions of sepiolite channels may be altered by the substitution of Fe^{3+}, and to a lesser extent by the substitution of Al^{3+}, for Mg^{2+} (Post and Crawford, 2006). In addition, studies have shown that the morphology of sepiolite varies considerably in form and fiber size from one deposit to another (Alvárez, 1984; Simonton *et al.*, 1988; Bellmann *et al.*, 1997; Viseras and López-Galindo, 1999). Colour may vary from white to cream to grey to brown (Alvárez, 1984; Galan, 1996; Santarén, 1996; Karakaya *et al.*, 2004; Post and Crawford, 2006). Finally, sepiolite can readily adsorb considerable amounts of potentially toxic elements, such as As, Sb,

Cd, Co, Cu, Pb, Ni, Hg, Se, Te, Tl, Ba, and other less dangerous elements (Li, Rb, Sr, Cr, Mo, V, Zr) (Brigatti et al., 1996; López- Galindo et al., 2006; Post and Crawford, 2006). Alternatively, these trace elements can be located within the structure of the clay mineral or in their accompanying accessory phases (López-Galindo *et al.*, 2006). The presence of excessive levels of such toxic elements would preclude its use in pharmaceuticals.

The rheological yield strength of sepiolite gels has been reported to be specifically dependent upon fiber length, specific surface area and degree of crystallinity (Simonton *et al.*, 1988). Its sorptive properties have also been linked to its surface area, porosity, crystal morphology, structure and composition (Galan, 1996; Goktas *et al.*, 1997; Cerezo *et al.*, 2001). Given the enormous textural and compositional variability of sepiolite, the chemical and mineralogical composition of the clay sample under investigation in this thesis, together with its basic physical and physico-chemical parameters, must be determined for the results of the tabletting and rheological studies undertaken subsequently to be meaningful and permit reproduction.

4.2 CONFIRMATION OF IDENTITY AND IDENTIFICATION OF IMPURITIES

pXRD and FT-IR were used as a means of confirming the mineralogical identity of the sample and to determine the presence of accessory quantities of other clay minerals. EDXA and ICP-MS permitted the determination of the major elements and trace elements respectively.

4.2.1 Powder X-ray Diffraction (pXRD)

4.2.1.1 Introduction

pXRD can be used to identify many different types of clay. When an incident X-ray beam encounters a crystal lattice, general scattering occurs. Although most scattering interferes with itself and is eliminated (destructive interference), diffraction occurs when scattering in a certain direction is in phase with scattered rays from other atomic planes. Under this condition the reflections combine to form new enhanced wave fronts that mutually reinforce each other (constructive interference). The relation by which diffraction occurs is

known as the Bragg equation. The Bragg equation for X-ray reflection from a parallel set of lattice planes with spacing, *d,* is

$$n\lambda = 2d \sin \theta \qquad \textbf{Equation 4.2a}$$

where θ is half the angle between the incident and diffracted beams, λ is the wavelength of the radiation and n is the order of the reflection which takes the values 1, 2, 3....., n (Battey and Pring, 1997).

Hence, a family of planes of a particular spacing can reflect X-rays of a given wavelength at one angle of incidence only and, as a corollary, each crystalline material, given its unique and characteristic atomic structure, will diffract X-rays in a unique characteristic pattern. Hence X-ray diffractograms can act as a fingerprint in mineral identification (Moore and Reynolds, 1989). To aid identification of clay minerals there is a comprehensive index of powder patterns of crystalline substances which is maintained by the Joint Committee on Powder Diffraction Standards (JCPDS). The JCPDS Index consists of a series of cards each containing a list of the interplanar crystalline spacings (*d* spacings) of the lines recorded, with their intensities and Miller (*hkl*) indices, together with compositional data (Battey and Pring, 1997).

In powder diffraction studies, it is usual to grind the sample to a very fine powder, such that there will be grains in every conceivable orientation, thus permitting reflections from each of the numerous families of planes that transect the crystal lattice to be recorded (Battey and Pring, 1997). Where the intention is to identify a clay mineral, oriented aggregate mounts prove more useful (Poppe *et al.*, 2001). By the orientation process, specimens are obtained in which the particles are mainly oriented with their basal planes parallel to the plane of sedimentation (Nagelschmidt, 1941). A diffractometer pattern from a very strongly oriented clay specimen may only show the *001* series of basal reflections with little or no evidence of *hkl* reflections (Nagelschmidt, 1941). It is these reflections that show the extent of the *d*-spacing expansion and/ or contraction indicative of certain clay minerals during glycolation and heating treatments (Poppe *et al.*, 2001) and hence are particularly diagnostic. Sepiolite is fibrous and so cannot be oriented so that *00l* reflections dominate the diffraction patterns (Moore and Reynolds, 1989). Consequently many lines from the *hkl* series are present and are relatively weak, thus they cannot be detected unless the sample is rich in sepiolite. Sepiolite is most easily identified by the strong basal

reflections at low 2θ values. Strong reflections from the *110* planes produce intense peaks at 12 – 12.5 Å in sepiolite (Brindley, 1959; Moore and Reynolds, 1989; Poppe *et al.*, 2001). As these and other peaks are near the diffraction angles for many of the mixed-layered and expandable clays, further treatments such as heating and ethylene glycol solvation are necessary to conclusively differentiate between them. The *110* peak of sepiolite is unaffected by solvation with ethylene glycol but changes during heat treatments. After heating to 400 °C, the *110* peak is reduced in intensity, further heating to 550 °C results in total destruction of the original peaks and the emergence of two new peaks at 10.4 Å and 8.2 Å (Moore and Reynolds, 1989; Poppe *et al.*, 2001; Karakaya *et al.*, 2004).

The U.S. Geological Survey Open File Report 01-041 describes a method for the conclusive identification of sepiolite of high purity using pXRD (Figure 4.2a).

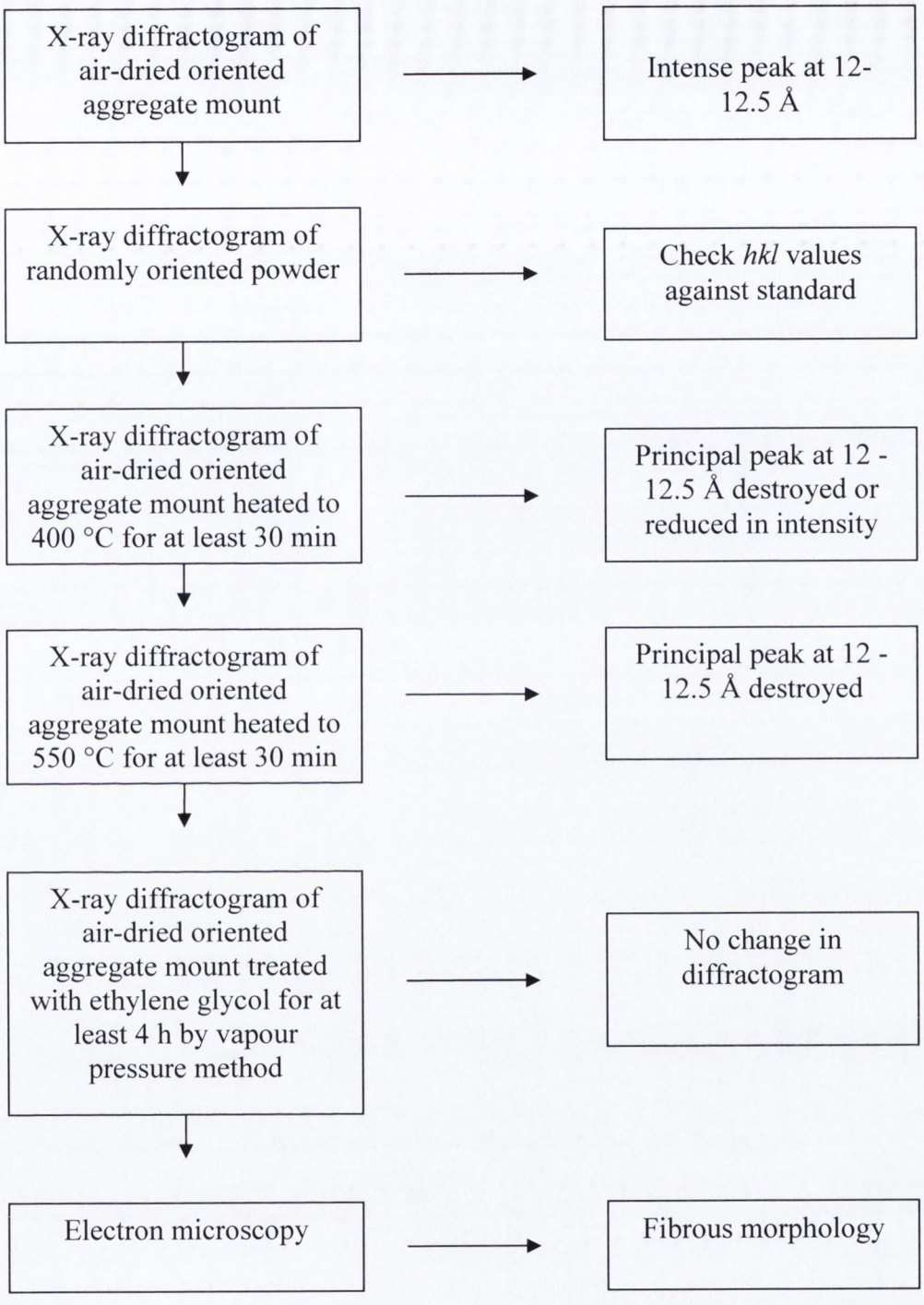


Figure 4.2a. Identification of sepiolite using pXRD (Reproduced from the U.S. Geological Survey Open File Report 01-041).

4.2.1.2 X-ray diffractograms of Pangel®-S9

The X-ray diffractograms of randomly oriented powder mounts of Pangel®-S9, together with oriented mounts subjected to the described glycolation and heat treatments, are presented in Figure 4.2b below.

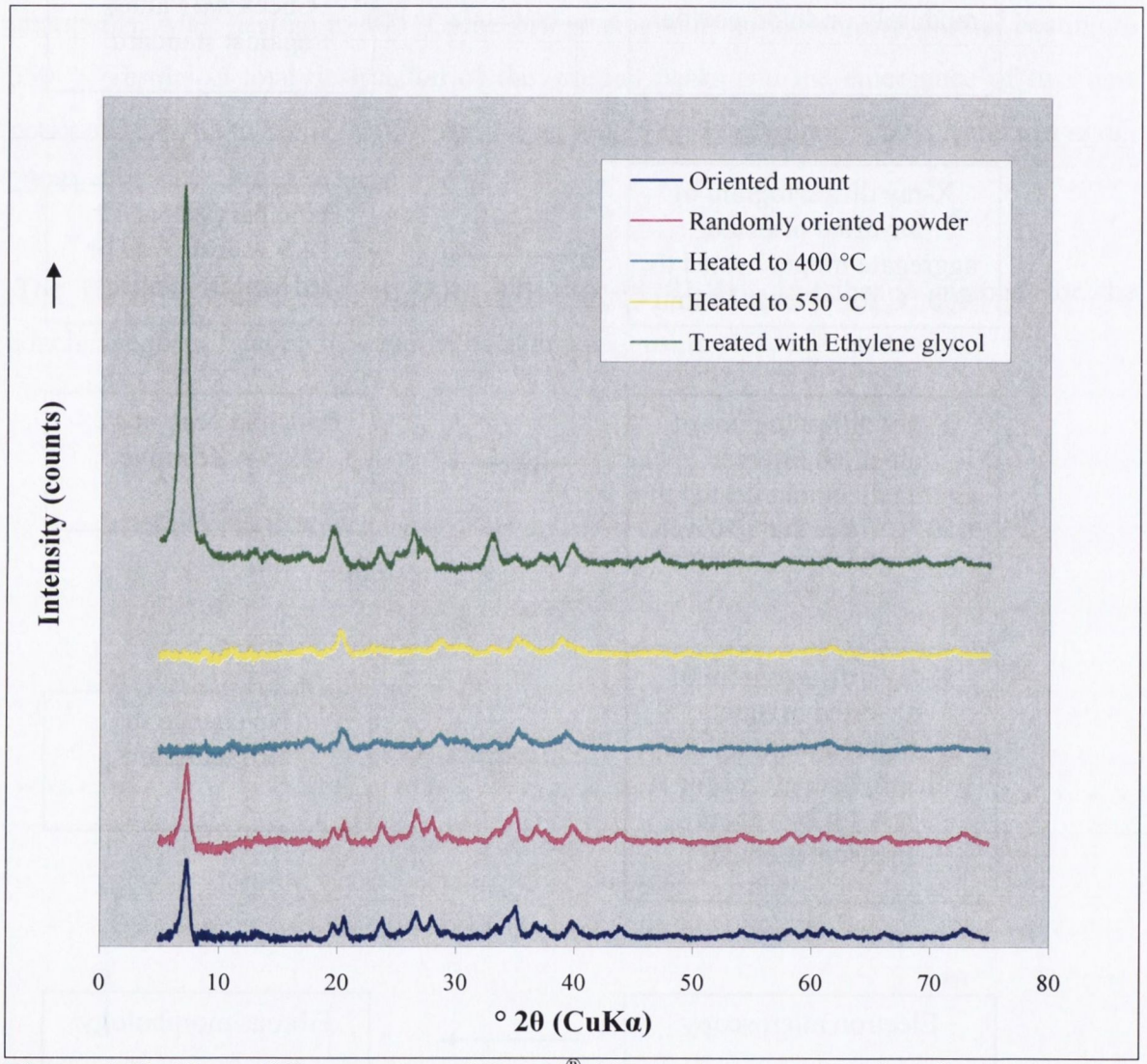


Figure 4.2b. X-ray diffractograms of Pangel®-S9 samples treated as described in the U.S. Geological Survey Open File Report 01-041.

The X-ray diffractograms of the oriented and randomly oriented Pangel®-S9 mounts were identical indicating that the orientation process, aimed at enhancing the *00l* reflections, proved unsuccessful, as would be expected given the fibrous nature of sepiolite (Brindley, 1959; Moore and Reynolds, 1989; He *et al.*, 1996). Such a result would also suggest the absence of platy clays in the sample. The most intense peak in both XRD patterns was at 7.3° 2θ corresponding to a d-spacing of 12.1 Å i.e. the *110* reflection (see Figure 4.2c).

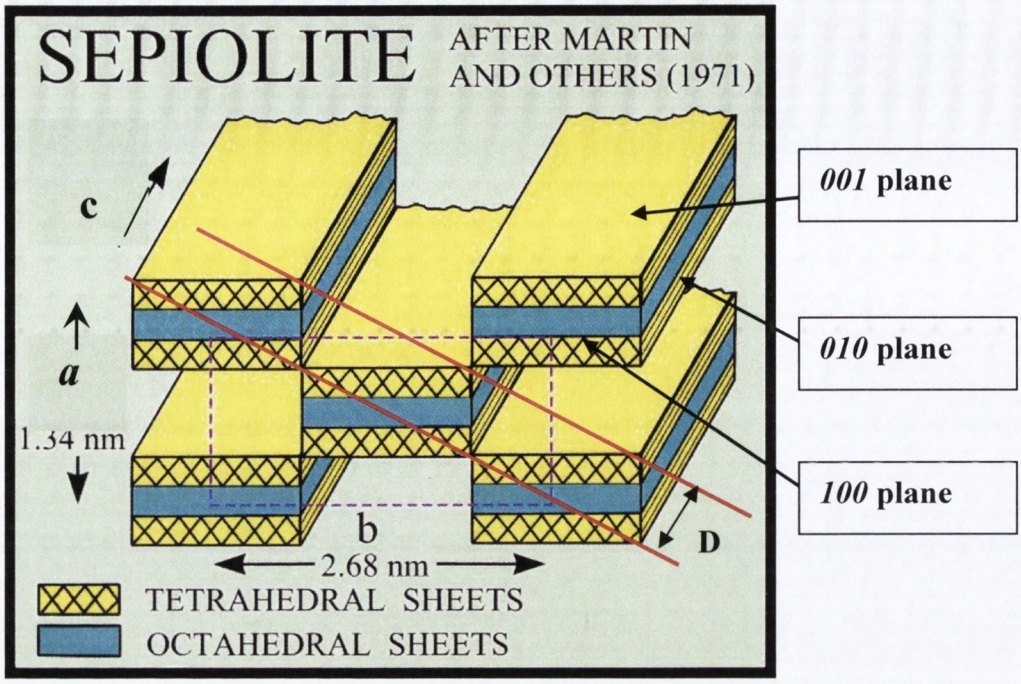


Figure 4.2c. Schematic representation of the different planes of sepiolite fibers; parallel red lines illustrate the *110* plane responsible for the strong peak at 7.3° 2θ (Adapted from Poppe *et al.*, 2001). The perpendicular distance between two adjacent *110* planes (denoted by D) may be theoretically calculated to be 12 Å using the dimensions of the sepiolite unit cell proposed by Brauner and Preisinger (1956).

The *d*-spacings of the peaks in the oriented mount were compared to those of JCPDS powder diffraction card 29-1492, which corresponds to a sepiolite sample from Eskişehir, Turkey. Peaks marked with an asterisk in Table 4.2a were of particular interest given that they are common to several different specimens of sepiolite and are free from interferences of other clay minerals common in the clay-size fraction (Moore and Reynolds, 1989).

The data from Pangel®-S9 corresponded well with that of JCPDS standard 29-1492 bearing in mind that a good deal of variation in spacings and intensities can occur from one sepiolite sample to the next depending on the extent of crystallinity (Brindley, 1959; Moore and Reynolds, 1989). The sample may be classed as one of intermediate crystallinity in accordance with Brindley (1959).

Table 4.2a. Comparison of X-ray diffraction data for JCPDS standard 29-1492 and Pangel®-S9.

JCPDS Standard 29-1492			Pangel®-S9		
2θ (°)	***d* (Å)**	**Intensity (%)**	**2θ (°)**	***d* (Å)**	**Intensity (%)**
6.9*	12.8	100	7.30	12.100	100
11.6*	7.6	4	11.62	7.609	4.35
17.5*	5.1	8	17.40	5.092	9.53
20.0	4.4	35	20.64	4.304	31.71
23.6*	3.77	20b	23.60	3.767	21.88
26.6	3.35	30vb	26.64	3.343	35.84

Note: b = broad, vb = very broad; asterisk denotes peaks common to several different specimens of sepiolite and free from interference by other clay minerals.

Peaks at 24.04° 2θ (*d* = 3.703 Å) and 30.80° 2θ (*d* = 2.900 Å) were indicative of the presence of small amounts of dolomite ($CaMg(CO_3)_2$) in the sample. Many authors (Karakaya *et al.*, 2004; Özcan *et al.*, 2004; Yalçin and Bozkaya, 2004) have reported traces of dolomite in sepiolite samples and have suggested that sepiolite may be formed from dolomite as follows:

$$8CaMg(CO_3)_2 + 12H_4SiO_4 \rightarrow Si_{12}O_{30}Mg_8(OH)_4(OH_2)_4.8H_2O + 16HCO^{3-} + 2H_2O + 16O_2 + 8Ca^{2+}$$

dolomite **silicic acid** **sepiolite** **Equation 4.2b**

Upon heating to 400 °C, the *110* peak at 7.30° 2θ (*d* = 12.1 Å) and the *031* peak at 19.8° 2θ (*d* = 4.475 Å) were destroyed and replaced by peaks at 8.74 and 11.18° 2θ (*d* = 10.117 and 7.957 Å respectively). Similar changes in the XRD pattern of sepiolite were noted by a number of authors following thermal treatment of this nature (Moore and Reynolds, 1989; He *et al.*, 1999; Poppe *et al.*, 2001; Karakaya *et al.*, 2004). Frost and Ding (2003) stated that the four molecules of crystal water from each structural formula unit of sepiolite were lost in two steps at ~330 °C and 530 °C due to different bonding energy. Serna *et al.* (1975a) reported that the changes in the X-ray diffractogram upon heating above 370 °C were indicative of the folding and collapse of the interspace of the sepiolite structure upon removal of the first portion of crystal water. No further changes in the X-ray diffractogram were observed following heating to 550 °C. This concurs with the findings of Serna *et al.* (1975a) and He *et al.* (1996) both of whom reported that heating above 530 °C to remove

the remainder of the crystal water (thereby producing sepiolite anhydride) caused little additional structural change.

No new reflections or peak shifts were evident following treatment of Pangel®-S9 with ethylene glycol confirming the absence of swelling clays (smectites, some mixed-layer clays and vermiculite) in the clay sample. Smectites can admit organic compounds of a polar nature, such as ethylene glycol, between the layers resulting in an expansion of the basal spacing (van Olphen, 1977). Ethylene glycol may access the intracrystalline channels of sepiolite (Ruiz-Huitzky, 2001) but cannot alter the channel dimensions due to the covalent nature of the bonding which produces the channels. The resolution of peaks occurring close together was reduced, presumably due to the amorphous scattering of X-rays by the presence of excess ethylene glycol (Poppe *et al.*, 2001).

Electron microscopy (Section 4.4) confirmed the fibrous morphology of sepiolite. Consequently, in accordance with the USGS clay mineral identification system, sepiolite was demonstrated to be the primary constituent of Pangel®-S9. The absence of swelling clays was also demonstrated conclusively.

4.2.2 Fourier Transform Infra-red Analysis (FT-IR)

FT-IR is primarily used for the qualitative and quantitative analysis of organic compounds but may also be used to determine the chemical structure of inorganic materials. It is mainly used as a complementary method to pXRD to investigate clays and clay minerals (Madejová and Komadel, 2001). Correlation of the IR spectrum of a material with its reference spectrum is frequently employed by the pharmacopoeias as a means of identification. An IR spectrum can served as a fingerprint for mineral identification, but it can also give unique information about the mineral structure, including the family of minerals to which the specimen belongs and the degree of regularity within the structure, the nature of isomorphic substituents, the distinction of molecular water from constitutional hydroxyl groups and the presence of both crystalline and non-crystalline impurities (Madejová and Komadel, 2001). Frost *et al.* (1998) noted that despite the similarity of the morphology and chemical composition of palygorskite and sepiolite, their IR spectra are considerably different. The FT-IR spectrum of Pangel®-S9 is presented in Figure 4.2d.

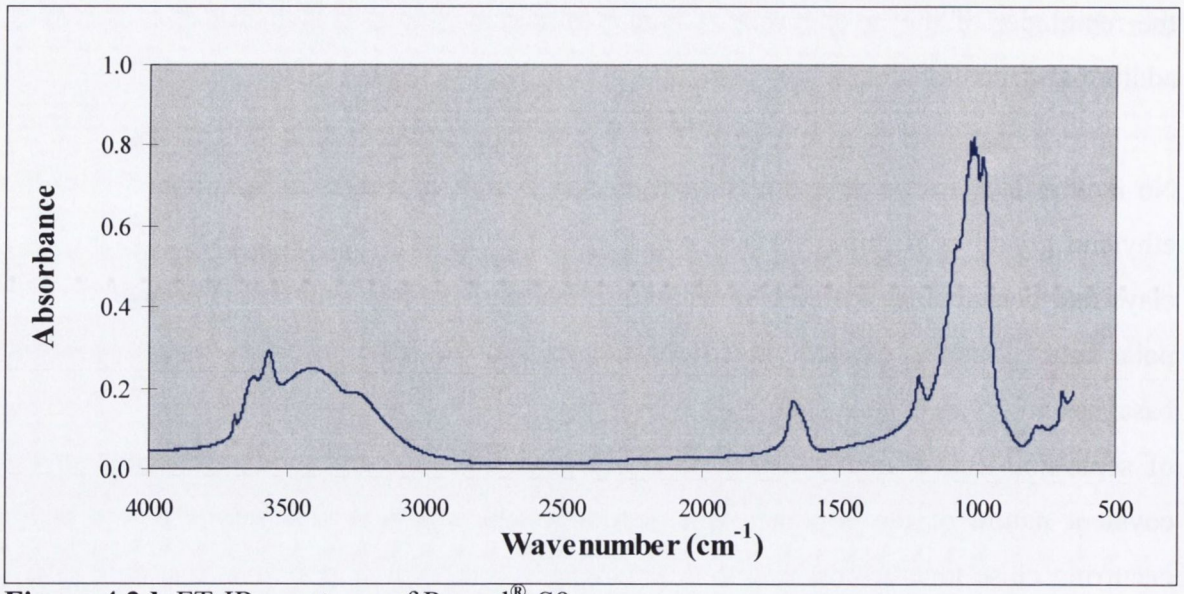


Figure 4.2d. FT-IR spectrum of Pangel®-S9.

The FT-IR spectrum of Pangel®-S9 correlates closely (r^2 = 0.9657) with a reference spectrum for sepiolite sourced in Two Crows, Nevada (FDM reference spectra, Appendix 3), thus acting as a further confirmation of the identity. Two Crows sepiolite is a rather pure sepiolite (Post, 1978) and is considered a useful standard in comparing sepiolites from different sources (Post and Janke, 1984). High correlation would be expected despite the different geologic source given that the host rock in both cases is sedimentary in nature and of similar geologic age (Post and Crawford, 2006). Band component analysis of the FT-IR spectrum of sepiolite has been carried out by a number of authors (Vicente-Rodríguez *et al.*, 1996; Frost *et al.*, 1998, 2001; Akyüz and Akyüz, 2003; Akçay, 2004). Four main regions may be distinguished in the FT-IR spectrum, namely the OH stretching region (3000-4000 cm^{-1}), the OH bending region (1600-1700 cm^{-1}), the Si-O stretching region (850-1300 cm^{-1}) and the Si-O-Si bending region (400-550 cm^{-1}) (Akyüz and Akyüz, 2003). Closer examination of the sample and reference spectra indicated that the 600-1300 cm^{-1} regions (i.e. silicate regions) correlated extremely closely (r^2 = 0.9672) while correlation in the 3000-4000 cm^{-1} region was poorer (r^2 = 0.9365). Higher correlation in the silicate regions than in the MgOH and co-ordinated water OH-stretching region would also be expected given the higher tendency for substitution of Mg in the brucite sheet than for Si in the silicate sheet (Karakaya *et al.*, 2004). Results published by Post and Crawford (2006) indicated that sepiolite from Two Crows, Nevada had lower Al and Fe contents than sepiolite from Vallecas, Spain. As Al and Fe are most likely to replace Mg in the brucite layer, differences in the 3000-4000 cm^{-1} region of the spectrum would be expected, thus accounting for the poorer correlation. Furthermore, the presence

of trace amounts of dolomite, as indicated by pXRD analysis, could provide a further source of variation in this region of the spectrum.

Table 4.2b. IR absorption bands of Pangel®-S9 and Eskişehir sepiolite[1] as obtained from band component analysis.

Probable Assignments[2]	**Pangel®-S9**	**Eskişehir sepiolite[1]**
SiOH/ MgOH (trioctahedral) hydroxyl stretch	3689.74	3689
MgOH (dioctahedral) stretch	3628.33	3629
OH stretch from co-ordinated water	3565.72	3570
Zeolithic water OH stretch	3396.69	3420
Zeolithic water OH stretch	3245.01	3221
Water OH bend	1653.58	1660
Si-O stretch	1212.17	1207
Si-O stretch	1080.17	1080
Si-O stretch	1018.39	1020
OH deformation	977.61	977
OH deformation	785.20	787
OH deformation	690.40	691

[1]Data for Eskişehir sepiolite from Akyüz and Akyüz (2003). [2] Assignments after Akyüz and Akyüz (2003) and Frost *et al.* (1998, 2001).

The positions and probable assignments of the 11 eleven principal peaks (absolute threshold 0.04, sensitivity 70) in the spectrum of Pangel®-S9 are presented in Table 4.2b. Assignments were made following the consideration of the work of Akyüz and Akyüz (2003) and Frost *et al.* (1998, 2001). Although the brucite layer in sepiolite is octahedral in form, the band at 3620 cm^{-1} is characteristic of dioctahedral systems. Ahlrichs *et al.* (1975) has reported that this is due to some vacant octahedral sites. The corresponding results for Eskişehir sepiolite (Akyüz and Akyüz, 2003) are included for comparative purposes and again indicate a high degree of correlation. FT-IR, therefore, conclusively confirmed the identity of the Pangel®-S9 sample as sepiolite.

4.2.3 Energy Dispersive X-ray Analysis (EDXA)

Semi-quantitative EDXA was used to determine the major elemental composition of Pangel®-S9. From Figure 4.2e, it is evident that the principal elements in Pangel®-S9 were silicon, oxygen, magnesium and aluminium. These results concur with the reported formula of the unit cell of sepiolite ($Si_{12}O_{30}Mg_8(OH)_4(OH_2)_4.8H_2O$; Cerezo *et al.*, 2001) and with the findings of Karakaya *et al.* (2004). Lower levels of calcium, potassium and iron were also present in Pangel®-S9. Low levels of aluminium and iron in samples of sepiolite from Vallecas, Spain have been reported by other authors (Post and Crawford, 2006). López-Galindo *et al.* (2006) also noted the existence of small amounts of iron, calcium and potassium in sepiolite samples. The tetrahedral Al can substitute for Si and also for Mg in the brucite layer (Karakaya *et al.*, 2004). Fe can also occupy the octahedral Mg position. Ca and K may be present as interlayer cations (Karakaya *et al.*, 2004). Alternatively the small amounts of dolomite ($CaMg(CO_3)_2$) present in the sample could account for all or part of the calcium content.

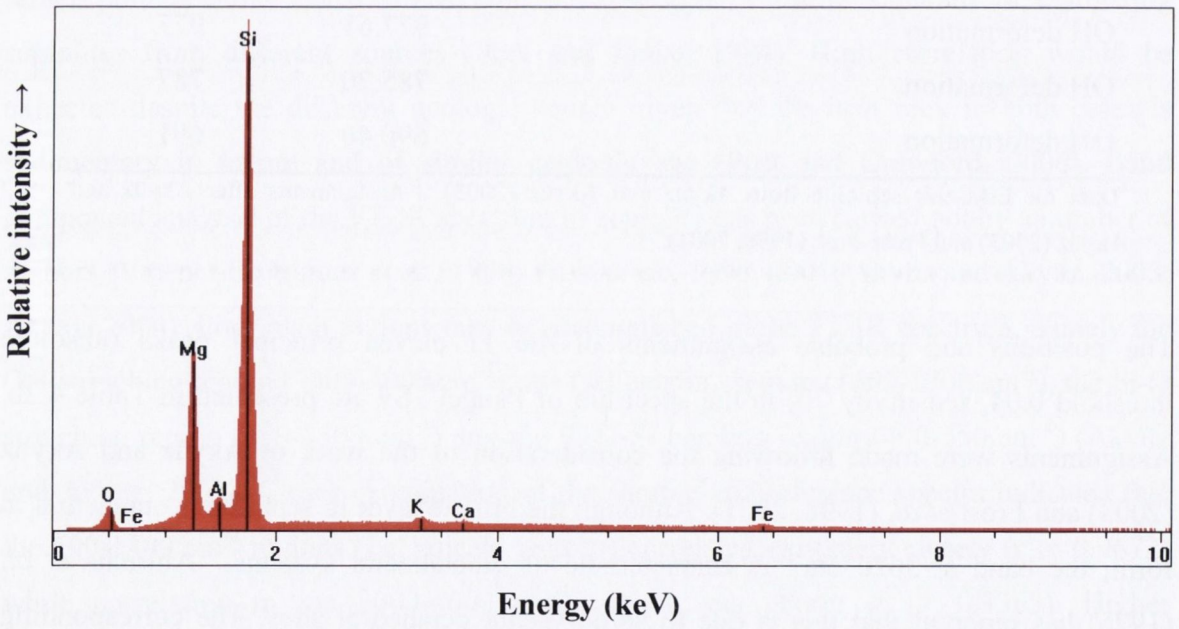


Figure 4.2e. Semi-quantitative EDX analysis of Pangel®-S9.

4.2.4 Inductively Coupled Plasma-Mass Spectroscopy (ICP-MS)

ICP-MS is ideally suited to the rapid and simultaneous analysis of multiple elements in geological materials including soils and most rock types (Longerich *et al.*, 1990; Eggins *et al.*, 1997) and more recently has been applied to clay minerals (Kogel and Lewis, 2001). Results of trace elemental analysis of Pangel®-S9 are presented in Table 4.2c. The clay sample was assayed for content of arsenic, barium, beryllium, cadmium, calcium, cobalt, chromium, caesium, copper, gallium, iron, lead, lithium, manganese, mercury, nickel, potassium, rubidium, selenium, silver, sodium, strontium, thallium, uranium, vanadium and zinc.

The results of trace element analysis of sepiolite mined from the same region as Pangel®-S9 (published by Post and Crawford, 2006) are also included in Table 4.2c for comparative purposes. From Table 4.2c it is evident that the principal trace elements in Pangel®-S9 were iron, potassium, calcium, sodium, lithium and manganese. Comparison of the trace elemental content of Vallecas sepiolite (Post and Crawford, 2006) with that of Pangel®-S9 indicated that although the level of rubidium was higher, those of strontium and chromium were similar and those of lead, nickel, arsenic, copper, zinc and vanadium were markedly less in the Pangel®-S9 sample. These differences may reflect variations in sepiolite mined from different sites within the Vallecas valley or alternatively that the purification process employed by Tolsa SA was successful in terms of reducing the heavy metal content.

The European, British and American Pharmacopoeias place limits on the levels of Pb, As and heavy metals in clays for pharmaceutical applications. The BP and PhEur (2007) impose limits of ≤ 4 ppm arsenic and ≤ 40 ppm heavy metals on Magnesium Trisilicate, which although is typically synthesized from sodium silicate and magnesium sulphate, can also refer to naturally occurring sepiolite (Anonymous, 1998). The USP (2006) limits for arsenic and heavy metals are 8 ppm and 30 ppm respectively. Consequently, the arsenic content of Pangel®-S9, although complying with USP requirements, exceeded BP and PhEur limits. Post and Crawford (2006) did note that the arsenic in some geological samples is strongly bound and hence not leachable when processed for commercial use and thus need not be considered hazardous. They did however concede that the arsenic bonding capacity of sepiolite has not yet been sufficiently investigated to deem this to be the case.

Table 4.2c. Results of trace element analysis of Pangel®-S9, Vallecas sepiolite[1] and Pharmasorb® regular[2] (elements listed in order of decreasing content in Pangel®-S9).

Metal	Pangel®-S9 (ppm)	Spanish (Vallecas) sepiolite[1] (ppm)	Pharmasorb® regular[2] (ppm)
Fe	5024	n.a.*	n.a.*
K	1824	n.a.*	n.a.*
Ca	958.7	n.a.*	n.a.*
Na	313.5	n.a.*	n.a.*
Mn	280.1	n.a.*	n.a.*
Li	97.55	n.a.*	25.4
V	31.15	82	122.3
Ba	33.32	425	125.0
Cr	28.38	31	153.2
Zn	24.00	2169	96.2
Sr	18.46	17	62.0
Rb	15.35	9	41.9
Cu	7.55	1540	8.4
As	6.03	90	n.a.*
Ga	5.03	n.a.*	13.2
Ni	4.80	31	21.5
Pb	3.16	715	8.2
Co	2.53	n.a.*	6.8
Be	<2**	n.a.*	2.1
Se	<2**	n.a.*	n.a.*
Ag	<2**	n.a.*	n.a.*
Cd	<2**	n.a.*	n.a.*
Cs	<2**	n.a.*	n.a.*
Tl	<2**	n.a.*	0.4
U	<2**	n.a.*	3.0
Hg	<0.2	n.a.*	n.a.*

[1] From Post and Crawford, 2006; [2] From Viseras and López-Galindo, 1999; *n.a. = not analysed; ** 2 ppm represents the limit of detection for Be, Se, Ag, Cd, Cs, Tl, U and Hg.

Neither the Pharmacopoeias nor the IUPAC Compendium of Chemical Terminology define clearly which metals are encompassed by the term "heavy metal". Any definitions found elsewhere were inconsistent; the term referring in some definitions to metals with high atomic weights (National Safety Council), in others to metals with a specific density >5 g /cm^3 (Jarüp, 2003) while more related it to metals with a specific density >4 g /cm^3 (Grant and Grant, 1987). Duffus (2002) has reviewed extensively the various definitions of a "heavy metal" and rendered the term meaningless and misleading due to the tendency to assume that all so-called heavy metals and their compounds have highly toxic properties.

Jarüp (2003) reported that the main threats to human health from heavy metals are associated with exposure to lead, cadmium, mercury and arsenic. Other authors have also included chromium and nickel in the toxic line-up. Duffus (2002) stated that the toxicity of metals and their compounds must be individually assessed based on their chemical properties, their bioavailability and the biological properties of the organism at risk. Consequently, given the inexact nature of the term "heavy metal", the compliance, or lack thereof, of the Pangel®-S9 sample with pharmacopoeial limits cannot be commented upon in any meaningful manner other than to note that the content of V, Ba, Cr, Zn, Sr, Rb, Cu Ga, Ni, Pb, Co, Be, Tl and U were markedly lower than the corresponding values in Pharmasorb® (a palygorskite pharmaceutical preparation) reported by Viseras and López-Galindo (1999).

4.3 THERMOGRAVIMETRIC ANALYSIS (TGA)

TGA was used to determine the amount and type of water present in Pangel®-S9. The TG profile of sepiolite (Pangel®-S9) is given in Figure 4.3a. Four distinct weight losses were observed, consistent with the findings of del Hoyo *et al.* (1996), Vučelić *et al.* (2002) and Frost and Ding (2003).

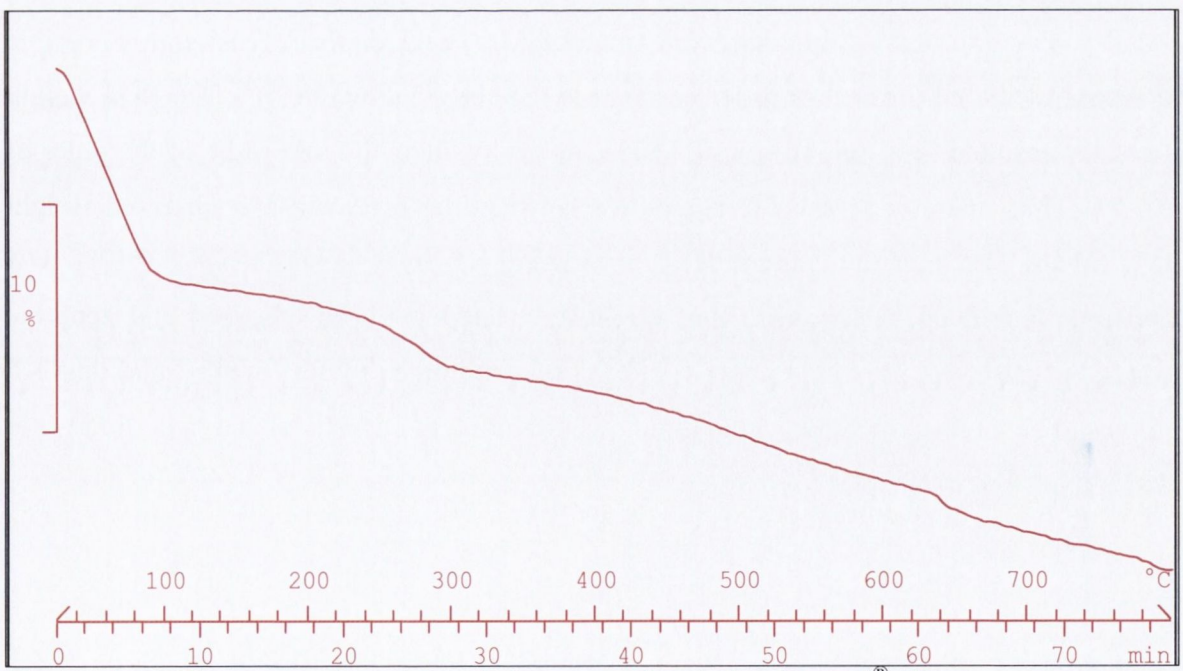


Figure 4.3a. Thermogravimetric analysis curve of sepiolite (Pangel®-S9).

The first step occurred over the temperature range 25-90 °C and has been attributed by Frost and Ding (2003) to the loss of adsorbed/ superficial water. Surface silanol groups act as centres for adsorption of water molecules. Water can associate by H-bonding with all types of surface silanols (Flörke *et al.*, 2002). The second, third and fourth steps occurred over the temperature ranges 120-300 °C, 300-640 °C and 640-800 °C respectively. Nagata *et al.* (1974) proposed that these four steps corresponded to (1) the loss of water adsorbed to the external surfaces, (2) the loss of zeolithic (hydration) water, (3) the loss of co-ordination water to form sepiolite anhydride and (4) the loss of edge silanol and structural Mg-OH groups through dehydroxylation. Such a scheme may be represented by the following equations (adapted from Frost and Ding, 2003):

- Step 1 and 2: $Si_{12}Mg_8O_{30}(OH)_4(OH_2)_4.8H_2O \rightarrow Si_{12}Mg_8O_{30}(OH)_4(OH_2)_4 + 8H_2O$
- Step 3(a): $Si_{12}Mg_8O_{30}(OH)_4(OH_2)_4 \rightarrow Si_{12}Mg_8O_{30}(OH)_4(OH_2)_2 + 2H_2O$
- Step 3(b): $Si_{12}Mg_8O_{30}(OH)_4(OH_2)_2 \rightarrow Si_{12}Mg_8O_{30}(OH)_4 + 2H_2O$
- Step 4: $Si_{12}Mg_8O_{30}(OH)_4 \rightarrow 8MgSiO_3 + 4SiO_2 + 2H_2O$

The theoretical weight loss occurring over steps 1 and 2 is 11.12% but will depend on the relative humidity under which the sample is stored (Alvarez, 1984). The observed weight loss was 13.10% (component steps: 8.99% and 4.11%). The theoretical weight loss for step 3 is 5.55% compared with the observed value of 5.00%. Given these results, it is possible that loss of the co-ordination water commenced slightly below 300 °C. The final weight loss step resulted in a weight loss of 3.91%, theory predicts the loss to be of the order of 2.77%. Thus, there is reasonable agreement between the predicted and observed weight loss values. The moisture content determined using KF analysis was 12.28 ± 0.22% w/w and thus correlated closely with the weight associated with the adsorbed and zeolithic water. As expected, structural water could not be determined by this method and thus KF proves to be a useful method for the rapid quantification of superficial and hydration water and is exploited in Chapter 5.

4.4 MACROSCOPIC AND MICROSCOPIC APPEARANCE OF SEPIOLITE (PANGEL®-S9)

4.4.1 Introduction

The aim of this Section was to study the macroscopic and microscopic appearance of Pangel®-S9 to confirm its fibrous morphology and the absence of non-fibrous contaminants. The change in appearance in response to mechanical and thermal treatment was also examined.

4.4.2 SEM of sepiolite (Pangel®-S9)

Pangel®-S9 is a lightweight cream-coloured powder. Alvarez (1984) notes that the colour of sepiolite when it occurs in compacted form is white or cream-coloured with grey, green, rose or even crimson tones, depending on the degree of contamination. The morphology and microstructure of sepiolite (Pangel®-S9) were investigated by means of SEM (Figures 4.4a-d). The fibrous nature of sepiolite was readily apparent. Two levels of organisation were evident – namely the parallel alignment of individual fibers along their *c*-axes to form bundles or sheaves, with lengths of ~ 0.25 – 1.5 μm (Figure 4.4c), and the aggregation of these bundles in a haphazard manner to form microagglomerates, of varied shape, and size typically of the order of ~ 30 – 42 μm across the longest diameter (Figure 4.4a). Several lots of Pangel®-S9 selected at random from the composite batch of 18 kg were analysed to examine the batch for uniformity of content. No difference in appearance at any level of magnification was observed between samples taken from different parts of the batch.

The fibers exhibit a column-like morphology with a rectangular cross section (Figure 4.4d) consistent with the structural model proposed by Brauner and Preisinger (1956). The tendency for bundles to interweave to form felted mats in one, two or three dimensions, noted by Alvárez (1984), is also apparent from Figures 4.4b and 4.4d.

Similar morphological characteristics and levels of structural architecture were reported by other authors (Viseras and López-Galindo, 1999; Vučelić *et al.*, 2002; Kojdecki *et al.*, 2005) indicating that the physico-chemical purification processes used by Tolsa SA did not alter the microstructure of the clay or the manner of fibrous association. Fiber dimensions, estimated from SEM, were ~ 40 nm wide (i.e. *b*-axis), 10-20 nm high (i.e. *a*-axis) and

250-1500 nm long (i.e. *c*-axis) and correlate well with those reported by Bellmann *et al.* (1997) and Santarén (1996) for sepiolite from Vallecas-Vicálvaro.

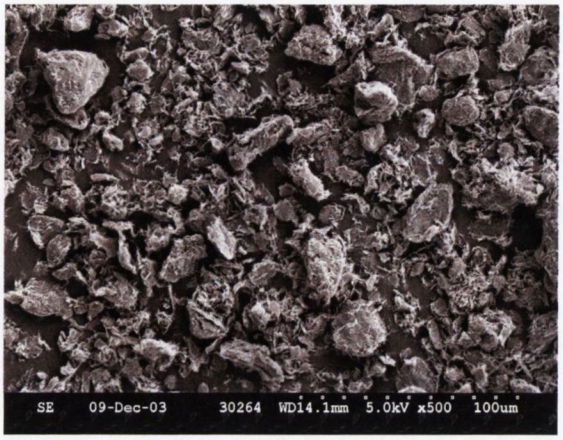


Figure 4.4a. SEM of sepiolite (magnification x 500).

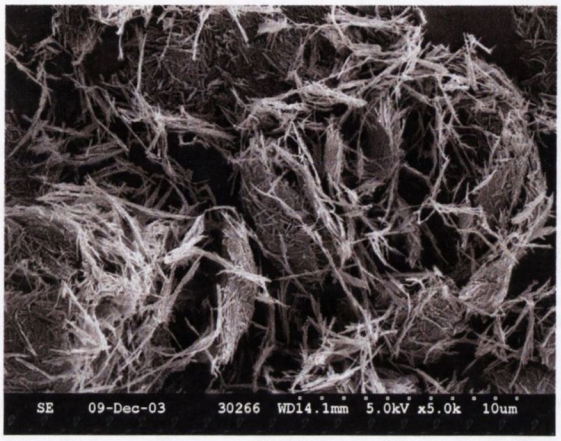


Figure 4.4b. SEM of sepiolite (magnification x 5,000).

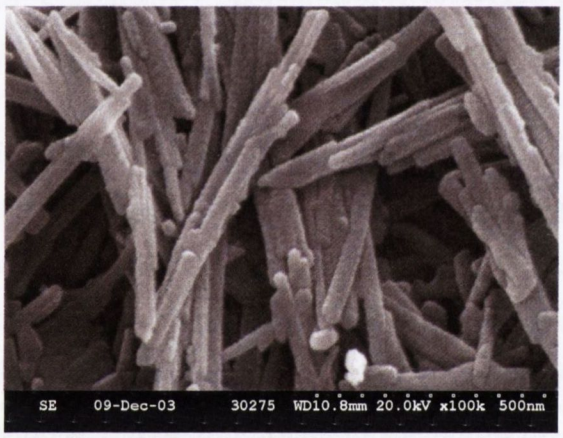


Figure 4.4c. SEM of sepiolite (magnification x 100,000).

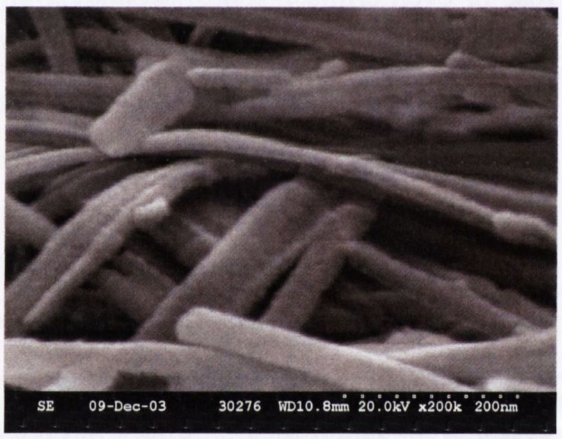


Figure 4.4d. SEM of sepiolite (magnification x 200,000).

López-Galindo *et al.* (2006) noted that in the specific case of fibrous clays, and although not a requirement of any pharmacopoeia, particle size must be strictly controlled because it is reportedly the decisive factor in the carcinogenic potential of fibrous clays following inhalation. The IARC (1997) has reported limited evidence in experimental animals for the carcinogenicity of long sepiolite fibers, defined as those greater than 5 μm in length. Stanton *et al.* (1981) reported that inactivation via phagocytosis occurred readily in the case of short fibers and those of large diameter while inactivation of long, thin fibers was negligible. The carcinogenic potential is linked to biodurability which in turn is dictated by fibrous dimensions. A high tumor incidence has been reported for a sepiolite from Finland but studies have revealed no evidence of carcinogenic potential (following either

intraperitoneal or intratracheal instillation) for sepiolite from Vallecas-Vicálvaro (Bellmann *et al.*, 1997). The low biological activity of Vallecas-Vicálvaro sepiolite, relative to the Finnish sample, has been attributed to the short length of the fibers and low *in vivo* persistence. This difference in the length distribution between Vallecas-Vicálvaro sepiolite and Finnish sepiolite was explained by Santarén and Alvárez (1994) as the different geological origins of the two types of sepiolite. Vallecas sepiolite is a sedimentary sepiolite of moderate crystallinity and fibers with an average length < 2 μm. The small crystal size is attributed to the presence of a higher number of crystallization nuclei during chemical precipitation in the sedimentary environment, compared to the non-sedimentary Finnish sepiolite, which is formed by hydrothermal processes (Galan, 1996). The IARC (1997) has indicated inadequate evidence in experimental animals for the carcinogenicity of short sepiolite fibers (< 5 μm). Consequently, two conclusions may be drawn from microscopic evaluation of sepiolite (Pangel®-S9); firstly, the fibrous form and dimensions of the clay are in concordance with those reported by other authors and secondly, the fiber length typically did not exceed 1.5 μm, thus predictive of low biodurability and carcinogenic potential.

4.4.3 The effects of dry grinding on the microscopic appearance of sepiolite

As sepiolite has a fibrous morphology, different methods of grinding may produce various structural changes (thinning of the fibers, distortion of the parallel units, and/or disruption of the structure) (Vučelić *et al.*, 2002). Consequently, three different methods of grinding were employed here to assess the robustness of the physical structure to processes typical in the pharmaceutical industry. Grinding was performed using a mortar and pestle, a ball mill and an ultracentrifugal mill (UCM).

Grinding of Pangel®-S9 using a mortar and pestle for 5 min resulted in the loss of definition of the microagglomerate perimeters (Figure 4.4e) due to separation of bundles of fibers from the microagglomerate structures. After longer grinding times (10 min), the once rounded aggregates became almost laminar, presumably due to thinning/ compaction of the aggregates in a direction perpendicular to the shearing action (Figure 4.4f). The dimensions of the *a*-axis and *b*-axis remained similar to that in the untreated sample; however, the average length of the fibers (i.e. the *c*-axis) was reduced with a noticeably larger proportion of fibers having lengths < 0.2 μm (Figure 4.4g).

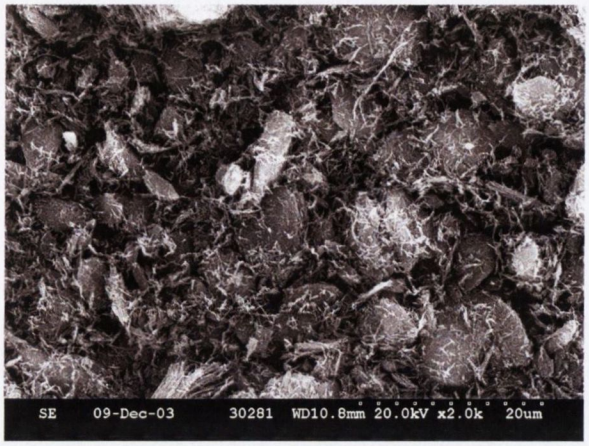


Figure 4.4e. SEM of sepiolite ground for 5 min using a mortar and pestle (magnification x 2,000).

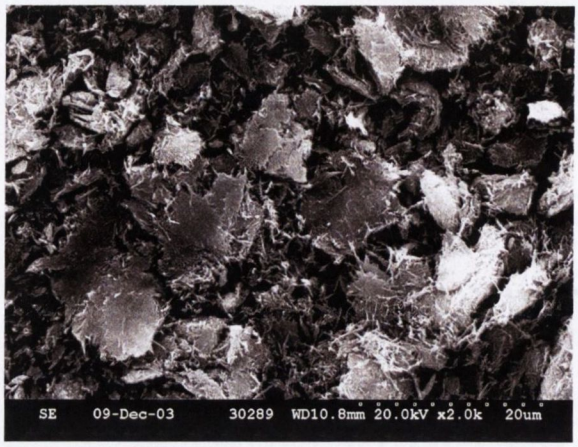


Figure 4.4f. SEM of sepiolite ground for 10 min using a mortar and pestle (magnification x 2,000).



Figure 4.4g. SEM of sepiolite ground in a mortar for 5 min (magnification x 100,000).



Figure 4.4h. SEM of sepiolite ground in a ball mill for 5 min (magnification x 100,000).



Figure 4.4i. SEM of sepiolite ground in an UCM at 14,000 rpm using a 0.5 mm sieve ring (magnification x 100,000).

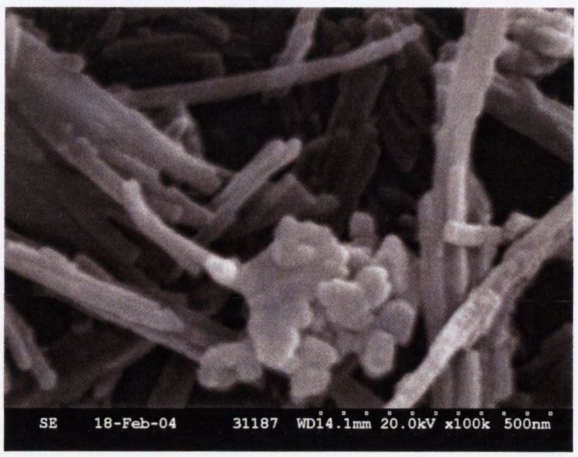


Figure 4.4j. SEM of sepiolite ground in an UCM at 18,000 rpm using a 0.5 mm sieve ring (magnification x 100,000).

Similar results were seen with samples milled in the ball mill, in that microagglomerates were flattened and bundles of fibers became displaced. The effect on the length of the fibers was not however as pronounced as in the case of the samples ground in the mortar and pestle (Figure 4.4h). Departure of the structure from that of the unmilled sample again became more evident after longer milling times.

After grinding in the ultracentrifugal mill, the aggregates appeared less fibrous and more rounded at low magnifications. The size and size range of the aggregates was reduced. The proportion of long fibers was again reduced and decreased further by milling at higher speeds (Figure 4.4i). The parallel association of fibers to form bundles was slightly disrupted in that a small proportion of bundles were partly separated into free fibers, which then oriented randomly relative to one another to form clumps (Figure 4.4j).

It was proposed from the persistence of the bundle-type level of organisation, despite the intensive mechanical trauma posed by the various grinding procedures, that they are not simply mechanical aggregates but are strongly bonded, most likely via the external silanol and silanol-derived groups which occur at ~5 Å intervals along the *c*-axis (Ahlrichs *et al.*, 1975).

4.4.4 The effects of thermal treatment on the microscopic appearance of sepiolite

The microscopic appearance of sepiolite samples heated to 400 °C and 550 °C was examined using SEM and results are presented in Figures 4.4k and 4.4l below. The results of TGA confirmed the loss of co-ordinated water had begun at 300 °C and was virtually complete by 600 °C. pXRD confirmed that this loss of co-ordinated water led to a change in the dimensions of the zeolithic channels, which has been attributed to folding of the structure, thus permitting magnesium ions to complete their co-ordination with oxygen atoms of neighbouring surfaces to form sepiolite anhydride (Figure 4.4m) (Weir *et al.*, 2001).



Figure 4.4k. SEM of sepiolite heated to 400 °C (magnification x 100,000).

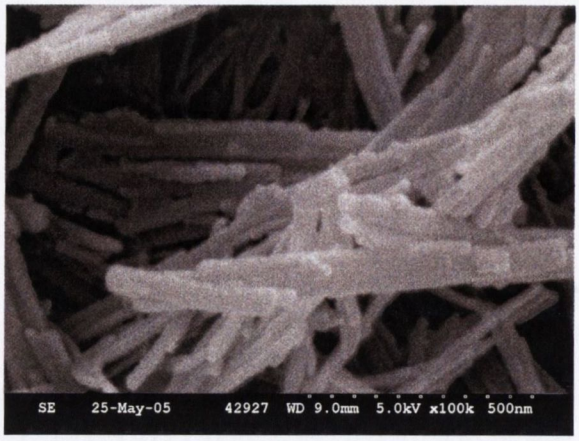


Figure 4.4l. SEM of sepiolite heated to 550 °C (magnification x 100,000).

From SEM, the fibrous appearance of sepiolite was retained despite heating to 400 °C, whereupon the first two water molecules co-ordinated to the octahedral sheet were lost (Ruiz *et al.*, 1996). Heating to 550 °C, facilitating the loss of the second pair of co-ordinated water molecules (Serna *et al.*, 1975a, 1975b; He *et al.*, 1996; Ruiz *et al.*, 1996), did not produce any notable change in the microscopic fibrous morphology (Figure 4.4l). The closer packing of the fibers following heating to 550 °C may be indicative of the commencement of the sintering process.

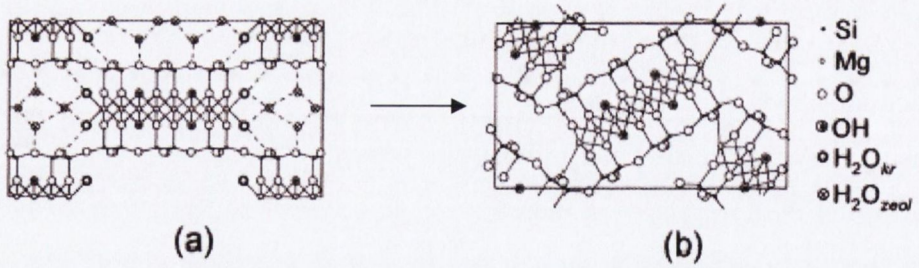


Figure 4.4m. Schematic representation of the folding of sepiolite, (a), upon heating to form sepiolite anhydride, (b). (Adapted from Weir *et al.*, 2001).

Formation of sepiolite anhydride would be expected to result primarily in a decrease in the height of the fibers (Figure 4.4m) given the inward collapse of the channels, however no change in average fiber dimensions was observed insofar as could be discerned from SEM.

4.5 TEXTURAL ANALYSIS

4.5.1 Introduction

The aim of this Section was to determine the textural characteristics of the sepiolite sample; namely the specific surface area and the pore size distribution. Minerals are typically highly porous as a result of their complex structure and the granular character of the solid phase (Jozefaciuk and Matyka-Sarzynska, 2006). The basic characteristic of such bodies is provided by a pore-size distribution function showing fractions of pores of different radii, while the overall quantity of pores is characterised by the pore volume and bulk density of the material (Rouquerol *et al.*,1994). The pore size distribution was determined using mercury intrusion porosimetry and the specific surface area was determined using N_2 adsorption. The surface area and adsorptive properties of sepiolite have been extensively studied but the studies devoted to discriminate the microporosity from the external surface area are scarce (Molina-Sabio *et al.*, 2001). Furthermore, even fewer relate specifically to sepiolite from the Vallecas-Vicálvaro region. The textural properties can be altered by thermal treatment (Kojdecki *et al.*, 2005). Therefore, the influence of heating on the textural properties was also investigated.

4.5.2 Specific surface area determination

4.5.2.1 Establishing ideal degassing conditions

Removal of all adsorbed gases, together with superficial and zeolithic water, is necessary for the accurate determination of the specific surface area. It is important to verify that the outgassing conditions chosen reproduce the original surface as closely as possible (USP, 2006). Special care must be taken in removing water from microporous zeolites as they can be particularly sensitive to a particular form of structural damage called steaming (Webb and Orr, 1997). A review of the literature on the determination of the specific surface area of sepiolite indicated that there was no one set of degassing conditions that was universally used and accepted. Most authors degassed under vacuum (Jiménez-López *et al.*, 1978; Molino-Sabio *et al.*, 2001; Radojević *et al.*, 2002a; Vučelić *et al.*, 2002; Hubbard *et al.*, 2003; Kojdecki *et al.*, 2005) at temperatures ranging from room temperature (Jiménez-López *et al.*, 1978; Hubbard *et al.*, 2003) to 150 °C (Kojdecki *et al.*, 2005). Degassing under N_2 flow was occasionally reported (Valentín *et al.*, 2006). Consequently, ideal degassing conditions were established from first principles. Galan (1996) reported that the

surface area of sepiolite is maximal after heating at 150 °C. Hence samples of sepiolite were degassed at 150 °C under N_2 flow for different lengths of time prior to surface area analysis in order to establish the optimum degassing time. Table 4.5a presents the specific surface areas, calculated from N_2 adsorption data using the BET equation, as a function of degassing time.

Table 4.5a. BET surface area of sepiolite as a function of degassing time (n = 2).

Degassing time (h)	BET surface area (m^2 /g)
0.5	186.195 ± 6.697
3	284.961 ± 15.804
5	282.115 ± 0.792
24	282.723 ± 5.193
48	293.414 ± 12.574

One-way ANOVA confirmed that the BET surface area of the sample following degassing for 0.5 h was significantly lower than the surface areas following degassing steps of 3 h or longer ($p < 0.05$). The surface areas obtained following degassing times of 3 h, 5 h, 24 h and 48 h were not significantly different from one another ($p > 0.05$). Furthermore, repeated analysis of the same sample degassed for 3 h (i.e. sample left in place and second adsorption cycle run) led to no further change in the surface area confirming that degassing was complete. Consequently the degassing time was set at 3 h for all further surface area analyses of this material.

4.5.2.2 Nitrogen adsorption isotherms

Nitrogen adsorption isotherms for untreated sepiolite and samples heated to 400 °C and 550 °C are presented in Figure 4.5a. The isotherms are similar in shape to those reported by other authors (Jiménez-López *et al.*, 1978; Molina-Sabio *et al.*, 2001; Radojević *et al.*, 2002a; Hubbard *et al.*, 2003; Güngör *et al.*, 2006; Jozefaciuk and Matyka-Sarzynska, 2006). Classification of the isotherms into one of the five types proposed by Brunauer *et al.* (1938) proves somewhat difficult in that they exhibit properties characteristic of both Type I (interpreted to contain significant microporosity) and Type II isotherms (interpreted as non-porous or containing meso- and/ or macropores) (Lowell and Shields,

1991; Webb and Orr, 1997). For the purposes of all further discussion, the IUPAC convention (1972) will be adopted, which characterises pores according to their diameter such that micro- (< 2 nm), meso- (2-50 nm) and macropores (> 50 nm) are identified.

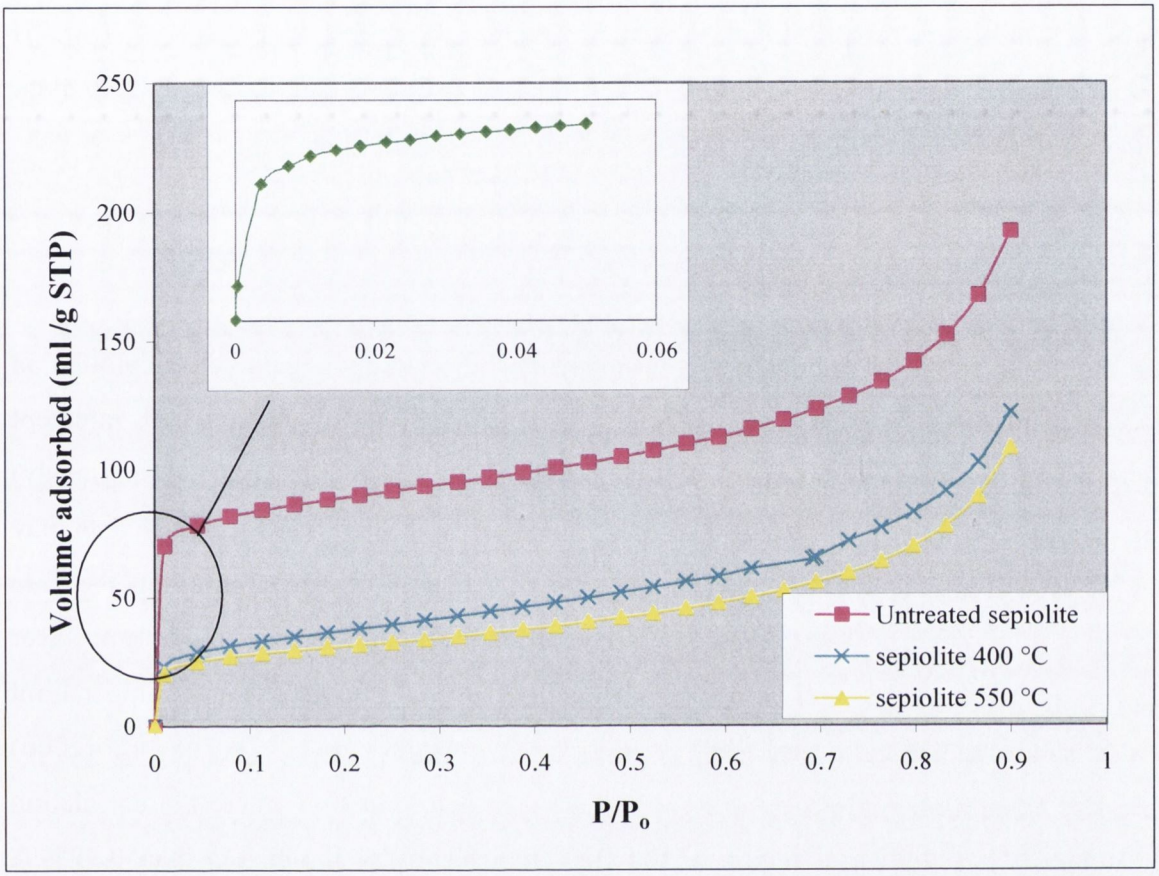


Figure 4.5a. Nitrogen adsorption isotherms for untreated sepiolite and samples heated to 400 °C and 550 °C for 1 h. Inset graph is a magnification of the low pressure region for nitrogen adsorption on untreated sepiolite at very low relative pressures.

The low pressure region of all three isotherms corresponds closely to a Type I isotherm. In a Type I isotherm, the curve rises almost vertically before levelling out to a long nearly horizontal section followed by a rise as saturation is approached and bulk condensation begins to occur (Webb and Orr, 1997). This curve is indicative of a material in which the exposed surface resides almost exclusively within the micropores, which once filled with adsorbate leaves little or no external surface for additional adsorption (Lowell and Shields, 1991). In the case of the adsorption isotherm for sepiolite, the rapid and extensive adsorption at low relative pressures is indicative of the presence of micropores (presumably the intrafibrous channels) (Sing, 2004). Condensation can occur within micropores at relative pressures less than 0.1 owing to their unusually high adsorption

potentials due to the overlapping potential from the walls of the micropores (Orr, 2001). The adsorption isotherms for sepiolite differ from classical Type I isotherms in that the volume adsorbed continues to rise consistently, albeit more gradually, in the relative pressure range 0.2 to 0.7 thereby indicating extensive surface area of non-microporous origin. This adsorption profile at relative pressures above 0.2 is typical of Type II isotherms. The rapid rise seen above ~ 0.7 relative pressure can be ascribed to bulk condensation.

4.5.2.3 BET surface area determination

Isotherm data for most solids (using nitrogen as the adsorptive gas), when plotted in accordance with the BET equation (Section 3.1.9.1), yield a straight line with intercept $1/V_mC$ and slope $(C-1)/V_mC$ (where V_m and C have the meanings as explained previously) between relative pressure values of 0.05 to 0.35 (Lowell and Shields, 1991). Such data may then be used in the surface area determinations. This range of pressures represents the state at which most of the high energy sites have been occupied and extensive multilayer adsorption has not yet begun (Lowell and Shields, 1991). In some cases the upper limit may be as low as 0.2 and occasionally even lower (Webb and Orr, 1997). The USP (2006) considers adsorption data acceptable for surface area determination where the correlation coefficient, r^2, of the linear region of the BET transform plot is not less than 0.995. A sample BET transform plot is presented in Appendix 4. For all samples, the BET transform plot was linear ($r^2 \geq 0.995$) in the relative pressure range of 0.078 to 0.2502 and so BET multipoint surface area was determined using the volumes of nitrogen adsorbed in this pressure range. The BET surface area was calculated using Equation 3.1b and the results are presented in Table 4.5b.

Table 4.5b. BET surface area of sepiolite samples (n = 2).

Sample	**BET surface area (m^2 / g)**
Untreated sepiolite	284.961 ± 15.804
Sepiolite heated to 400 °C	130.340 ± 1.104
Sepiolite heated to 550 °C	113.704 ± 2.540

The BET surface area value for untreated sepiolite was found to be very high (284.96 m^2 /g) and correlated well with those values reported by other authors where nitrogen was used as the sorbate molecule (range 243 – 334 m^2 /g; Jiménez-López *et al.*, 1978; Alvárez, 1984; Molina-Sabio *et al.*, 2001; Ruiz-Hitzky, 2001; Radojević *et al.*, 2002a; Vučelić *et al.*, 2002; Hubbard *et al.*, 2003; Güngör *et al.*, 2006). The relative contribution of the external surface area and the microporous surface area to the total surface area and the effect of heat treatment on both components are discussed in the next section.

4.5.2.4 Determination of the external surface area, micropore surface area and micropore volume

The t-plot method (Harkins-Jura, 1943; de Boer *et al.*, 1966) was used for the qualitative assessment of microporosity. Representative t-plots for each of the three samples are presented in Figure 4.5b. The t-plots of microporous materials exhibit a non-linear region at low t-values, and a linear region at higher t-values which corresponds to the relative pressures at which micropore filling has been completed. Extrapolation of the linear region to the adsorption axis will yield a positive intercept (Webb and Orr, 1997). All three t-plots exhibited the shape characteristic of a microporous material, although the deviation from linearity at low t-values was much more marked, and the magnitude of the positive intercept much higher, in the case of the untreated sample, indicative of more extensive microporosity. Using Equations 3.1e, 3.1f and 3.1g the external surface area, microporous surface area and volume were calculated. Results are presented in Table 4.5c.

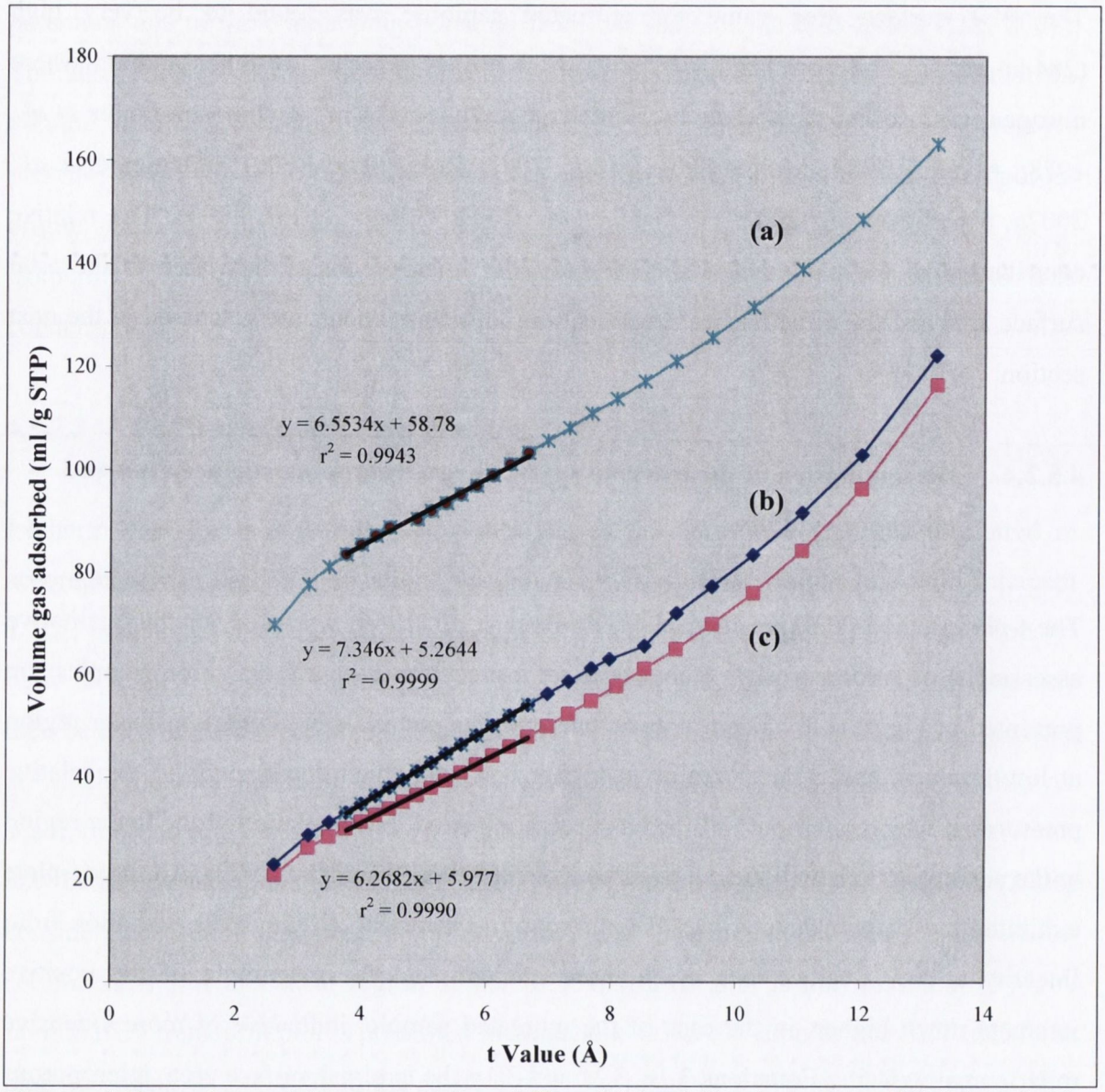


Figure 4.5b. t-plots of (a) untreated sepiolite, (b) sepiolite heated to 400 °C and (c) sepiolite heated to 550 °C. Linear regions (and associated regression equations) used in the determination of the external surface area are indicated by black lines.

In untreated sepiolite the micropore surface area (170.6 m^2 /g) was much larger than the external surface area (114.3 m^2 /g); similar trends and absolute values were reported by Alvarez (1984), Molina-Sabio *et al.* (2001) and Radojević *et al.* (2002) for sepiolite from Vallecas (Spain), Yunclillos (Spain) and Kosovo (Yugoslavia) respectively. A huge reduction in the surface area was noted following heat treatment (Table 4.5b), the change being attributable solely to the loss of the micropore structure as the external surface area did not change significantly on heating to either 400 °C or 550 °C ($p = 0.237$). These results correlated well with the findings of the authors (Alvarez, 1984; Ruiz *et al.*, 1996) and with images from SEM which did not reveal any changes in fiber dimensions

following thermal treatment at 400 ºC and 550 ºC. From TGA, these changes can be attributed to the loss of co-ordinated water. Serna *et al.* (1975a) and He *et al.* (1996) noted that further heating above 530 °C to remove the remainder of the crystal water (thereby producing sepiolite anhydride) caused little additional structural change. Textural results from N_2 adsorption and results from pXRD would concur with this.

Table 4.5c. External surface area, micropore surface area and micropore volume of sepiolite samples determined by applying the t-plot method to nitrogen adsorption data (n = 2).

Sample	BET surface area (m^2 /g)	External surface area (m^2 /g)	Micropore surface area (m^2 /g)	Micropore volume (mL /g)
Untreated sepiolite	284.961±15.804	114.329±15.077	170.632±0.726	0.085±0.001
Sepiolite heated to 400 °C	130.340 ± 1.104	111.896±0.907	18.444±0.197	0.009±0.001
Sepiolite heated to 550 °C	113.704 ± 2.540	96.029±4.094	17.675±1.554	0.008±0.001

In conclusion, ~60% of the extensive surface area of sepiolite resides within micropores. Heating to 400 °C caused the loss of the less tightly bound component of the co-ordination water, thereby provoking folding of the structure, the compression of the microporous channels and a consequent loss of surface area. Further heating to 550 °C drove off the more tightly bound co-ordination water, completing transformation to sepiolite anhydride (Figure 4.4m) but caused no further loss of surface area.

4.5.3 Helium Pycnometry and Mercury Intrusion Porosimetry (MIP)

4.5.3.1 Introduction

Helium pycnometry was used to measure the skeletal density, a property characteristic of the mineralogical composition of clay minerals (Salter, 2003; Byrne, 2004). Hence, if the skeletal densities of the different samples varied considerably then it could be deduced that the samples contained unrelated minerals and can therefore further aid identification of different clays when used in conjunction with other techniques.

Mercury porosimetry is a popular technique used in the characterisation of porous materials which is often used alongside nitrogen adsorption (Orr, 2001; Denoyel *et al.*, 2004). The zeolithic channels running parallel to the fiber axis are reported to be of approximate dimensions 3.6 x 10.6 Å (Brauner and Preisinger, 1956), which is below the lower limit of mercury porosimetry (Lowell and Shields, 1991; Webb and Orr, 1997). Consequently MIP was used to determine the mesopore-macropore size distribution of untreated sepiolite. An Autopore IV 9500 mercury intrusion porosimeter was used, which allowed pores of diameter $\geq$ 7.2 nm to be measured. The presence of macro- and mesopores play a significant role in the mass transfer to the micropores and hence may enhance or restrict a given application (Balci, 1996).

4.5.3.2 Results

The skeletal density of untreated sepiolite was found to be 2.424 ± 0.016 g /cm^3 and was in agreement with results quoted by Balci (1996; 2.429 g /cm^3). Cumulative and incremental mercury intrusion curves for the untreated sepiolite samples obtained from MIP are presented in Figure 4.5c below. A summary of the intrusion data is presented in Table 4.5d.

Table 4.5d. Summary of data derived from MIP of untreated sepiolite.

Intrusion Data Summary	
Total intrusion volume (mL /g)	4.7813
Total pore area (m^2 /g)	91.384
Median pore diameter (Volume) (μm)	9.0063
Median pore diameter (Area) (μm)	0.0186

In principle it is possible to evaluate the macropore and mesopore size distribution from the incremental volumes of mercury which enter the structure as the applied pressure is progressively increased (Webb and Orr, 1997; Sing, 2004). Two inflection points can be identified on the cumulative intrusion curve (Figure 4.5c), corresponding to three rates of pore filling and hence a trimodal pore size distribution. The trimodal pore distribution is presumably attributable to the filling of spaces between fibers within bundles ('intrabundle' spaces), the porous networks within microagglomerates caused by the haphazard arrangement of bundles ('interbundle' spaces) and between adjacent microagglomerates ('intermicroagglomerate' spaces). The large total volume of Hg

intruded (4.7813 mL /g) was indicative of a highly porous structure. Pores in the mesopore size range amenable to scrutiny using MIP (i.e. 7.2 nm – 50 nm) accounted for less than 0.346 mL /g. The median pore diameter determined from a plot of the cumulative volume intruded against pore diameter was 9.0063 μm. Consideration of these results together with images from SEM, revealed that the porous volume studied by MIP was largely accounted for by interstitial void spaces formed as a consequence of inefficient fiber packing within and between microagglomerates rather than pores within the fiber structure.

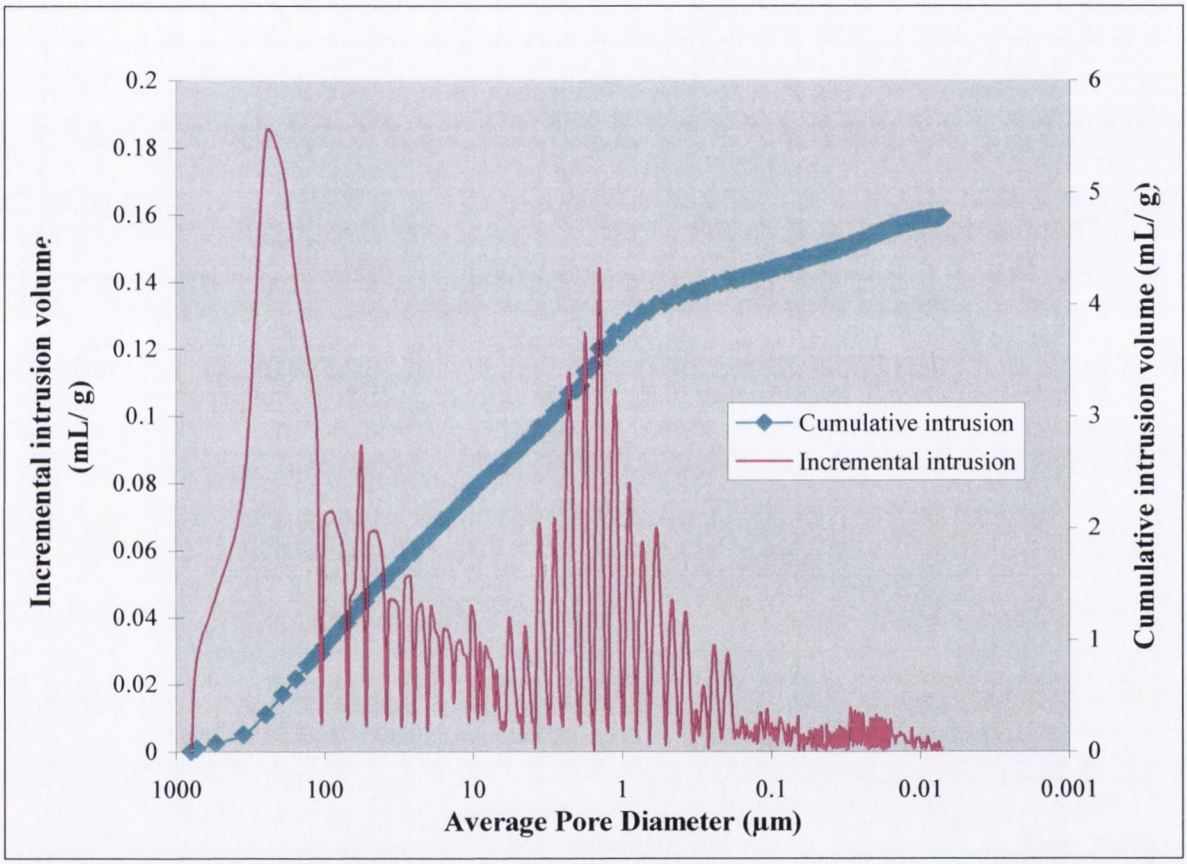


Figure 4.5c. Cumulative and incremental mercury intrusion versus mean pore diameter for untreated sepiolite.

The low median pore diameter by area (0.0186 μm) reflected the fact that the total pore area determined from MIP (91.384 m^2 /g) was largely accounted for by pores of diameter less than 0.1 μm (Figure 4.5d). As these pores are larger than the zeolithic channels, but account for the majority of the 'pore' surface area it was postulated that they may be attributable to lattice imperfections (Figure 4.5e, point X) or to void volumes enclosed by adjacent fibers within a bundle (Figure 4.4d and Figure 4.5e, point Y).

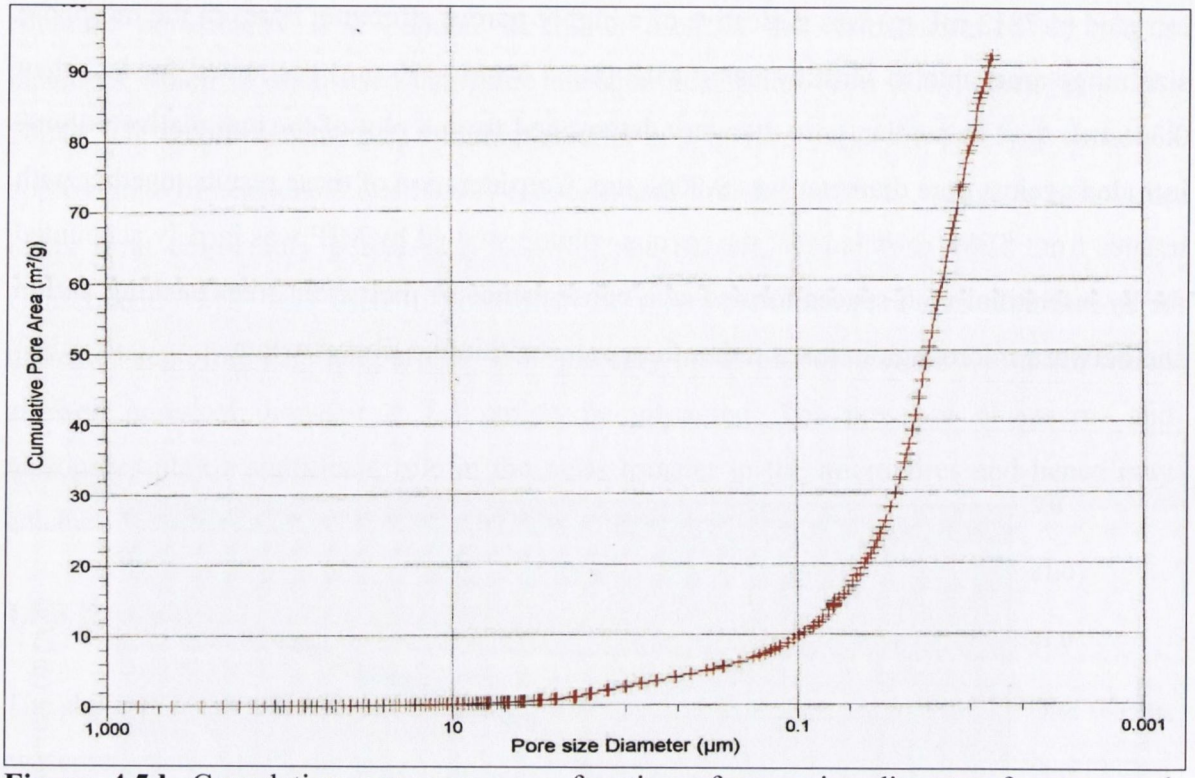


Figure 4.5d. Cumulative pore area as a function of pore size diameter for untreated sepiolite.

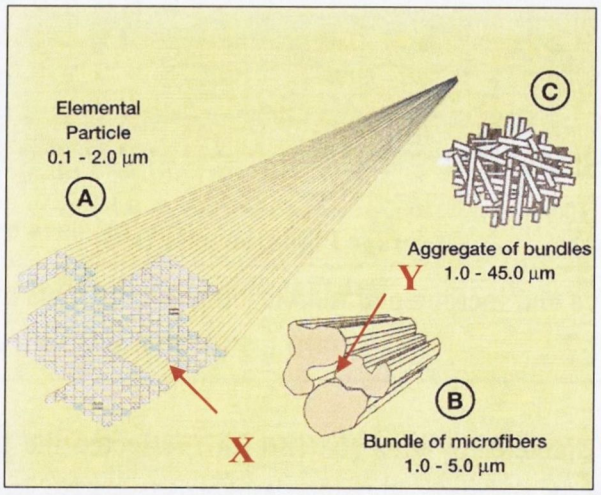


Figure 4.5e. Schematic of sepiolite morphology and levels of structural organisation. (The dimensions of the particles are not to scale). Adapted from Tolsa, 1999.

4.5.4 Correlation of surface area results from N_2 adsorption and MIP

Given that all pores sized by MIP are not true pores in that they have their origin in the void volume between adjacent fibers/ bundles/ microagglomerates rather than in the intrinsic elemental structure of the fibers, the surface area of all such 'pores' can be termed the 'external surface area' consistent with the term used for the determination of the same area by N_2 adsorption. There is a reasonable level of agreement between the two values for external surface area determined by N_2 adsorption and MIP (91.384 m^2 /g and 114.329 ± 15.077 m^2 /g, respectively) bearing in mind that comparable results are often not obtained in the overlapping or common range of both techniques (Orr, 2001). The slightly lower value from MIP may be accounted for by a consideration of the lower limit of detection of the instrumentation used in this technique. The surface area of pores of diameter less than 7.2 nm is not included in the value calculated by MIP. Conversely the value from nitrogen adsorption encompasses all surface area of non-microporous origin. Hence the difference in the two values may be due to the surface area of pores of diameter greater than 2 nm but less than 7.2 nm.

4.6 CONCLUSIONS

The use of a combination of complementary analytical techniques (pXRD, FT-IR, EDXA, SEM, TGA and helium pycnometry) conclusively identified the principal component of Pangel®-S9 to be sepiolite. The sample was of high mineralogical purity and free from swelling clays. pXRD suggested the presence of small amounts of dolomite, which given that it can be a precursor in sepiolite genesis, would not be unexpected. pXRD also indicated that the sample was of intermediate crystallinity, a finding consistent with the relatively short fiber lengths (relative to samples of high crystallinity) exposed using SEM. EDXA indicated that the principal elements were silicon, magnesium and oxygen, consistent with chemical formula of sepiolite. Smaller but appreciable amounts of calcium, aluminium, potassium and iron were also present, most likely as replacements for Mg in the octahedral sheet and also possibly for Si in the tetrahedral sheet. ICP-MS indicated the presence of an extensive array of metals at low ppm levels. Levels are lower than those reported by other authors for sepiolite mined from the same region and may reflect a reasonable level of success on the part of the Tolsa patented purification process or simply a site-to-site variation. These elements are most likely to be adsorbed rather than constitutive elements. Levels of As exceeded those permitted by the BP (2007) and PhEur

(2007) but complied with those imposed by the USP (2006) for Magnesium Trisilicate. Compliance with the heavy metals limit specified by the pharmacopoeias could not be commented upon in any meaningful manner owing to the ambiguity associated with the term "heavy metal". Levels of all trace elements determined, apart from Li, were lower in Pangel®-S9 than in Pharmasorb® regular, a palygorskite preparation currently employed in a pharmaceutical context.

TGA indicated that weight loss occurred in four discrete steps upon heating, which could be attributed to the loss of adsorbed water, zeolithic water, co-ordination water and dehydroxylation (Frost and Ding, 2003). Observed weight losses correlated well with the theoretical weight losses predicted using the chemical formula of sepiolite. SEM confirmed the fibrous morphology of sepiolite, the approximate dimensions of the fibers being 40 nm wide, 10-20 nm high and 250-1500 nm long. These elemental particles associated in a parallel manner along their longest axis to form bundles, which in turn were arranged in a haphazard manner to produce three-dimensional microagglomerate structures of up to 42 μm in diameter. The carcinogenic potential of Pangel®-S9 following inhalation was predicted to be low, in accordance with the IARC classification criteria. The microscopic appearance following grinding/ milling processes was altered, the manner and extent to which depended on the milling equipment and duration of milling. Grinding in a mortar and pestle and milling in a ball mill produced similar structural changes, namely the compaction of microagglomerates, the displacement of fibers from the microagglomerate structure and shortening of the fibers along their *c*-axis. Changes in the fiber dimensions along the *a*- and *b*-axes were not evident, indicating that the *c*-axis was the most vulnerable. Milling in an ultracentrifugal mill did not cause flattening of the microagglomerates, although changes at the bundle- and fiber-level were similar to those noted for the other two milling procedures.

The BET surface area of sepiolite determined using N_2 adsorption data was extensive (285 m^2 /g), with over 60% accounted for by the internal surface area of the zeolithic channels. Heating to 400 and 550 °C, despite not producing any discernible change in the microscopic appearance as determined by SEM, caused a dramatic reduction in the surface area which was largely attributable to the loss of microporosity as the sepiolite structure was forced to fold in order that magnesium ions, having lost their co-ordinated water, could complete their co-ordination via association with oxygen atoms of neighbouring surfaces. MIP indicated considerable porosity of trimodal nature in the meso- and

macropore range, which was ascribed to interstitial void space between fibers, between bundles and between microagglomerates rather than 'true' pores. Consequently, the total pore area derived from MIP could be equated to the external surface determined from gas adsorption. Reasonable agreement between the two values was evident, bearing in mind the minimum pore size amenable to determination using MIP.

Chapter 5

PREPARATION AND EVALUATION OF MODIFIED GRADES OF SEPIOLITE AS MULTIPURPOSE EXCIPIENTS IN TABLETTING BY DIRECT COMPRESSION

5.1 INTRODUCTION

Tablets comprise the largest group of delivery systems for all prescribed and over-the-counter drugs (Marshall, 1999). The European Pharmacopoeia (2007) defines tablets as 'solid preparations each containing a solid dose of one or more active ingredients and obtained by compressing uniform volumes of particles. They are intended for oral administration. Some are swallowed whole, some after being chewed, some are dissolved or dispersed in water before being administered and some are retained in the mouth, where the active ingredient is 'liberated'. The most popular of these is the immediate release tablet, intended to be swallowed whole and release the medicament rapidly in the stomach'. This Chapter focuses on those tablets to be swallowed whole to facilitate systemic drug delivery.

As outlined in Chapter 1, tablets are manufactured primarily by either direct compression or granulation-compression (Nachaegari and Bansal, 2004). The simplest tablet production method is that of direct compression, where the active ingredient is mixed with the required excipients (typically a disintegrant and lubricant) in the required quantities prior to compression. Whilst some drugs (e.g. ascorbic acid, thiamine hydrochloride) are available in grades suitable for direct compression and hence need only to be mixed with a disintegrant and lubricant prior to tabletting, the vast majority lack the necessary flowability and compactibility. This problem was addressed by the advent of direct compression bases (DCBs), which are chemically and pharmacologically inert, and possess the ideal properties required for the preparation of compact tablets. These bases can be used to disguise and overcome the poor tablettability of many drugs.

The original DCBs were composed of one material, which may or may not have undergone some form of physical modification to improve tablettability. Current advancements in the tabletting field have involved the production of DCBs by co-processing of two or more excipients, the objective of which is to provide a synergy of functionality improvements as well as masking the undesirable properties of individual excipients (Reimerdes, 1993). Co-processed excipients are prepared by incorporating one excipient into the particle structure of another using processes such as co-drying. Due to this interaction at a subparticle level, co-processing leads to the formation of excipient granulates with superior properties compared with corresponding physical mixtures of the components.

In the case of a drug which lacks suitable tabletting characteristics, an alternative to tabletting by direct compression, although much more labour intensive, is wet granulation. Wet granulation of the drug together with a suitable filler will permit an increase in bulk density, improved flowability (both of which are important for reproducible filling of the die), reduced risk of powder segregation and improved compactibility (Alderborn, 2002).

The objectives of this Chapter are two-fold; firstly to examine whether it is possible to prepare a DCB through physical processing of sepiolite and secondly to determine whether it is possible to prepare a co-processed excipient with merit using sepiolite and Kollidon® VA 64. The potential of sepiolite to act as a filler-binder in a wet granulation tabletting process is investigated in Chapter 6.

5.2 PRELIMINARY ASSESSMENT OF THE COMPRESSION PROPERTIES OF SEPIOLITE

The aim of preliminary studies was to establish the compression properties of sepiolite, as is, and therefore guide further work. When a compressive force is first applied to the material in the die of a tablet press, there will be some degree of repacking of the particles leading to a higher bulk density. At a certain load, the packing characteristics of the particles or a high interparticulate friction prevent any further interparticulate movement. Thereafter materials tend to deform plastically or by fragmentation with some materials exhibiting elastic recoil following removal of the compression force (Bolhuis and Chowhan, 1996). Ideally material to be tabletted should be predominantly plastic, i.e. capable of permanent deformation, but should also exhibit a degree of brittleness

(fragmentation). Accordingly if a drug has a high dose and behaves plastically, the excipients should fragment. If the drug is brittle or elastic, then other excipients should be plastic (Wells, 1988). Knowledge of the compression behaviour of sepiolite is therefore required.

Interpretation of the results of the preliminary compression study necessitates an appreciation of the role of magnesium stearate in tabletting. Magnesium stearate is a lubricant, the primary function of which is to reduce friction between granules or powders and the die wall during the compression and ejection cycles (Kikuta and Kitamoura, 1994). Studies by Otsuka *et al.* (2001) demonstrated that mixing of magnesium stearate with microcrystalline cellulose succeeded in improving powder flowability and reducing die friction. However, Bolhuis *et al.* (1975) reported that the degree of mixing of particulate solids with magnesium stearate can greatly reduce the strength of the resulting tablets. This phenomenon is a result of the adhesion of magnesium stearate to the substrate surface, thereby forming a hydrophobic lubricant film which precludes strong bonding. This somewhat disadvantageous property of magnesium stearate can be exploited to differentiate between those materials that undergo compression via fragmentation and those that deform plastically. In the case of a material that is primarily fragmenting, new lubricant-free surfaces will be generated during compression and consequently neither mixing time nor dwell time should affect tablet strength (Wells, 1998). In the case of a material which deforms plastically, an increase in the duration of mixing will increase the proportion of magnesium stearate-coated surfaces and hence have a deleterious effect on tablet strength. Furthermore, as plastic deformation is time dependent, an increase in the dwell time (i.e. duration of applied compressive force) will significantly increase tablet strength in the case of plastically deforming materials while having a negligible effect on fragmenting materials (Wells, 1998). As the lubricating ability of magnesium stearate is directly affected by its moisture content, which has been in turn related to the ability of this compound to form species of different hydration (Sharpe *et al.*, 1997); it should be noted that the dihydrate form of magnesium stearate was used in all work conducted for this thesis. It had been reported that the thermal behaviour of the anhydrate, dihydrate and trihydrate forms is markedly different (Sharpe *et al.*, 1997). The DSC of the dihydrate form is characterised by two thermal events; the first being an endotherm with a maximum of ~92.3°C with an associated weight loss of ~5.9% corresponding to a dehydration step and the second an endotherm at ~115°C, which is not accompanied by any measurable

weight loss, corresponding to the melting endotherm of the sample (Sharpe *et al.*, 1997). Consequently, the hydration state was verified using DSC and TGA after Sharpe *et al.* (1997) (Appendix 5).

Results of the compression study detailed in Section 3.5.1 are presented in Table 5.2a. Following from the discussion above, the crushing strengths of compacts A, B, C and D would be similar in the case of a material which is predominantly fragmenting. Conversely, for a plastically deforming material, tablet crushing strength would be expected to decrease with increasing mixing time, i.e. D > A > C and increase with an increase in dwell time, i.e. B > A (Wells, 1998).

Table 5.2a. Tablet hardness as a function of mixing time and compression dwell time.

Sample	Mixing time (min)	Compression dwell time (s)	Compact hardness (N)
A	5	1	88.00 ± 4.52
B	5	30	114.00 ± 6.48
C	30	1	79.33 ± 6.59
D	2.5	1	99.00 ± 4.24

Statistical analysis of the tablet crushing strength data indicated that crushing strength was dependent on both mixing time (D > A) and compression dwell time (B > A). Therefore it was concluded that sepiolite undergoes plastic deformation on compression and so is particularly suited to the tabletting of fragmenting and elastic drugs, of which paracetamol is a classic example.

Although tablet strength was quite high, the following problems were encountered with sepiolite during the preliminary study; firstly, the very low bulk density required a very large die cavity to accommodate the compression volume and secondly, tablets had a dusty appearance and exhibited high friability. Hence it was not suitable for use as a direct compression base in its untreated state. Two strategies were used to manipulate sepiolite and hence improve its tabletting properties; namely spray drying, the results of which are discussed imminently, and wet granulation, which is addressed in Chapter 6.

5.3 DIRECT COMPRESSION – REQUIREMENTS FOR EXCIPIENTS AND THE SEARCH FOR NEW EXCIPIENTS

5.3.1 Introduction

The development of new tabletting excipients to-date has been market-driven rather than marketing-driven and has not seen much activity as shown by the fact that, for the past many years, not a single new chemical excipient has been introduced into the market (Nachaegari and Bansal, 2004). Any advancements seen relate to minor modifications (e.g. changes in moisture content, particle size distribution) of DCBs already in existence. However functionality can be improved only to a certain extent because of the limited range of possible modifications. The principal reason for this lack of new chemical excipients is the relatively high cost involved in excipient discovery and development.

The most important requirements for DCBs have been addressed in Chapter 1. There is growing pressure on formulators to search for new excipients to achieve these desired set of functionalities as no single excipient currently available fulfils all of the optimum requirements.

Other factors driving the search for new excipients include the lack of excipients that address the needs of specific patients such as those with diabetes mellitus and lactose and sorbitol sensitivity, the growing popularity of the direct compression process and a demand for an ideal DCB which could substitute two or more of the excipients (Nachaegari and Bansal, 2004). The ability of one excipient to simultaneously perform the functions of two or more excipients is obviously highly desirable not only in terms of simplifying the manufacturing process but also in terms of reducing the potential for chemical incompatibilities.

Excipients with improved functionality can be prepared by developing new grades of existing materials, new chemical excipients and new combinations of existing materials (Moreton, 1996). The latter two strategies are addressed in this Chapter. First of all, sepiolite was examined as a potential DCB, bearing in mind the requirements cited by Bolhuis and Chowhan (1996) above. Secondly, sepiolite was co-processed with a commonly used tablet binder, Kollidon® VA 64, to examine whether the resultant product has any advantages over the individual components and a simple physical mixture of the

two components in the same ratio. The tabletting performance of the novel excipients was compared to those of a number of commercially available DCBs; namely Avicel® PH101, and a combination (9:1) of Ludipress®/ Kollidon® VA 64. Dibasic calcium phosphate dihydrate (Emcompress®) was initially included but discounted following the results of preliminary studies which exposed problems with capping post-ejection from the tablet press.

5.3.2 Preparation of modified sepiolite grades for use as DCBs

5.3.2.1 Introduction

In an analogous manner to most drugs, few excipients can be compressed directly into tablets without prior physical modification. Spray drying has been successfully used to produce filler-binders with enhanced physico-mechanical properties designed for direct compression into tablets (Bolhuis and Chowhan, 1996). A key characteristic of the process is that atomization produces spherical droplets which under ideal conditions dry to form spherical particles, producing a free flowing powder with a well-defined size distribution, hence its widespread use in the food and pharmaceutical industry (Oakley, 1997). Changes in solid-state characteristics of crystalline materials (e.g. the disordering of the crystal lattice of lactose) can result due to the rapid cooling and consequent imperfect recrystallisation (Corrigan, 1995) leading to increases in compressibility and compactibility, which are beneficial for direct compression (van der Voort Maarschalk and Bolhuis, 1989). Interestingly, spray drying has also found application in the ceramics industry where it is used to prepare the clay prior to pressing into tiles (Helsing, 1969; Oakley, 1997). Consequently it was expected that, in an analogous fashion, spray drying could be used prepare a grade of sepiolite which could be easily compressed into tablets.

5.3.2.2 Rationale for incorporation of Kollidon® VA 64 in a co-spray dried product

Co-processing is another way that new excipients are coming to the market without undergoing the rigorous safety testing required for a completely new chemical entity (Reimerdes and Aufmuth, 1992). It can be defined as combining two or more established excipients by an appropriate process (Reimerdes, 1993). As described in Chapter 1, the co-processed multi-component based excipients are developed to achieve better powder

characteristics and tabletting properties than a single substance or the physical mixture. One such co-processed multifunctional excipient is Ludipress® (Limwong *et al.*, 2004). Ludipress® consists of 93% α-lactose monohydrate, 3.5% polyvinylpyrrolidone as a binder (Kollidon® 30) and 3.5% crospovidone as a disintegrant (Kollidon® CL). The formulation of Ludipress® was used as a template for the development of the co-spray dried sepiolite product. From preliminary studies, it was clear that sepiolite compacts disintegrate rapidly in water; consequently the inclusion of a disintegrant in a co-processed excipient based on sepiolite was deemed unnecessary. Kollidon® VA 64 was selected as a binder for the co-processed excipient in preference to Kollidon® 30 for two reasons: firstly, it is much less hygroscopic and secondly, its plasticity is greater and so it produces tablets that are less brittle and less susceptible to capping following compression (Bühler, 2003).

From preliminary tabletting studies using paracetamol as the model drug, it was evident that capping was a problem when Ludipress® was used as the DCB. On consultation with BASF Pharma, the inclusion of 10% w/w Kollidon® VA 64 with Ludipress® was recommended to achieve the desired level of plasticity to preclude capping. Consequently the final formulation for the novel co-processed excipient was 10% w/w Kollidon® VA 64 and 90% w/w sepiolite.

5.3.2.3 Establishing optimum spray drying conditions for preparation of novel sepiolite grades

Establishing ideal spray drying conditions can be an onerous task owing to the many factors which impact on the yield and nature of the final product. The primary conditions which may be controlled directly by the operator are: (1) inlet temperature; (2) flow rate of liquid feed; (3) spray air flow rate and (4) aspirator speed.

The outlet temperature and relative humidity of the outlet air are also important, but can only be controlled indirectly through the adjustment of the primary conditions. These factors will have an important influence on final powder properties such as particle-size distribution, moisture content, density and particle strength, and also on product yield.

Initially aqueous suspensions of sepiolite (2% w/v) were spray dried at an inlet temperature of 175 °C, feed rate of 8%, air flow rate of 600 L /min and outlet temperature of 113 °C.

The resulting material demonstrated good compressibility and compactibility as evidenced by high tablet crushing strengths (in excess of 100 N following compression at 2000 kg). However, although the process demonstrated a potential to dramatically improve the tabletting characteristics of sepiolite, the yield was exceptionally low, with typically less than 1 g of product (corresponding to < 10% yield) resulting from a spray drying run of 5 h. Improvement of the yield was therefore essential.

The major loss of potential product was due to high levels of product deposition on the drying chamber walls. Such a problem could be overcome by the use of a spray dryer with a wider drying chamber, to ensure that the droplets are dried while still airborne. This problem of wall sticking is frequently encountered in the spray drying of ceramic slurries (Helsing, 1969; Lukasiewicz, 1989). Apart from the obvious implications for yield, long dryer down times result due to the difficulty associated with chamber cleaning. Masters (1991) reported that wall deposits may be classified as follows: (1) droplets that hit the chamber wall before a dry surface crust has been formed, resulting in the formation of a monolithic mass which hardens upon continued exposure to high temperatures, (2) dry granules which have a sticky surface at the drying temperatures, and (3) surface dusting of the chamber walls by dry granules. Those seen in the spray drying of sepiolite were a combination of Type 1 and Type 2 deposits. Type 1 deposits are caused by a large droplet size, improper airflow conditions or low solids-content slurry (Lukasiewicz, 1989). To address the problem of excessive wall deposits, the inlet temperature was increased to 180 °C and the suspension feed rate dropped to 5% to allow for more rapid and extensive drying of the droplets. These strategies did improve the yield slightly but not sufficiently so as to make the production of the required quantity (100 g) for tabletting studies feasible. Further increases in the inlet temperature were not attempted owing to safety concerns, particularly given the long duration of the spray drying run. Although an increase in the suspension concentration would reduce the amount of water to be evaporated, the viscosity of the suspension and the risk of nozzle blockage would be increased. Consequently suspension concentration was kept constant at 2% w/v.

The aqueous suspending medium was then replaced by an ethanol/ water mix (60:40 v/v). It was postulated that the higher volatility of this mixed solvent would result in faster drying times, thereby reducing the propensity to adhere to the chamber walls and increasing product yield. Continuous shear rheology, performed as described in Section

3.7.4, indicated the rheological behaviour of both the aqueous and hydroethanolic dispersions was best described by the Herschel-Bulkley model. Parameters derived from the rheological modelling indicated that the hydroethanolic dispersion had a much lower yield value and apparent viscosity than the aqueous suspension (Table 5.3a). This was advantageous in terms of consistent feed delivery to the nozzle. Furthermore, it has been noted that the size of the droplets formed during atomization is proportional to the feed viscosity (Lukasiewicz, 1989). A reduction in droplet size would also reduce the required drying time and reduce the extent of wall deposits. The hydroethanolic suspension was spray dried at the following conditions: inlet temperature of 95 °C, feed rate of 10%, air flow rate of 600 L /min and outlet temperature of 80 °C. The extent of product deposition on the chamber walls was markedly reduced and permitted an increase in the feed rate to 10%. Hence the use of the hydroethanolic feed improved yields substantially by two methods: firstly by reducing the product lost to the chamber walls and secondly by facilitating an increase in the quantity of material dried per unit time.

Table 5.3a. Rheological parameters of 2% w/v sepiolite suspensions prepared in different vehicles.

Ethanol: water ratio	Herschel-Bulkey yield value (Pa)	Apparent viscosity at 100 s^{-1} (Pa.s)
0:100	3.257 ± 0.290	0.0866 ± 0.0039
60:40	1.718 ± 0.249	0.0630 ± 0.0011

Identical spray drying conditions were used for the preparation of the co-spray dried product composed of 90% w/w sepiolite and 10% w/w Kollidon® VA 64. For the remainder of this thesis, this co-spray dried product is referred to as SepKoll.

5.4 CHARACTERISATION OF THE NOVEL SPRAY DRIED (SD) EXCIPIENTS

5.4.1 Introduction

The aim of this section was to characterize the novel spray dried grades of sepiolite. Comprehensive flowability studies and particle size analysis were conducted, given the importance of adequate flowability in the direct compression process. SEM, pXRD and

FTIR were used to ascertain the morphology, extent of crystallinity and any potential binding interaction between sepiolite and Kollidon® VA 64. These properties were compared with those of untreated sepiolite, Kollidon® VA 64 and a physical mixture of spray dried sepiolite and Kollidon® VA 64 in the same ratio as the SepKoll product. Such comparisons should facilitate determination of any effects that the spray drying process may have. KF was used to determine moisture content while DSC and TGA were used to determine the nature of any interaction between sepiolite and Kollidon® VA 64 when co-spray dried as opposed to simply blended together.

5.4.2 Assessment of powder properties relevant to tabletting

5.4.2.1 Flowability

Augsburger and Shangraw (1966) may have been the first to address the need to determine powder flow for pharmaceutical formulations. Good flow is essential for ease of pharmaceutical processing, as it will affect ease of mixing and transfer from intermediary containers to hoppers and die cavities. Reproducible filling of die cavities is essential to ensure uniformity of tablet weight and hence drug content (Alderborn, 2002). Consequently, the flow properties of the DCBs of interest were quantified using a number of flowability indices, namely the minimum orifice diameter, Carr's compressibility index and Hausner's ratio. The initial characterisation of the flow properties of solids was conducted by Carr (1965) and Jenike (1954). Carr (1965) evaluated interparticulate cohesive properties with angle of repose measurements and studied the effects of packing geometry of solids with bulk and tap density measurements. He found that the density of a powder depends on particle packing and that density changes as the powder consolidates. The degree of consolidation is unique to the powder and ratio of these densities is related to interparticulate friction. This ratio, percent compressibility, was used as an index of flow.

The flowability data for the DCBs are presented in Table 5.4a below. Density measurements performed on the bases indicated that Ludipress® had the highest bulk and tapped density, followed by Avicel® PH101, Kollidon® VA 64, SepKoll and finally by spray dried sepiolite and the physical mixture of spray dried sepiolite and Kollidon® VA 64 (Physmix).

Table 5.4a. Flow parameters and moisture contents of the different DCBs.

DCB	Bulk density (g/cm^3)	Tapped density (g/cm^3)	Angle of repose (°)	Carr's index (-)	Hausner ratio (-)	Critical orifice diameter (mm)	Moisture content (% w/w)	Taylor's Composite Index (-)
Sepiolite	0.12±0.00	0.13±0.01	62.4±0.7	9.21±0.94	1.10±0.01	>36	12.28±0.10	36.70
SD sepiolite	0.18±0.01	0.20±0.01	43.5±0.5	9.69±0.63	1.11±0.01	26	10.63±0.22	63.58
SepKoll	0.20±0.00	0.22±0.00	37.9±0.8	9.41±1.63	1.10±0.02	24	9.77±0.22	66.21
Physmix sepiolite and Kollidon® VA 64	0.17±0.00	0.20±0.00	36.7±0.8	14.13±1.00	1.16±0.01	26	9.50±0.28	63.89
Avicel® PH101	0.36±0.00	0.39±0.00	43.6±1.4	13.17±1.76	1.07±0.01	> 36	4.24±0.39	46.88
Ludipress®	0.55±0.01	0.59±0.00	31.7±0.6	7.12±0.50	1.08±0.01	4	5.17±0.24	91.13
Kollidon® VA 64	0.26±0.00	0.31±0.00	45.8±1.5	14.13±2.05	1.17±0.03	20	2.76±0.09	62.30
Ludipress®/Kollidon® VA 64 (9:1)	0.47±0.01	0.53±0.02	43.6±1.4	11.65±1.11	1.13±0.01	4	4.93±0.15	88.10

One-way ANOVA of the bulk and tapped densities of sepiolite before and after spray drying indicated that the spray drying process increased both the bulk density and tapped density significantly ($p < 0.05$). Images from SEM (Figures 5.4a - 5.4d below) confirmed that spray drying increased the number of aggregates present and the sphericity of such aggregates. Spheres have the smallest surface area to volume ratio and consequently, the adoption of a spherical habit as opposed to a less regular shape will reduce the surface area for interactions between aggregates, reduce cohesive forces and thereby improve flowability. Tsai *et al.* (1998) reported an improvement in the flowability of MCC following co-drying with β-cyclodextrin and attributed it to the increased roundness of the particles formed. The spray dried sepiolite particles were well defined, with fibers tending to follow the contours of the aggregate rather than protrude from the surface. The reduced number of these loose fibrous terminations will lead to a reduced risk of mechanical interlocking of the fibers which would tend to impede flow by producing powder arches.

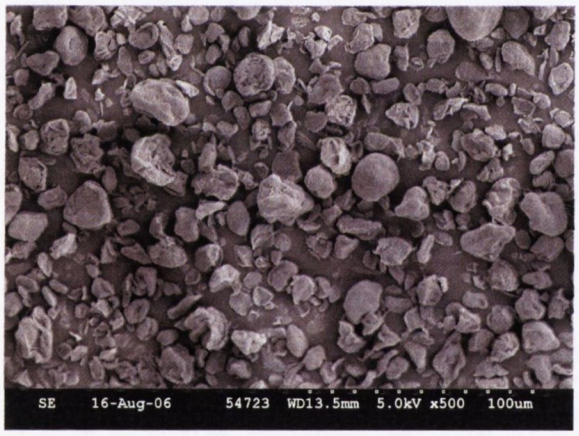


Figure 5.4a. SEM showing SD sepiolite (magnification x 500).

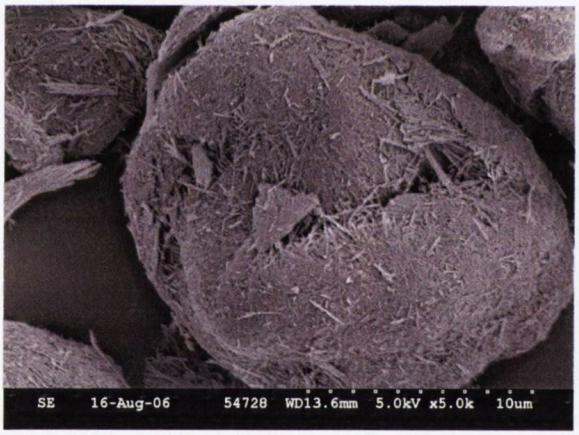


Figure 5.4b. SEM showing SD sepiolite (magnification x 5,000).

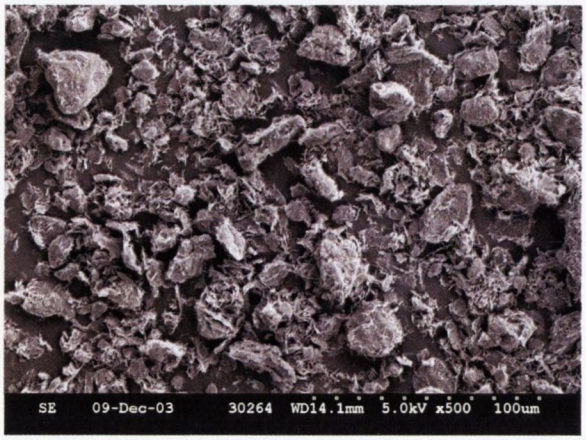


Figure 5.4c. SEM showing untreated sepiolite (magnification x 500).

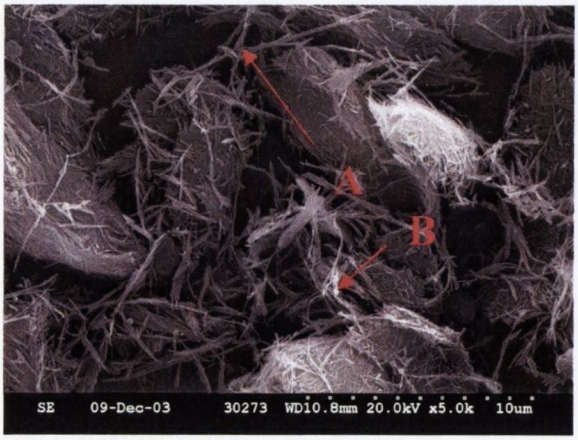


Figure 5.4d. SEM showing untreated sepiolite (magnification x 5,000).

The bulk and tapped densities of SD sepiolite and Physmix product were not significantly different; however those of SepKoll product were significantly higher ($p < 0.05$). Such a result would indicate that Kollidon® VA 64 interacts in a more intimate manner with sepiolite following co-spraying as opposed to physical mixing. The bulk and tapped densities of the spray dried sepiolite bases were very much lower than those of the commercially available DCBs. The low density measurements may be attributed to the highly porous nature of the individual sepiolite fibers, which even when closely packed into spherical aggregates following spray drying (Figure 5.3b), produce a lightweight high volume structure. Consequently the low values may not be reflective of poor packing of the sepiolite DCBs; a theory supported by Carr's indices and Hausner ratios within the range indicative of excellent flow (i.e. 5 - 15 and < 1.2, respectively; Wells, 1988). In contrast, the angle of repose and critical orifice diameter, although improved via the spray drying process, are still predictive of poor flow for all three spray dried sepiolite bases.

The angle of repose and Carr's compressibility index are both termed static methods of powder flow measurement, while the critical orifice diameter is a dynamic method. Correlation between the three parameters is poor in the case of Avicel® PH101 and the three sepiolite bases. Work carried out by Taylor *et al.* (2000) concluded that powder flow is a complex phenomenon which cannot be fully characterized by any single test methodology. Räsänen *et al.* (2003) also noted the difficulty associated with connecting indirect methods of flow analysis (i.e. Carr's compressibility index and Hausner ratio) with the in-process flow behaviour of powders. The failure of individual tests to fully and accurately characterize powder flow is not unexpected as each method challenges separate components of flow. Carr (1965) proposed that the angle of repose was a valid characterization of flow because it provided an indirect measurement of the shape, size, porosity, cohesion, fluidity, surface area and bulk properties of the material. He suggested that percent compressibility indicated the uniformity in size and shape, deformability, surface area, cohesion and moisture content of the test materials. The critical orifice diameter is a direct measure of powder cohesion and arch strength (Staniforth, 1987). Taylor *et al.* (2000) developed an empirical composite index which was correlated with powder flow in accordance with formulator experience. This empirical composite index was based on the results of the angle of repose, Carr's index and the critical orifice diameter (Equation 5.4a) and was found to be a more accurate determinant of likely flow behaviour than any one test.

$$\text{Composite Index} = \left(\frac{1120}{9}\right) - \left(\frac{10 \times COD}{9}\right) - \left(\frac{2 \times CI}{3}\right) - \left(\frac{2 \times AR}{3}\right) \qquad \textbf{Equation 5.4a}$$

where COD is the critical orifice diameter (mm), CI is Carr's compressibility index (%) and AR is the angle of repose (°).

Consequently Taylor's composite index was calculated and results are presented in Table 5.4a above. Taylor *et al.* (2000) recognized three categories of powder: those demonstrating good flow characteristics (corresponding to a composite index of 70-100), those with average flow characteristics (corresponding to a composite index of 61-70) and finally those with poor flow characteristics (composite index below 60).

The composite index indicated that only Ludipress® and the Ludipress®/ Kollidon® VA 64 blend exhibited 'good' flow properties. Untreated sepiolite exhibited extremely 'poor' flowability, which was improved by the spray drying process, such that flow after spray drying could be rated as 'average'. The flow properties of SepKoll were rated as 'average' and were similar to those of the individual components (i.e. SD sepiolite and Kollidon® VA 64) and also to a physical blend of the two components in the same ratio. Taylor's composite index for Avicel® PH101 was indicative of extremely poor flow. The poor flowability of MCC has been extensively reported in the literature (Bandelin, 1989; Banaker, 1994; Bolhuis and Chowhan, 1996; Buckton *et al.*, 1998; Tsai *et al.*, 1998) and is regarded as its biggest shortcoming. The poor flow has been attributed to the match-stick like form of the particles and the low bulk density (Bolhuis and Chowhan, 1996). While the flow properties of the novel spray dried bases are just average and will most likely necessitate the use of a flow aid, they are superior to Avicel® PH101.

5.4.2.2 Particle morphology and size distribution

The results of particle size analysis of the novel excipients, together with those of the other DCBs used as performance markers, are presented in Table 5.4b. The morphology of the spray dried bases was examined using SEM. These results are discussed in conjunction with those conclusions drawn from microscopy.

Table 5.4b. Particle size distribution by volume (n = 3).

Material	d10 (μm)	d50 (μm)	d90 (μm)
Sepiolite	2.597 ± 0.029	8.779 ± 0.154	21.332 ± 0.415
SD sepiolite	3.278 ± 0.240	10.058 ± 0.389	19.771 ± 0.555
SepKoll	4.298 ± 0.021	11.377 ± 0.003	21.582 ± 0.006
Physmix	3.368 ± 0.094	10.841 ± 0.069	23.415 ± 0.108
Avicel® PH101	20.110 ± 0.573	54.778 ± 0.165	122.524 ± 1.788
Ludipress®	32.333 ± 0.064	106.201 ± 2.395	288.879 ± 6.057
Kollidon® VA 64	11.929 ± 0.041	38.476 ± 0.191	104.566 ± 2.787
Ludipress®/Kollidon® VA 64 (9:1)	27.496 ± 0.572	103.304 ± 0.083	283.005 ± 1.507

SEMs of spray dried sepiolite are illustrated in Figures 5.4a, b, e and f. It is evident that the fibrous microstructure of sepiolite (as described in Chapter 4) was not destroyed by the spray drying process. The higher levels of architecture were, however, altered as a consequence. Prior to spray drying, sepiolite fibers associated along their longest dimension to form bundles, which in turn aggregate in a less ordered manner to form microagglomerates. The shape and size of these microagglomerates varied hugely; many were flattened and presented with fibers protruding from the surfaces which linked one 'tuft' to another (points A and B, Figure 5.4d). Following spray drying, the size and shape of the aggregates became much more uniform and the degree of sphericity increased (Figure 5.4e and b).

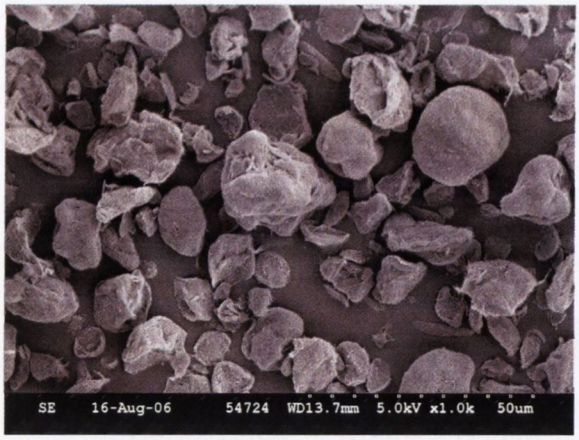


Figure 5.4e. SEM of spray dried sepiolite (magnification x 1,000).

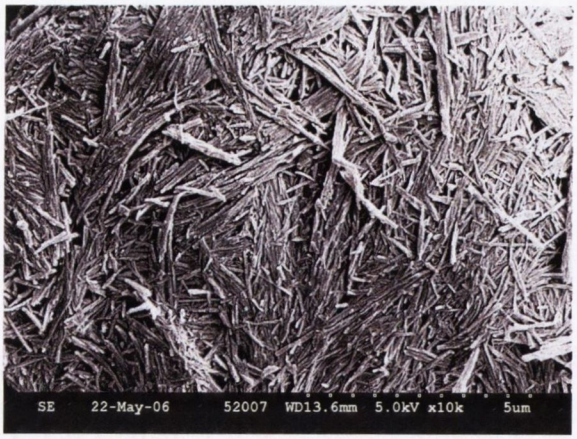


Figure 5.4f. SEM of spray dried sepiolite (magnification x 10,000).

SEMs of SepKoll are presented in Figures 5.4g – 5.4j. The morphology of these particles was clearly similar to that of spray dried sepiolite. Dense packing of the fibers within the rounded aggregates was again apparent (Figure 5.3i, 5.3j), as were the well-defined perimeters of the particles. The particles were slightly larger than those obtained following spray-drying of sepiolite on its own, as had been expected owing to the binding capabilities of Kollidon® VA 64. This visual observation was supported by the significantly larger ($p < 0.05$) d10, d50 and d90 values of SepKoll.

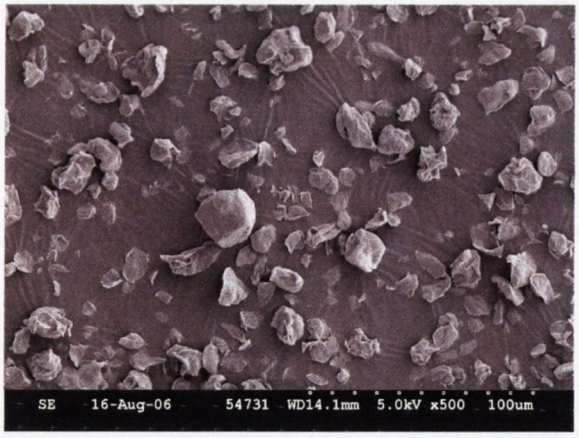


Figure 5.4g. SEM of SepKoll (magnification x 500).

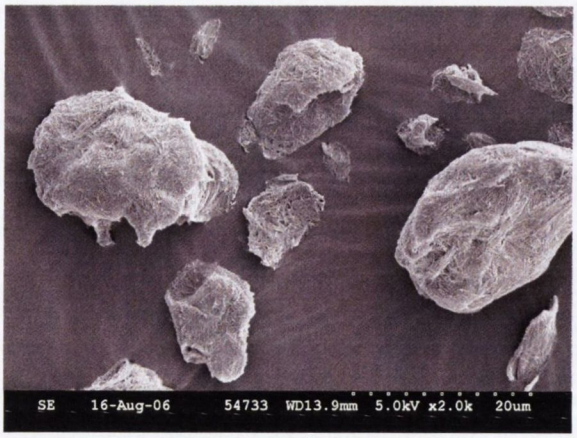


Figure 5.4h. SEM of SepKoll (magnification x 2,000).

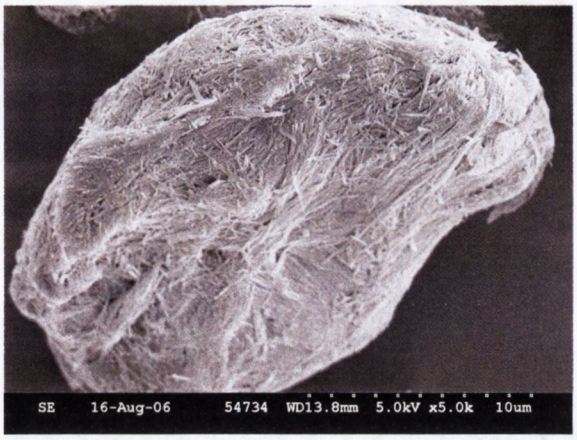


Figure 5.4i. SEM of SepKoll (magnification x 5,000).

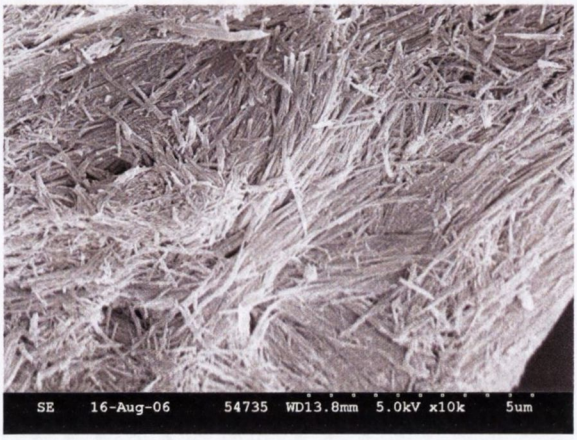


Figure 5.4j. SEM of SepKoll (magnification x 10,000).

SEM images of the physical mixture of spray dried sepiolite and Kollidon® VA 64 are presented in Figures 5.4k - 5.4n below. The characteristic hollow and broken spheres of Kollidon® VA 64 (Bühler, 2003) were apparent amongst the smaller sepiolite aggregates. The d10 and d50 values of the physical mixture were similar to those of SD sepiolite; the d90 was larger owing to the inclusion of the larger Kollidon® particles.

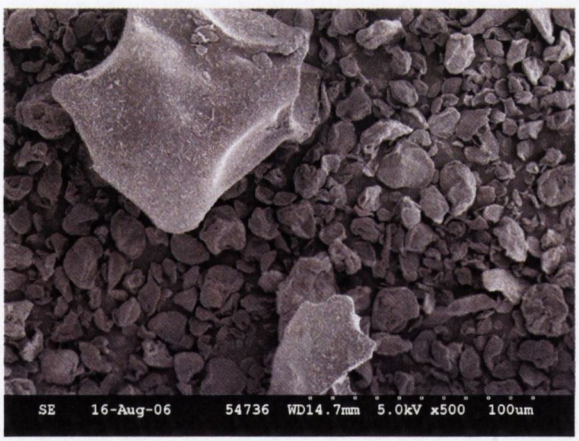


Figure 5.4k. SEM of Physmix (magnification x 500).

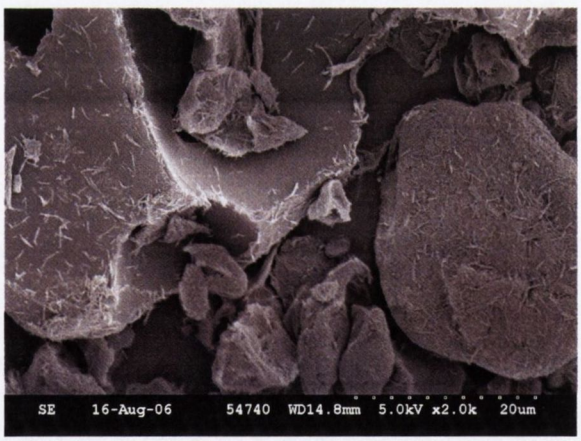


Figure 5.4l. SEM of Physmix (magnification x 2,000).

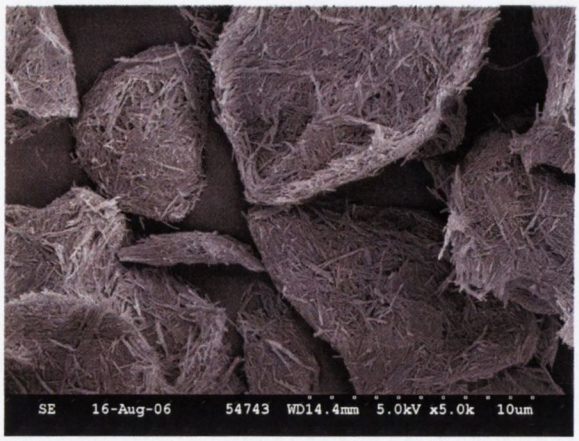


Figure 5.4m. SEM of Physmix (magnification x 5,000).

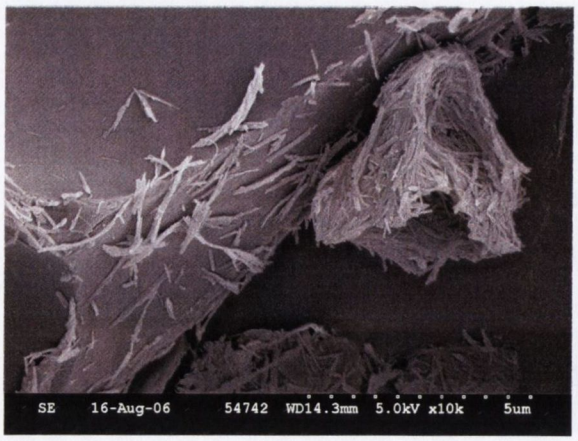


Figure 5.4n. SEM of Physmix (magnification x 10,000).

Relative to the other DCBs tested (Ludipress®, Avicel® PH101), the spray dried sepiolite products were very fine, with substantially lower d10, d50 and d90 values. Obviously a larger particle size would be preferable as it would enhance flowability. Manipulation of the particle size may be possible through the use of alternative spray drying equipment/ conditions. Such an approach has proved successful in the production of different size grades of MCC with improved flowability, resulting in reduced tablet weight variation and improved drug content uniformity (e.g. Avicel® PH102, PH200). However, the undertaking of such a process was considered outside the scope of this section, the primary aim of which was to assess the potential of sepiolite as a DCB by exploring the mechanisms by which it undergoes compression, its resultant compactibility and the impact of spray drying on these properties.

5.4.2.3 Powder X-ray Diffraction (pXRD) studies

pXRD was employed to determine whether any significant alteration in the crystalline structure of sepiolite occurred following spray drying. The thermal stability of sepiolite at temperatures of the order of 100 °C is well documented in the literature (Molino-Sabio *et al.,* 2001; Hubbard *et al.*, 2003). Consequently, no change in the crystalline structure was anticipated. The X-ray diffractograms of untreated sepiolite, SD sepiolite, SepKoll, the physical mixture and Kollidon® VA 64 are presented in Figure 5.4o below.

Several conclusions can be drawn from Figure 5.4o. Firstly, no differences in the peak positions or intensities were apparent on comparing the traces of SD sepiolite and

untreated sepiolite confirming that the crystalline structure was unaffected by spray drying. Secondly, Kollidon® VA 64 showed two slight diffuse halos over the 10° 2θ to 30° 2θ angular range with maximums at 15° 2θ and 22° 2θ, confirming the amorphous nature of the polymer. The diffractograms for both SepKoll and Physmix were identical indicating that Kollidon® VA 64 did not alter the crystalline state of sepiolite during the co-spray drying process, nor did the spray drying process bring about a change in the solid state form of Kollidon® VA 64.

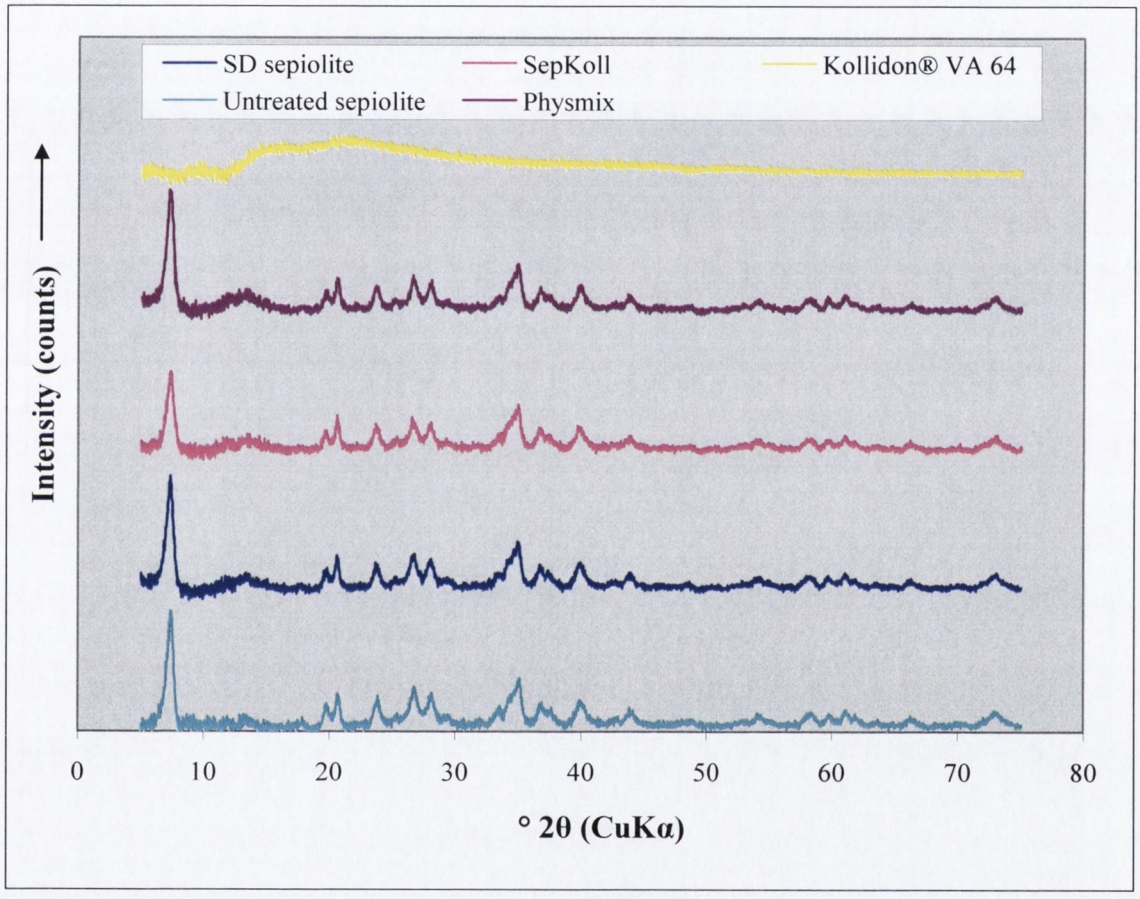


Figure 5.4o. X-ray diffractograms of untreated sepiolite, SD sepiolite, SepKoll, Physmix and Kollidon® VA 64.

5.4.2.4 FT-IR analysis

FT-IR has been used to study interactions in excipient–polymer blends. It can provide valuable information regarding the interactions of blends of two excipients at the molecular level. If an excipient and polymer interact then the functional groups in the FT-IR spectra of the blend will show the emergence of additional bands or alterations in wavenumber position or broadening compared to the spectra of the pure excipient and polymer (Takka,

2003). The FT-IR spectra of all the co-spray dried samples and physical mixtures are presented in Figure 5.4p. The position of the peaks in the spectrum of sepiolite did not shift obviously following spray drying, indicating no change in the nature of bonding within the structure. The major peaks assigned to the OH-stretching of water co-ordinated to magnesium cations (3565 cm^{-1}) and zeolithic water (3245 cm^{-1}, 3396 cm^{-1}) in untreated sepiolite were unaltered following spray drying, demonstrating that the manner of association of water molecules with the sepiolite structure was unchanged by the spray drying process. Furthermore, the position and intensity of the peak due to the water O-H bending (1653 cm^{-1}) was unaffected by the spray drying process.

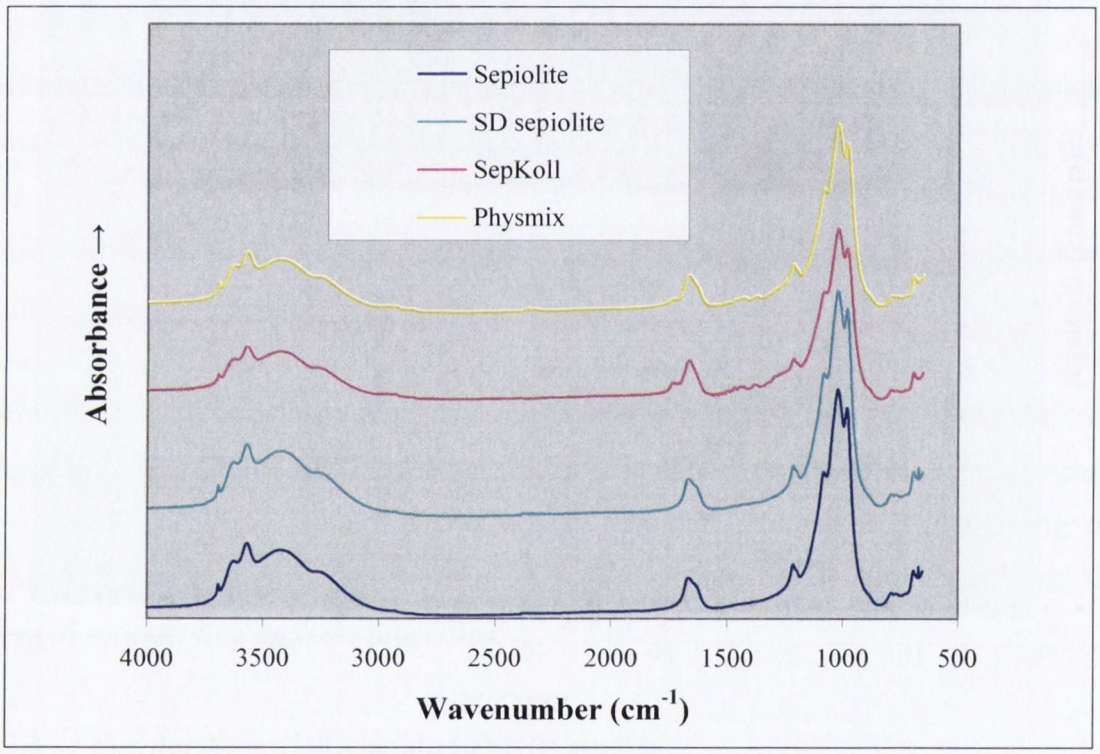


Figure 5.4p. FT-IR spectra of sepiolite, SD sepiolite, SepKoll and Physmix.

The peak positions in the FT-IR spectra of the physical mixture and co-spray dried sample were similar and differed from that of SD sepiolite only in the presence of an additional peak at 1750 cm^{-1} corresponding to the stretching frequency of the ester and pyrrolidone carbonyl groups of Kollidon® VA 64, thereby indicating that FT-IR appeared capable of detecting Kollidon® VA 64 at a concentration of 0.01% w/w. Given the similarity of the SepKoll and Physmix spectra, it is unlikely that interactions between Kollidon® VA 64 and sepiolite at a molecular level were facilitated by the co-spray drying process.

5.4.2.5 Thermal Analysis (TGA, DSC) and KF analysis

The three novel DCBs were subjected to thermal analysis (TGA and DSC) in order to investigate any potential interaction between SD sepiolite and Kollidon® VA 64. Thermal analysis is now a well developed technique used in the detection of incompatibilities in excipient mixtures (Ford and Rubenstein, 1981; Wissing *et al.*, 2000; Fathy *et al.*, 2002; Tomassetti *et al.*, 2004). DSC is a valuable tool used in preformulation studies to give fast and reliable information about possible interactions. Interactions may be deduced from DSC curves by observing changes in thermal events such as the disappearance of melting peaks, the appearance of new peaks, changes in peak shape, peak onset or peak maximum temperature (Fathy *et al.*, 2002).

TG and DSC thermograms for the three novel bases and Kollidon® VA 64 are presented in Figures 5.4q and 5.4r below. The TG profiles of the three novel bases were similar to each other and also to that of untreated sepiolite (Figure 4.3a), each one exhibiting a sharp weight loss over a temperature range of 25 to 90 °C, representing ~8.5% of the initial weight. Such an effect is due to the removal of water molecules adsorbed to the external surfaces of the fibers (del Hoyo *et al.*, 1996). This pronounced weight loss was followed by a more gradual weight loss which continued over the rest of the temperature range examined (i.e. to 300 °C) and may be attributed to the loss of the more strongly held water molecules from the channels (i.e. zeolithic water). The TG trace of Kollidon® VA 64 also displayed a pronounced weight loss over a temperature range of 25 °C to 50 °C due to polymer dehydration. The total weight loss over the temperature range examined correlated reasonably well with the water content determined using KF analysis (Table 5.4c), confirming that the weight loss on heating of the sepiolite bases was due to water loss.

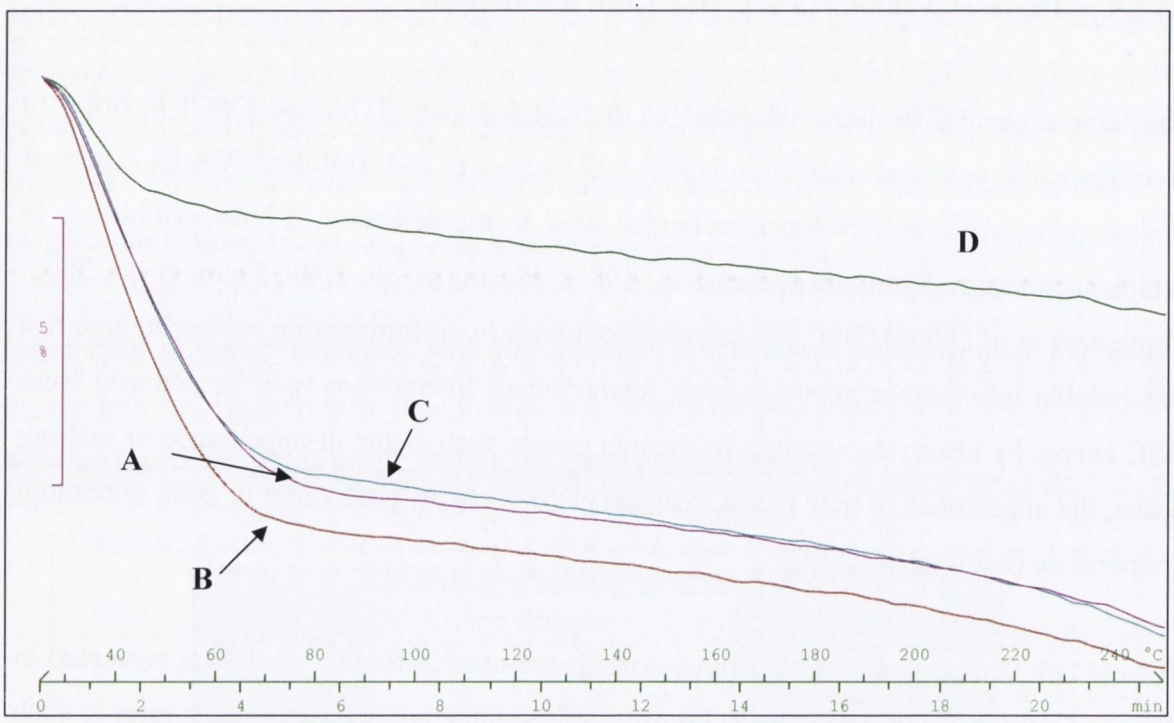


Figure 5.4q. TG thermograms of SepKoll (A), Physmix (B), SD sepiolite (C) and Kollidon® VA 64 (D).

Table 5.4c. Weight loss on heating and moisture content of the novel sepiolite DCBs.

Material	Weight loss over 25 - 250 °C[1] (% w/w)	Moisture content [2] (% w/w)
SD sepiolite	Range: 10.33 - 10.37	Range: 10.47 - 10.78
SepKoll	Range: 10.48 - 10.68	Range: 9.61 - 9.92
Physmix	Range: 10.97 – 11.27	Range: 9.30 - 9.70

[1]Determined from TG (n = 2).
[2]Determined from KF analysis (n =2).

The DSC profiles of the three sepiolite bases were again similar, each with a broad endotherm between 25 °C and 130 °C. Frost and Ding (2003) reported similar DSC traces and stated that this endotherm is composed of two overlapping endotherms centred at approximately 83-89 °C and 100-122 °C, corresponding to the energy required to remove the adsorbed and zeolithic water respectively. The DSC trace of Kollidon® VA 64 exhibited a shallow broad endothermic effect in the 40 to 130 °C range due to polymer dehydration. A comparatively small endothermic peak was also observed at ~ 114 °C, a temperature previously reported by Bühler (2003) to be the glass transition temperature of Kollidon® VA 64.

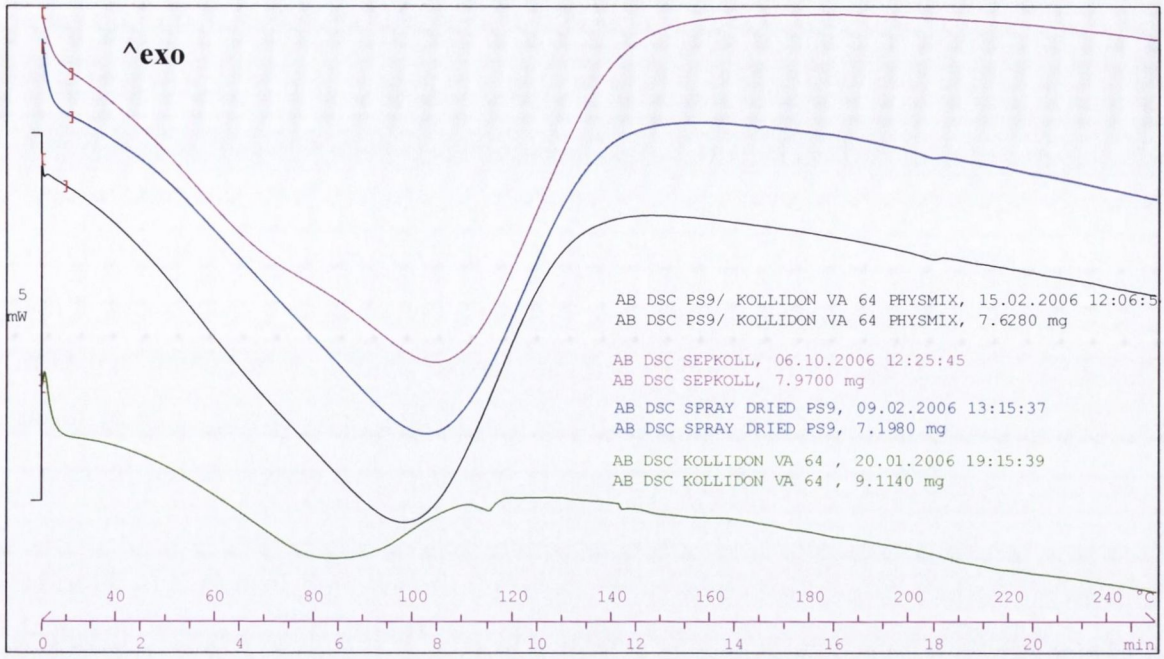


Figure 5.4r. DSC thermograms of SepKoll (purple), SD sepiolite (blue), Physmix (black) and Kollidon® VA 64 (green).

The DSC and TG traces of SD sepiolite, SepKoll and Physmix were quite similar, despite the inclusion of Kollidon® VA 64 (10% by weight) in the latter two samples. It is likely that the broad endotherms of the sepiolite component masked the thermal events associated with Kollidon® VA 64, given that these occur within the same temperature range and take the form of broad, shallow peaks. In conclusion, interpretation of the thermal data, according to appearance, shift or disappearance of endothermic/ exothermic peaks indicated that SD sepiolite was compatible with Kollidon® VA 64.

5.4.2.6 BET surface area and porosity

The adsorption isotherms for SD sepiolite, SepKoll and Physmix are presented in Figure 5.4s below. All three adsorption isotherms exhibited extensive nitrogen adsorption at extremely low relative pressures, representative of the filling of the micropores (i.e. the intracrystalline channels). Further increases in the relative pressure resulted in more gradual increases in the volume adsorbed corresponding to the progressive adsorption of nitrogen to the external surface area. A rapid rise was seen at very high relative pressures as saturation was approached and bulk condensation began to occur. Similar profiles were obtained by Jiménez-López *et al.* (1978) following heating of sepiolite to 110 °C for 10 h.

The data for all three spray dried samples was transformed in accordance with the BET equation (Equation 3.1a) to permit the determination of surface area. A negative BET C value was obtained in each case. The C value is a dimensionless constant related to the enthalpy of adsorption of the adsorbate gas on the powder sample. The value of C is most frequently between 50 and 300 when using nitrogen at 77 K (Webb and Orr, 1977). A negative C value is indicative of the presence of micropores, whose measurement is not amenable to analysis by the BET model without further modification (Webb and Orr, 1997; Brantley and Mellott, 2000). The modification of the BET model suggested by these authors was not clarified in any detail whatsoever. An extensive review of the literature was undertaken but yielded no further enlightenment. Measurements were repeated using a Quantachrome Nova 4200e Surface Area Analyser (Quantachrome Instruments, Florida, USA) together with a vacuum degassing station (Flowvac®). However, negative C values were still obtained, thus ruling out the possibility of a machine malfunction. In the absence of an alternative method, the adsorption isotherms were compared qualitatively with those of untreated sepiolite.

The isotherms for the three spray dried samples were identical in shape to that of the untreated sample of sepiolite. A substantial (~ 33%) reduction in the volume of nitrogen adsorbed per unit weight at low relative pressures was observed following spray drying of sepiolite, indicative of a reduction in the micropore surface area. The volume of nitrogen adsorbed per unit weight at relative pressures greater than 0.1 was identical in all cases indicating that the external surface area remained unchanged. XRD diffractograms indicated that the zeolithic channel structure was not altered by spray drying, ruling out the partial collapse of the channels as a consequence of spray drying. Serna and Van Scoyoc (1979) noted that ethanol can penetrate the intracrystalline structure and replace up to 50% of the co-ordinated water. It would be expected that this exchange would be accompanied by changes in the OH stretching region of the FT-IR spectrum following spray drying, but no changes were noted which may be a consequence of the complexity of this region due to the overlapping signals from many types of OH groups. Due to the larger molecular volume of ethanol, replacement of co-ordinated water by ethanol would cause a narrowing of the channels which would result in dramatically reduced access of nitrogen to the interior and consequently a reduction in micropore volume and surface area. Serna and Van Scoyoc (1979) also noted that co-ordinated water was mainly replaced by ethanol near the external surfaces. Consequently, only small amounts of co-ordinated water need be

replaced by ethanol in order to reduce the dimensions of channel opening and thereby hinder access to the entire channel volume. This could also explain the absence of changes in the hydroxyl stretching region of the FT-IR spectrum. Given the dimensions of the channels are of the order of 0.36 nm x 1.06 nm, any narrowing of the interior at either the entrance or along the channel length makes it possible that a molecule such as nitrogen, with dimensions 0.40 nm x 0.30 nm x 0.32 nm (Molina-Sabio *et al.*, 2001) could be in contact with two opposite sides of the channel rather than just one, thus providing surface area values lower than the true surface area.

Alternatively, it is possible that dispersion of sepiolite in a water-ethanol mixture, as was the case during spray drying, caused the dissolution of an organic contaminant/ amorphous silica (aqueous solubility = 120 mg /L; Freeze and Cherry, 1979) which if deposited at the channel openings or within the channels would lead to channel plugging, which would again result in dramatically reduced intracrystalline penetration of nitrogen and consequently a reduction in surface area.

Furthermore, Sing (2004) reported that two different micropore filling techniques can be identified, the manner of filling being dictated by the diameter of the micropores. In very narrow micropores of no more than ~1 nm in diameter (termed ultramicropores), the physisorption of nitrogen is energetically driven through the overlap of intermolecular forces and therefore takes place at extremely low pressures. The filling of wider micropores (termed supermicropores) takes place over a range of somewhat higher relative pressures; firstly, through incomplete monolayer adsorption on the pore walls and secondly, by a co-operative process. Any narrowing of the channels within the fibers could lead to a switch from the latter process to the former, hence proposing an explanation as to why the adsorption data from the spray dried samples is not amenable for analysis by the BET equation.

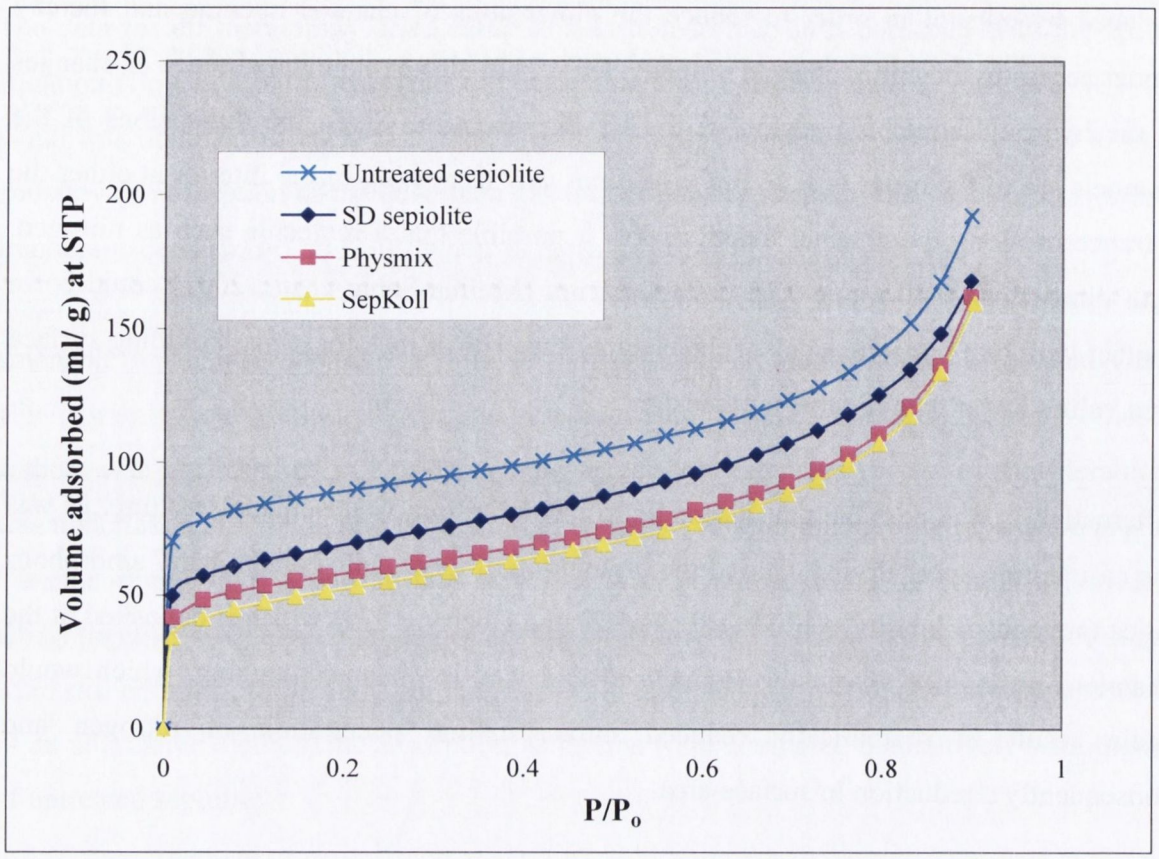


Figure 5.4s. Nitrogen adsorption isotherms for untreated sepiolite, SD sepiolite, SepKoll and Physmix.

For the physical mixture of sepiolite and Kollidon® VA 64, the volume adsorbed at low relative pressures was reduced relative to that of spray dried sepiolite as would be expected given the low surface area of Kollidon® (0.2125 m^2 /g) which accounted for 10% by weight of the sample. The volume adsorbed at low relative pressures in the case of SepKoll was lower again, and could possibly be attributed to the adhesive nature of the polymer which bound sepiolite fibers together following co-dispersion and drying (Figure 5.4i and 5.4j), and occluded pore openings. In conclusion therefore, the spray drying process was found to reduce the size of the micropores of sepiolite, possibly due to replacement of a fraction of the co-ordinated water by ethanol and/or by deposition of a dissolved contaminant. Co-spray drying with Kollidon® VA 64 reduced the micropore volume and surface area further presumably through partial occlusion of pore openings. Both suppositions are supported by the results of TGA, KF, pXRD and FT-IR, all of which indicate that a change in the crystalline structure of the channels did not occur upon spray drying.

5.5 COMPARISON OF THE TABLETTING PERFORMANCE OF NOVEL SEPIOLITE GRADES WITH OTHER DCBs USING PARACETAMOL AS AN ACTIVE INGREDIENT

5.5.1 Rationale for choice of paracetamol as model drug

Tablets were prepared by direct compression according to the formulations listed in Section 3.5.3. Paracetamol was chosen as a model drug for several reasons. First of all, it exhibits low flowability and poor compression ability tending to undergo elastic recoil following compression resulting in a high capping tendency (Hong-Guang and Ru-Hua, 1995; Lennartz and Mielck, 1998) and consequently poses quite a challenge to any potential DCB. Secondly, it was established from the preliminary compression studies that sepiolite deforms in a plastic manner and consequently is particularly suited to the tabletting of drugs which behave in an elastic manner (Wells, 1988). Finally paracetamol has a high pK_a value (9.5; Shaw *et al.*, 2005) and so the extent of ionization over the physiologically relevant pH range does not change considerably. In the case of drugs with pK_a values at physiologically relevant pH values, changes in ionization could affect the nature of any interaction between the clay and drug, thereby potentially altering tablet properties and making interpretation of the results very complex. In addition, changes in ionization could alter solubility, thereby complicating the results. Shaw and his co-workers (2005) observed that paracetamol solubility (approximately 20.3 mg/ mL) did not vary from pH 1.2 - 8.0, corresponding to the typical *in vivo* pH range in the gastrointestinal tract.

5.5.2 Uniformity of mixing

Tablet blends were prepared according to the formulations presented in Table 3.5a. Prior to tabletting, the uniformity of paracetamol content was established through random sampling of the tablet blend and subsequent UV analysis. The results are presented in Table 5.5a below.

Table 5.5a. Uniformity of content results for the DC blends.

Formulation	DCB	% Theoretical paracetamol content	
		Sample 1	Sample 2
TABDC1	SD sepiolite	102.28	101.91
TABDC2	SepKoll	94.95	98.28
TABDC3	Physmix	95.54	98.67
TABDC4	Avicel® PH101	113.48	116.69
TABDC5	Ludipress®/ Kollidon® VA 64 (9:1)	99.55	98.71
TABDC6	Kollidon® VA 64	96.23	95.84

All tablet blends contained within ± 5% of the stated paracetamol content with the exception of the Avicel® PH101 blend (TABDC4). A mixing time of 30 min failed to produce a sufficiently uniform tablet blend for further tabletting in the case of TABDC4. Lack of uniformity in the tablet blend will translate into tablets with varied drug contents and physical properties. The poor mixing properties of MCC most likely stem from its poor flowability (Bolhuis and Chowhan, 1996). Reus-Medina and Kumar (2006) noted that when preparing hydrochlorothiazide tablets using MCC as a DCB, the standard deviation associated with the uniformity of hydrochlorothiazide content was very large and attributed same to the poor flow and resultant poor mixing properties of MCC. The mixing time for TABDC4 blend was increased to 90 min, after which time the two random samples contained 102.10% and 99.55% of the theoretical paracetamol content. However, as described previously, a change in the mixing time with magnesium stearate can lead to significant alterations in tablet hardness (Kikuta and Kitamouri, 1994). In order to correct for this, all excipients, with the exception of magnesium stearate, were mixed for 90 min after which time magnesium stearate was added and mixing continued for a further 30 min. Repeated sampling of the blend at this stage confirmed the uniformity of the mix (101.32% and 102.89 % respectively).

In contrast, SD sepiolite, SepKoll and Physmix succeeded in producing a homogenous mixture within the specified mixing time. The d10, d50 and d90 values of the paracetamol used were as follows: 2.573 μm, 12.338 μm and 57.502 μm. Consequently the particle size

distribution was quite similar to those of SD sepiolite, SepKoll and Physmix, thereby facilitating the production of an intimate physical mix and also minimizing the likelihood of segregation. Indeed, Jivraj *et al.* (2000) stated that the ideal DCB should have a particle size equivalent to the active ingredients present in the formulation. The desire for a similar particle size distribution must not however be achieved at the cost of adequate flowability. In the case of the three novel SD bases, a reasonable balance between particle size and flow is realized.

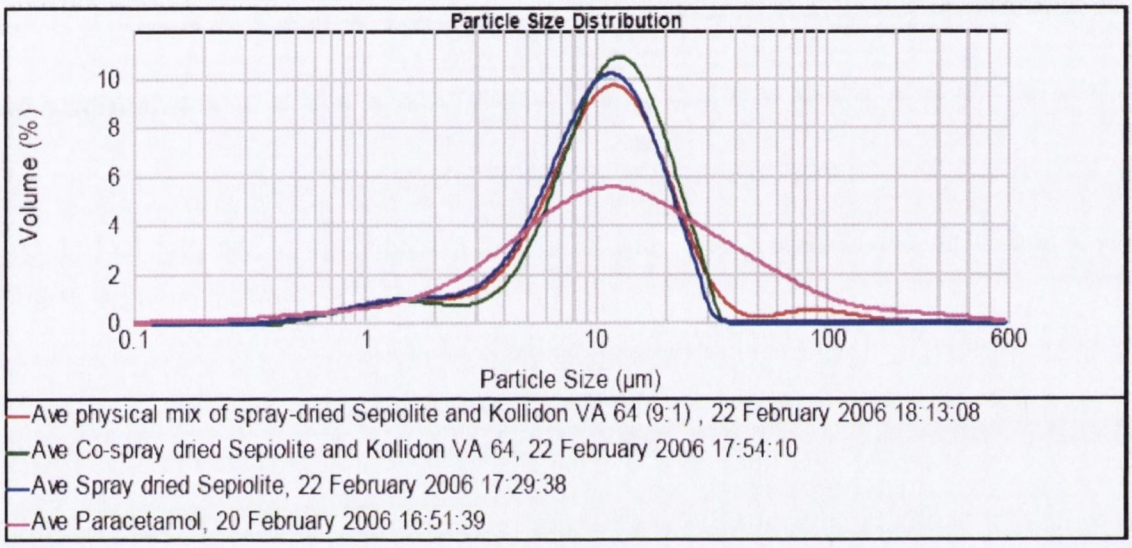


Figure 5.5a. Particle size distribution of SD sepiolite, SepKoll, Physmix and paracetamol (n = 3).

The excellent flow properties of Ludipress and Kollidon® VA 64 assured the rapid production of a uniform mix. The flowability indices determined in Section 5.4.2.1 were therefore an accurate predictor of mixing properties.

5.5.3 Compression Modelling

The development of a new direct compression base should include a rapid and comprehensive evaluation of its deformation properties. Numerous mathematical models may be applied to compaction data to investigate the change in the relative density of a powder bed as a function of the applied pressure (Paronen and Ilkka, 1996). Two equations have found particular application in the pharmaceutical industry, namely the Heckel and Kawakita equations.

5.5.3.1 Heckel Compression Analysis

5.5.3.1.1 Introduction

Heckel analysis is routinely performed to study the effect of applied pressure on the relative density of a powder bed during compaction and to determine the deformation mechanism of particles forming the compacts. According to Heckel (1961a), the compaction of powders may be considered analogous to a first-order chemical reaction, the pores being the reactant and the densification of the bulk the product. The equation takes the form:

$$\ln\left(\frac{1}{1-D}\right) = kP + A \qquad \textbf{Equation 5.5a}$$

where k and A are constants derived from the slope and intercept of the plot $\ln(1/(1\text{-}D))$ versus P, respectively, D is the relative density of a powder column at pressure P and consequently $(1\text{-}D)$ is the porosity of the compact at pressure P.

The Heckel equation exhibits linearity for many materials at high pressures (Çelik, 1992). At low pressures, the plots tend to be curved. Heckel (1961a, 1961b) attributed this non-linearity to the two processes of volume reduction, which take place firstly by die filling and secondly by particle rearrangement, before a coherent mass is formed by deformation and bonding of the discrete particles. Therefore, he concluded that the densification which is represented by the linear region of a plot of the natural logarithm of (1/Porosity) versus P occurs by plastic deformation of the compact. Consequently, k, the slope of the linear region, gives a measure of the ability of the compact to densify by plastic deformation. Heckel (1961b) demonstrated that the k value is linearly related to the reciprocal of the yield strength of the material, Y (Equation 3.5j).

Rather confusingly, Hersey and Rees (1971) subsequently proposed that the reciprocal of the constant k be termed the mean deformation pressure, designated P_y and defined as the pressure at which plastic behaviour becomes dominant. A review of the literature indicates that both the yield strength, Y, and the mean deformation pressure, P_y, are currently used as indices of the susceptibility of a material to deformation by plastic flow and it is their value relative to other materials rather than the absolute value that is of interest.

Furthermore, the area under the Heckel curve (AUHC) has been used by many authors (Rue and Rees, 1978; Kumar *et al.*, 2001) as a measure of compressibility (i.e. the extent of volume reduction following the application of a given stress).

The limitations of the Heckel model have been discussed by Rue and Rees (1971) and Carstensen and Hou (1985) and are largely attributable to the assumption that a non-porous state is achieved at infinite pressure. Given that several classes of porosity can exist in a material (interparticulate and intraparticulate porosity), it is not always valid to assume that they will respond to pressure in the same manner. This limitation is discussed with particular reference to the structure of sepiolite in the next section.

5.5.3.1.2 Results of Heckel Analysis

Compaction data from paracetamol tablets prepared using the different DCBs was subjected to Heckel analysis to permit determination and thereby comparison of the following parameters: mean deformation pressure (P_y), yield strength (Y) and compressibility (AUHC).

The relationship between compact porosity and compression pressure is presented in Figure 5.5b.

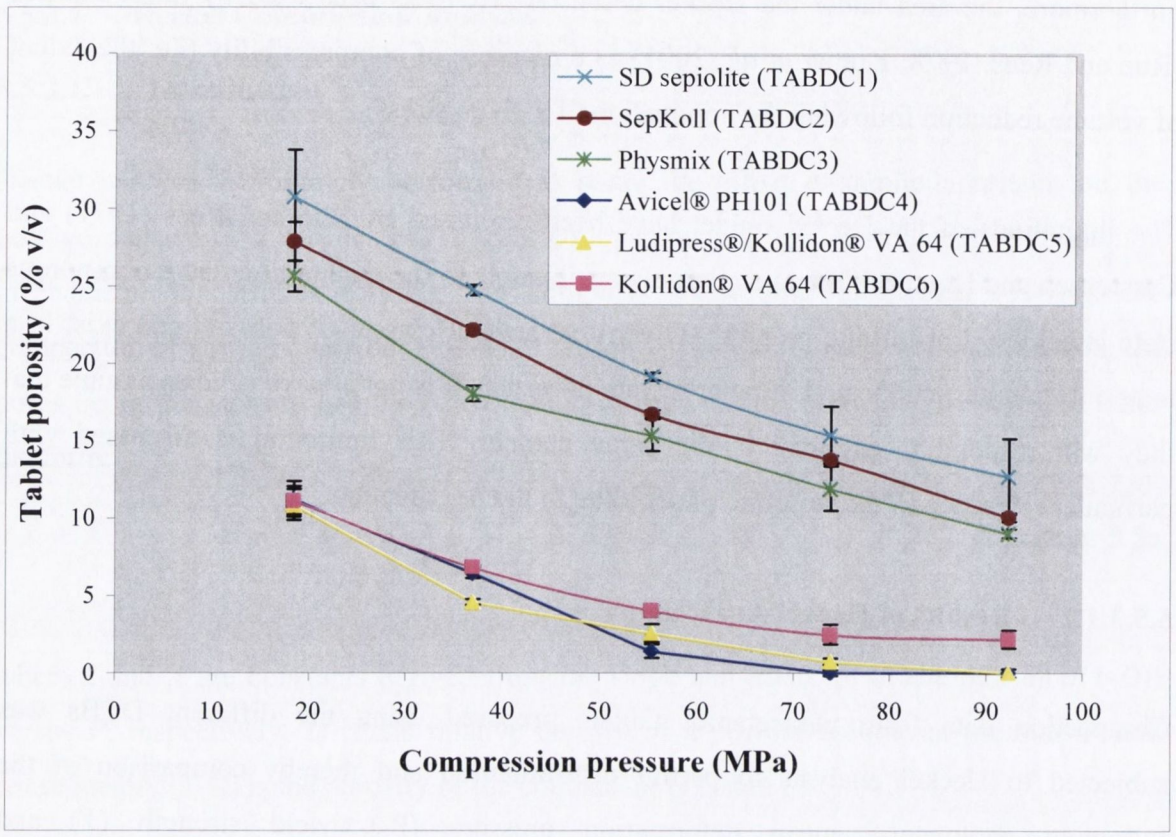


Figure 5.5b. Tablet porosity-applied pressure profiles for the different DC formulations (n = 3).

The tablet porosity decreased with increasing compaction pressure for all materials. At any given pressure, the blends containing sepiolite gave tablets of much higher porosity than the other DCBs. The high porosity is reflective of the extensive inter- and intra-particulate porosity of the sepiolite structure as determined using MIP and N_2 adsorption in Section 4.5. The porosity of compacts prepared using Kollidon® VA 64, Avicel® PH101 and the Ludipress®/ Kollidon® VA 64 blends was approximately zero at the maximum compression pressure studied, indicating that the Heckel assumption of a non-porous state at infinite pressure was likely to be valid. Our findings were consistent with those of Westermarck *et al.* (1999) and Badawy *et al.* (2006). Firstly, both authors reported that Avicel® PH101 has intraparticulate micropores; their volume being several-fold lower (0.0032 – 0.0040 mL/ g) than in the case of sepiolite and hence consistent with the lower porosity of Avicel® PH101-based compacts at low compression pressures. Secondly, Westermarck and his co-workers (1999) found that the volume of these pores does decrease on application of pressure and the extent of this reduction is related to the magnitude of the pressure applied.

The porosity of sepiolite-based compacts was of the order of 10% at the maximum compressive force. As addressed previously, the microporosity of sepiolite is due to the nature of covalent bonding within the material and so this element of the porosity is unlikely to yield to pressure. The retention of the fibrous morphology after compression at these pressures, as evidenced by SEM, indicates that a certain amount of interfibrous void space is also likely to be present. The residual total porosity at high compression pressures is therefore likely to represent primarily the pressure-independent nature of the microporosity of the sepiolite fibers and to a lesser extent the mesoporosity associated with interfibrous void space. The interpretation of Heckel plots and parameters is likely to be complicated by the existence of pore populations of varying pressure sensitivity. It cannot be excluded therefore that the Heckel model is unsuitable to assess the compressibility of the sepiolite bases, given that the compact porosity seems to tend toward a non-zero value at infinite pressure, thereby leading to an overestimation of the yield values and an underestimation of compressibility. Other authors (Carstensen and Hou, 1985 and Carstensen, 1990) have addressed this issue through a novel treatment of porosity-pressure measurements, whereby the density of a powder column was considered to approach a value different from the particle density. This involved an assumption that only pores and voids having a diameter larger than a threshold value, as measured by mercury porosimetry, were considered to take part in volume reduction. This corrective measure was not undertaken here due to the difficulty associated with defining a threshold pore value, but rather the results are discussed bearing this factor in mind. Moreover, the data was fitted to an alternative compression model developed by Lüdde and Kawakita (1966), which describes the change in volume as a function of the bulk volume rather than the skeletal volume and thereby avoids the assumption of zero porosity at infinite applied pressure.

Heckel plots for the different paracetamol blends are presented in Figure 5.5c. Regression analysis was performed over the compression pressure range 18-93 MPa. Heckel parameters are presented in Table 5.5b, together with the regression analysis results. High correlation coefficients for linearity ($r^2 > 0.9752$) were obtained for all formulations. Linear plots indicate deformation by plastic flow (Paronen and Ilkka, 1996).

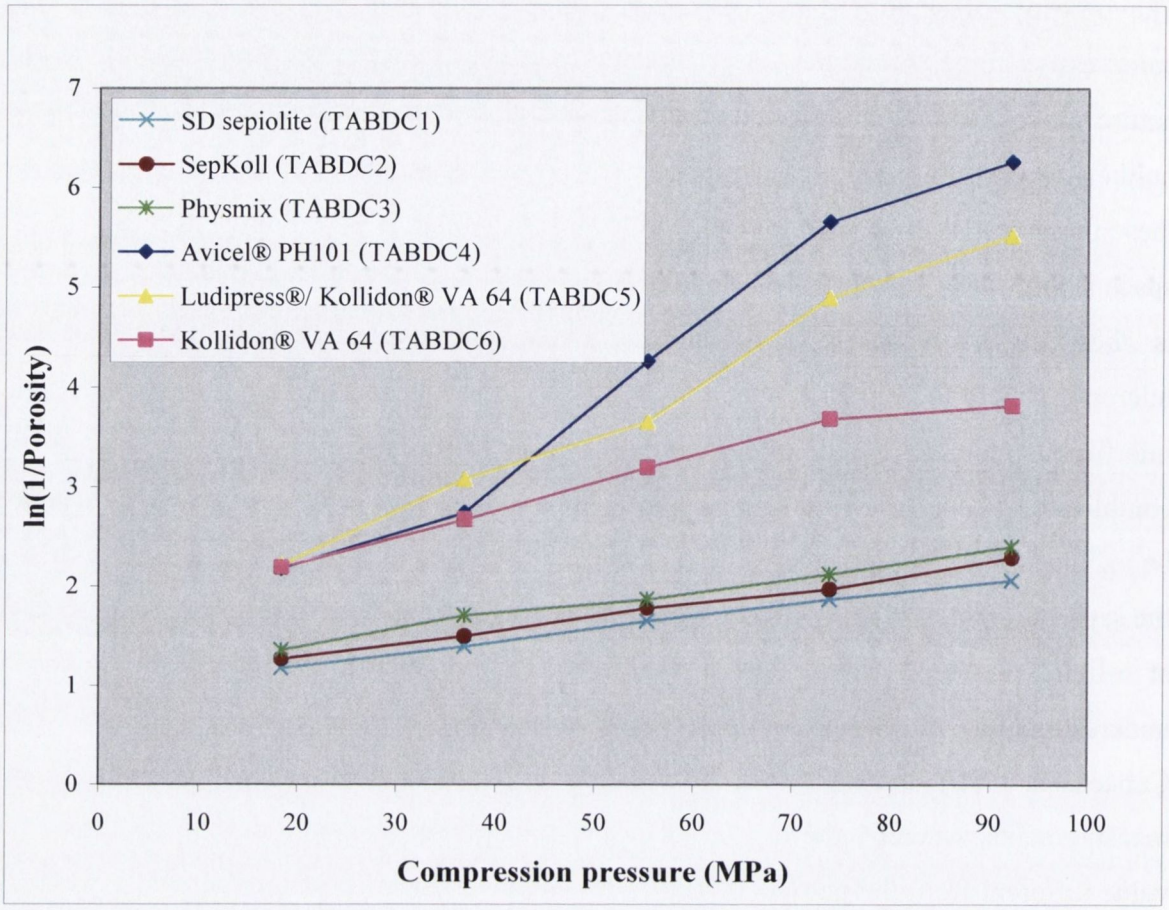


Figure 5.5c. "Out-of-die" Heckel profiles of the different DCBs (n = 3).

The mean deformation pressure (P_y) of the bases decreased in the following order: SD sepiolite > Physmix > SepKoll > Kollidon® VA 64 > Ludipress®/ Kollidon® VA 64 > Avicel® PH101. Podczeck and Revesz (1993) reported that materials with a P_y value of the order of 80 MPa or less deform mainly by plastic flow and as this value increases, materials become more and more brittle. The plastic nature of sepiolite established from the preliminary studies is therefore supported by the conclusions of Heckel analysis. The P_y of pure paracetamol has been reported by other authors to be 96.9 and 110 MPa (Roberts and Rowe, 1985; Hussan *et al.*, 1991). Hence SD sepiolite was capable of improving the deformability of the drug, albeit to a much lesser extent than either Avicel® PH101 or a Ludipress/ Kollidon® VA 64 (9:1) blend. The relative order of the P_y values indicated that the onset of deformation occurred at much lower pressures in the commercially available DCBs when compared to the novel SD sepiolite bases. Avicel® PH101 was clearly the most ductile of the materials examined. The AUHC values, which can be used as a measure of compressibility (Rue and Rees, 1978; Kumar *et al.*, 2001), confirmed this result. Many authors have also reported the extensive plastic flow occurring during compression of MCC and have attributed it to the numerous slip-planes and

dislocations present in its structure (Reier and Shangraw, 1966; Lamberson and Raynor, 1976; David and Augsburger, 1977).

Table 5.5b. Heckel plot constants of studied DCBs.

Formulation	DCB	r^2	k (MPa^{-1})	Y (MPa)	P_y (MPa)	AUHC (MPa)
TABDC1	SD sepiolite	0.9978	0.012	27.55	82.64	120.93
TABDC2	SepKoll	0.9956	0.014	24.51	73.53	130.48
TABDC3	Physmix	0.9897	0.014	24.69	74.07	140.31
TABDC4	Avicel® PH101	0.9752	0.060	5.56	16.67	312.00
TABDC5	Ludipress®/ Kollidon® VA 64	0.9881	0.046	7.31	21.93	286.55
TABDC6	Kollidon® VA 64	0.9707	0.023	14.43	43.29	232.26

The incorporation of Kollidon® VA 64 in the two novel sepiolite grades did succeed in improving plasticity, as was the rationale behind its inclusion in the formulation. Interestingly, similar reductions in the P_y values were observed (73.53 *vs* 74.07 MPa for SepKoll and Physmix respectively) irrespective of whether Kollidon® VA 64 was present as a component of a co-spray dried system (as in SepKoll) or simply as a component of a physical mixture (as in Physmix). It should be noted that Ludipress® and Emcompress® failed to produce sufficiently robust compacts when mixed in the same ratio with paracetamol and tabletted under identical conditions.

5.5.3.2 Kawakita Compression Analysis

5.5.3.2.1 Introduction

Although Heckel analysis is the most common model applied to compression data in order to elucidate compression mechanisms, many authors have cited the need to use it in conjunction with other models (Paronen and Ilkka, 1996).

By means of the Kawakita equation (Lüdde and Kawakita, 1966), further compression parameters can be derived. The Kawakita equation describes the relationship between the degree of compression of particles in a die (C) and the applied pressure (P) and is as follows:

$$\frac{P}{C} = \frac{P}{a} + \frac{1}{ab}$$ **Equation 3.5k**

The basis for the Kawakita equation is that particles subjected to a compressive load in a confined space are viewed as a system in equilibrium at all stages of compression, so that the product of the pressure term and volume term is a constant. The constants (a and b) can be evaluated from a plot of P/C versus P. The compression parameter denoted by a in the equation reflects the total degree of volume reduction of the powder at infinite applied pressure. The reciprocal of the compression parameter, b, i.e. $1/b$, has been suggested to give an indication of the stress at which the particles deform or fail during confined compression (Nicklasson and Alderborn, 2000), although the actual physical meaning of this constant has been in question (Paronen and Ilkka, 1996; Berggren *et al.*, 2004).

Many authors (Paronen and Ilkka, 1996) have urged caution in reliance on a single porosity-pressure function, given that no one equation can accurately model all stages of compression in all classes of materials. In contrast to Heckel plots, Kawakita plots give the best fit at low pressures and large to intermediate porosity and hence may be used to describe the initial stages of volume reduction (Çelik, 1992). Therefore the combined use of the two plots should provide a more comprehensive picture of the response to pressure over the entire pressure range. Furthermore, the Heckel compressibility parameters are derived through an assumption that the compact porosity tends towards zero, which may not be valid in the case of sepiolite bases. The Kawakita equation describes the change in

volume as a function of the initial bulk volume and so does not make this potentially erroneous assumption.

5.5.3.2.2 Results of Kawakita Analysis

The Kawakita profiles (Figure 5.5d) exhibit good linear correlation ($r^2 > 0.9999$) for all DCBs and therefore the equation may be used to predict the consolidation mechanisms of these bases. The compression parameters derived from the Kawakita equation are listed in Table 5.5c.

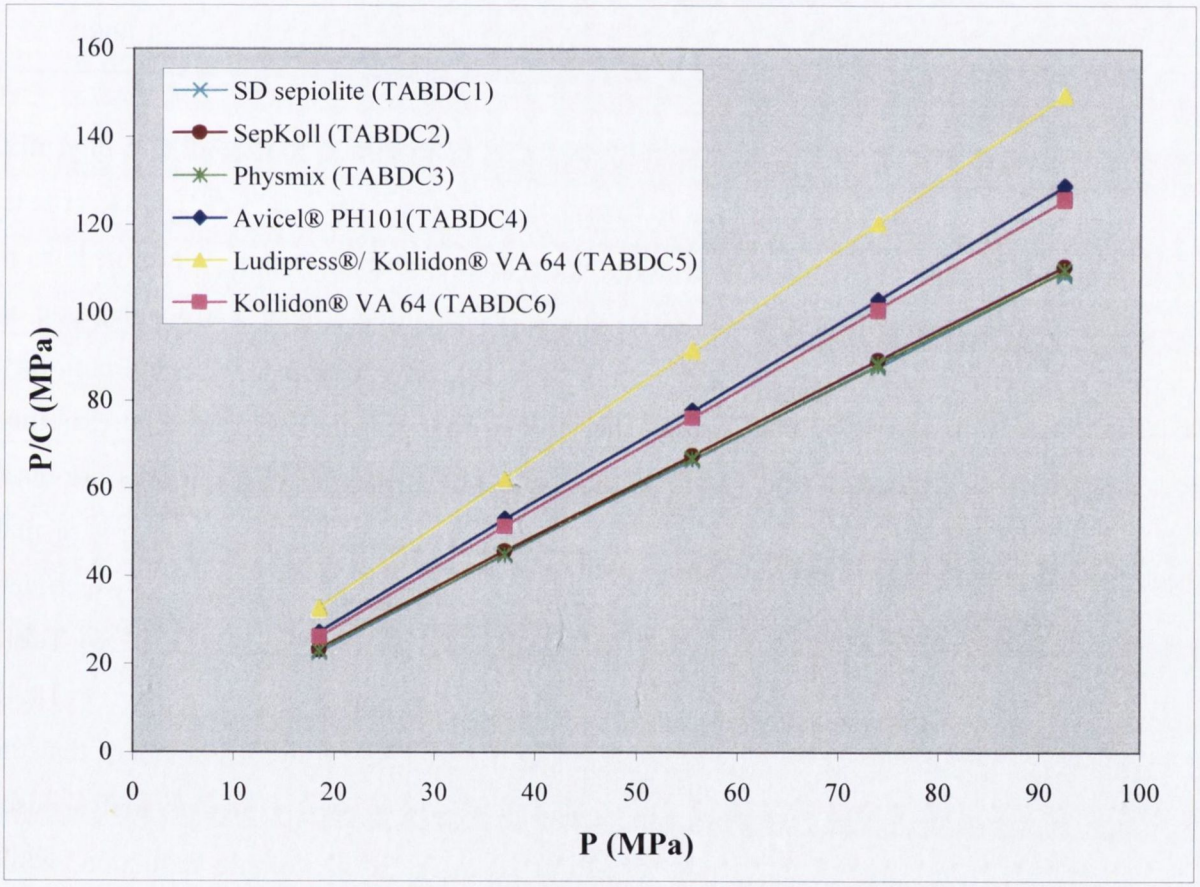


Figure 5.5d. Kawakita profiles of the different DCBs.

Table 5.5c. Kawakita constants of DCBs studied.

Formulation	DCB	Kawakita parameter, *a* (-)	Kawakita parameter, 1/*b* (MPa)	r^2
TABDC1	SD sepiolite	0.858	1.427	1.0000
TABDC2	SepKoll	0.847	1.468	0.9999
TABDC3	Physmix	0.847	1.198	0.9999
TABDC4	Avicel® PH101	0.728	1.328	0.9999
TABDC5	Ludipress®/ Kollidon® VA 64	0.631	2.105	0.9999
TABDC6	Kollidon® VA 64	0.743	0.982	1.0000

The parameter *a* (and hence compressibility) decreased as follows: SD sepiolite > Physmix = SepKoll > Kollidon® VA 64 > Avicel® PH101 > Ludipress/ Kollidon® VA 64. These results initially appear to be at odds with the compressibility values determined from Heckel analysis (AUHC), where the rank order was virtually the reverse. Consideration of the differences in the methods of calculating the Heckel and Kawakita compressibility parameters is necessary to explain this discrepancy. Firstly, the Heckel compressibility parameter is related to the response of a powder bed to further increases in pressure *after* initial packing of the powder column has occurred, while the Kawakita parameter is related to volume changes *including* those which accompany initial particle packing, which can account for the largest proportion of the volume decrease (Paronen and Ilkka, 1996). Table 5.5d presents the % volume reduction upon increasing the applied stress from zero to 18.48 MPa. From the results of Kawakita analysis and Table 5.5d below, it is evident that the total volume reduction was largest for the sepiolite blends. Secondly, Heckel analysis uses porosity (i.e. 1- (tablet density/ true density)) as an index of volume reduction, while Kawakita analysis measures volume reduction relative to the bulk volume (i.e. 1- (bulk density/ tablet density)). Hence, Heckel analysis is based on the principle that compact porosity tends toward zero, which is questionable in the case of microporous materials such as sepiolite, where the porosity tends towards a value larger than zero, and could lead to an underestimation of compressibility. The Kawakita function makes no such assumption and hence may be a more useful model to describe the compression of sepiolite.

Table 5.5d. Reduction in volume associated with initial compression at 18.48 MPa.

Formulation	DCB	Bulk volume of 505 mg DC blend (cm^3)	Compact volume at 18.48 MPa (cm^3)	% volume reduction on increasing pressure from 0 Pa to 18.48 MPa
TABDC1	SD sepiolite	2.224±0.060	0.432±0.019	80.58
TABDC2	SepKoll	2.107±0.025	0.431±0.007	79.54
TABDC3	Physmix	2.121±0.056	0.421±0.006	80.15
TABDC4	Avicel® PH101	1.253±0.025	0.399±0.005	68.16
TABDC5	Ludipress®/ Kollidon® VA 64	0.955±0.011	0.411±0.002	56.96
TABDC6	Kollidon® VA 64	1.543±0.035	0.451±0.005	70.77

The values of the Kawakita compression parameter, $1/b$, are included in Table 5.5c for completion, however, as stated earlier the actual physical meaning of this constant has been in question (Paronen and Ilkka, 1996; Berggren *et al.*, 2004). The $1/b$ parameter had previously been reported by some authors to be directly related to the yield strength of the particles which would imply that the yield strength of the formulations increased in the following order: Kollidon® VA 64 < Physmix < Avicel® PH101 < SD sepiolite < SepKoll < Ludipress/ Kollidon® VA 64. No correlation between these values and the Heckel model-derived P_y values could be made. Discrepancies between P_y values and Kawakita $1/b$ values have been reported for several excipients (Podczeck, 1996; Berggren *et al.*, 2004) and it now thought that the P_y values and $1/b$ parameters indicate different mechanical properties of the particles (Berggren *et al.*, 2004).

5.5.3.3 Correlation of results from Heckel and Kawakita Analysis

Both models appeared to fit the compression data well as indicated by high correlation coefficients. The conclusions relating to the relative order of compressibility of the bases were not consistent, and furthermore were really not comparable given their methods of calculation.

Kawakita analysis concluded that the compressibility of the sepiolite bases was of similar magnitude to Avicel® PH101; hence similar volume reduction occurred when Avicel® PH101, Kollidon® VA 64 or sepiolite powder blends were converted into compacts. The extent of this volume reduction was lower in the case of the Ludipress®/ Kollidon® VA 64 blend and may be attributed to good particle packing upon die filling such that the volume reduction associated with particle rearrangement is low.

Heckel analysis indicated that compressibility of the sepiolite bases is several times lower than Avicel® PH101, Kollidon® VA 64 and a Ludipress®/Kollidon® VA 64 blend. Hence at high pressures, where a compact had already been formed, the ability of the sepiolite blends to compress further to yield a compact of zero porosity was lower than Avicel® PH101, Kollidon® VA 64 and Ludipress®/ Kollidon® VA 64. This may be an artifact associated with the microporosity of the sepiolite structure and thus the possibility that the Heckel approach is unsatisfactory cannot be excluded. Indeed, Paronen and Ilkka (1996) noted that the Kawakita equation is generally found to provide a better fit to whole compression data than the Heckel equation, the reason being the nature of the scaling used by the Kawakita function.

Most importantly, it can concluded that the sepiolite bases underwent extensive volume reduction upon compression at reasonably low pressures resulting in sturdy compacts (refer to Section 5.5.4), indicating that the volume reduction observed was not simply associated with particle rearrangement but also brought the particle surfaces into sufficiently close contact to permit extensive bonding to take place.

5.5.4 Tensile strength profiles

Fell and Newton (1968, 1970) proposed a means of assessing the mechanical strength of tablets, which takes into account differences in compact thickness and diameter. The relationship between the tensile strengths of the compacts prepared and the relative compression pressure is shown in Figure 5.5e. The tensile strength of all tablets increased very rapidly with applied pressure, with the exception of those formulated with the Ludipress®/ Kollidon® VA 64 blend.

The areas under the tensile strength versus compression pressure plots (AUTSC) are presented in Table 5.5e. The AUTSC has been used as a direct measure of the compactibility of a material (Habib *et al.*, 1996; Kumar *et al.*, 2001). Compactibility may be defined as the ability of a powder bed to cohere into or form a compact and is usually described in terms of tablet strength as a function of applied compaction stress (Alderborn and Nyström, 1996). The AUTSC values clearly show that Avicel® PH101 formed the strongest tablets, followed closely by Physmix and SepKoll. Many authors have cited MCC as the DCB with the highest compactibility (Stamm and Mathis, 1977; Bolhuis and Chowhan, 1996). Sepiolite compares very favourably with Avicel® PH101 in terms of compactibility, particularly when combined with 10% by weight Kollidon® VA 64. The addition of Kollidon® VA 64 to SD sepiolite improved compactibility by the order of 16%. Clearly, no benefit in terms of compactibility stood to be gained from co-spray drying the two excipients as indicated by the similarity in the AUTSC values of the SepKoll and Physmix formulations, 246.98 and 248.94 MPa^2, respectively.

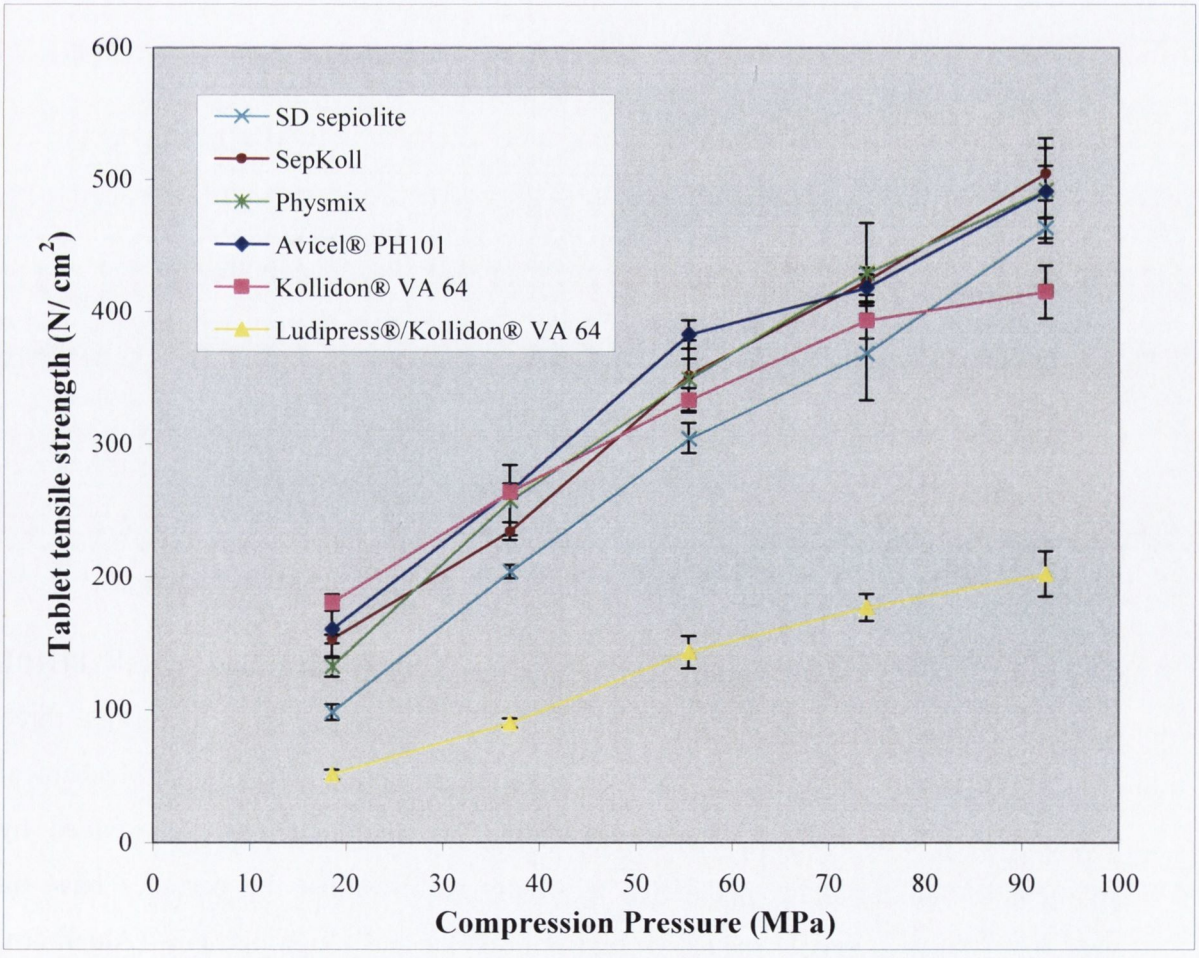


Figure 5.5e. Compactibility profiles for the different DCBs (n = 3).

The relationship between the Heckel yield values and compactibility (i.e. AUTSC) is poor (r^2 = 0.1381), indicating that while Heckel analysis can be used to assess the pressure required for deformation (i.e. compressibility), it does not necessarily give an insight into the strength of the binding forces which are formed upon application of this pressure (i.e. compactibility); a conclusion which has also been reached by other authors (Berggren *et al.*, 2004). Similarly, the Kawakita *a* parameter is not predictive of compactibility (r^2 = 0.4712). Berggren and his co-workers (2004) concluded that the compactibility of a material is largely dictated by two phenonema, namely particle deformability, which may be assessed using Heckel/ Kawakita analysis, and surface properties of the particles (roughness, surface tension), which will affect the strength of particle-particle adhesive joints. Differences in compactibility are not primarily due to a variation in the deformability/ compressibility of the particles in this instance. Führer (1977) proposed that three types of interactions may be considered to occur between particles to produce a composite; namely solid bridges, mechanical interlocking and intermolecular forces.

Table 5.5e. Compactibility data for the different DC formulations.

Formulation	**DCB**	**AUTSC (MPa^2)**
TABDC1	SD sepiolite	213.80
TABDC2	SepKoll	246.98
TABDC3	Physmix	248.94
TABDC4	Avicel® PH101	256.92
TABDC5	Ludipress®/ Kollidon® VA 64	99.19
TABDC6	Kollidon® VA 64	237.85

The very strong compacts formed by SD sepiolite, SepKoll, Physmix and Avicel® PH101 may be attributed to mechanical interlocking of the component fibers to form a three dimensional scaffold with many points of adhesion and intertwining. Mechanical interlocking is the term used to describe a situation where strength is provided by interparticulate hooking. This phenomenon usually requires that the particles have an atypical shape such as needle-shaped or highly irregular and rough particles (Alderborn, 2002). Avicel® PH101 is a direct compression base with superior bonding properties attributed to the filamentous structure of the cellulose micro-crystals (Bolhuis and Lerk,

1973). It is composed of matchstick-like particles that are mechanically interlocked and bonded by hydrogen bridges under compression (Reier and Shangraw, 1966). Sepiolite fibers bear a high concentration of silanol groups on their external surfaces, similarly providing a means of locking the fibers together through hydrogen bonding to produce very strong compacts. In addition, the external surface area of sepiolite is extremely high, providing a very large area for bonding. Furthermore, the presence of moisture within the porous structure of sepiolite acts as an internal lubricant, facilitating slippage and flow of the individual fibers during plastic deformation. The increase in compact strength on inclusion of Kollidon® VA 64 may be attributed to the extreme plastic nature of this polymer, which would facilitate filling of any void spaces to form a less porous compact in which the fibers were embedded and thereby further immobilised.

The compacts produced using Ludipress®/Kollidon® VA 64 (9:1) were comparatively weak, given the high susceptibility to deformation predicted by the low Heckel yield value. Kawakita analysis does indicate poorer compressibility, but as explained previously, this is likely to be due to highly efficient packing at zero pressure. Kah-Helbig and Lang (1987) and Goto *et al.* (1999) reported that Ludipress® particles exhibited a spherical morphology with a smooth surface. These particles will have little tendency to interlock in the manner characteristic of Avicel® PH101 (Nyström and Karehill, 1996). The occurrence of capping prior to the inclusion of Kollidon® VA 64 would support the theory of weak interparticulate adhesive bonds between Ludipress® and paracetamol particles. The incorporation of Kollidon® 30 and Kollidon® VA 64 will increase the extent of plastic deformation, however given the highly elastic nature of paracetamol, not sufficiently so as to produce a strong compact.

5.5.5 Tablet hardness and friability testing

The BP (2007) cites a requirement for testing the resistance of tablets to crushing to ensure that they possess a suitable mechanical strength to avoid crumbling or breaking on handling or subsequent processing. For each DC formulation, ten tablets, each compressed at 2000 kg (36.5 MPa), were assessed and the average result is reported in Table 5.5f below.

Table 5.5f. Results of hardness and friability testing of tablets.

Formulation	DCB	Hardness (N)	Friability (%)
TABDC1	SD sepiolite	125.00 ± 12.35	0.98
TABDC2	SepKoll	143.60 ± 3.03	0.59
TABDC3	Physmix	145.50 ± 18.01	0.70
TABDC4	Avicel® PH101	136.80 ± 14.16	0.93
TABDC5	Ludipress®/ Kollidon® VA 64	54.70 ± 4.22	12.95
TABDC6	Kollidon® VA 64	183.70 ± 14.07	0.64

One-way ANOVA confirmed that SD sepiolite, SepKoll, Physmix and Avicel® PH101 produced tablets of similar hardness, while Ludipress®/Kollidon® VA 64 produced significantly weaker tablets and Kollidon® VA 64 produced significantly stronger tablets ($p < 0.001$). Hardness values for SD sepiolite, SepKoll, Physmix and Avicel® PH101 compare favourably with hardness values for commercially available tablets cited by other authors (Bühler, 1996; Nunthanid *et al.*, 2004). The results correlate well with the tensile strength profiles above in that a similar rank order is evident. However, the tensile strength plots did not indicate that Kollidon® VA 64 produced stronger tablets than SD sepiolite, SepKoll, Physmix and Avicel® PH101. Closer inspection of the data indicated that an equal weight of Kollidon® VA 64 produced thicker compacts (average thickness values for Kollidon® VA 64, SD sepiolite, SepKoll, Physmix and Avicel® PH101 were 3.29, 3.00, 3.03, 2.93 and 2.90 mm respectively) which translated into reduced tensile strength results despite the higher hardness values.

Friability values (n = 20 tablets) are also presented in Table 5.5f. All formulations met the BP requirement (< 1 % weight loss) with the exception of Ludipress®/ Kollidon® VA 64-based tablets. Given the poor compactibility of this formulation, for reasons discussed previously, a high friability value was expected. Most importantly, the friability values of the SepKoll and Physmix formulations were lower than those of the SD sepiolite and Avicel® PH101. The inclusion of Kollidon® VA 64 therefore increases resistance to surface abrasion, again through acting as an amorphous matrix in which the sepiolite fibers are pitted.

5.5.6 Disintegration testing of tablets

The results of disintegration testing of tablets compressed at 2000 kg are presented in Table 5.5g below. One-way ANOVA indicated that all three sepiolite based formulations have similar disintegration times, while Avicel® PH101 and Ludipress®/ Kollidon® VA 64 compacts required a significantly longer time to disintegrate ($p < 0.05$). Kollidon® VA 64 compacts produced the longest disintegration times and failed to meet the 15 min limit imposed by the BP (2007) for uncoated tablets. Tablet hardness was not found to be a predictor of tablet disintegration times as indicated by a low correlation coefficient ($r^2 = 0.4554$).

Table 5.5g. Average disintegration time of paracetamol tablets prepared using the different DCBs (n = 6).

Formulation	DCB	Disintegration time (min)
TABDC1	SD sepiolite	1.11 ± 0.13
TABDC2	SepKoll	1.16 ± 0.10
TABDC3	Physmix	1.19 ± 0.06
TABDC4	Avicel® PH101	1.63 ± 0.30
TABDC5	Ludipress®/ Kollidon® VA 64	1.73 ± 0.31
TABDC6	Kollidon® VA 64	101.77 ± 2.61

It was postulated that the average disintegration time may be more closely linked with tablet porosity than tablet hardness, as this parameter will influence the rate and extent to which water can permeate the compact to promote disintegration. A strong inverse relationship between tablet porosity and disintegration rates was found for all formulations (with the exception of Kollidon® VA 64) as indicated by a linear regression coefficient (r^2) of 0.9699 (Figure 5.5f). The rapid disintegration of the sepiolite-based formulations may be attributed to the rapid uptake of water by the hydrophilic sepiolite fibers via capillary action; Alvárez (1984) reported that sepiolite is the most absorptive of all clays and is capable of absorbing more than 100% of its own weight of water. The uptake of water disrupts the interparticulate hydrogen bonding and breaks the tablet into fine pieces. The disintegration behaviour of the sepiolite compacts in hexane, a fluid with a very low dielectric constant, was studied. The dielectric constant of a solvent is a measure of a

solvent's polarity or ability to form dipoles and is, consequently, a measure of a compound's ability to hydrogen bond, since this phenomenon is a particular kind of dipole-dipole interaction (Reier and Shangraw, 1966). Hexane has been demonstrated to penetrate the sepiolite structure readily, at least to a mesoporous level (Barry, 2005). No disintegration was evident even after 8 h, thus indicating that disintegration is caused by the disruption of hydrogen bonds by the ingressing medium rather than by an explosive force generated by swelling due to medium ingression (Reier and Shangraw, 1966). MCC disintegrates via a similar wicking action (Patel *et al.*, 1994). Clearly, sepiolite functions successfully as both a filler-binder and a disintegrant.

The very long disintegration time of Kollidon® VA 64 compacts cannot be explained in terms of low porosity values; indeed the porosity of these compacts is comparable to those of Avicel® PH101. The ingression of water which precedes disintegration may be retarded in cases where the DCB is not especially hydrophilic. The hydrophobic vinyl acetate moiety of Kollidon® VA 64 may consequently slow the rate of water uptake and prolong disintegration. Furthermore, the particle-particle adhesive joints in these compacts may not take the form of hydrogen bonds which consequently are less likely to be easily disrupted by water.

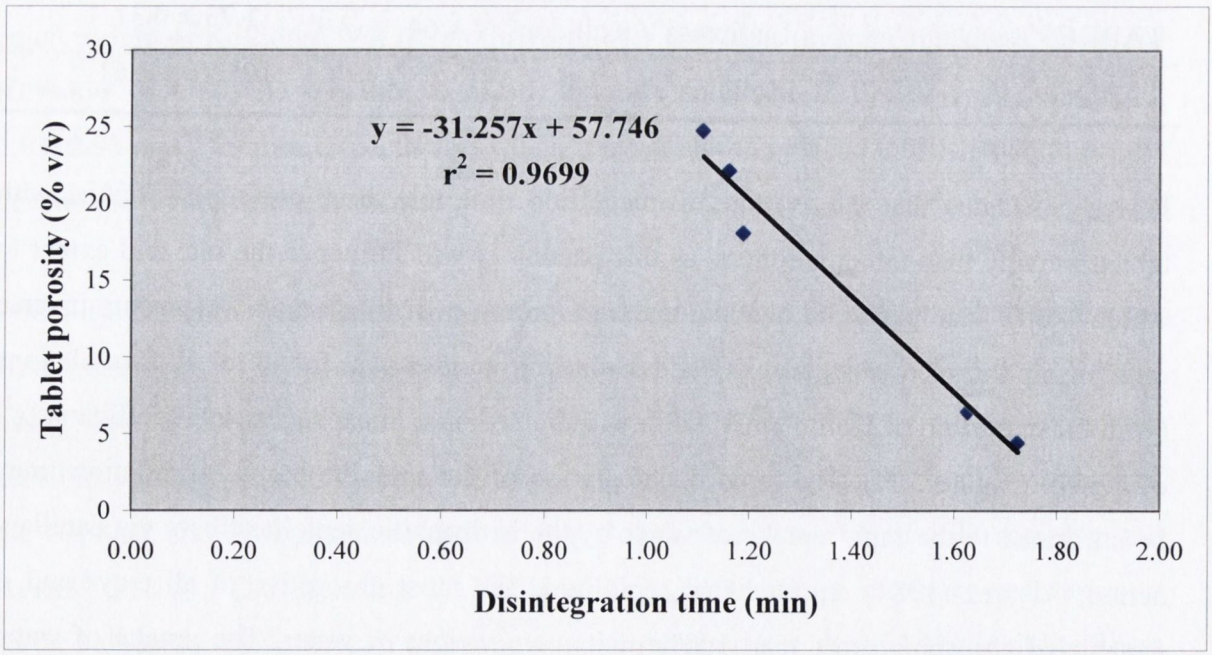


Figure 5.5f. Relationship between tablet porosity (compression at 2000 kg) and disintegration time.

5.5.7 *In vitro* drug release study

The release profiles of paracetamol from the tablets prepared are shown in Figure 5.5g. f_2 similarity factors have been used to investigate differences between release profiles (Moore and Flanner, 1996; Shah *et al.*, 1998), however their applicability is reduced in the case of products which are rapidly dissolving i.e. more than 85% in 15 min or less. As f_2 values are sensitive to the number of dissolution time points, only one measurement should be considered after 85% dissolution of the product (Shah *et al.*, 1998). Consequently, the similarity factor comparison cannot be applied meaningfully to the paracetamol release profiles shown below.

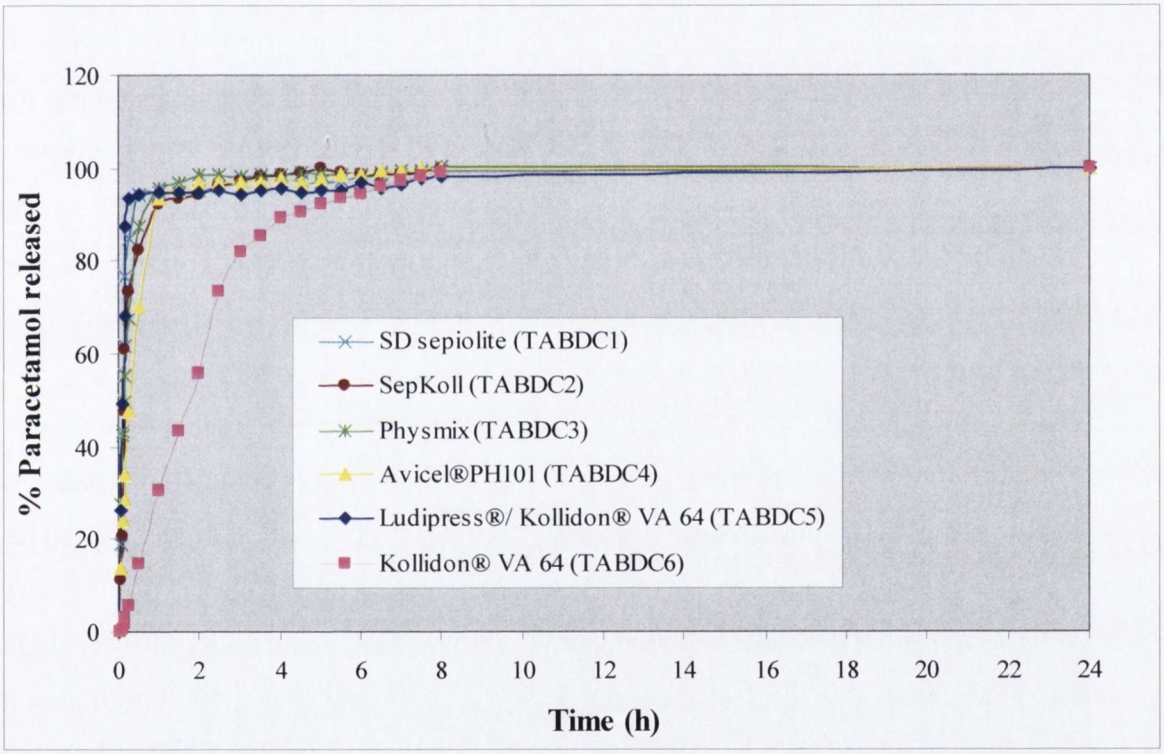


Figure 5.5g. Paracetamol release profiles from different DC tablets compressed at 2000 kg (n = 3).

It can be seen from the release profiles that paracetamol release from the three sepiolite-based formulations was rapid, with in excess of 90% drug release occurring within the first hour. Sepiolite did not therefore retard paracetamol dissolution rate as has been reported following co-administration of paracetamol with "synthetic" magnesium trisilicate (Iwuagwu and Aloko, 1992). Paracetamol release from the Ludipress®/ Kollidon® VA 64 and Avicel® PH101 formulations was comparably quick, with 95% and 94% of the total drug content released at t = 1 h. Given the similarity of the mean disintegration times, similar release profiles would be expected. The release profile from the Kollidon® VA 64

formulation was much slower, as drug availability in the dissolution medium was delayed by the robustness of the tablet which hindered exposure of the drug to the dissolution medium.

5.5.8 Surface profiling using non-contact optical profilometry

5.5.8.1 Introduction

Non-contact laser profilometry was used to quantify and characterise the surface morphology of the compacts. The roughness of the surface is a very important parameter in the case of tablets that are to be coated with a release-modifying or taste-masking film. The efficacy of such a film will be dependent on the thickness of the film which in turn is related to the nature (roughness/ smoothness) of the surface to be coated, assuming the volume of coating material remains constant (Rowe, 1978; Rowe, 1979). The surface characteristics have also been reported to be closely related to tablet porosity (Ozkan and Briscoe, 1996), dissolution rate (Healy *et al.*, 1995), compaction pressure (Toyoshima *et al.*, 1988; Riippi *et al.*, 1998; Podczeck *et al.*, 1999) and lubricant added during tabletting (Toyoshima *et al.*, 1988; Peltonen *et al.*, 1997).

SEM provides qualitative information about the surface characteristics of compacts (Karehill *et al.*, 1990). Quantitative methods may also be used and include stylus profilometry, atomic force microscopy (AFM) and non-contact optical (laser) profilometry (NOP) (Narayan and Hancock, 2003). AFM allows data acquisition at very high resolution, tending towards the molecular level. Stylus profilometry and NOP both permit data acquisition in the submicron to micron range. Although providing similar data, the stylus method requires direct contact with the surface and has been documented to cause damage (Poon and Bhushan, 1995), while NOP is based on the principal of light interference from reflected laser sources, requires minimal sample preparation and is non-destructive (Riippi *et al.*, 1998). Many researchers have used non-contact profilometry to determine the surface roughness of their tablets (Newton *et al.*, 2001; Narayan and Hancock, 2003; Bashaiwoldu *et al.*, 2004).

Surface roughness parameters are well standardised and they have been used for a long time, especially in the characterisation of metal surfaces and have recently been found to have practical importance in tablet surface studies. There are many ways of quantitatively

expressing surface roughness values including R_a (average rugosity/ roughness), R_q (RMS roughness), R_q/R_a (ratio describing surface variability), R_t (maximum peak to valley height) and R_p (distance between the highest peak and the centre line) (Rowe, 1979; Narayan and Hancock, 2003). Rowe (1979) advocates assessment of more than one parameter in order to permit comprehensive comparisons to be made between surfaces.

5.5.8.2 Results of surface profiling

Surface profiling results for the upper and lower surfaces of the compacts compressed at 2000 kg (i.e. 36.95 MPa) are presented in Table 5.5h and represent the average of measurements on three different tablets. Samples of the actual non-contact laser profiles are presented in Figure 5.5h and 5.5i. Interpretation of these profiles requires a consideration of the colour scale presented to the left of each profile as the colour scale varies from profile to profile.

Table 5.5h. Surface parameters of tablets prepared under 2000 kg compression pressure using different DCBs (n = 3).

Formulation	DCB	R_a (µm)		R_q (µm)		R_q/R_a (-)	
		Upper	Lower	Upper	Lower	Upper	Lower
TABDC1	SD sepiolite	0.67 ± 0.05	0.68 ± 0.03	0.87 ± 0.06	0.87 ± 0.03	1.31 ± 0.04	1.28 ± 0.01
TABDC2	SepKoll	0.97 ± 0.06	0.84 ± 0.03	1.32 ± 0.14	1.20 ± 0.07	1.36 ± 0.06	1.42 ± 0.08
TABDC3	Physmix	0.87 ±0.03	0.73 ± 0.04	1.17 ± 0.07	1.05 ± 0.02	1.41 ± 0.03	1.43 ± 0.06
TABDC4	Avicel® PH101	0.94 ± 0.05	0.95 ± 0.04	1.36 ± 0.02	1.41 ± 0.06	1.34 ± 0.07	1.45 ± 0.09
TABDC5	Ludipress®/ Kollidon® VA 64	0.92 ± 0.15	1.20 ± 0.28[a]	1.26 ± 0.26	1.73 ± 0.15	1.36 ± 0.06	1.43 ± 0.09
TABDC6	Kollidon® VA 64	1.04 ± 0.03[a]	1.14 ± 0.14[a]	1.47 ± 0.06	1.63 ± 0.21	1.41 ± 0.03	1.43 ± 0.06

[a]Significantly different from the R_a values of SD sepiolite ($p < 0.05$).

R_a values represent the arithmetic mean of all deviations from the central line; consequently, the closer to zero, the smoother the surface. R_a values for all compacts are quite low (0.67 – 1.20 μm) indicating the production of relatively smooth compacts. This is in agreement with Narayan and Hancock (2003), who noted that materials compressed above their yield pressure values (as all materials were in this case), should produce smooth surfaces. Paired t-tests were used to assess whether there was any significant difference between the R_a values of the upper and lower surfaces of tablets of a given formulation. Salako *et al.* (1998) noted that lower surfaces may exhibit higher R_a values as the compaction force is not fully transmitted from the upper to the lower punch. However, the R_a values of the upper surfaces did not differ significantly ($p > 0.05$) from the lower surfaces, indicating that compression force was conveyed efficiently through the powder bed for all formulations. Tukey's HSD was used to compare R_a values of the upper and lower surfaces of tablets of different formulations. The upper and lower surfaces of Kollidon® VA 64 and lower surfaces of Ludipress®/ Kollidon® VA 64 compacts were found to be significantly rougher ($p < 0.05$) than either the upper or lower surface of SD sepiolite compacts. This result was unexpected, given that the ratio of the compression pressure to the yield pressure is high, but may be a reflection of the much larger initial particle size of the Ludipress® and Kollidon® VA 64 powders. All other surfaces were not significantly different ($p > 0.05$). Analogous conclusions may be drawn from statistical analysis of the R_q values.

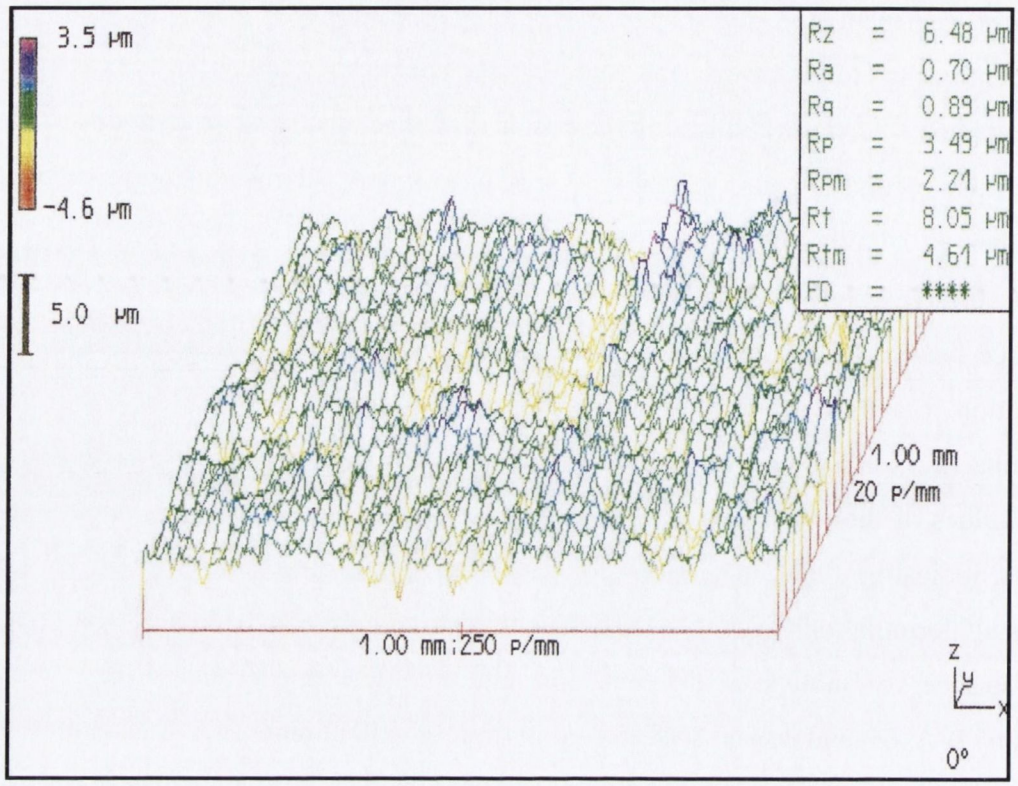


Figure 5.5h. Profile of the upper surface of a SD sepiolite/ paracetamol tablet compressed at 2000 kg.

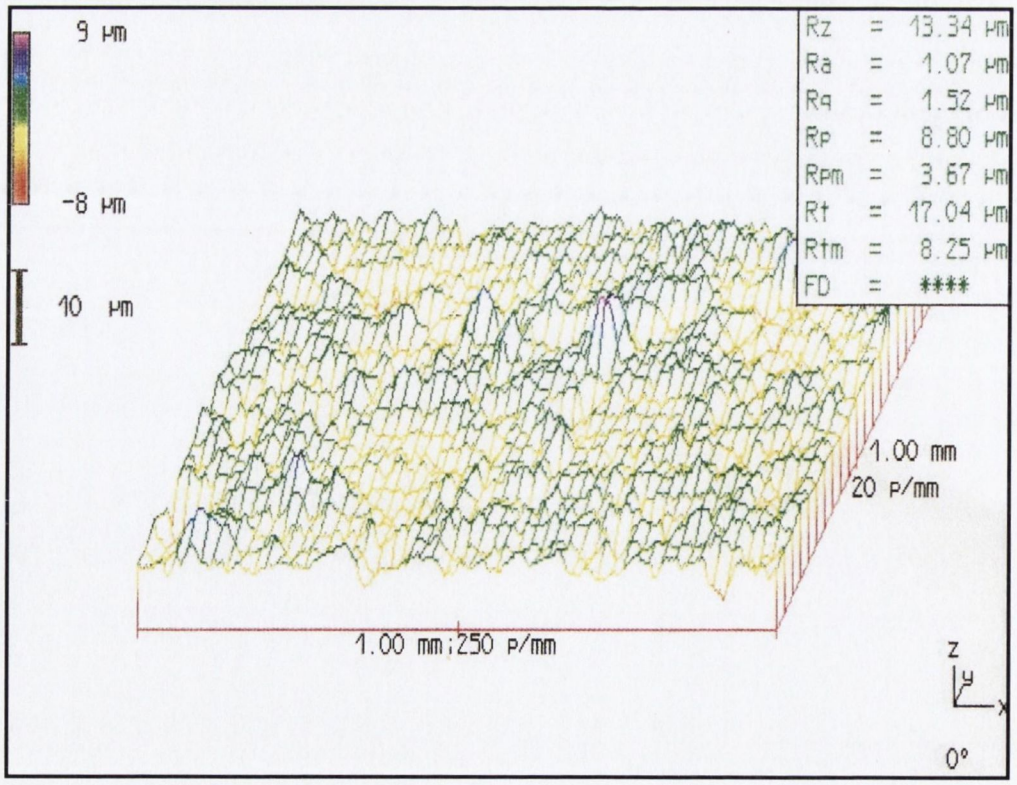


Figure 5.5i. Profile of the upper surface of a Ludipress®/ Kollidon® VA 64/ paracetamol tablet compressed at 2000 kg.

R_q/R_a may be used as an index of surface variability; if the roughness profile has regular deviations from the mean plane, then this ratio tends toward unity. An irregular spread of height deviations results in a large ratio as the RMS values are weighted higher than the arithmetic mean (Narayan and Hancock, 2003). Paired t-tests and Tukey's HSD confirmed that the surface variability did not differ between the upper and lower surfaces of a given tablet or the surfaces of tablets of different formulations, respectively. All ratios do tend toward unity (maximum value of R_q/R_a is 1.45) indicating that surface irregularity is low and the departures from the central line can be accounted for by regular deviations of similar magnitude. Low surface variability coupled with low R_a values are anticipated in the case of ductile materials compressed above their yield values as the powder particles will flatten irreversibly without fracturing upon compression, producing a compact with a smooth regular surface (Figure 5.5j; Narayan and Hancock, 2003). Consequently, the plastic nature of the materials established by Heckel analysis is further substantiated by the surface topography. Brittle materials tend to produce low R_a values but exhibit high surface irregularity due to fragmentation of most of the particles, which subsequently re-orientate to produce a smooth yet irregularly patterned surface (Narayan and Hancock, 2003).

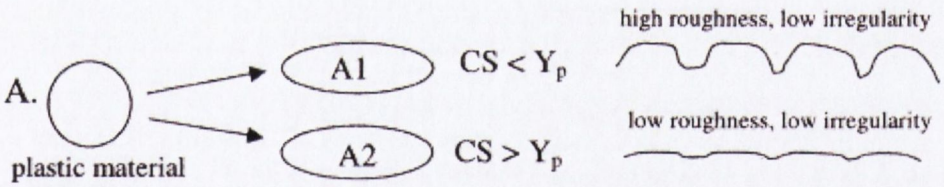


Figure 5.5j. Relationship between a plastic material, A, compressed at pressures (CS) above and below its yield pressure (Y_p) and the surface roughness and variability (Reproduced from Narayan and Hancock, 2003).

Several conclusions may be drawn from the results above; namely the three sepiolite-based formulations deform plastically to generate compacts with smooth and regular surfaces, comparable to those of the commercially available DCBs, with minimal inter-compact variation as indicated by low standard deviations associated with the surface parameters.

The effect of varying compression pressure on the surface morphology was examined for the SD sepiolite, SepKoll and Physmix formulations. Paired t-tests again confirmed that the upper and lower surfaces for a given formulation compressed at a particular pressure were not significantly different ($p > 0.05$). Hence, for simplicity, results quoted refer to the

lower surfaces of the compacts in all cases. Figures 5.5k and 5.5l illustrate the change in R_a values and R_q/R_a values with increasing compression pressure, respectively.

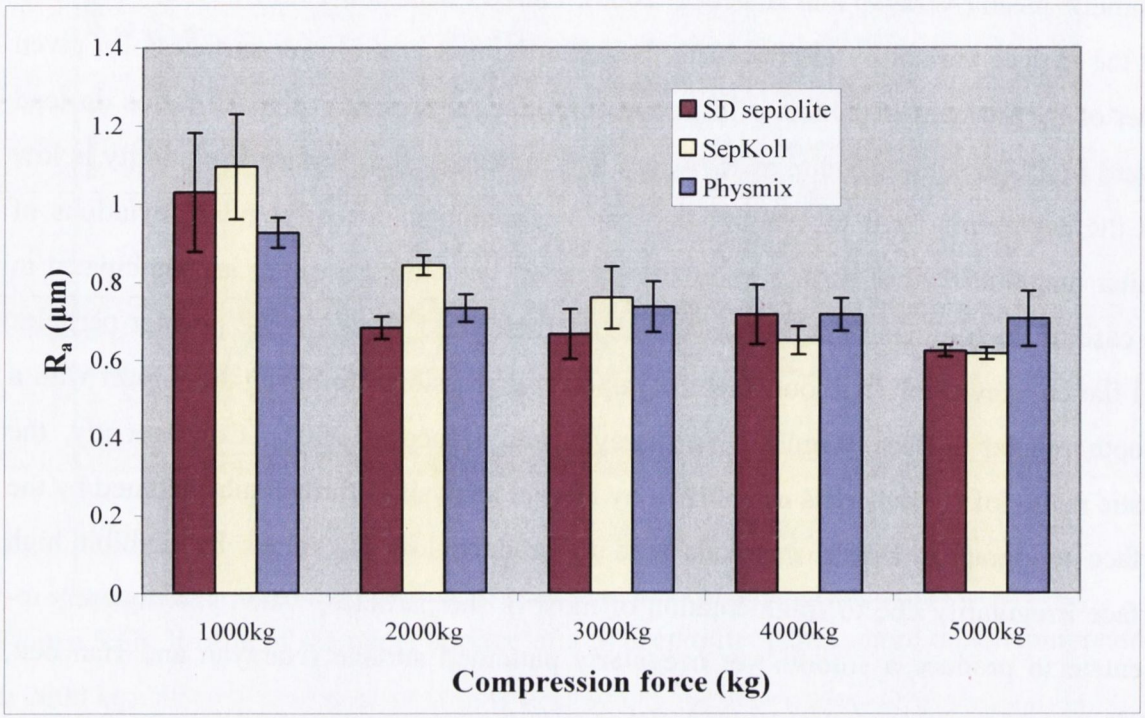


Figure 5.5k. The relationship between R_a values and compression force (n = 3).

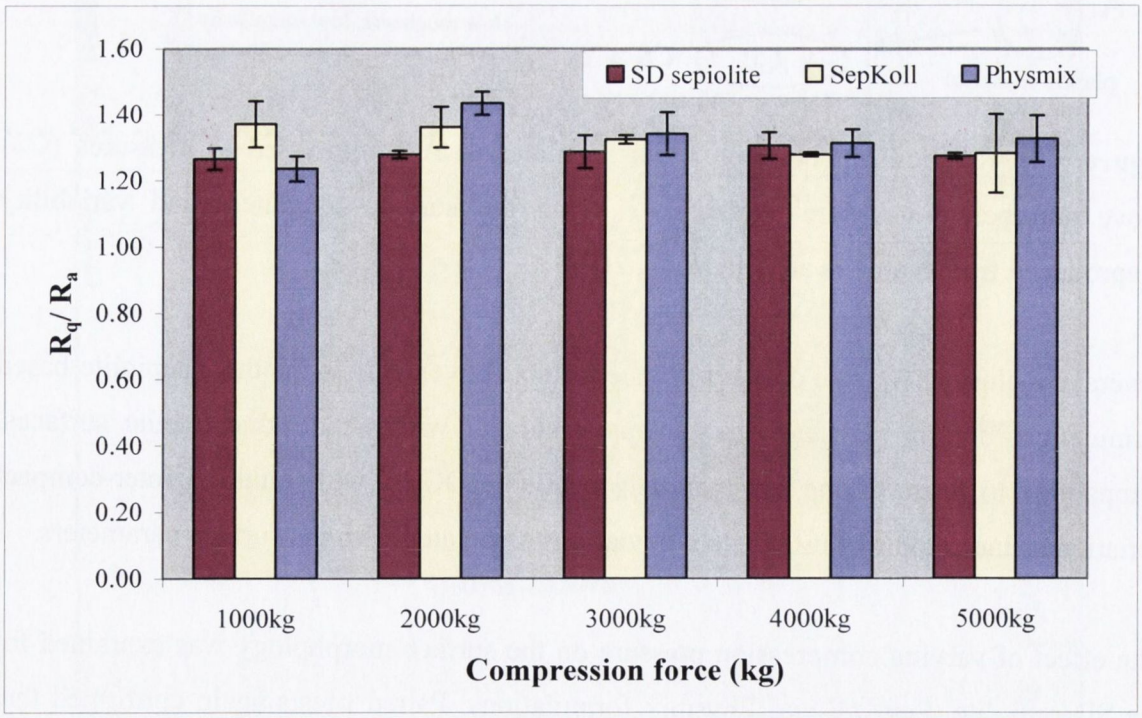


Figure 5.5l. The relationship between R_q/R_a values and compression force (n = 3).

All three formulations responded identically to an increase in the compression force. A significant reduction in the R_a value ($p < 0.05$) was observed on increasing the compression force from 1000 kg to 2000 kg (i.e. 18.35 MPa to 36.5 MPa). Other authors have also noted a reduction in surface rugosity of ethylene glycol and erythromycin acistrate compacts with increasing compression force (Rowe, 1979; Podczeck, 1998; Riippi *et al.*, 1998). However, further increases in pressure above 2000 kg did not alter the R_a value significantly. Tukey's HSD confirmed that there was no significant change ($p > 0.05$) in the surface variability (R_q/R_a) upon alteration of the compression pressure. These results may be easily explained in terms of the Narayan and Hancock model (2003) depicted above (Figure 5.5j). On increasing the compression force from 1000 to 2000 kg (i.e. 18.35 MPa to 36.5 MPa), the yield strength of the three blends was exceeded. Below the yield strength, the powder particles would be expected to retain much of their original shape and produce a rough yet regular surface profile (i.e. high R_a, $R_q/R_a \approx 1$). Above the yield strength, deformation of the original particles produces a smooth and regular surface (i.e. lower R_a, $R_q/R_a \approx 1$). In addition, it may be concluded from these results that the incorporation of Kollidon® VA 64, either as a dry powder or a co-spray dried product, did not alter surface characteristics, given that the R_a values and R_q/R_a values for the three formulations at each compression pressure were not significantly different ($p > 0.05$).

5.6 EXCIPIENT COMPATIBILITY

The successful formulation of a stable and effective solid dosage form depends on the careful selection of excipients (Indrayanto *et al.*, 1994). As outlined in Section 5.4.2.5, thermal analysis, with a particular emphasis on DSC, has been widely used in the detection of drug-excipient and excipient-excipient interactions (Ford and Rubenstein, 1981; Wissing *et al.*, 2000; Mura *et al.*, 2003).

This study was undertaken to establish the compatibility of sepiolite with paracetamol and a number of commonly used tablet excipients. A 1:1 mixture of sepiolite and the substance in question was prepared. Although this ratio was unlikely to be used in practice, 1:1 mixtures were studied to maximize the likelihood of observing possible interactions (Malan *et al.*, 1997; Fathy *et al.*, 2002). Thermograms obtained by DSC and TG analyses of the individual components were compared to those of combinations of sepiolite and the excipients (paracetamol, Kollidon® 25, Kollidon® 30, Kollidon® 90F, Kollidon® VA 64,

magnesium stearate, Explotab® and Aerosil® 200) and are presented in Appendix 5. Interpretation of the thermal data, according to appearance, shift or disappearance of endothermic or exothermic peaks indicated that sepiolite appeared to be compatible with paracetamol, Kollidon® 25, Kollidon® 30, Kollidon® 90F, magnesium stearate and Explotab® and Aerosil® 200.

5.7 CONCLUSIONS

Preliminary compression studies indicated that sepiolite deforms plastically upon compression and consequently is ideally suited to the tabletting of elastic and fragmenting drugs. Its low bulk density and poor intrinsic flowability made its use as a DCB in its untreated state unfeasible. Spray drying was investigated as a means of surmounting these shortcomings. Sepiolite was successfully spray dried from an aqueous dispersion of low solids content but yields were extremely low. The main loss of product was due to deposition on the drying chamber walls due to unsuitable drying conditions. Increases in the inlet temperature and reductions in the feed rate failed to produce any marked improvement in the yield. Use of a hydroethanolic dispersion medium reduced the extent of wall deposits, presumably by improving drying efficiency. Two mechanisms were proposed; firstly the volatility of the hydroethanolic dispersion medium was higher than the aqueous dispersion medium and hence was more easily driven off and secondly, the inclusion of ethanol reduced the apparent viscosity of the dispersion at all shear rates which translated into a reduced droplet size, thereby enhancing the mass transfer processes associated with drying. A co-spray dried product containing sepiolite and Kollidon® VA 64 (SepKoll) was also successfully produced under identical dispersion and drying conditions.

The spray drying procedure improved flowability as determined by both static (angle of repose, Carr's compressibility index and Hausner ratio) and dynamic methods (critical orifice diameter). The improvement in flowability was accounted for by an alteration in the packing of fibers within agglomerates. SEM indicated that the fibrous morphology was preserved during spray drying and the sphericity of microagglomerates improved. Increased sphericity would reduce the effective surface area for flow-hindering interactions between agglomerates. The extent of fibrous projections from the surfaces of the agglomerates was also reduced; minimizing the risk of mechanical interlocking of the fibers and powder arching. Powder-in-air particle sizing confirmed a narrowing of the size

range distribution (by volume) of the microagglomerates. The increased regularity of the size and shape of the microagglomerates led to improved packing and a consequent increase in the bulk and tapped density. Inclusion of Kollidon® VA 64 in the spray dried product (i.e. SepKoll) improved the flow properties further and shifted the particle size (by volume) distribution to slightly higher values. Flow properties of SepKoll were slightly better than the Physmix product. The flowability of modified sepiolite grades was rated as 'average' on Taylor's scale where Ludipress® represented 'excellent' flow, Kollidon® VA 64 'average' flow and Avicel® PH101 'poor' flow. Particle sizing indicated that the median particle size of the sepiolite bases was much smaller than that of the commercial DCBs. There is further scope for refinement of the spray drying process to facilitate increased particle size and improved flowability.

pXRD confirmed that the crystalline structure of sepiolite was unaltered following spray drying with or without Kollidon® VA 64. FT-IR further corroborated the conclusions of pXRD. A combination of DSC and TGA confirmed the compatibility of Kollidon® VA 64 and sepiolite. N_2 adsorption studies indicated that the external surface area was unaffected by spray drying while the micropore surface area was reduced by the order of 33%. It was postulated that this could be attributed to plugging/ narrowing of the channel cross section, possibly by replacement of some of the co-ordination water by bulkier ethanol molecules or by deposition of contaminants dissolved during the dispersion process. The adsorption data was not amenable to analysis by the BET equation. Following Sing (2004), it was proposed that the filling mechanism of the narrowed pores may be altered with a reduction in diameter, such that the assumptions underlying the BET model are no longer valid. Co-spray drying with Kollidon® VA 64 reduced the micropore surface area further presumably due to deposition of Kollidon on the fiber surfaces, thereby occluding channel openings.

The mixing properties of the novel sepiolite bases were comparable to those of Ludipress® and Kollidon® VA 64, and superior to those of Avicel® PH101. The Heckel and Kawakita equations were applied to compression data to determine the mean deformation pressure and compressibility. The Heckel method defines compressibility based on the rate at which the porosity approaches zero with increasing compression pressure, while the Kawakita model defines compressibility based on the volume reduction relative to the initial bulk volume. Heckel analysis concluded that the novel sepiolite bases exhibited poorer compressibility and higher deformation yield pressures than the commercial DCBs. The

Heckel model assumes attainment of a non-porous state at infinite compression pressure and consequently, its applicability to the compression of the novel sepiolite bases was questionable based on the presence of pressure-responsive and relatively pressure-independent pore populations within sepiolite corresponding to the interfibrous void spaces and microporous channels. Kawakita analysis concluded that the extent of volume reduction upon conversion of Avicel® PH101, Kollidon® VA 64 and novel sepiolite DCBs powders to compacts was comparable, indicative of similar compressibility. Tablet tensile strength testing indicated that the SD sepiolite DC formulation produced very sturdy compacts even at the lower end of the compression pressure range. Inclusion of Kollidon® VA 64 improved compactibility; the SepKoll and Physmix formulations exhibited compactibility comparable to the Avicel® PH101 formulation and far superior to the Ludipress®/ Kollidon® VA 64 formulation. The mechanical interlocking afforded by the fibrous and matchstick morphology of sepiolite and Avicel® PH101 respectively was one reason proposed for the more robust nature of these compacts relative to those composed of the mixture of Ludipress®/ Kollidon® VA 64. Results of friability testing confirmed the high resistance to attrition displayed by the novel sepiolite formulations. The inclusion of Kollidon® VA 64 increased resistance to surface abrasion, presumably by acting as an amorphous matrix in which the sepiolite fibers were embedded. The three sepiolite-based formulations disintegrated more quickly in water than all other formulations. The disintegration rate in hexane was several orders of magnitude lower and given the fact that hexane percolates reasonably readily through the structure, it was proposed that disintegration of sepiolite-based compacts is principally mediated via H-bond perturbation rather than through an explosive force generated by the medium ingression. The disintegration rate was found to correlate much more closely with tablet porosity than tablet hardness. Rapid release of paracetamol from sepiolite-based based compacts was observed.

Surface profiling indicated that the topography of the upper and lower surfaces of sepiolite-based compacts was comparable thus indicating efficient conveyance of the compression force through the thickness of the powder bed. The surface smoothness of sepiolite-based compacts was comparable, and in some cases superior, to those of the commercially available DCBs investigated. The low surface rugosity and variability exhibited by sepiolite-based compacts was again indicative of plastic deformation.

Thermal analysis (TGA and DSC) confirmed the compatibility of sepiolite with a host of commonly used tabletting excipients, including Kollidon® 25, Kollidon® 30, Kollidon® 90F, Kollidon® VA 64, magnesium stearate and Explotab®.

In conclusion therefore, spray drying successfully produced a grade of sepiolite which showed great potential as a DCB and as a disintegrant. The inclusion of Kollidon® VA 64 did improve compactibility and resistance to attrition. The similar performance of SepKoll and Physmix indicated that no advantage was gained by a co-spray drying step.

EVALUATION OF SEPIOLITE AS A MULTIPURPOSE EXCIPIENT IN TABLETTING BY WET GRANULATION

6.1 INTRODUCTION

As discussed in Chapter 5, few drugs possess the necessary flowability, compressibility and compactibility to permit direct compression into a robust compact (Alderborn and Wikberg, 1996). Use of a DCB to mask these undesirable attributes has been addressed in the previous Chapter. An alternative approach to conferring the necessary tabletting attributes involves pretreatment of the drug, either alone or in combination with a filler, to form granules that lend themselves to tabletting (Bandelin, 1989). Granulation confers an increase in bulk density, improved flowability, reduced risk of segregation of excipients and actives, reduced dust generation and improved compactibility through binder addition relative to a simple physical blend of the powders in the same ratio (Alderborn, 2002). Granulation processes currently employed fall into two categories: dry granulation and wet granulation, the latter being the method of interest in this Chapter.

Wet granulation is the oldest and most conventional way of making granules (Bandelin, 1989). At the most simplistic level, wet granulation involves the use of a filler, a binder, a solvent, a disintegrant and a lubricant. The aim of the wet granulation studies was to assess the merits of sepiolite as a filler, and to determine the ability of sepiolite to act simultaneously as a filler, a binder and a disintegrant. The ability of one excipient to perform these three functions would simplify the wet granulation process considerably and reduce the cost price of the raw materials and the number of suppliers to be accredited. Cole (1998) has observed that the cost of quality control (QC) associated with a product is proportional to the number of excipients; consequently, a reduction in the number of excipients translates into reduced analytical time and cost.

6.2 PRELIMINARY STUDIES - DEVELOPMENT OF FORMULATIONS AND DETERMINATION OF OPTIMUM PRODUCTION PARAMETERS

6.2.1 Development of suitable wet granulation formulations

Granulates were prepared according to the formulations described in Table 3.5b. The rationale behind each formulation is explained below.

TABF4, TABF5 and TABF6 were used to assess the merits of sepiolite as a filler for wet granulation. These formulations included paracetamol (50% w/w) as a model drug. Given that fillers are typically used in conjunction with a binder, Kollidon® 25, Kollidon® 30 and Kollidon® 90F were incorporated at concentrations of 5% w/w in TABF4, TABF5 and TABF6 respectively. Kollidon® was chosen based on its extensive use as a binder in the wet granulation of paracetamol-containing formulations (Albertini *et al.*, 2003; Odeku and Itiola, 2003; Simons *et al.*, 2005). The concentration of Kollidon® to be used was based on a review of the literature. BASF Pharma recommends the incorporation of 2 - 5% of tablet weight for Kollidon® 25 and Kollidon® 30 (BASF Soluble Kollidon® grades, 2002). Albertini *et al.* (2003) used 5% w/w Kollidon® 30 as a binder in a formulation composed of paracetamol (15% w/w), cornstarch (45% w/w), α-lactose monohydrate (30% w/w) and orange flavour (5% w/w). Liu *et al.* (1994) used 5% w/w Kollidon® 30 to develop a directly compressible free flowing grade of paracetamol.

Based on these results, it was decided to incorporate 5% w/w Kollidon® 25 / 30/ 90F in the formulation. Bühler (2003) did note that Kollidon® 90F exhibits a greater binding efficiency when compared to the lower molecular weight grades, which would permit the use of concentrations lower than 2 - 5% of the tablet weight. It was decided however that identical concentrations of all three binders would be used so as to maintain a standard concentration of sepiolite in the three formulations.

The incorporation of the binder can take a number of forms. Bühler (2003) described four different variations of the procedure:

1. Granulation of the active substance (+ filler) with a binder solution.

2. Granulation of a mixture of the active substance (+ filler) and the binder with pure solvent.
3. Granulation of a mixture of the active substance (+ filler) and a portion of the binder with a solution of the remaining binder.
4. Granulation of the active substance (+ filler) with a solution of a portion of the binder followed by dry addition of the remaining binder to the finished granulate.

Method 2 was adopted in this case (i.e. the binders were added in the dry state to the powder mass to be granulated and the mixture subsequently moistened by the required quantity of water) for a number of reasons. Firstly, use of binders in the dry state ensured a constant binder concentration in all batches; in contrast the use of a solution of Kollidon® may lead to minor fluctuations in the amount of binder added to different batches owing to variations in the quantity of liquid required to reach the granulation end point (Schmidt, 1999). Constant binder addition is essential as the mean granule size has been demonstrated to be very sensitive to the quantity of binder added (Holm *et al.*, 1996) and so minor fluctuations in the amount of binder present add a further layer of complexity when interpreting differences between different batches and formulations. Secondly, D'Alonzo *et al.* (1990) reported that the percentage of fines was reduced when Kollidon® was added as a dry powder rather than as a solution to a MCC model system in a high shear mixer. Somewhat confusingly, Alkan *et al.* (1983; cited in Schmidt, 1999) noted that the dry binder addition method produced granules with a smaller mean particle size when dealing with a lactose/starch (80%: 12%) mixture in a fluidized bed granulator. Schmidt (1999) attributed these seemingly contradictory results to the nature of the excipients and the equipment used. MCC absorbs high quantities of water before agglomeration starts allowing rapid, uniform wetting and binder dissolution to occur, while a mixture containing 80% lactose and 12% starch agglomerates immediately. The use of a high shear mixer is also preferable to a fluidized bed arrangement as it generates a better kneading action, which facilitates more intensive contact between the binder, excipients and water leading to dense packing of the material and a better distribution of the liquid (Schmidt, 1999). Given the tendency of sepiolite to absorb large quantities of water prior to agglomeration (in a similar manner to MCC) and the nature of the mixing equipment available (Kenwood planetary mixer with the kneading 'K' attachment), it was proposed that the dry binder addition method be used in the current study.

The TABF7 formulation was designed to evaluate sepiolite as a filler-binder. Assessment of the ability of sepiolite to act concurrently as a filler and a binder was prompted by the reports of a decrease in the friability of pellets composed of animal feed stuffs on incorporation of sepiolite (Angulo *et al.*, 1995). The tensile strength results for DC compacts presented in Section 5.5.4 indicated that sepiolite was capable of generating very strong compacts with low friability in the absence of any binder. The binding capacity was attributed firstly to the extremely high concentration of silanol groups on the very large external surface area, which permitted extensive hydrogen bonding to take place and secondly to the ability of the fibers to physically intertwine and interlock to rivet the compact together. It was postulated that sepiolite may be capable of producing granules of similarly low friability and high compactibility in the absence of a binder. The poor flowability of untreated sepiolite is unlikely to be hugely problematic as the densification and agglomeration processes occurring during granulation generate reasonably spherical particles of increased mean particle size and consequently good flowability.

The TABF8 formulation is based on the TABF7 formulation but includes 2.4% w/w sodium starch glycolate (Explotab®) as a disintegrant. Half the disintegrant was included intragranularly and half extragranularly to facilitate the break-up of the tablet into granules and then into the primary particles. In a study conducted by Shangraw *et al.* (1987), sodium starch glycolate was rated by formulators as one of the top four disintegrants on account of its compatibility with a wide range of drugs and excipients and its superb disintegration action; hence its selection in this study. In addition it has been demonstrated to be an effective disintegrant in the case of insoluble filler-binders (Van Kamp *et al.*, 1986). Comparison of the properties (in particular disintegration time and paracetamol release profile) of TABF7 and TABF8 would indicate whether the incorporation of a disintegrant conferred any benefits on the formulation.

MCC (Avicel® PH101) has been extensively used in the wet granulation process of tablet making (Bandelin, 1989; Propst, 2002) for reasons addressed in detail in Chapter 1. Avicel® PH101 represents an 'all-in-one' standard against which the filler/binder/disintegrant properties of sepiolite can be assessed; hence the rationale for the TABF9 formulation, which differs from TABF7 only in the replacement of sepiolite by Avicel® PH101.

6.2.2 Establishing suitable production parameters

The mixing times, speeds and quantity of granulating solvent used were based on the conditions required to produce a cohesive plastic mass with a uniform paracetamol content throughout. Both mixing time and speed were kept constant for all formulations as there are many reports of variations in the finished product characteristics following changes in granulation times (Soyeux *et al.*, 1998; Suzuki *et al.*, 2001) and mixing speeds (Knight *et al.*, 2000). The quantity of granulating liquid required did vary between formulations, given the different nature of the excipients, but was kept constant for all batches of a given formulation. Other researchers have also observed changes in the wettability of formulations when the components were changed (Jaiyeoba and Spring, 1980; Eerikäinen, 1991; Elbers *et al.*, 1992). Drying of the moist granulate was concluded when the granule moisture content lay in the range 4 - 5% w/w. The weight loss associated with water evaporation was used to give an indication of the drying end-point which was then confirmed by KF analysis. This final moisture content range was selected for a number of reasons. Firstly Bolhuis and Chowhan (1996) reported that the compactibility of MCC depends on the moisture content; they proposed that at its equilibrium moisture content (5% w/w), most of the water will be within the pores of the MCC structure thus facilitating slippage and plastic flow upon compression. Reduction in the moisture content results in a decrease in compactibility due to the reduced number of hydrogen bond bridges formed (Khan *et al.*, 1981). Secondly, Garr and Rubinstein (1992) noted that moisture content had a considerable impact on the consolidation and compaction characteristics of paracetamol. Their studies concluded that the capping tendency and mean yield pressure were reduced, and tablet apparent density and crushing strength increased with increasing moisture content up to 6% w/w. Further increases in the moisture content resulted in a reduction in compact strength.

Finally, the influence of moisture content on the compaction properties of sepiolite was investigated. Five batches of the TABF7 formulation were prepared in an identical fashion but dried to different extents so as to produce granulates with moisture contents in the range 3.2 to 10.6% w/w. The resulting flowability parameters, tablet friabilities and hardness values were determined and compared. The flowability indices are presented in Table 6.2a. Figure 6.2a correlates the friability values with tablet hardness values. It should be noted that fines in excess of 10% w/w were excluded from the granules to be

compressed and the compression weight was adjusted for granulates of different moisture content in order to ensure a constant paracetamol content of 250 mg per tablet.

One-way ANOVA of the tablet hardness results indicated that formulations B, C and D (moisture contents of 4.0, 6.2 and 8.5% w/w, respectively) produced significantly harder tablets ($p < 0.05$) than formulations E and F (moisture contents of 9.8 and 10.6% w/w), which in turn produced harder tablets than formulation A (moisture content 3.2% w/w). Hence, the optimum moisture content for tablet hardness is of the order 4 – 8.5% w/w. Our findings are qualitatively similar to those of Garr and Rubinstein (1992), who reported that a certain moisture content is necessary as it acts as a lubricant promoting compaction force transmission and formation of strong hydrogen bonds. Moisture contents in excess of this optimum reduce particle-particle contact area, surface energy and corresponding adhesive forces.

From Figure 6.2a it is evident that the resistance of formulations B, C and D to attrition was higher than that of formulations A, E and F, providing further evidence of a reduction in particle-particle adhesive joint strength with moisture contents outside the optimum range of 4 – 8.5% w/w.

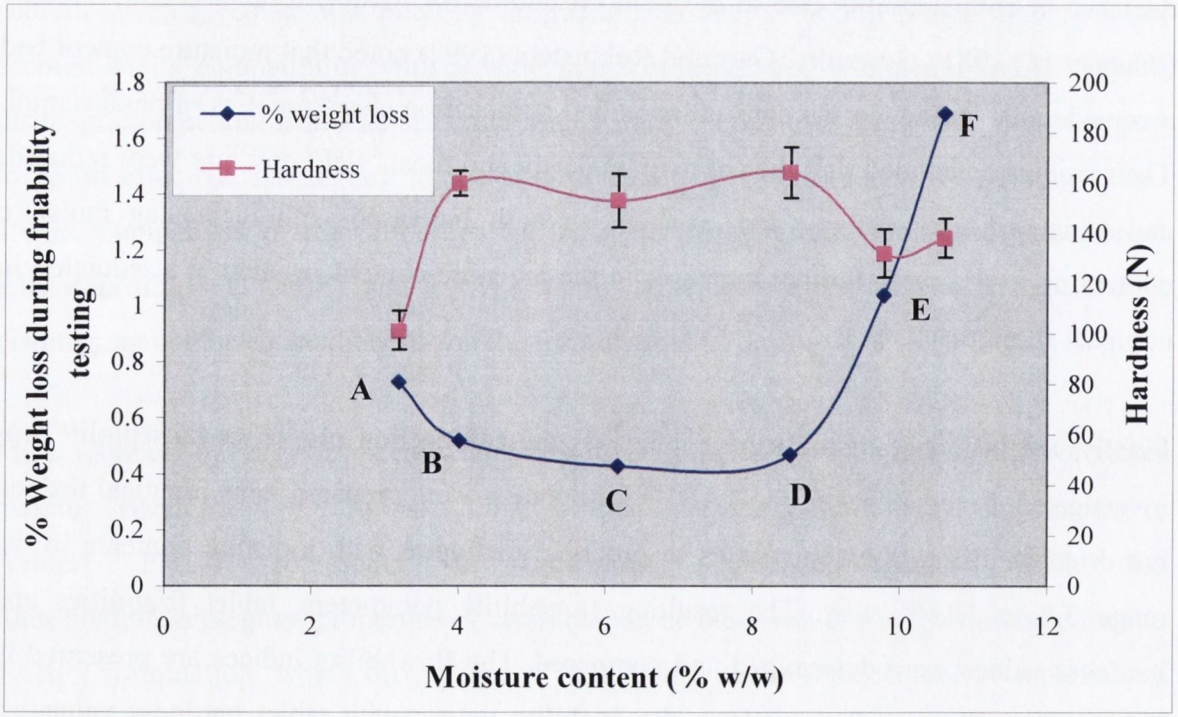


Figure 6.2a. Relationship between moisture content, % weight loss during friability testing and tablet hardness testing (n = 10) for TABF7 formulations.

Taylor's composite index predicts excellent flowability for all formulations, in particular for formulation B (Table 6.2a). The differences between the tapped and bulk densities for each formulation were calculated. Comparison of these differences using ANOVA indicated that the difference between the tapped and bulk density was significantly lower in the case of formulation B ($p < 0.05$). This translates into significantly lower Carr's indices and Hausner ratios for this formulation. Large differences in the tapped and bulk densities can lead to significant processing problems, in particular with achieving uniformity of tablet weight. One-way ANOVA of the angle of repose results indicate that those of formulations A-D are comparable ($p > 0.05$), while that of formulation E is higher and that of formulation F is higher again ($p < 0.05$). The critical orifice diameter is the same for all formulations. The optimum moisture content for flowability is therefore of the order of 4% w/w.

Hence consideration of results from the literature for MCC and paracetamol, together with experimental results for sepiolite, indicates that a final granulate moisture content of 4-5% w/w is appropriate; given that it is within this range that optimum compactibility (and additionally in the case of sepiolite, optimum flowability) was observed.

Table 6.2a. Flow properties of TABF7 granulates as a function of moisture content (Flow properties were evaluated following removal of fines in excess of 10% by volume).

Formulation	Moisture content (% w/w)	Bulk density (g/cm^3)	Tapped density (g/cm^3)	Angle of repose (°)	Carr's index (-)	Hausner ratio (-)	Critical orifice diameter (mm)	Taylor's composite flow index (-)
A	3.2	0.43 ± 0.00	0.51 ± 0.01	32.2 ± 0.3	15.98 ± 0.97	1.19 ± 0.01	5	86.70
B	4.0	0.48 ± 0.01	0.53 ± 0.02	31.2 ± 0.8	9.08 ± 0.98	1.10 ± 0.01	5	91.40
C	6.2	0.45 ± 0.00	0.54 ± 0.01	31.2 ± 0.5	16.41 ± 1.20	1.20 ± 0.02	5	87.14
D	8.5	0.46 ± 0.02	0.56 ± 0.01	31.6 ± 0.0	16.99 ± 2.03	1.21 ± 0.03	5	86.49
E	9.8	0.45 ± 0.01	0.53 ± 0.02	33.9 ± 0.3	14.74 ± 1.26	1.17 ± 0.02	5	86.46
F	10.6	0.47 ± 0.01	0.54 ± 0.00	35.5 ± 0.0	14.42 ± 0.19	1.17 ± 0.00	5	85.59

6.3 CHARACTERISATION OF GRANULATES

6.3.1 Uniformity of drug content

Prior to compaction of the granules, the uniformity of mixing was confirmed by assaying random samples of weight equal to the calculated compression weight for paracetamol content by UV spectroscopy. In accordance with other authors (Odeku and Itiola, 2003), uniform mixing was deemed to have been achieved where the actual paracetamol content was within ± 5% of the theoretical content (i.e. 250 mg). The results of two samplings of each of three batches of each formulation are presented in Table 6.3a below.

Table 6.3a. Uniformity of drug content results for the dry granulate.

Formulation	% theoretical paracetamol content					
	Batch 1		Batch 2		Batch 3	
	Sample 1	Sample 2	Sample 1	Sample 2	Sample 1	Sample 2
TABF4	95.49	98.44	102.26	104.65	99.02	104.69
TABF5	96.51	99.17	101.37	100.09	96.64	96.24
TABF6	96.44	101.75	98.69	97.50	103.75	102.35
TABF7	98.32	96.01	103.94	104.24	102.73	104.24
TABF8	97.25	100.09	99.70	97.35	99.21	97.93
TABF9	103.07	99.91	103.83	104.02	100.15	104.35

All granules contained within ± 5% of the stated paracetamol content, confirming that adequate mixing was achieved under the mixing conditions cited in Section 3.5.6.1.

6.3.2 Granulate flowability

One of the principal aims of wet granulation is to improve flowability through densification of the mixture and increasing particle size and sphericity. A number of static measures of flow (angle of repose, Carr's compressibility index, Hausner's ratio) and dynamic measures (critical orifice diameter) were used to ascertain if this aim had been accomplished. The results are outlined in Table 6.3b below. It should be noted that the bulk densities of the dry mixes were of the order of 0.16 - 0.18 g /cm^3 for TABF4 to TABF8 and 0.40 g/ cm^3 for TABF9. It is evident that the bulk densities of all sepiolite granulates were approximately three-fold higher than the dry mixes of the excipients in the same

ratio. Consequently densification of the material was successfully achieved through wet granulation. One-way ANOVA indicated that there was no significant difference in the bulk density values of any of the six granulates ($p > 0.05$). In addition, the standard deviations, which represent batch-to-batch variation in bulk density, were small indicating that the granulation process and formulations were robust.

Similarly, no significant difference in the tapped density values of the six formulations was evident. Carr's compressibility indices were all within the range indicative of excellent flow (i.e. 5-15; Carr, 1965). Hausner ratios of < 1.11 in all cases were predictive of good flow as were the angle of repose values (Copley scientific website, 2002). Dynamic measures of flow (critical orifice diameter) further corroborate the conclusions of the static measures. Finally, calculation of Taylor's composite flow indices (Taylor *et al.*, 2000) yielded values close to the perfect score of 100, indicating that the granulate flowability is on a par with commercial products such as spray dried lactose monohydrate USP (Super Tab®). Taylor's composite indices for the initial dry powder blends are of the order of 50, indicative of extremely poor flow. As expected, the poor flowing initial blend of powders acquired very good flow through wet granulation.

Table 6.3b. Flowability data for the TABF granulates (n = 3; each sample is representative of a different batch).

Formulation	Bulk density (g/cm^3)	Tapped density (g/cm^3)	Angle of repose (°)	Carr's index (-)	Hausner ratio (-)	Critical orifice diameter (mm)	Taylor's Composite Index (-)
TABF4	0.49 ± 0.02	0.53 ± 0.01	28.2 ± 1.0	7.25 ± 0.62	1.08 ± 0.01	5	95.25
TABF5	0.48 ± 0.01	0.53 ± 0.02	31.2 ± 0.8	9.08 ± 0.98	1.10 ± 0.01	5	92.02
TABF6	0.49 ± 0.00	0.54 ± 0.01	32.7 ± 0.5	8.87 ± 0.91	1.11 ± 0.03	5	91.18
TABF7	0.47 ± 0.01	0.51 ± 0.01	32.6 ± 0.5	8.68 ± 0.86	1.10 ± 0.01	5	91.40
TABF8	0.44 ± 0.00	0.48 ± 0.01	31.9 ± 1.2	8.37 ± 1.61	1.10 ± 0.02	5	92.04
TABF9	0.41 ± 0.03	0.45 ± 0.03	33.3 ± 1.3	7.17 ± 1.10	1.08 ± 0.01	6	90.81

6.3.3 Microscopic structure of granules

SEMs of granules from the six TABF formulations, taken prior to the removal of excessive fines, are presented in Figures 6.3a – 6.3f below. There was little evidence of debris in any of the SEMs, which is suggestive of reasonable binding capacity and high granule robustness in all formulations. All SEMs were taken at the same magnification (x 50) and so permit a qualitative comparison of particle size and shape. The individual granules appeared to have a more oblong than spherical appearance, which was probably attributable to the nature of the granulation process, where the width of the granules was dictated by the sieve aperture and the length by the cohesive nature of the wet mass being forced through the sieve. The surface of TABF8 granules appeared to be more rugged than that of the other formulations. Granule size appeared to be similar in all formulations.

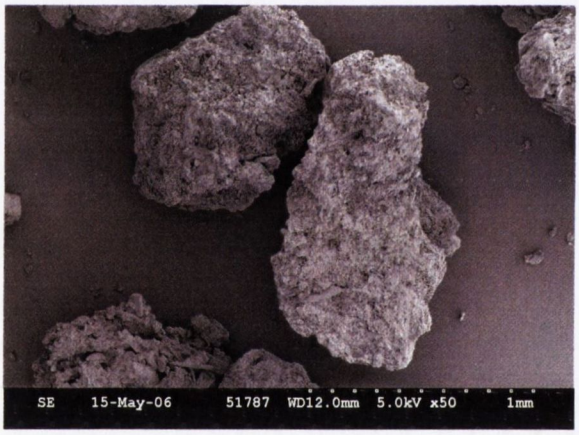


Figure 6.3a. SEM of TABF4 granules (magnification x 50).

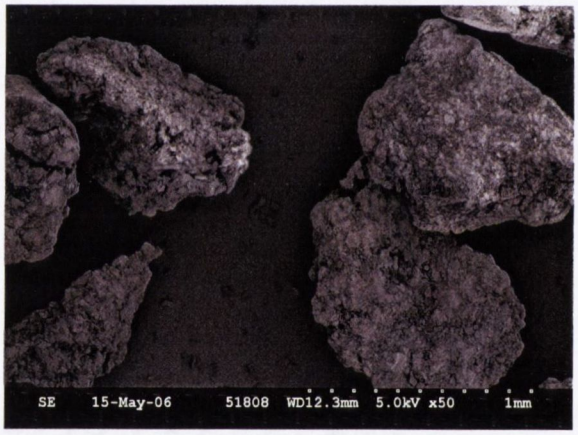


Figure 6.3b. SEM of TABF5 granules (magnification x 50).

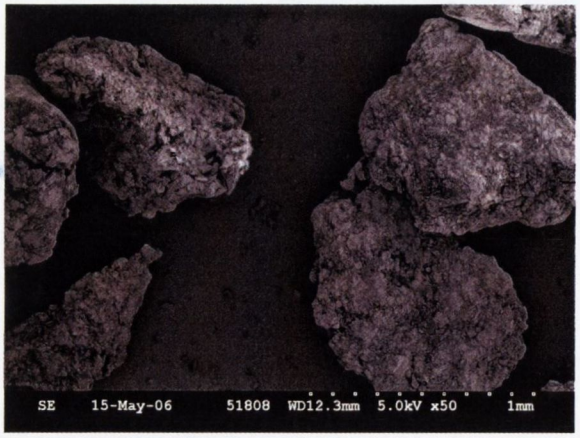


Figure 6.3c. SEM of TABF6 granules (magnification x 50).

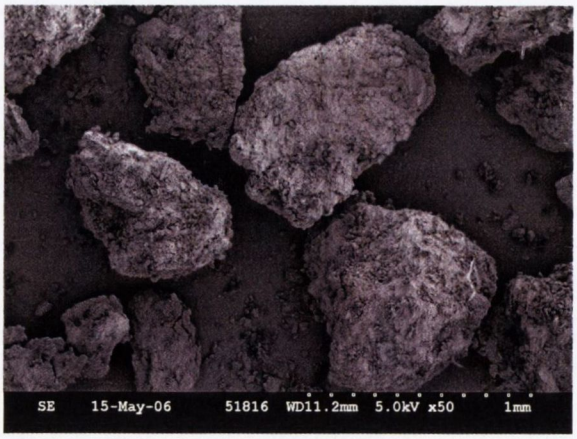


Figure 6.3d. SEM of TABF7 granules (magnification x 50).

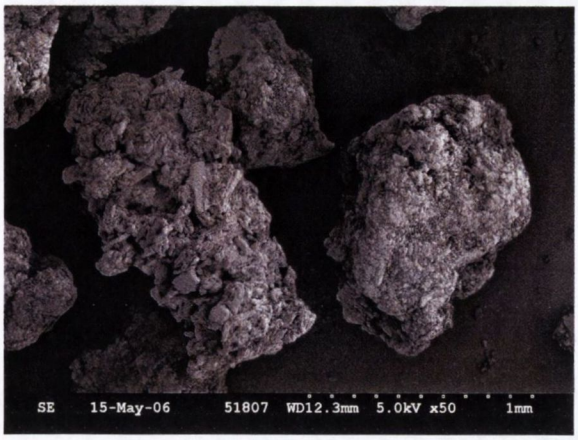


Figure 6.3e. SEM of TABF8 granules (magnification x 50).



Figure 6.3f. SEM of TABF9 granules (magnification x 50).

6.3.4 Granule sizing

Comprehensive quantitative analysis of the granule size distribution was carried out using the Malvern Mastersizer 2000 with the powder-in-air cell (Scirocco® 2000). Measurements were initially made at 60% vibration and 2 bar pressure. However, huge variability between batches was found to exist and in addition, there was huge variability on repeated sampling from the same batch. Qualitative assessment of the granule size from SEM did not corroborate the quantitative results. It was postulated that the dispersive air pressure used was too high and led to a milling effect prior to sizing. As granules are composed of a number of primary particles, they would be particularly vulnerable to this milling effect. Size analyses were repeated using a lower vibration (50%) and dispersive air pressure (0.5 bar) which led to improved repeatability and correlation with the SEM images. Keleb *et al.* (2004) also noted the need to measure granule size at minimal air pressures to avoid deagglomeration and/or disintegration of the granules during the test. These results are presented in Table 6.3c below. The standard deviations quoted represent between batch variability.

Table 6.3c. Granule size distribution by volume (% volume undersize; n = 3).

Formulation	d10 (µm)	d50 (µm)	d90 (µm)
TABF4	281 ± 21	581 ± 8	1071 ± 8
TABF5	236 ± 24	567 ± 5	1038 ± 20
TABF6	367 ± 32	667 ± 24	1159 ± 46
TABF7	234 ± 10	612 ± 26	1146 ± 59
TABF8	213 ± 24	574 ± 9	1072 ± 21
TABF9	128 ± 15	523 ± 31	1004 ± 55

The particle size distributions may be used as a means of assessing the strength of the cohesive binding forces within the formulation. The greater the binding, the smaller the volume of fines (i.e. high d10 values) and the larger the coarse fraction (i.e. high d50, d90 values). One way ANOVA was carried out on the d10, d50 and d90 values and the results presented in Figures 6.3g - 6.3i below.

TABF9	TABF8	TABF7	TABF5	TABF4	TABF6
128	213	234	236	281	367

Figure 6.3g. ANOVA comparison of d10 values for each formulation (There is no significant difference (i.e. $p > 0.05$) between products joined by a black line).

TABF9	TABF5	TABF8	TABF4	TABF7	TABF6
523	567	574	581	612	667

Figure 6.3h. ANOVA comparison of d50 values for each formulation (There is no significant difference (i.e. $p > 0.05$) between products joined by a black line).

TABF9	TABF5	TABF4	TABF8	TABF7	TABF6
1004	1038	1071	1072	1146	1159

Figure 6.3i. ANOVA comparison of d90 values for each formulation (There is no significant difference (i.e. $p > 0.05$) between products joined by a black line).

From one-way ANOVA of the d10 values, it was evident that the d10 values of TABF4, TABF5, TABF7 and TABF8 did not differ significantly. The d10 value of TABF6 was significantly higher than the rest, while that of TABF9 was significantly lower ($p < 0.05$). It may be concluded that TABF6 produced the smallest volume of fines. Given that low levels of fines are reflective of high binding capacity within the formulation, it is evident that the TABF6 formulation exhibits superior binding ability. Furthermore, the d50 value of the TABF6 formulation was significantly higher than all other formulations, while the d90 value was higher than all formulations apart from TABF7, which is indicative of a large coarse fraction.

Comparison of the particle size distributions of TABF4, TABF5 and TABF6 permits an assessment of the relative binding properties of Kollidons® 25, 30 and 90F, respectively. The d10, d50 and d90 values of TABF4 and TABF5 did not differ significantly, while the corresponding values for TABF6 were significantly higher. Hence Kollidon® 90F exhibits superior binding properties when compared to Kollidon® 30 or Kollidon® 25, while these two lower molecular weight grades exhibit similar binding action. This result is in agreement with the BASF product literature and also with the work of Bühler (2003), who observed that the coarse fraction of a corn-starch granulate prepared using 5% w/w Kollidon® 25 /30 / 90F increased and the fine fraction reduced to a greater extent with Kollidon® 90F than with the other two grades of lower molecular weight. He also noted no major differences in the particle size distribution of the granules produced by Kollidon® 25 and Kollidon® 30. As the relative order of binding efficiency is consistent with other literature, it may be concluded that the Kollidons® were capable of performing their binding action within these formulations.

The ability of sepiolite to act as a sufficiently strong binder to permit exclusion of a traditional binder such as Kollidon® from the formulation may likewise be evaluated by a

review of the particle size distributions of TABF4, TABF5, TABF6 and TABF7. The d10 and d50 values of TABF7 were not significantly different from those of TABF4 and TABF5 ($p > 0.05$), while the d90 value was significantly higher ($p < 0.05$). Hence the addition of 5% w/w Kollidon® 25 or 30 did not produce a discernible increase in the strength of binding above that already achieved through incorporation of sepiolite within the formulation. In contrast, Bühler (2003) has noted a considerable shift in the particle size distribution to higher values following the inclusion of 5% w/w (and in some cases < 5% w/w) Kollidon® 25 or 30 in other formulations. The fact that the resulting size distribution cannot be improved further through addition of the recommended amount of Kollidon® 25 or 30 indicated that the binding influence of sepiolite is similar to that of these low molecular weight Kollidons®. Comparison of the particle size distributions of TABF6 and TABF7 indicated that the incorporation of 5% w/w Kollidon® 90F did reduce the proportion of fines significantly and so did improve the strength of binding within the formulation. From our results, it may be concluded that sepiolite is an extremely good binder, on a par with Kollidons® 25 and 30 but weaker than Kollidon® 90F. Kollidon® may therefore be omitted from the formulation entirely, certainly without detriment to the particle size distribution or flowability. The impact of such a formulation change on the resultant tablet properties will need to be evaluated before it may be definitively concluded that the inclusion of a traditional binder is unnecessary.

Comparison of the particle size distributions of TABF7 and TABF9 allowed the binding ability of sepiolite to be rated against that of MCC. The binding action of MCC in a wet granulation context has been well documented (Bandelin, 1989; Bolhuis and Chowhan, 1996; Propst, 2002). The d10, d50 and d90 values of TABF9 were significantly lower than those of TABF7, suggesting that the binding action of sepiolite is superior to that of MCC. Although the mechanism of binding is likely to be similar in both cases (i.e. a combined effort of hydrogen bonding and mechanical interlocking), the much larger external surface area of sepiolite (~114 m^2 /g *vs.* 1.3 m^2 /g (Zografi *et al.*, 1984)) could potentially facilitate a greater number of hydrogen bonding interactions per unit weight, thus explaining the difference in binding efficiency.

6.3.5 Granule friability

A second parameter used to assess the quality of granules is resistance to attrition i.e. granule friability. The resistance of granules toward attrition is of huge importance during the handling and processing of granules (Wikiberg and Alderborn, 1996). Reports in the literature do correlate reduced friability levels with greater binder efficiency. Watano *et al.* (2001) observed an inverse relationship between friability of lactose, MCC and corn starch pellets and the extent of binder dispersion. Cutt *et al.* (1986) did note that increased concentration of binder in granules led to increased resistance to attrition. The friability of granules is a function of both the surface geometry, with particles of regular geometric shape and smooth surface texture being more likely to display high resistance to attrition, and the bonding forces of interparticulate attraction. The relative importance of these two variables appears to be formulation dependent (Wikberg and Alderborn, 1996). Low friability, whether attributable to a more regular surface shape or higher binding efficiency or a combination of both, is desirable. The friability results for the different TABF formulations are presented in Table 6.3d below and represent the average and standard deviation of three determinations, each one on a different batch of the formulation in question.

Table 6.3d. Granule friability results.

Formulation	Friability (%)
TABF4	13.09 ± 1.89
TABF5	15.15 ± 2.31
TABF6	13.96 ± 3.55
TABF7	16.96 ± 0.77
TABF8	25.48 ± 4.50
TABF9	26.12 ± 1.51

Tukey's HSD indicated that the friabilities of TABF4, TABF5, TABF6 and TABF7 were not significantly different ($p > 0.05$), indicating that incorporation of a traditional binder does not improve granule quality above that achieved using sepiolite alone. Friability

values associated with TABF8 and TABF9 were significantly different from TABF7 ($p < 0.05$) and very significantly different from TABF4, TABF5 and TABF6 ($p < 0.01$). The quality of granules produced in the absence of a binder i.e. TABF7, TABF8 and TABF9 differed quite substantially. As granule friability is in part related to the regularity of particle shape and surface, the superior friability of TABF7 formulations cannot be ascribed solely to the superior binding properties of sepiolite when compared to Avicel® PH101. What may be concluded however is that replacement of Avicel® PH101 by sepiolite results in an improvement in the quality of the granules produced.

The high friability of the TABF8 formulation indicates that the binding influence of sepiolite is somewhat disturbed by the inclusion of the disintegrant, sodium starch glycolate (Explotab®), within the formulation. The major function of a disintegrant is to oppose the efficiency of the tablet binder to permit the tablet to break apart when placed in an aqueous environment (Bandelin, 1989). In order to fulfill this role, sodium starch glycolate (Explotab®) hydrates and swells such that there is an enormous increase in granule volume. Souto *et al.* (2005) did report a four-fold increase in the micropore volume following incorporation of 2.5% w/w sodium starch glycolate in MCC/ hydrochlorothiazide pellets produced by extrusion-spheronisation. Internal addition of sodium starch glycolate may therefore have resulted in a change in the surface morphology or granule regularity due to swelling during the wet granulation process. SEMs of the granules (Figures 6.3d/e above and Figures 6.3j/k below) do support the conclusion that the surface topologies of TABF7 and TABF8 granules differ, that of TABF8 appears to be much more rugged and less well compacted and hence more susceptible to erosion during the friability test.

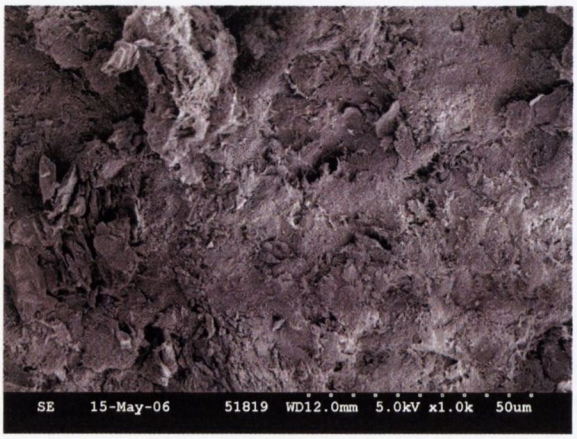


Figure 6.3j. Surface topography of TABF7 granule (magnification x 1,000).

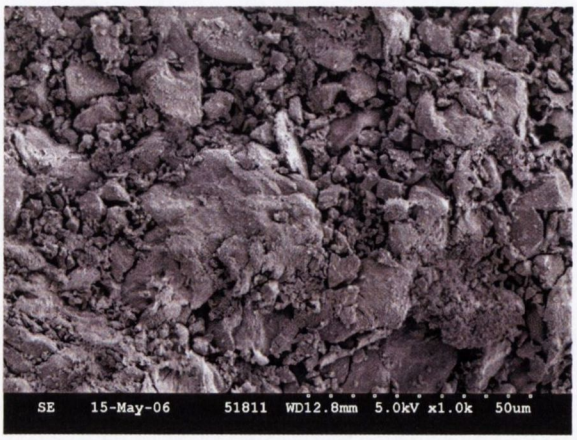


Figure 6.3k. Surface topography of TABF8 granule (magnification x 1,000).

6.4 CHARACTERISATION OF THE TABLETS PRODUCED BY GRANULATE COMPRESSION

6.4.1 Compression Modelling

6.4.1.1 Heckel Compression Analysis

The Heckel equation was used to model the compression data and provide a means of elucidating the compression mechanisms and associated compression parameters; mean deformation pressure (P_y), yield strength (Y) and compressibility (AUHC).

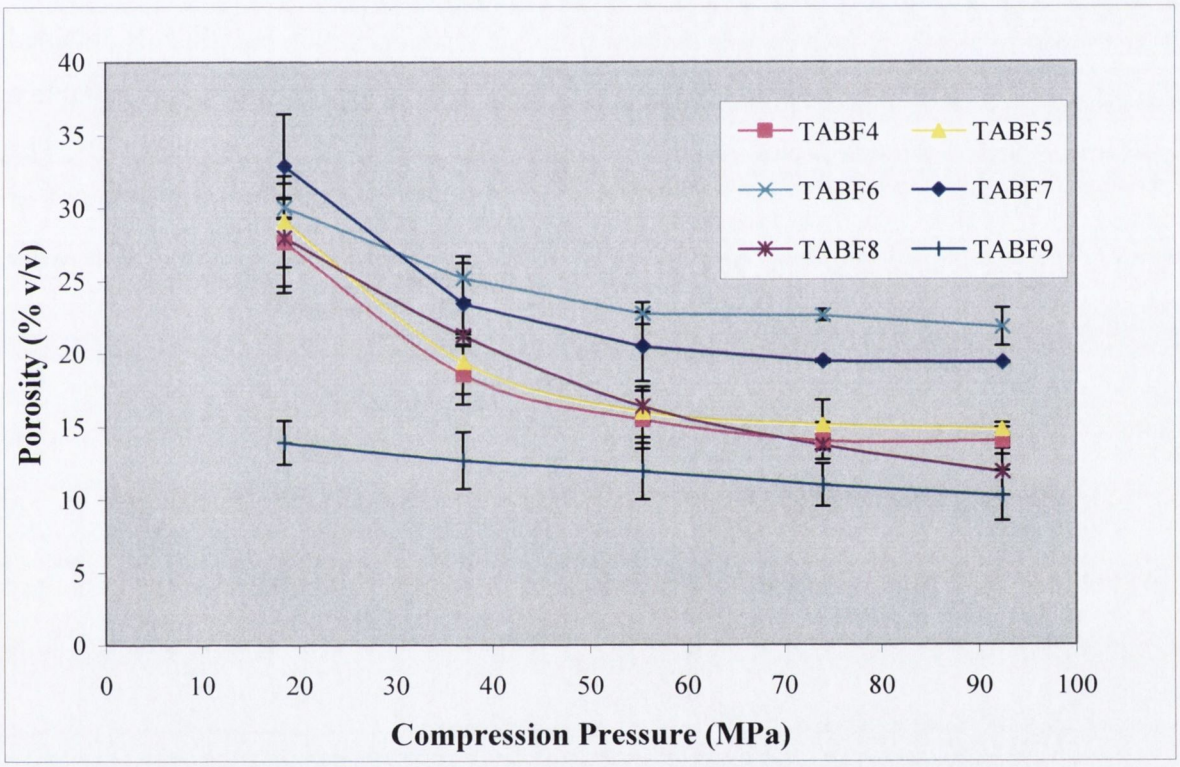


Figure 6.4a. Tablet porosity-applied pressure profiles for the TABF formulations (n = 3).

A plot of total tablet porosity against compression pressure is presented in Figure 6.4a. The porosities of all sepiolite based formulations (i.e. TABF4 - TABF8 inclusive) did not differ significantly from one another ($p > 0.05$) when compressed at the lowest compression pressure used (18.35 MPa). One-way ANOVA confirmed that the porosity of the Avicel® PH101 based compacts, TABF9, was statistically significantly lower ($p < 0.05$) than all other formulations at 18.35 MPa. This result was similar to that obtained during the direct compression studies and the same rationale for this difference may be applied; namely that the tablet porosity represented the sum of the intergranular, intragranular and intraparticulate porosities. The intraparticulate porosity is much larger in the case of

sepiolite as opposed to Avicel® PH101 and this inflates the total porosity value. However, unlike the results obtained in the DC studies, the porosity of the Avicel® PH101 based compacts did not decrease substantially on increasing the compression pressure to 92.4 MPa, indicating that the compressibility of Avicel® PH101 was reduced following wet granulation.

Heckel plots for the TABF formulations and the corresponding compression parameters are presented in Figure 6.4b and Table 6.4a, respectively. Table 6.4a also lists the compression pressure ranges over which the regression analysis was performed, together with the regression analysis results. Correlation coefficients were high for the TABF8 and TABF9 formulations. However, it is evident from the low correlation coefficients obtained with TABF4, TABF5, TABF6 and TABF7 that the Heckel equation was not as suitable a model to describe the manner of volume reduction as it was in the case of the DCBs. The reduced appropriateness of this model may be attributed to the greater number of layers of complexity associated with the process of granular compression as opposed to powder compaction.

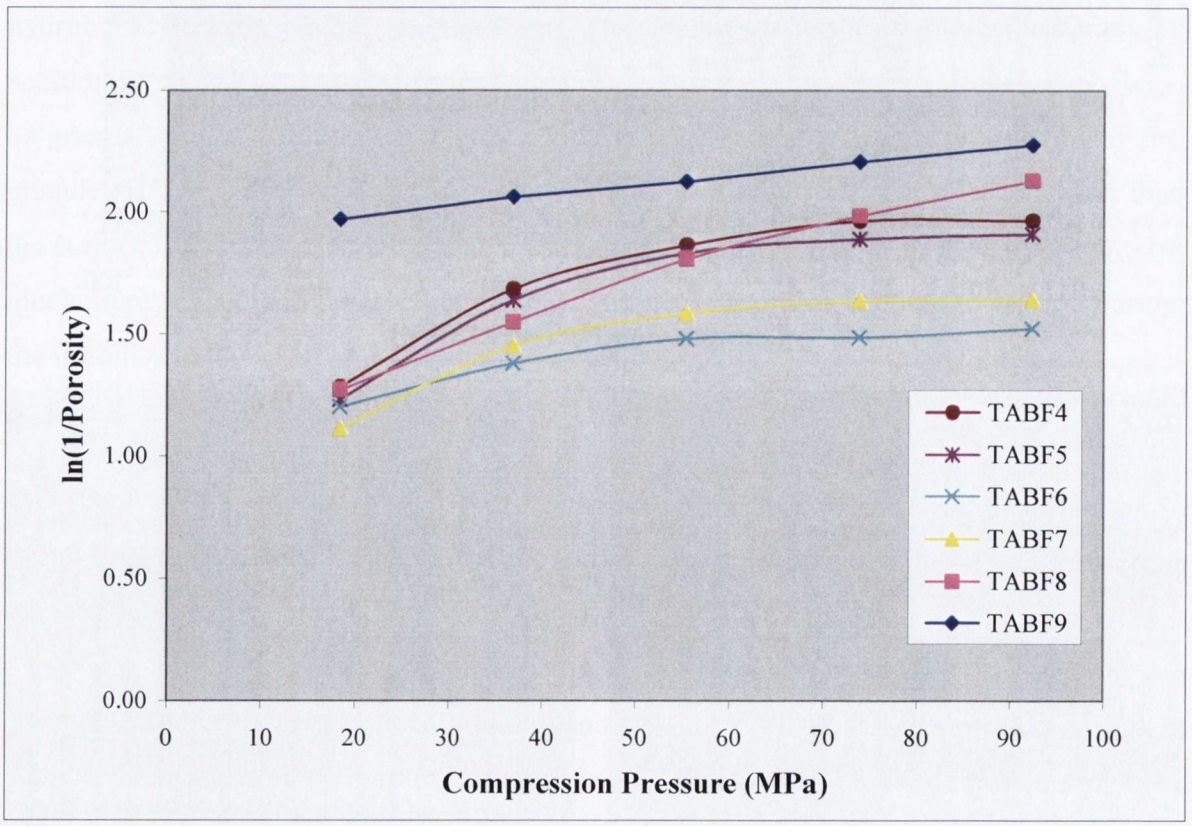


Figure 6.4b. "Out-of-die" Heckel profiles of the different TABF formulations (n = 3).

Van der Zwan and Siskens (1982) proposed that the compaction of granules to form tablets involves the following processes:

1. Filling of holes between the granules by rearrangement (results in the reduction of intergranular porosity)
2. Fragmentation and plastic deformation of the granules
3. Filling of holes between the primary particles (hence producing a reduction in the intragranular porosity or an increase in granule density)
4. Fragmentation and plastic deformation of the primary particles.

They stressed that all mechanisms can occur simultaneously in a powder bed during compaction and will not necessarily occur in sequence. Hence the compaction of granules is a more complex process than the compaction of powders involving the reduction of both intergranular and intragranular porosities, which respond differently to the application of pressure. Wikberg and Alderborn (1996) have urged caution in the application of the Heckel equation to wet granulation systems, given that it assumes that porosity responds uniformly to applied pressure which is not necessarily true of the dualistic pore distributions of these systems.

Table 6.4a. Heckel plot constants of wet granulate formulations.

Formulation	**Compression pressure range (MPa)**	**r^2 (-)**	***k*** **(MPa^{-1})**	***Y*** **(MPa)**	**P_y (MPa)**	**AUHC (MPa)**
TABF4	18-93	0.8250	0.0089	37.45	112.36	131.99
TABF5	18-93	0.8071	0.0087	38.31	114.94	128.17
TABF6	18-93	0.8287	0.0040	83.33	250.00	105.43
TABF7	18-93	0.7812	0.0067	49.75	149.25	111.78
TABF8	18-93	0.9815	0.0116	28.74	86.21	130.28
TABF9	18-93	0.9967	0.0041	81.30	243.90	157.44

Despite the poorness of the data fit, the conclusions from Heckel analysis were consistent with expected results. The mean deformation pressures (and yield values) increased in the following order: TABF8 < TABF4 = TABF5 < TABF7 < TABF9 < TABF6. The

compressibility parameter (AUHC) increased as follows: TABF6 < TABF7 < TABF5 ≈ TABF4 ≈ TABF8 < TABF9.

Firstly, the incorporation of the disintegrant, sodium starch glycolate, in the formulation reduced the mean deformation pressure (86.21 MPa *vs.* 149.25 MPa) as it opposed the binding action of the sepiolite through swelling to increase granule volume. As a consequence of this increase in granule volume it is possible that the framework of the resulting granules may have been weakened and hence permit more extensive compression at lower pressures.

Following the incorporation of Kollidon® 25 and Kollidon® 30 in the formulation, the mean deformation pressure was also reduced and the compressibility slightly increased. The reduction in deformation pressure was attributed to the extremely plastic nature of these amorphous polymers which deform readily upon compression to fill voids, thereby reducing compact porosity and increasing Heckel compressibility. The large increase in the mean deformation pressure upon the incorporation of Kollidon® 90F therefore seems anomalous. However, Bühler (2003) and Schmidt (1999) both noted that on a weight-per-weight basis, Kollidon® 90F will double granule hardness when compared to Kollidon® 25 and Kollidon® 30. Consequently, a doubling of the mean deformation pressure as seen above would not be unexpected. As porosity reduction (i.e. Heckel compressibility) is governed by the ease of deformation of the TABF6 granules, low deformability will translate into reduced Heckel compressibility.

TABF9 had a much higher Heckel compressibility than the other TABF formulations. In terms of an ability to produce a compact of nearing zero porosity, TABF9 was much more successful than any of the other TABF formulations as the porosity of the TABF9 granules was much lower than corresponding values for the other TABF formulations at all compression pressures. Again, it is possible that the use of total porosity as opposed to interparticle porosity as a measure of compressibility is not appropriate in the case of the sepiolite formulations and may result in an underestimation of the compressibility. Confusingly, the Heckel equation also predicts a much higher yield value for TABF9 than for any other formulation. The yield value is a reflection of the rate or ease with which porosity tends toward zero in response to an increased compression pressure. This seemingly contradictory result may be explained by scrutiny of the porosity versus

compression pressure plot (Figure 6.4a). The porosity of TABF9 does not reduce as dramatically as in the case of the sepiolite-based formulations, explaining the higher yield value. Therefore, although the other sepiolite-based wet granulation formulations undergo more extensive reductions in porosity over the compression pressure ramp than TABF9, the final porosities are still higher than the TABF9 compact porosity at the lowest compression pressure; this occurrence translates into lower yield values and lower AUHC compressibilities respectively.

The lower mean yield pressure of the TABF7 formulation when compared to the TABF9 formulation is advantageous in that it translates into reduced compression pressures, reduced energy expenditure and reduced wear and tear of the compression equipment.

6.4.1.2 Kawakita Compression Analysis

As described in section 5.5.3.2.2, the Kawakita equation may be a more appropriate equation to model the volume reduction associated with compression of porous systems as it uses the ratio of bulk density to compact density as a measure of volume reduction as opposed to the ratio of compact density to skeletal density as is the case for Heckel analysis. Hence modelling using the Kawakita equation does not assume zero compact porosity at infinite applied pressure. The Kawakita plots and volume reduction parameter, *a*, are presented in Figure 6.4c and Table 6.4b respectively.

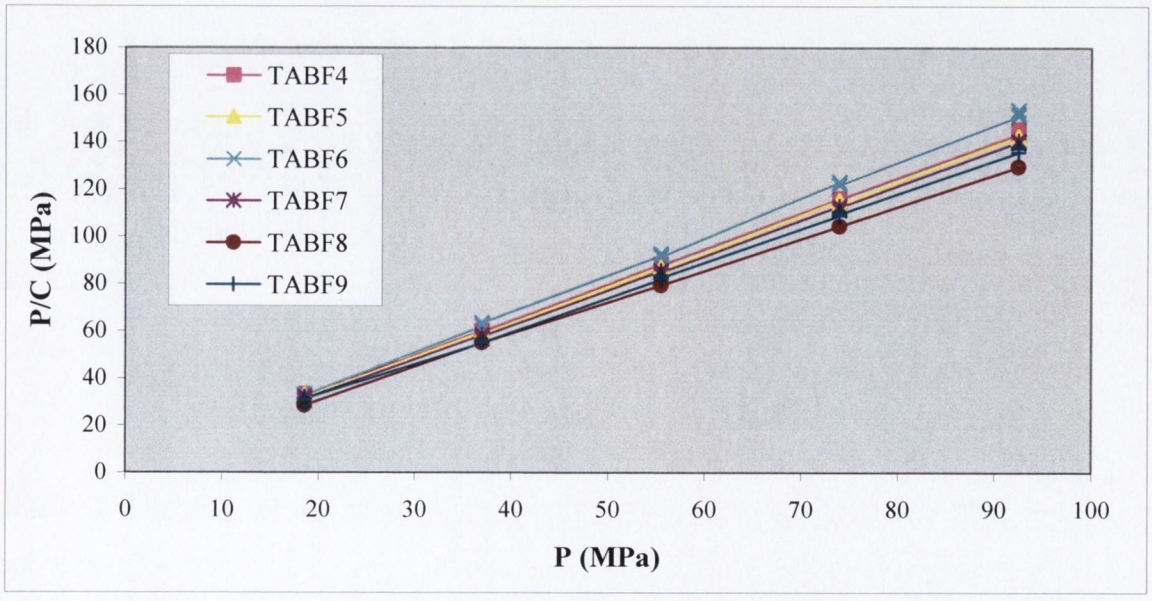


Figure 6.4c. Kawakita plot for the different TABF formulations (n = 3).

The Kawakita equation fitted the compression data well as indicated by high correlation coefficients ($r^2 > 0.9982$). The Kawakita parameter, *a*, which is a measure of the relative volume reduction associated with compression is comparable for formulations TABF4, TABF5, TABF7 and TABF9. TABF8 undergoes slightly more volume reduction than the other formulations while TABF6 undergoes less.

Table 6.4b. Kawakita parameters for the different TABF formulations.

Formulation	Kawakita parameter, *a (-)*	Kawakita parameter, 1/*b* (MPa)	r^2
TABF4	0.6601	2.574	0.9995
TABF5	0.6691	2.589	0.9995
TABF6	0.6177	2.475	0.9997
TABF7	0.6778	2.425	0.9996
TABF8	0.7345	2.947	0.9982
TABF9	0.6868	1.657	0.9992

On comparison of the Kawakita compressibility parameters (i.e. *a*) of TABF7 and TABF9 with those of the corresponding direct compression formulations, (SD sepiolite and Avicel® PH101, respectively; Section 5.5.3.2.2), it is evident that the compressibility was reduced following wet granulation.

The Kawakita compression parameters, 1/*b*, are also presented in table 6.4b. As discussed previously in section 5.5.3.2.2, a review of recent literature has indicated that this parameter has not been satisfactorily reconciled with a particular physical property/ event during the compression process (Paronen and Ilkka, 1996; Podczeck, 1996; Berggren *et al.*, 2004). Consequently, these values are not addressed in any detail.

6.4.1.3 Correlation of results from Heckel and Kawakita Analysis

The rank order of granulate compressibility predicted by both Heckel and Kawakita analysis is presented in Figure 6.4d. Again, as noted in Section 5.5.3.2.3, the relative orders of granulate compressibilities calculated using the two models are not consistent, and furthermore are really not comparable given the assumptions underlying their calculation.

Kawakita analysis concluded that the compressibilities of TABF4, TABF5, TABF7 and TABF9 were of similar magnitude; hence similar volume reduction occurs when these granulates were converted into compacts. The extent of this volume reduction was lower in the case of TABF6. With respect to TABF6, Heckel analysis also indicated reduced compressibility with respect to the other sepiolite based formulations. The difference in the compressibility of TABF6 granules is most likely attributable to the granular strength. It has been well documented that Kollidon® 90F produces very hard granules. Heckel analysis predicted high yield values for TABF6, which is indicative of high granular strength and hence a higher inherent resistance to deformation/ porosity reduction under pressure, i.e. reduced compressibility.

Kawakita Compressibility

TABF6 < TABF4 = TABF5 = TABF7 = TABF9 < TABF8

Heckel Compressibility

TABF6 < TABF7 < TABF5 = TABF4 = TABF8 < TABF9

Figure 6.4d. Relative order of increase of the Kawakita and Heckel compressibility parameters.

Kawakita analysis indicated that TABF8 underwent the greatest volume reduction on conversion to a compact; Heckel analysis rated it as similar to TABF4 and TABF5. Hence it may be concluded that TABF8 undergoes extensive compression upon application of pressure to the granulate bed, possibly due to a weaker granular structure; while at high pressures where a compact had already been formed, the ability of TABF8 to compress further to yield a compact of zero porosity was comparable to TABF4 and TABF5.

Heckel analysis indicated that the compressibility of TABF9 was significantly higher than TABF4, TABF5 and TABF7; Kawakita analysis rated the compressibility of TABF9 as similar to that of TABF4, TABF5 and TABF7. Hence a similar volume reduction was observed on conversion of the granules to a compact for each of these formulations. However, in the case of TABF9 the resulting compacts had a lower porosity, which was most likely related to the lower intraparticulate porosity of the constituent filler-binder, Avicel® PH101.

6.4.2 Tensile strength profiles

The relationship between tensile strength and compression pressure is shown in Figure 6.4e. In contrast to the tensile strength profiles of the DCBs where the tablet strength tended to increase over the whole of the pressure range used, the tensile strength of the wet granulated formulations tended to level off with increasing applied pressure and reach a plateau at higher applied pressures. This plateau was reached after approximately 55 MPa for all wet granulated formulations. Similar compactibility profiles, i.e. with a pressure-dependent region and a plateau, have been reported previously for tablets formed from sodium chloride and polyethylene glycol (Adolfsson and Nyström, 1996) and from spray dried lactose and PVP (Berggren *et al.*, 2004).

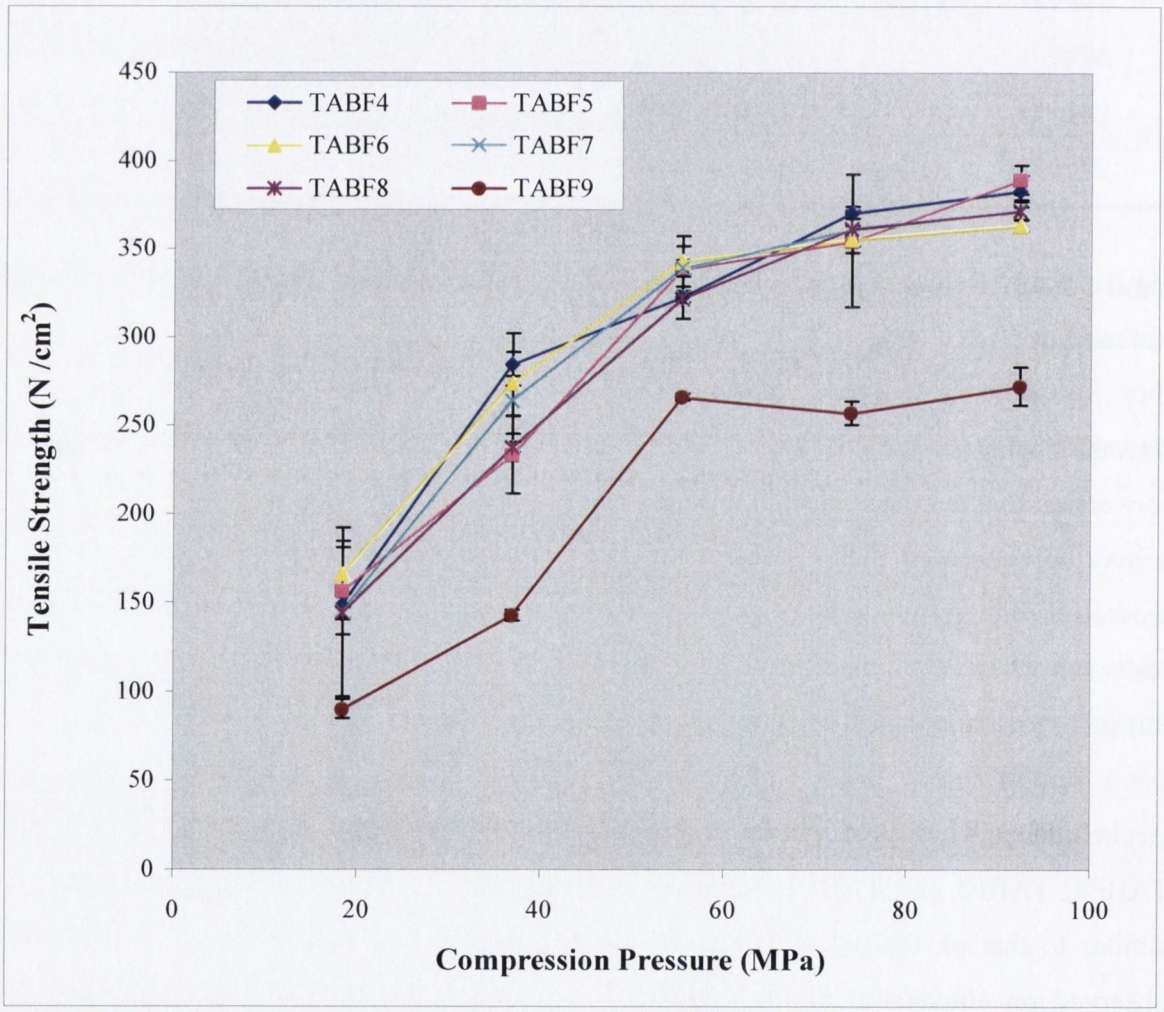


Figure 6.4e. Compactibility profiles for the different TABF formulations.

The AUTSC values, which are indicative of the compactibilities of the formulations (Habib *et al.*, 1996; Kumar *et al.*, 2001), are presented in Table 6.4c. It is evident that the

compactibilities of TABF4, TABF5, TABF6, TABF7 and TABF8 are similar but all are substantially higher than that of TABF9.

Table 6.4c. Compactibility data for the different TABF formulations

Formulation	AUTSC (MPa^2)
TABF4	229.80
TABF5	221.74
TABF6	228.52
TABF7	225.82
TABF8	217.98
TABF9	156.57

Several conclusions may be drawn from these results. First of all, the inclusion of Kollidons® 25, 30 and 90F in the formulation did not alter compactibility. Consequently, it was proposed that the mechanical strength of compacts is principally derived from the strong binding characteristics of sepiolite rather than the Kollidon®, which therefore may be excluded from the formulation without consequence for the compactibility. The high compactibility associated with sepiolite based formulations has already been explained by virtue of the extensive hydrogen bonding and mechanical interlocking, which are facilitated by the abundant surface silanol groups and fibrous habit, respectively.

Despite the slightly lower compressibility and higher yield value associated with the TABF6 formulation, the compactibility was not lower than that of TABF4, TABF5 and TABF7. Conversely, the greater binding capacity of Kollidon® 90F relative to the lower molecular weight Kollidons® would have been expected to translate into higher compactibility (Bühler, 2003). As discussed previously here and by other authors (Berggren *et al.*, 1994), the relationship between compressibility and compactibility is complex. A certain level of compressibility is necessary to bring surfaces into sufficiently close proximity to permit the formation of a compact through bonding. Hence the extent of compressibility will influence the number of bonds which may be formed but it is the strength, in addition to the quantity, of these particle-particle adhesive joints that will influence compactibility. Kollidon® 90F is typically used in concentrations of 1 - 3% w/w (Schmidt, 1999; Bühler, 2003). A higher concentration was used in TABF6 to permit the

relative binding capacities of Kollidon® 25, 30 and 90F to be easily assessed without needing to correct for differing binder concentrations. Use of this high concentration of Kollidon® 90F produced a very hard granulate with a reduced compressibility, which antagonized the binding capacity of Kollidon® 90F with the consequence that one effect negated the other and so the compactibility did not differ from that of TABF4 and TABF5.

The inclusion of sodium starch glycolate (Explotab®) did not impact negatively on compactibility. In order to explain the increased friability and compressibility of these granules, it was proposed that Explotab® weakened the granular scaffold as a consequence of swelling during the wet granulation process. This adverse effect would have been overcome upon compression as the sepiolite fibers are readily brought into sufficiently close contact to physically intermesh and form hydrogen bonds to rivet the structure together in a similar manner to TABF7.

Compactibility of TABF9 is significantly lower than that of TABF7. Irrespective of the compression force used, it is not possible to prepare tablets of comparable tensile strength using TABF9. In terms of its potential as a filler-binder, sepiolite has demonstrated superior compressibility and compactibility relative to the extensively used Avicel® PH101.

6.4.3 Influence of wet granulation on compressibility and compactibility of MCC and sepiolite

The Heckel mean deformation pressure of the Avicel® PH101 based formulation was much higher and the compressibility (AUHC) much lower than that associated with the corresponding DC formulation. The Kawakita compressibility parameter, *a*, was similarly reduced following wet granulation. Other authors (Staniforth *et al.*, 1988; Bolhuis and Chowhan, 1996; Buckton *et al.*, 1998) have noted that the compressibility of MCC deteriorates following wet granulation; a phenomenon which has been termed "hornification". Buckton and his co-workers (1998) ascribed this deterioration in the compression properties to a change in internal bonding/ packing within the MCC structure as indicated by a change in the enthalpy of water sorption at low relative humidity and a change in the near infra red (NIR) spectrum in the region which relates to C-H bonding. Badawy *et al.* (2006) also attributed the reduced deformability following wet granulation

to a change in packing resulting in a reduction in the primary particle porosity. Westermarck *et al.* (1999) likewise credited the reduction in compressibility to densification of MCC during wet granulation through reduction in the pore volume in the pore diameter range 3 – 200 nm. Staniforth *et al.* (1988) related the loss of compressibility to the fact that less plastic deformation occurred during compaction of granules in comparison with compaction of powder particles as a large proportion of compaction energy was probably utilized in breaking up primary granule structures, a process which must proceed before deformation of the individual MCC fibers. Comparison of TABF7 with the SD sepiolite formulation indicated that the increase in mean deformation pressure upon wet granulation was not a phenomenon unique to Avicel® PH101. This change is not as dramatic in the case of sepiolite and it is postulated that it relates to improved packing following wet granulation (as indicated by the increased bulk and tapped densities), which translates into a reduction in the extent of volume reduction that can be achieved through the application of a given pressure.

The influence of wet granulation on the compactibility of sepiolite and Avicel® PH101 was also assessed by comparison of the AUTSC values of TABF7 and TABF9 with the corresponding values for the SD sepiolite and Avicel® PH101 direct compression formulations. In the case of Avicel® PH101, wet granulation resulted in a 39% reduction in the compactibility. Given the dramatic deterioration in compressibility following granulation (AUHC decreased by ~ 50%), the intergranular separation distance is unlikely to favour the forging of extensive bonding. Maganti and Çelik (1993) similarly attributed the decreased bonding of MCC to changes in shape, size and possibly a reduction in the number of bonding sites. Interestingly, sepiolite retains its compactibility following wet granulation. Wet granulation therefore serves only to augment the tabletting characteristics of sepiolite: flowability is improved, dust generation reduced, compressibility is slightly reduced but compactibility remains unaffected.

6.4.4 Tablet hardness and friability testing

For each formulation, ten tablets compressed at 2000 kg (36.95 MPa) were crushed diametrically and the tablet strength noted. These results are shown in Table 6.4d.

Table 6.4d. Tablet hardness and friability values for the TABF formulations.

Formulation	Hardness (N)	Friability (%)
TABF4	156.80 ± 5.20	0.42 ± 0.26
TABF5	153.80 ± 7.90	0.50 ± 0.36
TABF6	184.60 ± 11.54	0.73 ± 0.17
TABF7	159.90 ± 4.93	0.52 ± 0.07
TABF8	149.90 ± 15.51	0.31 ± 0.18
TABF9	94.60 ± 7.23	0.27 ± 0.17

One-way ANOVA confirmed that TABF4, TABF5, TABF7 and TABF8 produced tablets of similar hardness, while TABF9 produced significantly weaker tablets and TABF6 produced significantly harder tablets ($p < 0.001$). The similarity of the TABF4, TABF5, TABF7 and TABF8 results indicated that the inclusion of a classical binder is not necessary to ensure adequate tablet hardness, nor does the inclusion of sodium starch glycolate antagonize tablet hardness. The low hardness value of the TABF9 formulation is a reflection of the deterioration in compressibility and compactibility associated with wet granulation of MCC discussed previously. The hardness values followed the same rank order as the AUTSC compactibility values except in the case of TABF6. The AUTSC compactibility value of TABF6 was comparable to those of TABF4, TABF5, TAB7 and TABF8 yet the tablet hardness was significantly higher. Tablet tensile strength is directly proportional to tablet hardness but inversely related to tablet thickness (Fell and Newton, 1968). The reduced compressibility of TABF6 resulted in the production of thicker compacts relative to the other sepiolite-based formulations for a given compression weight. The increase in tablet hardness and thickness thereby offset one another resulting in similar tensile strengths to the other formulations.

Friability results for the TABF formulations are also shown in Table 6.4d and represent the average of three runs, each one on a different batch of the formulation in question. All formulations met the BP requirement of < 1 % weight loss during the friability run.

6.4.5 Disintegration testing of tablets

The results of disintegration testing of the TABF formulations are presented in Table 6.4e below. Six tablets from each of three batches of each formulation were tested and the average disintegration time was calculated. The standard deviation represents the batch-to-batch variation in the disintegration time. All formulations comply with the BP limit of 15 min for the disintegration of uncoated tablets with the exception of TABF9.

Table 6.4e. Average disintegration times in water for TABF formulations.

Formulation	Disintegration time (min)
TABF4	2.35 ± 0.43
TABF5	2.20 ± 0.23
TABF6	3.45 ± 0.42
TABF7	1.37 ± 0.19
TABF8	0.84 ± 0.11
TABF9	> 15

The results of ANOVA on the disintegration results are illustrated in Figure 6.4f.

TABF8	TABF7	TABF5	TABF4	TABF6	TABF9
0.84	1.37	2.20	2.35	3.45	> 15

Figure 6.4f. ANOVA comparison of the disintegration times for each formulation (There is no statistically significant difference (i.e. $p > 0.05$) between products joined by a black line).

The disintegration times of TABF7 and TABF8 were low and not significantly different ($p > 0.05$), indicating that sepiolite alone was capable of ensuring rapid tablet disintegration, hence obviating the need for a separate disintegrant. The disintegration

times of TABF4 and TABF5 were slightly longer, presumably due to the binding effects of Kollidon® 25 and 30 which tended to oppose tablet break-up (Bandelin, 1989). The disintegration time of TABF6 was longer again and may be attributed to the stronger binding action of Kollidon® 90F relative to the lower molecular weight Kollidons®.

The disintegration time of TABF9 was in excess of 15 min, indicating that the wet granulation process not only reduced MCC compressibility and compactibility, but also its ability to act as a disintegrant. Conversely, Wu *et al.* (2001) observed an improvement in disintegration properties of MCC following wet granulation and correlated it to the reduction in tablet hardness. The disintegrant properties of MCC have been attributed to the penetration of water by means of the capillary action of the pores and the consequent disruption of intermolecular bonding (Bolhuis and Chowhan, 1996) and/or generation of an internal mechanical stress following a moderate level of swelling (Ek *et al.*, 1995). As discussed previously, many authors (Staniforth *et al.*, 1988; Buckton *et al.*, 1998; Westermarck *et al.*, 1999) have reported a change in the internal packing of MCC following wet granulation resulting in an increase in primary particle density. It is possible that the resultant rate of water ingression via capillary action is reduced due to an alteration in the pore structure, leading to a prolongation of disintegration time. Many authors (Kleinebudde, 1994; Tho *et al.*, 2003; Souto *et al.*, 2005) have noted a deterioration in the disintegration properties of MCC following extrusion-spheronisation, a process not dissimilar to wet granulation. Kleinebudde (1994) reported that MCC/ paracetamol pellets obtained by extrusion/spheronisation did not retain their swelling potential after the manufacturing process and only disintegrated when the amount of drug was larger than the capacity of the MCC for keeping the structure together. At this point, when the drug had been dissolved, the structure collapsed, but this was not a true disintegration. Souto *et al.* (2005) noted a similar loss of disintegrating ability (which could not be overcome by the inclusion of superdisintegrants) in the case of MCC/ hydrochlorothiazide pellets.

Unlike in the case of the DCBs, there is no linear relationship between total porosity and tablet disintegration time ($r^2 = 0.4200$), even after exclusion of TABF9 data. This may be due to the more complex nature of the pore structure with three levels of organization, namely intergranular, intragranular and intraparticulate porosities, in the wet granulated samples; as opposed to two (interparticulate and intraparticulate) in the case of the DCBs.

6.4.6 *In vitro* drug release profiles

The release profiles of paracetamol from the tablets prepared are shown in Figure 6.4g.

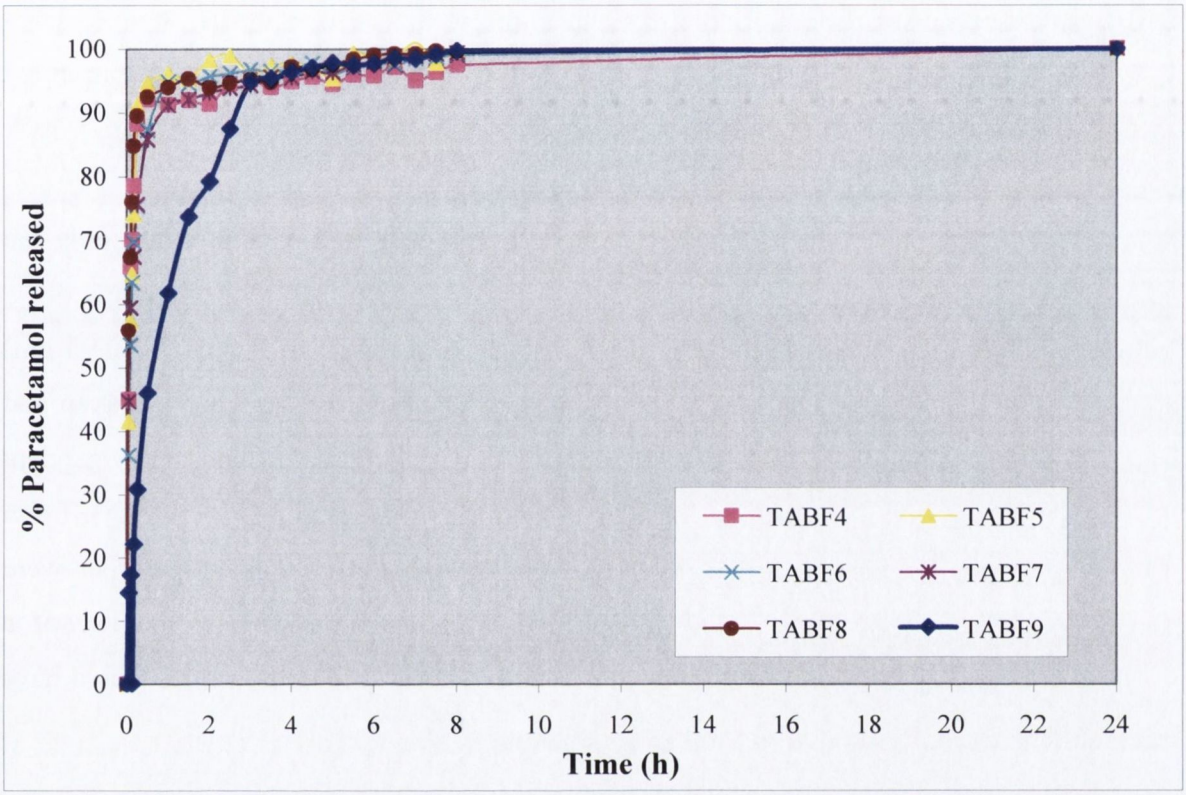


Figure 6.4g. Paracetamol release profiles from TABF tablets compressed at 2000 kg (n = 3).

It is evident from the release profiles above that the release of paracetamol from all sepiolite-based TABF formulations was similar and extremely rapid with in excess of 70% of the total drug content present in solution after 15 min for each replicate. The standardised BP (2007) criteria for conventional release solid oral dosage forms requires, for each unit tested, that not less than 70% of the active ingredient or ingredients dissolves within 45 min. Consequently all sepiolite-based formulations complied with the BP specifications. In the case of TABF9, 70% of the stated paracetamol content was not present in solution until 120 min after the commencement of the dissolution test. Thus TABF9 fails to meet BP requirements for conventional release solid oral dosage forms.

6.4.7 Surface profiling using non-contact optical profilometry and SEM

Surface profiling results for the upper and lower surfaces of the compacts compressed at 2000 kg (i.e. 36.95 MPa) are presented in Table 6.4f and represent the average of measurements on three different tablets. An example of the surface profile obtained from non-contact laser surface profiling of the upper surface of a TABF9 compact is presented in Figure 6.4h.

The R_a values for all TABF formulations lay in the range 1.18-1.65 μm, confirming the production of tablets with reasonably smooth surfaces. Comparison with the range of R_a values obtained for SD sepiolite and Avicel® PH101 DCB formulations (0.67 – 0.95 μm) indicated that the surfaces of the wet granulated formulations were rougher. Narayan and Hancock (2003) reported that, in the case of plastic materials, low R_a values are dependent on exceeding the yield pressure of the material during compression (Figure 5.5j). From Heckel analysis, it was evident that the yield values of the wet granulated materials were much higher than those of the DC blends and were not exceeded by the use of a compression pressure of 2000 kg (36.95 MPa). Consequently, higher R_a values would have been anticipated in the case of the wet granulated materials.

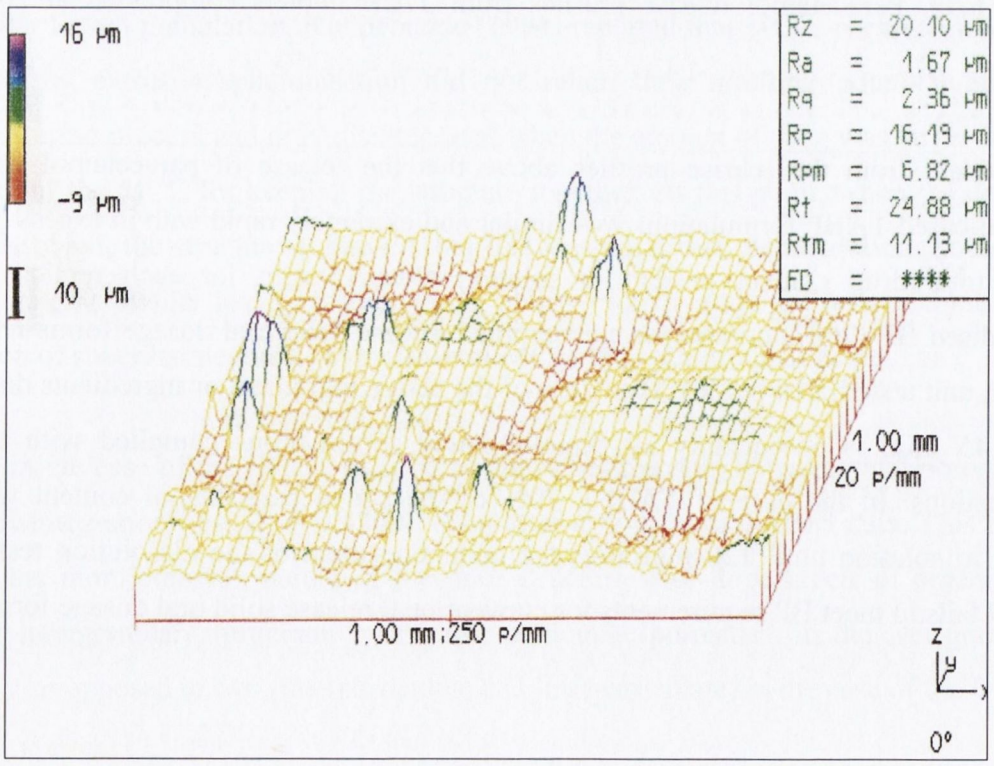


Figure 6.4h. Profile of upper surface of TABF9 tablet compressed at 2000 kg.

From ANOVA, it was evident that the R_a values of all TABF compacts were not statistically significantly different ($p = 0.643$) and the surface roughness characteristics were therefore comparable. Furthermore, R_q values of all TABF compacts were similar ($p = 0.548$). Inclusion of Kollidons® or Explotab® did not therefore alter the surface topography.

Paired t-tests indicated that there was no significant difference in the R_a and R_q values of the upper and lower surfaces of a particular tablet of a given formulation. Two conclusions may be drawn from this observation; firstly the compression force was efficiently transmitted through the powder bed for all granulates and secondly, none of the TABF granulates displayed a tendency to segregate vertically within the die based on granular size (i.e. larger granules near the upper punch and fines towards the lower punch or *vice versa*). If this were the case, the R_a value of the upper surface would be expected to be notably different from that of the lower surface.

Surface variability was assessed using the ratio R_q/R_a. Paired t-tests and one-way ANOVA ($p = 0.326$) confirmed that the surface variability did not differ between the upper and lower surfaces of a given tablet or the surfaces of tablets of different formulations, respectively. All R_q/R_a ratios were low (maximum value of R_q/R_a is 1.41) indicating that variation from the central line could be accounted for by periodic deviations of similar size. Consultation of the Narayan and Hancock (2003) model for compression of ductile materials indicates that the higher R_a values may be ascribed to retention of the original granular shape upon compression at a sub-yield pressure (evident from Figure 6.4h), which in turn leads to a regular and uniform distribution of peaks and valleys and consequently a low surface irregularity.

SEMs of the upper surfaces of TABF7 and TABF9 are presented in Figures 6.4i – 6.4k below. At high magnifications (x 1,000), spaces between individual granules could still be identified, indicating that compression forces in excess of the yield values were not used, a finding consistent with the results of Heckel analysis and with the high R_a values from non-contact optical profilometry.

Table 6.4f. Surface parameters for the TABF compacts compressed at 2000 kg (n = 3).

Formulation	R_a (µm)		R_q (µm)		R_q/R_a (-)	
	Upper	Lower	Upper	Lower	Upper	Lower
TABF4	1.65 ± 0.26	1.49 ± 0.11	2.10 ± 0.27	1.96 ± 0.18	1.28 ± 0.04	1.31 ± 0.04
TABF5	1.47 ± 0.17	1.53 ± 0.27	1.92 ± 0.19	2.02 ± 0.38	1.30 ± 0.04	1.32 ± 0.03
TABF6	1.49 ± 0.34	1.49 ± 0.32	2.08 ± 0.27	1.95 ± 0.46	1.41 ± 0.14	1.31 ± 0.04
TABF7	1.38 ± 0.16	1.31 ± 0.13	1.87 ± 0.09	1.73 ± 0.14	1.36 ± 0.10	1.32 ± 0.07
TABF8	1.52 ± 0.44	1.45 ± 0.43	1.98 ± 0.52	1.86 ± 0.54	1.31 ± 0.06	1.28 ± 0.00
TABF9	1.22 ± 0.10	1.18 ± 0.08	1.55 ± 0.15	1.62 ± 0.04	1.27 ± 0.03	1.37 ± 0.06

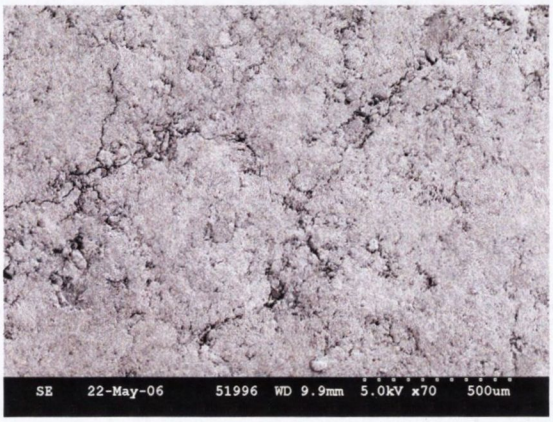


Figure 6.4i. SEM of the upper surface of TABF7 compact compressed at 2000 kg (magnification x 70).

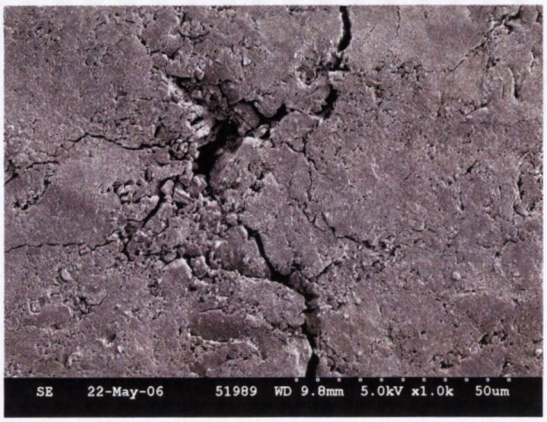


Figure 6.4j. SEM of the upper surface of TABF7 compact compressed at 2000 kg (magnification x 1,000).



Figure 6.4k. SEM of the upper surface of TABF9 compact compressed at 2000 kg (magnification x 70).

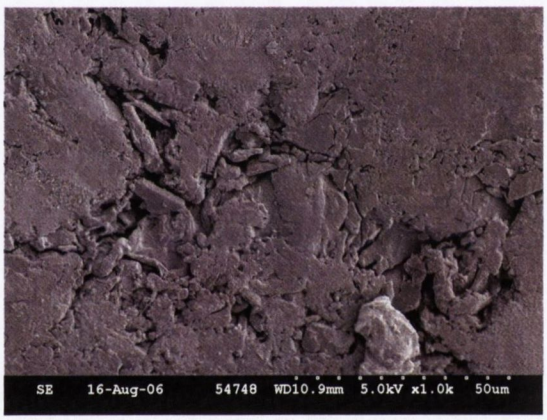


Figure 6.4l. SEM of the upper surface of TABF9 compact compressed at 2000 kg (magnification x 1,000).

In conclusion, all sepiolite-based TABF formulations produced slightly rougher compacts than comparable DC formulations on account of the failure to exceed the higher yield values of these wet granulated samples during compression. Surface irregularity was however comparable and hence the wet granulated formulations produced compacts with surface characteristics consistent with the Narayan and Hancock model (2003) for the compression of plastic materials at pressures below the Heckel yield pressure. Surface characteristics of all sepiolite-based compacts were comparable with those of MCC (Avicel® PH101).

6.5 CONCLUSIONS

Preliminary studies indicated that a granulate of reasonable quality could be produced by wet granulation of a paracetamol-sepiolite (50:50 w/w) blend in the absence of a traditional binder (i.e. TABF7). The moisture content of the granulate had a significant influence on flowability and on the hardness and friability of the tablets produced by its compression. The optimum moisture content for high flowability, low friability and high tablet hardness was of the order of 4 - 5% w/w which coincided with the reported ranges for maximal compactibility of MCC and paracetamol (Garr and Rubinstein, 1992; Bolhuis and Chowhan, 1996).

Increases in bulk density of the order of 300% were achieved following wet granulation of the sepiolite-based formulations (i.e. TABF4 to TABF8). Marked improvements in the flow properties of both sepiolite- and Avicel® PH101-based formulations were also evident following wet granulation. The flowability of all granulates was rated as 'excellent' using Taylor's composite flowability index. SEM indicated that the granules of all formulations were of similar shape, and were typically longer than they were wide. This oblong shape was attributed to the nature of the granulation process, where the width of the granules was dictated by the size aperture and the length by the cohesiveness and plasticity of the moist powder mass. From granule sizing and granule friability testing, it was evident that sepiolite was a more efficient intragranular binder than Avicel® PH101. Use of sepiolite together with Kollidon® 25 or Kollidon® 30 did not improve the intragranular binding efficiency further. A combination of sepiolite and Kollidon® 90F produced maximal intragranular binding efficiency; this did not improve compactibility or tablet friability above that seen with sepiolite alone and was achieved at the cost of an increased yield value, reduced compressibility and prolonged disintegration time. Inclusion of either Kollidon® 25 or Kollidon® 30 decreased the yield value relative to sepiolite alone, although this did not translate into increased compactibility or reduced tablet friability and furthermore led to a retardation of disintegration. The incorporation of any of the three Kollidons® did not alter or improve compact surface rugosity or variability relative to the sepiolite-only formulation.

Consequently, it was concluded that a traditional binder, typified by the Kollidon® range, could be excluded from the sepiolite-based formulation without detriment to intragranular

binding efficiency, flowability, granule friability, granulate compactibility and tablet surface roughness. Furthermore, exclusion of a traditional binder resulted in an increase in tablet disintegration rates.

The inclusion of a disintegrant (Explotab®) in the sepiolite-based formulations was deemed unnecessary; disintegration was suitably rapid in its absence. Furthermore, the inclusion of Explotab® increased granule friability which would lead to undesirable increases in the proportion of fines during transfer processes.

The replacement of Avicel® PH101 by sepiolite led to improved intragranular binding efficiency as evidenced by the granule size distribution, reduced granule friability, a reduced yield value, increased compactibility, comparable tablet surface topography and more rapid disintegration and drug release without the loss of good flowability. Negligible changes in the bulk density of the TABF9 formulation were observed following granulation. Despite this, the compressibility and compactibility of Avicel® PH101 were reduced following granulation as was its ability to act as a disintegrant; the compressibility of sepiolite was reduced (presumably due to improved packing) but the compactibility and disintegrant properties were retained.

In summary, therefore, sepiolite can act simultaneously as a filler, binder and a disintegrant in the wet granulation tabletting process, thereby simplifying the tabletting process considerably and reducing associated analytical times and costs.

Chapter 7

THE EFFECT OF pH, TEMPERATURE AND ELECTROLYTES ON THE RHEOLOGY AND STABILITY OF AQUEOUS SEPIOLITE SUSPENSIONS

7.1 INTRODUCTION

The main aim of this Chapter was to assess the rheological properties of sepiolite (Pangel®-S9) with a view to exploiting them in a pharmaceutical context either as a means of facilitating suspension stabilization and/or gel formation. Clay-based mineral thickeners and rheological additives have been used for decades to modify the viscosity or flow properties of paints and other coatings (Santarén, 1993). A review of the literature indicates that the most commonly used clays for these purposes are the plate-like smectite group, in particular Na^+-montmorillonite (commonly referred to as bentonite; Luckham and Rossi, 1999). Their usefulness is related to two properties; firstly, to their ability to swell when placed in water as water molecules penetrate the interlayer spaces and become adsorbed and immobilized, and secondly, to the formation of three-dimensional structures (termed "house of cards") throughout the medium, which further restrict flow and increase viscosity (van Olphen, 1977; Abend and Lagaly, 2000).

The rheological properties of fibrous clays such as sepiolite and attapulgite (palygorskite) have been less well reviewed and less extensively exploited. The reason for our interest in sepiolite stems from the fact that the gelling mechanism of sepiolite is quite different from that of the smectites in spite of their similar chemical composition (Santarén, 1993; Viseras *et al.*, 2006). This difference may be ascribed to differences in the arrangement of the tetrahedral silica sheets and the octahedral magnesia or alumina sheets, producing fibrous non-swelling particles in the case of sepiolite and plate-like expandable particles in the case of smectites. Gelling of bentonite particles is limited to aqueous media of low electrolyte concentration and requires interlayer saturation with sodium cations (Santarén, 1993). In contrast, Tolsa SA, the producers of sepiolite-based rheological additives (Pangel®) derived from deposits in Spain, claim that the rheological properties of sepiolite are independent of electrolyte concentration and are retained over a wide pH range (from 4

to 14) and temperature range (to 300 °C). The purported robustness of sepiolite suspensions would be of huge benefit in a pharmaceutical context, where major physical stability issues can result from even minor changes in electrolyte concentration, pH or temperature. Although Nash (1996) has listed sepiolite as a pharmaceutically useful suspending agent, a review of the literature reveals very little information on its rheological behaviour with relevance to pharmaceutical formulation.

In this Chapter, we therefore propose to investigate the ease of suspension formation, the rheological behaviour of sepiolite suspensions and finally the response of these suspensions to changes in the pH, temperature and concentration of electrolytes. The gelling mechanism of bentonite (as the most commonly used smectite) is also reviewed in more detail as a means of understanding the difference in the response of these two systems to various environmental stresses and to thereby determine whether sepiolite may be used as a replacement for bentonite.

In Chapter 8, a novel grade of sepiolite, SepCMC, composed of sepiolite and the polymer sodium carboxymethylcellulose (NaCMC) is likewise evaluated. Polymers have been used in combination with clays in order to enhance the rheological properties of both the clay and the polymer (Ciullo, 1981; Ciullo and Braun, 1991). Having established the pertinent functional, rheological and incompatibility characteristics of sepiolite and SepCMC suspensions, their ability to act as suspending agents in a model pharmaceutical formulation (calamine lotion) is assessed using other traditional suspending agents (bentonite, Avicel® RC-591 and CL-611) as standards against which their performance can be rated.

7.2 GELLING MECHANISM OF BENTONITE

Bentonite is a 2:1 layer silicate. Each layer is composed of two sheets of silicon-oxygen tetrahedra in between which lies a sheet of aluminium-oxygen-hydroxyl octahedra. The resulting plate-like layers are stacked upon one another. The trivalent Al in the octahedral layer may be replaced by Mg, Fe, Cr, Zn or Li atoms due to their similarity in size; hence the process is termed isomorphous substitution (van Olphen, 1977). In cases where an atom of lower positive valency replaces Al, a net negative charge results. Part of this negative charge is compensated for by adsorbed cations such as Na^+, Ca^{2+}, Li^+ or Mg^{2+}.

These compensating cations can be readily exchanged with other cations when available in solution; hence they are termed "exchangeable cations". In the stack of layers that make up a bentonite particle, the exchangeable cations are located on both sides of each layer in the stack; hence they are present, not only at the external surfaces of the particle, but also in between the layers. On addition of water to bentonite, it penetrates between the bentonite layers resulting in an increase in the interlayer thickness. For gel formation to occur, the adjacent layers must be separated, which in turn requires that the hydration energy of the interlayer exchangeable cations is large enough to overcome the electrostatic attraction of the adjacent clay layers (van Olphen, 1977; Luckham and Rossi, 1999). If the interlayer cations are monovalent and strongly hydrated (e.g. Na^+ and Li^+), the interplatelet repulsion is sufficient to cause plate separation.

The formation of the "house of cards" structure following separation of the layers may be explained by consideration of the surface charge of the bentonite plates. The faces of the plate-like layers bear a negative charge, the magnitude of which is determined by the type and degree of isomorphous substitution. At the edges of the plates, the tetrahedral silica sheets and the octahedral alumina sheets are disrupted and primary bonds are broken (van Olphen, 1977). The exposed aluminium and silicon oxides (denoted by *Sur*-OH) can ionise as illustrated in Equation 7.1a (Levis and Deasy, 2002):

$$Sur-OH_2^+ \xleftarrow{H^+} Sur-OH \xrightarrow{OH^-} Sur-O^- \qquad \textbf{Equation 7.1a}$$

Alumina exhibits amphoteric behaviour and consequently, the equilibrium of the reaction will be dictated by the pH, leading to a negative charge at more alkaline pHs and a positive charge at acidic pH values. The point of zero charge (PZC) does not necessarily occur at neutral pH, but rather is dependent on the crystal structure of the alumina particle (van Schuylenborgh, 1951). Silica, as an acidic oxide, has a greater tendency to accept hydroxyl groups, thereby generating a net negative charge over a more substantial range of pH values (van Olphen, 1977). However, it is known that in the presence of very small amounts of Al atoms in the suspension, as may occur due to the slight solubility of the clay, the silica surface double layer can become positive. van Olphen (1977) postulated that the silica sheets are preferentially broken at sites where aluminium atoms have substituted silicon, such that the exposed surface at the edge is effectively that of an alumina surface and typically carries a positive double layer. Thiesson (1942; cited in van

Olphen, 1977) investigated the interaction of a negatively charged gold sol with kaolinite and found that the gold particles were exclusively adsorbed at the edges, further supporting the concept of a positive edge charge. The positively charged edges are attracted to the negatively charged faces producing a "house of cards" structure on standing (Figure 7.2a), within which the liquid is immobilized resulting in a high viscosity system. The high viscosity of bentonite dispersions has also been partly attributed an electroviscous effect whereby the extended diffuse ionic layers around the particles restrict the translational and rotational freedom of the particles increasing the yield value (Rand *et al.*, 1980; Güven, 1992).

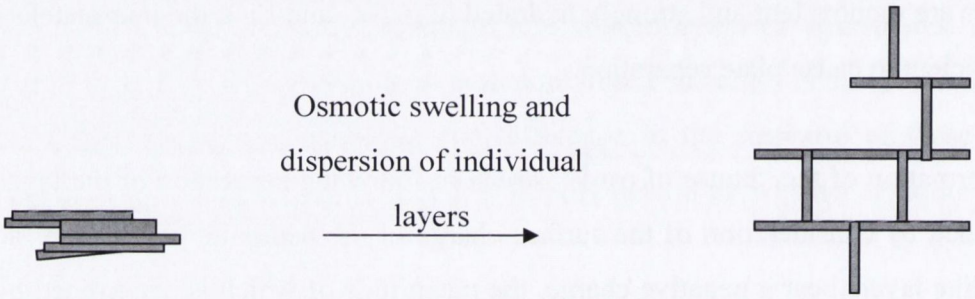


Figure 7.2a. Osmotic swelling of bentonite resulting in the separation of layers and the production of a "house of cards" arrangement through association of the positively charged edges with the negatively charged faces.

The tenuous "house of cards" structure may be broken down on application of a shear stress. The extent of structure breakdown (and consequently the viscosity) is typically proportional to the stress applied, hence bentonite dispersions may be termed pseudoplastic (Viseras *et al.*, 2006). Dispersions of bentonite display a time-dependent recovery of the viscosity and hence are also thixotropic (Viseras *et al.*, 2006). The importance of pseudoplasticity and thixotropy in the context of pharmaceutical suspensions has already been discussed in Chapter 1. The shortcomings of bentonite as a suspending agent are as follows:

1. Addition of water to bentonite does not produce any gel (Viseras *et al.*, 2006). Gelling of bentonite is limited to aqueous media of low electrolyte concentration and requires interlayer saturation by Na^+ or Li^+ ions (Simonton *et al.*, 1988). Swelling must occur before a high viscosity system can be obtained (Viseras *et al.*, 1999). As a consequence, development of a suitable viscosity requires a standing

time typically of the order of 24 h (Rowe *et al.*, 2005). Systems employing bentonite as a suspending/ gelling agent must be made in a two-step process where the bentonite suspension is prepared and allowed to stand in advance of the addition of the other excipients.

2. Once formed, bentonite gels are extremely sensitive to the addition of electrolytes. Electrolytes can augment and depress surface charges, thereby altering interparticulate repulsion and the net energy of particle interaction (Permien and Lagaly, 1994a). Their addition may result in changes in the flocculated/deflocculated state of the system and consequently can alter the rheological behaviour of the system, not only quantitatively but also qualitatively.
3. Furthermore, the stability of bentonite gels is highly influenced by pH due to the pH-dependency of components of the surface charge. At pH < 6, bentonite suspensions are unstable (Rowe *et al.*, 2005; Viseras *et al.*, 2006).
4. The addition of significant amounts of alcohol will also lead to the coagulation of bentonite particles primarily due to the compression of the diffuse ionic layer surrounding the particles permitting them to associate in the primary attraction minimum in accordance with the DLVO theory (Permien and Lagaly, 1994a, 1994b).

The stability of bentonite suspensions is therefore somewhat precarious, being both easily and dramatically influenced by minor changes in the environmental conditions.

7.3 GELLING MECHANISM OF SEPIOLITE

7.3.1 Introduction

The gelling mechanism of fibrous clays, including sepiolite, is not well understood (Viseras *et al.*, 1999). Simonton *et al.* (1988) reported that the gelling properties of sepiolite are dependent on the fibrous nature of these particles, which when thoroughly dispersed in water, form a three dimensional structure consisting of randomly intermeshed elongated particles. This lattice entraps the liquid which is further immobilised by sorption on the large external surface area of the clay as well as within the internal channels (Santarén, 1993; Tolsa product brochure, 1999). Systems of high viscosity are thus produced. Simonton and his co-workers (1988) did not attribute the interparticulate

electrostatic forces any role in the formation and stability of fibrous gel systems. They furthermore stated that sepiolite gels could be prepared in aqueous and organic solvents without concern for the chemistry of exchangeable cations or electrolytes present in the clay or the solvent. Tolsa claims that the main advantage of sepiolite over bentonite is that sepiolite suspensions do not flocculate in the presence of electrolytes and are stable over a wide pH range and at high salt concentrations. These claims relating to the formation and stability of sepiolite gels/suspensions focus on Simonton's theory where rheology is a consequence of physical entanglement of the fibers and minimal importance is ascribed to the electrostatic interactions between fibers. However, Chang *et al.* (1993) related the stability of fibrous clay gels to electrostatic interactions similar to those responsible in laminar clay systems. Furthermore, Viseras *et al.* (1999) noted that sepiolite systems were indeed sensitive to pH indicating that electrostatic interactions do play a role in stability. An extensive evaluation of the influence of pH and electrolytes on electrostatic interactions between sepiolite fibers, which will dictate rheological and sedimentation behaviour, has not been published. Consequently, such a study has been performed here.

7.3.2 Ease of sepiolite gel formation – the influence of mixing speed and time on the resultant rheological properties

Simonton *et al.* (1988) reported that there were very few publications relating to the formation of sepiolite gels but given the need for physical entanglement of individual fibers to generate viscosity, separation of the fibers would be necessary. Separation of the plate-like bentonite particles is achieved via swelling of the interlayer cations. Swelling is not involved in the separation of sepiolite fibers. Exchangeable cations do reside within the microporous channels of sepiolite; however these channels are held together via covalent Si-O-Si bonds and hence intracrystalline swelling does not occur. The individual fibers are held together by hydrogen bonds and van der Waals forces (Santarén, 1993). Separation of the individual fibers is achieved relatively easily by mechanical means which is much less time-consuming than the process of hydrating the interlayer cations which must occur in bentonite (Simonton *et al.*, 1988). The rheological grade of sepiolite used here (Pangel®-S9) is produced by a wet micronisation process which Tolsa claims facilitates the separation of microbundles of sepiolite particles into the individual particles without causing damage to their characteristic elongated shape. From SEM studies of Pangel®-S9 (Chapter 4), it was evident that fiber association at the bundle-level persisted. Moreover,

these bundles associate in a haphazard manner to form microagglomerates. Disruption of these two higher levels of microarchitecture would be necessary to achieve high viscosity. Furthermore, the extent of disruption would therefore be expected to affect the rheological parameters (Viseras *et al.*, 1999; Figure 7.3a).

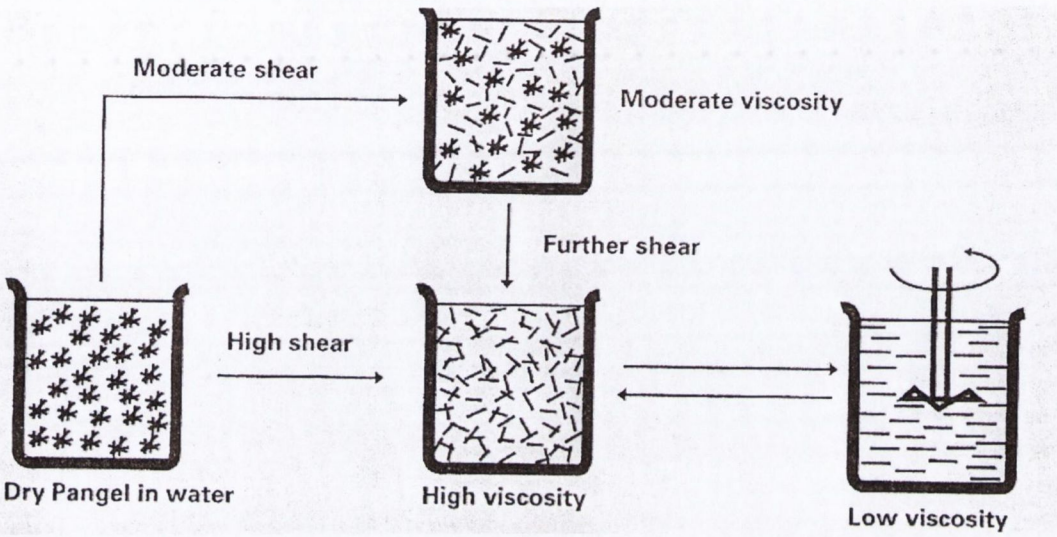


Figure 7.3a. Schematic of sepiolite (Pangel®) dispersion in water at different rates of shear. (Reproduced from Pansil-Pangel product sheet, Tolsa SA, 1999).

Tolsa SA (1999) advocates the use of high shear mixers to ensure maximum deagglomeration of the particles, the highest possible degree of dispersion and therefore maximum rheological effectiveness. Hence the use of different mixing times and mixing speeds (i.e. different mechanical energies) would be expected to produce sepiolite suspensions with different rheology. Viseras *et al.* (1999) reported that the apparent viscosity of sepiolite samples was related to mixing power (i.e. speed), the influence of mixing time being somewhat more minor. A 2^2 factorial experimental design was used to investigate the effect of mixing time and mixing speed on the Herschel-Bulkley yield of a 1% w/v aqueous sepiolite suspension (Section 3.7.4.2). The Herschel-Bulkley model was the "best fit" model as indicated by the lowest standard error. ANOVA was carried out to determine: (1) the conditions necessary for maximum dispersion, and; (2) whether the extent of dispersion is more closely related to mixing speed or time or is dependent on their product. The average Herschel-Bulkley yield values (n = 3) at each of the four design points and the results of ANOVA are presented in Table 7.3a and 7.3b below.

Table 7.3a. The Herschel-Bulkley yield values (Pa) of 1% w/v sepiolite suspensions as a function of the mixing speed and time used during initial dispersion (n = 3).

Mixing time	Mixing speed	
	13,500 rpm	24,000 rpm
30 min	0.228 ± 0.015	0.718 ± 0.015
60 min	0.416 ± 0.014	0.755 ± 0.010

Table 7.3b. Analysis of variance table for Herschel-Bulkley yield values.

Source	df	SS	MS	F	p
Mixing speed	1	0.51406	0.51406	2751.82	0.000
Mixing time	1	0.03780	0.03780	202.35	0.000
*Mixing speed*Mixing time*	1	0.01727	0.01727	92.47	0.000
Error	8	0.00149	0.00019		
Total	**11**	**0.57053**			

The two factor interaction between mixing time and speed was statistically significant (p = 0.000). Consequently both factors must be considered simultaneously. Figure 7.3b shows the interaction plot. Means were compared using Tukey's HSD at a significance level of 0.05. At the low mixing speed, increasing the mixing time from 30 min to 60 min produced a significant increase in the Herschel-Bulkley yield value. At high speeds, the yields were significantly higher than those at low speeds, but an increase in mixing time from 30 min to 60 min at the high mixing speed did not produce a significant increase in the Herschel-Bulkley yield value.

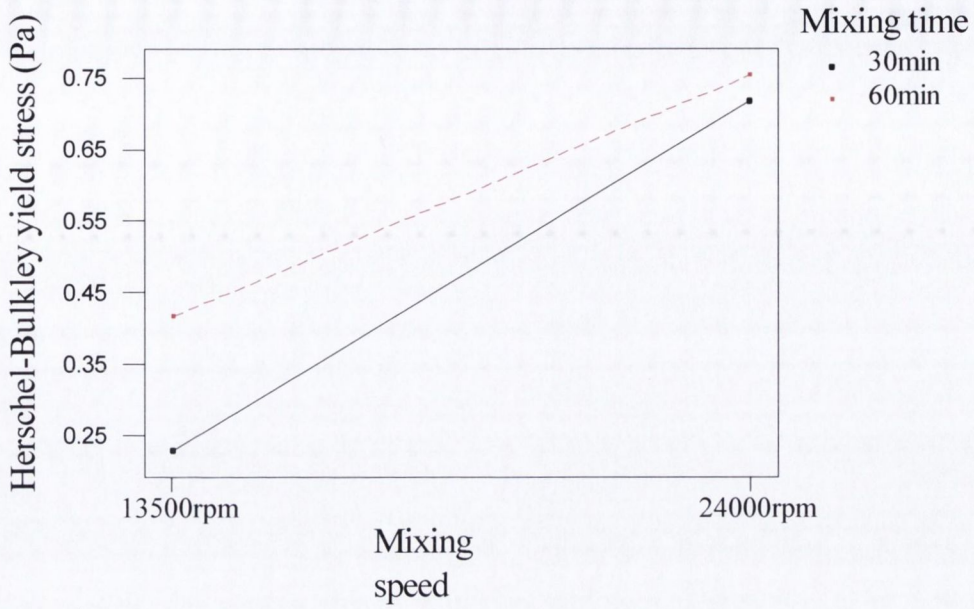


Figure 7.3b. Interaction plot illustrating the effect of different dispersion conditions on the Herschel-Bulkley yield value of 1% w/v aqueous sepiolite suspensions.

The development of a three dimensional structure within the suspension was therefore dependent on both the mixing time and the mixing speed used during the formation of the suspension, thereby supporting the "swelling-independent" gelling mechanism proposed for sepiolite. The influence of mixing speed on dispersion appeared to be more profound than the mixing time as the Herschel-Bulkley yield value at the lower speed and longer time was significantly lower than the corresponding value at the higher speed and shorter time, even though a reasonably similar amount of mixing energy would have been imparted in both cases. This finding is consistent with that of Viseras *et al.* (1999). It is probable that very high levels of shear are required to separate individual fibers from the microagglomerates and that it is the magnitude, more so than the duration, of these shearing forces that will determine whether the interparticulate forces will be overcome. Doubling the mixing time at 13,500 rpm almost doubled the Herschel-Bulkley yield value, however no significant increase in the Herschel-Bulkley yield value was observed on doubling the mixing time at the higher mixing rate, indicating that the dispersion was virtually complete after 30 min at high shear.

SEM studies of the dried suspensions (Figures 7.3c and 7.3d) also confirmed that these dispersion conditions (24,000 rpm, 30 min) were successful in terms of disruption of the

microagglomerate and bundle structures. In addition, it is evident that the use of the high shearing forces did not appear to damage the fibrous nature of the individual sepiolite particles.

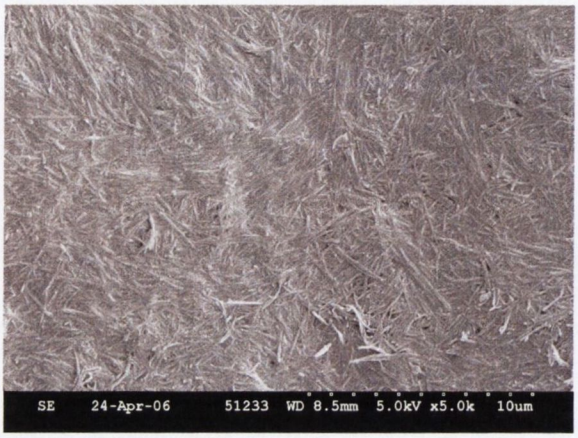


Figure 7.3c. SEM of dried sepiolite suspension prepared using a mixing speed of 24,000 rpm for 30 min (magnification x 5,000).

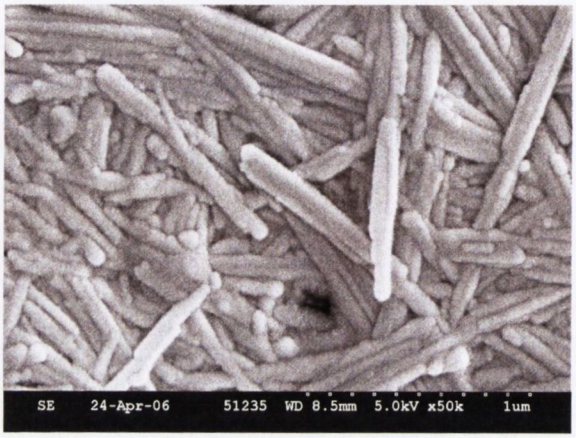


Figure 7.3d. SEM of dried sepiolite suspension prepared using a mixing speed of 24,000 rpm for 30 min (magnification x 50,000).

Furthermore, powder-in-liquid size analysis (Table 7.3c) confirmed significant reductions ($p < 0.05$) in the d10, d50 and d90 values occurred on increasing the mixing speed from 13,500 rpm to 24,000 rpm at a constant mixing time; consistent with the observed increasing trends in yield value. Increasing the mixing time at the low shear level did succeed in improving the degree of dispersion as indicated by a significant reduction in the d10, d50 and d90 values. Only minor changes in the d10, d50 and d90 values were recorded on increasing the mixing time from 30 to 60 min at a mixing speed of 24,000 rpm, indicating minimal changes in the level of dispersion which translated into insignificant changes in the yield values.

Table 7.3c. Results of powder-in-liquid size analysis on sepiolite suspensions prepared using different dispersion times and speeds (n = 3).

Mixing speed (rpm)	Mixing time (min)	d10 (µm)	d50 (µm)	d90 (µm)
13,500	30	4.242 ± 0.068	9.770 ± 0.078	21.470 ± 0.225
13,500	60	3.971 ± 0.071	8.489 ± 0.035	20.354 ± 0.825
24,000	30	3.010 ± 0.057	7.690 ± 0.283	17.778 ± 0.940
24,000	60	2.893 ± 0.002	7.531 ± 0.017	17.627 ± 0.304

In conclusion, the dispersion time and, in particular, mixing speed need to be strictly controlled owing to their profound influence on the extent of dispersion and consequently the viscosity. Results from rheological studies, SEM and particle sizing confirmed that complete dispersion was achieved following shear at 24,000 rpm for 30 min. Thus, to ensure optimum dispersion of the suspensions and reproducibility of the rheological behaviour from batch to batch, a mixing time of 30 min together with a mixing speed of 24,000 rpm was set as standard for the production of all future sepiolite suspensions. Although samples were allowed to settle for 24 h after preparation to allow for shear recovery, a visible increase in the viscosity of the systems was noted immediately after dispersion confirming that in contrast to the laminar clays, sepiolite does not require a swelling period to produce a gel, which is of major importance where 'in situ' interposition of the dispersion is required.

7.4 THE RELATIONSHIP BETWEEN SEPIOLITE CONCENTRATION, RHEOLOGICAL BEHAVIOUR AND SUSPENSION STABILITY

7.4.1 Introduction

It would be anticipated that increases in the concentration of sepiolite would translate into increased yield values and increased apparent viscosities. Knowledge of the manner in which these rheological parameters change with concentration is of importance for gel/ suspension formulation. Continuous shear rheology was used to ascertain this relationship and also to establish the type of flow behaviour (i.e. Newtonian, plastic, pseudoplastic etc.) exhibited by suspensions of different sepiolite concentration. Fitting of the flow data to the

rheological models provided a means of quantifying the changes in flow behaviour with an increase in concentration (section 3.7.4.1).

7.4.2 Rheological behaviour of sepiolite suspensions of different concentration

Flow curves of aqueous sepiolite suspensions of concentration 0.25% - 4% w/v are presented in Figure 7.4a below. It must be noted that these flow curves were generated by running each concentration over a different shear stress range beginning at the minimum shear stress required to move a sample of that particular concentration and stepped up to the maximum shear stress possible before the angular velocity became too high. The nature of the change in viscosity with an increase in shear rate will be addressed for each concentration (refer to Figure 7.4b). The best mathematical fit of the flow data was afforded by the Herschel-Bulkley model at all concentrations, as indicated by the relative order of the standard error for each of the five rheological models (Table 7.4a). The Herschel-Bulkley parameters at each concentration are presented in Table 7.4a.

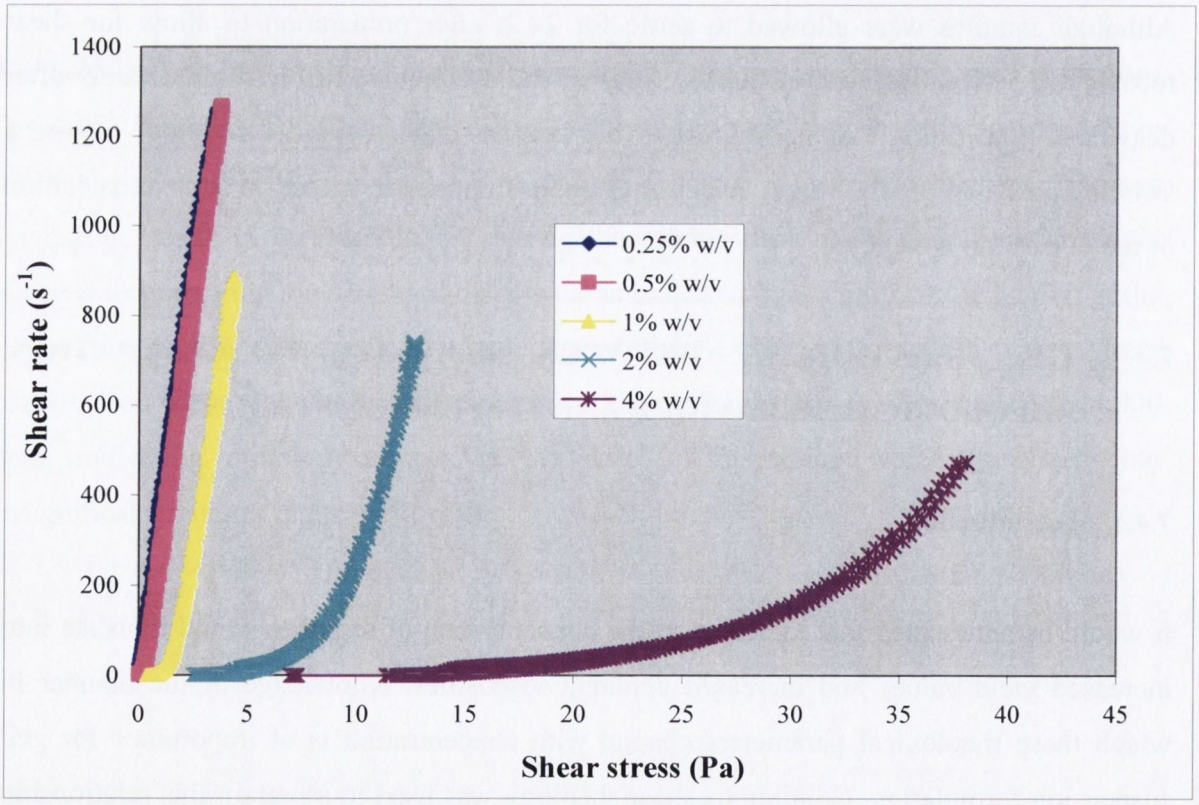


Figure 7.4a. Flow curves of aqueous sepiolite suspensions of different concentration.

From Figure 7.4a it is evident that the 0.25% w/v sepiolite suspension exhibited approximate plastic behaviour, a conclusion supported by the similarity of the standard

error of fit for the Bingham model and Herschel-Bulkley model. Furthermore, the flow behaviour index, n, obtained by data fitting to the Herschel-Bulkley model was approximately 1, confirming quantitatively the absence of pseudoplastic behaviour. A small initial stress (of the order 0.0718 Pa) was necessary to move the sample following which a direct linear relationship between stress and strain resulted, which is indicative of a constant apparent viscosity (see Figure 7.4b). Existence of a yield point is indicative of the presence of a three dimensional structure (Matijaŝić and Glasnović, 2002). Hence, even at this low concentration, fiber entanglement to generate a three dimensional network was possible. The magnitude of the yield point depends on the number and strength of bondages between particles per unit volume of suspensions (Firth and Hunter, 1976). Therefore at this concentration, the number of the interfibrous connections, be they of either purely physical, electrostatic or hydrogen bonding nature or a combination of all three, were few. A small stress resulted in complete and immediate breakdown of the structure to generate a free flowing liquid of constant viscosity in which the fibers were aligned parallel to the direction of shear, thereby proffering the lowest hydrodynamic drag. Application of shear may, in addition, have caused some of the water molecules associated with the sepiolite fibers to be released resulting in an apparent reduction in the size of the dispersed molecules. This, too, would effect a lowering of the apparent viscosity (Martin, 1993; Papo *et al.*, 2002). The released water would act as a lubricant, easing the movement of one particle relative to another.

From Figure 7.4a, it is evident that the rheological behaviour of the 0.5% w/v sepiolite suspension was qualitatively similar to that of the 0.25% w/v sample. The Herschel-Bulkley yield value was approximately three times higher than the corresponding value for the 0.25% w/v suspension (refer to Table 7.4a) as a more extensively interlinked network could be formed given the doubling of the number of fibers per unit volume. Complete breakdown of the three-dimensional structure did not occur instantaneously at a given shear stress as in the case of the 0.25% w/v (Figure 7.4b) and hence the sample may be regarded as having an element of shear-thinning behaviour at low shear stresses.

Table 7.4a. Rheological parameters of sepiolite suspensions of different concentration.

Sepiolite concentration (% w/v)	HB yield value, σ_{HB} (Pa)	HB Flow behaviour index, n (-)	HB Consistency index, K ($Pa.s^n$)	*HB correlation coefficient, r^2 (-)	HB model standard error (-)	Newtonian model standard error (-)	Bingham model standard error (-)	Power law standard error (-)	Casson model standard error (-)
0.25	0.0718 ± 0.0088	0.9613 ± 0.0991	0.0047 ± 0.0009	0.86279	19.12	38.37	20.62	27.81	25.42
0.5	0.2541 ± 0.0141	0.9524 ± 0.0191	0.0037 ± 0.0006	0.96470	16.73	67.24	17.89	29.94	19.36
1.0	0.7140 ± 0.0562	0.4733 ± 0.0059	0.1705 ± 0.0133	0.92534	24.80	288.9	88.58	70.45	44.03
2.0	3.2570 ± 0.2901	0.3346 ± 0.0108	1.0675 ± 0.1178	0.91872	32.44	622.6	140.3	77.28	80.02
4.0	11.5167 ± 1.1960	0.4246 ± 0.0327	1.9700 ± 0.1998	0.91771	52.04	455.4	124.4	113.1	78.18

* The lowest correlation coefficient of all replicates was quoted. The highest standard error of all replicates was quoted.

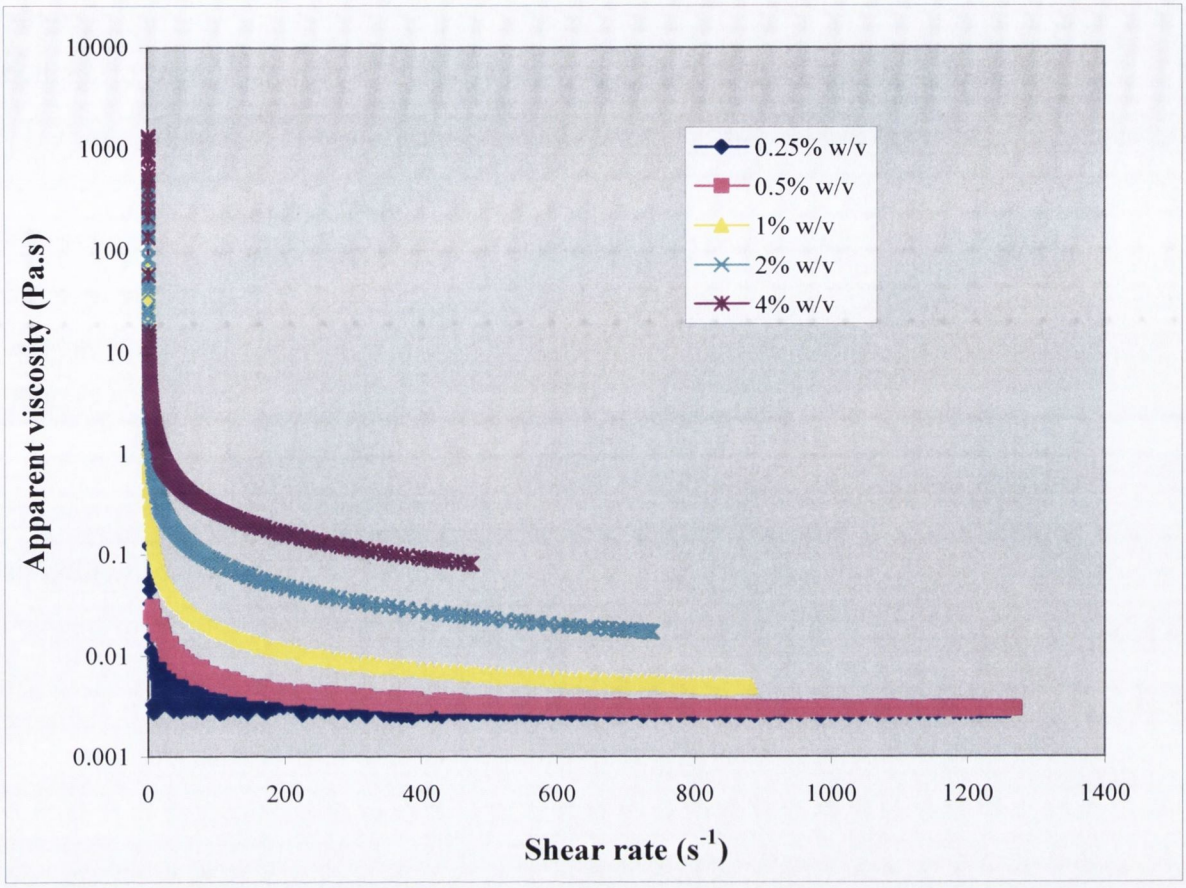


Figure 7.4b. Relationship between apparent viscosity and shear rate for sepiolite suspensions of different concentration.

From Figure 7.4a and 7.4b, it is evident that the flow behaviour of 1% w/v sepiolite suspensions may be described as pseudoplastic as the viscosity continued to decrease with an increase in the applied shear stress. Rheological modelling confirmed that the Herschel-Bulkley model was the most appropriate model to describe the flow data. Pseudoplastic behaviour is typical of clay suspensions (van Olphen, 1977). The value of the flow consistency index was 0.4788, indicating that the extent of pseudoplasticity was considerable. The change from plastic to pseudoplastic flow behaviour with increasing sepiolite concentration may be explained as follows: an increase in concentration translates into an increase in the number of fibers per unit volume and a reduction in the distance between adjacent fibers, both of which will facilitate more extensive entanglement of the fibers and increased opportunity for electrostatic and non-covalent interconnections to occur resulting in a single giant 'floc' rather than a larger number of smaller flocs.

In more concentrated suspensions, therefore, the increased number of interfibrous connections will translate into an increased apparent yield value and furthermore, given

that these connections are infinitely more complex and presumably of varying strength, they do not all yield at one particular applied stress but rather over a range of applied stresses, hence the resultant pseudoplastic behaviour.

From Figures 7.4a and 7.4b it is evident that the extent of pseudoplastic character increased as the concentration of sepiolite was increased above 1% w/v. Similar results were reported for Na-bentonite suspensions, which exhibited approximate Newtonian flow at low concentrations (1% w/v) and pseudoplastic flow at suspension concentrations of 2.5% w/v (Shainberg and Otoh, 1968; Keren, 1988).

A plot of Herschel-Bulkley yield values as a function of sepiolite concentration is presented in Figure 7.4c.

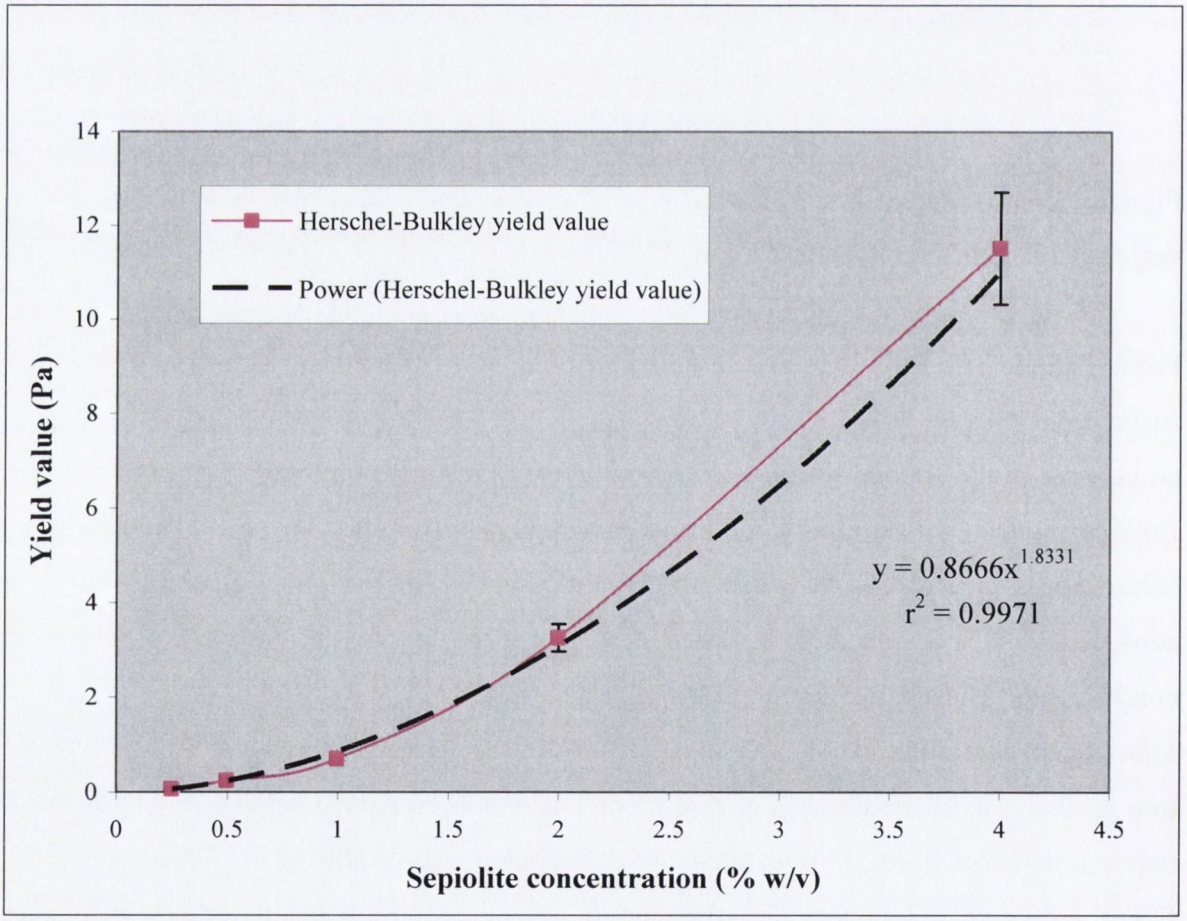


Figure 7.4c. Herschel-Bulkley yield values as a function of sepiolite concentration.

Herschel-Bulkley yield values increased with increasing concentration, but in a non-linear manner, confirming the role of interparticulate forces in the development of rheology within these suspensions. Indeed, a strong relationship between the approximate square of

concentration and both sets of yield values was observed. Matijašić and Glasnović (2002) also reported disproportionate increases in the yield value of kaolin suspensions with increasing kaolin concentration. The disproportionate increase in the yield value with an increase in concentration indicated that the framework became disproportionately more intricate and extensive with an increase in the number of fibers. As a consequence the shear thinning behaviour was evident over a much wider shear stress range.

7.4.3 Relationship between concentration and thixotropy

At low sepiolite concentrations (i.e. 0.25 - 0.5% w/v), complete structural breakdown occurred at relatively low shear stresses and thereafter flow curves became linear (Figure 7.4a). The down-curves of these rheograms were superimposable on the up-curves at high shear rates but were displaced to the left of the up-curves at very low shear rates. Such a result would be expected given that the fibrous framework had been completely destroyed at high shear and could not be reformed under shear. Following a rest time of 5 min, repeated shear of a sample produced a virtually identical flow curve with similar rheological parameters indicating that complete recovery of the three dimensional structure within the sample did occur over time (Figure 7.4d). The time dependency was attributed to the time taken for particles to come into contact via Brownian motion to restore the connective framework (Martin, 1993). At low sepiolite concentrations therefore, thixotropic behaviour was observed.

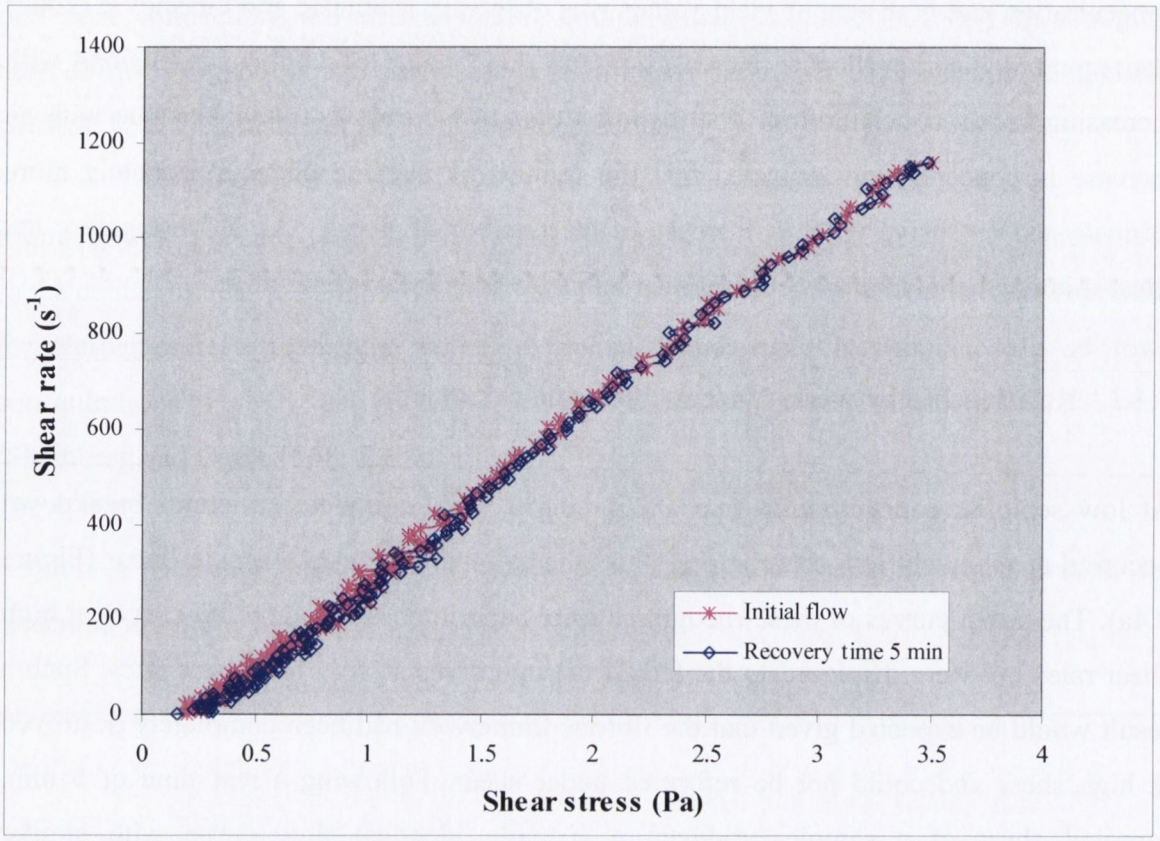


Figure 7.4d. Flow curves illustrating the repeated shear of a 0.5% w/v sepiolite sample following a recovery period of 5 min.

At higher concentrations however (≥ 1% w/v), slight displacement of the down-curve to the right of the up-curve (Figure 7.4e) was seen. This indicated that the apparent viscosity, which decreased with increasing rates of shear, recovered once the rate of shear was reduced. That the down-curve was displaced to the right of the up-curve indicated that the apparent viscosity at a given shear rate on the up-curve was lower than the apparent viscosity at the same shear rate on the corresponding down-curve i.e. the rate of structural recovery was faster than the rate of structural breakdown. Furthermore, the extent of recovery was greater than 100%. Samples subjected to two shear cycles exhibited a higher apparent viscosity at all shear rates on the up-flow curve of the second shear cycle when compared to the up-flow curve of first shear cycle (Figure 7.4e).

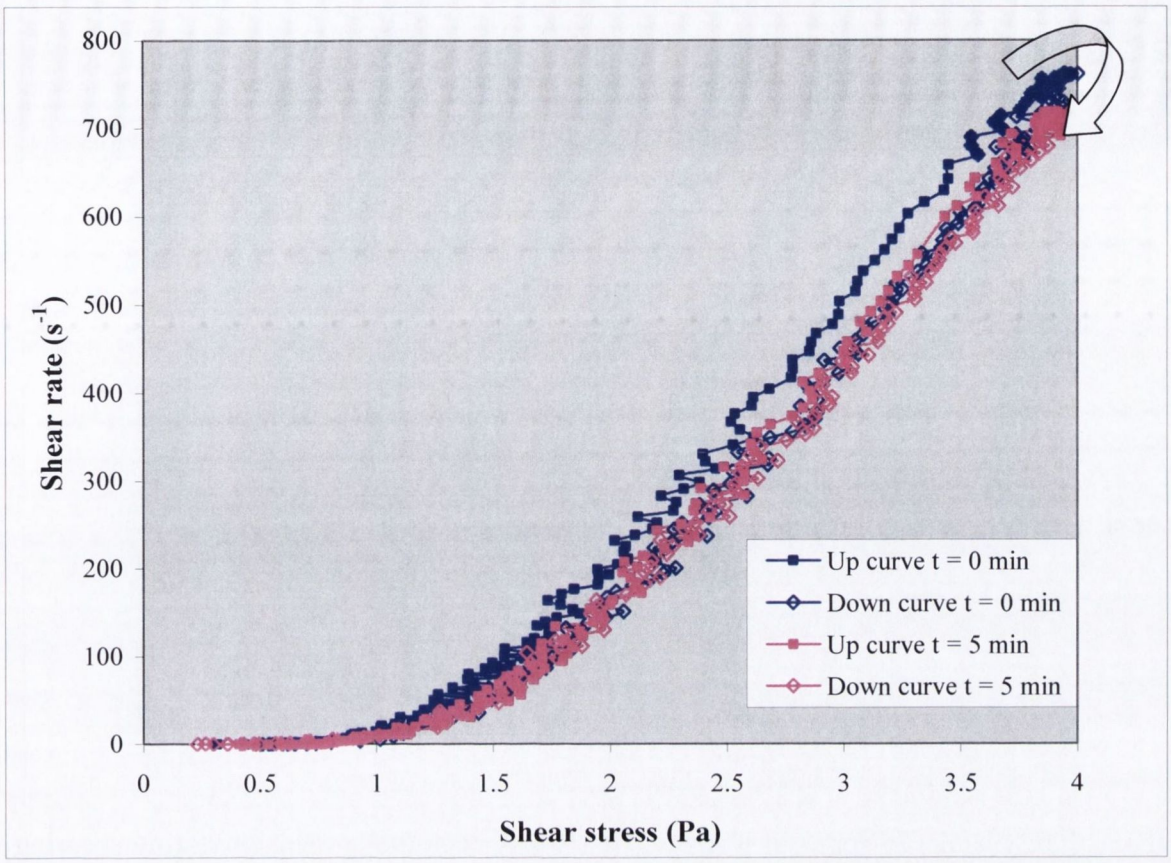


Figure 7.4e. Flow curves of a 1% w/v sepiolite suspension demonstrating antithixotropic behaviour upon first shearing cycle and absence of same upon repeated shearing following a recovery time of 5 min. (Block arrow indicates displacement of the down-curve relative to the up-curve for the first shear cycle).

Flow curves generated at a constant shear rate indicated that the apparent viscosity decreased with increasing duration of shear (Figure 7.4f). Samples sheared at a constant shear rate and allowed to rest before shear was repeated exhibited higher apparent viscosities during the second shear when compared to the initial shear (Figure 7.4f). A reversible time-dependent decrease in viscosity at a constant shear rate is defined as thixotropy. Recovery of the structure takes time such that displacement of the down-curve to the left of the up-curve would be expected in the case of a thixotropic material subjected to a shear cycle (Radebaugh *et al.*, 1996; Luckham and Rossi, 1999). Clearly, the situation in the case of sepiolite suspensions is more complex than this. While the sepiolite suspension does display a time-dependent decrease in viscosity at a constant shear rate, the change cannot be classed as truly reversible as the extent and rate of sample recovery is such that the rheological parameters of the 'recovered' sample are altered relative to the initial unsheared sample.

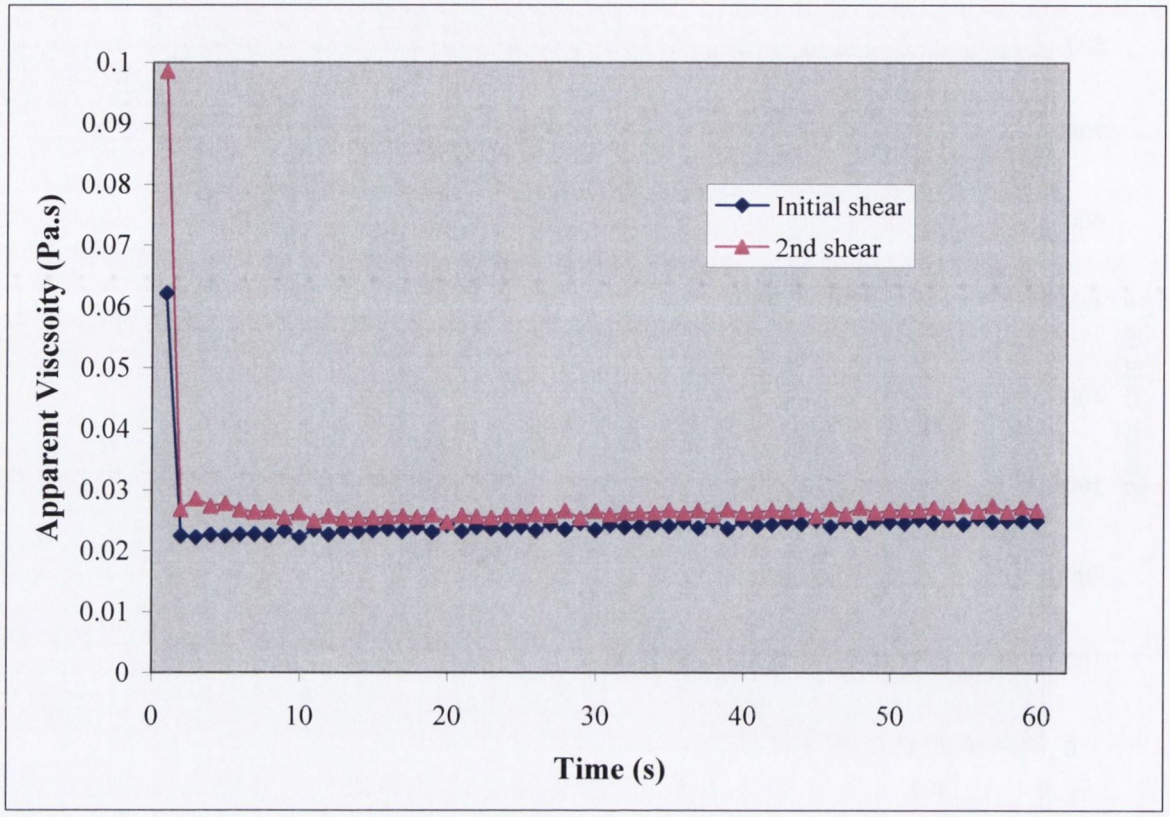


Figure 7.4f. Change in apparent viscosity of 1% w/v sepiolite suspension during shearing at a constant rate of 100 s^{-1}. Recovery time prior to application of second shear was 5 min.

Chong *et al.* (1960) reported an unusual rheological phenomenon in the rheological analysis of magnesia magma USP (7.5% w/v $Mg(OH)_2$ in water). Chong and his co-workers observed that when magnesium magma was alternately sheared at increasing and then decreasing rates of shear, the magma continuously thickened over time but at a decreasing rate, finally reaching an equilibrium state in which further cycles of increasing-decreasing shear rates no longer increased the consistency of the material (Figure 7.4g). On standing, the material returned to its initial state. This was similar to the behaviour observed in the case of 1% w/v sepiolite suspensions (Figure 7.4e). However, recovery of the sepiolite sample to its initial consistency did not occur within a time frame of 30 min. Assessment of recovery times in excess of this were not possible as the sample tended to dry out on the peltier plate of the rheometer.

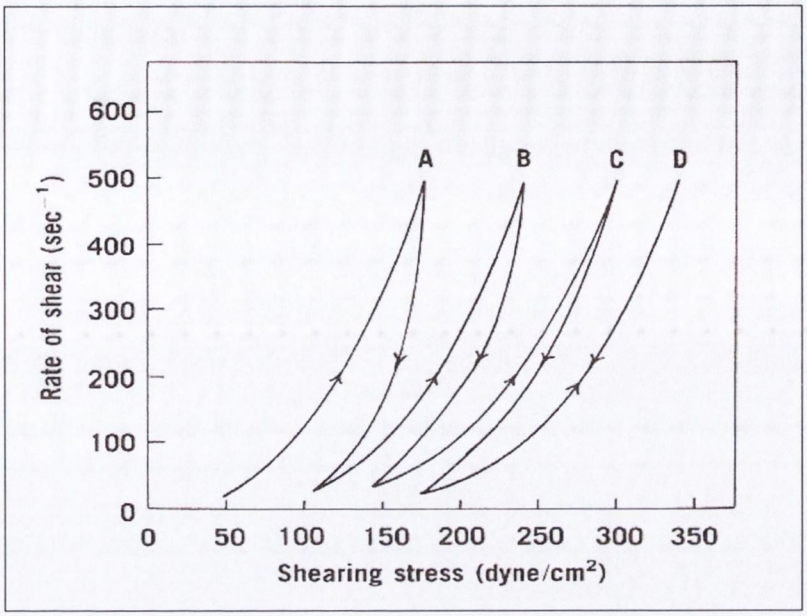


Figure 7.4g. Rheogram of magnesia magma. The material is sheared at repeated increasing and then decreasing rates of shear. At stage D, further cycling no longer increased consistency, and the up- and down-curves coincided (Reproduced from Chong *et al.*, 1960).

Classification of this unusual rheological behaviour of sepiolite suspensions ($\geq$ 1% w/v) has proved difficult. Despite the similar behaviour of magnesia magma upon shear cycling, Chong *et al.* (1960) noted that a pronounced increase in consistency could also be induced upon subjecting the material to a constant shear rate in excess of 30 s^{-1}. He termed this sol-gel-sol transformation "antithixotropy" or negative thixotropy; the sol representing the equilibrium form. Freundlich and Juliusberger (1935) noted that suspensions containing strongly anisotropic particles show different thixotropic properties depending on the change in orientation of the particles caused by the shear applied. Up-down violent shaking of a gypsum paste in a test tube caused liquefaction; solidification of the sample occurred on standing after ~ 40 min. In contrast, rolling the test tube to and fro between the palms of the hand, thus causing a regular circular movement of the liquid following violent shaking as described above led to solifidification within 20 s. Freundlich and Juliusberger (1935) deduced that the gentle circular movement caused orientation of the rod-shaped particles with their long axes lying horizontally; a condition which facilitated spontaneous solidification. This accelerated structural build-up brought about by small shear rates they termed 'rheopexy'. Rheopexy differs from dilatancy in that dilatancy is dependent on the rate of shear only. Furthermore, in the case of dilatancy the new state formed by dislocation of the particles on shear is not in a state of equilibrium; on the contrary, the

material returns to its more liquid state as soon as the external forces are removed. In contrast in a rheopectic system, the solidified structure represents the state of equilibrium; the material does not turn liquid again on standing (Freundlich and Juliusberger, 1935; Chong *et al.*, 1960).

It appears that neither the term antithixotropy nor rheopexy adequately describes the flow properties of sepiolite suspensions ($\geq$ 1% w/v). Sepiolite suspensions do not display an increase in viscosity with time when subjected to a constant shear rate, as is the requirement for the flow behaviour to be termed antithixotropic (Chong *et al.*, 1960). The definition of rheopexy is not wholly satisfied either in that accelerated structural build-up is observed following the application not only of low shear rates, but also of very high shear rates (displacement of the down-curve relative to the up-curve in Figure 7.4e was particularly pronounced at high shear rates). Further confusion results from the fact that the terms rheopexy and antithixotropy are used interchangeably in the literature (Chong *et al.*, 1960; Cheng and Evans, 1965; Radebaugh, 1996). Several authors have noted that this proposed equivalence of the terms is unjustified (Chong *et al.*, 1960; Cheng and Evans, 1965) while others note that for practical purposes, the two terms may be used interchangeably (Radebaugh, 1996; Neaman and Singer, 2000).

A review of the literature indicated that similar phenomena have been reported by Viseras *et al.* (1999) and Neaman and Singer (2000) in the case of palygorskite suspensions prepared in deionised water. Palygorskite is a fibrous magnesium silicate, differing only in structure from sepiolite in the width of the interfibrous channels. Both sets of authors referred to this behaviour as antithixotropic. Neaman and Singer (2000) use the terms antithixotropy and rheopexy interchangeably in their description of palygorskite flow behaviour. Furthermore Samyn and Jung (1967) and Radebaugh (1996) note however that clay suspensions may show negative thixotropy and such antithixotropic systems have low solids content (1-10%) and are flocculated. Moreover, Tombácz and Szekeres (2006) reported plastic and antithixotropic behaviour (which they define as an apparent viscosity on the downward flow curve higher than that at the same shear rate on the upward flow curve) for 15% w/v aqueous kaolinite suspensions at pH 6. Consequently, the increased rate and extent of structural recovery, as indicated by the formation of a hysteresis loop in which the downward flow curve is displaced to the right of the upward flow curve upon shear cycling, is throughout the rest of this thesis referred to as antithixotropic behaviour. It

is accepted that this definition is not consistent with that of Chong *et al.* (1960) but is consistent with the behaviour termed antithixotropy (albeit inappropriately) by more recent publications particularly those involving clay suspensions.

The antithixotropic behaviour of sepiolite suspensions was surprising given that Viseras *et al.* (1999, 2006) and Alvárez (1984) have reported that sepiolite suspensions demonstrate thixotropic properties. The qualitative explanation of the flow behaviour observed with sepiolite may be explained in terms of the changes in fiber association upon shear. Antithixotropic behaviour indicates that a more extensive interfibrous framework existed at a given shear stress on the down-curve when compared with the up-curve, which initially seemed somewhat implausible, given that the application of shear has been demonstrated to cause structural disruption. Neaman and Singer (2000) explained this phenomenon in the case of palygorskite as follows: the palygorskite fibers possess a net negative surface charge in deionised water which hinders intimate interaction of the fibers. The increase in the rate of stiffening of the suspension following shear is a consequence of the increased collision rate such that fibers can become linked together to reform the three-dimensional network more easily than upon standing. The pH of an aqueous sepiolite suspension is of the order of 8.2, Martínez-Ramírez *et al.* (1996) attribute this to a hydrolytic phenomenon which liberates some OH^- ions from the silanol groups present in the sepiolite structure. At this pH, the particles have a zeta potential of ~ -20 mV (Figure 7.5a). Consequently, in accordance with the Derjaguin-Landau-Verwey-Overbeek (DLVO) theory, the primary maximum energy barrier to coagulation, which is dependent on the magnitude of the zeta potential, will be reasonably large and fibers will tend to interact in the secondary attractive minimum to form three dimensional networks which are responsible for the existence of a yield value. Dilute sepiolite suspensions in distilled water produce a clear supernatant (see Section 7.4.4) and a loose fluffy sediment upon standing thereby supporting this theory of secondary minimum flocculation. Application of shear causes these three dimensional flocs to disperse such that individual fibers become aligned in the direction of shear. As the shear stress is then reduced, the particles are forced to slow, and given that all particles are unlikely to slow at the same rate, the tendency for particles to collide is increased. The velocities of the particles are such that they can cause the particles to collide with sufficient energy to overcome the repulsive barrier and rapidly form a stable three-dimensional structure with increased viscosity, hence the antithixotropic behaviour. Our theory is supported by two observations; firstly that antithixotropic behaviour was

only observed at clay concentrations ≥ 1% w/v - an increased collision frequency would be expected with an increase in the number of fibers per unit volume, and secondly, the extent of antithixotropic behaviour (as determined by the area of the hysteresis loop) was variable owing to the random nature of the particle-particle collisions required to generate a structure of increased viscosity.

7.4.4 Relationship between sedimentation behaviour and concentration

Continuous shear rheology provides a means of elucidating and quantifying the behaviour of a suspension upon application of an external stress. The majority of factors that govern the physical stability of a suspension are dependent upon the motion of the particles induced by gravity (i.e. sedimentation) (Bhargava *et al.*, 1996). In order that sepiolite may be used as a suspending agent, the concentration used must be high enough to form an interfibrous network or structured vehicle that is stable under gravity and is thus capable of retarding the sedimentation of the insoluble drug via entrapment. While rheological assessment provides a means of ascertaining the yield value of the suspension, the magnitude of the yield value necessary to prevent sedimentation – i.e. the gradual collapse of the structure under gravity - is unknown. Hence, the purpose of these preliminary sedimentation studies was to assess the sedimentation characteristics of sepiolite suspensions (i.e. sedimentation rate, quality and volume of sediment, ease of redispersion) and thus establish a suitable concentration range for use in the preparation of oral and cutaneous suspensions.

The change in the relative sediment volume, F, over time for sepiolite suspensions of different concentration is presented in Figure 7.4h. 0.25% w/v and 0.5% w/v suspensions sedimented rapidly, producing a loose fluffy sediment and a clear supernatant. Martin (1993) reported that the absence of caking and the production of a clear supernatant are indicative of a flocculated system. Despite the rapid sedimentation, the sediments in both cases were readily redispersed requiring only one to two inversions to achieve complete redispersion even after 1 month of standing. The sedimentation rate decreased dramatically with an increase in concentration, a result in keeping with the increasing trend in Herschel-Bulkley yield values with concentration in Table 7.4a. 2% w/v and 4% w/v suspensions showed no evidence of sedimentation after 1 month, and hence may be said to be in 'flocculation equilibrium'. In practical terms, the 4% w/v suspension was difficult to pour

even after a moderate amount of shaking and consequently was deemed more suitable for the preparation of semi-solid formulations. In contrast, 1% w/v and 2% w/v suspensions were readily pourable after a moderate amount of agitation. Following consideration of these results and those of the rheological studies (Section 7.4.2), the optimum concentration of sepiolite for use as a suspending agent in liquid formulations was deemed to be of the order of ~ 1% - 2% w/v. After 28 days of standing at room temperature, the relative sediment volumes of sepiolite suspensions of concentration 1% - 2% w/v were of the order of 0.88 or higher, these systems were readily redispersed and the yield values sufficiently low to ensure the production of free flowing products following a moderate level of agitation.

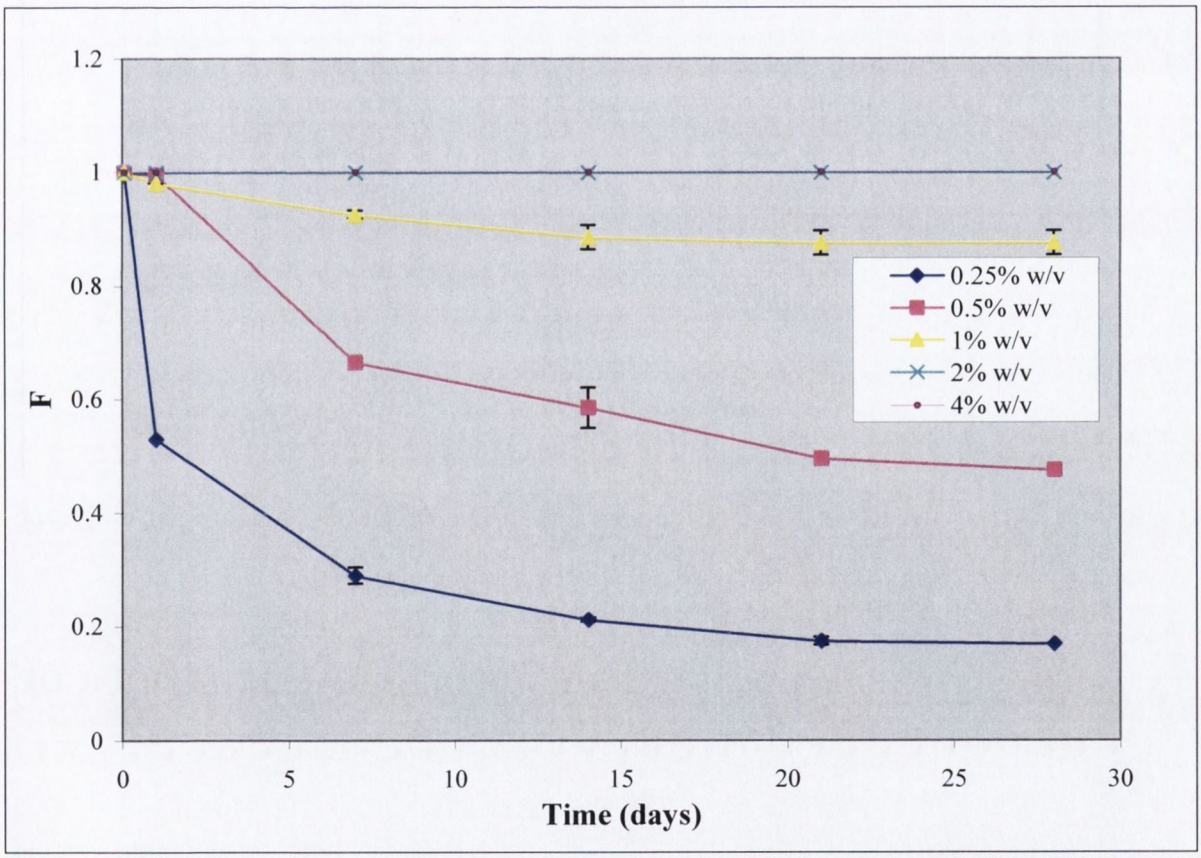


Figure 7.4h. The relative sediment volume, F, of sepiolite suspensions of different concentration as a function of time.

The sedimentation rate can be altered by vibration, as may occur during transportation. Evaluation of vibration on the physical stability of the suspension is essential (Dell and Colliopoulos, 2000). The sedimentation rate was monitored following the application of a vibrational stress for 40 min. Results are presented in Figure 7.4i below. ANOVA

confirmed that the sediment volume was comparable or indeed higher at each time point following the vibration. It is evident that the sedimentation rate was not adversely affected by the simulated transportational stress. These results augur well for the efficacy of sepiolite as a suspending agent.

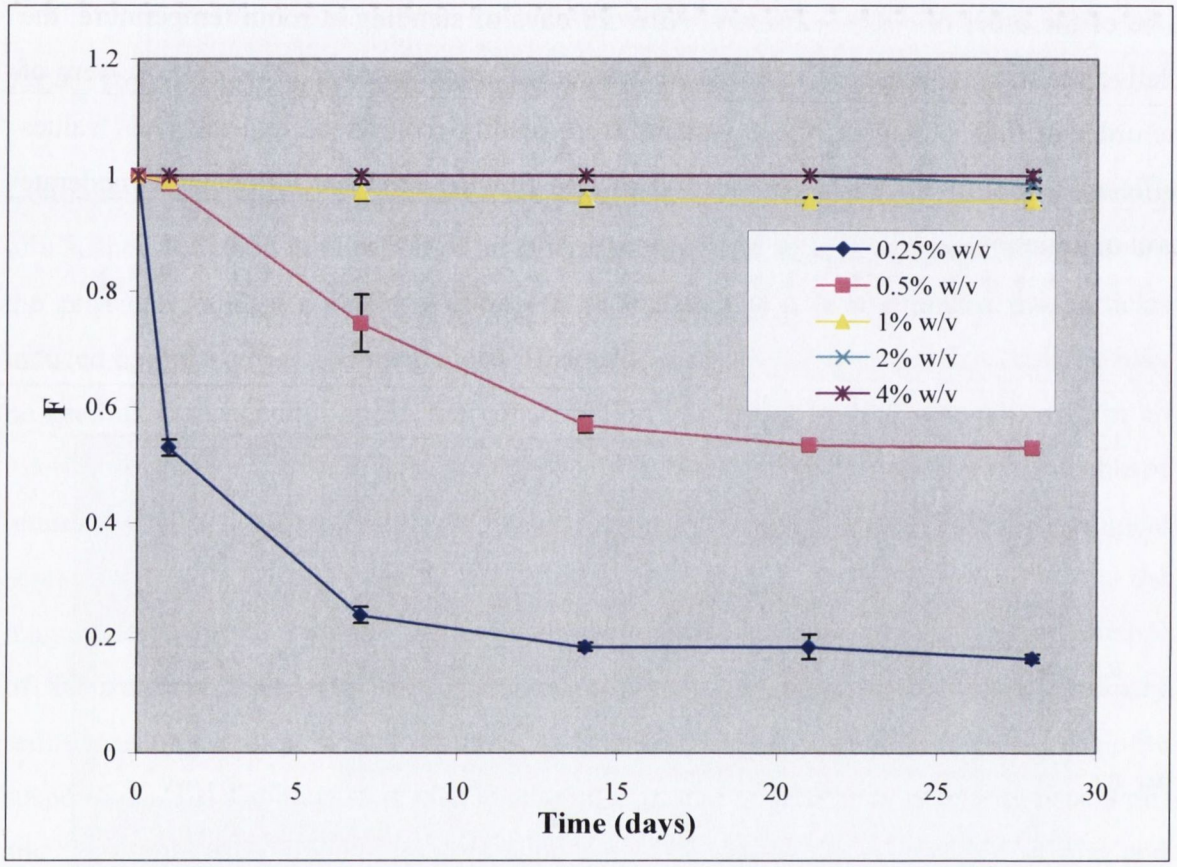


Figure 7.4i. The relative sediment volume, F, of sepiolite suspensions of different concentration as a function of time following simulated transportational stress.

7.5 THE INFLUENCE OF pH ON THE RHEOLOGICAL BEHAVIOUR OF SEPIOLITE

7.5.1 Introduction

The influence of pH on the rheological behaviour of sepiolite was also investigated. Preliminary investigations revealed that the rheological parameters were altered considerably by changes in pH. This variation was indicative of changes in the interparticulate interactions at different pHs, highlighting the importance of surface charge in the development of viscosity.

7.5.2 Zeta potential as a function of pH

In order to understand the variation in rheological behaviour with pH, the zeta potential of sepiolite fibers at different pH values was determined and the results are presented in Figure 7.5a below. From Figure 7.5a it is evident that the zeta potential of sepiolite was slightly positive at a very low pH but became increasingly negative as the pH was increased. The point of zero zeta potential is termed the isoelectric point (i.e.p.) (Lyklema, 1991). The i.e.p. represents the sum of interactions occurring at the mineral/water interface, e.g. H^+ and OH^- adsorption, distribution of dissolved lattice ions, if present, or hydrolytic reactions of H^+ and OH^- with the dissolved lattice ions at the interface (Dobias and Witika, 1995). The i.e.p. of sepiolite occurs in the pH range 2.6 – 3 and agrees well with the value quoted by Knapp *et al.* (1997) for Spanish sepiolite.

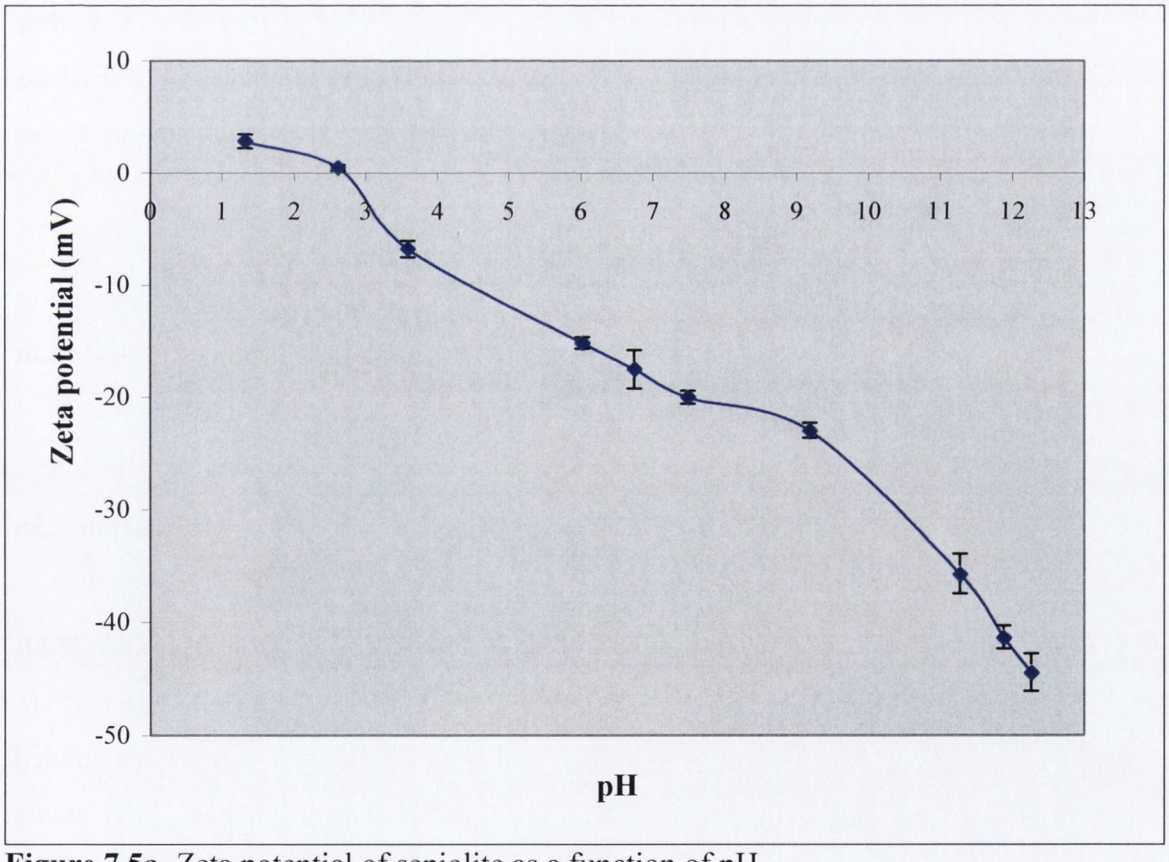


Figure 7.5a. Zeta potential of sepiolite as a function of pH.

The influence of pH on the zeta potential can be explained by considering the elemental composition of sepiolite and the origin of surface charge. Several mechanisms are involved in the development of surface charge in sepiolite:

1. **Isomorphous substitution**. Exchange of Mg in the brucite layer and Si in the silica layer by cations of lower valency results in a deficiency of positive charge (Lyklema, 1991). The extent of isomorphous substitution of sepiolite tends to be low (Simonton *et al.*, 1988) and so the magnitude of this permanent negative surface charge and the CEC are quite low. Because this charge is intrinsic to the layer structure, its sign and magnitude are independent of pH (Neaman and Singer, 2000).

2. **Surface hydroxyl groups**. Octahedral Mg-OH and tetrahedral Si-OH are situated at the broken edges and exposed hydroxyl-terminated planes of the clay particles (Tombácz and Szekeres, 2004). Silanol groups are present on the external fiber surface at intervals of 5 Å (Ahlrichs *et al.*, 1975). Silanol groups are formed as a result of broken Si-O-Si bonds at external surfaces balancing their residual charge by accepting either protons or hydroxyl groups to form Si-OH groups (Galan, 1996). Silanol groups may be protonated or deprotonated under acidic (Equation 7.5a) and alkaline (Equation 7.5b) conditions, respectively (Stumm *et al.*, 1976). Hence the portion of surface charge, the origin of which lies in the silanol groups, is pH-dependent and as an extension of this, so too is the zeta potential. The pKa for Equation 7.5a is -1, while that for Equation 7.5b is 4.0 (Duval *et al.*, 2002). The surface concentration of $Si\text{-}OH_2^+$ is highest at pH 0, while the surface concentration of $Si\text{-}O^-$ increases with increasing pH. Consequently, Equation 7.5b predominates over a wide pH range, the equilibrium lying to the right hand side of the equation at pH values exceeding 4.

$$Si - OH_2^+ \Leftrightarrow Si - OH + H^+ \qquad \textbf{Equation 7.5a}$$

$$Si - OH \Leftrightarrow Si - O^- + H^+ \qquad \textbf{Equation 7.5b}$$

Where the octahedral layers end, charges can also form on the hydroxyl groups bonded to Mg atoms. The magnesium hydroxyl groups can become protonated under acidic conditions (Equation 7.5c) and deprotonated under basic conditions (Equation 7.5d; Vico, 2003). The Mg-OH groups in sepiolite are weaker acids than the Si-OH groups (Vico, 2003) and consequently, Equation 7.4c will predominate over a wide pH range.

$$Mg - OH_2^+ \Leftrightarrow Mg - OH + H^+ \qquad \textbf{Equation 7.4c}$$

$$Mg-OH \Leftrightarrow Mg-O^{-}+H^{+} \qquad \textbf{Equation 7.4d}$$

It is unclear whether a heterogenous surface charge exists in sepiolite i.e. that there are domains of predominant positive charge and of predominant negative charge in a manner analogous to the oppositely charged faces and edges of bentonite platelets. Certainly, a study of the structure to assess the relative exposure of Mg-OH and Si-OH groups at the surface indicates that the situation is infinitely more complicated than in the case of bentonite. The permanent negative charge arising from isomorphous substitution of Mg/ Si for cations of lower valency and from unoccupied octahedral sites can be compensated for by cations adsorbed within the zeolithic channels as well as to the external surface area. Whether the zeolithic cations contribute significantly, or indeed at all, to the nature of the electrical double layer surrounding the elemental fibers is unknown. The external surface of the fibers along the *c*-axis (termed the face of the fiber, in keeping with the terminology used for bentonite) is principally composed of silicon-oxygen-hydroxyl sheets (Figure 4.2c) while the external surface at the particle edges (i.e. *100* face) is comprised of a considerable amount of exposed octahedral brucite sheets in addition to the silicon sheets. van Olphen (1977) postulated that in the case of bentonite, the silica sheets were preferentially broken at sites where aluminium atoms have substituted silicon, such that the resultant exposed surface is effectively that of an alumina surface and typically carries a positive double layer. This may also be true of sepiolite, where magnesium/ aluminium/ iron have been reported to substitute for silicon, such that the surface charge at the edges is somewhat less negative than that on the faces and even possibly electroneutral or positive. Three different modes of particle association could then occur: face-to-face (FF), edge-to-face (EF) and edge-to-edge (EE) (Figure 1.5c). As described in Chapter 1, the electrical interaction energy for the three types of association is governed by three different combinations of the two double layers. Additionally the rate of diffusion of the particles as they approach each other in these three ways is not the same and they may not occur simultaneously or to the same extent in the flocculated state (Luckham and Rossi, 1999).

3. **Ion adsorption.** Ions may be adsorbed onto the fiber surface from a bulk electrolyte solution.

At high pH, therefore, the abundant silanol groups will tend to be deprotonated, producing a negative charge. Isomorphous substitution of Mg by atoms of lower valence also results in a permanent negative charge. The small number of edge Mg-OH groups will tend to act as bases and accept protons producing a small positive charge. The sum of all these charges results in a net negative zeta potential at high pH. Given that the surface silanol groups are far more abundant than the surface Mg-OH groups and that the charge due to isomorphous substitution is constant and negative, the extent of deprotonation of the silanol groups will be the main determinant of zeta potential at any given pH (assuming the absence of specifically adsorbing ions). As the silanol groups are acidic oxides, they will tend to be deprotonated over a very wide pH range and as a consequence the zeta potential is negative over a very wide pH range (pH > 3). The extent of deprotonation of Si-OH groups will decrease as the pH drops and so the surface charge becomes less negative. Below the i.e.p., the electrokinetic charge becomes positive as Equations 7.5a and 7.5c predominate. Analogous results were reported by Flörke *et al.* (2005) who reported that silanol groups of precipitated silica were protonated at very low pH values (pH 2). Furthermore, the i.e.p. for silica was reported to be 3.0 (Knapp *et al.*, 1997) reflective of the importance of the silanol groups in the development of electrokinetic charge in sepiolite. The zeta potential at the native pH of the clay (pH 8.2) was ~ -20 mV.

7.5.3 Rheological behaviour of sepiolite suspensions as a function of pH

The rheological behaviour of 1% w/v sepiolite suspensions of different pH values was investigated. The pH values investigated (pH = 1.2, 5.8 and 13.1) were chosen based on work conducted by Dressman *et al.* (1993). These values represent those of gastric fluid at three extreme conditions (i.e. pH before lunch, after lunch, highly anomalous pH, respectively). The temperature used was 37 °C, again with the aim of mimicking physiological conditions. The rheological behaviour of an aqueous suspension of sepiolite of unadjusted pH (i.e. pH 8.2) was also investigated as a control. Flow curves for these suspensions are shown in Figure 7.5b.

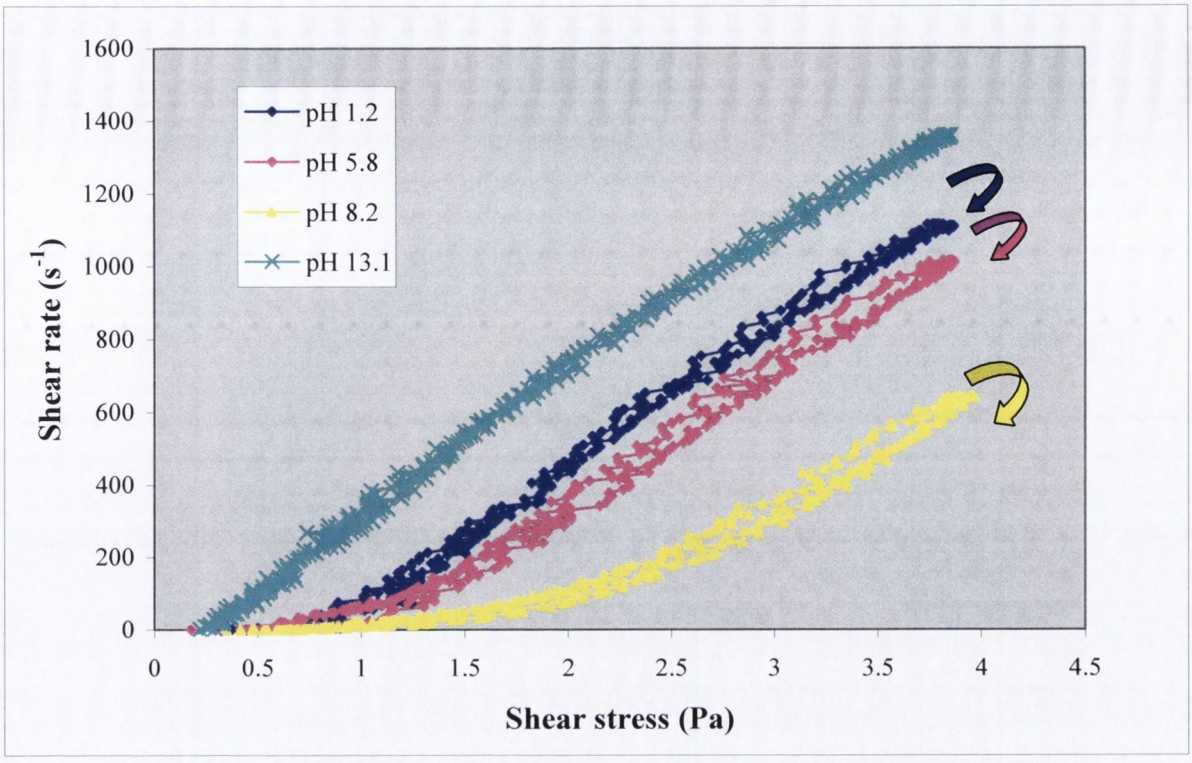


Figure 7.5b. Flow curves of 1% w/v sepiolite suspensions as a function of pH. (Colour-coded block arrows indicate the displacement of the downward flow curve relative to the upward flow curve).

Fitting of each data set to the rheological models was also carried out as described in section 3.7.4.1. In all instances, the lowest standard error was associated with the fit of the Herschel-Bulkley model to the data (Table 7.5a). The Herschel-Bulkley parameters are presented in Table 7.5a below. The change in Herschel-Bulkley yield stress as a function of pH is summarized in Figure 7.5c. The results are discussed relative to the behaviour of the unadjusted suspension of sepiolite (i.e. pH 8.2).

Table 7.5a. Rheological parameters for 1% w/v sepiolite suspensions of different pH at 37 °C.

Sepiolite suspension pH (-)	HB yield value, σ_{HB} (Pa)	HB Flow behaviour index, n (-)	HB Consistency index, K ($Pa.s^n$)	HB correlation coefficient, r^2 (-)	HB model standard error (-)	Newtonian model standard error (-)	Bingham model standard error (-)	Power law standard error (-)	Casson model standard error (-)
1.2	0.958 ± 0.046	0.979 ± 0.007	0.0223 ± 0.0023	0.83423	44.97	304.8	55.11	144.3	70.25
5.8	0.343 ± 0.113	0.824 ± 0.220	0.0150 ± 0.0003	0.93087	20.92	189.9	56.81	55.25	23.61
8.2	0.836 ± 0.035	0.532 ± 0.100	0.1719 ± 0.0198	0.94166	25.25	266.3	99.84	111.8	48.47
13.1	0.264 ± 0.014	1.071 ±0.036	0.0015 ± 0.0003	0.89950	14.81	58.67	18.30	34.82	26.23

Note: The lowest correlation coefficient of all replicates was quoted. The highest standard error of all replicates was quoted.

From Figure 7.5b it is evident that the rheological behaviour is altered considerably by changes in the pH. At very high pH values, suspensions exhibited near Newtonian flow with a very small yield value (~ 0.264 Pa). At this pH the sepiolite fibers tend to repel one another because the magnitude of the zeta potential is high. Consequently, interfibrous network formation will be unlikely. Bhargava *et al.* (1996) reported that zeta potentials of 25 mV or more typically result in the production of deflocculated systems as the repulsive forces exceed the attractive van der Waals forces. The existence of a yield value may be reflective of the large amounts of water associated with the fiber surfaces, resulting in an effective increase in the size of the dispersed fibers, hence hindering their relative movement, similar to the electroviscous effect proposed by Rand *et al.* (1980) and Güven (1992). Upon shear, the associated solvent molecules can be released thus reducing dispersed particle size and lowering the apparent viscosity (Martin, 1993). As individual particles can move independently upon shear, Newtonian behaviour is observed once the yield stress has been exceeded.

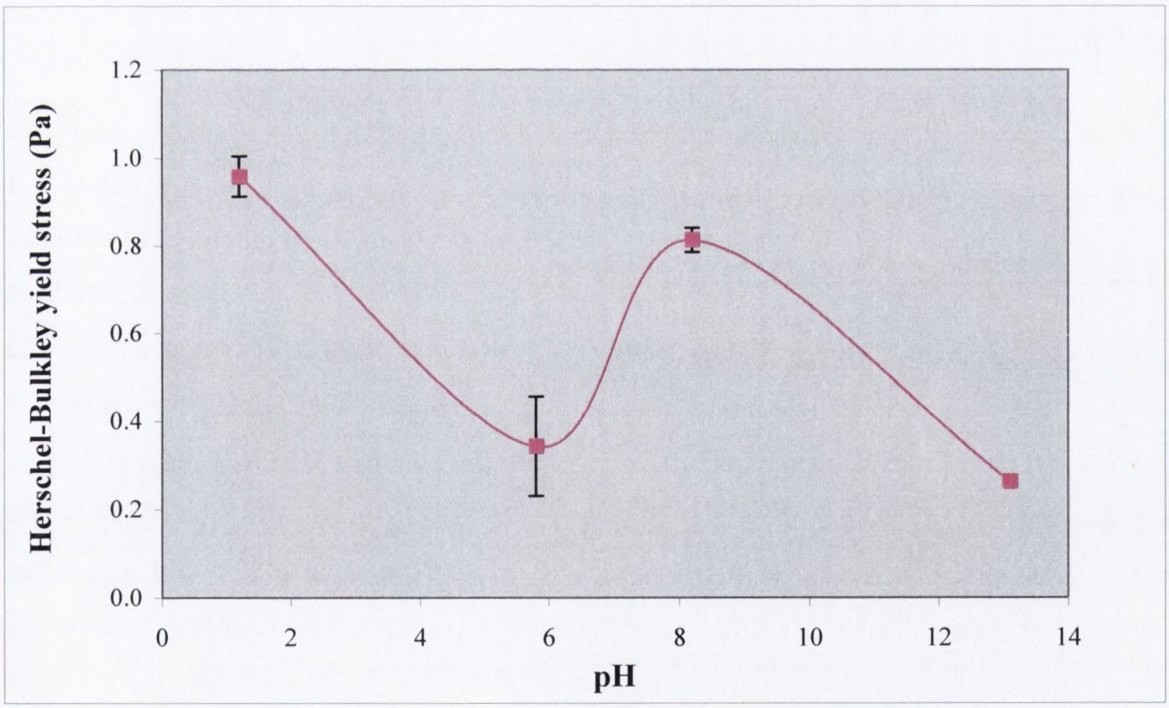


Figure 7.5c. The influence of pH on the Herschel-Bulkley yield values of 1% w/v sepiolite suspensions.

The zeta potential at pH 8.2 was of the order of -20 mV. The low value of the HB flow index (0.532) confirmed considerable pseudoplastic behaviour. The yield value was much higher than that at pH 13.1. Viseras *et al.* (1999) also reported a drastic reduction in yield

stress following treatment of 10 % w/v sepiolite suspensions with basic solutions. Changes in pH caused similar qualitative changes in the rheological behaviour of palygorskite and bentonite suspensions. Neaman and Singer (2000) noted a switch from pseudoplastic flow to near-Newtonian flow on increasing the pH of 3% w/v palygorskite suspensions from 7 to 9. Keren (1988) reported that both the apparent viscosity and yield stress of 2.5% w/v suspensions of Na-montmorillonite decreased with increasing pH from 7 to 10. Non-Newtonian flow and Newtonian flow were observed at pH 7 and pH 10, respectively. From the zeta potential study it was evident that the magnitude of the negative electrokinetic charge of sepiolite was reduced by ~ 50% with the drop in pH from 13.1 to 8.2. As a consequence, interparticulate repulsion was reduced to such a degree that an extensive three dimensional network could be established producing a system with a high yield value which was gradually destroyed under shear, hence the pseudoplastic behaviour. These findings are in agreement with those of Bhargava *et al.* (1996) and Ofner *et al.* (1996) who reported that for colloids in general, the reduction of the zeta potential below 25 mV resulted in attractive forces exceeding repulsive forces and consequently flocculation as the particles came together in the secondary attractive minimum.

The zeta potential at pH 5.8 was of the order of -14 mV, thereby reducing the magnitude of the primary repulsive barrier to particle agglomeration. It would have been anticipated that this reduction in interparticulate repulsion would translate into an increased yield value as more intimate entanglement of the fibers could occur. However, the Herschel-Bulkley yield value was lower than the corresponding values at pH 8.2. Santarén (1993) did observe a reduction in the yield stress of sepiolite suspensions on decreasing the pH from 7 to 6 but did not propose any explanation for same. It may be the case that a threshold value for interparticulate repulsion exists, below which the reduced repulsion hinders the independent orientation of one fiber relative to another consequently producing a less voluminous three dimensional structure, although this is purely supposition. Alternatively, the anomalous rheological behaviour observed at pH 5.8 can be explained by the presence of a heterogeneous edge-face surface charge. At pH 8.2, the edge Mg-OH groups may be protonated/ neutral while the more acidic silanol counterparts on the faces are predominantly negatively charged. This surface charge heterogeneity may favour EF interactions at pH values ~ 8.2, which will lend themselves to the formation of a porous voluminous scaffold with a high yield value (van Olphen, 1977). At pH values ~ 5.8, the acidity of the environment may be such that ionization of the silanol groups is depressed

and FF associations are facilitated. FF associations would result in the formation of thicker dispersed units, thereby fragmenting the three dimensional network and reducing the yield value. As further support for this theory, scanning electron micrographs of palygorskite at low pH revealed domains of parallel orientated fibers arranged in the suspension by FF contacts (Neaman and Singer, 2000).

At very low pH, the flow behaviour index, n, obtained from data fitting to the Herschel-Bulkley model is 0.979; the yield value is high (0.958 Pa), consequently rheological behaviour at this pH may best be described as plastic. The zeta potential at pH 1.2 is slightly positive, hence the repulsive energy barrier is reduced relative to that at pH 8.2 and so fiber coagulation would be expected to occur, resulting in a high yield structure which fails to break down upon shear as the coagulation process is irreversible. This is in agreement with the observed plastic-like flow behaviour. An alternative explanation for the plastic behaviour of sepiolite at low pH may be extracted from a consideration of the effect of strong acid treatment on the structure of sepiolite. Several authors (Aznar *et al.*, 1995; Radojević *et al.*, 2002; Santarén, 2003) have noted that very strongly acidic conditions cause the leaching of octahedral magnesium ions, leaving the more stable tetrahedral layer unchanged. Where the acid treatment is sufficiently severe and prolonged, complete dissolution of the octahedral cations yields highly porous silica in which the fibrous morphology is preserved. Colloidal silicas have been documented to display pseudoplastic-plastic flow behaviour depending on the concentration (Ofner *et al.*, 1996) and consequently it is possible that the altered rheological parameters at low pH may be in part reflective of a change in the elemental composition of sepiolite.

7.5.4 SEM of sepiolite suspensions at different pH values

It is assumed in the preparation of these samples that the nature of the fibrous interaction is not altered. SEMs of the sepiolite at pH 1.2, 5.8, 8.2 and 13.1 are presented in Figures 7.5d to 7.5g respectively. It should be noted that the magnification of the sample at pH 8.2 (Figure 7.5f) is lower that at the other pH values.

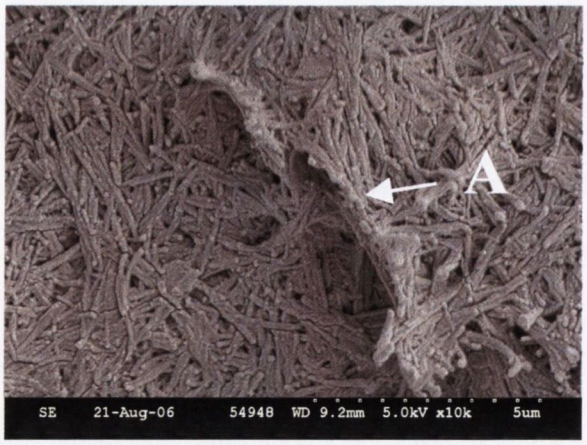


Figure 7.5d. Sepiolite at pH 1.2 (magnification x 10,000).



Figure 7.5e. Sepiolite at pH 5.8 (magnification x 10,000).

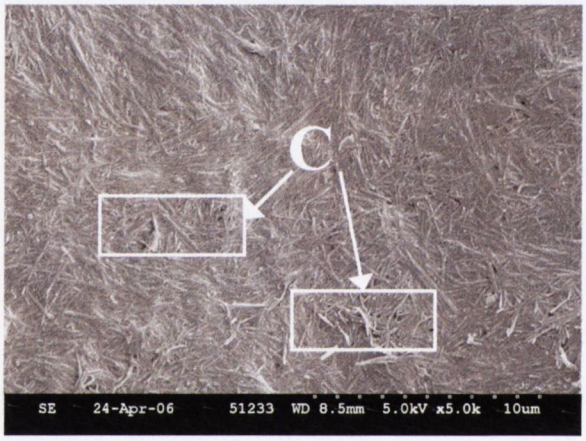


Figure 7.5f. Sepiolite at pH 8.2 (magnification x 5,000).

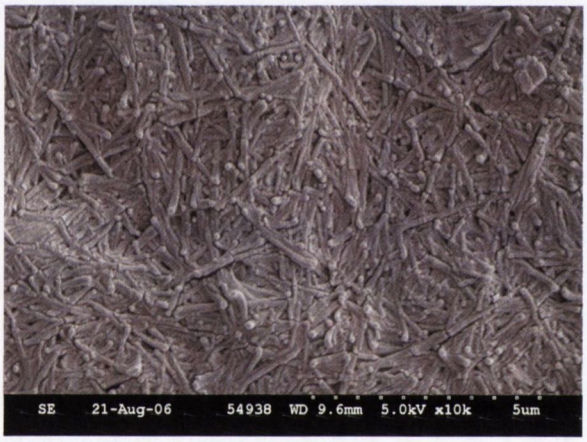


Figure 7.5g. Sepiolite at pH 13.1 (magnification x 10,000).

At pH 1.2 FF, EF and EE associations of the sepiolite fibers were evident and hence confirmed the coagulated state predicted by both the zeta potential and rheological parameters. The network of fibers built in the Z-direction (i.e. perpendicular to the surface of the microscopic stub) was retained (Point A) during the traumas of filtration, sample mounting and coating, emphasizing the mechanical strength of the scaffold.

At pH 5.8, bundles of parallel-orientated fibers were evident (point B), again in agreement with the observed rheological parameters and zeta potential measurements. The absence of FF associations in the sample at pH 8.2 is indicative of the fact that the zeta potential at this pH facilitates EF and EE associations (which serve to increase the yield value) but hinders formations of bundles (which reduce the yield value). The three dimensional nature of the scaffold was again evident (point C). At pH 13.1, minimal, if indeed any, interfibrous interaction would be anticipated given the rheological and zeta potential

results. Drying of such a highly peptized sample will not maintain the disperse nature of the fibers, but a haphazard orientation of one fiber relative to another in the dried sample, reflecting the absence in particular of extensive FF associations would be expected, and was found to be the case.

7.5.5 Antithixotropy, thixotropy and pH

Antithixotropic behaviour was observed in the case of 1% w/v sepiolite suspensions at pH 5.8 and pH 8.2. Application of a second shear cycle led to an equilibrium state in which the up-curve was superimposed on the down-curve (similar to Figure 7.4e) indicating that a maximum consistency had been reached. Again, recovery of initial sample consistency was not seen within 30 min of completion of the initial shear.

Figure 7.5h illustrates the response of a sepiolite sample at pH 13.1 to a second shear cycle 5 min after the completion of the first. Markedly different behaviour was witnessed on repeated shear at this pH. The rheogram associated with the second shear cycle was displaced to the left of the first. Comparison of the rheological parameters for these two flow curves (Table 7.5b) indicated that the yield value was 50% lower on the second shear cycle relative to the first but that the consistency and flow behaviour indices were similar. The magnitude of the yield value is dependent on the extent to which the initial structure was restored; and as the flow behaviour index in both cases is ~1, the consistency index can be regarded as a measure of the viscosity of the system at high shear rates when structural breakdown has been completed. It was concluded therefore that only partial restoration of the structure had occurred during the 5 min recovery period. Extension of the recovery time to 30 min (in the case of a fresh sample subjected to one shear cycle) resulted in complete recovery of the sample as indicated by the similarity of the flow curves and yield values for the first and second shear cycles. Thus sepiolite may be regarded as exhibiting positive thixotropy at high pH. This result is consistent with the findings of Samyn and Jung (1967), who reported that magnesium aluminium silicate (Veegum® HV) suspensions demonstrated antithixotropic behaviour when flocculated and positive thixotropic behaviour when deflocculated.

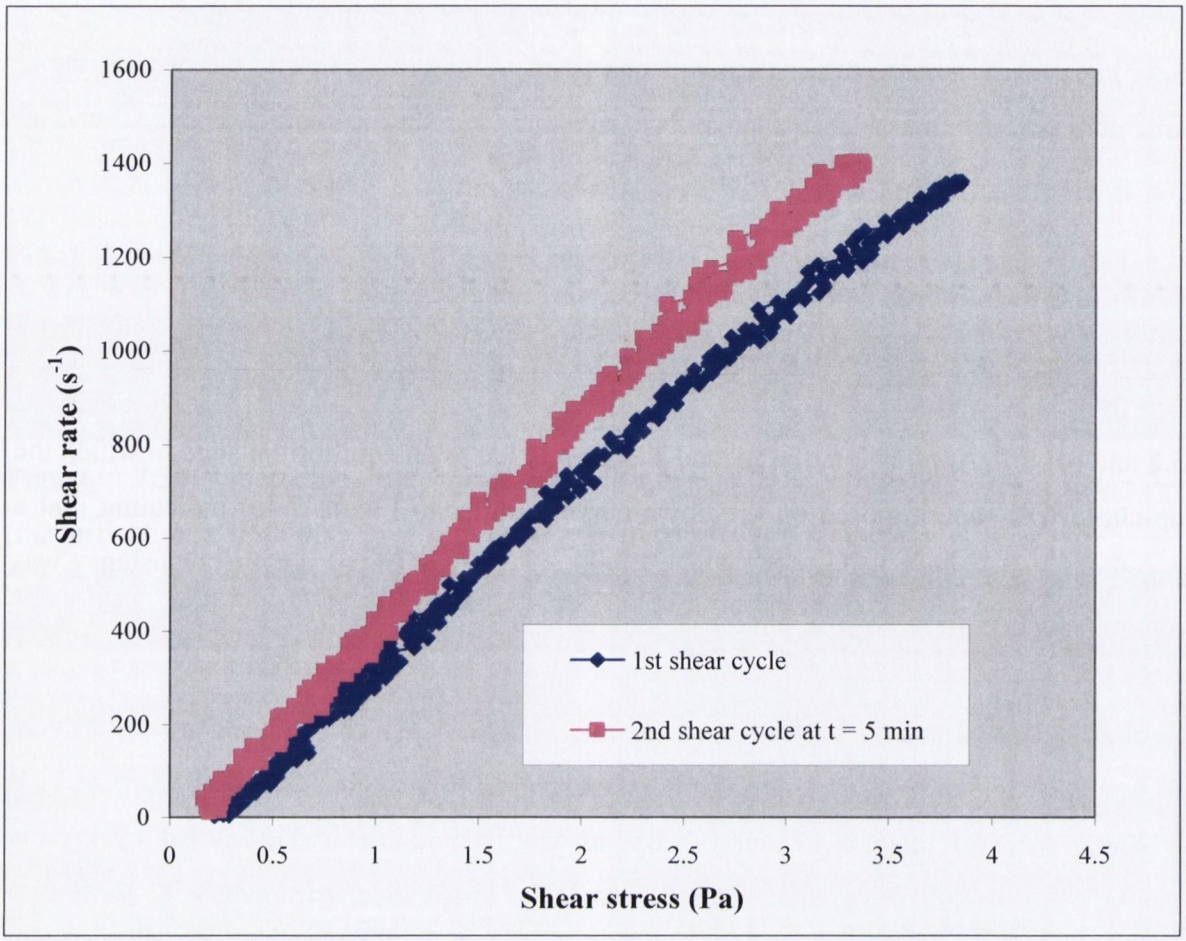


Figure 7.5h. Flow curves of a 1% w/v sepiolite suspension at pH 13.1 demonstrating failure of the sample to fully recover from the effects of the 1st shear cycle within a 5 min recovery period.

Table 7.5b. Herschel-Bulkley rheological parameters for flow curves presented in Figure 7.5h.

Herschel-Bulkley parameters	**1st shear cycle**	**2nd shear cycle at t = 5 min**
Yield value, σ_{HB} (Pa)	0.2792	0.1322
Flow behaviour index, n (-)	1.039	1.022
Consistency index (Pa.s^n)	0.001843	0.001756
Correlation coefficient, r^2 (-)	0.9957	0.9967

The difference in the rheological behaviour on repeated shear at different pH values is most likely linked to the differences in surface charge. At pH 13.1 the fibers exhibit a highly disperse nature on account of the large negative zeta potential, and as a consequence

the likelihood of them colliding with a velocity sufficient to overcome the repulsive energy barrier to facilitate rapid and extensive interparticle bonding, as is believed to be the cause of antithixotropy, is low. The reduction in the magnitude of the zeta potential as the pH is decreased reduces the interparticulate repulsion making rapid structural recovery under decreasing rates of shear (i.e. antithixotropy) possible.

7.6 THE INFLUENCE OF TEMPERATURE ON THE RHEOLOGY AND STABILITY OF SEPIOLITE SUSPENSIONS

7.6.1 Introduction

During the normal processes of transport, storage and distribution, pharmaceutical products will be subjected to fluctuations in temperature. Consequently, the influence of changes in temperature on the stability of such products must be evaluated. The flow behaviour of 1% w/v sepiolite suspensions at 4 °C, 20 °C and 40 °C was evaluated. 4 °C is reflective of the temperature of a refrigerated unit and 40 °C is the temperature used for accelerated stability testing of pharmaceutical products in accordance with the ICH guidelines (2003). In addition, storage temperatures of the order of 40 °C may be encountered in tropical areas (Zatz *et al.*, 1996).

7.6.2 Rheological behaviour of sepiolite suspensions at different temperatures

Flow curves of 1% w/v sepiolite suspensions at 4 °C, 20 °C and 40 °C and their corresponding rheological parameters are presented in Figure 7.6a and Table 7.6a respectively. In the construction of the flow curves, the applied shear stress range was kept constant and the resultant shear rate measured. Antithixotropic behaviour was observed at each of the three temperatures under investigation. From the flow curves, it was evident that increasing the temperature from 20 °C to 40 °C resulted in an increase in the resultant shear rate at any given shear stress, i.e. a reduction in the apparent viscosity. A slight increase in the apparent viscosity at high shear stresses was observed on reducing the temperature from 20 °C to 4 °C.

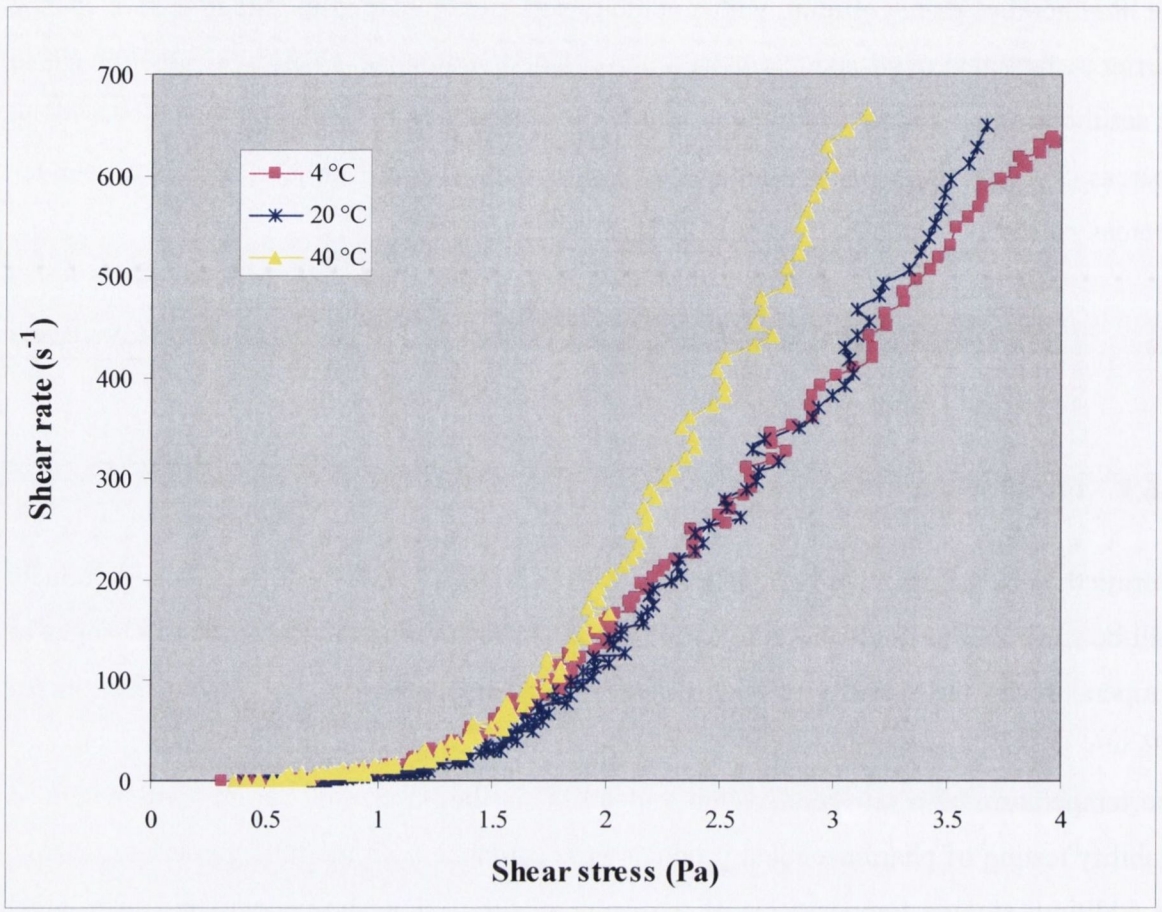


Figure 7.6a. Upward flow curves of 1% w/v sepiolite suspensions as a function of temperature.

Table 7.6a. Herschel-Bulkley (σ_{HB}) yield values of 1% w/v sepiolite suspensions at different temperatures (This rheological model provided the best fit of all those examined).

	Temperature (°C)		
	4	**20**	**40**
σ_{HB} (Pa)	0.4754 ± 0.0123	0.7410 ± 0.0562	0.6539 ± 0.0506

Changes in the temperature principally affect two parameters: namely the extent of Brownian motion and the viscosity of the suspending medium, i.e. water. Brownian motion arises from collisions of water molecules with suspended particles of diameter less than 5 μm (Martin, 1993). If numerous successive unbalanced collisions occur, the particles will move rapidly. The process, if repeated, produces random translation and rotation of the clay particles (McBride and Baveye, 2002). Brownian motion in clay suspensions therefore tends to randomize particle orientations, destroying alignment and increasing the apparent viscosity (Chang *et al.*, 1993). Brownian motion is composed of both rotational and

translational velocities (Chang *et al.*, 1993; McBride and Baveye, 2002). For spherical particles, the translational diffusion coefficient, D, is given by the Stokes-Einstein equation:

$$D = k_B T / 6\pi\eta_s r \qquad \textbf{Equation 7.6a}$$

where k_B is the Boltzmann constant, T is the absolute temperature, η_s is the viscosity of the solvent and r is the radius of the suspended particles (Einstein, 1956; cited in McBride and Baveye, 2002).

The rotational diffusion coefficient of disc-shaped (anisometric) particles, D_R, is given by:

$$D_R = 3k_B T / 32\eta_s r^3 \quad \text{(Hunter, 1989)} \qquad \textbf{Equation 7.6b}$$

where k_B, T, η_s and r have the meanings explained previously.

Consequently, both translational and rotational velocities are directly proportional to the temperature. The effect of rotational Brownian motion is most significant for suspensions of elongated particles (Chang *et al.*, 1993). A higher temperature would be expected to increase rotational and translational velocities, increasing fiber entanglement, network formation and consequently the yield value.

The temperature dependence of the viscosity of water also needs to be taken into account as the viscosity of a suspension (η) is directly related to the viscosity of the suspending medium (Barnes *et al.*, 1989). The viscosity of water (η_s) decreases in a non-linear manner with temperature; the relationship is expressed approximately by an equation analogous to the Arrhenius equation of chemical kinetics (Martin, 1993):

$$\eta_s = Ae^{E_v / RT} \qquad \textbf{Equation 7.6c}$$

where A is a constant depending on molecular weight and molar volume of the liquid, R is the absolute gas constant, T is the absolute temperature and E_v is an activation energy required to initiate flow between the molecules upon the application of an external stress.

Table 7.6b quotes the values for the viscosity of water at the three temperatures under investigation. Consequently an increase in temperature will not only decrease the viscosity of the suspending medium, but will also increase the translational and rotational diffusional velocities of the suspended particles which will act to increase the yield value and suspension apparent viscosity at low shear rates where destruction of the fibrous network is incomplete.

In order to predict the effect of temperature on the development of a yield value from first principles, the influence of temperature on the Brownian motion coefficients must be considered. The magnitudes of the Brownian motion coefficients are inversely proportional to the viscosity of the suspending medium, water, and directly proportional to the absolute temperature, which in turn is inversely related to the logarithm of the viscosity of the suspending medium. For our purposes, Equation 7.6a, 7.6b and 7.6c may be rewritten as:

$$D = \frac{K_1 T}{\eta_s} \qquad \textbf{Equation 7.6d}$$

and

$$D_R = \frac{K_2 T}{\eta_s} \qquad \textbf{Equation 7.6e}$$

and

$$\ln \eta_s \propto \frac{1}{T} \qquad \textbf{Equation 7.6f}$$

and for a given suspension

$$D_{rel} \quad \text{and} \quad D_{R_{rel}} = \frac{T_1 \eta_{s2}}{T_2 \eta_{s1}} \qquad \textbf{Equation 7.6g}$$

where D_{rel} is the relative translational diffusion coefficient (i.e. the ratio of the translational diffusion coefficient at temperature, T_1, to that at T_2), D_{Rrel} is the relative rotational diffusion coefficient (i.e. the ratio of the rotational diffusion coefficient at temperature, T_1, to that at T_2), η_{s1} and η_{s2} represent the viscosity of the suspending medium at temperatures, T_1 and T_2 respectively, and K_1 and K_2 are temperature independent constants for particles of given radius, r.

Applying Equation 7.6g at the three temperatures under study here allows calculation of a relative translational and rotational diffusion coefficient i.e. the translational (or rotational) diffusion coefficient at temperature 1, (T_1), divided by that at 20 °C (T_2). Results are presented in Table 7.6b. The relationship between temperature, η_s and D_{Rrel} is presented in Figure 7.6b.

Table 7.6b. The dynamic viscosity of water and the relative rotational diffusion coefficient, D_{Rrel}, at the three experimental temperatures (relative to that at 20 °C).

Temperature (°C)	**Dynamic Viscosity of water*** **(Pa.s)**	**D_{Rrel}[§]** **(-)**
4	0.001569	0.604
20	0.001003	1.000
40	0.000653	1.641

*Values from ThermExcel (2003).

[§]The magnitude of the relative rotational diffusion coefficient will be identical to the relative translational diffusion coefficient.

It is expected that the magnitude of the yield value of the system will be a function of D and D_R as described previously and therefore D_{Rrel} would predict an increase in the yield value with increasing temperature. Consequently, the D_{Rrel} value would predict an increase in the yield point with an increase in temperature. One-way ANOVA confirmed that the Herschel-Bulkley yield value at 4 °C was indeed significantly lower than that at either 20 °C or 40 °C ($p < 0.05$). However, the Herschel-Bulkley yield value at 20 °C was not significantly different from that at 40 °C. An increase in the thermal energy of the system will not only increase the frequency of fiber-fiber collisions, which serve to build the three dimensional network, it will also increase the frequency of water-fiber collisions, which may hinder formation of the fibrous framework where such collisions cause the displacement of a fiber from a point of contact with another fiber. Furthermore, the more energetic water molecules will offer a higher resistance to immobilization within the structured vehicle; a challenge to which the fibrous network may, in part, succumb. The failure of the yield value to increase with a further increase in temperature from 20 °C to 40 °C would indicate that the more violent fiber-water collisions at the higher temperature antagonized the positive effect of an increased fiber-fiber collision frequency on network formation.

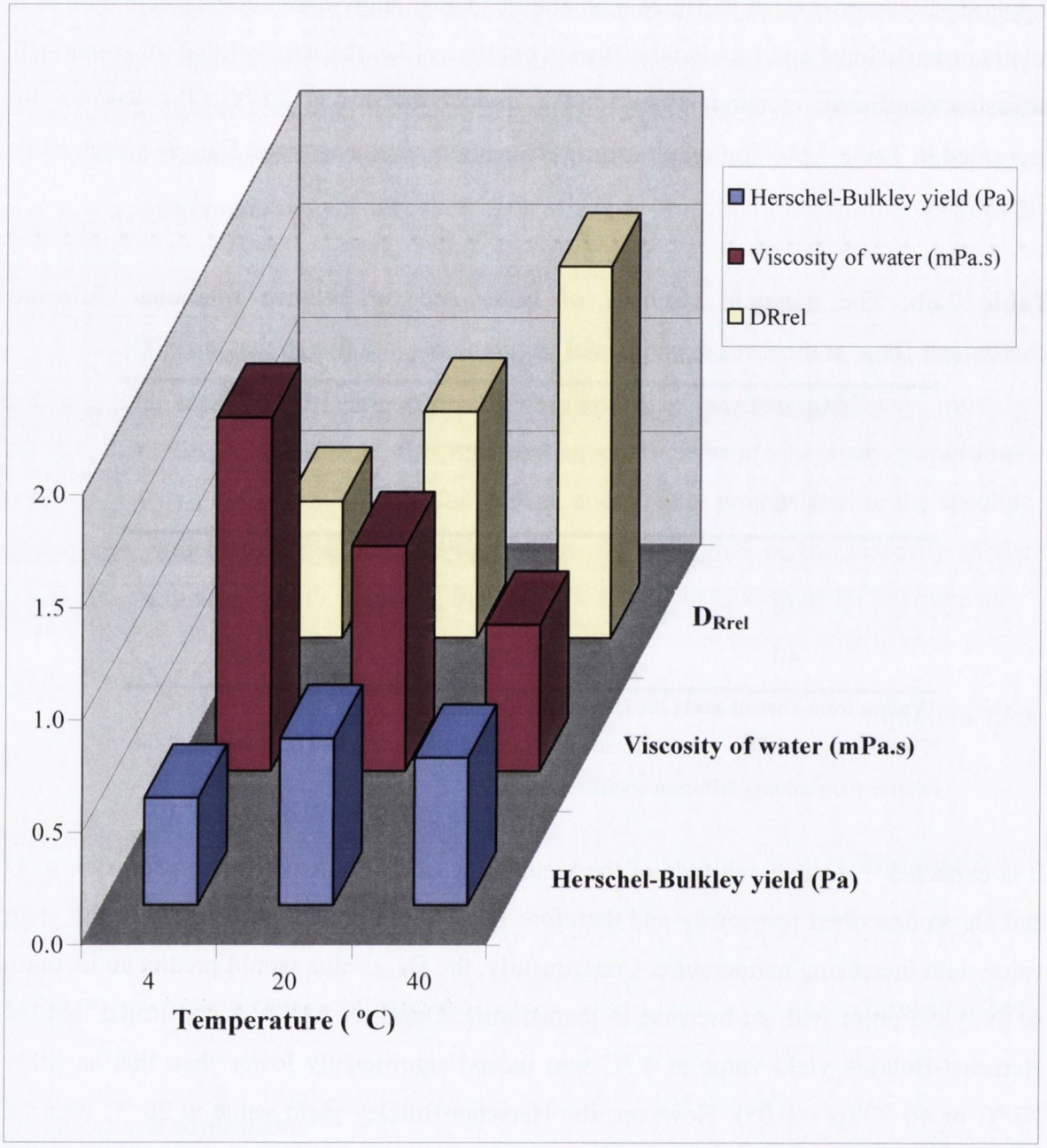


Figure 7.6b. The relationship between temperature, η_s and D_{Rrel} for a 1% w/v aqueous sepiolite suspension.

The apparent viscosity at any point on the flow curve is the quotient of the shear stress and shear rate. Consequently it is evident that at high shear rates (~ 600 s^{-1}), the apparent viscosity decreases in the order 4 °C > 20 °C > 40 °C. For systems subject to shear, the effects of Brownian motion and shear on the system viscosity are superimposed. The influence of shear is to force alignment of the particles in the direction of flow, thereby reducing viscosity. Conversely, the rotational Brownian motion tends to randomize the particle orientations thereby opposing this alignment and raising the viscosity (Chang *et al.*, 1993). The effect of shear would be expected to dominate over that of Brownian

motion at high shear stresses and consequently, the apparent viscosity follows the same trend as the absolute viscosity of the suspending medium, water, at the different temperatures investigated.

7.6.3 The influence of temperature on the sedimentation behaviour of sepiolite suspensions of different concentration

Sedimentation studies were also carried out at 4 °C and 40 °C to ascertain the effect of temperature on the settling rate of sepiolite suspensions of different concentration. From the rheological results above, it is evident that sepiolite suspensions offer more resistance to an applied shear stress at 20 °C and 40 °C than at 4 °C, given the relative order of the yield values. Upon standing, the actions of Brownian motion and motion induced by gravity will oppose and augment settling respectively. As discussed in Chapter 1, the factors influencing the sedimentation rate of insoluble spherical particles in a suspension can be described using Stokes Law (Equation 1.7a). The rate of settling of non-spherical particles will be slower than predicted by Stokes Law as their increased surface area relative to their 'equivalent' spheres will result in an increased drag (Rawle, 2003).

As described above the Brownian motion, which serves to increase the yield point via increased entanglement of fibers, increases with temperature. The sedimentation rate contains two temperature dependent terms, namely the density of the liquid and the viscosity of the continuous phase, both of which will decrease with increasing temperature, thereby increasing the predicted sedimentation rate. Consequently the physical stability of the suspension as temperature increases will be the result of the interaction between these two opposing motions.

Figures 7.6c - 7.6g illustrate the change in relative sediment volume, F, over time as a function of temperature for sepiolite suspensions of different concentration. At sepiolite concentrations of 0.25% w/v, storage at 4 °C resulted in more rapid sedimentation than at 20 °C indicating that the effect of gravity-induced motion was dominant. Increasing the storage temperature to 40 °C increased the initial sedimentation rate indicating that the reduction in aqueous viscosity, which increased gravity-induced settling, cannot be counteracted adequately by the increase in Brownian motion.

In the case of 0.5% w/v sepiolite suspensions, the rate of sedimentation was similar at 20 °C and 40 °C but much more rapid at 4 °C. The similarity of the sedimentation behaviour at 20 °C and 40 °C indicated that the increase in erratic Brownian motion with temperature increased the interaction between the fibers and the connectivity of the interfibrous framework to an extent sufficient to offset the fall in viscosity of water. The marked increase in the sedimentation rate at 4 °C indicated that the Brownian motion was decreased to such a degree at this temperature that the increase in aqueous viscosity was unable to retard sedimentation. This result again emphasizes the importance of Brownian motion in the development of a yield value through increased interfibrous collisions.

Results for 1% w/v sepiolite suspensions (Figure 7.5e) were qualitatively similar to those for 0.5% w/v suspensions and support the trend in yield values reported in Section 7.6.2. The resistance of a sepiolite system to sedimentation under zero applied external forces, apart from those due to gravity, may therefore be predicted using these rheological yield values.

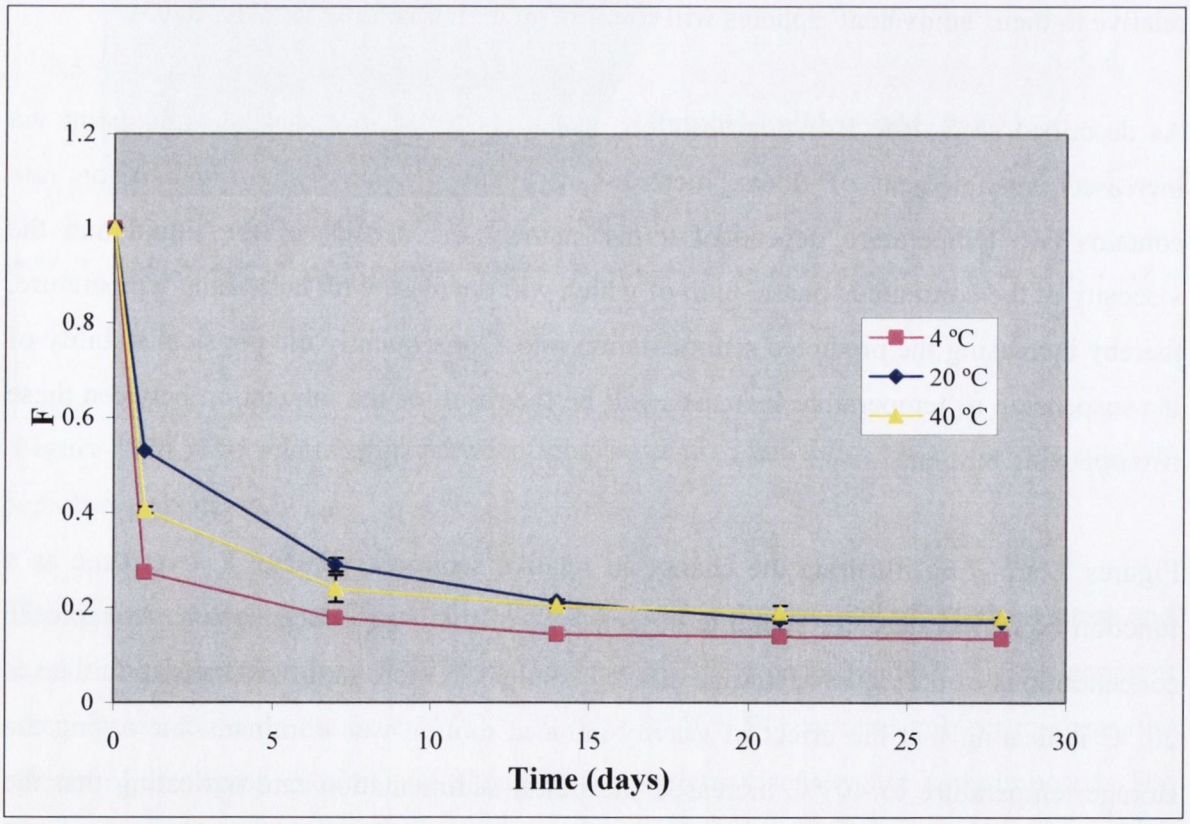


Figure 7.6c. The relative sediment volume, F, as a function of time and temperature for a 0.25% w/v sepiolite suspension.

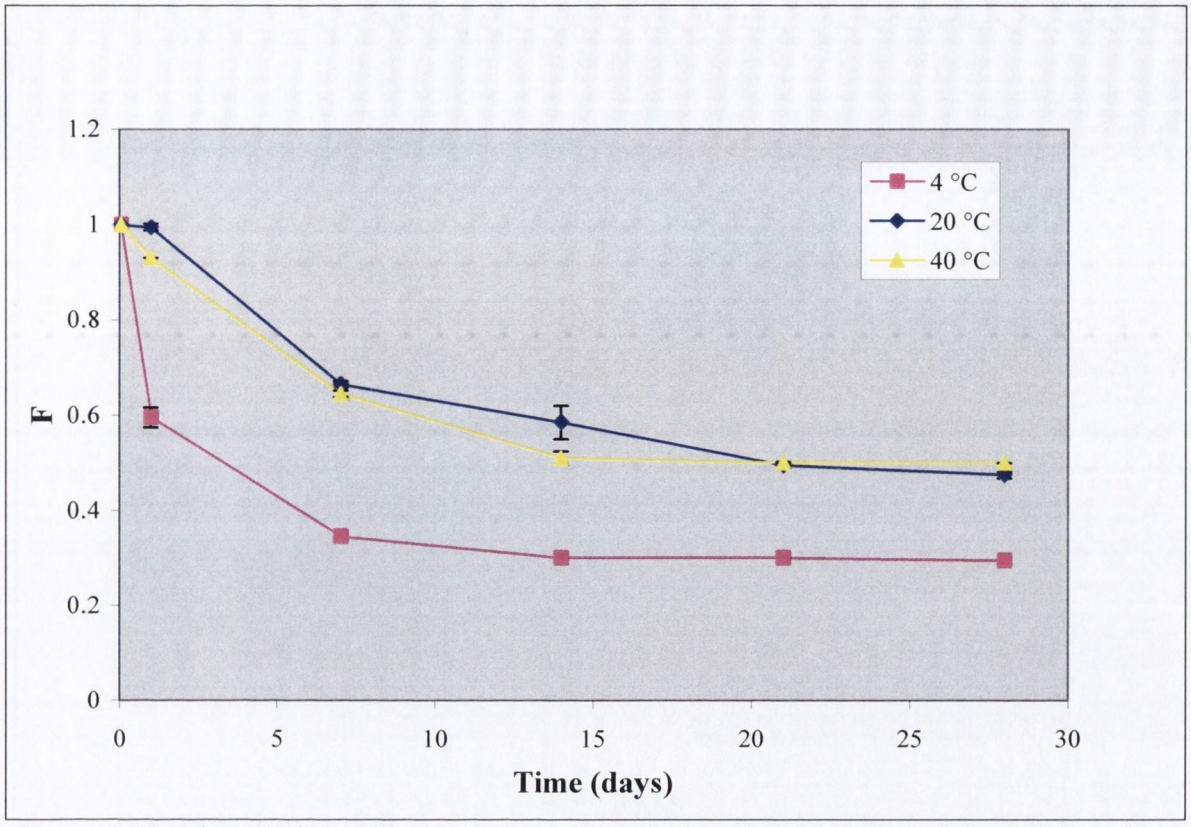


Figure 7.6d. The relative sediment volume, F, as a function of time and temperature for a 0.5% w/v sepiolite suspension.

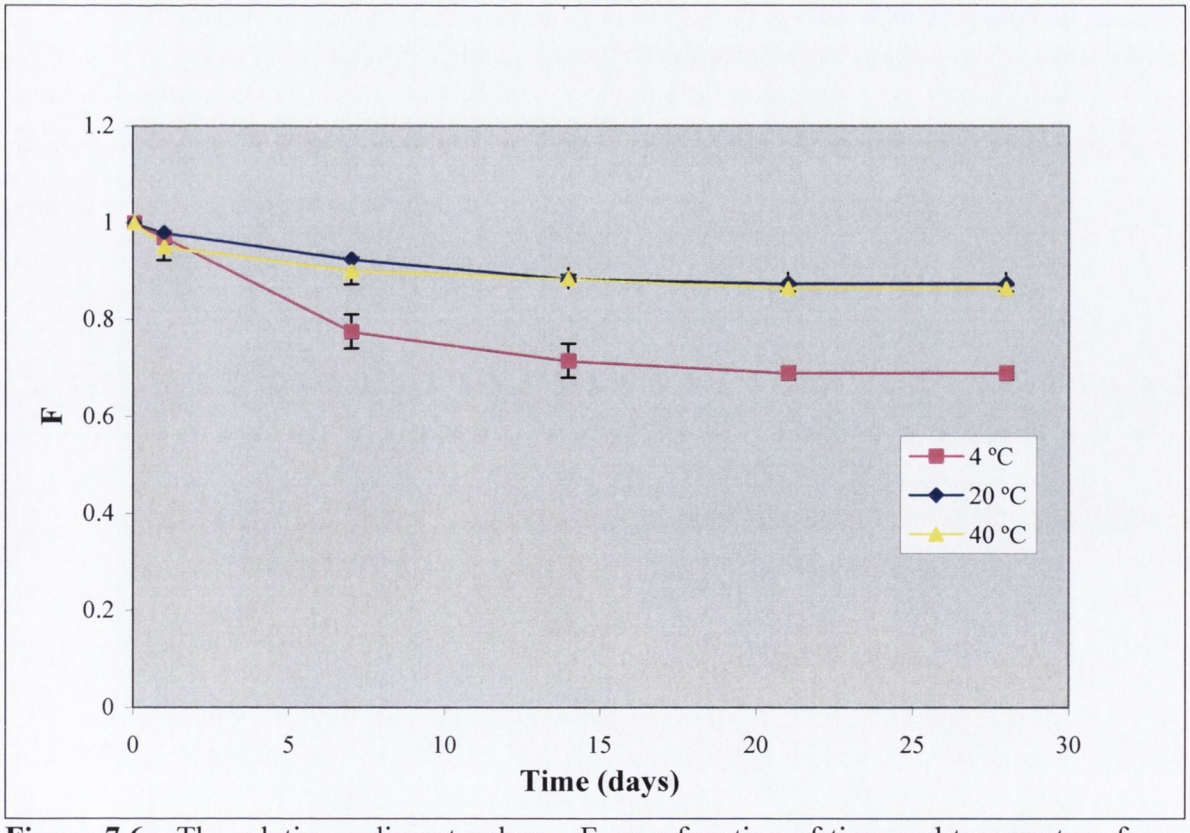


Figure 7.6e. The relative sediment volume, F, as a function of time and temperature for a 1% w/v sepiolite suspension.

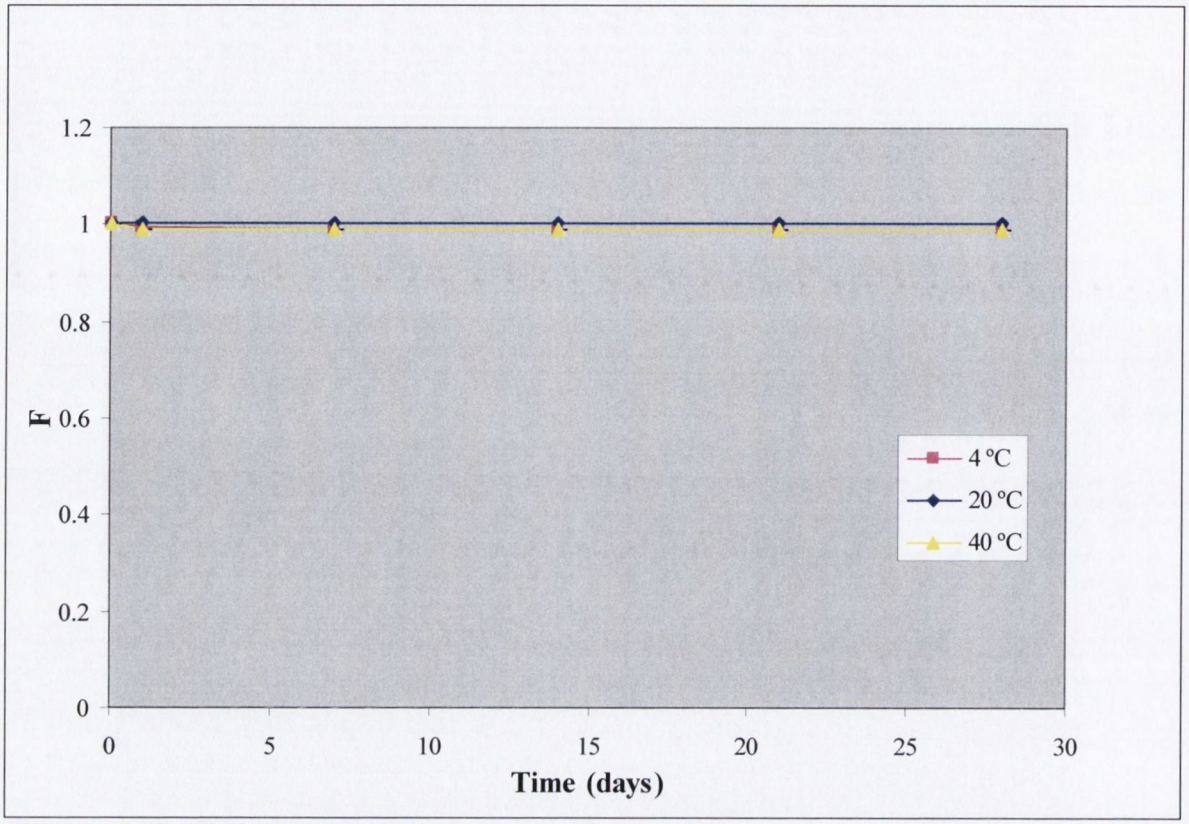


Figure 7.6f. The relative sediment volume, F, as a function of time and temperature for a 2% w/v sepiolite suspension.

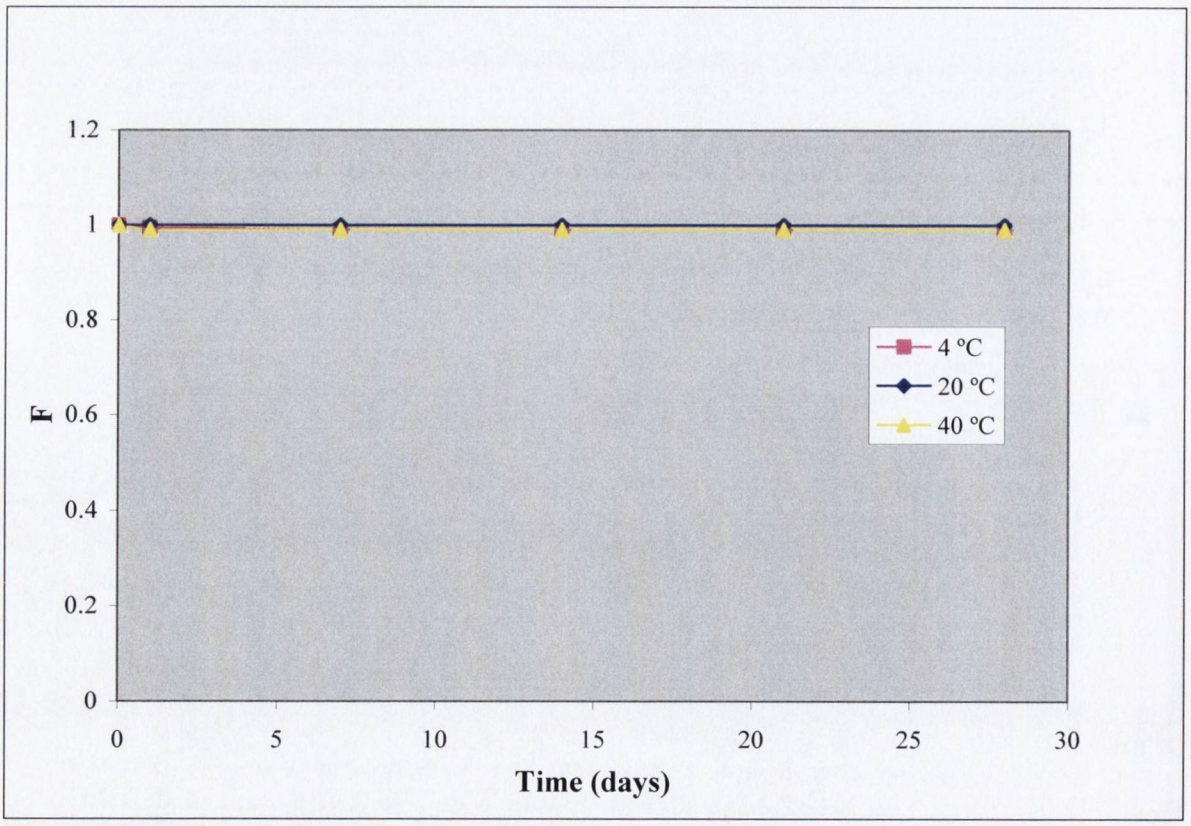


Figure 7.6g. The relative sediment volume, F, as a function of time and temperature for a 4% w/v sepiolite suspension.

Sedimentation studies indicated that 2% w/v and 4% w/v suspensions were equally stable at 4 °C, 20 °C and 40 °C with no sedimentation evident after 28 days. The decrease in Brownian motion associated with a decrease in the storage temperature did not adversely affect stability. It was postulated that the dependence of the development of the fibrous scaffold (and as a consequence the yield value) on Brownian motion decreases as the concentration of sepiolite increases. It stands to reason that as the number of fibers per unit volume increases, the distance between fibers is reduced and consequently their collision and entanglement is less hindered by a reduction in the magnitude of Brownian motion than in cases where the concentration is low and as a result distance between fibers large. In addition, the increase in the complexity of the network will cause more extensive immobilization of the water molecules through entrapment and adsorption, thus opposing the temperature induced decrease in the viscosity of water.

7.7 THE INFLUENCE OF AGEING ON SEPIOLITE SUSPENSIONS

The shelf-life of a dispersion depends on the physical stability of the system, as well as the chemical stability of the ingredients. Because of the importance of viscosity in terms of stability and certain in-use characteristics, major changes in viscosity over time are cause for concern (Zatz *et al.*, 1996). The influence of standing time on the rheological behaviour, pH and particle size of a 1.5% w/v sepiolite suspension was therefore investigated. Results are presented in Table 7.7a. The Herschel-Bulkley rheological model afforded the best data fit and consequently only rheological parameters derived from this model are presented in Table 7.7a.

It is evident that there was a tendency for the Herschel-Bulkley yield to increase over time. A downward trend in the flow behaviour index with time was also seen, indicative of the development of more pronounced pseudoplastic character. Furthermore, the consistency index increased markedly over time. Marked changes in thixotropic character were also observed. One-way ANOVA indicated that the yield values, flow behaviour and consistency indices at 0 h and 28 d were significantly different ($p < 0.05$). Fluctuations in the pH were minimal (0.26 units) and did not display any trend with time and hence could not account for the change in rheological behaviour observed. It is possible that the percolation of water through the microporous volume of the fibers may require time. This theory was supported by the tendency to observe a small drop (< 1% v/v) in the volume of

the suspensions on standing after 24 h in well-sealed containers. Such an occurrence would result in an apparent increase in concentration and therefore an increase in the apparent yield values. However, it alone would fail to explain the change in thixotropic character with time. The increases in the yield value and consistency index do not appear to be associated with irreversible coagulation of fibers as the particle size distribution is constant over the time period in question. From the rheological data, it appears that time affords the formation of a greater number of stronger interfibrous connections. It is postulated that Brownian motion-related interparticle collisions, over time, result in increased association of fibers in the secondary attractive minimum, thereby tending from a system composed of a large number of smaller floccules to one composed of a single giant floc extending throughout the entire volume of the suspension with corresponding increases in the yield value, consistency and flow behaviour indices. The results of particle sizing over time do not support this conclusion. However, the nature of the particle sizing process is such that it requires the repeated circulation of a dilute particle-in-liquid sample through a glass cell using a pump, which serves to disperse the sample, separate aggregates and prevent sedimentation. Typical pumps speeds are of the order of 500 to 1750 rpm, which even at the lower end of the range would most likely cause deaggregation of flocs/interfibrous networks. Thus such a change in the size/number of floccules may not be reflected in the measured particle size distribution, given the nature of the particle size measurement process.

Table 7.7a. The change in Herschel-Bulkley model parameters, thixotropic behaviour, pH and particle size of 1.5% w/v sepiolite suspension as a function of time.

Time	HB yield value, σ_{HB} (Pa)	HB Flow behaviour index, n (-)	HB Consistency index, K ($Pa.s^n$)	HB correlation coefficient, r^2 (-)	HB model standard error (-)	Area of thixotropic loop ($Pa.s^{-1}$)	pH (-)	d10 (µm)	d50 (µm)	d90 (µm)
0 h	1.136±0.285	0.4156±0.0069	0.4410±0.0363	0.99747	32.58	-761.6±26.4	8.79	2.937±0.003	7.544±0.006	18.478±0.100
8 h	1.326±0.078	0.4168±0.0114	0.4135±0.0655	0.98436	28.67	-711.9±13.1	8.81	2.938±0.007	7.541±0.059	18.569±0.466
24 h	1.864±0.052	0.3972±0.0144	0.4984±0.0702	0.95492	47.90	-575.2±42.1	8.89	3.002±0.004	7.676±0.018	18.576±0.064
48 h	2.043±0.201	0.4056±0.0118	0.4958±0.0469	0.93018	21.64	-406.0±38.8	9.05	3.012±0.002	7.702±0.014	18.232±0.135
7 d	2.241±0.133	0.3728±0.0004	0.7048±0.0047	0.93525	27.58	-207.6±12.2	8.93	3.051±0.007	7.797±0.029	18.802±0.053
14 d	2.564±0.218	0.3631±0.0075	0.8148±0.0413	0.94065	30.22	-95.5±22.6	9.02	3.145±0.018	8.091±0.099	19.827±0.637
28 d	2.485±0.049	0.3771±0.0010	1.0800±0.0665	0.94141	39.46	+11.4±5.5	8.95	2.971±0.014	7.596±0.083	18.197±0.486

Note: The lowest correlation coefficient of all replicates was quoted. The highest standard error of all replicates was quoted.

Interestingly, the antithixotropic behaviour of the suspension decreased dramatically with an increase in time, switching to slight thixotropic behaviour after 28 days. This observation provides support for an increased level of connectivity within the fibrous network (i.e. increased flocculation) over time. Antithixotropic behaviour is evidence of suboptimal fibrous interactions in the initial suspension, the level of which may be optimized by increasing the frequency of particle collisions as occurs upon shear cycling. The outcome of both agitation and prolonged standing times is ironically the same; both reduce antithixotropic behaviour by increasing the intimacy of fiber entanglement. In the case of agitation, increased fiber interlinking is a consequence of the increased collision frequency caused by the imparted shear kinetic energy, while in the case of standing, it is related to Brownian motion-induced collisions. The rate of increase of fibrous entanglement is much faster following shear cycling (Figure 7.4e) than upon standing, as the collision frequency is a function of particle velocity (Silcom, 2006). Once an optimum level of particle entanglement is reached, agitation-induced or Brownian motion-induced collisions cannot enhance fiber-fiber associations further. Consequently, the area of the hysteresis loop seen on shear cycling, formerly negative, now tends toward zero, or indeed a positive value. These results support the findings in Section 7.4.3.

It is noted and accepted that these results indicate that the flow behaviour of sepiolite suspensions may be more appropriately termed rheopectic (in accordance with the definition of Freundlich and Juliusberger (1935)) than antithixotropic (in accordance with the definition of Chong *et al.*, 1960) given that the equilibrium state is one of increased consistency relative to the initial suspension, the increase in consistency occurring more rapidly following (albeit high) shear than on standing at zero shear. For reasons cited in Section 7.4.3, the term 'antithixotropic' is used and defined in accordance with Tombácz and Szekeres (2006).

7.8 THE INFLUENCE OF ELECTROLYTES AND DEFLOCCULATING AGENTS ON THE RHEOLOGY AND SEDIMENTATION BEHAVIOUR OF SEPIOLITE SUSPENSIONS

7.8.1 Introduction

In accordance with the DLVO theory, the stability of clay suspensions (i.e. extent of aggregation/ flocculation/ deflocculation) is dependent on the electrical charges on the surfaces of the clay particles and hence will be influenced by the addition of electrolytes (Martin, 1993; van Olphen, 1977). Furthermore, adsorption of polymers or surfactants on the particle surfaces will change interparticle interactions and thereby alter the colloidal stability and rheological properties (Sjöberg *et al.*, 1999).

Ions capable of adsorbing specifically to the charged surface of colloidal particles are termed potential determining ions or specifically adsorbed ions. Potential determining ions have a 'chemical' affinity for the surface in addition to the Coloumb interaction, where 'chemical' is a collective adjective, embracing all interactions other than purely Coloumbic (i.e. van der Waals, hydrophobic bonding, complex formation, etc.) (Lyklema, 1991). Not only are they capable of altering the surface potential and consequently the zeta potential, they are capable of bringing about a reversal of surface charge (van Olphen, 1977; Alkan *et al.*, 2005a).

In contrast, other electrolytes which do not engage in any sort of specific reaction with the surface, apart from Coloumbic interaction, may be termed indifferent or inert electrolytes (van Olphen, 1977; Lyklema, 1991). Indifferent ions adsorb through Coloumb forces only; hence they are repelled by surfaces of like charge, attracted by surfaces of opposite charge, and do not adsorb on an uncharged surface (Lyklema, 1991). On account of the Coloumbic attraction, indifferent electrolytes accumulate as counterions in the outer diffuse region (Gouy layer) of the electrical double layer (EDL) of charged colloidal particles. The effective thickness of the double layer (also termed the Debye length, denoted $1/\kappa$) is related to the rate of potential decay (Falkiewicz, 1996) which in turn is related to the concentration of electrolyte present in accordance with the following equation (IUPAC, 1972):

$$1/\kappa = \left(\frac{\varepsilon_r RT}{4\pi F^2 \Sigma_i c_i z_1^2} \right)^{1/2}$$ **Equation 7.8a**

where $1/\kappa$ is the Debye length in Å, ε_r is the relative static permittivity of solution, R is the gas constant, T is the absolute temperature, F is the Faraday constant, c_i is the molar concentration of species *i* and z_i is the valency of species *i*.

Thus the effective thickness of the double layer is an inverse function of both the valency of the electrolyte and the square root of the electrolyte concentration (Vanderhoff, 1996). If ion concentration and/or valency are increased, the double layer will be compressed. The generalisation that the flocculating power of cations for negative hydrophobic sols increases with valency is termed the Schulze-Hardy rule. As the repulsion between two particles depends on the distance between them, the EDL thickness will be a key parameter in the determination of V_R (Falkiewicz, 1996). Patton (1979) expressed the relationship between a decrease in the double layer thickness and the magnitude of the interparticle repulsive force, V_R as follows:

$$\frac{V_R}{kT} = 0.01 Dd\zeta^2 \ln[1 + \exp(-S\kappa)]$$ **Equation 7.8b**

where D is dielectric constant of the medium, d is the particle diameter (μm), ζ is the zeta potential (mV), S is the separation between the surfaces (Å) and $1/\kappa$ is the double layer thickness (Å).

Increases in the electrolyte concentration/ valency cause a decrease in the thickness of the EDL, and a consequent reduction in repulsive interparticle forces thereby facilitating more intimate entanglement/ association of the particles; i.e. flocculation/ coagulation depending on the extent of zeta potential reduction. The yield value, which is proportional to the mechanical strength of the physical network of particles formed in suspensions (Tombácz and Szekeres, 2004), will therefore be influence by the electrolyte concentration as will the apparent viscosity at low shear rates.

Santarén (1993) claims that sepiolite suspensions are stable even at high electrolyte concentrations. He attributes this behaviour to the unique shape of the sepiolite particles

and the low CEC; such that the needle-like sepiolite particles form a voluminous structure stabilized not only by electrostatic forces, but also by hydrogen bonding and mechanical entanglement. Galan (1996) reports that sepiolite has the advantage over other clays such as bentonite in that it is much less sensitive to salt. Suspensions of sepiolite in distilled water have been shown to exhibit properties consistent with those of a flocculated suspension (high yield value, clear supernatant upon settling, zeta potential ~ -20 mV). The dramatic changes in rheological behaviour as a function of pH presented in Section 7.5.3 indicate that changes in the zeta potential have a striking impact on the occurrence of interfibrous interaction and furthermore, the manner of this interaction. Given that the rheology and stability of sepiolite suspensions is charge-dependent, it would be anticipated that electrolytes would influence stability through compression of the electrical double layer (indifferent electrolytes) and possibly via adsorption to the fiber surface (potential determining ions). The influence of simple electrolytes (i.e. NaCl, $CaCl_2$, sodium citrate) and more complex molecules (cetrimide and sodium polyphosphate) on the rheological and sedimentation behaviour of 1% w/v sepiolite suspensions was investigated. Indeed, Biggs *et al.* (1995) observed that rheological yield stress data can give a sensitive measure of interparticle interactions and moreover permit determination of steric barrier sizes for a wide range of small molecules and polymeric dispersants. In addition, the results should permit further elucidation of the manner of interfibrous interaction.

7.8.2 Sodium chloride

The appearance of sepiolite suspensions treated with NaCl in the concentration range 5 μM to 1.5 M is presented in Figure 7.8a. There was no discernible difference in the appearance of the suspensions after 28 days; all suspensions appeared identical to the control suspension containing no NaCl. SEMs of samples at the lowest (5 μM) and highest NaCl (1.5 M) concentrations are illustrated in Figures 7.8b and 7.8c. The nature of interfibrous interactions, insofar as it can be extrapolated from the SEMs, did not appear to be altered in any way.



Figure 7.8a. Appearance of sepiolite suspensions treated with different concentrations of NaCl at 28 days. Tube A = control, i.e. no NaCl; Tubes 1-8 represent decreasing concentration of NaCl from left to right in accordance with Table 3.7c.



Figure 7.8b. SEM of sepiolite treated with 5 μM NaCl (magnification x 20,000).



Figure 7.8c. SEM of sepiolite treated with 1.5 M NaCl (magnification x 20,000).

Finally the flow curves of samples treated with the eight different NaCl concentrations were studied; those at the highest and lowest salt concentrations are presented in Figure 7.8d. Qualitatively similar rheological properties were observed in all cases, in that all samples exhibited similar degrees of pseudoplasticity (flow rate index ranged from 0.4685-0.5491) upon application of a supra-yield stress. The data were fitted to all rheological models - the Herschel-Bulkley afforded the best data fit as adjudged by the relative magnitudes of the standard errors. Figure 7.8e relates the change in the Herschel-Bulkley yield values as a function of NaCl concentration. All parameters from this rheological modeling are presented in Table A6a in Appendix 6. The pH of the suspensions was

monitored over time and was found to be quite stable and similar in the case of all suspensions (range 8.13 - 8.51).

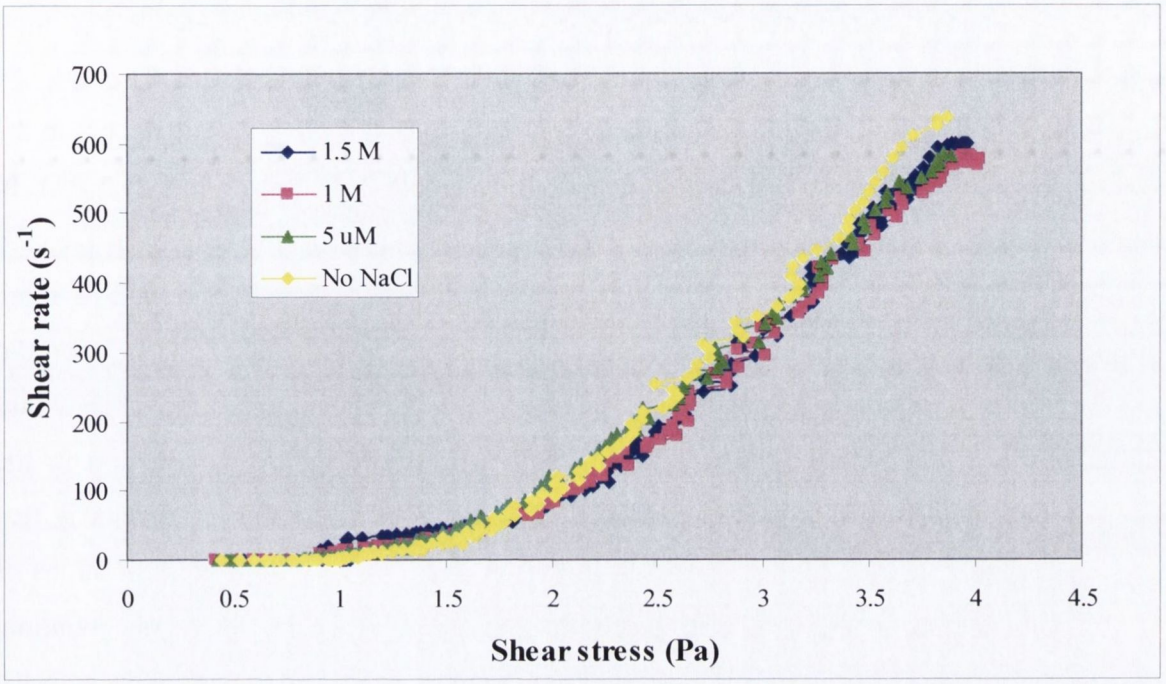


Figure 7.8d. Up-flow curves of 1% w/v sepiolite suspensions containing different concentrations of NaCl.

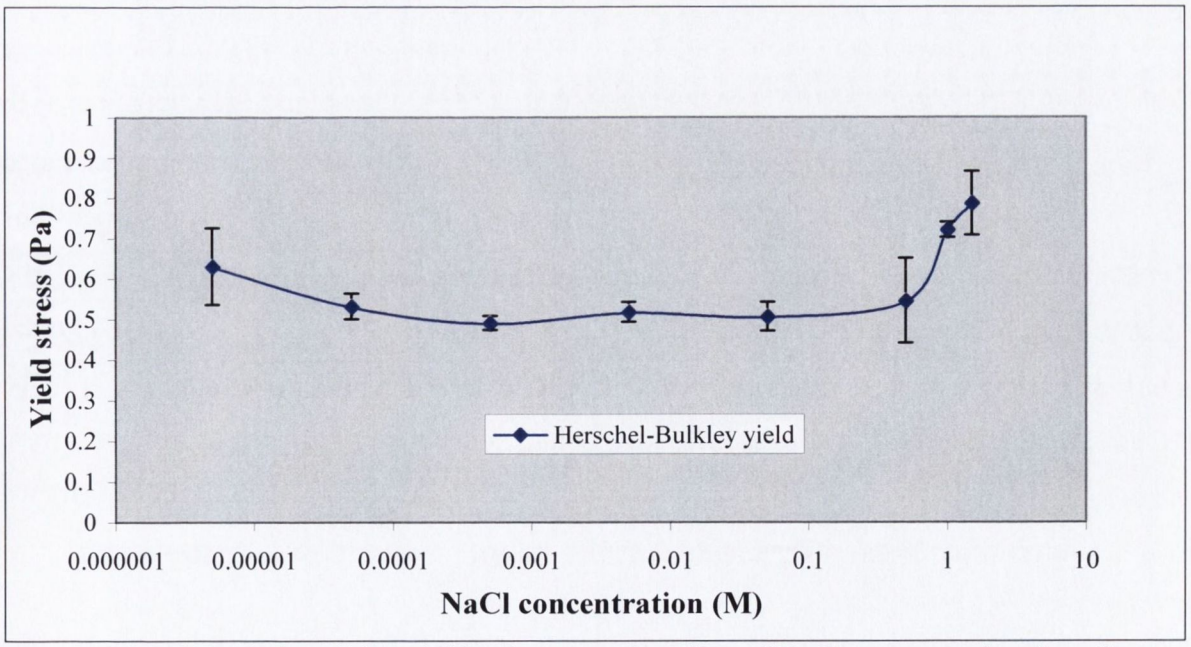


Figure 7.8e. Herschel-Bulkley yield values as a function of NaCl concentration (n = 3).

Alkan *et al.* (2005a) noted that Na^+ acts as an 'indifferent electrolyte', in that Na^+ is incapable of adsorbing specifically to the surface of the negatively charged sepiolite fibers but may cause compression of the EDL through accumulation in the more diffuse region. Hence NaCl may "screen" the negative charge of the sepiolite fibers facilitating more intimate fibrous entanglement and an increased yield value. It is evident from Figure 7.8e above that the ability of NaCl to compress the EDL was weak, with minimal changes in the yield value upon increasing the NaCl concentration 100,000-fold from 5 μM to 0.5 M. In addition the magnitude of antithixotropic behaviour was similar to the control in the case of all samples containing 0.5 M NaCl or less, indicating that the occurrence of more intimate fibrous interaction was unlikely. Further increases in the NaCl concentration did translate into slightly increased yield values and slightly reduced antithixotropic behaviour, presumably attributable to enhanced fibrous interaction induced by a reduction in the interparticle repulsion. The conclusion from sedimentation and rheological data is that sepiolite suspensions are extremely stable in the presence of very high concentrations of NaCl. The persistent pseudoplastic behaviour observed at each NaCl concentration, together with the SEMs, confirm that the slightly increased yield values seen at NaCl concentrations of the order of 1 - 1.5 M may be attributed to enhanced flocculation rather than irreversible coagulation of the suspension.

7.8.3 Calcium chloride

The appearance of sepiolite suspensions treated with $CaCl_2$ in the concentration range 5 μM to 1.5 M is presented in Figure 7.8f. After 1 h, the viscosity of suspensions containing 50 mM $CaCl_2$ or more had visibly increased, suggesting aggregation of the sample had occurred. Upon holding these suspensions in front of a light source, increased turbidity relative to the control suspension was apparent in samples containing $CaCl_2$ in the concentration range 50 mM to 1.5 M. Air bubbles, indicative of a gel-like structure, were entrained in samples containing 1 M and 1.5 M $CaCl_2$. No further changes in appearance were evident after 28 days of standing.



Figure 7.8f. Appearance of sepiolite suspensions treated with different concentrations of $CaCl_2$ at 28 days. Tube A = control, i.e. no $CaCl_2$; Tubes 1-8 represent decreasing concentration of $CaCl_2$ from left to right in accordance with Table 3.7c.

SEMs of samples at the lowest (5 μM) and highest $CaCl_2$ (1.5 M) concentrations are illustrated in Figures 7.8g and 7.8h. At low $CaCl_2$ concentrations, the individual fibers can be easily distinguished and their haphazard arrangement is indicative of the collapse of the three dimensional network upon dehydration of the structure. At high concentrations, coagulation of the sample is evident, indicative of a drastic reduction in interparticle repulsion. The borders between fibers were no longer clearly defined due to agglomeration.

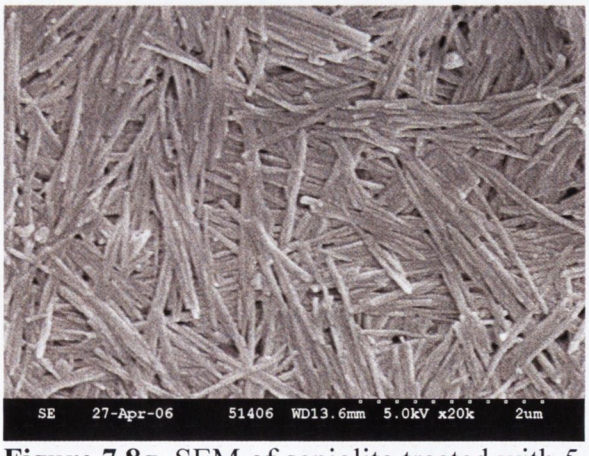


Figure 7.8g. SEM of sepiolite treated with 5 μM $CaCl_2$ (magnification x 20,000).

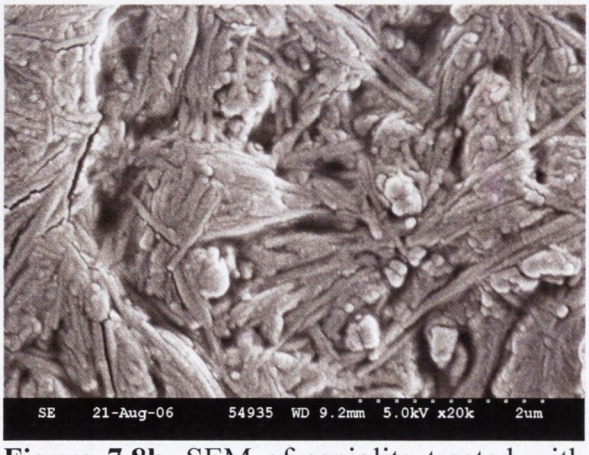


Figure 7.8h. SEM of sepiolite treated with 1.5 M $CaCl_2$ (magnification x 20,000).

These results are consistent with those of Alkan *et al.* (2005a) who reported that Ca^{2+} can act as a potential determining ion for sepiolite and hence is capable of reducing the interparticle repulsion in two ways; firstly via accumulation in the more diffuse outer electrical layer bringing about its compression and secondly via adsorption onto the surface of negatively charged sepiolite particles. Alkan and his coworkers (2005a) looked at the influence of Ca^{2+} concentration on the zeta potential of sepiolite and found that concentrations of the order of 0.01 M were capable of reducing the zeta potential of sepiolite to zero. A reversal of charge was not apparent at the maximum calcium concentration studied by Alkan (0.1 M). The agglomeration observed in samples containing 1.5 M $CaCl_2$ indicates that it was unlikely that charge reversal occurred even at this concentration and if indeed it did, the magnitude of the resulting positive zeta potential was insufficiently high to prevent particle coagulation.

Flow curves of samples treated with the eight different concentrations of $CaCl_2$ were studied; those at the highest and lowest salt concentrations are presented in Figure 7.8i. The data were fitted to all rheological models - the Herschel-Bulkley afforded the best data fit as adjudged by the relative magnitudes of the standard errors. Figure 7.8j illustrates the change in the Herschel-Bulkley yield values as a function of $CaCl_2$ concentration. All parameters from this rheological modeling are presented in Table A6b in Appendix 6. The flow behaviour at all $CaCl_2$ concentrations examined is pseudoplastic; however the extent of pseudoplastic character at a $CaCl_2$ concentration of 1.5 M is lower relative to that at all other concentrations evaluated. Furthermore the degree of antithixotropy decreases markedly with an increase in $CaCl_2$ concentration such that at 1.5 M, the up-curve is virtually superimposable on the down-curve. At high concentrations of $CaCl_2$, the sample is visibly coagulated, and consequently a reduced responsiveness to shear manifesting as a reduction in pseudoplastic behaviour, an increase in yield value (Figure 7.8j) and a reduction in thixotropic character would be expected.

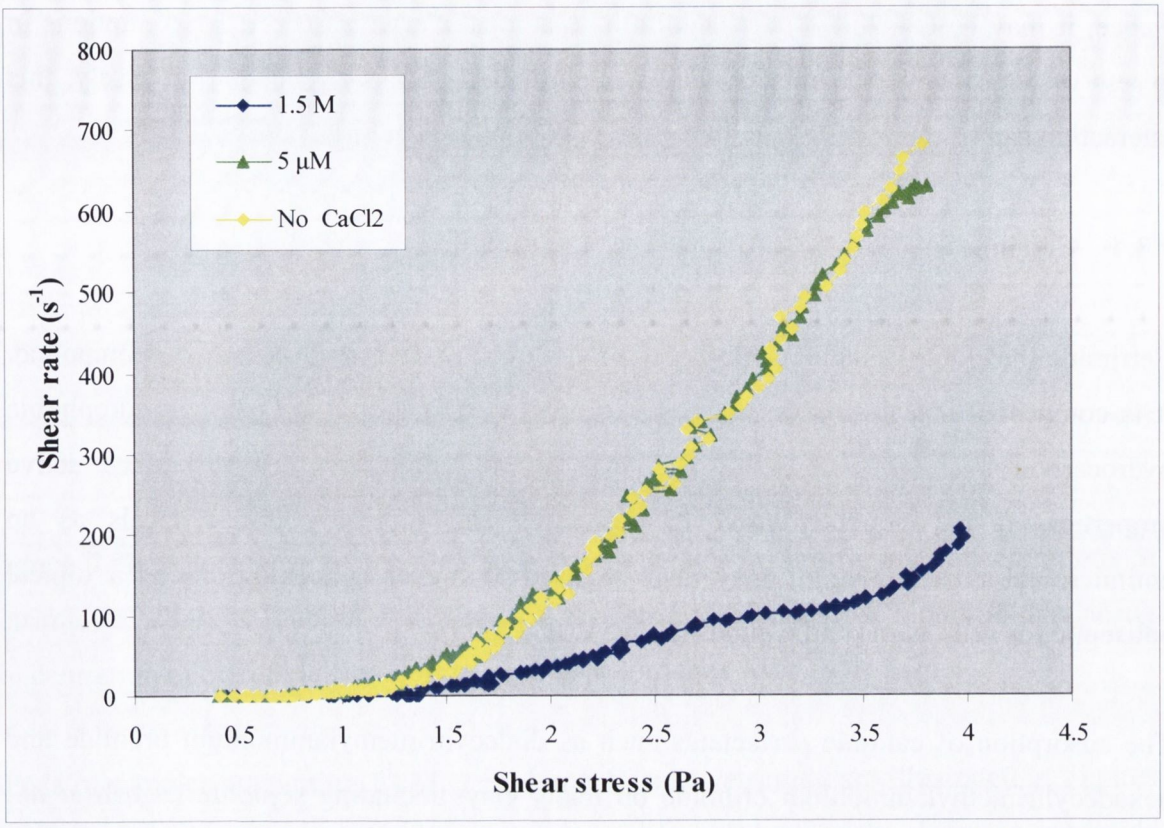


Figure 7.8i. Up-flow curves of 1% w/v sepiolite suspensions containing different concentrations of $CaCl_2$.

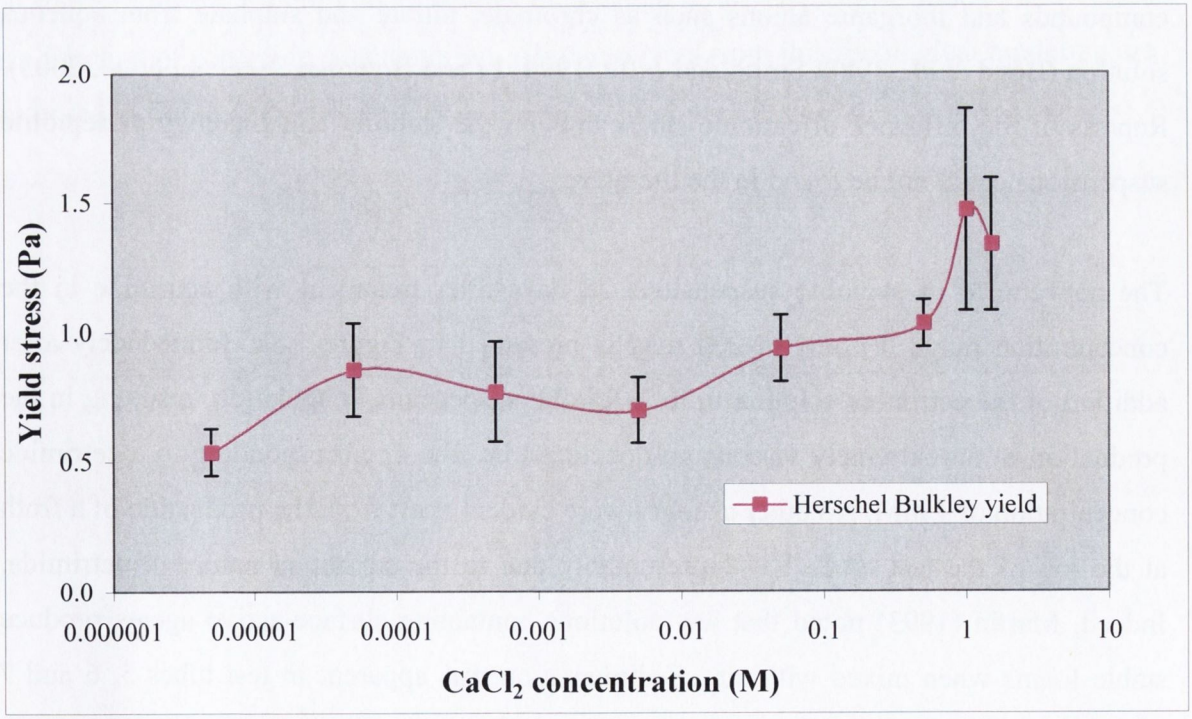


Figure 7.8j. Herschel-Bulkley yield values as a function of $CaCl_2$ concentration.

Hence, it may be concluded that sepiolite is incompatible with Ca^{2+} at concentrations in excess of 50 mM; the manner of the interaction being charge related. Conversely, this interaction can be exploited to facilitate the production of a gel-like base.

7.8.4 Cetrimide

Cetrimide (hexadecyltrimethylammonium bromide) is a quaternary ammonium compound. It is composed of a positively charged hydrophilic head group and a long hydrophobic hydrocarbon tail. On account of this amphoteric nature, it exhibits surface active properties. It is frequently used in cosmetics and topical pharmaceuticals as an antimicrobial preservative. It may also be used at higher concentrations as a topical antiseptic for skin, burns and wounds (Rowe *et al.*, 2005).

The adsorption of cationic surfactants such as dodecyltrimethylammonium bromide and hexadecyltrimethylammonium bromide on many clays including sepiolite (Sabah *et al.*, 2002; Li *et al.*, 2003) has been studied with a view to removing cationic surfactants from wastewaters (Sabah *et al.*, 2002) and producing cationic-surfactant modified clays for use in environmental remediation given their enhanced ability to sorb non-ionic organic compounds and inorganic anions such as chromate, nitrate and sulphate from aqueous solution (Boyd *et al.*, 1988; Smith and Jaffe, 1994; Li and Bowman, 1997; Li *et al.*, 2003). Reports of the influence of cationic surfactants on the stability and rheology of sepiolite suspensions could not be found in the literature.

The appearance of sepiolite suspensions 28 days after treatment with cetrimide in the concentration range 0.1 μM to 200 mM is presented in Figure 7.8k. Immediately after addition of the cetrimide solution to the sepiolite suspension, coagulation, resulting in the production of an extremely viscous gel, occurred in tube 4, corresponding to a cetrimide concentration of 1 mM. No other changes were evident apart from the production of a froth at the top of the test tubes 1 – 3 presumably due to the surfactant nature of cetrimide. Indeed, Martin (1993) noted that any solutions containing surface-active agents produce stable foams when mixed with air. Sedimentation was apparent in test tubes 5, 6 and 7 after 7 days.



Figure 7.8k. Appearance of sepiolite suspensions treated with different concentrations of cetrimide at 28 days. Tube A = control, i.e. no cetrimide; Tubes 1-8 represent decreasing concentration of cetrimide from left to right in accordance with Table 3.7d.

SEMs of samples containing 1 μM, 1 mM and 10 mM cetrimide are illustrated in Figures 7.8l-7.8q below. Flow curves of samples treated with the eight different cetrimide concentrations are presented in Figure 7.8r. The data were fitted to all rheological models - the Herschel-Bulkley afforded the best data fit as adjudged by the relative magnitudes of the standard errors. Figure 7.8s illustrates the change in the Herschel-Bulkley yield values as a function of cetrimide concentration. All parameters from this rheological modeling are presented in Table A6c in Appendix 6.

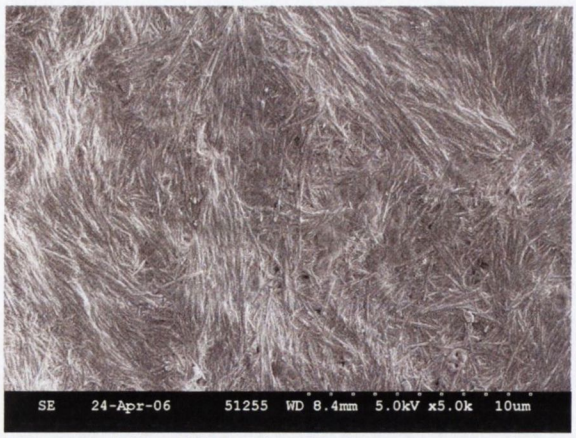


Figure 7.8l. SEM of sepiolite treated with 1 μM cetrimide (magnification x 5,000).

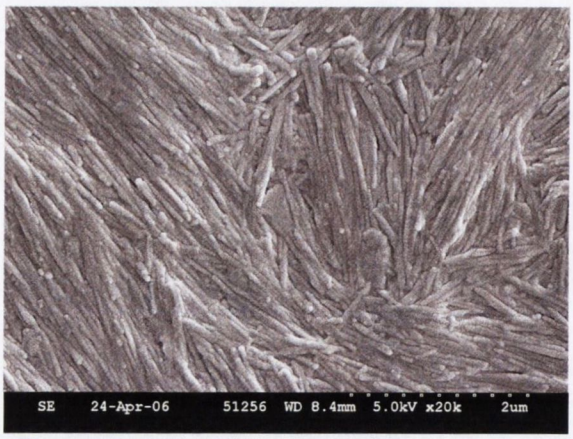


Figure 7.8m. SEM of sepiolite treated with 1 μM cetrimide (magnification x 20,000).

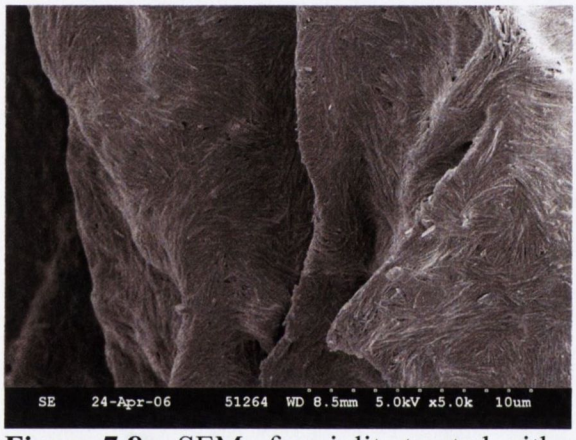


Figure 7.8n. SEM of sepiolite treated with 1 mM cetrimide (magnification x 5,000).

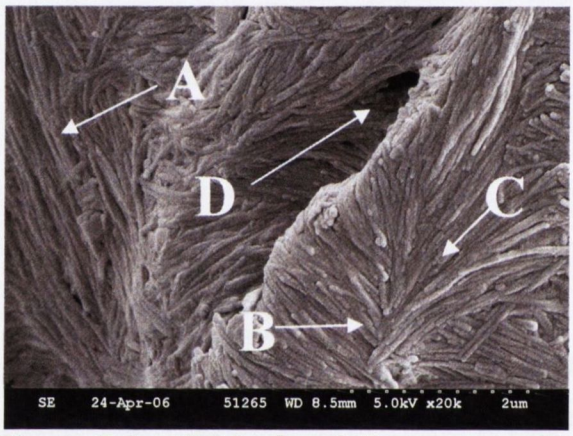


Figure 7.8o. SEM of sepiolite treated with 1 mM cetrimide (magnification x 20,000).

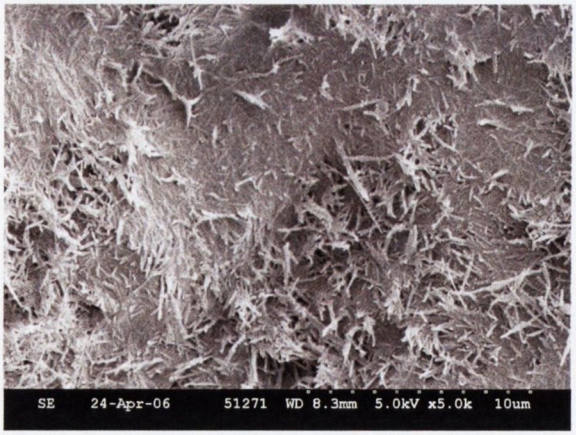


Figure 7.8p. SEM of sepiolite treated with 10 mM cetrimide (magnification x 5,000).

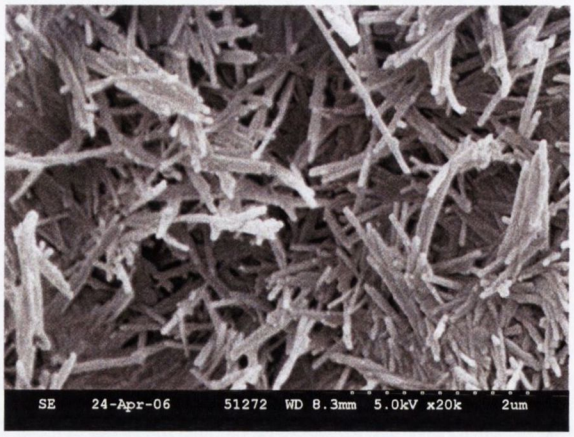


Figure 7.8q. SEM of sepiolite treated with 10 mM cetrimide (magnification x 20,000).

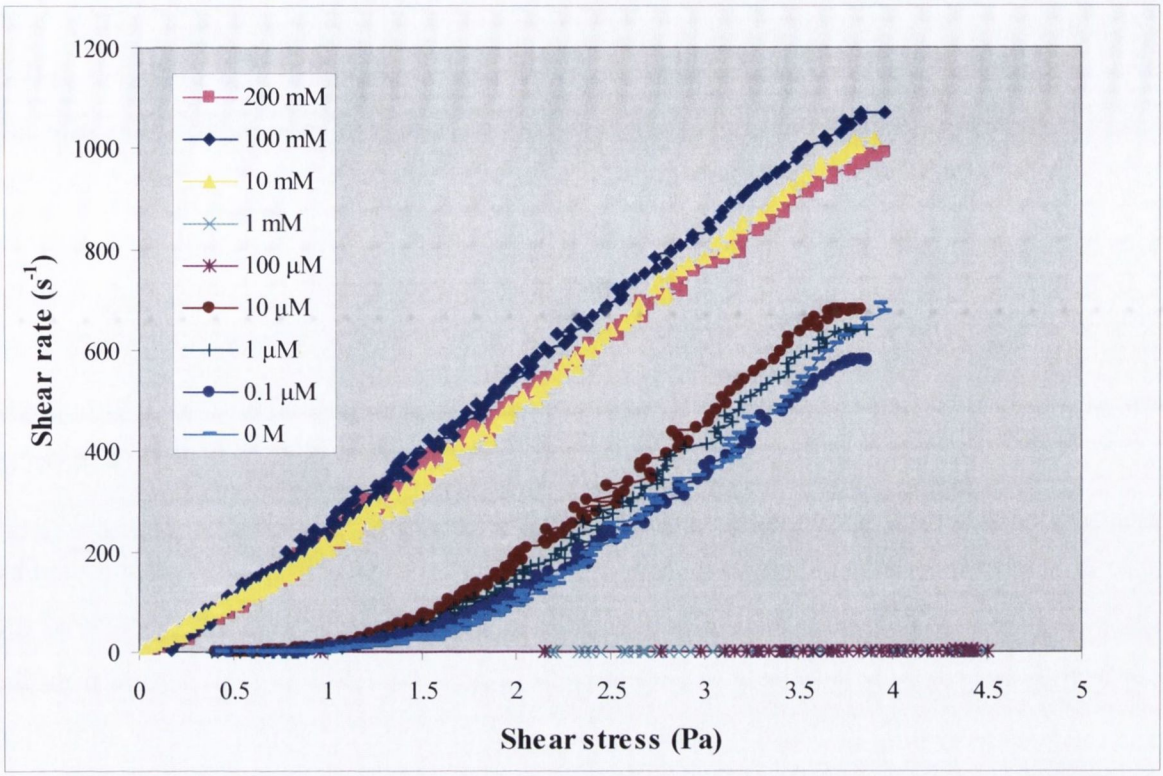


Figure7.8r. Up-flow curves of 1% w/v sepiolite suspensions containing different concentrations of cetrimide.

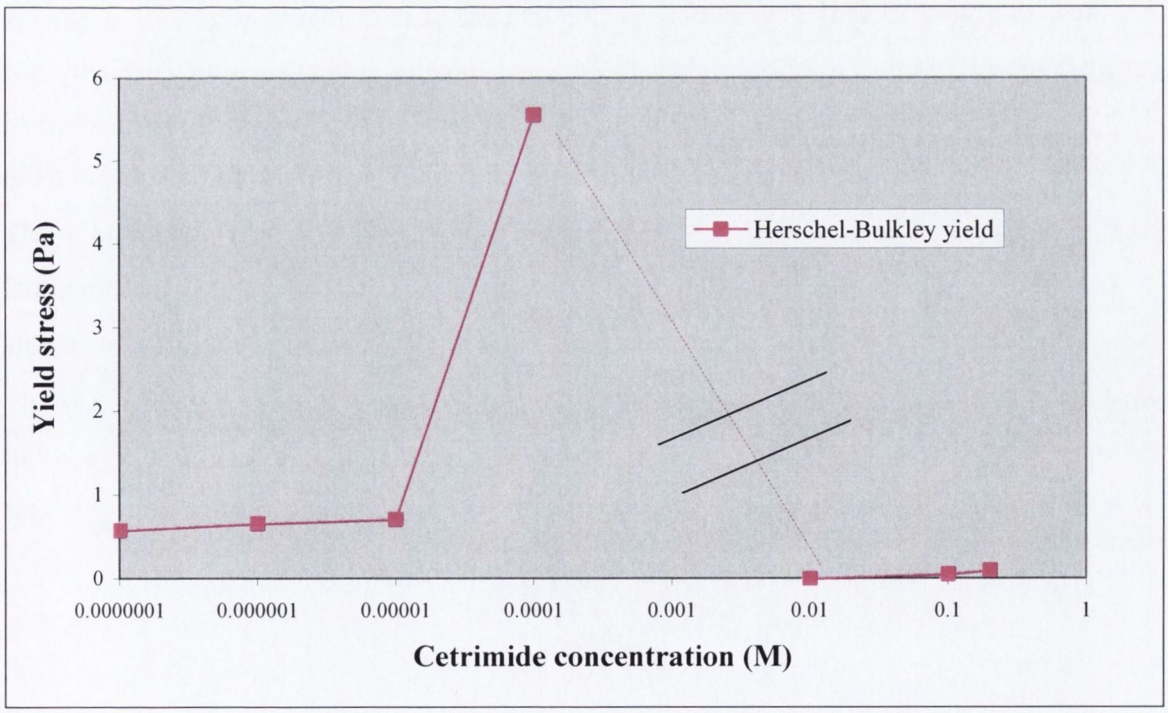


Figure 7.8s. Herschel-Bulkley yield values as a function of cetrimide concentration. (It should be noted that the sample containing 1mM cetrimide did not yield to even the highest applied shear stress investigated, consequently no yield stress is presented for this sample in the figure above).

The inclusion of cetrimide in sepiolite suspensions has profound and very much concentration-dependent effects. Sabah *et al.* (2002) reported that cetrimide adsorption onto sepiolite exhibits two distinct phases. The first stage is characterized by a low rate and governed through an ion exchange process between ammonium ions and exchangeable ions associated with the sepiolite surface. The amount sorbed during this stage was, however, several times larger than the CEC of sepiolite. Rytwo *et al.* (1998) attributed this excess organic cation uptake to sorption on neutral sites or negative sites originating from silanol groups. The second stage of adsorption is ascribed to a combination of hydrophobic chain-chain interactions through van der Waals forces and an ion exchange process resulting in the production of bilayers. Li *et al.* (2003) determined that the amount of cetrimide sorbed by hydrophobic bonding in the second stage was four-fold greater than by ion exchange in the first stage. Furthermore, Li and his coworkers (2003) discovered the ratio of sorbed bromide counterion to sorbed cetrimide to be 4:5, a large departure from the 1:2 ratio observed in the case of platy clay minerals where classical bilayer formation occurs. From these observations, it was concluded that multiple cetrimide molecules in the upper layer of the bilayer formation may attach to a single cetrimide molecule in the lower layer via hydrophobic bonding, forming cylindrical admicelles as depicted in Figure 7.8t (Manne and Gaub, 1995). The end of the second stage is typically observed when the equilibrium solute concentration equals the critical micelle concentration (CMC) for the cetrimide (0.9 mM; Liu and Ducker, 1999; El Kadi *et al.*, 2003). Li *et al.* (2003) also noted that the sorption maximum was 260 mmoles/ kg sepiolite. Interestingly, this corresponds to a ratio of sepiolite to cetrimide between that of test tubes 3 (10 mM) and 4 (1 mM). Furthermore, using the figures reported by Li *et al.* (2003), it is postulated that maximal adsorption should be possible in test tube 3 with a resulting equilibrium solute concentration of the order 7.4 mmoles/ L, i.e. in excess of the CMC.

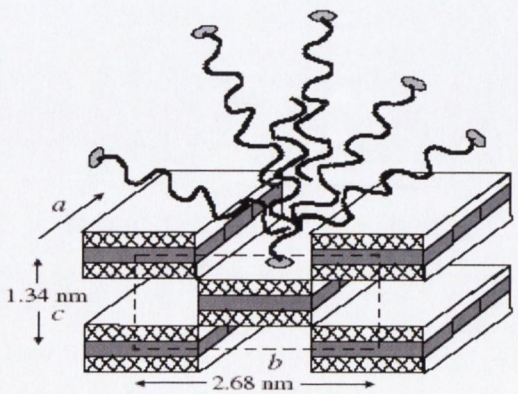


Figure 7.8t. Hypothesized surfactant admicelles on fibrous mineral surfaces such as sepiolite (Reproduced from Li *et al.*, 2003).

At the lowest cetrimide concentration investigated (0.1 μM), no sedimentation was evident. The cetrimide concentration per unit weight of sepiolite was 0.01 mmoles/ kg, far below the sorption maximum. From Figures 7.8r and 7.8s and Table A6c, it was evident that the adsorbed surfactant caused a slight reduction in the Herschel-Bulkley yield value relative to the control suspension; however the flow behaviour index compared favourably indicating no qualitative change in the rheological behaviour. Similar antithixotropic behaviour to the control was also noted providing further evidence of minimal changes in the nature of fiber-fiber interactions.

At slightly higher cetrimide concentrations (1 to 10 μM; test tubes 7 and 6 respectively), sedimentation was observed resulting in the production of a viscous, poorly redispersible sediment by day 7. Surprisingly, the rheological behaviour was unaltered; pseudoplastic and antithixotropic behaviour was still evident and one-way ANOVA confirmed that the yield values were not significantly different ($p > 0.05$) from that of the control (Figures 7.8r and 7.8s). The quantities of cetrimide per unit weight of sepiolite were 0.1 and 1 mmoles/ kg, respectively. The hydrophobicity of the fiber faces would be expected to increase with an increase in the quantity of cetrimide sorbed. This increasing hydrophobic nature was most likely the reason for sedimentation, which acted as a means of excluding water from the vicinity of the fibers, and for the poorly redispersible nature of the sediment. SEM studies indicated a dramatic change in the nature of particle interactions. The random orientation of one fiber relative to another was lost and replaced by predominantly face-to-face associations. At this concentration, it was likely that the second stage of sorption resulting in admicelle formation on the surface of the sepiolite fibers would not occur. The faces of the fibers, therefore, were effectively covered by a hydrophobic layer as in Figure 7.8u. Face-to-face arrangements were consequently favoured as they facilitated reduced interaction of the hydrophobic hydrocarbon tails with the surrounding aqueous environment. The preference for FF associations would be expected to cause a reduction in the yield value. It is possible however that this effect may be offset by the reduced ability of water to lubricate the movement of the increasingly hydrophobic fiber surfaces relative to another.

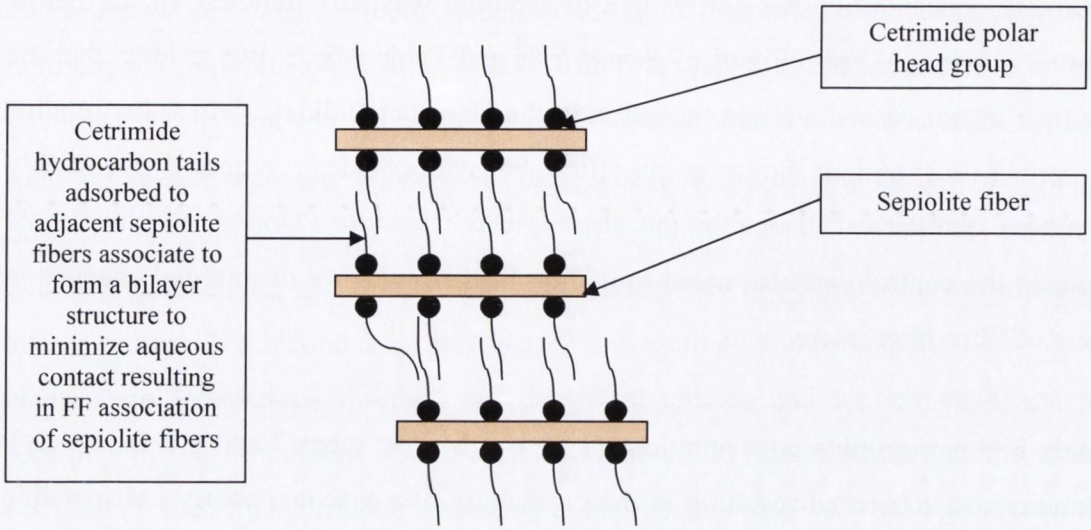


Figure 7.8u. The mechanism of FF associations between sepiolite fibers at low cetrimide concentrations.

At a cetrimide concentration of 100 μM (test tube 5), the ratio of cetrimide to sepiolite was 10 mmole/ kg. Sedimentation was apparent; the sediment was composed of two distinct layers, a caked lower layer and a more porous upper region. The rheology of the suspension was dramatically altered; appreciable rates of shear were not obtained over the shear stress range examined. This behaviour can be explained by the ever-increasing hydrophobic nature of the clay surface as the quantity of cetrimide adsorbed via ionic mechanisms increased. The surface could no longer be wetted by water and the clay precipitated. The layering evident within the sediment may be due to the compression of the lower region of the sediment by the weight of that above it, thus forcing water out of the sediment to form a caked layer. The driving force for the exclusion of water would be greater than that in test tubes 6 and 7 owing to the increased hydrophobicity. In addition, the sorption of cetrimide to negative sites on the sepiolite fiber surface will reduce interfibrous repulsion to a greater extent, thereby further facilitating the closer association of fibers within the sediment. The huge increase in apparent viscosity may be explained as follows: the relative movement of fibers on application of shear is typically lubricated by water molecules, this process is now impeded by the poor wettability of the organic-clay complex and a huge resistance to flow is observed.

At 1 mM cetrimide concentrations (test tube 4), a highly viscous gel with large amounts of entrained air was produced immediately. At this concentration, the cetrimide/sepiolite ratio (100 mmoles/ kg) is close to the maximum sorption ratio, as quoted by Li *et al.* (2003), hence 100% occupation of all negatively charged silanol adsorption sites is likely. The loss of the net negative surface charge and the hydrophobic nature of the particles both promote extensive agglomeration; Figures 7.8n and 7.8o illustrate the highly aggregated three dimensional structures formed by FF, EF and EE associations (points A, B and C respectively). The volume occupied by an entrained air bubble was also evident at point D. Poor flow could therefore be attributed to the coagulated state of the suspension. Coagulation was also observed by Pakter (1972) in palygorskite (attapulgite) suspensions treated with cetrimide and he attributed it to complete neutralization of the surface negative charge of the dispersed clay particles.

At 10 mM cetrimide concentrations (test tube 3), cetrimide adsorption was most likely complete as mentioned earlier, resulting in the production of admicelle structures, as in Figure 7.8v. Due to the hydrophilic external shield afforded by the outer layer of charged quaternary ammonium head groups, the polar nature of the fibers is restored. The organic cations and the anions of the ionic groups together form a more or less diffuse electrical double layer, and the adsorption complex now assumes a positive charge (van Olphen, 1977). However, due to the electrical repulsion between the positively charged shields surrounding the fibers, particle association will be hindered and a disperse suspension would be expected to result. The absence of a yield value and of thixotropy (Figure 7.8s) confirms the disperse nature of the suspension. Images from SEM (Figures 7.8p and 7.8q) further supported the disperse nature of the fibers. These essentially peptized particles will settle slowly and form a compact cake. Although not readily apparent from Figure 7.8k, a small volume of caked sediment was present at the base of test tube 3. Similar sedimentation and rheological behaviour was observed at higher cetrimide concentrations (100 mM and 200 mM; equivalent to 10,000 mmoles/ kg and 20,000 mmoles/ kg sepiolite, respectively). One-way ANOVA confirmed the yield values of these suspensions were not significantly different ($p > 0.05$) from that at 10 mM. (i.e. zero). This observation indicated that cetrimide adsorption reached a maximum at concentrations of the order of 100 – 1000 mmoles cetrimide/ kg sepiolite; a range which is in agreement with that quoted by Li *et al.* (2003).

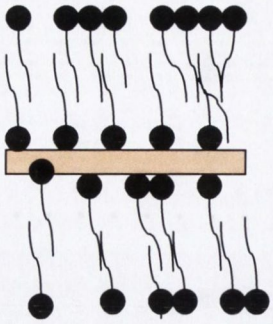


Figure 7.8v. Admicelle formation on the surface of the sepiolite fibers producing an organo-clay complex with a net positive charge.

7.8.5 Sodium citrate

Sodium citrate (tri-sodium 2-hydroxy propane-1,2,3-tricarboxylate dihydrate) is widely used in the pharmaceutical industry as a deflocculating agent (Biggs *et al.*, 1995) and has been successfully used to deflocculate kaolin and halloysite (Salter, 2003). Kaolin and halloysite are aluminosilicates and exhibit a plate-like and tubular morphology respectively (van Olphen, 1977). At neutral pH, the faces of the kaolinite plates and the halloysite tubules are negatively charged due to the combined effect of isomorphous substitution of Al^{3+} for ions of lower valence and the abundance of acidic surface silanol groups. In contrast, the edges in both cases are positively charged due to the tendency for alumina, present at the edges due to discontinuity of the gibbsite sheet, to accept protons at this pH (van Olphen, 1977). Consequently both kaolin plates and halloysite tubules tend to associate in an edge-to-face (EF) arrangement because of the electrical attraction caused by the difference in the charge of the edges and faces (Salter, 2003). Sodium citrate is a salt of citric acid and dissolves in water to form both citrate and sodium ions. The trivalent citrate ions are negatively charged and can neutralize/ render negative the positive end charges of kaolin plates and halloysite tubules, thus hindering EF associations and producing a deflocculated suspension.

As proposed in Section 7.5.2 above, the faces of the sepiolite fibers possess a negative charge when dispersed in distilled water whilst the edges of the fibers may possess a positive charge on account of the basic $Mg(OH)_2$ groups produced by the disruption of the octahedral brucite layer. The effect of $CaCl_2$ was demonstrated above and it appears that Ca^{2+} ions were capable of depressing the negative charge associated with the fiber faces,

thereby facilitating FF associations and coagulation of the sample. In contrast, citrate ions would be expected to interact preferentially with the small positive charge associated with the edges and in neutralizing same would be expected to cause deflocculation of the system as EF associations are disrupted. The results of SEM, sedimentation studies and rheological testing are outlined below (all parameters from this rheological modeling are presented in Table A6d in Appendix 6) and subsequently interpreted in terms of the interactions between the citrate ions and the sepiolite fibers. The appearance of sepiolite suspensions treated with sodium citrate in the concentration range 0.1 μM to 200 mM were identical to the control suspension containing no sodium citrate after 24 h of standing. However, after 7 days, marked changes in the appearance were noted and were further accentuated after 28 days of standing. The appearance of the samples at 28 days is presented in Figure 7.8w.

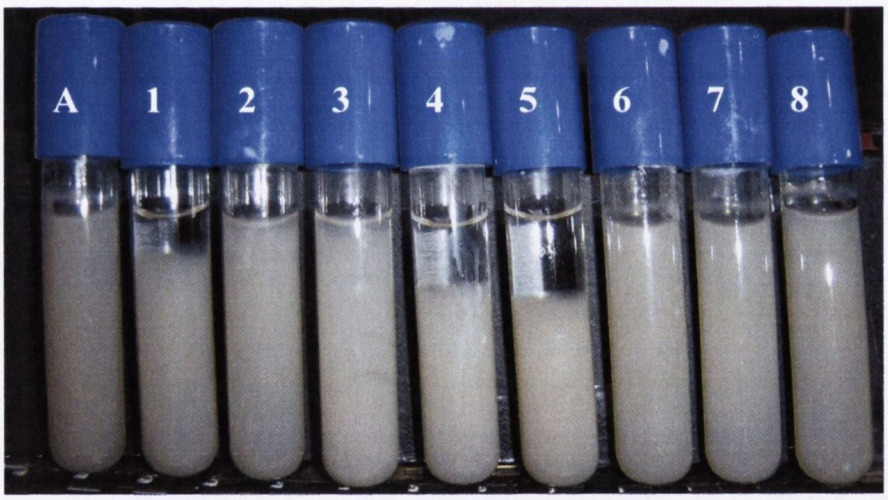


Figure 7.8w. Appearance of sepiolite suspensions treated with different concentrations of sodium citrate at 28 days. Tube A = control, i.e. no sodium citrate; Tubes 1-8 represent decreasing concentration of sodium citrate from left to right in accordance with Table 3.7d.

From Figure 7.8w above, it is evident that the presence of sodium citrate in the concentration range 0.1 – 10 μM (test tubes 8 – 6 respectively) caused no visible change in the stability of the sepiolite suspensions relative to the control. In contrast, citrate concentrations of 100 μM – 1 mM (test tubes 5 and 4) caused a marked increase in sedimentation rate. The resulting sediments were loose, fluffy and readily redispersed. The absence of caking together with the production of a clear supernatant was indicative of a flocculated system composed of a large number of small flocs as opposed to a single giant

floc. Further increases in citrate concentration (10 mM – 100 mM) caused the production of a small volume of a cloudy supernatant, characteristic of a deflocculated system. Increasing the citrate concentration to 200 mM surprisingly led to the production of a flocculated system, with a clear supernatant and loose sediment.

SEMs of samples at the lowest (0.1 μM) and highest (200 mM) sodium citrate concentrations are presented in Figures 7.8x - 7.8aa. At high magnification, the samples have a very similar appearance to one another and also to the control. Fibers were reasonably well dispersed and no agglomeration was evident. At low magnification, the three dimensional nature of the scaffold formed via fibrous interaction was evident in the case of the sample treated with 200 mM sodium citrate. Retention of this structure despite the trauma involved in sample preparation is indicative of its high mechanical strength.

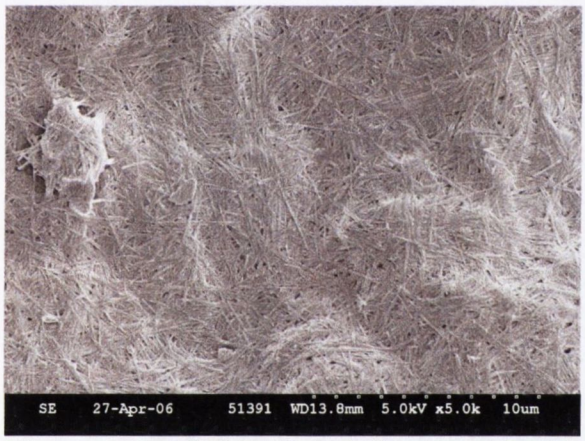


Figure 7.8x. SEM of sepiolite treated with 0.1 μM sodium citrate (magnification x 5,000).



Figure 7.8y. SEM of sepiolite treated with 0.1 μM sodium citrate (magnification x 20,000).

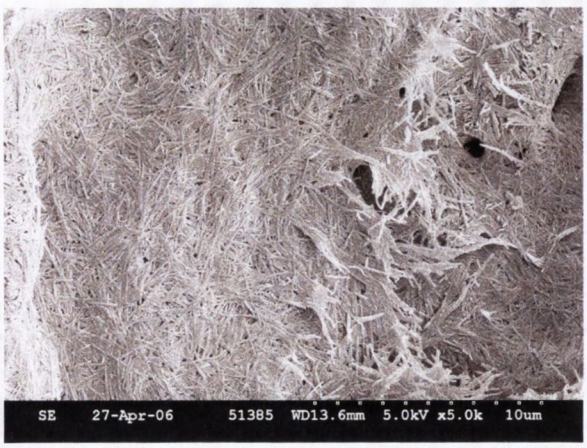


Figure 7.8z. SEM of sepiolite treated with 200 mM sodium citrate (magnification x 5,000).



Figure 7.8aa. SEM of sepiolite treated with 200 mM sodium citrate (magnification x 20,000).

Flow curves of samples treated with the eight different sodium citrate concentrations were studied; those at the highest and lowest salt concentrations are presented in Figure 7.8ab. The data were fitted to all rheological models - the Herschel-Bulkley afforded the best data fit as adjudged by the relative magnitudes of the standard errors. Figure 7.8ac illustrates the change in the Herschel-Bulkley yield values as a function of sodium citrate concentration. All parameters from this rheological modeling are presented in Table A6d in Appendix 6. The influence of sodium citrate on the resultant rheology of the systems was extremely concentration dependent. Low concentrations (0.1 μM – 100 μM) exhibited a qualitatively similar rheology to the control sample in that they were pseudoplastic and antithixotropic, but exhibited slightly reduced yield values relative to the control suspension. For samples with citrate concentrations in the range 1 mM to 100 mM, the standard error of fit of the Herschel-Bulkley model and the Bingham model were similar in magnitude indicating that these suspensions displayed approximate plastic behaviour. Yield values were significantly reduced relative to the control suspension. The Herschel-Bulkley yield values for samples containing sodium citrate at 1 mM, 10 mM and 100 mM were significantly lower ($p < 0.001$) than the corresponding values at all other citrate concentrations studied. Furthermore, the magnitude of the yield at 10 mM citrate was significantly lower ($p < 0.05$) than that at either 1 mM or 100 mM citrate. At the highest citrate concentration studied (200 mM), the rheological behaviour reverted to markedly pseudoplastic (flow behaviour index = 0.210) with a significant degree of positive thixotropy.

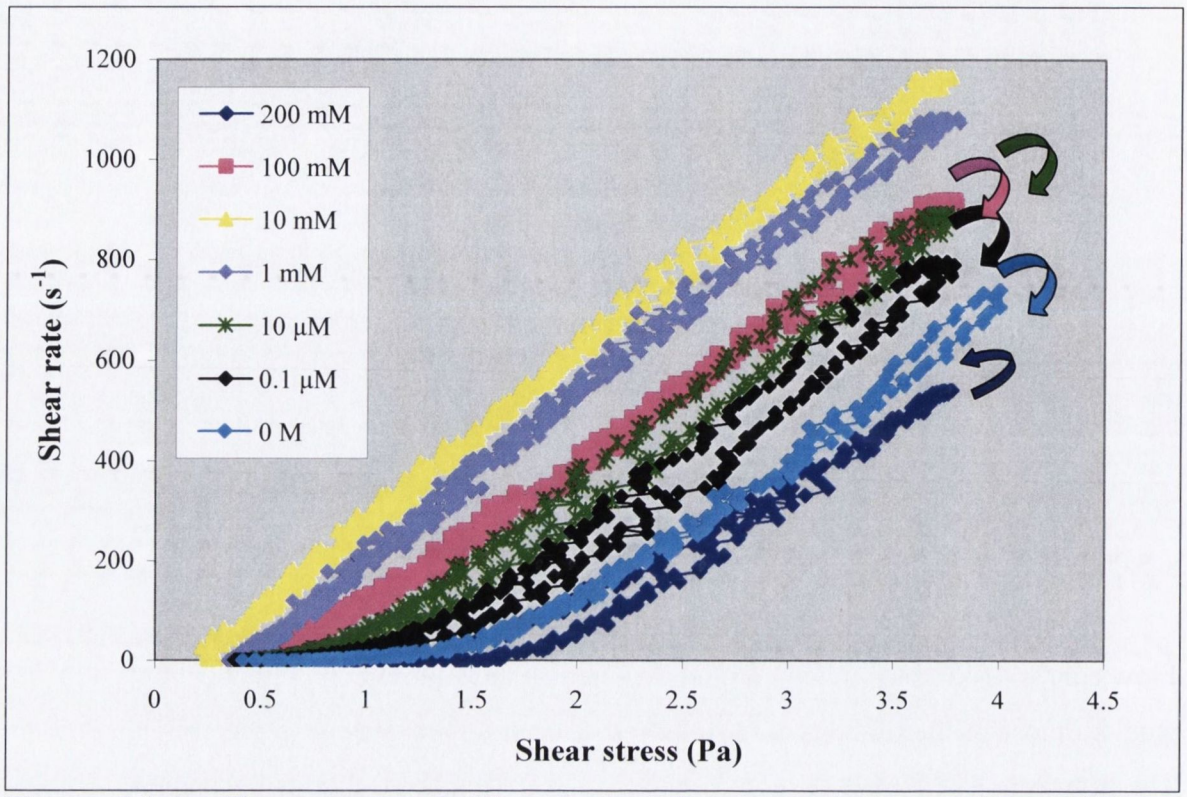


Figure 7.8ab. Flow curves of 1% w/v sepiolite suspensions containing different concentrations of sodium citrate (colour-coded arrows illustrate the displacement of the down-curves relative to the up-curves).

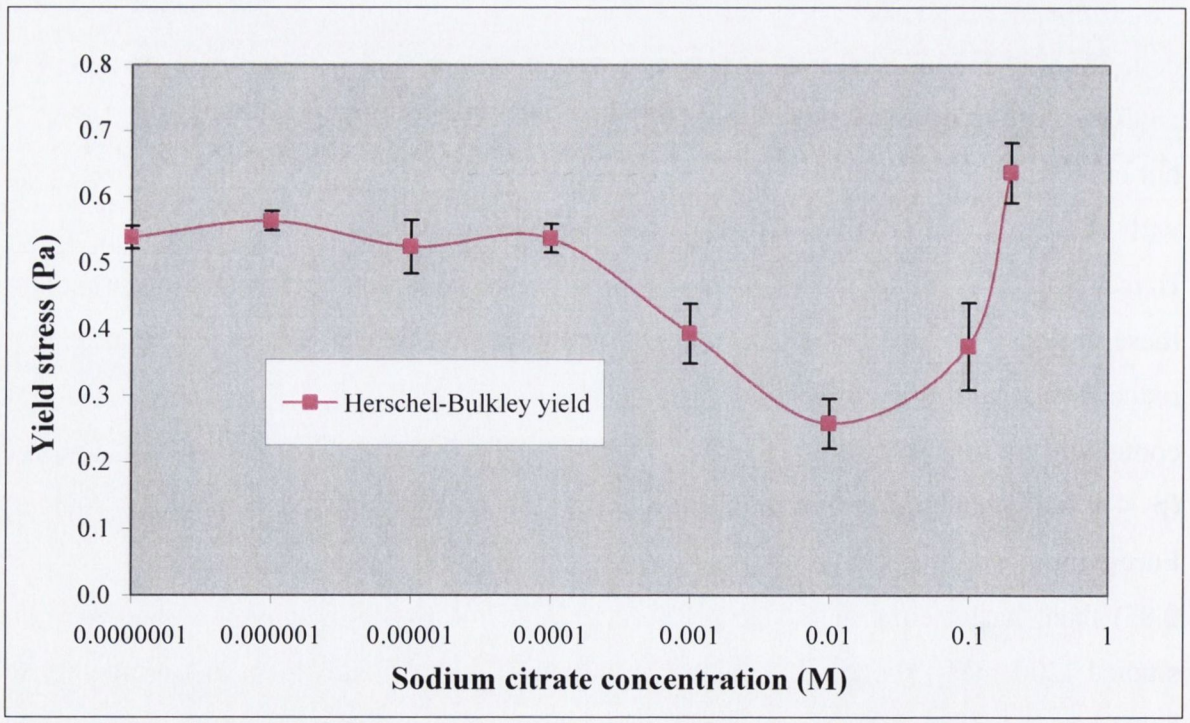


Figure 7.8ac. Herschel-Bulkley yield values as a function of sodium citrate concentration.

The effect of sodium citrate on sepiolite suspensions is clearly complex and multifaceted. Ca^{2+} ions exerted two actions; namely neutralization of negative face charges via specific adsorption and compression of the EDL, both of which produced a reduction in interparticle repulsion as evidenced by the change in sedimentation and flow behaviour. Charge neutralization and EDL compression would also be anticipated in the case of citrate ions, however, in this case the actions will oppose rather than augment one another in terms of their effect on interparticle repulsion. Neutralization of the positive edge charges would serve to increase the negativity of the zeta potential and hinder network formation. Compression of the EDL would serve to decrease the interparticle repulsion, facilitating network formation. It is anticipated that the effect of EDL compression would be overshadowed by the effect of edge charge neutralization at low citrate concentrations but would become increasingly dominant as the citrate concentration is increased. In terms of interparticle interactions, the system would be expected to exhibit increasingly deflocculated character as the citrate concentration increased to a certain point where thereafter, further increases in citrate concentration would cause a return to a flocculated state.

At low citrate concentrations (0.1 μM – 100 μM) the dominant effect, as expected, appears to be that of neutralization of the positive edge charge, resulting in reduced network formation as indicated by the decreased Herschel-Bulkley yield values (0.5243 – 0.5635 Pa) relative to the control (0.7140 Pa). At 100 μM, the reduction of the interfibrous interaction was such that the giant single floc was replaced by a large number of small flocs, which settle due to gravity roughly in accordance with Stokes' Law (Figure 7.8w, test tube 5).

At a citrate concentration of 1 mM, the yield value of the suspension was reduced further (0.393 Pa) indicating a further reduction of the degree of fiber association and floccule size. The rate index is approximately 1 indicating the absence of pseudoplastic character. The plastic type behaviour may be explained in terms of the rapid breakdown of these small loosely bound flocs and alignment of the elemental fibers in the direction of flow upon shear. Increasing the citrate concentration to 10 mM produced a deflocculated system in which the low yield value (0.258 Pa) may be attributed to the force required to align the fibers in the direction of shear. The rheology of these samples was qualitatively similar to that of sepiolite samples at high pH (~13.1), further corroborating the proposed increase in

the negativity of the zeta potential. The small volume of cloudy supernatant formed is reflective of the slow rate of settling of the highly peptized suspension (van Olphen, 1977; Martin, 1993).

Increasing the citrate concentration to 100 mM increased the Herschel Bulkley yield value (0.374 Pa) relative to that at 10 mM (0.258 Pa). It is proposed that at this high concentration, the adsorption capacity of sepiolite for citrate had been exceeded and consequently, the effect of compression of the EDL on the interparticle repulsion became dominant so that particle interaction was again facilitated. A further increase in sodium citrate concentration to 200 mM would therefore be expected to further decrease the interparticle repulsion. The observed increase in the yield value (0.637 Pa), together with the restoration of pseudoplastic behaviour (flow behaviour index = 0.210) supports this theory. However, the sedimentation and thixotropic behaviour observed would not have been anticipated. It is probable that the nature of interfibrous interactions (i.e. relative number of EE, EF and FF associations) in this system is altered relative to that in distilled water. Adsorption of citrate ions to the edges will lead to the formation of a barrier of approximate thickness equal to the diameter of a hydrated trivalent citrate ion i.e. 10 Å (Biggs *et al.*, 1995), thus hindering EE and EF associations. Furthermore, compression of the EDL at high citrate concentrations would be expected to facilitate increased FF associations. FF interactions will tend to facilitate the production of multiple small flocs rather than a single giant floc extending throughout the volume of the structure, thus explaining the tendency for sedimentation to occur. The occurrence of positive thixotropy further supports the proposed change in the nature of interparticle interactions.

7.8.6 Sodium polyphosphate (NaPP)

Sodium polyphosphate is a commercial deflocculating agent and has been successfully used to deflocculate kaolin suspensions (Lagaly, 1989; Papo *et al.*, 2002; Andreola *et al.*, 2006), bentonite suspensions (Keren, 1988) and palygorskite suspensions (Pakter, 1962). The addition of negatively charged dispersants to kaolin suspensions affects the particles' surface charge by favouring repulsion among the particles until the saturation adsorption limit of the dispersing agent is attained. van Olphen (1977) noted that an anion with a high valence, such as the polyphosphate anion which may have a valence of 30 or more, may become attached with only a fraction of its ionic groups actually bound to the particle

surface, conferring a distinctly negative charge as in Figure 7.8ad below. The magnitude of the interparticle repulsion is thereby dramatically increased and is such that it exceeds the attractive force at all interparticle distances. As a result electrostatic stabilization occurs. Furthermore, the employment of polymeric deflocculants induces a mechanism of particle stabilization, which results from steric interactions combined with electrostatic repulsions (Ituare, 2005). Moreover, Andreola and his co-workers (2006) note that sodium polyphosphate will complex any dissolved alkaline earth metals in the EDL and replace them with Na^+ ions, therefore increasing the EDL thickness and increasing interparticle repulsion.

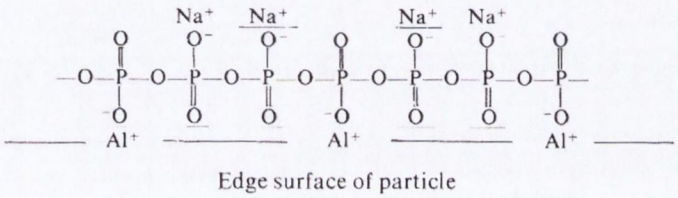


Figure 7.8ad. Schematic of a polymetaphosphate anion adsorbed to the surface of an aluminosilicate illustrating its ability to become attached to the surface of a clay particle through neutralization of positive surface charges involving only a fraction of its ionised groups, the other fraction thereby capable of conferring an extremely large negative charge such that the overall particle charge may be reversed rather than just neutralized.

The appearance of sepiolite suspensions treated with varying concentrations of sodium polyphosphate and allowed to stand for 28 days is presented in Figure 7.8ad. A caked sediment was evident within an hour in the case of tubes 1 – 5; corresponding to a sodium polyphosphate concentration range of 200 mM to 100 μM. No changes in the appearance of sepiolite suspensions treated with 0.1 μM to 10 μM were apparent at this stage. Over time, further sedimentation occurred in test tubes 1 – 5 resulting in the production of an increased volume of caked sediment and the formation of a cloudy supernatant. The appearance of test tubes 6 – 8 was identical to the control even after 28 days of standing.



Figure 7.8ae. Appearance of sepiolite suspensions treated with different concentrations of sodium polyphosphate at 28 days. Tube A = control, i.e. no sodium polyphosphate; Tubes 1 – 8 represent decreasing concentration of sodium polyphosphate from left to right in accordance with Table 3.7d.

SEMs of sepiolite samples treated with 0.1 μM sodium polyphosphate are presented in Figures 7.8af – 7.8ag. SEMs of the sediment produced on addition of 200 mM sodium polyphosphate are presented in Figures 7.8ah – 7.8ai. Flow curves of samples treated with the eight different sodium polyphosphate concentrations were studied and are presented in Figure 7.8aj. The data were fitted to all rheological models - the Herschel-Bulkley afforded the best data fit as determined by the relative order of magnitude of the standard errors; Figure 7.8ak describes the change in these yield values as a function of deflocculant concentration. All parameters from this rheological modeling are presented in Table A6e in Appendix 6.

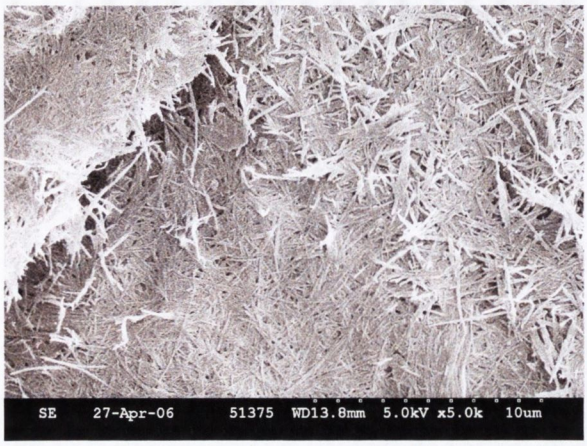


Figure 7.8af. SEM of sepiolite treated with 0.1 μM sodium polyphosphate (magnification x 5,000).

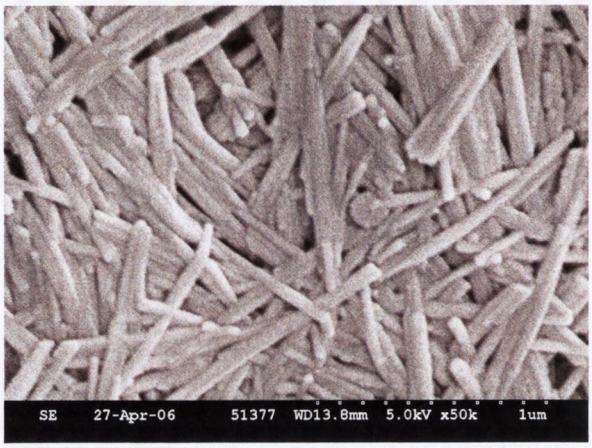


Figure 7.8ag. SEM of sepiolite treated with 0.1 μM sodium polyphosphate (magnification x 50,000).

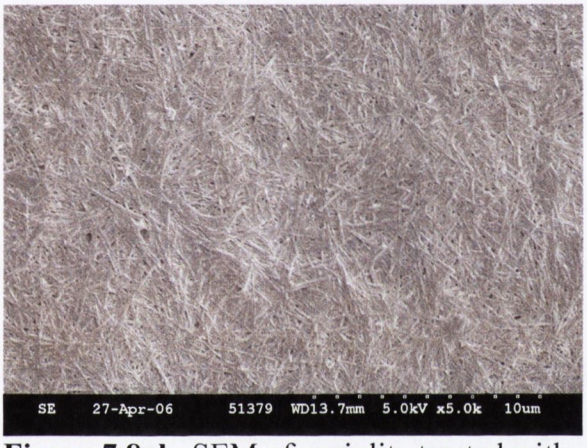


Figure 7.8ah. SEM of sepiolite treated with 200 mM sodium polyphosphate (magnification x 5,000).

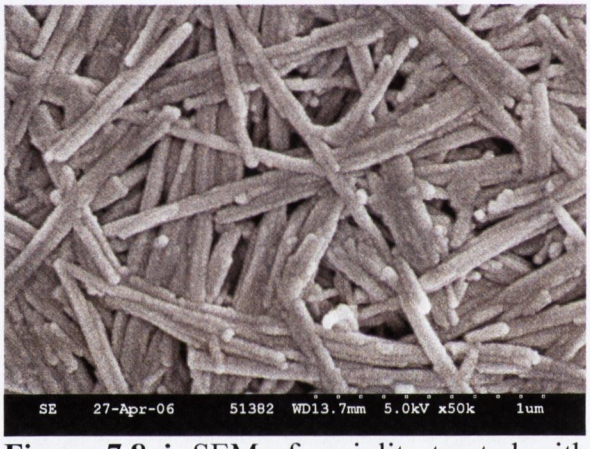


Figure 7.8ai. SEM of sepiolite treated with 200 mM sodium polyphosphate (magnification x 50,000).

In the case of the sample treated with 0.1 μM sodium polyphosphate, the three dimensional nature of the scaffold formed via fibrous interaction was evident at low magnification, indicating that the extent of NaPP adsorption at these concentrations did not alter fiber association markedly. At high magnification, the samples had a very similar appearance to the control as would be expected given the similar appearance of the dispersions on standing for 28 days. Furthermore, the samples containing 0.1 – 10 μM NaPP exhibited qualitatively similar rheological behaviour to one another and also to the control; namely pseudoplastic behaviour upon exceeding a yield value. Data fitting to the Herschel-Bulkley rheological model indicated that the yield values were slightly lower than those of the control and that the pseudoplastic character, as quantified by the flow behaviour index, decreased over the NaPP concentration range of 0.1 – 10 μM.

This may be explained in terms of the adsorption of NaPP to positive sites thus increasing the magnitude of the zeta potential and reducing the strength of interparticle associations. Antithixotropic behaviour decreased with increasing NaPP concentration and was negligible at concentrations above 10 mM, indicating that the magnitude of interparticulate repulsion was such that it hindered particle collisions which underlie the development of a yield value and antithixotropic behaviour.

At higher sodium polyphosphate concentrations, marked changes in the flow behaviour were observed. The rheological behaviour at 100 μM NaPP became less pseudoplastic and the yield value was dramatically reduced. Such behaviour may be attributed to the increased adsorption of NaPP onto the fiber surfaces, increasing interparticle repulsion. The production of a caked sediment provided further evidence of the increasingly deflocculated nature of the suspension. At NaPP concentrations of 1 mM to 100 mM, flow behaviour approaches that of a Newtonian fluid, the absence of a yield value and loss of pseudoplastic character (flow behaviour index $\approx$ 1) indicating the complete loss of interparticulate association, consistent with a deflocculated suspension. The apparent viscosity at all shear rates decreased on increasing NaPP concentration from 1 mM to 100 mM. Such a result indicated that the NaPP adsorption saturation limit had not yet been reached. On increasing the NaPP concentration to 200 mM, the apparent viscosity was higher than that of the 10 mM and 100 mM NaPP-treated suspensions at all shear rates (Figure 7.8aj). Papo *et al.* (2002) reported that when the saturation adsorption limit of the NaPP dispersant has been attained, a minimum viscosity value is reached. Thereafter further increases in NaPP concentration lead to an excess concentration in solution, which is not adsorbed on the suspended particles and causes an increase in viscosity. Hence, it was concluded that saturation of the clay surface with NaPP occurred at concentrations between 100 mM and 200 mM, corresponding to a NaPP/ sepiolite ratio of 10,000 – 20,000 mmoles/ kg.

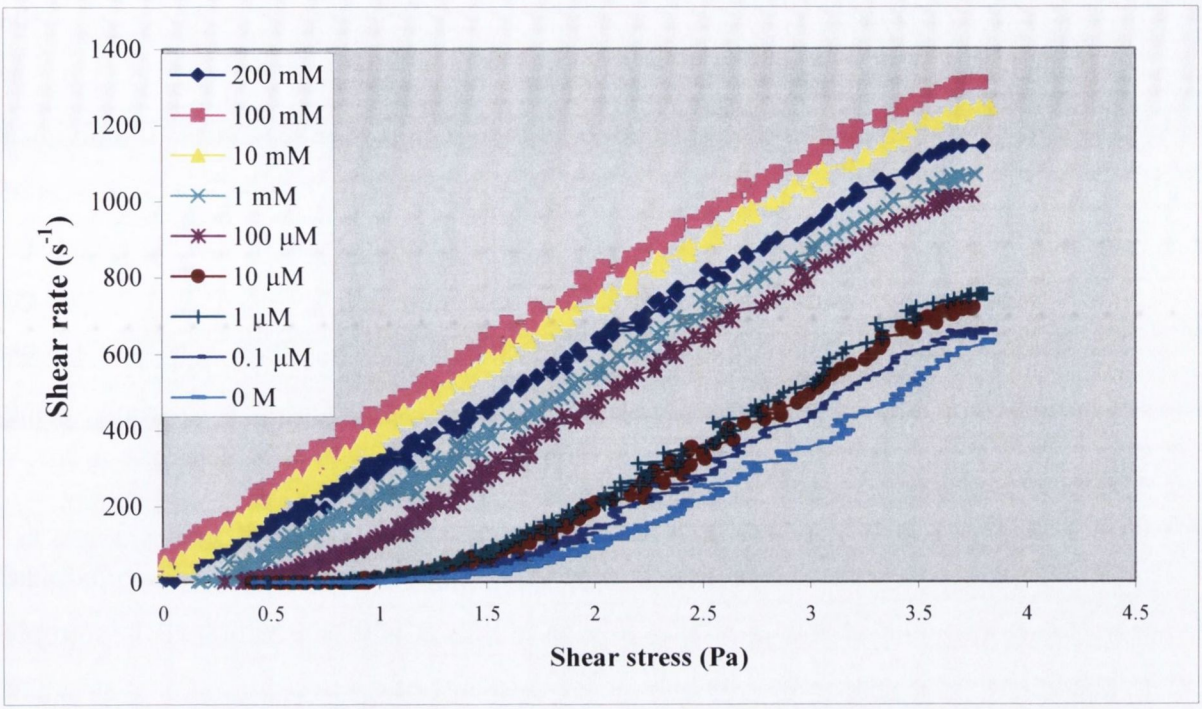


Figure 7.8aj. Up-flow curves of 1% w/v sepiolite suspensions containing different concentrations of sodium polyphosphate.

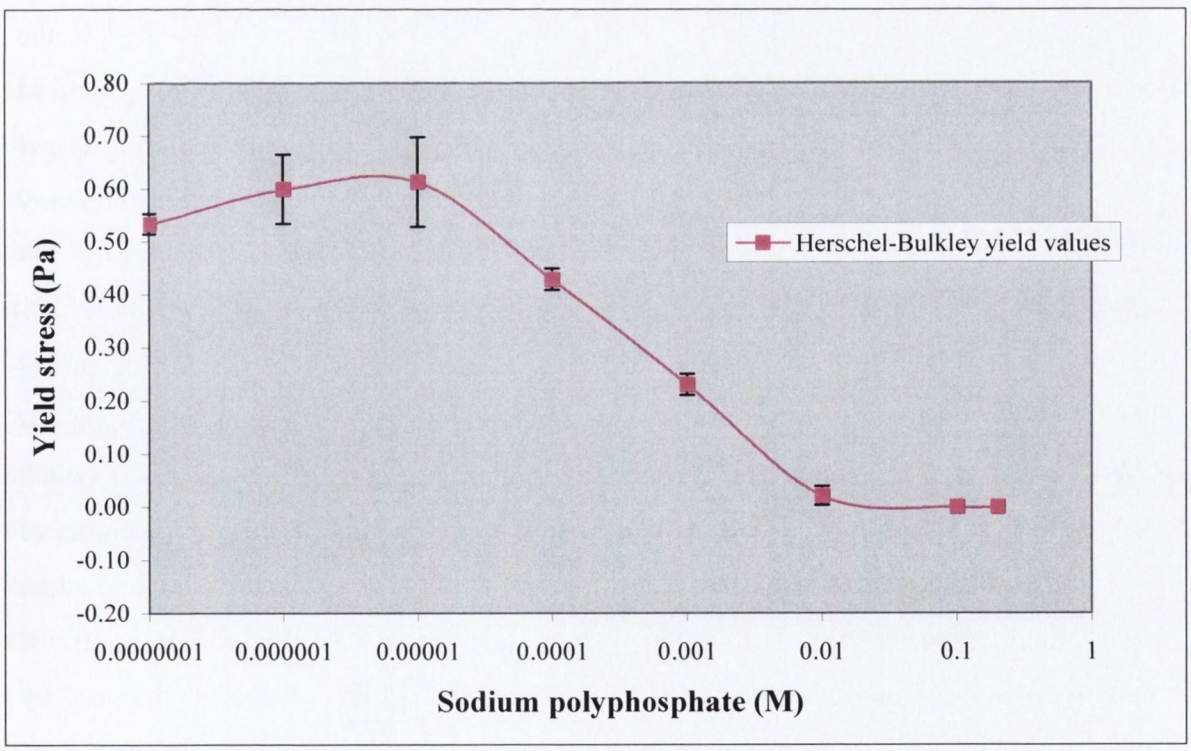


Figure 7.8ak. Herschel-Bulkley yield values as a function of sodium polyphosphate concentration.

7.9 CONCLUSIONS

Effective dispersion of sepiolite in water to form a gel requires the separation of individual fibers and therefore the use of high shear mixing equipment. The rheological properties of the resultant dispersion were demonstrated to be dependent on both the mixing speed and duration thereby supporting the 'swelling-independent' gelling mechanism proposed previously by other authors (Simonton *et al.*, 1988). Higher mixing speeds and longer mixing times ensured greater dispersion of the fibers, as evidenced by particle sizing results, and a resultant increase in the rheological yield value.

Aqueous sepiolite suspensions of low concentration ($\leq$ 0.5% w/v) exhibited approximate plastic flow behaviour characterized by low yield values with superimposed thixotropic character. The yield value was evidence of the presence of a three-dimensional structure formed by fiber-fiber interactions. The plastic behaviour indicated that a small stress resulted in the complete breakdown of the structure and the alignment of the constituent fibers in the direction of shear. At higher concentrations, flow behaviour became pseudoplastic. The change from plastic to pseudoplastic behaviour may be ascribed to the increasing number and complexity of 'joints' within the three-dimensional fibrous scaffold with an increase in concentration such that breakdown is more difficult, requiring larger stresses, and occurs over a range of shear stresses due to the varying strength of the many constituent fiber-fiber connections.

The Herschel-Bulkley yield values increased disproportionately with increasing concentration. All suspensions exhibited a decrease in the viscosity with time upon the application of a constant shear rate. An increase in concentration also resulted in a switch from positive thixotropic behaviour to antithixotropic behaviour (defined in accordance with Tombácz and Szekeres (2006)). Thixotropic behaviour was ascribed to the time taken for structural re-establishment following shear breakdown. At high concentrations, structural re-establishment was facilitated by the increased collision frequency induced by the shearing action such that apparent viscosity values were higher at equivalent shear rates on the down-curve than on the up-curve (i.e. antithixotropy). A reduced sedimentation rate was observed with an increase in sepiolite concentration. Sediments formed were fluffy and easily redispersed; the associated supernatants were clear thus confirming the flocculated state of these suspensions as indicated by rheological testing. The rate of

sedimentation was not increased by a simulated transportational stress. No sedimentation was evident in suspensions of concentration ≥ 2% w/v. It was proposed that concentrations of this order permitted the formation of a single giant floc which extended throughout the suspension volume, while below this concentration the system was composed of a larger number of smaller flocs which settled in accordance with Stokes' law. It was concluded that concentrations in the range 1-2% w/v could, by the formation of a structured vehicle, retard the sedimentation of insoluble drugs by entrapment and thus act as suspending agents.

The rheological and sedimentation behaviour of sepiolite suspensions was altered by changes in temperature, highlighting the importance of Brownian motion in the development of three-dimensional fibrous networks. The change in the yield value with temperature could be explained in terms of the temperature dependence of the translational and rotational Brownian motion diffusion coefficients. The change in apparent viscosity at high shear stresses with temperature mirrored the change in the viscosity of the suspending medium with temperature.

The zeta potential at the native pH of sepiolite was distinctly negative (-20 mV) but within the range reported to facilitate particle association in the secondary minimum in accordance with the DLVO theory. The proximity of the i.e.p of sepiolite (~ 2.6 to 3) to that of silica (~3.0; Knapp *et al.*, 1997) highlights the importance of the silanol groups in the development of surface charge. Indeed, it appears that in the absence of specifically adsorbing ions, it is the principal determinant of the sign and magnitude of the zeta potential with a change in pH. Over most of the pH range (3-14), sepiolite has a negative zeta potential which decreases in magnitude with decreasing pH. Flow behaviour changes markedly with pH. At very high pH, the magnitude of the zeta potential was such that particle-particle associations were considerably hindered and a relatively disperse system exhibiting Newtonian-like flow behaviour resulted. At very low pH, plastic flow behaviour characterized by a high yield value was observed. Furthermore at intermediate pH (~5.8), the yield value was reduced relative to that at pH 8.2 despite the reduction in the interparticulate repulsive force predicted by the change in zeta potential. Although it has been reported elsewhere that the rheological properties of fibrous clay suspensions are dependent on the mechanical interference between the long fibers (Bradley, 1940; Simonton *et al.*, 1988; Santarén, 1993), rather than on electrostatic interparticle forces,

these results indicated that these two phenomena are not mutually exclusive as has been proposed, but rather the extent of mechanical entanglement of the fibers is dependent on the nature and magnitude of the electrostatic interparticulate forces. The deviation of the flow behaviour at pH 5.8 from that predicted by the DLVO theory indicates that the relative proportion of EE, EF and FF fiber-fiber associations changes with pH and supports the existence of a heterogeneous edge-face charge. FF interactions are only facilitated at acidic pH values where ionization of the silanol groups on the fiber faces is suppressed. At higher pH values, EE and EF associations are favoured. van Olphen (1977) reported that FF associations do not make the same positive contribution to the development of a yield value and viscosity as EE and EF associations (van Olphen, 1977), thus explaining the anomalous low yield value observed at pH 5.8.

Despite literature reports to the contrary, the stability of sepiolite suspensions was shown to be influenced by the presence of electrolytes. The susceptibility of sepiolite suspensions to the effect of electrolytes does appear to be less than that of plate-like clays in that higher concentrations of electrolytes were required to effect changes. Two mechanisms were demonstrated to be involved; namely, the compression of the EDL via accumulation of the ions within the diffuse outer layer and the active sorption of ions onto the fiber surface thereby altering the magnitude and in some case affecting a reversal of surface charge. Ions which caused compression of the EDL only were termed "indifferent" electrolytes and were capable of screening but not reversing the charge of the surface. Na^+ ions belonged to this category. Even at very high NaCl concentrations (1.5 M) sepiolite suspensions were extremely stable, indicating that the effect of Na^+ on the EDL was relatively weak. At low Ca^{2+} concentrations, sepiolite suspensions were stable, however high concentrations caused marked coagulation of the fibers via a combination of both EDL compression and adsorption. The effect of cationic surfactants, exemplified by cetrimide, was more complex and predominantly governed by specific adsorption to the sepiolite fiber surface; increased flocculation, coagulation and deflocculation were observed as the negative surface charge of the fibers was initially reduced, eradicated and reversed, respectively, with increasing concentrations of cetrimide. Trivalent anions, typified by citrate ions, were similarly capable of decreasing the size of floccules, presumably by reducing the positive edge charge, and at sufficiently high concentrations, a deflocculated system was produced. Finally, the influence of polyanionic materials was examined using sodium polyphosphate,

which was demonstrated to cause increasing deflocculation of the suspension with increasing concentration.

In conclusion, therefore, the rheological behaviour of sepiolite suspensions is dependent upon the physical intermeshing of the fibers as described previously by other authors. This physical intermeshing is facilitated by Brownian-motion induced collisions at zero shear. The pH and electrolyte dependency of the flow and sedimentation behaviour indicates that the nature and extent to which these fiber-fiber interactions can occur is a function of the zeta potential (and consequently the surface charge). This work therefore supports the theory previously described by Chang *et al.* (1993), namely that the stability of fibrous clay gels may, in analogous manner to laminar clay gels, be described in terms of electrostatic interparticulate interactions.

Chapter 8

EVALUATION OF THE PERFORMANCE OF DIFFERENT GRADES OF SEPIOLITE AS SUSPENDING AGENTS IN A MODEL PHARMACEUTICAL SUSPENSION

8.1 PREPARATION OF A NOVEL RHEOLOGICAL GRADE OF SEPIOLITE

8.1.1 Introduction

The theory of protective colloids has been described in Chapter 1. van Olphen (1977) reported that polyelectrolytes can increase the salt tolerance of hydrophobic sols including clay suspensions. This protective effect was exemplified by the protective action of the anion of sodium carboxymethylcellulose (NaCMC) on a bentonite suspension. Indeed, a combination of magnesium aluminium silicate and carboxymethylcellulose has been used as a stabilizing system in liquid makeups for over 30 years (Ciullo, 1981).

FMC Corporation has exploited this protective action of NaCMC in the production of a number of MCC-based suspending agents; including Avicel® RC-591 and CL-611 (Sissen, 1965). In addition to improving electrolyte tolerance, NaCMC also aids dispersion of colloidal MCC (Avicel® R) (Dell and Colliopoulos, 2001; Rowe *et al.*, 2005). Furthermore, incorporation of 10% NaCMC (relative to the dry weight of colloidal Avicel®) produced a marked increase in viscosity and yield stress of Avicel® R suspensions (Sissen, 1965). Avicel® RC-591 and CL-611 are spray dried blends of NaCMC and colloidal MCC (Rudraraju and Wyandt, 2005a) and exhibit both pseudoplastic and thixotropic behaviour (Dolz-Planas *et al.*, 1988; Dolz *et al.*, 1991; Dolz-Planas *et al.*, 1992; Dell and Colliopoulos, 2001). The viscosity of colloidal Avicel® grades has been attributed to the physical interference of the rod-shaped particles with one another, in a manner comparable to the development of viscosity in sepiolite suspensions. Hence, it was postulated that in an analogous manner to Avicel® RC and CL grades, inclusion of NaCMC may aid dispersion in sepiolite suspensions and furthermore act as a protective colloid. Avicel® RC-591 and CL-611 contain NaCMC (medium viscosity grade) 8.3 - 13.8% w/w (average:

11.05% w/w) and 11.3 - 18.8% w/w (average: 15.05% w/w) respectively and require only low to moderate shear mixing to achieve dispersion. Using the formulation of Avicel® CL-611 as a template, a novel rheological product containing NaCMC/sepiolite in the ratio 15.05: 84.95% by weight was produced by spray-drying. For the remainder of this thesis, this co-spray dried product is referred to as SepCMC.

8.1.2 Establishing optimum spray drying conditions for the preparation of SepCMC

The spray drying conditions used to prepare SD sepiolite and SepKoll in Chapter 5 were used as a starting point for the establishment of optimum drying conditions for SepCMC. The use of an ethanol-water (60:40 v/v) dispersion medium proved necessary to achieve reasonable yields of SD sepiolite and SepKoll. 2% w/v sepiolite suspensions were used previously and consequently would require the inclusion of 0.354% w/v NaCMC to achieve the final dry weight ratio of 84.95% sepiolite to 15.05% NaCMC in the co-spray dried product. NaCMC, despite being readily dispersible in water (solubility 20 mg /mL, Sigma-Aldrich MSDS), is practically insoluble in ethanol (Rowe *et al.*, 2005). Aqueous slurries were used for the preparation of SepCMC in preliminary studies but resulted in exceptionally poor yields. Consequently, the solubility of NaCMC in a 60:40 ethanol/ water mixture was investigated. Given the aqueous solubility of the polymer, the volume of water present in the mixture should be sufficient to disperse 0.354% w/v NaCMC. Direct addition of 0.354% w/v NaCMC to the hydroalcoholic mixture resulted in immediate agglomeration. Dispersion of 0.354 g NaCMC in 40 mL water, followed by the very gradual addition of ethanol, while stirring, to a final volume of 100 mL produced a clear dispersion. Following overnight storage at room temperature, a small amount of precipitate was evident. Consequently, all NaCMC-sepiolite dispersions were prepared immediately before the spray drying process as follows: NaCMC was dispersed in the aqueous component of the dispersion medium, sepiolite in the ethanolic component and the sepiolite suspension added gradually to the NaCMC dispersion while stirring. The hydroethanolic suspension was spray dried using the following conditions: inlet temperature of 95 °C, feed rate of 10%, atomising air flow rate of 600 L/ min and outlet temperature of 74 °C. The yield was of the order of 15%.

8.2 CHARACTERISATION OF SepCMC

8.2.1 Introduction

SEM and laser diffraction analysis were used to elucidate the morphology and particle size distribution of SepCMC. pXRD was used to ascertain whether any changes in the crystalline nature of sepiolite occurred upon co-spray drying with NaCMC. FT-IR was used to investigate the nature of any binding interaction occurring between sepiolite and NaCMC. These properties were compared to those of untreated sepiolite, NaCMC and a physical mixture of spray dried sepiolite and NaCMC in the same ratio as the co-spray dried product (termed Physmix_NaCMC).

8.2.2 SEM

Images of SepCMC and NaCMC obtained from scanning electron microscopy are presented in Figures 8.2a - 8.2c and Figure 8.2d respectively. As expected from the results obtained in Chapter 5, an increase in the number and sphericity of aggregates was evident on comparing SepCMC to untreated sepiolite. In terms of morphology, SepCMC aggregates were similar to those of SD sepiolite (Figure 5.3a). The nature of the surface of the aggregates differed between SD sepiolite and SepCMC. In the case of SepCMC, the fibers appeared to be impregnated in an amorphous matrix, presumably NaCMC, producing a very smooth surface. The characteristic string-like appearance of NaCMC (Figure 8.2d) was not evident in SepCMC, providing further evidence that it had been successfully dispersed to a molecular level in the hydroethanolic vehicle.

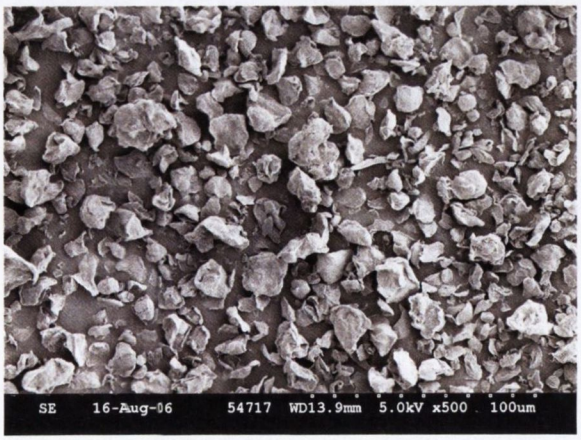


Figure 8.2a. SEM of SepCMC (magnification x 500).

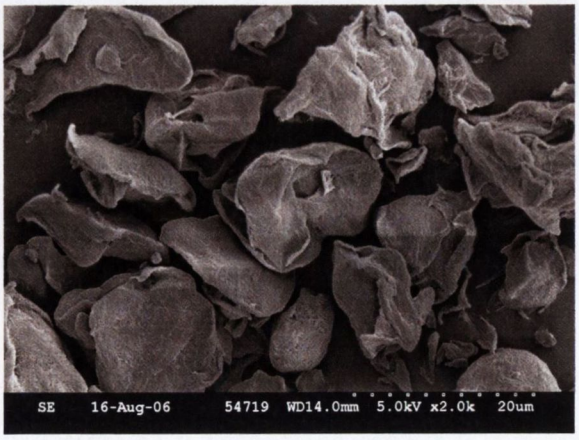


Figure 8.2b. SEM of SepCMC (magnification x 2,000).



Figure 8.2c. SEM of SepCMC (magnification x 10,000).



Figure 8.2d. SEM of NaCMC (magnification x 70).

8.2.3 Particle sizing

The results of particle sizing of SepCMC are presented in Table 8.2a. The particle size distributions of NaCMC, Physmix_NaCMC and SD sepiolite are included for comparative purposes.

Table 8.2a. Particle size distribution by volume (% volume undersize; n = 3).

Material	d10 (µm)	d50 (µm)	d90 (µm)
SepCMC	3.986 ± 0.067	11.014 ± 0.068	21.778 ± 0.109
SD sepiolite	3.278 ± 0.240	10.058 ± 0.389	19.771 ± 0.555
NaCMC	39.073 ± 0.291	106.515 ± 0.983	266.283 ± 0.715
Physmix_NaCMC	4.371 ± 0.146	12.262 ± 0.178	33.366 ± 0.609

One-way ANOVA confirmed that the d10, d50 and d90 values of SepCMC were significantly larger than those of SD sepiolite ($p < 0.01$). This result is unsurprising given that NaCMC firstly acts as a tablet binder at concentrations in the range 1.0 - 6.0% (Rowe *et al.*, 2005) and secondly will increase the viscosity of the dispersion slurry and size of the resultant droplets (Lukasiewicz, 1989). The d10, d50 and d90 values of Physmix_NaCMC were biased upwards relative to those of SepCMC due to the presence of the larger NaCMC particles.

8.2.4 pXRD

pXRD was used to assess whether any significant alteration in the crystalline structure of sepiolite occurred on co-spray drying with NaCMC. From the results in section 5.4.2.3 it was evident that spray drying of sepiolite alone or in combination with Kollidon® VA 64 did not alter the crystalline structure of sepiolite and consequently no changes would be anticipated on co-spray drying with NaCMC. The X-ray diffractograms of SepCMC, SD sepiolite, NaCMC and Physmix_NaCMC are presented in Figure 8.2e below.

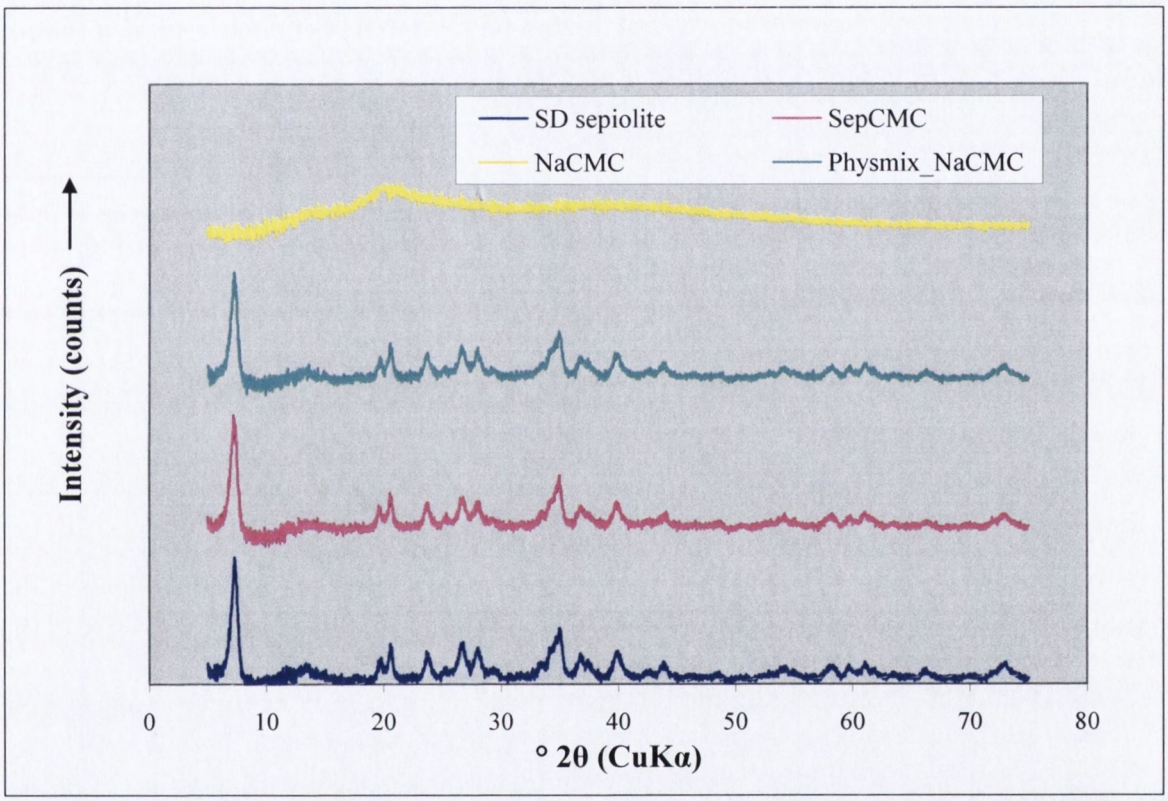


Figure 8.2e. X-ray diffractograms of SD sepiolite, SepCMC, Physmix_NaCMC and NaCMC.

The X-ray diffractogram of NaCMC showed two broad features over the 12° 2θ to 30° 2θ angular range indicative of an amorphous physical state. The peak positions and intensities in the X-ray diffractograms of SD sepiolite, SepCMC and Physmix_NaCMC were identical indicating that the crystalline structure of sepiolite remained unchanged by co-spray drying with NaCMC. Furthermore, changes in the solid state form of NaCMC following spray drying were unlikely given the similarity of the SepCMC and Physmix_NaCMC traces.

8.2.5 FT-IR

The infrared spectra of SepCMC, NaCMC, Physmix_NaCMC and SD sepiolite are presented in Figure 8.2f. Xiao *et al.* (2000) assigned the bands centred at 1616 cm^{-1} in the IR spectrum of NaCMC to asymmetric stretching vibration of the carboxyl group. Broad bands in the region 3100 to 3400 cm^{-1} were assigned to stretching of the secondary alcohol groups of NaCMC. Any interaction between NaCMC and sepiolite in the co-spray dried product would be expected to involve the carboxy groups of NaCMC and the surface silanol groups and possibly Mg(OH) groups of sepiolite and thereby produce changes in the OH-stretching (3000-4000 cm^{-1}), the carbonyl and OH-bending region (1600-1700 cm^{-1}) and the Si-O stretching region (850-1300 cm^{-1}).

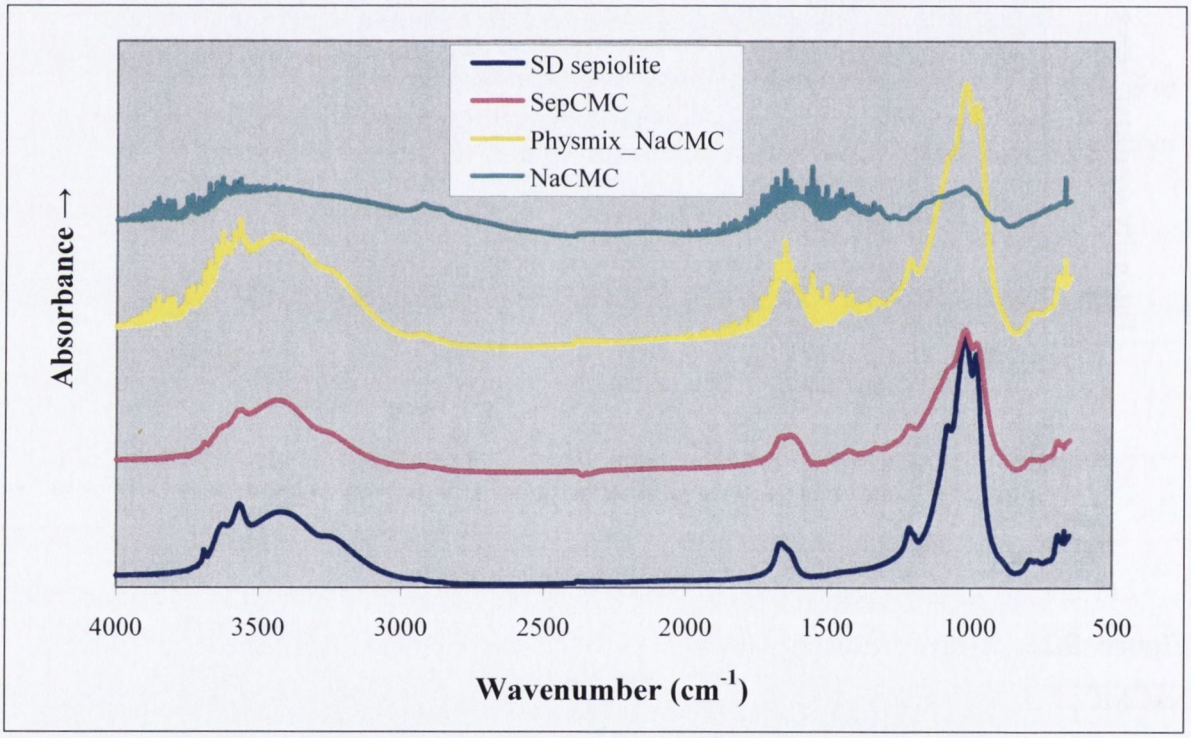


Figure 8.2f. FT-IR spectra of SD sepiolite, SepCMC, Physmix_NaCMC and NaCMC.

The FT-IR spectrum of Physmix_NaCMC (i.e a physical mixture of spray dried sepiolite and NaCMC in the same ratio as the co-spray dried product) is effectively a composite of that of NaCMC and SD sepiolite. The major peaks of both excipients are visible in the spectrum of the physical mixture. The major peak positions were unchanged, suggesting that bonding interactions between the functional groups of the excipients did not occur during the physical mixing process. The FT-IR spectrum of SepCMC is markedly different from that of the physical mixture. Substantial changes in the OH-stretching (3000-4000

cm^{-1}), carbonyl and OH-bending region (1600-1700 cm^{-1}) and the Si-O stretching region (850-1300 cm^{-1}) were evident. Peaks in these regions were typically broadened and decreased in intensity. The shoulder at 1080 cm^{-1} attributable to Si-O stretching in SD sepiolite was not evident in the SepCMC spectrum. Xiao *et al.* (2000) noted that the width and intensity of the spectral bands, in addition to the position of the peaks, are sensitive to environmental changes and intermolecular interactions. Spectral bands associated with hydroxyl and carbonyl functional groups are typically broadened when these groups participate in hydrogen bonding. The conclusion from FT-IR studies is that bonding interactions do take place between NaCMC and sepiolite during co-spray drying. These interactions seem to involve the silanol groups and Mg(OH) groups of sepiolite and the carbonyl and possibly the secondary alcohol groups of NaCMC.

8.3 PRELIMINARY RHEOLOGICAL INVESTIGATIONS

The rheology of SepCMC was investigated with a specific focus on its potential use as a suspending agent. In-use tests should use a shear rate which replicates the property being tested (Zatz and Kushla, 1996). A shear rate of 100 s^{-1} is the approximate shear rate associated with moderate shaking necessary prior to administration of a suspension, while a rate of 1000 s^{-1} may be correlated with the high shear experienced by a topical product upon rubbing into the skin (Zatz and Kushla, 1996; IFSCC Monograph number 3, 1997; Practical Techniques I, Applied Rheology Symposium 2002). Consequently, the samples were subjected to a shear rate of 0-1000 s^{-1} increased over 1 min and then returned to zero over the same time period. 2% w/v and 4% w/v suspensions were prepared. Given the results of earlier work on sepiolite (section 7.4.4) these concentrations reflect a range suitable for use in suspensions and in gels. Flow curves of the 2% w/v and 4% w/v SepCMC dispersions are presented in Figure 8.3a below. For comparative purposes, the rheograms of 2% and 4% w/v sepiolite suspensions are included; as are those of dispersions containing both 1.7% w/v untreated sepiolite and 0.3% w/v NaCMC or 3.4% w/v untreated sepiolite and 0.6% w/v NaCMC. The Herschel-Bulkley model afforded the best fit for all data sets. Rheological parameters derived from the Herschel-Bulkley model are presented in Table 8.3a.

From Figure 8.3a, it is evident that the rheological behaviour of SepCMC suspensions was markedly different from that of sepiolite suspensions and furthermore, that the rheological behaviour of SepCMC was qualitatively different at different concentrations.

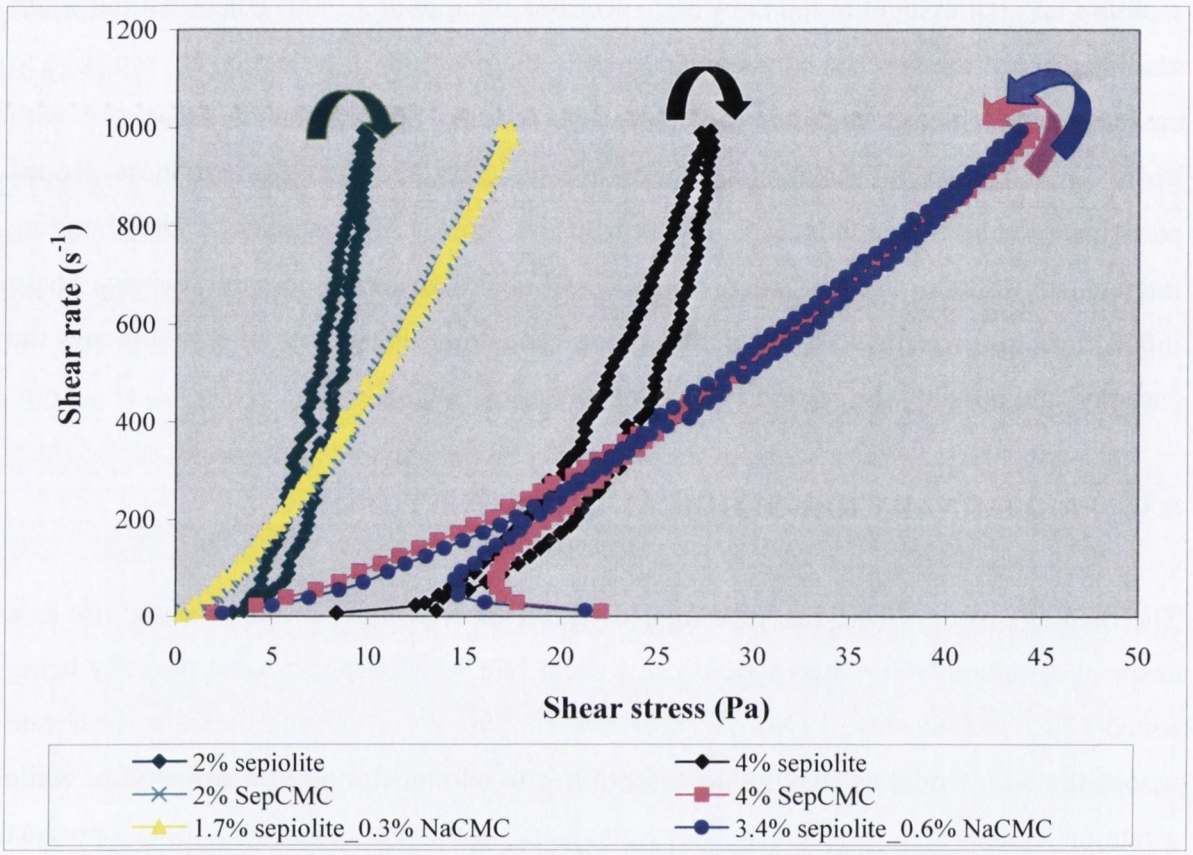


Figure 8.3a. Flow curves of 2% and 4% w/v SepCMC suspensions and relevant contr

Table 8.3a. Rheological parameters for SepCMC suspensions together with relevant controls (n = 3).

Sample (% w/v)	HB yield value, σ_{HB} (Pa)	HB Flow behaviour index, n (-)	HB Consistency index, K ($Pa.s^n$)	*HB correlation coefficient, r^2 (-)	Thixotropy ($Pa.s^{-1}$)	HB model standard error (-)	Newtonian model standard error (-)	Bingham model standard error (-)	Power law standard error (-)	Casson model standard error (-)
2% sepiolite	3.307±0.112	0.3765±0.0098	0.1698±0.0125	0.98692	-734 ± 152	18.45	295.8	98.22	37.58	45.23
2% SepCMC	0.575±0.195	0.7299±0.0345	0.1636±0.0262	0.99603	-158 ± 54	8.803	86.85	31.68	12.65	14.88
1.7% sepiolite/ 0.3% NaCMC	0±0	0.7356±0.0017	0.1012±0.0129	0.99297	-112 ± 24	9.092	67.98	30.78	9.095	17.47
4% sepiolite	11.010±0.800	0.4556±0.0287	1.2254±0.1225	0.97584	-1612 ± 87	34.11	315.4	138.5	78.69	55.29
4% SepCMC	19.797±0.855	0.7480±0.0726	0.0024±0.0003	0.97641	1947 ± 190	56.47	253.8	69.28	136.6	99.07
3.4% sepiolite/ 0.6% NaCMC	14.807±1.855	0.7173±0.0395	0.0457±0.0067	0.99396	828 ± 368	47.00	269.1	54.09	120.7	82.52

* The lowest correlation coefficient of all replicates was quoted. The highest standard error of all replicates was quoted.

At the lower concentration investigated, sepiolite, SepCMC and the physical mixture of sepiolite and NaCMC exhibited pseudoplastic flow behaviour. The yield values decreased in the order: sepiolite > SepCMC > physical mixture. The yield value of a suspension is a function of both the number of particle-particle linkages and the energy required to break those linkages (Keren, 1988). The incorporation of NaCMC therefore reduced the number and/or strength of interparticulate bonds per unit volume of suspension. The reduction in the yield value of the physical mixture was significantly more marked than in the case of SepCMC. This indicated that the co-spray drying process did affect the interaction between NaCMC and sepiolite. It is evident from Figure 8.3b and from the relative magnitudes of the flow behaviour indices in Table 8.3a that the 2% w/v sepiolite-only suspension displayed more marked pseudoplastic behaviour than those samples containing NaCMC, presumably reflective of the more intricate scaffold which can be established in the absence of polymer.

The apparent viscosity of 2% w/v SepCMC is higher than that of the corresponding physical mixture at shear rates less than 100 s^{-1} but thereafter is similar. Furthermore, the apparent viscosity of the 2% w/v sepiolite-only suspension was higher than that of the 2% w/v SepCMC suspension at all shear rates below 230 s^{-1}. The flow curves intersect at a shear rate of approximately 230 s^{-1}, such that above this shear rate, the apparent viscosity of the SepCMC dispersion was higher than that of the sepiolite-only suspension (Figure 8.3b). Sjöberg *et al.* (1999) studied the adsorption of NaCMC on kaolin particles and reported that the extent of sorption was typically low and led to an increase in the magnitude of the negative zeta potential, stronger electrostatic interparticle repulsion and a lower relative viscosity. Hence NaCMC acts in a manner akin to sodium polyphosphate (Section 7.8.6). This observation explains the lower yield values and lower apparent viscosity of the NaCMC-containing dispersions at shear rates below the point of intersection.

At shear rates above the intersection point, destruction of the interfibrous network in the 2% w/v sepiolite-only suspension was extensive but not yet complete, as indicated by the continuing downward trend in apparent viscosity (Figure 8.3b). The apparent viscosity at this point and beyond represented the resistance of small fibrous aggregates/ individual fibers to flow, while in the case of NaCMC-containing dispersions, the apparent viscosity at and beyond this intersection point represented the resistance to flow of the larger

polymer-clay composite particles. The larger particles are likely to offer increased resistance to shear, hence the higher relative apparent viscosity.

At the lower concentration examined, the degree of antithixotropic behaviour of both NaCMC-containing dispersions was much reduced relative to that of sepiolite alone. The extent of thixotropy seen under these experimental conditions depends on the number and efficiency of particle collisions upon decreasing shear. The decreased antithixotropy may be reflective of the increased zeta potential of the polymer-clay particles (relative to sepiolite fibers) which increases interparticulate repulsive forces, thereby decreasing the proportion of agitation-induced collisions which result in particle interlinking and structural re-establishment.

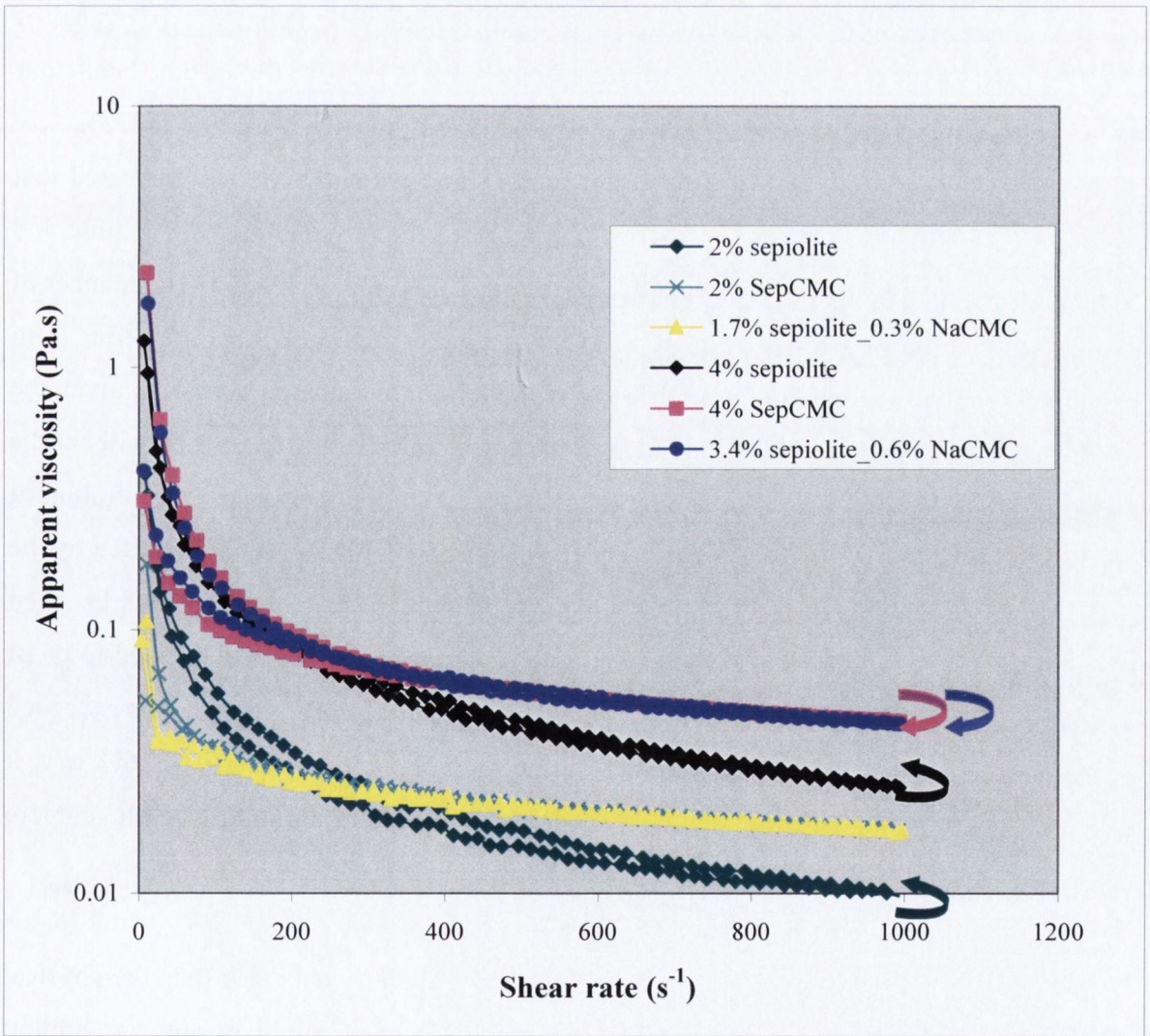


Figure 8.3b. Relationship between apparent viscosity and shear rate (Colour-coded arrows indicate the displacement of the down-curve relative to the up-curve).

As would be expected the yield values of all three systems increased with an increase in concentration from 2% w/v to 4% w/v. The rheological behaviour of 4% w/v sepiolite was pseudoplastic at supra-yield stress values; that of SepCMC and the physical mixture of sepiolite and NaCMC could similarly be described as shear-thinning. The rate of reduction in apparent viscosity with increasing shear rate was similar in all three systems at shear rates below 230 s^{-1}. Thereafter, the rate and extent of reduction in apparent viscosity with increasing shear rate was much greater in the sepiolite-only sample. The higher apparent viscosity of the NaCMC-containing systems at very high shear rates may again be attributed to the greater resistance to flow posed by the clay-polymer complexes as opposed to individual sepiolite fibers.

Both NaCMC-containing systems displayed remarkable positive thixotropic behaviour at a 4% w/v concentration (Figure 8.3a and Table 8.3a). Thixotropic behaviour is typical of NaCMC dispersions (Harwood *et al.*, 1996). The increase in positive thixotropic behaviour did not come at the cost of a reduced yield value, as was the case for the 2% w/v dispersions; in fact the results of data fitting to the Herschel-Bulkey model indicated that the yield values of the 4% w/v SepCMC dispersion and the physical mix of sepiolite and NaCMC were significantly higher than that of the sepiolite-only dispersion. The manner of particle association in 2% w/v NaCMC-containing dispersions must therefore differ from that at 4% w/v. As the extent of adsorption of NaCMC was anticipated to be low, given the results reported by Sjöberg (1999) in the case of kaolin, this positive thixotropy without the expected reduction in yield value at 4% w/v may be due to the increased concentration of unadsorbed NaCMC in the solution phase of the dispersion. This theory is supported by the findings of Erikson *et al.* (1991) who reported that NaCMC forms polymer networks when in solution at concentrations above the overlap concentration, which they deemed to be of the order of 0.2-0.3% w/v. While it is possible that the overlap concentration was exceeded in the case of the 4% w/v dispersions, where the total NaCMC content was 0.6% w/v, it was unlikely to be the case for the 2% w/v dispersions, where the total NaCMC content was 0.3% w/v.

At 2% w/v, the spray dried composite, SepCMC, had a higher yield value than the physical mixture of untreated sepiolite and NaCMC, while the degree of antithixotropy was similar. At 4% w/v, SepCMC displayed both a superior yield value and an increased level of thixotropy relative to the physical mixture. These results would suggest that the extent of

NaCMC adsorption onto sepiolite was reduced or the manner altered by the spray drying process. The reduced level of adsorption would result in a less pronounced increase in the magnitude of the zeta potential and reduced hindrance of particle association. Furthermore, the concentration of NaCMC in the solution phase would be increased such that at 4% w/v SepCMC concentration, the overlap concentration would be well exceeded, producing a substantial NaCMC network, which has been previously reported to display thixotropic behaviour.

Several conclusions may be drawn from this study; firstly the combination of NaCMC with sepiolite, either as a simple physical mixture or as a co-spray dried composite, changed the rheological behaviour markedly. A reduction in yield value and apparent viscosity was seen at 2% w/v concentrations. However, at 4% w/v, SepCMC had the advantage of positive thixotropy without loss of yield strength and thus may prove to be of use in the production of suspension and gel systems.

8.4 EVALUATION OF THE PERFORMANCE OF SEPIOLITE AND SepCMC AS SUSPENDING AGENTS USING CALAMINE LOTION AS A MODEL SYSTEM

8.4.1 Introduction

The factors influencing the stability of sepiolite suspensions have been extensively reviewed in Chapter 7. Having thus established the relevant functional and rheological characteristics, the ability of sepiolite and the novel rheological grade, SepCMC, to act as suspending agents will be evaluated in this section using calamine lotion BP as a model formulation. The impact of the incorporation of these novel suspending agents on the rheological behaviour and sedimentation rate of the lotion will be investigated.

8.4.2 Development of suitable formulations

The BP formulation incorporates 3% w/v bentonite as a suspending agent, together with 0.5% w/v (i.e. 0.017 M) sodium citrate to control the degree of flocculation. Modified formulations of calamine lotion BP were produced in which bentonite was replaced by sepiolite, SepCMC and other suspending agents (Avicel® RC-591 and CL-611) in accordance with Table 8.4a. The colloidal Avicel® grades were included in the study to act

as standards against which the performance of sepiolite and, in particular, SepCMC (given the similarity of their formulation) could be rated.

Table 8.4a. Modified calamine lotion formulations, differing from the BP formulation only in terms of the suspending agent used and the quantity of sodium citrate present in the formulation. (Note: This table is a replicate of Table 3.8b).

Product	Suspending agent	Sodium citrate concentration	
		(M)	(% w/v)
1	No suspending agent	BP[1]	BP[1]
2	3% w/v bentonite (Calamine lotion BP -Ovelle®)	BP[1]	BP[1]
3	2% w/v Avicel® RC-591	BP[1]	BP[1]
4	2% w/v Avicel® CL-611	BP[1]	BP[1]
5	2% w/v sepiolite	0	0
6	2% w/v sepiolite	0.010	0.2941
7	2% w/v sepiolite	0.025	0.7353
8	2% w/v sepiolite	0.050	1.4705
9	2% w/v sepiolite	0.100	2.9410
10	2% w/v SepCMC	0	0
11	1.7% w/v spray dried sepiolite + 0.3% w/v NaCMC	0	0
12	1.7% w/v sepiolite + 0.3% w/v NaCMC	0	0
13	0.3% w/v NaCMC	0	0

[1]BP: as per BP formulation.

In preliminary studies, sodium citrate was excluded from formulations containing sepiolite as a suspending agent, given its deleterious effect on the rheological and sedimentation behaviour of sepiolite as outlined in section 7.8.5. However, the resultant products were extremely viscous and entrained large volumes of air, indicative of a coagulated system. Zinc oxide (the primary constituent of calamine) and ferric oxide (present at concentrations of ~ 0.5% w/w in calamine) have been reported to be practically insoluble in water (BP, 2007). However, as discussed in section 7.8.3, Ca^{2+} concentrations as low as 50 mM can lead to agglomeration of sepiolite fibers. Presumably, comparable concentrations of Zn^{2+}

ions and even lower concentrations of Fe^{3+}, on account of its higher valency, could produce agglomeration in an analogous fashion. Consequently, sodium citrate was included in the revised formulation to increase the negativity of the zeta potential and reduce susceptibility to surface charge neutralization and resultant agglomeration caused by the zinc and iron cations. Citrate concentrations in the range 0.01 to 0.1 M were investigated. This range was selected for two reasons: firstly, it included the concentration of citrate in the BP formulation; and secondly, it was evident from the results in section 7.8.5 that the presence of 0.01 M citrate in a 1% w/v sepiolite suspension produced a deflocculated system.

It was also evident from preliminary studies that lotions prepared using 2% w/v SepCMC as a suspending agent in the absence of sodium citrate did not agglomerate, thus confirming the protective electrosteric influence of NaCMC and obviating the need for sodium citrate in the formulation.

8.4.3 Evaluation of the rheological behaviour of the modified calamine lotion formulations

The modified calamine lotions were subjected to continuous shear rheology as described in section 8.3. Flow curves for the various products are presented in Figures 8.4a, 8.4c and 8.4d. The data were fitted to all rheological models - the Herschel-Bulkley afforded the best data fit as adjudged by the relative magnitudes of the standard errors (Appendix 7, Table A7a). Herschel-Bulkley rheological parameters are presented in Table 8.4b.

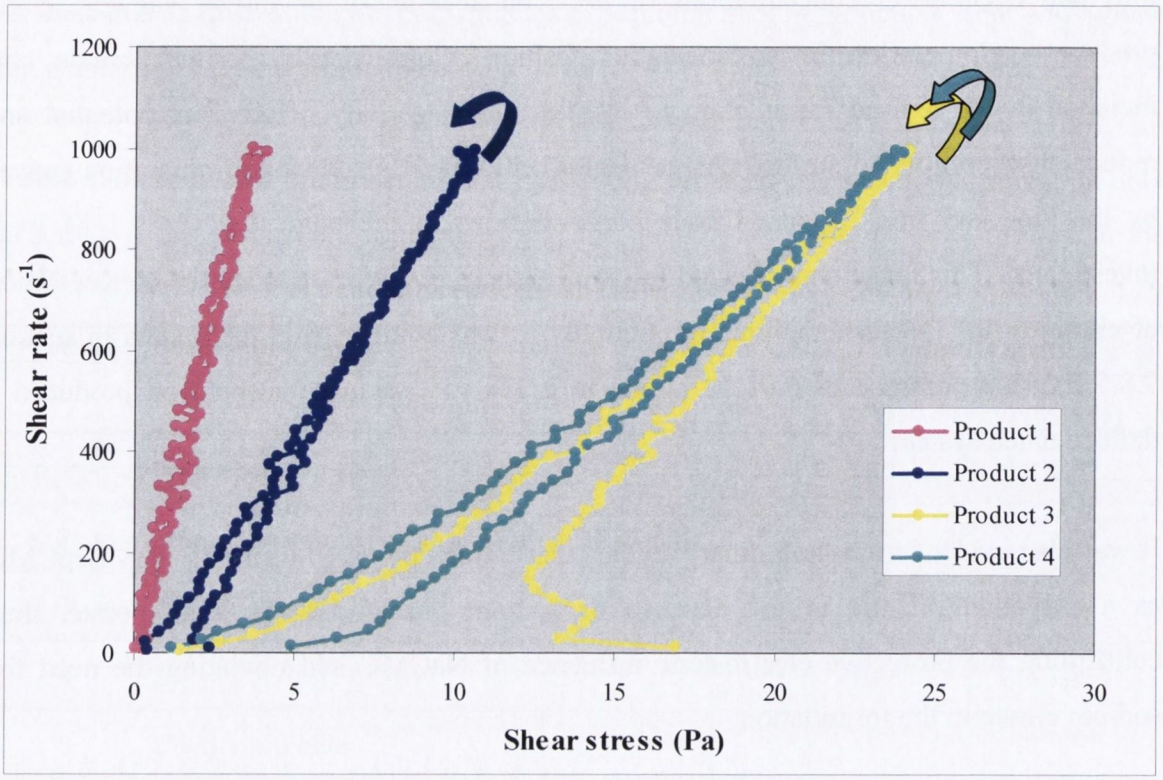


Figure 8.4a. Flow curves of calamine products 1 – 4 (Colour-coded arrows indicate the displacement of the down-curve relative to the up-curve).

From Figure 8.4a, it was evident that in the absence of any suspending agent (i.e. product 1), the formulation exhibited Newtonian-like behaviour, as confirmed by the absence of a yield value, the similarity of the apparent viscosity values at 93 and 995 s^{-1}. The standard errors of data fit for the Herschel-Bulkley, Bingham, Casson and Newtonian models were also comparable. Addition of 3% w/v bentonite (i.e. product 2, BP formulation) produced a system with a yield value and increased apparent viscosity. Existence of a yield point is indicative of the presence of a three dimensional structure (Matijašić and Glasnović, 2002). Consequently, it may be concluded that bentonite particles were associated by EF or EE associations to form a voluminous house-of-cards structure, which was dispersed on application of shear as indicated by the reduction in apparent viscosity on increasing the shear rate from 93 to 995 s^{-1} (van Olphen, 1977).

Use of the colloidal Avicel® grades, RC-591 and CL-611 (as in products 3 and 4 respectively), resulted in products with considerable pseudoplastic character ($n < 1$ in both cases) and led to marked increases in the yield stress, apparent viscosity at all shear rates and extent of positive thixotropy relative to product 1. The yield stresses and thixotropic character of product 3 were twice those of product 4 indicating that, on an

equal weight basis, the RC-591 grade was a more efficient rheological modifier than the CL-611 grade, consistent with the product information brochure (FMC, 2005). The rheological properties of these grades may again be attributed to the establishment of a three-dimensional network (Figure 8.4b), held together by weak hydrogen bonding (FMC, 2005).

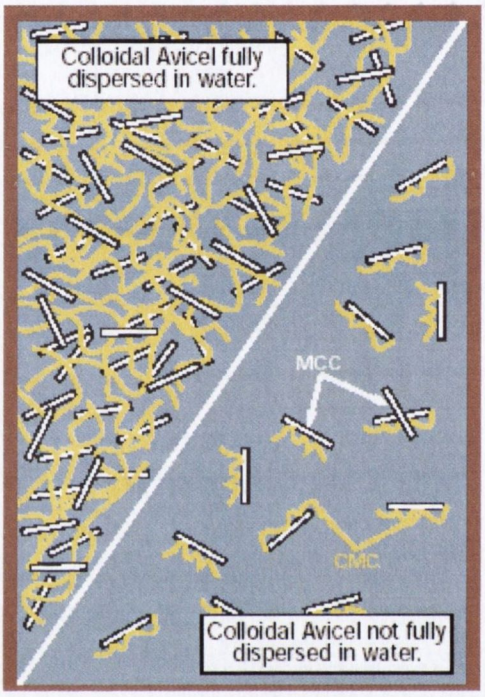


Figure 8.4b. Schematic representation of the manner of particle association in Avicel colloidal grades dispersed in water (Reproduced from FMC, 2005).

Table 8.4b. Rheological parameters for modified calamine lotion formulations (n = 3).

Product	HB yield value, σ_{HB} (Pa)	HB Flow behaviour index, n (-)	HB Consistency index, K ($Pa.s^n$)	* HB correlation coefficient, r^2 (-)	Thixotropy ($Pa.s^{-1}$)	**Apparent viscosity at 93 s^{-1} (mPa.s)	**Apparent viscosity at 995 s^{-1} (mPa.s)
1	-0.005 ± 0.009	0.9939 ± 0.0762	0.0032 ± 0.0012	0.95733	-239.1 ± 25.2	3.69 ± 0.73	3.40 ± 0.26
2	1.303 ± 0.317	0.9790 ± 0.0442	0.0094 ± 0.0022	0.91566	249.1 ± 13.4	20.01 ± 2.90	9.17 ± 0.84
3	13.560 ± 0.538	0.6977 ± 0.1145	0.0751 ± 0.0000	0.70051	2966.3 ± 144.8	154.03 ± 5.03	24.40 ± 0.08
4	5.707 ± 0.296	0.8393 ± 0.0294	0.0551 ± 0.0135	0.93099	1698.7 ± 104.4	84.06 ± 4.65	23.37 ± 0.66
5	10.162 ± 0.912	0.5456 ± 0.0221	0.3356 ± 0.0582	0.95699	197.4 ± 13.0	155.67 ± 6.23	24.75 ± 0.50
6	2.153 ± 0.141	0.9363 ± 0.0229	0.0083 ± 0.0007	0.93053	476.1 ± 26.0	28.08 ± 1.55	7.51 ± 0.61
7	1.791 ± 0.100	1.0074 ± 0.033	0.0070 ± 0.0017	0.91569	339.8 ± 18.6	24.58 ± 1.81	9.07 ± 0.10
8	1.391 ± 0.211	0.8922 ± 0.0176	0.0137 ± 0.0028	0.90841	337.2 ± 20.8	21.25 ± 1.46	7.17 ± 0.43
9	1.948 ± 0.110	0.9599 ± 0.0579	0.0073 ± 0.0014	0.90362	353.7 ± 28.1	28.75 ± 1.27	9.38 ± 0.66
10	3.094 ± 0.391	0.7250 ± 0.0267	0.1640 ± 0.0317	0.98920	1362.7 ± 77.0	81.37 ± 3.27	27.43 ± 1.77
11	2.772 ± 0.189	0.7173 ± 0.0136	0.7105 ± 0.0094	0.98880	1343.3 ± 115.8	93.51 ± 1.74	35.83 ± 0.07
12	0.088 ± 0.011	0.7105 ± 0.0094	0.1878 ± 0.0084	0.99399	666.6 ± 33.2	54.25 ± 3.03	27.10 ± 0.25
13	0.127 ± 0.010	0.9458 ± 0.0305	0.0124 ± 0.0032	0.95887	-172.7 ± 21.3	8.72 ± 1.10	8.35 ± 0.58

*The lowest correlation coefficient of three replicates was quoted. ** Apparent viscosity values were determined from the up-flow curve.

Flow curves of products 5 – 9 are presented in Figure 8.4c and allow assessment of the effect of sepiolite together with different concentrations of sodium citrate on the rheology of the calamine system. Firstly it should be noted that during the preparation of products 6 – 9 inclusive, the order of addition of citrate and calamine/ zinc oxide was extremely important. It was necessary to add the citrate to an aqueous dispersion of sepiolite, prior to the addition of calamine and zinc oxide. Addition of calamine and zinc oxide to the sepiolite dispersion prior to addition of sodium citrate resulted in a very frothy and viscous product indicating that the state induced by the divalent zinc and trivalent iron ions was irreversible.

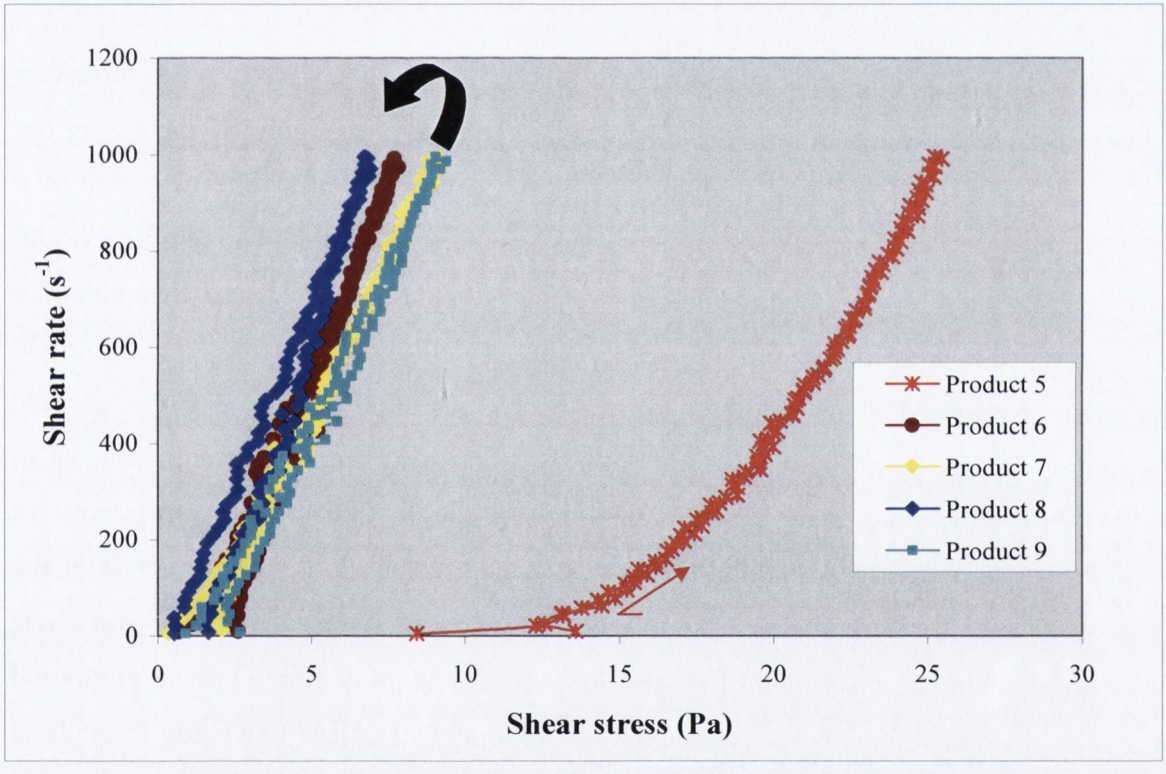


Figure 8.4c. Flow curves of calamine products 5 – 9. (Block arrow indicates that the down flow curve was displaced to the left of the up-flow curve in the case of products 6 – 9).

The addition of sodium citrate in the range 0.01 to 0.1 M produced a substantial (>80%) reduction in the Herschel-Bulkley yield values relative to product 5 (no citrate). One-way ANOVA revealed that the Herschel-Bulkley yield value for product 7 was significantly lower ($p = 0.001$) than those for products 6, 8 and 9 which, in turn, did not differ from one another. The thixotropic behaviour of products 7, 8 and 9 was similar, while that of product 6 was significantly higher ($p < 0.001$).

The changes in the magnitude of the yield value and thixotropy may be explained through a consideration of the effects of the citrate ion when present at different concentrations. As described previously in section 7.8.5, the citrate ion will exert two opposing effects: firstly, neutralization of the positive edge charges of sepiolite, thereby increasing the negativity of the zeta potential and interparticle repulsion and secondly, compression of the EDL, which would serve to reduce the interparticle electrostatic repulsion. From section 7.8.5, the first effect appeared to dominate at low citrate concentrations whilst the second was more pronounced at higher citrate concentrations. In terms of counteracting the pro-agglomeration effect of the zinc and ferric ions, a citrate concentration which promotes a net increase in the negativity of the zeta potential is desirable.

The reduced yield value and increased level of thixotropy of product 6 relative to product 5 indicated that the citrate ion afforded a 'protective' effect, presumably by increasing the magnitude of the zeta potential through adsorption to positive sites. The existence of a yield point confirmed that a three-dimensional structure was formed in product 6 and therefore that the presence of citrate at this concentration did not increase the zeta potential to a magnitude that precluded interfibrous associations entirely. The increase in thixotropic behaviour confirmed that the three-dimensional structure was formed via particle flocculation rather than agglomeration. Further increases in citrate concentration, as in product 7 (0.025 M), led to significant reductions in the yield value and thixotropy relative to product 6 (0.01M). At these higher citrate concentrations, the dispersive effect of the citrate ions may have exceeded the pro-agglomerative influences of the zinc and ferric cations, thus reducing the extent of fibrous interaction and producing a system composed of a large number of small flocs rather than a voluminous scaffold extending throughout the entire volume of the system. Increasing the citrate concentration to 0.05 M (as in product 8) led to a recovery of the yield value to that seen in product 6. The thixotropic behaviour failed to recover to levels seen in product 6. At this concentration, it appears that compression of the EDL by citrate ions became the predominant effect, thus reducing interparticle repulsion and facilitating increased levels of fiber interaction relative to product 7. The failure of thixotropy to recover suggested that the nature of the fibrous interactions (i.e. the relative proportion of EF, FF and EE associations) in product 6 differed from that in products 8 and 9.

In terms of suitable rheology for a topical lotion, all calamine lotion formulations containing sepiolite in combination with sodium citrate exhibited a reasonable yield stress i.e. that which is large enough to prevent rapid sedimentation of the suspension and small enough to be overcome by shaking such the structure can be broken down generating a readily pourable liquid. The apparent viscosity values at 93 s^{-1} were similar to one another and also to that of the BP product thus predicting similar 'pourability'. Furthermore, apparent viscosity values of products 6 – 9 were also comparable to the BP product at the high shear rate thus suggesting similar 'spreadability'. Moreover, all samples exhibited positive thixotropy, thus indicating that rethickening did not occur immediately on cessation of shaking, hence ensuring that the pouring viscosity was comparable to the shaking viscosity (i.e. apparent viscosity at 95 s^{-1}).

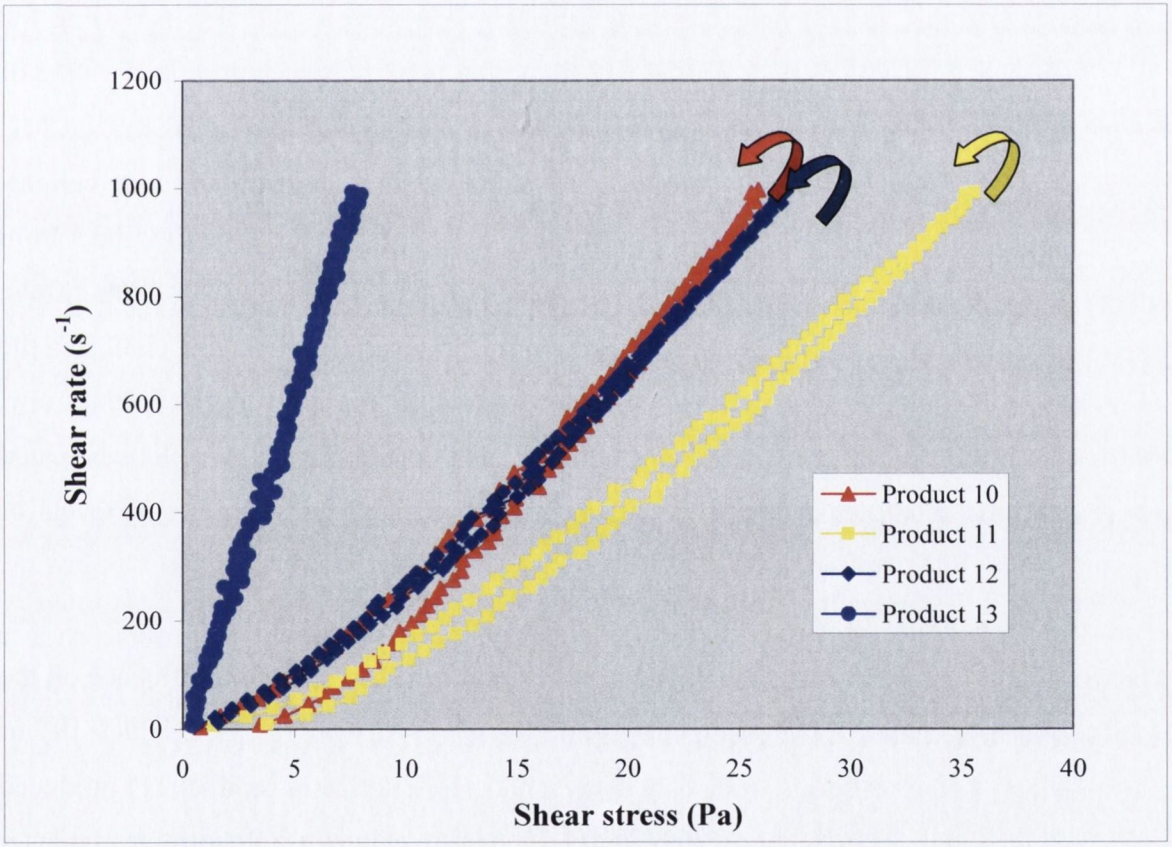


Figure 8.4d. Flow curves of calamine products 10 – 13 (Colour-coded arrows indicate the displacement of the down-curve relative to the up-curve).

The flow curves of products 10–13 are presented in Figure 8.4d. Incorporation of 0.3% w/v NaCMC in the calamine formulation (as in product 13) led to the production of a low yield system with poor thixotropic properties. It is evident from the flow curves of products 5 and 13 that, at the concentrations used here, neither sepiolite (in the absence of sodium

citrate) nor NaCMC alone were capable of conferring suitable rheological properties on the calamine system to permit its use as a lotion. When used in combination, however, as in products 10, 11 and 12, systems with more pharmaceutically relevant rheological behaviour were obtained (i.e. pseudoplastic flow associated with high levels of thixotropy) relative to systems where the two excipients were used individually (products 5 and 13). A comparison of the rheological parameters of the sepiolite/ NaCMC systems with those of the standards (i.e. products 2 – 4) indicated that the rheological behaviour of SepCMC (product 10), in qualitative terms, was similar to that of Avicel® CL-611 (product 4).

Comparison of the flow parameters for 2% w/v aqueous dispersions of sepiolite and SepCMC in section 8.3 indicated that the inclusion of NaCMC reduced the yield value of the system. This effect was attributed to the association of the negative carboxymethylcellulose molecules with the sepiolite fiber surface, thereby increasing the magnitude of the negative zeta potential and hindering particle association. In the case of the calamine formulation, the increase in zeta potential negativity promoted by NaCMC opposed the decrease in zeta potential negativity promoted by the iron and zinc cations. Hence the effect of sodium carboxymethylcellulose was to protect the sepiolite fibers from agglomeration induced by the zinc and iron cations, in a manner akin to sodium citrate. The resultant zeta potential in these products favoured extensive particle association in the secondary minimum, as indicated by the high yield value and high level of thixotropy. Furthermore, the presence of the long polymer chains of carboxymethylcelluose created the possibility of increased entanglement, further increasing yield values and levels of thixotropy.

The manner in which NaCMC and sepiolite were combined had a marked influence on the rheological behaviour of the resultant system. Co-spray drying (as in product 10) or combination of NaCMC with previously spray dried sepiolite (as in product 11) produced systems with significantly higher yield values ($p < 0.001$) and greater thixotropic character than when NaCMC was combined with untreated sepiolite (i.e. product 12). It was proposed in section 8.2 that the spray drying process reduced the adsorptive capacity of sepiolite for NaCMC. Reduced adsorption would dampen the dispersive effect of NaCMC, thereby increasing interparticulate attraction. In this instance, the increased interparticulate attraction resulted in increased flocculation rather than agglomeration. Hence, the relative performance and suitability of SepCMC, a physical mix of spray dried sepiolite and

NaCMC and a physical mix of untreated sepiolite and NaCMC will be influenced considerably by the ionic composition of the system as it is this factor that will dictate the importance (and hence the required magnitude) of the protective effect of NaCMC on sepiolite. In systems where the protective influence required is higher due to a higher concentration of cations, the performance of the simple physical mixture of untreated sepiolite and NaCMC is likely to be superior.

In conclusion, the rheological characteristics (flow indices, consistency indices, apparent viscosities) conferred by 2% w/v sepiolite combined with sodium citrate were comparable to those proffered by 3% w/v bentonite. The performance of 2% w/v SepCMC (product 10), as adjudged by estimates of spreadability, pourability and thixotropy from rheological studies, was similar to that of 2% w/v Avicel® CL-611 (product 4). Products 4 and 10 should be considered when a lotion of slightly higher viscosity than the BP formulation is required.

8.4.4 Sedimentation behaviour of modified calamine lotion formulations

The relative sediment volume, F, of the thirteen calamine lotion preparations was determined as a function of time and the results presented in Figure 8.4e below. In addition, the physical appearance of the formulations after 50 days of standing (i.e. nature of sediment, appearance of supernatant) was also recorded and results presented in Table 8.4c. The number of standard 'shakes' required to redisperse any sediment present and generate a uniformly distributed, readily pourable liquid after 50 days of standing was determined as described in sections 3.7.5.3 and 3.8.3.

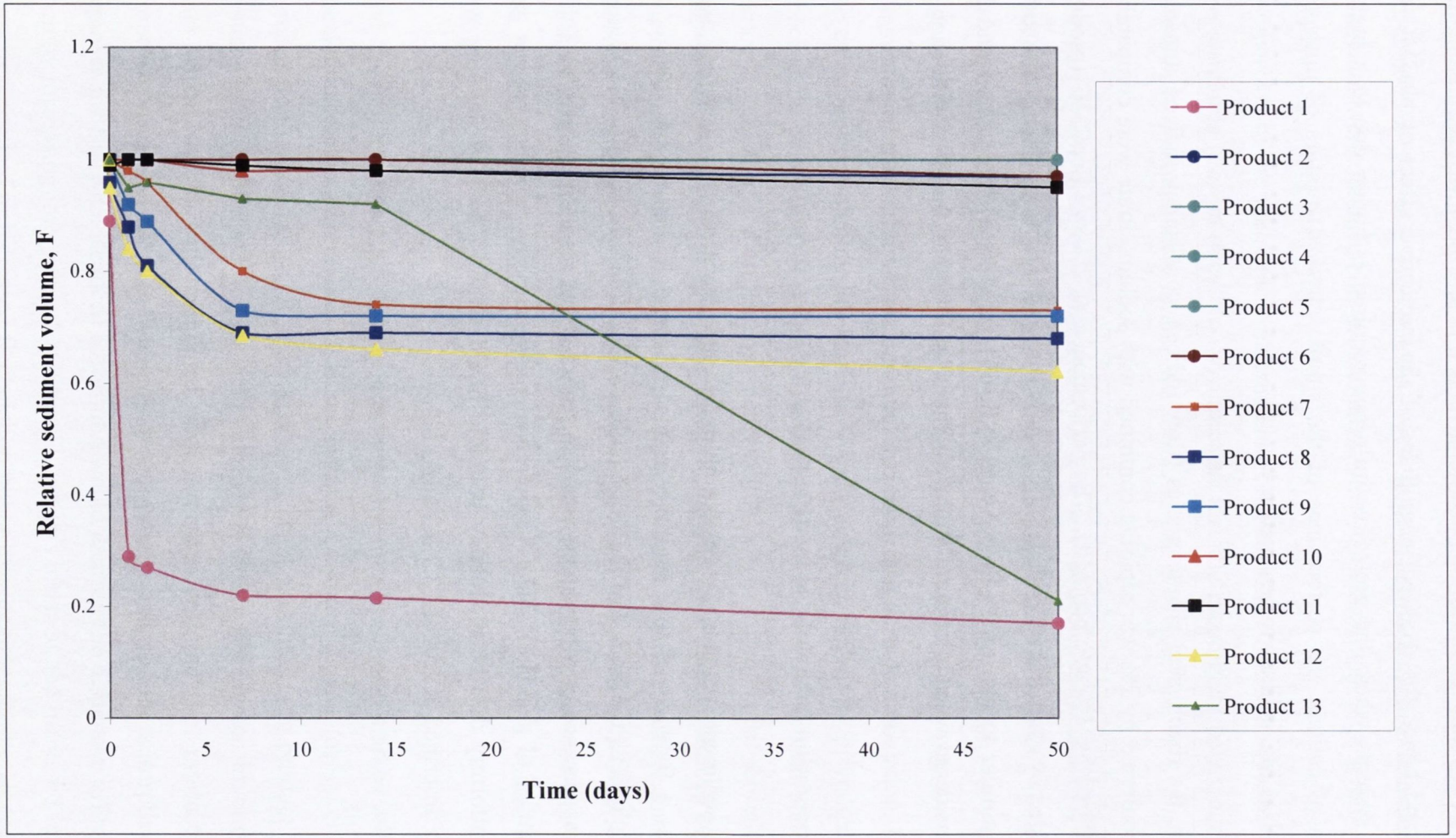


Figure 8.4e. Relative sediment volumes, F, of the modified calamine lotion preparations over time. It should be noted that the behaviour of products 3, 4 and 5 were identical in that sediment ratio (F) was 1 for the duration of the study and consequently, the same symbol is used to represent these three formulations.

Table 8.4c. Physical appearance of modified calamine lotions after 50 days of standing at room temperature.

Product number	Sediment volume (ml)	Appearance of supernatant	Appearance of sediment	Standard shakes required[§]
1	17	Clear	Caked	27
2	97	Clear	Loose, fluffy	5
3	100	None	None	10
4	100	None	None	6
5	100	None	None	13
6	97	Clear	Loose, fluffy	3
7	73	Clear	Loose, fluffy	8
8	68	Clear	Loose, fluffy	17
9	72	Clear	Loose, fluffy	11
10	95	Clear	Loose, fluffy	7
11	95	Clear	Loose, fluffy	6
12	62	Clear	Loose, fluffy	6
13	21	Cloudy	Increasingly caked with depth	> 40

[§]This number reflects the total number of standard shakes required to firstly redisperse any sediment formed on standing and secondly permit ready pouring of the suspension from the graduated cylinder into a beaker.

Ofner and Schnaare (2001) noted that if the yield value developed by a suspending agent is greater than the stress exerted in the suspending fluid by a suspended particle, the suspended particle cannot move though the suspension and sedimentation cannot take place. They reported that the theoretical minimum yield value required to permanently suspend a particle can be calculated from the following equation:

$$YV = \frac{V_p(\rho_2 - \rho_1)g}{A} \qquad \textbf{Equation 8.4a}$$

where YV is the theoretical minimum yield value, V_p is the particle volume given by $\pi d^3/6$ (where d is the particle diameter), A is the cross-sectional area of the particle given by $\pi d^2/4$, ρ_2 is the particle density, ρ_1 is the dispersion medium density and g is acceleration due to gravity.

From dry powder particle sizing, it was evident that 100% by volume of zinc oxide particles were below 138.038 μm, whilst 100% by volume of the calamine particles were below 39.811 μm. The densities of zinc oxide, zinc carbonate and ferric oxide are 5.60 g/ cm^3, 4.40 g/ cm^3 and 5.25 g/ cm^3 respectively (Webelements, 2007a, 2007b). Consequently, the zinc oxide particles, by virtue of their larger size and higher density, will be the most susceptible to sedimentation. Hence the theoretical yield value required to prevent sedimentation of even these particles, (assuming particles were spherical and that particle amalgamation did not occur in suspension), is 4.15 Pa. From the results in Tables 8.4b and 8.4c it was evident that there was reasonably good agreement between the theoretical minimum YV required to prevent sedimentation and the Herschel-Bulkley yield value – sedimentation did not occur in products 3, 4 and 5, which were the only products in which the Herschel-Bulkley yield value exceeded 4.15 Pa.

In the absence of any suspending agent (i.e. product 1), rapid sedimentation resulting in the production of a caked, poorly redispersible sediment occurred. All suspending agents tested succeeded in reducing the rate of sedimentation and, apart from 0.3% w/v NaCMC (product 13), all improved the redispersibility of any sediment formed.

The BP formulation (product 2) exhibited a slow sedimentation rate despite the low yield value and required a moderate amount of agitation to generate a uniformly dispersed, free-flowing liquid. The appearance of product 3 was that of a gel, which again required a large amount of agitation to overcome the high yield value and produce a free-flowing suspension. Product 4 also required a moderate level of agitation to convert to a free-flowing liquid, although as mentioned earlier, the apparent viscosity was considerably higher than the BP formulation. Product 5, as described previously, was extremely viscous and required an excessive amount of agitation to overcome the high yield value and produce a free-flowing lotion, which would undoubtedly impact on patient acceptability. Simultaneous consideration of the rheological characteristics and the sedimentation behaviour indicated that product 6, containing 2% w/v sepiolite together with 0.01 M sodium citrate, represented the optimum formulation in terms of reproducing the properties of the BP formulation. The apparent viscosity values at low and high shear rates (Table 8.4b) and the sedimentation rate (Figure 8.4e) were comparable to those of the BP formulation, whilst the ease with which the product could be redispersed following prolonged periods of standing was higher.

Products 7 – 9 and product 12, despite their promising rheological behaviour, underwent reasonably rapid and extensive sedimentation. Although the sediment formed could be readily redispersed in the case of products 7 and 12, the unsightly inelegant product appearance would be likely to reduce patient confidence in the product.

Products 10 and 11 exhibited comparable sedimentation characteristics to the BP formulation and were readily redispersed following a moderate level of agitation, indicating SepCMC or spray dried sepiolite plus NaCMC may be used as alternative suspending agents to bentonite, although the resulting products will have a higher apparent viscosity.

8.3 CONCLUSIONS

A novel rheological grade of sepiolite incorporating NaCMC was successfully produced by co-spray drying a hydroalcoholic dispersion of the two excipients. SEM and particle sizing of the co-spray dried product indicated that the NaCMC bound sepiolite fibers together, improving the smoothness of the aggregate surface and increasing the aggregate size. No changes in the solid state of sepiolite or NaCMC were observed following co-spray drying. FT-IR indicated bonding interactions occurred between NaCMC and sepiolite following co-spray drying and most likely involved the silanol and Mg-OH groups of sepiolite and the carbonyl and alcohol groups of NaCMC. The rheological properties of sepiolite were altered on combination with NaCMC. Flow behaviour was consistently pseudoplastic. However, relative to 2% w/v sepiolite suspensions, a reduction in yield value, apparent viscosity at low shear rates and antithixotropic behaviour was evident in the case of 2% w/v SepCMC suspensions. Inclusion of NaCMC affords an electrostatic protective effect at these concentrations, increasing the negativity of the zeta potential of sepiolite through surface adsorption and hindering particle-particle interaction. The reduction of all three parameters was more marked in the case of physical mixes of untreated sepiolite and NaCMC at the same ratio and concentration. It was concluded that spray drying reduces the adsorption capacity of sepiolite for NaCMC and thus hinders the protective effect of NaCMC. At higher suspension concentrations (~ 4% w/v), the reduced adsorption of NaCMC to sepiolite as a result of spray drying has very interesting consequences. It resulted in a very large concentration of unadsorbed NaCMC in solution which was free to partake in the formation of polymer networks. This interpenetrating network of linked

polymer chains and connected fibers resulted in markedly increased yield values and positive thixotropy relative to sepiolite-only suspensions of comparable concentration.

2% w/v sepiolite (in combination with 0.01 M sodium citrate) could be used as an alternative suspending agent to 3% w/v bentonite in the preparation of calamine lotion BP. The resultant product exhibited comparable rheological characteristics, sedimentation behaviour and redispersibility confirming that, on an equal weight basis, sepiolite is a more efficient rheological modifier than bentonite. SepCMC and a physical mixture of spray dried sepiolite and NaCMC proved to be suspending agents with merit in the calamine lotion model system. The inclusion of sodium citrate proved unnecessary in these two systems, providing further confirmation of the electrostatic influence of NaCMC. The performance of SepCMC was comparable to that of Avicel® CL-611.

The manner in which sepiolite and NaCMC were combined affected the yield values and thixotropic character of the resultant system. Spray drying of sepiolite reduced its adsorptive capacity for NaCMC irrespective of whether NaCMC was co-spray dried with sepiolite or added subsequent to the spray-drying of sepiolite alone. Reduced adsorption had two consequences; firstly it reduced the protective effect of NaCMC and secondly it facilitated increased polymer network formation. Hence by interchanging untreated sepiolite and spray dried sepiolite, and also by varying the amount of NaCMC added, a suspending agent tailored to the requirements of a particular system (i.e. required protective effect and desired rheological characteristics) may be readily attained.

GENERAL DISCUSSION

The research presented in this thesis focused on the potential pharmaceutical applications of a clay mineral called sepiolite. Clay minerals have been widely used in medicinal products, both as active principles and excipients, since the origin of mankind (Carretero, 2002). The clay minerals currently used in medicinal products are generally confined to kaolin, bentonite, saponite, talc and palygorskite (attapulgite). The use of halloysite in pharmaceuticals has recently gained credence following work by Levis (2000), Kelly (2002), Salter (2003), Byrne (2004) and Ryan (2006). Kaolin, talc, bentonite and palygorskite (attapulgite) are the subject of independent monographs in the pharmacopoeias (USP, 2006; BP, 2007). Despite the structural similarity of sepiolite and palygorskite, and the consequent practice of using them interchangeably in numerous other fields, sepiolite had not been used in any pharmaceutical preparation at the commencement of this work (Carretero, 2002).

Reports on palygorskite-sepiolite properties and uses are found in widely disseminated fields including those of soil science, paint manufacture, fertilizer suspension formulation and wastewater remediation, to mention but a few. Applications of sepiolite have traditionally been based on two properties, namely its sorptive capacity and its unusual rheology. More recent work in the area of animal husbandry has established its ability to act as a binder with a food-replacing value in animal feedstuffs (Castaing, 1994; Angulo *et al.*, 1995; Angulo *et al.*, 1996; Castaing and Noblet, 1997; Parisini *et al.*, 1999; Ouhida, 2000a; Ouhida, 2000b; Ouhida, 2000c; Sardi *et al.*, 2004). A review of the applications of sepiolite exposed binding and rheological properties that could be exploited in pharmaceutical formulations. That the potential of sepiolite as a pharmaceutical aid has gone untapped is something of a mystery, but given the large number of publications in this area since the start of this work (Sardi *et al.*, 2004; Köse *et al.*, 2005; Ruiz-Hitzky *et al.*, 2005; López-Galindo *et al.*, 2006) and its recent inclusion in Aivlosin®, it is unlikely to remain the case for much longer. Pifferi *et al.* (1999) reported that, with regards to the

development of pharmaceutical excipients, three main approaches are adopted by industry: (1) physical or chemical manipulation of materials already known; (2) combination of two or more marketed excipients in order to reduce unwanted defects and; (3) preparation of new chemical entities. The last option is generally prohibitively expensive due to the extensive toxicity testing involved coupled with the high risk and cost of an unfavourable outcome. While sepiolite may essentially represent a new chemical entity, the necessary testing may not be as costly as in the case of other new excipients for a number of reasons as described below.

Firstly, sepiolite is chemically, mineralogically and morphologically similar to palygorskite (van Olphen, 1977; Cerezo *et al.*, 2001). Palygorskite has already gained regulatory approval; it is used in a number of commercially available pharmaceutical products, including those for ingestion, and furthermore, it is the subject of a monograph in the BP and USP. As mentioned previously, these two clay minerals are used interchangeably in other fields and consequently, the experience gained with palygorskite in pharmaceutical applications should help to establish the pharmaceutical acceptability of sepiolite. Reference must also be made to two other facts, both of which would be likely to further support any application for pharmaceutical acceptability of sepiolite. Firstly, deposits of palygorskite are rarely more than 75% pure, however sepiolite deposits can often be up to 97% pure (López-Galindo *et al.*, 2006). Mineralogical purification of mined sepiolite would be expected, therefore, to prove less difficult than that of mined palygorskite. Furthermore, the level of cationic substitution of Mg in the brucite layer is generally much higher in palygorskite than in sepiolite (Brindley and Brown, 1980; Galan and Carretero, 1999). Thus variation in elemental composition between lots would be anticipated to be more marked in the case of palygorskite.

Secondly, it has been reported by a number of authors that sepiolite complies with the pharmacopoeial definition of magnesium trisilicate BP and thus may be regarded as a naturally occurring form of magnesium trisilicate BP (Anonymous, 1998; Rowe *et al.*, 2003). Magnesium trisilicate BP is a compound of variable composition corresponding to the approximate formula, $Mg_2Si_3O_8.xH_2O$, containing not less than 29% of magnesium oxide and not less than the equivalent of 65% of silicon dioxide, both calculated with reference to the ignited substance (BP, 2007). Pifferi *et al.* (1999) has reported that pharmacopoeial monographs for excipients are based to too great an extent on simple

identification tests and often outdated chemical assays for purity, with no sort of testing of the functionality of the excipient in question. Consequently, they have called for their review and up-dating to include tests which assess the technological properties and functionality of the excipients. The inadequacy of the pharmacopoeial monographs for excipients is highlighted by the technical legitimacy of the proposed equivalence of magnesium trisilicate BP and sepiolite, the validity of which in functionality terms is somewhat dubious. While the acceptability of this proposed equivalence is questionable, it may be possible to bypass/ circumvent certain registration steps as a consequence, thereby facilitating the introduction of sepiolite as a pharmaceutical excipient.

Peck *et al.* (1988) observed that pharmaceutical excipients for use in either tablets or other oral dosage forms generally fall into one of the following categories: (1) excipients permitted in foodstuffs; (2) excipients described in pharmacopoeias; and (3) newer excipients with no official status, but registered with the health authorities in various countries of the world, and approved for use in some of these countries. Sepiolite has been an EU registered additive (E-562), permitted for use in feedstuffs for all animal species, including food-producing animals, for almost two decades (Santarén, 1996). Excipients permitted for use in foodstuffs are generally regarded as acceptable for like uses in drug products. These materials have typically been extensively used in food and will be employed in relatively low amounts as a tablet or pharmaceutical component compared to their use as food components (Peck *et al.*, 1988).

Finally, extensive toxicity testing has already been performed during the assessment of a sepiolite-collagen complex as a biomaterial (Olmo *et al.*, 1985; Lizarbe *et al.*, 1987a; Lizarbe *et al.*, 1987b; Olmo *et al.*, 1987; Olmo *et al.*, 1988; Olmo *et al.*, 1992; Herrera *et al.*, 1995; Olmo *et al.*, 1996). The conclusion from these studies, which involved *in vitro* and *in vivo* testing (namely subcutaneous, intramuscular and intratrabecular inoculation), was that sepiolite-collagen complexes were biocompatible. The health-related effects of sepiolite have also been studied by Stanton *et al.* (1981) and Bellmann *et al.* (1997). They reported that following inhalation of short fibers (< 5 μm) and those of large diameter, inactivation via phagocytosis occurred readily, while inactivation of long, thin fibers was negligible. The evidence for the carcinogenicity of short sepiolite fibers (< 5 μm) in experimental animals has been deemed inadequate (IARC, 1997). The IARC has reported limited evidence in experimental animals for the carcinogenicity of long sepiolite fibers

(> 5 μm). Sepiolite fiber lengths typically only exceed 5 μm in deposits of non-sedimentary origin (Galan, 1996). Sepiolite from Vallecas-Vicálvaro is a sedimentary sepiolite of moderate crystallinity and fibers with an average length < 2 μm. *In vivo* testing of sepiolite from this region carried out by Santarén and Alvárez (1994) and Bellmann *et al.* (1997) indicated that it had a low intrinsic biological activity with no evidence of carcinogenic potential following either intraperitoneal or intratracheal instillation.

Thus, the regulatory and toxicological testing barriers to the introduction of sepiolite as a pharmaceutical adjuvant are not likely to be as taxing as in the case of a 'true' new chemical entity given that much of the data required to support registration is already in existence.

Given the numerous and complex functions that a modern excipient must fulfil, its characterisation must go well beyond the simple tests for identity and purity as prescribed in the pharmacopoeial monographs, and be extended to testing the technological functionality of the material (Pifferi *et al.*, 1999). López-Galindo *et al.* (2006) have recently presented a comprehensive review of the compositional, technical and safety specifications of clays to be used in pharmaceutical and cosmetic products. They noted that as these substances can vary widely in composition, texture and crystallinity, with significant effects on their properties, some of the tests included in the pharmacopoeias may be obsolete, inaccurate and imprecise because they are usually qualitative or semi-quantitative. Moreover, other properties such as specific surface area or ion-exchange capacity, which determine the functionality and suitability of phyllosilicates, are rarely taken into account. The first part of this work focused on a comprehensive examination of the material and positive identification of the main component as sepiolite and the identification of any mineralogical and chemical impurities as would be typical of the requirements cited in current excipient monographs. In recognition of the valid points made by Pifferi *et al.* (1999), the solid state character, moisture content, particle shape, particle size distribution, specific surface area, porosity and compatibility with a number of other pharmaceutical excipients were evaluated. These tests reflected properties at the molecular- and particle-level (Pifferi *et al.*, 1999; Nachaegari and Bansal, 2004). Properties of the bulk powder (packing behaviour, flowability, compressibility, compactibility) were also determined.

pXRD and FT-IR confirmed conclusively that sepiolite was the principal mineralogical component of Pangel®-S9. pXRD also established the absence of accessory mineral phases. EDXA confirmed a high level of chemical purity. The level of isomorphous substitution of Si/ Mg atoms was low. The principal substituting atoms were Fe, Ca, Al and K. ICP-MS indicated the presence of an array of metals at ppm levels. Compliance with pharmacopoeial limits for heavy metals could not be commented upon in a meaningful manner given the ambiguity associated with the term "heavy metal". The term "heavy metal", as used in the pharmacopoeias, must be defined as a matter of urgency. In addition to the recommendations made by Pifferi *et al.* (1999) with regards to pharmacopoeial testing requirements for excipients, we propose that the current colourimetric assay for heavy metals be replaced by a method such as ICP-MS, which can identify the quantities of each individual metal present. Meaningful limits based on the toxicity and bioavailability of each individual "heavy" metal could then be introduced. In the case of the sepiolite sample tested, the quantity of the trace metals present was demonstrated to be lower than in pharmaceutical-grade activated attapulgite (palygorskite) intended for ingestion. SEM confirmed the fibrous morphology and the absence of fibers of length ≥ 5 μm. Thus *in vivo* persistence and carcinogenic potential following inhalation is likely to be extremely low. The introduction of instruments such as the Morphologi G2 (Malvern Instruments, UK), which permit the virtually instantaneous imaging of thousands of particles using a small sample size, would be ideally suited to such a determination on an industrial scale. Particle length, aspect ratio, circularity and convexity can be rapidly determined and compiled by the Morphologi G2. The absence of fibers exceeding biologically safe lengths and foreign matter of a different shape/ size could be rapidly established. The specific surface area was extremely large (~ 280 m^2/ g), and mainly attributable to the surface area of the intracrystalline channels. Porosity was extensive, accounting for over half of the bulk volume. The porosity was largely a result of the dislocation of bundles of fibers relative to one another, thereby producing large void spaces. Compatibility with a number of tabletting excipients was established using DSC and TGA.

Given its purported binding ability, sepiolite was first evaluated as a tabletting aid. Tabletting excipients, particularly those which can account for a substantial portion of tablet weight, are required to exhibit high flowability, mixability, compressibility and compactibility (Bandelin, 1988). Untreated sepiolite (i.e. Pangel®-S9) exhibited extremely

poor flowability due to the irregular shape of the fibrous aggregates, which tended to interlock via protruding fibrous terminations. The bulk density of untreated sepiolite was prohibitively low for tabletting applications, and would necessitate the use of over-sized blending containers and tablet press tooling. Preliminary compressibility studies were indicative of a high degree of plastic deformation, compressibility and compactibility. Strategies to improve its technological functionality therefore focused on engineering particles with improved packing behaviour, increased bulk density, enhanced flowability and mixability. Particle engineering via spray drying was explored. Sepiolite was spray dried on its own and in combination with a binder (Kollidon® VA 64).

Spray drying of sepiolite was successful in improving flowability and increasing bulk density. Improvements in bulk-level properties were reflective of particle-level changes. Changes in the crystalline state and fibrous habit following spray drying were ruled out using XRD, FT-IR, DSC, TGA and SEM. SEM revealed that the sphericity of the microagglomerates was increased and prevalence of fibrous protrusions much reduced. Powder arching was much less problematic as a direct consequence. These improvements occurred as a result of changes in the arrangement of fibers within the microagglomerate. In a manner akin to the Avicel® PH product range, different grades of spray dried sepiolite, which vary in particle size and moisture content, could be prepared and evaluated. Scale-up to industrial production would be possible, given that clays are frequently spray dried at rates of 25 tons/hr during the production of ceramic tiles (Helsing, 1969). The continuity of the process also lends itself very readily to automatic control. Such a scale-up should focus not only on optimizing the shape, size and moisture content of the product but also on optimizing efficiency. At pilot scale, the efficiency of the drying process was poor, with a considerable amount of product lost as wall deposits. The surface of the particle must be dry before it reaches the chamber walls, otherwise it will stick. The free trajectory of the particle before it touches the wall of the drying chamber will consequently influence process efficiency. Improved yield is therefore likely to be seen with a wider drying chamber and higher inlet temperatures.

The performance of SD sepiolite and the co-processed product, SepKoll, as DCBs was evaluated using paracetamol as a model drug. Avicel® PH101 and Ludipress® were used as performance indicators. Avicel® PH101 was chosen as a comparator for a number of reasons. Firstly, it is one of the most widely used DCBs on account of its high

compressibility and compactibility, and disintegrating properties (Shangraw and Dermarest, 1993; Pifferi *et al.*, 1999). Secondly, in many respects, it bears a close resemblance to sepiolite in that it consists of "needle-like" particles which interweave and reticulate to form mechanical rivets which are further secured in place by hydrogen bonds (Bolhuis and Lerk, 1973). Ludipress® was representative of co-processed excipients, and combines the desirable qualities of the filler, α-lactose monohydrate; the binder, Kollidon® 30; and the disintegrant, Kollidon® CL. Flowability studies revealed that the flow properties of SD sepiolite, SepKoll and Physmix, although improved relative to untreated sepiolite, were inferior to those of Ludipress®. Flowability of the novel bases was superior to that of Avicel® PH101, the poor flowability of which is rated as its biggest shortcoming (Bolhuis and Chowhan, 1996). There is scope within the spray drying process to improve flowability of the sepiolite DCBs further by biasing the microagglomerate size distribution upwards. Mixability of SD sepiolite, SepKoll and Physmix was comparable to a Ludipress®/Kollidon® VA 64 (90:10 w/w) blend and superior to Avicel® PH101. Compressibility of the DCB/paracetamol blends was assessed using Heckel and Kawakita analysis. Heckel analysis concluded that the novel sepiolite bases exhibited poorer compressibility and higher deformation yield pressures than the commercial DCBs. Conversely, Kawakita analysis predicted similar compressibility for Avicel® PH101, Kollidon® VA 64 and the novel sepiolite DCBs. The inconsistency in these conclusions may indicate that the assumption of zero porosity at an infinite applied pressure, which underpins the Heckel equation, is somewhat questionable where sepiolite DCBs are concerned. The novel sepiolite DCBs produced tablets with good mechanical properties. Tensile strength and friability were comparable, and in some cases actually superior, to the commercial DCBs used as performance indices. The remarkable strength of the sepiolite DCB compacts was ascribed to plastic deformation coupled with mechanical interlocking of the fibers and extensive hydrogen bonding in a manner analogous to that seen with Avicel® PH101. Inclusion of Kollidon® VA 64, either through co-processing or physical blending improved tensile strength and resistance to attrition further and it was postulated that the Kollidon® acted as a matrix in which the interlocking fibers were impregnated and further immobilized. Good mechanical strength was not achieved at the cost of fast disintegration rates; disintegration occurred rapidly by a mechanism similar to that of Avicel® PH101, involving disruption of the hydrogen bonds following water ingression due to capillary action of the pores. Paracetamol release from the sepiolite-based compacts was rapid as indicated by its detection in the dissolution medium. Sepiolite did not

interfere to any significant extent with the rate of paracetamol dissolution (as indicated by the availability of dissolved paracetamol in the dissolution medium). The total quantity of paracetamol released was comparable to the theoretical paracetamol content, confirming that sepiolite did not irreversibly bind paracetamol. Finally, surface profiling confirmed that the sepiolite DCBs produced tablets of comparable, and in some cases, reduced surface rugosity and variability relative to the commercial DCBs. The smoothness of these sepiolite-based compacts would facilitate their coating with release-modifying and taste-masking polymers.

Further research in this area should focus on challenging the capability and versatility of the sepiolite DCBs using drugs with alternative compression properties (e.g. plastically deforming drugs, fragmenting drugs). Dilution potential, defined as "the ability of a given quantity of an excipient to bind a specified amount of an active ingredient to form an acceptable tablet" also needs to be established (Propst, 2002). Current studies have verified that the sepiolite DCBs can mask the poor compression properties of 50% w/w paracetamol. The stability of the sepiolite-based dosage forms has yet to be established under accelerated (40°C/ 75% RH) and long-term (25°C/ 60% RH) storage conditions. Comparison of the tabletting performance of SepKoll and the corresponding physical blend indicated that the co-processing step conferred no additional benefits. However, it was postulated that the incorporation of Kollidon® VA 64 during spray drying may, once spray drying conditions have been suitably optimized, facilitate further upward biasing of the particle size distribution. Furthermore, it may be the case that the sepiolite/ Kollidon® VA 64 ratio used was suboptimal and hence, alternative ratios should be explored with the principal aim of enhancing flowability further. Consideration of the disintegration of the sepiolite-based and Kollidon® VA 64-based compacts would suggest that the use of increased amounts of Kollidon® VA 64 relative to sepiolite will result in the retardation of the disintegration rate of the resultant compacts. This combination could perhaps be exploited to achieve the sustained release of drugs; the rate of release may be controlled by the ratio of Kollidon® VA 64 to sepiolite present. Comprehensive studies on the impact of sepiolite on the bioavailability of drugs need to be carried out. Initial studies should focus on those drugs reported to be involved in binding interactions with other clays and magnesium trisilicate. In cases where drug bioavailability is unaltered, sepiolite may be used as a DCB. It is possible that where binding interactions occur between sepiolite and a drug, they could be exploited in the development of sustained release formulations (Aguzzi

et al., 2006). Finally, different grades of sepiolite are produced by Tolsa. Bulk-level properties such as flowability, mixability and bulk density may differ between grades and those grades displaying promising bulk properties should be investigated as tabletting excipients. It may be the case that use of a different grade of sepiolite may obviate the need to spray dry sepiolite entirely and thereby increase the commercial viability of the project.

Untreated sepiolite was investigated as an "all-in-one" filler-binder-disintegrant for tabletting of paracetamol by wet granulation. The resultant sepiolite-based granules exhibited extremely high flowability, low friability and extremely high compactibility. Compacts formed by granule compression displayed high tensile strengths, rapid disintegration and *in vitro* drug release rates. Inclusion of Kollidon® 25, Kollidon® 30 or Kollidon® 90F in the sepiolite-paracetamol blend did not improve the characteristics of the resultant granules/ tablets above those seen with sepiolite alone. Indeed, the use of these binders actually prolonged disintegration times. The performance of sepiolite during wet granulation was also compared to Avicel® PH101 (MCC). One of the major shortcomings of MCC is the reduction in compressibility and compactibility observed following wet granulation (Staniforth *et al.*, 1988; Bolhuis and Chowhan, 1996; Buckton *et al.*, 1998). This "hornification" process is thought to relate to the replacement of hydrogen bonds between the polar hydroxyl groups on the cellulose fibers and water molecules by interfibrous hydrogen bonds with a consequent loss of capillaries and an increase in particle density (Luukkonen, 2001). Hornification of MCC was observed during the wet granulation studies and had unfavourable consequences, not only for tablet strength, but also for disintegration and *in vitro* drug release rates. Although a decrease in the compressibility of sepiolite was observed following wet granulation, due to the more efficient packing of fibers within the granules, it was not associated with diminished compactibility or *in vitro* drug release rates. Sepiolite demonstrated remarkable efficacy in the tabletting of poorly compressible paracetamol by wet granulation, producing granules of high flowability and rapidly disintegrating compacts with good mechanical properties. The use of sepiolite would therefore permit a remarkable simplification of any wet granulation tabletting formulation, in that only the active and a lubricant are required in addition to sepiolite. Furthermore, analytical and production time requirements and associated costs will also be reduced considerably.

Future work in the area of wet granulation should involve extensive stability testing of the manufactured tablets to establish their commercial viability. Studies evaluating the content of active, content of active-related substances, moisture content, tablet hardness, friability and organoleptic properties as a function of time, temperature and relative humidity must be carried out. In an analogous manner to the novel spray dried DCBs, the "capacity" of sepiolite as a filler-binder for wet granulation needs to be determined, as does its ability to successfully tablet drugs of varying physicochemical properties where immediate drug release is required.

The use of sepiolite as a spheronisation aid has also been investigated and the results published elsewhere (Barry, 2005). A summary of the major findings is presented in Appendix 8. Most drugs do not possess the properties required for successful pelletisation by extrusion-spheronisation (ES). Addition of an aiding excipient is therefore required to produce formulations with the necessary rigidity, plasticity and water-absorbing capacity to allow the production of spheres (Tho *et al.*, 2003). MCC has come to be regarded as an essential component for successful ES; it acts by favourably altering the rheological properties of the wet mass (Ghebre-Sellassie, 1989; Lustig-Gustafsson *et al.*, 1999). MCC pellets prepared by ES usually fail to disintegrate, resulting in a prolonged matrix-type drug release (Kleinebudde, 1994; Tho *et al.*, 2002; Tho *et al.*, 2003; Souto *et al.*, 2005; Thommes and Kleinebudde, 2006a). For drugs of low solubility, the time for complete release may be longer than the gastrointestinal passage time resulting in decreased bioavailability (Thommes and Kleinebudde, 2006a). Alternatives to this commonly used pelletisation aid have therefore been sought (Tho *et al.*, 2002; Tho *et al.*, 2003; Thommes and Kleinebudde, 2006a, 2006b). Pectin was one such alternative spheronisation aid investigated by Tho *et al.* (2002). However, spherical pellets could not be formed using water as a granulating agent due to an unsuitable plasticity-rigidity ratio, which hindered breaking of the extrudate into spherical pieces (Tho *et al.*, 2002). Pure chitosan was pelleted using acetic acid as a granulating agent (Steckel *et al.*, 2004). Studies on the mechanical properties of drug-loaded chitosan pellets and drug release profiles from same have not been published. Glyceryl monostearate has been successfully used in the pelletisation by ES of certain drugs (e.g. diclofenac) but has proved unsuitable in a number of other drugs (paracetamol, ibuprofen, indomethacin) (Chatchawalsaisin *et al.*, 2005). It therefore lacks the universality of MCC. To date, there is no suitable alternative or substitute for MCC (Thommes and Kleinebudde, 2006a). The results of our preliminary ES

studies indicated that sepiolite pellets with a high degree of sphericity (Form PE: 0.922 ± 0.051; width-to-length ratio: 0.945 ± 0.051; Appendix 7) can be produced using water as the granulating agent. This result was not unanticipated given the high plasticity, compactibility and rapid wicking action of sepiolite evident from wet granulation studies. Furthermore, these pellets disintegrated rapidly and consequently could be used for the fast delivery of drugs of low solubility (Tho *et al.*, 2003). Alternatively, the pellets could be overcoated with release-retardant polymers to permit a more refined control of release rate than can be achieved with uncoated MCC pellets. More extensive work to optimize the yield of sepiolite pellets in the desired range will be necessary as preliminary yields were of the order of 50%. Universality of sepiolite needs to be investigated, as does the maximum weight of drug that can be incorporated without exceeding the capacity of sepiolite to successfully spheronize the mixture. Recently, Dreu *et al.* (2006) has highlighted the importance of being able to use non-aqueous granulation liquids in the case of granulation/ ES of drugs sensitive to moisture. Sepiolite has been successfully spheronized using 2.5% w/v ethylcellulose in ethanol as a granulating agent. Pellets produced in this manner disintegrate rapidly in water (Barry, 2005). Tabletting of moisture-sensitive drugs by wet granulation using sepiolite as a filler-binder and ethanol as the granulating liquid may therefore prove possible and should be the subject of further investigation. Non-disintegrating sepiolite pellets were also prepared by ES using an ethanolic solution of Eudragit® E PO as the granulating agent. Sepiolite pellets prepared using Eudragit® RS 30D as a granulating agent swelled in water but did not disintegrate. Results of preliminary ES studies indicate that sepiolite shows considerable promise as a spheronisation aid; disintegrating, non-disintegrating and swelling pellets may be produced by appropriate selection of the granulating agent. This work is very much at an exploratory stage and more comprehensive investigations are required to firmly establish sepiolite's role in the ES of drugs at a commercially viable scale.

Sepiolite is currently employed as a rheological modifier in many industrial processes including paint manufacture, fertilizer suspension formulation and the drilling industry. The development of rheology in sepiolite dispersions is dependent upon adequate mechanical dispersion of the fibers rather than on swelling as is the case for laminar clays. This fact represents a potential time (and thus cost) saving, given that the time taken for mechanical dispersion of sepiolite is considerably shorter than that required for completion of swelling in laminar clays. Preliminary studies indicated that the efficiency of the

dispersion process was more closely linked to mixing speed than mixing time. Hence the use of high shear mixers would permit the rapid preparation of viscous sepiolite suspensions on an industrial scale. Aqueous sepiolite dispersions were found to display interesting rheology ranging from plastic, low-yield systems at low concentrations to pseudoplastic, high-yield systems at higher concentrations. The rheological efficiency of sepiolite was found to higher than palygorskite and bentonite; i.e. at equal concentrations in water, the yield and apparent viscosity of sepiolite dispersions were higher than those of the other two clays. Hence the use of sepiolite as a rheological modifier would not only reduce suspension preparation times, it would also permit a reduction in the amount (and presumably cost) of suspending agent required.

The rheological behaviour of sepiolite suspensions has been explained by a number of authors in terms of the physical interference of the fibers, which generate three dimensional interlinked systems on standing which are destroyed upon application of shear (Alvárez, 1984; Santarén, 1993; Viseras *et al.*, 1999). Furthermore, sepiolite dispersions have been reported to be stable over a wide pH range, temperature range and at high electrolyte concentrations (Alvárez, 1984; Santarén, 1993, Santarén, 1996; Tolsa, 1999). Very little evidence to support these claims can be found in the literature. Consequently, extensive investigation into the influence of temperature, pH and electrolytes on the rheological and sedimentation behaviour was undertaken and attempts were made to correlate the observed behaviour with factors influencing the number of fiber-fiber collisions and interactions, namely Brownian motion and zeta potential. The importance of Brownian motion-induced collisions in the establishment of these interweaving fibrous frameworks was verified by the increase in yield and reduction in antithixotropic character observed during ageing of the suspensions. Furthermore, the yield value of 1% w/v sepiolite suspensions was found to increase with temperature from 4 °C to 20 °C and thereafter remain reasonably constant with a further increase to 40 °C, indicative of the importance of thermal motion in driving particles into contact positions.

Having established the importance of Brownian motion in yield stress development, the influence of changes in the zeta potential on both the yield stress and apparent viscosity was studied. Sepiolite was found to have a net negative zeta potential at its native pH (~8.2). This potential was of the order of -20 mV. In accordance with the DLVO theory, which describes the stability of hydrophobic colloids in terms of the net total of the

interparticle electrostatic repulsive forces and van der Waals attractive forces, zeta potentials of the order of 25 mV typically result in the production of flocculated systems where particles interact in the secondary attractive minimum (Bhargava *et al.*, 1996). The presence of a yield value and the production of a loose sediment and clear supernatant on standing confirmed that sepiolite suspensions are indeed flocculated at pH 8.2. The zeta potential of sepiolite increased with increasing pH and decreased with decreasing pH. The i.e.p. was of the order of pH 2.6 – 3. The similarity of the i.e.p. to that of silica indicated the importance of silanol groups in the development of surface charge. The rheological behaviour could be reasonably well predicted through consideration of the influence of the zeta potential on interparticle repulsion. At pH 13, the zeta potential was markedly negative; interparticle repulsion increased to an extent that hindered interparticle associations. The resultant suspension displayed near Newtonian flow behaviour. Although the brucite layer of sepiolite can be dissolved under very acidic conditions, predictions from the DLVO theory still hold true in that at this pH, the zeta potential was low and the yield values of the sepiolite suspensions were high. Predictions from the DLVO theory proved incorrect at pH values of the order of 5.8. An increase in the yield value relative to that seen at pH 8.2 would have been expected in accordance with the decrease in the magnitude of the zeta potential. However, a relative reduction in the yield value was observed. The somewhat anomalous behaviour at this pH is thought to be a reflection of the contribution of the edge Mg-OH groups to surface charge. At pH 8.2, these groups may be protonated/ neutral while the silanol counterparts on the faces are predominantly negatively charged. This surface charge heterogeneity may favour EF interactions at pH values ~ 8.2, which will lend themselves to the formation of a porous voluminous scaffold. At pH values ~ 5.8, the acidity of the environment may be such that ionization of the silanol groups is depressed and FF associations are facilitated. FF associations resulted in the formation of thicker dispersed units rather than a network; hence the reduction in yield value.

Having determined the response of sepiolite systems to fluctuations in pH, the influence of electrolytes was examined. Electrolytes are frequently included in pharmaceutical formulations as buffering agents, dispersing agents, antioxidants, tonicity adjusters, preservatives and active ingredients. Despite literature reports to the contrary, the stability of sepiolite suspensions was shown to be influenced by the presence of electrolytes. In terms of the effect on stability, two types of ions could be distinguished; namely

"indifferent" ions and "potential determining" ions. Indifferent ions reduced interparticle repulsion by accumulating in the outer region of the EDL. Potential determining ions were specifically adsorbed to the charged fiber surface and hence were capable, not only of altering the magnitude of surface charge, but also of reversing its sign. Consequently, potential determining ions, depending on their charge and concentration could both increase and decrease interparticle repulsion. Sepiolite suspensions were remarkably stable in the presence of very high concentrations of NaCl, an indifferent electrolyte. Ca^{2+} ions caused such a reduction in interparticle repulsion that fiber agglomeration occurred. The effect of cationic surfactants, exemplified by cetrimide, was much more complex. Cetrimide has previously been reported to be a potential determining ion for sepiolite; indeed, cetrimide-treated sepiolite has been used in removal of anions such as chromate, nitrate and sulphate from industrial wastewaters (Li *et al.*, 2003). With increasing cetrimide concentration, the yield value increased sharply to a maximum and then decreased again. The increase corresponded to an increased amount of adsorbed cetrimide cations, such that the fibers were bristling with alkyl chains which intertwined with a resultant increase in the yield stress to a maximum. The sharp decrease of the yield stress at still higher cetrimide concentrations was indicative of recharging of the fibers following the formation of cetrimide bilayers on their surfaces. In the case of trivalent anions, such as citrate, the yield value decreased to a minimum with increasing citrate concentration and subsequently recovered with further increases in citrate concentration. Finally, the influence of polyvalent anions such as sodium polyphosphate was investigated. Increasing deflocculation of the suspension was evident with an increase in the concentration of NaPP, indicating its ability to selectively bind to the fiber surface.

The implication of these stability studies for the use of sepiolite as a suspending agent is that the temperature and, in particular the pH, must be carefully controlled through the use of compatible buffering agents and appropriate storage conditions. It should however be noted that sepiolite, in itself, tended to act as a buffer. Changes in the pH of sepiolite suspensions were very difficult to effect, and suspensions tended to revert to the native pH over time. However, sepiolite suspensions of pH 5 were prepared using McIlvaine's buffer (pH 5), thus indicating that it is possible to alter and control sepiolite suspension pH.

Instability in the presence of electrolytes is generally less easily overcome as the electrolytes may be essential components of the formulation and it may not be possible to

alter their concentration. The use of a protective colloid to increase stability of sepiolite suspensions in the presence of electrolytes was therefore pursued. NaCMC, given its pharmaceutical acceptability, was used as the protective colloid, and several different rheological grades of sepiolite were prepared by co-spray drying sepiolite and NaCMC (SepCMC), by physical blending of spray dried sepiolite with NaCMC and finally by physical blending of untreated sepiolite with NaCMC. Again, spray drying conditions need to be further optimized to produce commercially viable yields. The inclusion of NaCMC caused changes in rheological behaviour akin to those seen with NaPP when 2% w/v suspensions were prepared, indicating that interparticle repulsion had been successfully increased. It seems that at the NaCMC/ sepiolite dry weight ratio investigated the sorptive capacity of sepiolite for NaCMC was exceeded, such that a proportion of the NaCMC present was unadsorbed. At the higher dispersion concentration examined, significant increases in the yield value and thixotropic character were observed. It appeared that when the concentration of unadsorbed NaCMC in the dispersion was sufficiently high, it contributed positively to the rheology of the overall system as these polymer chains became involved in the development of a three dimensional network. Interestingly, spray drying of sepiolite, either alone or in combination with NaCMC, caused a reduction in its sorptive capacity for NaCMC. The mechanism by which this occurs was not elucidated and is a matter warranting further investigation. There were two consequences of this reduced sorption; firstly, the protective influence afforded by NaCMC was reduced and secondly, the increased unadsorbed NaCMC fraction contributed more significantly to the rheology of the overall system. Having established the factors affecting the stability of sepiolite suspensions, the performance of these novel rheological grades was assessed in a model pharmaceutical system, namely calamine lotion. The use of sepiolite, in combination with an appropriate amount of citrate to control the degree of flocculation, produced a product with rheological characteristics, sedimentation behaviour and redispersibility comparable to calamine lotion BP. SepCMC and a physical mixture of spray dried sepiolite and NaCMC also proved to be suspending agents with merit in the calamine lotion model system. The performance of SepCMC, as adjudged by sedimentation characteristics and estimates of spreadability and pourability from rheological studies, was similar to that of Avicel® CL-611. Future work should explore the performance of alternative dry weight ratios of sepiolite and NaCMC. The universality of these novel rheological agents also needs to be established. Studies should be extended to investigate the use of these rheological modifiers as gelling agents. The viscoelastic properties of such systems could

be established using oscillatory rheology; while textural analysis would allow the determination of in-use properties such cohesiveness and adhesiveness (Ryan, 2006).

In conclusion, sepiolite, together with grades prepared by spray drying and co-processing, represent a novel class of pharmaceutical excipients, with applications ranging from tabletting to extrusion-spheronisation to suspension formulation. The wealth of data relating to toxicity, the similarity of its chemical composition to that of pharmaceutically acceptable clays and the extensive experience with its use in other fields would provide considerable evidence to support any registration applications. It is expected that the research presented in this thesis will act as a stimulus for further research in this area, especially given the renewed interest in the role and functionality of pharmaceutical excipients (Pifferi *et al.*, 1999). Thus, the potential of sepiolite generates a new and exciting area, requiring further development with commercial exploitation being a likely outcome.

REFERENCES

Abend, S., Lagaly, G., (2000),
Sol-gel transitions of sodium montmorillonite dispersions,
Appl. Clay Sci., **16**, 201-227.

Aguzzi, C., Cerezo, P., Viseras, C., Caramella, C., (2006),
Use of clays as drug delivery systems: possibilities and limitations,
Appl. Clay Sci., In Press, doi:10.1016/j.clay.2006.06.015.

Ahlrichs, J.L., Serna, C., Serratosa, J.M., (1975),
Structural hydroxyls in sepiolite,
Clays Clay Miner., **23**, 119-124.

Aivlosin®, Product information, Schering-Plough Animal Healthcare [Online],
http://www.noahcompendium.co.uk/Schering-Plough_Animal_Health/Aivlosin_42_5mg_g_Premix/-41176.html. and
http://www.emea.eu.int/vetdocs/PDFs/EPAR/Aivlosin/V-083-PI-en.pdf.
Accessed: 25/01/07.

Akçay, M., (2004),
FT-IR spectroscopic investigation of the adsorption of pyridine on the raw sepiolite and Fe-pillared sepiolite from Anatolia,
J. Mol. Struct., **694**, 21-26.

Akyüz, S., Akyüz, T., (2003),
FT-IR spectroscopic investigations of surface and intercalated 2-aminopyrimidine adsorbed on sepiolite and montmorillonite from Anatolia,
J. Mol. Struct., **651-653**, 205-210.

Akyüz, S., Akyüz, T., (2004),
FT-IR spectra of natural loughlinite (Na-sepiolite) and adsorption of pyrimidine on loughlinite,
J. Mol. Struct., **705**, 147-151.

Al-Achi, A., Clark, T.J., Greenwood, R., Mafu, S.S., (2003),
Human insulin interaction with soybean powder,
Pharmaceut. Eng., **23**, 1-5.

Al-Achi, A., Greenwood, R., Akin-Isijola, A., Bullard, J., (1999),
Calamine lotion: experimenting with a new suspending agent,
Int. J. Pharm. Compounding, **3**, 490-492.

Albertini, B., Carmella, C., Passerini, N., Voinovich, D., González-Rodríguez, M., Magarotto, L., Rodriguez, L., (2004),
Characterization and taste-masking evaluation of acetaminophen granules: comparison between different preparation methods in a high-shear mixer,
Eur. J. Pharm. Sci., **21**, 295-303.

Alderborn, G., (2002),
Tablets and compaction,
pp. 289-305 in: *Pharmaceutics, The Science of Dosage Form Design,* 2nd Edition, Aulton, M.E., (Ed.), Churchill Livingstone, Edinburgh.

Alderborn, G., Nyström, C., (1996),
Nomenclature,
pp. vii-viii in: *Pharmaceutical Powder Compaction Technology,* Alderborn, G., Nyström, C., (Eds.), Marcel Dekker, New York.

Alderborn, G., Wikberg, M., (1996),
Granule properties,
pp. 323-374 in: *Pharmaceutical Powder Compaction Technology,* Alderborn, G., Nyström, C. (Eds.), Marcel Dekker, New York.

Alebiowu, G., Itiola, O.A., (2001),
Effects of natural and pregelatinized sorghum, plantain and corn starch binders on the compressional characteristics of a paracetamol tablet formulation,
Pharm. Technol., Drug delivery supplemental edition, 26–30.

Alebiowu, G., Itiola, O.A., (2003),
The effect of starches in mechanical properties of paracetamol tablet formulations. I. Pregelatinization of starch binders,
Acta Pharm., **53**, 231-237.

Al-Gohary, O.M., (1990),
An *in vitro* study of the interaction between mebeverine hydrochloride and magnesium trisilicate powder,
Int. J. Pharm., **67**, 89-95.

Al-Gohary, O.M., Lyall, J., Murray, J.B., (1987),
Adsorption of antihypertensives by suspensoids. Part 1. Adsorption of propranolol hydrochloride by attapulgite, charcoal, kaolin and magnesium trisilicate,
Pharm. Acta Helv., **62**, 66-72.

Al-Gohary, O.M., Lyall, J., Murray, J.B., (1988),
Adsorption of antihypertensives by suspensoids. Part 2. The adsorption of acebutolol, metoprolol, nadolol, oxprenolol and timolol by attapulgite, charcoal, kaolin and magnesium trisilicate,
Pharm. Acta Helv., **63**, 13-18.

Alkan, M., Demirbaş, Ö., Çelikçapa, S., Doğan, M., (2004),
Sorption of acid red 57 from aqueous solution onto sepiolite,
J. Hazard. Mater., **B116**, 135-145.

Alkan, M., Demirbaş, Ö., Doğan, M., (2005a),
Electrokinetic properties of sepiolite suspensions in different electrolyte media,
J. Colloid Interface Sci., **281**, 240-248.

Alkan, M., Tekin, G., Namli, H., (2005b),
FTIR and zeta potential measurements of sepiolite treated with some organosilanes,
Microporous Mesoporous Mater., **84**, 75-83.

Alkan, H., Ulusoy, A., (1987),
Granulation in a fluidized bed. I. Effect of addition of binder in solution or in dry form,
DOGA TU J. Med. Pharm., **11**, 1-7.

Allwood, M.C., (1982),
The adsorption of esters of p-hydroxybenzoic acid by magnesium trisilicate,
Int. J. Pharm., **11**, 101-107.

Alvárez, A., (1984),
Sepiolite: properties and uses,
pp. 253-287 in: *Palygorskite-Sepiolite: Occurrences, genesis and uses, Developments in Sedimentology, Volume 37*, Singer, A., Galan, E., (Eds.), Elsevier, Amsterdam.

Al-Zoubi, N., Koundourellis, J.E., Malamataris, S., (2002),
FT-IR and Raman spectroscopic methods for identification and quantitation of orthorhombic and monoclinic paracetamol in powder mixes,
J. Pharm. Biomed. Anal., **29**, 459-467.

Andreola, F., Castellini, E., Ferreira, J.M.F., Olhero, S., Romagnoli, M., (2006),
Effect of sodium hexametaphosphate and ageing on the rheological behaviour of kaolin dispersions,
Appl. Clay Sci., **31**, 56-64.

Angulo, E., Brufau, J., Esteve-Garcia, E., (1995),
Effect of sepiolite on pellet durability in feeds differing in fat and fibre content,
Anim. Feed Sci. Technol., **53**, 233-241.

Angulo, E., Brufau, J., Esteve-Garcia, E., (1996),
Effects of a sepiolite product on pellet durability in feeds differing in particle size and in broiler starter and finisher diets,
Anim. Feed Sci. Technol., **63**, 25-34.

Anonymous, (1998),
The silicates: attapulgite, kaolin, kieselguhr, magnesium trisilicate, pumice, talc,
Int. J. Pharm. Compound., **2**, 162-163.

Araki, J., Wada, M., Kuga, S., Okano, T., (1998),
Flow properties of microcrystalline cellulose suspension prepared by acid treatment of native cellulose,
Colloids Surf., **A142**, 75-82.

Araki, J., Wada, M., Kuga, S., Okano, T., (1999),
Influence of surface charge on viscosity behaviour of cellulose microcrystal suspension,
J. Wood Sci., **45**, 258-261.

Augsburger, L., Shangraw, R.F., (1966),
Effect of glidants in tabletting,
J. Pharm. Sci., **55**, 418-423.

Aulton, M., (2002),
Drying,
pp. 397-396 in: *The Science of Dosage Form Design, 2nd Edition*, Aulton, M.E., (Ed.), Churchill Livingstone, Edinburgh.

Aznar, A.J., Gutiérrez, Díaz, P, Alvárez, A., Poncelet, G., (1996),
Silica from sepiolite: Preparation, textural properties and use as support to catalysts,
Microporous Mater., **6**, 105-114.

Babhair, S.A., Tariq, M., (1983),
Effect of magnesium trisilicate and kaolin-pectin on the bioavailability of trimethoprim,
Res. Commun. Chem. Pathol. Pharmacol., **40**, 165-168.

Badawy, S.I.F., Gray, D., Hussain, M.A., (1994),
A study on the effect of wet granulation on microcrystalline cellulose particle structure and performance,
Pharm. Res., **23**, 634-640.

Bain, D.C., Smith, B.F.L., (1994),
pp. 300-327 in: *Clay Mineralogy: Spectroscopic and chemical determinative methods*, 1st Edition, Wilson, M.J. (Ed.), Chapman and Hall, London.

Balci, S., (1999),
Effect of heating and acid pre-treatment on pore size distribution of sepiolite,
Clay Miner., **34**, 647-655.

Banaker, U.V., (1994),
Role of ingredients and excipients in developing pharmaceuticals,
Manuf. Chem., **65**, 32-35.

Bandelin, F.J., (1989),
Compressed tablets by wet granulation,
pp. 131-193 in: *Pharmaceutical Dosage Forms: Tablets, Volume 1*, Lieberman, H.A., Lachman, L., Schwartz, J.B., (Eds.), Marcel Dekker, New York.

Barnes, H.A., Hutton, J.F., Walters, K., (1989),
An introduction to rheology, Elsevier Publishers, Amsterdam.

Barrer, R.M., Mackenzie, N., (1954),
Sorption by attapulgite. Part I. Availability of intracrystalline channels,
J. Phys. Chem., **58**, 560-567.

Barrer, R.M., Mackenzie, N., MacLeod, D.M., (1954),
Sorption by attapulgite. Part II. Selectivity shown by attapulgite, sepiolite and montmorillonite for n-paraffins,
J. Phys. Chem., **58**, 568-562.

Barry, A., (2005),
Pharmaceutical applications of sepiolite,
Ph.D. Transfer Report, Trinity College, University of Dublin.

Bashaiwoldu, A.B., Podczeck, F., Newton, J.M., (2004),
The application of non-contact laser profilometry to the determination of permanent structural change induced by compaction of pellets: II. Pellets dried by different techniques,
Eur. J. Pharm. Sci., **22**, 55-61.

Battey, M.H., Pring, A., (1997),
Mineralogy for students, 3rd Edition, Longman Publishers, London.

Baykara, T., Duman, G., Ozesener, K. S., Ordu, S., Ozates, B., (1991),
Comparing the compressibility of Ludipress with other direct tabletting agents by using acetaminophen as an active ingredient,
Drug Dev. Ind. Pharm., **17**, 2359-2371.

Bellmann, B., Muhle, H., Ernst, H., (1997),
Investigations on health-related properties of two sepiolite samples,
Environ. Health Perspect., **105** (Suppl. 5), 1049-1052.

Berggren , J., (2003),
Engineering of pharmaceutical particles: modulation of particle structural properties, solid-state stability and tabletting behaviour by the drying process,
PhD. Thesis, Uppsala University, Sweden.

Berggren, J., Frenning, G., Alderborn, G., (2004),
Compression behaviour and tablet-forming ability of spray-dried amorphous composite particles,
Eur. J. Pharm. Sci., **22**, 191-200.

Beyer, T., Day, G.M., Price, S.L., (2001),
The prediction, morphology and mechanical properties of the polymorphs of paracetamol,
J. Am. Chem. Soc., **123**, 5086-5094.

Bhargava, H.N., Nicolai, D.W., Oza, B.J., (1996),
Topical suspensions,
pp.183-242 in: *Pharmaceutical Dosage Forms: Disperse Systems, Volume 2*, 2nd Edition, Lieberman, H.A., Rieger, M.M., Banker, G.S., (Eds.), Marcel Dekker Inc., New York.

Biggs, S., Scales, P., Leong, Y.K., Healy, T.W., (1995)
Effects of citrate adsorption on the interactions between zirconia surfaces,
J. Chem. Soc. Faraday Trans., **91**, 2921-2928.

Birsoy, R., (2002),
Formation of sepiolite-palygorskite and related minerals from solution,
Clays Clay Miner., **50**, 736-745.

Bivings, M.D.L., (1946),
Acute infectious urticaria,
J. Pediatr., **28**, 602-604.

Bolhuis, G.K., Chowhan, Z.T., (1996),
Materials for direct compression,
pp. 419–500 in: *Pharmaceutical Powder Compaction Technology,* Alderborn, G., Nyström, C., (Eds.), Marcel Dekker, New York.

Bolhuis, G.K., Eissens, J.C., Adrichem, T.P., Wesseling, J.A., Frijlink, H.W., (2003),
Hollow filler-binders as excipients for direct compression,
Pharm. Res., **20**, 515-518.

Bolhuis, G.K., Lerk, C.F., (1973),
Comparative evaluation of excipients for direct compression,
Pharm. Weekbl., **108**, 469-481.

Bolhuis, G.K., Lerk, C.F., Zijlstra, H.T., de Boer, A.H., (1975),
Film formation by magnesium stearate during mixing and its effect on tabletting,
Pharm. Weekbl., **110**, 317-325.

Bork, P., (2001),
Spray drying plants for manufacture of dustless powders – A technical note,
J. Therm. Spray Technol., **10**, 578-583.

Bosch, M., Ruiz Sánchez, A.J., Sánchez Rojas, F., Bosch Ojeda, C., (2006),
Determination of paracetamol: Historical evolution,
J. Pharm. Biomed. Anal., **42**, 291-321.

Botting, (2000),
Mechanism of action of acetaminophen: Is there a Cyclooxygenase 3?,
Clin. Infect. Dis., **31**, S202-210.

Botting, R., Ayoub, S.S., (2005),
COX-3 and the mechanism of action of paracetamol/ acetaminophen,
Congrès COX isoenzymes, Annual Symposium N° 12, **72**, 85-87.

Boutaud, O., Aronoff, D.M., Richardson, J.H., Marnett, L.J., Oates, J.A., (2002),
Determinants of the cellular specificity of acetaminophen as an inhibitor of prostaglandin H_2 synthases,
Proc. Natl. Acad. Sci. USA, **99**, 7130-7135.

Boyd, S.A., Mortland, M.M., Chiou, C.T., (1988),
Sorption characteristics of organic compounds on hexadecyltrimethylammonium-smectite,
Soil Sci. Soc. Am. J., **52**, 652-657.

Bradley, W.F., (1940),
The structural scheme of attapulgite,
Am. Mineral., **25**, 405-410.

Brantley, S., Mellott, N., (2000),
Surface area and porosity of primary silicate materials,
Am. Mineral., **85**, 1767-1783.

Brauner, K., Preisinger, A., (1956),
Struktur and Enstehung des Sepioliths,
Tschermaks miner. petrogr. Mitt., **6**, 120-140.

Brigatti, M.F., Franchini, G., Frigieri, P., Gardinali, C., Medici, L., Poppi, L., (1999),
Treatment of industrial wastewater using zeolitite and sepiolite, natural microporous materials,
Can. J. Chem. Eng., **77**, 163-168.

Brigatti, M.F., Medici, L., Poppi, L., (1996),
Sepiolite and industrial waste-water purification: removal of Zn^{2+} and Pb^{2+} from aqueous solutions,
Appl. Clay Sci., **11**, 43-54.

Brindley, G.W., (1959),
X-ray and electron diffraction data for sepiolite,
Am. Mineral., **44**, 495-500.

Brindley, G.W., Brown, G., (1980),
Crystal Structures of Clay Minerals and their X-ray Identification, Mineralogical Society Monograph No. 5, Mineralogical Society, London.

British National Formulary, (2006),
British National Formulary, 52nd Edition, British Medical Association and the Royal Pharmaceutical Society of Great Britain, The Pharmaceutical Press, London.

British Pharmacopoeia, (2007),
British Pharmacopoeia, Volumes I, II, III and IV, The Pharmaceutical Press, London.

Broadhead, J. Rouan, E.S.K., Rhodes, C.T., (1992),
The spray drying of pharmaceuticals,
Drug Dev. Ind. Pharm., **18**, 1169-1206.

Brunauer, S., Deming, L.S., Deming, W.S., Teller, E., (1938),
Adsorption of gases in multimolecular layers,
J. Am. Chem. Soc., **60**, 309-319.

Büchi spray drying training papers, [Online],
http://www.buchi.com/Mini-Spray-Dryer-B-290.179.0.html. Accessed: 20/05/2005.

Buckton, G., Yonemochi. E., Yoon, W.L., Moffat, A.C., (1998),
Water sorption and near IR spectroscopy to study the differences between microcrystalline cellulose and silicified microcrystalline cellulose before and after wet granulation,
Int. J. Pharm., **181**, 41-47.

Bueno, P., Villafranca Sanchéz, M., González Pradas, E., López González, J.D., (1984),
Adsorcion de amoniaco, metilamina y etilamina sobre una sepiolite,
An. Quim., **81**, 18-21.

Bühler, V., (2003),
Kollidon®- Polyvinylpyrollidone for the pharmaceutical industry, 7th Edn.,
BASF AG Ludwigshafen, Germany.

Bühler, V., (2004),
Pharmaceutical technology of BASF excipients, 2nd Edition,
BASF AG Ludwigshafen, Germany.

Buitenhuis, J., Pönitsch, M., (2003a),
Negative thixotropy of polymer solutions. 1. A model explaining time-dependent viscosity,
Colloid Polym. Sci., **281**, 253-259.

Buitenhuis, J., Pönitsch, M., (2003b),
Negative thixotropy of polymer solutions. 1. A systematic study of the time-dependent viscosity of partially hydrolyzed polyacrylamide,
Colloid Polym. Sci., **281**, 260-266.

Byrne, R.S., (2004),
Characterisation and use of porous aluminosilicate pellets for extended drug delivery,
PhD. Thesis, Trinity College, University of Dublin.

Calamine MSDS, (2002),
[Online],
http://www.jmloveridge.com/cosh/Calamine.pdf
Accessed: 10/12/2004.

Carr, R.L., (1965),
Classifying flow properties of solids,
Chem. Eng., **72**, 69-72.

Carretero, M.I., (2002),
Clay minerals and their beneficial effects upon human health. A review.
Appl. Clay Sci., **21**, 155-163.

Carstensen, J.T., Geoffrey, J.M., Dellamonica, C., (1990),
Compression characteristics of binary mixtures,
Powder Technol., **62**, 119-124.

Carstensen, J.T., Hou, X.P., (1985),
The Athy-Heckel equation applied to granular agglomerates of basic tricalcium phosphate [$3Ca_3(PO_4)_2.Ca(OH)_2$],
Powder Technol., **42**, 153-157.

Casal, B., Merino, J., Serratosa, J.-M., Ruiz-Hitzky, E., (2001),
Sepiolite-based materials for the photo- and thermal- stabilization of pesticides,
Appl. Clay Sci., **18**, 245-254.

Castaing, J., (1994),
Effet de l'introduction de sépiolite EXAL selon teneurs en cellulose brute et matiere grasse d'aliment pour porc charcutiers,
Journées Rech. Porcine en France, **26**, 199-205.

Castaing, J., Noblet, J., (1997),
Conséquences de l'introduction de sepiolite sur l'utilisation digestive d'aliment et les performances du porc en croisance,
Journées Rech. Porcine en France, **29**, 213-220.

Çelik, M., (1992),
Overview of compaction data analysis techniques,
Drug Dev. Ind. Pharm., **18**, 767-810.

Çelik, M., Driscoll, C. E., (1993),
An overview of the effects of some physico-chemical and mechanical characteristics of particulates on the compaction and post-compaction properties of compacts,
Drug Dev. Ind. Pharm. **19**, 2119-2141.

Cerezo, P., Viseras Iborra, C., López-Galindo, A., Ferrari, F., Caramella, C., (2001),
Use of water uptake and capillary suction time measures for evaluation of the anti-diarrhoeic properties of fibrous clays,
Appl. Clay Sci., **20**, 81-86.

Chang, S.H., Ryan, M.E., Gupta, R.K., (1993),
The effect of pH, ionic strength and temperature on the rheology and stability of clay suspensions,
Rheol. Acta, **32**, 263-269.

Chatchawalsaisin, J., Podczeck, J.F., Newton, J.M., (2005),
The preparation by extrusion-spheronisation and the properties of pellets containing drugs, microcrystalline cellulose and glyceryl monostearate,
Eur. J. Pharm. Sci., **24**, 35-48.

Cheng, D. C.-H., Evans, F., (1965),
Phenomenological characterization of the rheological behaviour of inelastic reversible thixotropic and antithixotropic fluids,
Br. J. Appl. Phys., **16**, 1599-1617.

Chong, C.W., (1962),
Factors influencing the selection of suspending agents,
J. Soc. Cosmet. Chem., **14**, 123-133.

Chong, C.W., Erikse, S.P., Swintosky, J.V., (1960),
Antithixotropic behaviour of magnesia magma,
J. Am. Pharm. Assoc., Sci. Ed., **49**, 547-552.

Ciullo, P.A., (1981),
Rheological properties of magnesium aluminium silicate/xanthan gum dispersions,
Cosmet. Chem, **32**, 275-285.

Ciullo, P.A., Braun, D.B., (1991),
Clay/carbomer mixtures enhance emulsion stability,
Cosmet. Toiletries, **106**, 89-95.

Cole, E.T., Rees, J.E., Hersey, J.A., (1975),
Relations between compaction data for some crystalline pharmaceutical materials,
Pharm. Acta Helv., **50**, 28-32.

Cole, G., (1998),
Evaluating development and production – Costs: tablets versus capsules,
Pharmaceut. Tech. Eur., May, 17-24.

Collett, J., Moreton, C., (2002),
Modified-release peroral dosage forms,
pp. 289-305 in: *Pharmaceutics: The Science of Dosage Form Design, 2nd Edition*, Aulton, M.E., (Ed.), Churchill Livingstone, Edinburgh.

Copley Scientific product information, [Online],
http://www.copleyscientific.co.uk/copleycatalogue.asp.
Accessed: 12/12/2006.

Corma, A., García, H., Leyva, A., Primo, A., (2004),
Alkali-exchanged sepiolites containing palladium as bifunctional (basic sites and noble metal) catalysts for the Heck and Suzuki reactions,
Appl. Catal., **A257**, 77-83.

Cornejo, J., Hermosin, M.C., White, J.L., Peck, G.E., Hem, S.L., (1980),
Oxidative degradation of hydrocortisone in presence of attapulgite,
J. Pharm. Sci., **69**, 945-948.

Corrigan, O.I., (1995),
Thermal analysis of spray dried products,
Thermochim. Acta, **248**, 245-258.

Cutt, T., Fell, J.T., Rue, P.J., Spring, M.S., (1986),
Granulation and compaction of a model system. I: Granule properties,
Int. J. Pharm., **37**, 81-87.

D'Alonzo, G.D., O'Connor, R.E., Schwartz, J.B., (1990),
Effect of binder concentration and method of addition on granule growth in a high intensity mixer,
Drug Dev. Ind. Pharm., **16**, 1931-1944.

Dandy, A.J., (1968),
Sorption of vapors by sepiolite,
J. Phys. Chem., **72**, 334-339.

David, S.T., Augsburger, L.L., (1977),
Plastic flow during compression of directly compressible fillers and its effect on tablet strength,
J. Pharm. Sci., **66**, 155-159.

de Boer, J.H., Lippens, M.G., Linsen, B.C., Broekhoff, J.C.P., van den Heuvel, A. and Osinga, T.V., (1966),
The t-curve of multimolecular N_2–adsorption,
J. Colloid Interface Sci., **21**, 405-414.

Deer, W.A., Howie, R.A., Zussman, J., (1992),
Sheet silicates,
pp. 277-387 in: *An Introduction to the Rock Forming Minerals*, *2nd Edition*, Longman Publishers, London.

del Hoyo, C., Rives, V., Vicente, M.A., (1996a),
Thermal studies of pharmaceutical clay systems. Part I. Montmorillonite-based systems,
Themochim. Acta, **286**, 89-103.

del Hoyo, C., Rives, V., Vicente, M.A., (1996b),
Thermal studies of pharmaceutical clay systems. Part II. Sepiolite-based systems,
Thermochim. Acta, **286**, 105-117.

Dell, S.M., Colliopoulos, J.A., (2001),
Avicel® RC/ CL, Microcrystalline cellulose and carboxymethylcellulose sodium, N.F., B.P., [Online],
http://www.fmcbiopolymer.com/Portals/bio/content/Docs/Pharmaceuticals/Problem%20Solver/Section%2014%20PS%20Avicel%20RC%20CL.pdf.
Accessed: 10/10/2004.

Denoyel, R., Llewellyn, P., Beurroies, I., Rouquerol, J., Rouquerol, F., Luciani, L., (2004),
Comparing the basic phenomena involved in three methods of pore-size characterization: gas adsorption, liquid intrusion and thermoporometry,
Part. Part. Syst. Charact., **21**, 128-137.

Derjaguin, B.V., Landau, L.D., (1941),
Theory of the stability of strongly charged lyophobic sols and of the adhesion of strongly charged particles in solution of electrolytes,
Acta Physicochim. URSS, **14**, 633-662.

DeSimone, E.M., Triplett, C.A., (1997),
OTC products for relieving itch,
US Pharmacist, **22**, 1.

Di Martino, P., Conflant, P., Drache, M., Huvenne, J.-P., Guyot-Hermann, A.-M., (1997),
Preparation and physical characterisation of forms I and II of paracetamol,
J. Therm. Anal. Calorim., **48**, 447-458.

Dobias, B., Witika, L.K., (1995),
Electrochemistry of sulphide materials,
pp. 207-259 in: *Flotation Science and Engineering*, Matis, K.A., (Ed.), Dekker, New York.

Doelker, E., (1993),
Comparative compaction properties of various microcrystalline cellulose types and generic products,
Drug Dev. Ind. Pharm., **19**, 2399-2471.

Dolz., M., Belda, R., Herraez, M., Harraez, J.V., Sobrino, P., (1991),
The effect of electrolyte concentration on thixotropic behaviour of MCC-NaCMC gels,
J. Dispersion Sci. Technol., **12**, 453-466.

Dolz-Planas, M., Gonzalez-Rodriguez, F., Belda-Maximino, R., Harraez-Dominguez, J.V., (1988),
Thixotropic behaviour of MCC-NaCMC gel,
J. Pharm. Sci., **77**, 799-801.

Dolz-Planas, M., Roldan, C., Belda-Maximino, R., Harraez-Dominguez, J.V., Sobrino, P., (1992),
Rheological behaviour of microcrystalline cellulose hydrogels,
J. Dispersion Sci. Technol., **13**, 95-113.

Dressman, J.B., Bass, P., Rischel, W.A., Friend, D.R., Rubinstein, A., Ziv, E., (1993),
Gastrointestinal parameters that influence oral medication,
J. Pharm. Sci., **82**, 857-872.

Dreu, R., Širca, J., Pinyte-Hodi, K., Burjam, T., Planinšek, O., Srčič, S., (2005),
Physicochemical properties of granulating liquids and their influence in microcrystalline cellulose pellets obtained by extrusion-spheronisation technology,
Int. J. Pharm., **291**, 99-111.

Drever, J.I., (1973),
The preparation of oriented clay mineral specimens for X-ray diffraction analysis by a filter-membrane peel technique,
Am. Mineral., **58**, 553-554.

Drummer, O.H., (2004),
Pharmacokinetics and metabolism,
pp. 172-201 in: *Clarke's Analysis of Drugs and Poisons*, *Volume 1*, 3rd Edition,
Moffat, A.C., Osselton, M.D., Widdop, B., (Eds.), The Pharmaceutical Press, London.

Dufus, J.H., (2002),
"Heavy metals" – a meaningless term?,
Pure Appl. Chem., **74**, 793-807.

Dukić, A., Mens, R., Adriaensens, P., Foreman, P., Gelan, J., Remon, J.P., Vervaet, C., (2006),
Development of starch-based pellets via extrusion/ spheronisation,
Eur. J. Pharm. Biopharm., In Press, doi:10.1016/j.ejpb.2006.08.015.

Duval, Y., Mielczarski, J. A., Pokrovsky, O. S., Mielczarski, E., Ehrhardt, J. J., (2002),
Evidence of the Existence of Three Types of Species at the Quartz-Aqueous Solution Interface at pH 0-10: XPS Surface Group Quantification and Surface Complexation Modeling,
J. Phys. Chem., **B106**, 2937-2945.

Ece, Ö.I., Çoban, F., (1994),
Geology, occurrence and genesis of Eskişehir sepiolites, Turkey,
Clays Clay Miner., **42**, 82-92.

Eerikäinen, S., (1991),
Effects of spheronization on some properties of uncoated and coated granules containing different kinds of fillers,
Int. J. Pharm., **77**, 89-106.

Eggins, S.M., Woodhead, J.D., Kinsley, L.P.J., Mortimer, G.E., Sylvester, P., McCulloch, P., Hergt, M.T., Handler, M.R., (1997),
A simple method for the precise determination of ≥40 trace elements in geological samples by ICP-MS using enriched isotope internal standardization,
Chem. Geol., **134**, 311-326.

Einstein, A., (1956),
Investigations on the theory of the Brownian movement,
Dover Publications, New York. (English translation of original publication).

Ek, R., Lennholm, H., Davidson, R., Nyström, C., Ragnarsson, G., (1995),
Pore swelling in beads made of cellulose fibre and fiber fragments,
Int. J. Pharm., **122**, 49-56.

Elbers, J.A.C., Bakkenes, H.W., Fokkens, J.G., (1992),
Effect of amount and composition of granulating liquid on mixing, extrusion and spheronization,
Drug Dev. Ind. Pharm., **18**, 501-517.

El Kadi, N., Martins, F., Clausse, D., Schulz, P.C., (2003),
Critical micelle concentrations of aqueous hexadecyltrimethylammonium bromide-sodium oleate mixtures,
Colloid Polym. Sci., **281**, 353-362.

El-Obeid, H.A., Al-Badr, A.A., (1985),
Acetaminophen,
pp. 551-596 in: *Analytical profiles of drug substances, Volume 14*, Florey, K., (Ed.), Academic Press, New York.

Erikson, U., Järnström, L., Engström, G., Rigdahl, M., (1991),
pp. 97, PTS-Streicherei Symposium.

Etman, M.A., Naggar, V.F., (1990),
Thermodynamics of paracetamol solubility in sugar-water cosolvent systems,
Int. J. Pharm., **58**, 177-184.

European Pharmacopoeia, (2007),
5th Edition, European Directorate for the Quality of Medicines, Strasbourg.

Falkiewicz, M.J., (1996),
Theory of suspensions,
pp. 17-52 in: *Pharmaceutical Dosage Forms: Disperse Systems, Volume 2*, 2nd Edition, Lieberman, H.A., Rieger, M.M., Banker, G.S., (Eds.), Marcel Dekker Inc., New York.

Fasihi, A.R., Parker, M.S., (1987),
Inimical effects of compaction speed on micro-organisms in powder systems with dissimilar compaction,
J. Pharm. Sci., **76**, 468-470.

Fathy, M., Hassan, M.A., Mohammed, F.A., (2002),
Differential scanning calorimetry to investigate the compatibility of ciprofloxacin hydrochloride with excipients,
Pharmazie, **57**, 825-828.

FDM Reference Spectra,
Sepiolite in KBr, Nevada: CMS SEPNev-1, [Online],
http://www.fdmspectra.com. Accessed: 16/08/2004.

Fell, J.T., Newton, J.M., (1968),
The tensile strength of lactose tablets,
J. Pharm. Pharmacol., **20**, 657-758.

Fell, J.T., Newton, J.M., (1970),
Determination of tablet strength by the diametral-compression test,
J. Pharm. Sci. **59**, 688-691.

Fersman, A.G., (1913),
Research on magnesium silicates,
Zap. Imp. Akad. Nauk., **32**, 321-430.

Firth, B.A., Hunter, R.J., (1976),
Flow properties of coagulated colloidal suspensions I, II and III,
J. Colloid Interface Sci., **57**, 248-275.

Fleck, C.A., (2006),
Palliative dilemmas: Wound odour,
Wound Care Canada, **4**, 10-13.

FMC, (2005),
Microcrystalline cellulose/ cellulose gels – dispersible grades, [Online],
http://www.fmcbiopolymer.com/PopularProducts/FMCMicrocrystallineCellulose/ColloidalGrades/tabid/808/Default.aspx. Accessed: 10/02/06.

FMC, (1995),
Avicel® RC-591. Product information brochure, [Online],
http://www.fmcbiopolymer.com/Portals/bio/Content/Docs/Pharmaceuticals/Avicel%20RC-591.pdf. Accessed: 20/01/2006.

Flörke, O.W., Graetsch, H., Brunk, F., Benda, L., Paschen, S., Bergna, H.E., Roberts, W.O., Welsh, W.A., Chapman, D.M., Ettinger, M., Kerner, D., Maier, M., Meon, W., Schmoll, R., Gies, H., Schiffman, D., (2005),
Silica,
In: *Ullmann's Encyclopedia of Industrial Chemistry*, 5th Edition, (electronic version), Gerhartz, W., (Ed.), Wiley Interscience, New York.

Ford, J.L., Rubinstein, M.H., (1981),
An investigation into some pharmaceutical interactions by differential scanning calorimetry,
Drug Dev. Ind. Pharm., **7**, 675-682.

Freeze, R.A., Cherry, J.A., (1979),
Groundwater, 1st Edition, Prentice-Hall, Inc., New Jersey.

Freundlich, H., Juliusberger, F., (1935),
Thixotropy influenced by the orientation of anisometric particles in sols and suspensions,
Trans. Faraday Soc., **31**, 920-921.

Frost, R.L., Cash, G.A., Keoprogge, J.T., (1998),
'Rocky Mountain leather', sepiolite and attapulgite – an infrared emission spectroscopic study,
Vibr. Spectrosc., **16**, 173-184.

Frost, R.L., Ding, Z., (2003),
Controlled rate thermal analysis and differential scanning calorimetry of sepiolite and palygorskites,
Thermochim. Acta, **397**, 119-128.

Frost, R.L., Locos, O.B., Ruan, H., Kloprogge, J.T., (2001),
Near-infrared and mid-infrared spectroscopic study of sepiolites and palygorskites,
Vibr. Spectrosc., **27**, 1-13.

Führer, C., (1977),
Substance behaviour in direct compression,
Labo. Pharms. Probl. Techn., **269**, 759-762.

Fukumoto, K., (1999),
Development of a honeycomb filter using porous materials,
pp. 100 in: *Proc. 12th Annual Meeting of odour research and engineering of Japan.*

Gabaude, C.M., Guillot, M., Gautier, J.C., Saudemon, P., Chulia, D., (1999),
Effects of true density, compacted mass, compression speed and punch deformation on the mean yield pressure,
J. Pharm. Sci., **88**, 725-730.

Galan, E., (1996),
Properties and applications of palygorskite-sepiolite clays,
Clay Miner., **31**, 443-453.

Galan, E., Carretero, M.I., (1999),
A new approach to compositional limits for sepiolite and palygorskite,
Clays Clay Miner., **47**, 399-409.

Galan, E., Castillo, A., (1984),
Sepiolite-palygorskite in Spanish tertiary basins: genetical patterns in continental environments,
pp. 87-136 in: *Palygorskite-Sepiolite: Occurrences, genesis and uses, Developments in Sedimentology, Volume 37*, Singer, A., Galan, E., (Eds.), Elsevier, Amsterdam.

Garekani, H.A., Ford, J.L., Rubinstein, M.H., Rajabi-Siahboomi, A.R., (2000a),
Highly compressible paracetamol: I: crystallization and characterization,
Int. J. Pharm., **208**, 87-99.

Garekani, H.A., Ford, J.L., Rubinstein, M.H., Rajabi-Siahboomi, A.R., (2000b),
Highly compressible paracetamol: II: compression properties,
Int. J. Pharm., **208**, 101-110.

Garr, J.S.M., Rubinstein, M.H., (1992),
The influence of moisture content on the consolidation and compaction properties of paracetamol,
Int. J. Pharm., **81**, 187-192.

Gehring, A.U., Fry, I.V., Luster, J., Sposito, G., (1994),
Vanadium in sepiolite: A redox-indicator for an ancient closed brine system in the Madrid Basin, Central Spain,
Geochim. Cosmochim. Acta, **58**, 3345-3351.

Ghebre-Sellassie, I., (1989),
Pharmaceutical Pelletization Technology, Ghebre-Sellassie, I., (Ed.), Marcel Dekker, Inc., New York.

Gioia, A., (1980),
Intrinsic flowability: a new technology for powder-flowability classification,
Pharm. Technol., February, 65-68.

Gohel, M.C., (2005),
A review of co-processed directly compressible excipients,
J. Pharm. Pharmaceut. Sci., **8**, 76-93.

Goktas, A.A., Misirili, Z., Baykara, T., (1997),
Sintering behaviour of sepiolite,
Ceram. Int., **23**, 305-311.

González, J.C., Molino-Sabio, M., Rodríguez-Reinoso, F., (2001),
Sepiolite-based adsorbents as humidity controller,
Appl. Clay Sci., **20**, 111-118.

Goto, K., Sunada, H., Danjo, K., Yonezawa, Y., (1999),
Pharmaceutical evaluation of multipurpose excipients for direct compressed tablet manufacture: comparisons of the capabilities of multipurpose excipients with those in general use,
Drug Dev. Ind. Pharm., **25**, 869-878.

Grant, R., Grant, C., (1987),
Grant and Hackh's Chemical Dictionary, McGraw-Hill Publishers, New York.

Güngör, N., Sevim, I., Ebru, G., Włodzimierz, M., Teterycz, H., Klimkiewicz, R., (2006),
Characterisation of sepiolite as a support of silver catalyst in soot combustion,
Appl. Clay Sci., **32**, 291-296.

Guo, H.X., (2002),
Compression behaviour and enteric film coating properties of cellulose esters,
Academic dissertation, University of Helsinki, Finland.

Güven, N., (1992),
Rheological aspects of aqueous smectite suspensions,
pp. 81-126 in : *Clay-Water Interface and its rheological implications*, Güven, N., Pollastro, R., (Eds.), CMS Workshop Lectures, Volume 4, The Clay Mineral Society, Boulder, Colorado.

Habib, Y., Augsburger, L., Reier, G., Wheatley, T., Shangraw, R., (1996),
Dilution potential: A new perspective,
Pharm. Dev. Technol., **1**, 205-212.

Haden, W.L., (1961),
Symposium on industrial applications: Attapulgite: properties and uses,
Clay Miner., **10**, 284-290.

Harkins, W.D., Jura, G., (1943),
An adsorption method for the determination of the area of a solid without the assumption of a molecular area and the area occupied by N_2 molecules on the surface of solids,
J. Chem. Phys., **11**, 431-432.

Harwood, R.J., Luber, J.R., Sunbery, E.W., (1996),
Antacids and clay products,
pp. 111-148 in: *Pharmaceutical Dosage Forms: Disperse Systems, Volume 2*, 2nd Edition, Lieberman, H.A., Rieger, M.M., Banker, G.S., (Eds.), Marcel Dekker Inc., New York.

He, C., Makociky, E., Osbæck, B., (1996),
Thermal treatment and pozzolanic activity of sepiolite,
Appl. Clay Sci., **10**, 337-349.

Healy, A.M., Corrigan, O.I., Allan, J.E.M., (1995),
The effect of dissolution on the surface texture of model solid-dosage forms as assessed by non-contact laser profilometry,
Pharm. Technol. Eur., **9**, 14-22.

Heckel, R.W., (1961a),
Density-pressure relationships in powder compaction,
Trans. Metal. Soc. AIME, **221**, 671-675.

Heckel, R.W., (1961b),
An analysis of powder compaction phenomena,
Trans. Metal. Soc. AIME, **221**, 1001-1008.

Helsing, H.J., (1969),
Advanced processing of oxide-ceramics by spray drying,
Powder Metall. Int., **1**, 62-65.

Hempel, K.F.B., (1969),
The restoration of two marble statues by Antonio Corradini,
Stud. Conservat., **14**, 126-131.

Hermosin, M.C., Cornejo, J., White, J.L., Hem, S.L., (1981),
Sepiolite, a potential excipient for drugs subject to oxidative degradation,
J. Pharm. Sci., **70**, 189-192.

Herrera, J.I., Olmo, N., Turnay, J., Sicilia, A., Bascones, A., Gavilanes, J.G., Lizarbe, M.A., (1995),
Implantation of sepiolite-collagen complexes in surgically created rat calvaria defects,
Biomaterials, **16**, 625-631.

Hersey, J. A., Rees, J.E., (1971),
Deformation of particles during briqueting,
Nature Phys., **230**, 96.

Hileman, G.A., Goskonda, S.R., Spalitto, A.J., Upadrashta, S.M., (1993),
Response surface optimisation of high dose pellets by extrusion and spheronization,
Int. J. Pharm., **100**, 71-79.

Holm, P., Bonde, M., Wigmore, T., (1996),
Pelletization by granulation in a roto-processor RP-2. Part 1. Effects of process and product variables on granule growth,
Pharm. Technol. Eur., **8**, 22-36.

Hong-Guang, W., Ru-Hua, Z., (1995),
Compaction behaviour of paracetamol powders of different crystal structure,
Int. J. Pharm., **21**, 863-868.

Hubbard, B., Kuang, W., Moser, A., Facey, G.A., Detellier, C., (2003),
Structural study of Maya blue: textural, thermal and solid-state multinuclear magnetic resonance characterization of the palygorskite-indigo and sepiolite-indigo adducts,
Clays Clay Miner., **51**, 318-326.

Hunter, R.J., (1989),
Foundation of Colloid Science, *Volume 1*, Oxford University Press, Oxford.

Hussan, M.S.H., York, P., Timmins, P., (1991),
Influence of commercial and high-purity magnesium stearates on sodium chloride and paracetamol DC granules during tabletting,
Int. J. Pharm. **70**, 103-109.

Ibrahim, Y.K., Olurinola, P. F., (1991),
Comparative microbial contamination levels in wet granulation and direct compression methods of tablet production,
Pharm. Acta Helv., **66**, 298-301.

Inagaki, S., Fukushima, Y., Dot, H., Kamigaito, O., (1990),
Pore size distribution and adsorption selectivity of sepiolite,
Clay Miner., **25**, 99-105.

Indrayanto, G., Mugihardijo, A., Handayani, R., (1994),
Compatibility study between famotidine and some excipients using differential scanning calorimetry,
Drug. Dev. Ind. Pharm., **20**, 911-920.

Ingelbrecht, S., Remon, J.P., (1997),
Instrumentation of a roll compactor and the evaluation of the parameter settings by neural networks,
Int. J. Pharm., **148**, 103-115.

International Agency for Research on Cancer (IARC) monograph, (1997),
Volume 68, Silica, Group 3, Sepiolite, [Online],
http://monographs.iarc.fr/ENG/Monographs/vol68/volume68.pdf.
Accessed 02/01/2007.

International Conference on Harmonization (ICH), (2003),
Topic Q 1 A (R2) Stability testing of new drug substances and products step 5,
http://www.emea.eu.int/pdfs/human/ich/273699en.pdf. Accessed: 06/11/2006.

International Federation of Societies of Cosmetic Chemists (IFSCC) Monograph no. 3, (1997),
An Introduction to Rheology, Micelle Press, Dorset.

International Union of Pure and Applied Chemistry (IUPAC),
Compendium of Chemical Terminology, [Online],
http://www.iupac.org/publications/compendium/H.html. Accessed: 29/12/2006.

International Union of Pure and Applied Chemistry (IUPAC), (1972),
Manual of symbols and terminology for physicochemical quantities and units,
Appendix 2, Definitions, terminology and symbols in Colloid and Surface Chemistry, Part 1.
Pure Appl. Chem., **31**, 578-638.

Ituare, N.N., (2005),
Atrazine adsorption at the air/silica interface,
M.Sc. Thesis, Ohio State University.

Iwuagwu, M.A., Aloko, K.S., (1992),
Adsorption of paracetamol and chloroquine by some antacids,
J. Pharm. Pharmacol., **44**, 655-658.

Jaiyeoba, K.T., Spring, M.S., (1980),
The granulation of ternary mixtures: the effect of the wettability of the powders,
J. Pharm. Pharmacol., **32**, 386-388.

Jarüp, L., (2003),
Hazards of heavy metal contamination,
Br. Med. Bull., **68**, 167-182.

Jenike, A.W., (1954),
Flow of solids in bulk handling system. Report on the development of a quantitative method of design,
ASME Meeting, June 20-24,
Bull. Univ. Utah., 64.

Jiménez-López, A., López-González, J., Ramīrez-Sāenz, A., Rodríguez-Reinoso, F., Valenzuela-Calahorro, C., Zurita-Herrera, L., (1978),
Evolution of surface area in a sepiolite as a function of acid and heat treatments,
Clay Miner., **13**, 375-384.

Jivraj, M., Martini, L.G., Thomson, C.M., (2000),
An overview of the different excipients useful for the direct compression of tablets,
Pharmaceut. Sci. Technol. Today, **3**, 58-63.

Johansson, B., Alderborn, G., (2001),
The effect of shape and porosity on the compression behaviour and tablet forming ability of granular materials formed from microcrystalline cellulose,
Eur. J. Pharm. Biopharm., **52**, 347-357.

Jozefaciuk, G., Matyka-Sarzynska, D., (2006),
Effect of acid treatment and alkali treatment on nanopore properties of selected minerals,
Clays Clay Miner., **54**, 220-229.

Kaerger, J.S., Edge, S., Price, R., (2004),
Influence of particle size and shape on flowability and compactibility of binary mixtures of paracetamol and microcrystalline cellulose,
Eur. J. Pharm. Sci., **22**, 173-179.

Kah-Helbig, A., Lang, S., (1987),
Ludipress, a new direct tabletting auxiliary, [Online],
BASF AG Ludwigshafen, Germany,
http://www.megglepharma.cn/es/literature/articles/208/208.pdf.
Accessed: 03/10/2005.

Kalantzi, L., Reppas, C., Dressman, J.B., Amidon, G.L., Junginger, H.E., Midha, K.K., Shah, V.P., Stavchansky, S.A., Barends, D.M., (2006),
Biowaiver monographs for immediate release solid oral dosage forms: Acetaminophen (paracetamol),
J. Pharm. Sci., **95**, 4-14.

Kara, M., Yuzer, H., Sabah, E., Çelik, M.S., (2003),
Adsorption of cobalt from aqueous solutions onto sepiolite,
Water Res., **37**, 224-232.

Karakaya, N., Çelik Karakaya, M., Temel, A., Küpeli, Ş., Tunoglu, C., (2004),
Mineralogical and chemical characterization of sepiolite occurrences at Karapinar (Konya basin, Turkey),
Clays Clay Miner., **52**, 495-509.

Karehill, P.G., Glazer, M., Nyström, C., (1990),
Studies on direct compression of tablets. XXIII. The importance of surface roughness for compactibility of some directly compressible materials with different binding and volume reduction properties,
Int. J. Pharm., **64**, 35-43.

Keleb, E.I., Vermeire, A., Vervaet, C., Remon, J.P., (2004),
Twin screw granulation as a simple and efficient tool for continuous wet granulation,
Int. J. Pharm., **273**, 183-194.

Kelessidis, V.C., Maglione, R., (2006),
Modeling rheological behavior of bentonite suspensions as Casson and Robertson–Stiff fluids using Newtonian and true shear rates in Couette viscometry,
Powder Technol., 168, 134-147.

Kelly, M.H., (2002),
Novel formulations for use in the oral cavity,
PhD. Thesis, Trinity College, University of Dublin.

Keren, R., (1988),
Rheology of aqueous suspensions of sodium/calcium montmorillonite,
Soil Sci. Soc. Am. J., **52**, 924-928.

Khan, K.A., Musikabhumma, P., Warr, J.P., (1981),
The effect of moisture content of microcrystalline cellulose on the compressional properties of some formulations,
Drug Dev. Ind. Pharm., **7**, 525-538.

Kikuta, J., Kitamori, N., (1994),
Effect of mixing time on the lubricating properties of magnesium stearate and the final characteristics of compressed tablets,
Drug Dev. Ind. Pharm., **20**, 343-355.

Kleinebudde, P., (1994),
Shrinking and swelling properties of pellets containing microcrystalline cellulose and low substituted hydroxypropylcellulose. I: Shrinking properties,
Int. J. Pharm., **109**, 209-219.

Knapp, C., Gil-Llambías, F.J., Guluppi-Cabra, M., Avila, P., Blanco, J., (1997),
Phase distribution in titania-sepiolite catalyst supports prepared by different methods,
J. Mater. Chem., **7**, 1641-1645.

Knight, P.C., Johansen, A., Kristensen, B., Schaefer, J.P.K., (2000),
An investigation of the effects on agglomeration of changing the speed of a mechanical mixer,
Powder Technol., **110**, 204-209.

Kogel, J.E., Lewis, S.A., (2001),
Baseline studies of the Clay Minerals Society source clays: chemical analysis by inductively coupled plasma-mass spectroscopy,
Clays Clay Miner., **49**, 387-392.

Kojdecki, M.A., Bastida, J., Pardo, P., Amorós, P., (2005),
Crystalline structure of sepiolite influenced by grinding,
J. Appl. Crystallogr., **38**, 888-899.

Köse, A., Karabagli, Y., Kürkçüoglu, M., Çetin, C., (2005),
Alpha sepiolite: An old clay mineral – A new dressing material,
Wounds, **17**, 114-121.

Koshy, K.T., Lach, J.I., (1961),
Stability of aqueous solution of *N*-acetyl-*p*-aminophenol,
J. Pharm. Sci., **50**, 113-118.

Kumar, V., Kothari, S., Banker, G., (2001),
Compression, compaction and disintegration properties of low crystallinity celluloses produced using different agitation rate during their regeneration from phosphoric acid solutions,
AAPS Pharm. Sci. Technol., **2**, Article 7.

Kumar, V., Reus-Medina, M., Yang, D., (2002),
Preparation, characterization and tabletting performance of a new cellulose-based pharmaceutical aid,
Int. J. Pharm., **235**, 129-140.

Kvech, S.J., (2001),
Formation of aluminum containing solids in drinking water: influence on Pb/Cu corrosion, Al solubility and enhanced softening,
M.Sc. Thesis, Virginia Polytechnic Institute and State University, USA.

Lagaly, G., (1989),
Principles of flow of kaolin and bentonite dispersions,
Appl. Clay Sci., **4**, 105-123.

Lagaly, G., (2001),
Pesticide-clay interactions and formulations,
Appl. Clay Sci., **18**, 205-209.

Lagaly, G., (2005),
Colloids,
In: *Ullmann's Encyclopedia of Industrial Chemistry*, 5th Edition, (electronic version), Gerhartz, W., (Ed.), Wiley Interscience, New York.

La Grega, M.D., Buckingham, P.L., Evans, J.C., (1994),
Hazardous Waste Management, McGraw Hill, New York.

Lamberson, R.L., Raynor, G.E., (1976),
Tabletting properties of microcrystalline cellulose,
Mfg. Chem. Aerosol News, June, 55-61.

Landin, R., Martinez-Pacheco, R., Gomez-Amoza, J.L., Souto, C., Concheiro, A., Rowe, R.C., (1993),
Effect of country of origin on the properties of microcrystalline cellulose,
Int. J. Pharm., **91**, 123-131.

Larney, J., (1971),
Ceramic restoration in the Victoria and Albert Museum,
Stud. Conservat., **16**, 69-82.

Lennartz, P., Mielck, J.B., (1998),
Mini-tabletting: improving the compactibility of paracetamol powder mixtures,
Int. J. Pharm., **173**, 75-85.

Leong, Y.K., Boger, D.V., Scales, P.J., Healy, T.W., Buscall, R., (1993),
Control of the rheology of concentrated aqueous colloidal systems by steric and hydrophobic forces,
J. Chem. Soc., Chem. Commun., **7**, 639-641.

Levis, S.R., (2000),
Novel pharmaceutical excipients,
PhD. Thesis, Trinity College, University of Dublin.

Levis, S.R., Deasy, P.B., (2001),
Pharmaceutical applications of size reduced grades of surfactant co-processed microcrystalline cellulose,
Int. J. Pharm., **230**, 25-33.

Levis, S.R., Deasy, P.B., (2002),
Characterisation of halloysite for use as a microtubular drug delivery system,
Int. J. Pharm., **243**, 125-134.

Li, Z., (1999),
Sorption of oxyanions and surface anion exchange by surfactant modified clay minerals,
J. Environ. Qual., **28**, 1457-1463.

Li, Z., Bowman, R.S., (1997),
Counterion effects on the sorption of cationic surfactant and chromate in natural clinoptilolite,
Environ. Sci. Technol., **31**, 2407-2412.

Li, Z., Willms, C., Kniola, K., (2003),
Removal of anionic contaminants using surfactant-modified palygorskite and sepiolite,
Clays Clay Miner., **51**, 445-451.

Liu, J.-F., Ducker, W.A., (1999),
Surface-induced phase behaviour of alkyltrimethylammonium bromide surfactants adsorbed to mica, silica and graphite,
J. Phys. Chem., **B103**, 8558-8567.

Limwong, V., Sutanthavibul, N., Kulvanich, P., (2004),
Spherical composite particles of rice starch and microcrystalline cellulose: A new co-processed excipient for direct compression,
AAPS Pharm. Sci. Technol., **5**, Article 30.

Lin, F.H., Lee, Y.H., Jian, C.H., Wong, J.-M., Shieh, M.-J., Wang, C.-H., (2002),
A study of purified montmorillonite intercalated with 5-fluorouracil as drug carrier,
Biomaterials, **23**, 1981-1987.

Liu, C.H., Chen, S.C., Lee, Y.C., Sokoloski, T.D., Sheu, M.T., (1994),
Directly compressible acetaminophen compositions prepared by fluidized bed granulation,
Drug Dev. Ind. Pharm., **20**, 1911-1922.

Lizarbe, M. A., Olmo, N., Gavilanes, J.G., (1987a),
Adhesion and spreading of fibroblasts on sepiolite-collagen complexes,
J. Biomed. Mater. Res., **21**, 137-144.

Lizarbe, M.A., Olmo, N., Gavilanes, J.G., (1987b),
Outgrowth of fibroblasts on sepiolite-collagen complexes,
Biomaterials, **8**, 35-37.

Longerich, H.P., Jenner, G.A., Fryer, B.J., Jackson, S.E., (1990),
Inductively coupled plasma-mass spectrometric analysis of geological samples: a critical evaluation based on case studies,
Chem. Geol., **83**, 105-118.

López-Galindo, A., Viseras, C., Cerezo, P., (2006),
Compositional, technical and safety specifications of clays to be used as pharmaceutical and cosmetic products,
Appl. Clay Sci., In Press, doi:10.1016/j.clay.2006.06.016.

Lowell, S., Shields, J.E., (1991),
Powder Surface Area and Porosity, 3rd Edition, Chapman and Hall Publishers, New York.

Luckham P.F., Rossi, S., (1999),
The colloidal and rheological properties of bentonite suspensions,
Adv. Colloid Interface Sci., **82**, 43-92.

Lüdde, K.H., Kawakita, K., (1966),
Die Pulverkompression,
Pharmazie, **21**, 393-403.

Ludipress® and Ludipress® LCE: One-step tabletting, [Online],
BASF Pharma, Germany,
http://www.pharma-solutions.basf.com/(m5s5wd2stnlwmuzf4zit1e3s)/pdf/brochures/3454_Ludipress.pdf. Accessed: 20/10/2006.

Lukasiewicz, S.J., (1989),
Spray-drying of ceramic powders,
J. Am. Ceram. Soc., **72**, 617-624.

Lustig-Gustafsson, C., Kaur Johal, H., Podczeck, F., Newton, J.M., (1999),
The influence of water content and drug solubility on the formulation of pellets by extrusion and spheronisation,
Eur. J. Pharm. Biopharm., **8**, 147-152.

Luukkonen, P., (2001),
Rheological properties and state of water of microcrystalline cellulose and silicified microcrystalline cellulose,
Dissertationes Biocentri Viikki Universitatis Helsingiensis, Finland.

Lyklema, J., (1991),
Nomenclature, symbols, definitions and measurements for electrified interfaces in aqueous dispersions of solids (IUPAC recommendations, 1991),
Pure Appl. Chem., **63**, 895-906.

Madejová, J., Komadel, P., (2001),
Baseline studies of the Clay Minerals Society Source Clays. Infrared methods,
Clays Clay Miner., **49**, 410-432.

Maganti, L., Çelik, M., (1993),
Compaction studies on pellets I. Uncoated pellets,
Int. J. Pharm., **95**, 29-42.

Maganti, L., Çelik, M., (1994),
Compaction studies on pellets II. Coated pellets,
Int. J. Pharm., **103**, 55-67.

Malan, C.E., de Villiers, M.M., Lötter, A.P., (1997),
Application of differential scanning calorimetry and high performance liquid chromatography to determine the effects of mixture composition and preparation during the evaluation of niclosamide-excipient compatibility,
J. Pharm. Biomed. Anal., **15**, 549-557.

Manne, S., Gaub, H.E., (1995),
Molecular organization of surfactants at solid-liquid interfaces,
Science, **270**, 1480-1482.

Margulies, L., Rozen, H., Cohen, E., (1985),
Energy transfer at the surface of clays and protection of pesticides from photodegradation,
Nature, **315**, 658-659.

Margulies, L., Stern, T., Rubin, B., Ruzo, L.O., (1992),
Photostabiliztion of Trifluralin adsorbed in a clay matrix,
J. Agric. Food Chem., **40**, 152-155.

Marshall, (1999),
Compression/ compaction, [Online],
http://www.fmcbiopolymer.com/Portals/bio/content/Docs/Pharmaceuticals/Problem%20Solver/Section%203%20Compression_Compaction.pdf.
Accessed: 12/04/2005.

Martin, A., (1993),
Physical Pharmacy, 4th Edition, Lippincott, Williams and Wilkins Publishers, Philadelphia.

Martinello, T., Kaneko, T.M., Velasco, M.V.R., Taqueda, M.E.S., Consiglieri, V.O., (2006),
Optimization of poorly compactable drug tablets manufactured by direct compression using the mixture experimental design,
Int. J. Pharm., **322**, 87-95.

Martinez-Ramirez, A., Puertas, F., Blanco-Varela, M.T., (1996),
Stability of sepiolite in neutral and alkaline media at room temperature,
Clay Miner., **31**, 225-232.

Martin-Vivaldi, J.L., Cano Ruiz, J., (1956),
Contribution to the study of sepiolite. II. Some considerations regarding mineralogical formulae,
Clay Miner., **4**, 173-176.

Masters, K., (1991),
Spray Drying Handbook, 5th Edition, Longman Scientific and Technical, UK.

Mathis, A., Stamm, A., (1976),
A study of the compression properties of direct compression excipients,
Sci. Techn. Pharm., **5**, 245-247.

Matijaŝić, G., Glasnović, A., (2002),
Influence of the disperse phase characteristics on rheological behaviour of suspensions,
Chem. Biochem. Eng. Q., **16**, 165-172.

Matthews, B.A., Rhodes, C.T., (1968),
Some studies of flocculation phenomena in pharmaceutical suspensions,
J. Pharm. Sci., **57**, 569-573.

McBride, M.B., Baveye, P., (2002),
Particle interactions in colloidal systems – diffuse double layer models, long-range forces and ordering in clay colloids,
Soil Sci. Soc. Am. J., **66**, 1207-1217.

McConnochie, K., Bevan, C., Newcombe, R.G., Lyons, J.P., Skidmore, J.W., Wagner, J.C., (1993),
A study of Spanish sepiolite workers,
Thorax, **48**, 370-374.

McElnay, J.C., D'Arcy, P.F., Leonard, J.K., (1982a),
The effect of activated dimethicone, other antacid constituents and kaolin on the absorption of propranolol,
Experientia, **38**, 605-607.

McElnay, J.C., Mukhtar, H.A., D'Arcy, P.F., Temple, D.J., Collier, P.S., (1982b),
The effect of magnesium trisilicate and kaolin on the *in vivo* absorption of chloroquine,
J. Trop. Med. Hyg., **85**, 159-163.

Mendelovici, E., Portillo, D.C., (1976),
Organic derivatives of attapulgite; I, Infrared spectroscopy and X-ray diffraction studies,
Clays Clay Miner., **23**, 177-182.

Micromeritics Application Note nº 78, (1991)
Selecting the appropriate minimum and maximum thickness values for micropore t-plots,
Micromeritics® Instrument Corporation, Georgia.

Molina-Sabio, M., Caturla, F., Rodríguez-Reinoso, F., Kharitonova, G.V., (2001),
Porous structure of a sepiolite as deduced from the adsorption of N_2, CO_2, NH_3 and H_20,
Microporous Mesoporous Mater., **47**, 389-396.

Moore, J.W., Flanner, H.H., (1996),
Mathematical comparison of curves with an emphasis on *in vitro* dissolution profiles,
Pharm. Tech., **20**, 64-74.

Moore, D.M., Reynolds, R.C., (1989),
X-ray Diffraction and the Identification and Analysis of Clay Minerals,
Oxford University Press, Oxford.

Moreton, R.C., (1996),
Tablet excipients to the year 2001: A look into the crystal ball,
Drug Dev. Ind. Pharm., **22**, 11-23.

Mullins, E., (2003),
Statistics for the Quality Control Chemistry Laboratory, 1st Edition, Royal Society of Chemistry, Cambridge.

Muñoz-Ruiz, A., Velasco-Antequera, M.V., Monedero-Peralse, M.C., Jiménez-Castellanos, M.R., (1994),
Tabletting properties of new granular microcrystalline celluloses,
Eur. J. Pharm. Biopharm., **40**, 36-40.

Mura, P., Maestrelli, F., Cirri, M., Furlanetto, S., Pinzauti, S., (2003),
Differential scanning calorimetry as an analytical tool in the study of drug-cyclodextrin interactions,
J. Therm. Anal. Calorim., **73**, 635-646.

Murray, H., (2000),
Tradition and new applications for kaolin, smectite and palygorskite: a general overview,
Appl. Clay Sci., **17**, 207-221.

Murray, H., (2002),
Industrial clays case study, [Online],
http://www.iied.org/mmsd/mmsd_pdfs/064_murray.pdf. Accessed: 29/01/2004.

Nachaegari, S.K., Bansal, A.K., (2004),
Co-processed excipients for solid dosage forms,
Pharm. Technol., **28**, 52-64.

Nadkarnai, D., Kildsig, D.O., Kramer, P.A., Banker, G.S., (1975),
Effect of surface roughness and coating solvent on film adhesion to tablets,
J. Pharm. Sci., **64**, 1554-1557.

Nagata, H., Shimoda, S., Sudo, T., (1974),
On dehydration of bound water of sepiolite,
Clays Clay Miner., **22**, 285-293.

Nagelschmidt, G., (1941),
The identification of clay minerals by means of aggregate X-ray diffraction diagrams,
J. Sci. Instrum., **18**, 100-101.

Naggar, V.F., Khalil, S.A., (1979),
Effect of magnesium trisilicate on nitrofurantoin absorption,
Clin. Pharmacol. Ther., **25**, 857-863.

Nagy, B., Bradley, W. F., (1954),
The structural scheme of sepiolite,
Acta Crystallogr., **7**, 683.

Nagy, B., Bradley, W. F., (1955),
The structural scheme of sepiolite,
Am. Mineral., **40**, 885-892.

Narayan, P., Hancock, B.C., (2003),
The relationship between the particle properties, mechanical behaviour and surface roughness of some pharmaceutical excipient compacts,
Mat. Sci. Eng., **A355**, 24-36.

Nash, R.A., (1996),
Pharmaceutical suspensions,
pp. 1-46 in: *Pharmaceutical Dosage Forms: Disperse Systems, Volume 2*, 2nd Edition, Lieberman, H.A., Rieger, M.M., Banker, G.S., (Eds.), Marcel Dekker Inc., New York.

National Safety Council,
Glossary, [Online],
http://www.nsc.org/ehc/glossary.htm. Accessed: 29/12/2006

Neaman, A., Singer, A., (2000),
Rheological properties of aqueous suspensions of palygorskite,
Soil Sci. Soc. Am. J., **64**, 427-436.

Newton, M., Petersson, J., Podczeck, F., Clarke, A., Booth, S., (2001),
The influence of formulation variables on the properties of pellets containing a self-emulsifying mixture,
J. Pharm. Sci., **90**, 987-995.

Nichols, G., Frampton, C.S., (1998),
Physicochemical characterisation of the orthorhombic polymorph of paracetamol crystallized from solution,
J. Pharm. Sci., **87**, 684-693.

Nicklasson, F., Alderborn, G., (2000),
Analysis of the compression mechanics of pharmaceutical agglomerates of different porosity and composition using the Adams and Kawakita equations,
Pharm. Res., **17**, 947-952.

Nolan, R.P., Langer, A.M., Herson, G.B., (1991),
Characterisation of palygorskite specimens from different geological locales for health hazard evaluation,
Br. J. Ind. Med., **48**, 463-475.

Nunthanid, J., Laungtanaanan, M., Sriamornsak, P., Limmatvapirat, S., Lim, L.Y., Puttipipatkhachorn. S., Khor, E., (2004),
Characterization of chitosan acetate as a binder for sustained release tablets,
J. Controlled Release, **99**, 15-26.

Nyström, C., Karehill, PG., (1996),
The importance of intermolecular bonding forces and the concept of bonding surface area,
pp. 17-54 in: *Pharmaceutical Powder Compaction Technology,* Alderborn, G., Nyström, C., (Eds.), Marcel Dekker, New York.

Oakley, D.A., (1997),
Produce uniform particles by spray drying,
Chem. Eng. Prog., **93**, 48-54.

Odeku, O.A., Itiola, O.A., (2003),
Effect of interacting variables on the tensile strength and release properties of paracetamol tablets,
Trop. J. Pharmaceut. Res., **2**, 147-153.

O'Driscoll, M., (1992),
European cat litter. Absorbing market growth,
Ind. Miner., **299**, 46-65.

Ofner, C.M., Schnaare, R., (2001),
Suspensions, [Online],
http://www.fmcbiopolymer.com/Portals/bio/content/Docs/Pharmaceuticals/Problem%20Solver/Section%209%20Suspensions.pdf. Accessed: 10/10/2004.

Ofner, C.M., Schnaare, R., Schwartz, J.B., (1996),
Oral aqueous suspensions,
pp. 149-182 in: *Pharmaceutical Dosage Forms: Disperse Systems, Volume 1*, 2nd Edition, Lieberman, H.A., Rieger, M.M., Banker, G.S., (Eds.), Marcel Dekker Inc., New York.

Ohta, S., Nagai, K., Maruyama, M., Inouem H., Katsuyama, Y., Atobe, O., Ogata, H., Yamato, S., Tachikawa, E., Zenda, H., (1999),
Preparation and characteristics of antibacterial sepiolite containing povidone-iodine as a useful pharmaceutical agent for patient care,
Biol. Pharm. Bull., **22**, 42-47.

Olmo, N., del Pozo, A.M., Lizarbe, M.A., Gavilanes, J.G., (1985),
Interaction of type I collagen with sepiolite (magnesium trisilicate),
Collagen Related Res., **5**, 9-16.

Olmo, N., Lizarbe, M.A., Gavilanes, J.G., (1987),
Biocompatibility and degradability of sepiolite-collagen,
Biomaterials, **8**, 67-69.

Olmo, N., Lizarbe, M.A., Turnay, J., Muller, K.P., Gavilanes, J.G., (1988),
Cell morphology, proliferation and collagen synthesis of human fibroblasts cultured on sepiolite-collagen complexes,
J. Biomed. Mater. Res., **22**, 257-270.

Olmo, N., Turnay, J., Gavilanes, J.G., Lizarbe, M.A., Herrera, J.I., (1992),
Subcutaneous and intramuscular implantation of sepiolite-collagen complexes,
J. Mater. Sci., **3**, 239-244.

Olmo, N., Turnay, J., Herrera, J.I., Gavilanes, J.G., Lizarbe, M.A., (1996),
Kinetics of *in vivo* degradation of sepiolite-collagen complexes: effect of glutaraldehyde treatment,
J. Biomed. Mater. Res., **30**, 77-84.

O'Neil, A.J., Jee, R.D., Moffat, A.C., (2003),
Measurement of the percentage volume particle size distribution of powdered microcrystalline cellulose using reflectance near-infrared spectroscopy,
Analyst, **128**, 1326-1330.

Otsuka, M., Sato, M., Matsuda, Y., (2001),
Comparative evaluation of tabletting compression behaviors by methods of internal and external lubricant addition: Inhibition of enzymatic activity of trypsin preparation by using external lubricant addition during the tabletting compression process,
AAPS Pharm. Sci., **3**, Article 20.

Ouhida, I., Pérez, J.F., Gasa, J., (2000a),
Sepiolite (EXAL) decreases microbial colonization in the gastrointestinal tract of young broilers fed barley-wheat based diets,
Arch. Zootec., **49**, 501-504.

Ouhida, I., Pérez, J.F., Gasa, J., Puchal, F., (2000b),
Enzymes (beta-glucanase and arabinoxylanase) and/or sepiolite supplementation and the nutritive value of maize-barley-wheat based diets for broiler chickens,
Br. Poult. Sci., **41**, 617-624.

Ouhida, I., Pérez, J.F., Piedrafita, J., Gasa, J., (2000c)
The effects of sepiolite in broiler chicken diets of high, medium and low viscosity. Productive performance and nutritive value,
Anim. Feed Sci. Technol., **85**, 183-194.

Özkan, A., Şahin, M., Özkan, A.S., (2004),
Adsorption of nitrate ions onto sepiolite and surfactant-modified sepiolite,
Adsorpt. Sci. Technol., **23**, 323-333.

Ozkan, N., Briscoe, B.J., (1996),
The surface topography of compacted agglomerates: a means to optimize compaction conditions,
Powder Technol., **86**, 201-207.

Pakter, A., (1962),
Studies in the rheology of clay-water systems. Part 5. Viscosity and gel strength of sodium attapulgite systems and their coagulation by electrolytes,
Rheol. Acta, **2**, 44-50.

Papo, A., Piani, L., Ricceri, R., (2002),
Sodium tripolyphosphate and polyphosphate as dispersing agents for kaolin suspensions: rheological characterization,
Colloids Surf., **A201**, 219-230.

Paracetamol Information Centre, [Online],
http://www.pharmweb.net/pwmirror/pwy/paracetamol/pharmwebpic1.html.
Accessed: 10/05/2004.

Parisini, P., Martelli, G., Sardi, L., Escribano, F., (1999),
Protein and energy retention in pigs fed diets containing sepiolite,
Anim. Feed Sci. Technol., **79**, 155-162.

Paronen, P., Ilkka, J., (1996),
Porosity-pressure functions,
pp. 55-76: in *Pharmaceutical Powder Compaction Technology,* Alderborn, G., Nyström, C. (Eds.), Marcel Dekker, New York.

Patel, N.K., Upadhyay, A.H., Bergum, J.S., Reier, G.E., (1994),
An evaluation of microcrystalline cellulose and lactose excipients using an instrumented single station tablet press,
Int. J. Pharm., **110**, 203-210.

Patton, T.C., (1979),
Paint Flow and Pigment Dispersion, 2nd Edition, Wiley, New York.

Peck, G.E., Baley, G.J., McCurdy, V.E., Banker, G.S., (1988),
Tablet formulation and design,
pp. 75-130 in: *Pharmaceutical Dosage Forms: Tablets, Volume 1*, Lieberman, H.A., Lachman, L., Schwartz, J.B., (Eds.), Marcel Dekker, New York.

Peltonen, L., Mannermaa, J.-P., Yliruusi, J., (1997),
Roughness analysis from tablet surfaces with a confocal laser scanning microscope,
Pharmazie, **52**, 860-863.

Pereira, M.A., Alves, M.M., Azeredo, J., Mota, M., Oliveira, R., (2000),
Influence of physico-chemical properties of porous microcarriers on the adhesion of an anaerobic consortium,
J. Ind. Microbiol. Biotechnol., **24**, 181-186.

Pérez-Rodríguez, J.L., Carretero, M.I., Maqueda, C., (1989),
Behaviour of sepiolite, vermiculite and montmorillonite as supports in anaerobic digestors,
Appl. Clay Sci., **4**, 69-82.

Permien, T., Lagaly, G., (1994a),
The rheological and colloidal properties of bentonite dispersions in the presence of organic compounds: I. Flow behaviour of sodium-bentonite in water-alcohol,
Clay Miner., **29**, 751-760.

Permien, T., Lagaly, G., (1994b),
The rheological and colloidal properties of bentonite dispersions in the presence of organic compounds: II. Flow behaviour of Wyoming bentonite in water-alcohol,
Clay Miner., **29**, 761-766.

Pharmaceutical Codex: Principles and Practice of Pharmaceutics, (1994),
12th Edition, Lund, W., (Ed.), The Pharmaceutical Press, London.

Pharmaceutical Handbook (1980),
19th Edition, Wade, A. (Ed.), The Pharmaceutical Press, London.

Pifferi, G., Santoro, P, Pedrani, M., (1999),
Quality and functionality of excipients,
Il Farmaco, **54**, 1-14.

Podczeck, F., (1996),
The development and optimization of tablet formulations using mathematical models,
pp. 577: in *Pharmaceutical Powder Compaction Technology,* Alderborn, G., Nyström, C. (Eds.), Marcel Dekker, New York.

Podczeck, F., (1998),
Measurement of surface roughness of tablets made from polyethylene glycol powders of various molecular weight,
Pharm. Pharmacol. Commun., **4,** 179-182.

Podczeck, F., Brown, S., Newton, M., (1999),
Monitoring film coating with surface profilometry,
Pharm. Technol., **23,** 48-56.

Podczek, F., Revesz, P., (1993),
Evaluation of the properties of microcrystalline and microfine cellulose powders,
Int. J. Pharm., **91**, 183-193.

Poon, C., Bhushan, B., (1995),
Comparison of surface roughness measurements by stylus profiler, AFM and non-contact optical profiler,
Wear, **190**, 76-88.

Poppe, L.J., Paskevich, V.F., Hathaway, J.C., Blackwood, D.S., (2001),
A laboratory manual for X-ray powder diffraction,
USGS OFR01-041, [Online],
http://pubs.usgs.gvo/of/of01041/htmldocs/flow/d4/d4f1.html. Accessed: 12/8/2004.

Post, J.L., (1978),
Sepiolite deposits of the Las Vegas, Nevada area,
Clays Clay Miner., **26**, 58-64.

Post, J.L., Crawford, S., (2006),
Varied forms of palygorskite and sepiolite from different geologic systems,
Appl. Clay Sci., In Press, doi:10.1016/j.clay.2006.10.003.

Post, J.L., Janke, N.C., (1984),
Ballarat sepiolite, Inyo County, California,
pp. 159-169 in: *Palygorskite-Sepiolite: Occurrences, Genesis and Uses, Developments in Sedimentology, Volume 37*, Singer, A., Galan, E., (Eds.), Elsevier, Amsterdam.

Practical Techniques I, Applied Rheology Symposium 2002,
TA Instruments, Leatherhead, UK.

Preisinger, A., (1959),
X-ray study of the structure of sepiolite,
pp. 61-67 in: *International Series of Monographs on Earth Sciences, Clays and Clay Minerals*, Swineford, A., (Ed.), Pergamon Press, Oxford.

Preisinger, A., (1963),
Sepiolite and related compounds: its stability and application,
pp. 365-371, *10th National Conference on Clays and Clay Minerals.*

Propst, C.W., (2002),
Tablet Processing – Problem Solver, [Online],
http://www.fmcbiopolymer.com/Portals/bio/content/Docs/Pharmaceuticals/Problem%20Solver/Section%202%20Tablet%20Processing.pdf. Accessed: 23/12/2002.

Puertas, R., (1993),
Escorias de alto horno: composición y comportamiento hidráulico,
Materiales de construcción, **43**, n° 229.

Radebaugh, G.W., (1996),
Rheological and mechanical properties of dispersed systems,
153-209 in: *Pharmaceutical Dosage Forms: Disperse Systems, Volume 1*, 2nd Edition, Lieberman, H.A., Rieger, M.M., Banker, G.S., (Eds.), Marcel Dekker Inc., New York.

Radojević, M., Jović, V., Vitorović, D., (2002a),
Study of sepiolite from Goleŝ (Kosovo, Yugoslavia). I. Sorption capacity,
J. Serb. Chem. Soc., **67**, 489-497.

Radojević, M., Jović, V., Karaulić, D., Vitorović, D., (2002b),
Study of sepiolite from Goleŝ (Kosovo, Yugoslavia). II. Acid activation,
J. Serb. Chem. Soc., **67**, 499-506.

Ramos, A.J., Hernández, E., Plá-Delfina, J.M., Merino, M., (1996),
Intestinal absorption of zearalenone and *in vitro* study of non-nutritive sorbent materials,
Int. J. Pharm., **128**, 129-137.

Rand, B., Pecenć, E., Goodwin, J.W., Smith, R.W., (1980),
Investigation into the existence of edge-face coagulated structures in Na-montmorillonite suspensions,
J. Chem. Soc., Faraday Trans. I, **76**, 225-235.

Räsänen, E., Antikainen, O., Yliruusi, J., (2003),
A new method to predict flowability using a microscale fluid bed,
AAPS Pharm. Sci. Technol., **4**, Article 53.

Rawle, A., (2003),
Basic principles of particle size analysis,
Technical note, Malvern Instrumentation, Worchester.

Reddy, K.R., Mutalik, S., Reddy, S., (2003),
Once-daily sustained release matrix tablets of nicorandil: formulation and *in vitro* evaluation,
AAPS Pharm. Sci. Technol., **4**, Article 61.

Reier, G.E., (2002),
Avicel® PH Microcrystalline cellulose, NF, Ph Eur., JP, BP,
http://www.fmcbiopolymer.com/Portals/bio/content/Docs/Pharmaceuticals/Problem%20Solver/Section%2011%20Avicel%20PH.pdf. Accessed: 15/01/2004.

Reier, G.E., Shangraw, R., (1966),
Microcrystalline cellulose in tabletting,
J. Pharm. Sci., **55**, 510-514.

Reimerdes, D., (1993),
The near future of tablet excipients,
Manuf. Chem., **64**, 14-15.

Reimerdes, D., Aufmuth, K.P., (1992),
Tabletting with co-processed lactose-cellulose excipients,
Manuf. Chem., **63**, 21-24.

Reus-Medina, M., Kumar, V., (2006),
Preparation, characterization and tabletting properties of a new cellulose-based pharmaceutical aid,
Int. J. Pharm., **235**, 129-140.

Rezwan, K., (1996),
Ceramic nanotechnology: adjusting suspension properties, [Online],
http://www.bioceramics.uni-bremen.de. Accessed: 29/01/2007.

Riippi, M., Antikainen, O., Niskanen, T., Yliruusi, J., (1998),
The effect of compression force on surface structure, crushing strength, friability and disintegration time of erythromycin acistrate tablets,
Eur. J. Pharm. Biopharm., **46**, 339-345.

Ritter, A., Sucker, H.B., (1980),
Studies of the variables that affect tablet capping,
Pharm. Technol., **3**, 57-65.

Roberts, R.J., Rowe, R.C., (1985),
The effect of punch velocity on the compaction of a variety of materials,
J. Pharm. Pharmacol., **37**, 377-389.

Robinson, R.L., Hollenbeck, R.G., (1991),
Manufacture of spherical acetaminophen pellets: comparison of rotary processing with multiple-step extrusion and spheronisation,
Pharm. Technol., **15**, 48-56.

Rouquerol, R., Avnir, D., Fairbridge, C.W., Everett, D.H., Haynes, J.H., Pernicone, N., Ramsay, J.D.F., Sing, K.S.W., Unger, K.K., (1994),
Recommendations for the characterization of porous solids,
Pure Appl. Chem., **66**, 1739-1758.

Rowe, R.C., (1978),
The effect of some formulation and process variables on the surface roughness of film coated tablets,
J. Pharm. Pharmacol., **30**, 669-672.

Rowe, R.C., (1979),
Surface roughness measurements on both uncoated and film-coated tablets,
J. Pharm. Pharmacol., **31**, 473-474.

Rowe, R.C., Sheskey, P.J., Weller, P.J., (Eds.), (2003),
Handbook of Pharmaceutical Excipients, 4th Edition,
Pharmaceutical Press and the American Pharmaceutical Association, London and Washington.

Rowe, R.C., Sheskey, P.J., Owen, S.C., (Eds.), (2005),
Handbook of Pharmaceutical Excipients, 5th Edition,
Pharmaceutical Press and the American Pharmaceutical Association, London and Washington.

Rubinstein, M.H., (1987),
Preface,
pp. 7-8 in: *Pharmaceutical Technology: Tableting Technology, Volume 1*, Ellis Horwood Ltd., Chichester.

Rudraraju, V.S., Wyandt, C.M., (2004a),
Rheological characterisation of microcrystalline cellulose/ sodium carboxymethyl cellulose hydrogels using a controlled stress rheometer: part 1,
Int. J. Pharm., **292**, 53-61.

Rudraraju, V.S., Wyandt, C.M., (2004b),
Rheological characterisation of microcrystalline cellulose/ sodium carboxymethyl cellulose hydrogels using a controlled stress rheometer: part 2,
Int. J. Pharm., **292**, 63-73.

Rue, P.J., Rees, J.E., (1978),
Limitations of the Heckel relation for predicting powder compaction mechanisms,
J. Pharm. Pharmacol., **30**, 642-643.

Ruiz, R., del Moral, J.C., Pesquera, C., Benito, I., González, F., (1996),
Reversible folding in sepiolite: study by thermal and textural analysis,
Thermochim. Acta, **279**, 103-110.

Ruiz-Huitsky, E., (2001),
Molecular access to intracrystalline tunnels of sepiolite,
J. Mater. Chem., **11**, 886-891.

Ruiz-Hitzky, E., Darder, M., Aranda, P., (2005),
Functional biopolymer nanocomposites based on layered solids,
J. Mater. Chem., **15**, 3650-3662.

Ryan, C., (2006),
Potential applications of halloysite for improved topical drug delivery,
PhD. Thesis, Trinity College, University of Dublin.

Rytwo, G., Nir, S., Margulies, L., Casal, B., Merino, J., Ruiz-Huitsky, E., Serratosa, J.M., (1998),
Adsorption of monovalent organic cations on sepiolite; experimental results and model calculations,
Clays Clay Miner., **46**, 340-348.

Rytwo, G., Nir, S., Crespin, M., Marguiles, L., (2000),
Adsorption and interactions of methyl green with montmorillonite and sepiolite,
J. Colloid Interface Sci., **222**, 12-19.

Sabah, E., Çelik, M.S., (2005),
Sepiolite: An effective bleaching adsorbent for the physical refining of degummed rapeseed oil,
J. Am. Oil Chem. Soc., **82**, 911-916.

Sabah, E., Turan, M., Çelik, M.S., (2002),
Adsorption mechanism of cationic surfactants onto acid- and heat-activated sepiolite,
Water Res., **36**, 3957-3964.

Salako, M., Podczek, F., Newton, J.M., (1998),
Investigations into the deformability and tensile strength of pellets,
Int. J. Pharm., **168**, 49-57.

Salter, A.E., (2003),
Use of halloysite for agrochemical applications,
PhD. Thesis, Trinity College, University of Dublin.

Salvador, R., Casal, B., Yates, M., Martín-Luengo, M.A., Ruiz-Huisky, E., (2002),
Microwave decomposition of a chlorinated pesticide (Lindane) supported on modified sepiolites,
Appl. Clay Sci., **22**, 103-113.

Samyn, J.C., Jung, W.Y., (1967),
Negative thixotropy in flocculated clay suspensions,
J. Pharm. Sci., **56**, 188-191.

Sanchez-Martin, M.J., Rodriguez-Cruz, M.S., Andrades, M.S., Sanchez-Camazano, M., (2005),
Efficiency of different clay minerals modified with a cationic surfactant in the adsorption of pesticides: Influence of clay type and pesticide hydrophobicity,
Appl. Clay Sci., **31,** 216-228.

Santarén, J., (1993),
Sepiolite: a mineral thickener and rheology additive,
Modern Paint and Coatings, September, 63-70.

Santarén, J., (1996),
Sepiolite - the Spanish special clay,
Ind. Clays, January, 27-35.

Santarén, J., Alvárez, A., (1994),
Assessment of the health effects of mineral dusts: the sepiolite case,
Ind. Miner., **319**, 101-114.

Sardi, L., Martelli, G., Escribano, F., Parazza, P., Parisini, P., (2004),
The effects of sepiolite-SPLF on piglet and heavy pig production,
Ital. J. Anim. Sci., **3**, 225-234.

Schmidt, P.C., (1999),
Kollidon® - a review on its use in granulation,
BASF ExAct, **2**, 5-13.

Schmidt, P.C., Rubensdörfer, C.J., (1994a),
Evaluation of Ludipress as a multipurpose excipient for direct compression. Part I: Powder characteristics and tabletting properties,
Drug Dev. Ind. Pharm., **20**, 2899-2925.

Schmidt, P.C., Rubensdörfer, C.J., (1994b),
Evaluation of Ludipress as a multipurpose excipient for direct compression. Part II: Interactive blending and tabletting with micronised glibenclamide,
Drug Dev. Ind. Pharm., **20**, 2927-2952.

Schnell, T.C., Lindemann, M.D., Kornegay, E.T., Blodgett, D.J., Doerr, J.A., (1993),
Effectiveness of different types of clay for reducing the detrimental effects of Aflatoxin-contaminated diets on performance and serum profiles of weanling pigs,
J. Anim. Sci., **71**, 1226-1231.

Schroder, M., Kleinebubbe, P., (1995),
Influence of formulation parameters in dissolution of propyphenazone pellets,
Eur. J. Pharm. Biopharm., **41**, 382-387.

Seitavuopio, P., Rantanen, J., Yliruusi, J., (2003),
Tablet surface characterization by various imaging techniques,
Int. J. Pharm., **254**, 281-286.

Serna, C., Ahlrichs, J.L., Serratosa, J.M., (1975a),
Sepiolite anhydride and crystal folding,
Clays Clay Miner., **22**, 285-293.

Serna, C., Ahlrichs, J.L., Serratosa, J.M., (1975b),
Folding in sepiolite crystals,
Clays Clay Miner., **23**, 452-457.

Serna, C., Fernández-Alvarez, T., (1974),
Adsorción de hidrocarburos en sepiolita. I. Penetración intracristalina,
Anal. Quim., **70**, 760

Serna, C.J., Van Scoyoc, G.E., (1979),
Infrared study of sepiolite and palygorskite surfaces,
Proc. Int. Clay Conf. Oxford, pp. 120.

Shah, V.P., Tsong, Y., Sathe, P., (1998),
In vitro dissolution profile comparison – statistics and analysis of the similarity factor, f_2,
Pharm. Res., **15**, 889-896.

Shah, V.P., Tsong, Y., Sathe, P., Williams, R.L.,
Dissolution profile comparison using similarity factor, f_2, [Online],
http://www.dissolutiontech.com/DTresour/899Art/DissProfile.html.
Accessed: 10/10/2006.

Shahjahan, M., Islam, I., (1998),
Preliminary evaluation of Shilajit as a suspending agent in antacid suspensions,
Drug Dev. Ind. Pharm., **24**, 1109-1112.

Shainberg, L., Otoh, H., (1968),
Size and shape of montmorillonite particles saturated with Na/Ca ions,
Isr. J. Chem., **6**, 251-259.

Shangraw, R.F., (1989),
Compressed tablets by direct compression,
pp. 195-246 in: *Pharmaceutical Dosage Forms: Tablets, Volume 1*, Lieberman, H.A., Lachman, L., Schwartz, J.B., (Eds.), Marcel Dekker, New York.

Shangraw, R.F., Dermarest, D.A., (1993),
Survey of current practices in the formulation and manufacture of tablets and capsules,
Pharm. Technol., **17**, 32-44.

Shangraw, R.F., Wallace, J.W., Bowers, F.M., (1981),
Morphology and functionality in tablet excipients for direct compression,
Pharm. Technol., **5**, 69-78.

Sharpe, S.A., Celik, M., Newman, A.W., Brittain, H.G., (1997),
Physical characterisation of the polymorphic variations of magnesium stearate and magnesium palmitate hydrate species,
Structural Chem., **8**, 78-84

Shaw, L.R., Irwin, W.J., Grattan, T.J., Conway, B.R., (2005),
The role of gastric mucus as a barrier to the absorption of ibuprofen or paracetamol and the effects of co-administered antacids and modified pH,
Int. J. Pharm., **290**, 145-154.

Sheen, C.L., Dillon, J.F., Bateman, D.N., Simpson, K.J., MacDonald, T.M., (2002),
Paracetamol toxicity: epidemiology, prevention and costs to the health care system,
Q. J. Med., **95**, 609-619.

Shiromani, P.K., (2006),
Tabletting tips,
Pharma and Bio Ingredients, January, 30-34.

Shivanand, P., Sprockel, O.L., (1992),
Compaction behaviour of cellulose polymers,
Powder Technol., **69**, 177-184.

Silcom, (2006),
Particle collisions and mean-free path, [Online],
http://www.silcom.com/~aludwig/Physics/Particle_collisions.htm.
Accessed: 10/01/2007.

Silvennoinen, R., Peiponen, K.E., Hyvärinen, V., Raatikainen, P., Paronen, P., (1999),
Optical surface roughness study of starch acetate compacts,
Int. J. Pharm., **182**, 213-220.

Simons, S.J.R., Rossetti, D., Pagliai, P., Ward, R., Fitzpatrick, S., (2005),
The relationship between surface properties and binder performance in granulation,
Chem. Eng. Sci., **60**, 4055-4060.

Simonton, T.C., Komarneni, S., Roy, R., (1988),
Gelling properties of sepiolite versus montmorillonite,
Appl. Clay Sci., **3**, 165-176.

Sing, K.S.W., (2004),
Characterization of porous materials: past, present and future,
Colloids Surf., **A241**, 3-7.

Singer, A., Stahr, K., Zarei, M., (1998),
Characteristics and origin of sepiolite (Meerschaum) from Central Somalia,
Clay Miner., **33**, 349-362.

Sissen, W.A., (1966),
Avicel microcrystalline cellulose – its production, properties and applications,
Avicel distributors' meeting, Geneva.

Sjöberg, M., Bergström, L., Larsson, A., Sjöström, E., (1999),
The effect of polymer and surfactant adsorption on the colloidal stability and rheology of kaolin dispersions,
Colloids Surf., **A159**, 197-208.

Smith, J.A., Jaffe, P.R., (1994),
Benzene transport through landfill liners containing organophilic bentonite,
J. Environ. Eng., **120**, 1559-1577.

Soluble Kollidon® grades (2002),
Product Information, BASF AG, Ludwigshafen.

Souto, C., Rodriguez, A., Parajes, S., Martinez-Pacheco, R., (2005),
A comparative study of the utility of two superdisintegrants in microcrystalline cellulose pellets prepared by extrusion-spheronisation,
Eur. J. Pharm. Biopharm., **61**, 94-99.

Soyeux, P., Delacourte, A., Delie, B., Lefevre, P., Boniface, B., (1998),
Influence and optimization of operating parameters with a new binder in wet granulation. I: use in powder form,
Eur. J. Pharm. Biopharm., **46**, 95-103.

Staniforth, J.N., (1987),
Powder Flow,
pp. 600-615 in: *Pharmaceutical Technology: Tabletting*, Rubinstein M.H., (Ed.), Halsted Press, New Jersey.

Staniforth, J.N., Baichwal, A.R., Hart, J.P., Heng, P.W., (1988),
Effect of addition of water on the rheological and mechanical properties of microcrystalline celluloses,
Int. J. Pharm., **41**, 231-236.

Staniforth, J.N., Rees, J.E., Kayes, J.B., Priest, R.C., Cotterill, N.J., (1981),
The design of a direct compression tabletting excipient,
Drug Dev. Ind. Pharm., **7**, 179-190.

Stanton, M.F., Layard, M., Tegeris, A., Miller, E., May, M., Morgan, E., Smith, A., (1981),
Relation of particle dimension to carcinogenicity in amphibole asbestoses and other fibrous minerals,
J. Natl. Cancer Inst., **67**, 965-975.

Steckel, H., Mindermann-Nogly, F., (2004),
Production of chitosan pellets by extrusion/ spheronisation,
Eur. J. Pharm. Biopharm., **57**, 107-114.

Stumm, W., Hohl, H., Dalang, F., (1976),
Interaction of metal ions with hydrous oxide surfaces,
Croat. Chem. Acta, **48**, 491-504.

Sugiura, M., Fukumoto, K., Inagaki, S., (1991a),
Adsorption of odorous vapors by sepiolite in ambient air,
Clay Sci., **8**, 129-145.

Sugiura, M., Fukumoto, Hayashi, H., Suzuki, T., (1991b),
Adsorption of ammonia by sepiolite in ambient air,
Clay Sci., **8**, 87-100.

Sun, A., de la Caillerie, J.B., Fripiat, J.J., (1995),
A new microporous material: aluminated sepiolite,
Microporous Mater., **5**, 135-142.

Sun, C., (2004),
A novel method for deriving the true density of pharmaceutical solids including hydrates and water-containing powders,
J. Pharm. Sci., **93**, 646-653.

Suzuki, T., Kikuchi, H., Yamamura, S., Terada, K., Yamamoto, K., (2001),
The change in the characteristics of microcrystalline cellulose during wet granulation using a high-shear mixer,
J. Pharm. Pharmacol., **53**, 609-616.

Sweetman, S.C., (2004),
Martindale: The Complete Drug Reference, 35th Edition, The Pharmaceutical Press, London.

Swierkosz, T.A., Jordan, L., McBride, M., McGough, K., Devlin, J., Botting, R.M., (2002),
Actions of paracetamol on cyclooxygenases in tissue and cell homogenates of mouse and rabbit,
Med. Sci. Monit., **8**, BR496-503.

Takka, S., (2003),
Propranolol hydrochloride – anionic polymer binding interaction,
Il Farmaco, **58**, 1051-1056.

Taylor, M.K., Ginsburg, J., Hickey, A., Gheyas, F., (2000),
Composite method to quantify powder flow as a screening method in early tablet or capsule formulation development,
AAPS Pharm. Sci. Technol., **1**, Article 18.

Tekin, N., Dinçer, A., Demirbas, Ö., Alkan, M., (2006),
Adsorption of cationic polyacrylamide onto sepiolite,
J. Hazard. Mater., **134**, 211-219.

Thermexcel, (2003),
Physical characteristics of water at atmospheric pressure, [Online],
http://www.thermexcel.com/english/tables/eau_atm.htm. Accessed:10/10/2006.

Thiesson, P.A., (1942),
Wechselseitige Adsorption von Kolloiden,
Z. Elektrochem., **48**, 675-681.

Tho, I., Sande, S.A., Kleinebudde, P., (2002),
Pectinic acid, a novel excipient for production of pellets by extrusion spheronisation: preliminary studies,
Eur. J. Pharm. Biopharm., **54**, 95-99.

Tho, I., Sande, S.A., Kleinebudde, P., (2003),
Disintegrating pellets from a water-insoluble pectin derivative produced by extrusion-spheronisation,
Eur. J. Pharm. Biopharm., **56**, 371-380.

Thomas, S., Fisher, B., Fram, P., Waring, M., (1998),
Odour absorbing dressings, a comparative laboratory study, [Online],
http://www.worldwidewounds.com/1998/march/Odour-Absorbing-Dressings/odour-absorbing-dressings.html.
Accessed: 29/04/2005.

Thommes, M., Kleinebudde, P., (2006a),
Use of κ-carrageenan as alternative pelletisation aid to microcrystalline cellulose in extrusion/spheronisation. I. Influence of type and fraction of filler,
Eur. J. Pharm. Biopharm., **63**, 59-67.

Thommes, M., Kleinebudde, P., (2006b),
Use of κ-carrageenan as alternative pelletisation aid to microcrystalline cellulose in extrusion/spheronisation. II. Influence of drug and filler type,
Eur. J. Pharm. Biopharm., **63**, 68-75.

Tobyn, M.J., McCarthy, G.P., Staniforth, J.N., Edge, S., (1998),
Physicochemical comparison between microcrystalline cellulose and silicified microcrystalline cellulose,
Int. J. Pharm., **169**, 183-194.

Tolsa, (1999),
Pansil-Pangel product brochure IT-140-02-ENG,
Grupo Tolsa, Madrid.

Tomassetti, M., Catalani, A., Rossi, V., Vecchio, S., (2004),
Thermal analysis study of the interactions between acetaminophen and excipients in solid dosage forms and in some binary mixtures,
J. Pharm. Biomed. Anal., **37**, 949-955.

Tombácz, E., Szekeres, M., (2004),
Colloidal behaviour of aqueous montmorillonite suspensions: the specific role of pH in the presence of indifferent electrolytes,
Appl. Clay Sci., **27**, 75-94.

Tombácz, E., Szekeres, M., (2006),
Surface charge heterogeneity of kaolinite in aqueous suspension in comparison with montmorillonite,
Appl. Clay Sci., **34**, 105-124.

Torres-Ruiz, J., López-Galindo, A., González-López, J.M., Delgado, A., (1994),
Geochemistry of Spanish sepiolite-palygorskite deposits: genetic considerations based on trace elements and isotopes,
Chem. Geol., **112**, 221-245.

Toyoshima, K., Yasumura, M., Ohnishi, N., Ueda, Y., (1988),
Quantitative evaluation of tablet sticking by surface roughness measurement,
Int. J. Pharm., **46**, 211-215.

Tsai, T., Wu, J.S., Ho, H., Sheu, M.T., (1998),
Modification of physical characteristics of microcrystalline cellulose by co-drying with β-cyclodextrin,
J. Pharm. Sci., **87**, 117-122.

UBM System Reference Guide, UBM measurement and analysis software for Windows, Rev 1.3, UBM Messtechnik GmbH, Ettlingen, 1996.

U.S. Geological Survey,
Open File Report 01-041: Identification of sepiolite - X-rays of Oriented Aggregates, [Online],
http://pubs.usgs.gvo/of/of01-041/htmldocs/flow/d4/d4f1.htm. Accessed 1/12/2003.

United States Pharmacopeia and National Formulary, (2006),
United States Pharmacopeia, 29th Edition, The National Formulary, 24th Edition, United States Pharmacopeial Convention, Inc., USA.

Usui, S., (1984),
Electrical Phenomena at Interfaces; Fundamentals, measurements and applications, pp. 15-46 In: *Surfactant Science Series*, *Volume 15*, Kitahara, A., Watanabe, A., (Eds.), Dekker, New York.

Valentín, J.L., López-Manchado, M.A., Rodríguez, A., Posadas, P., Ibarra, L., (2006),
Novel anhydrous unfolded structure by heating of acid pre-treated sepiolite,
Appl. Clay Sci., In Press, doi:10.1016/j.clay.2006.10.005.

Vanderbilt Report no. 920, (2004),
Rheology control additives, [Online],
http://rtvanderbilt.com/No920CD.pdf. Accessed: 09/01/2005.

Vanderhoff, J.W., (1996),
Theory of colloids,
pp. 91-152 in *Pharmaceutical Dosage Forms: Disperse Systems, Volume 1*, 2nd Edition, Lieberman, H.A., Rieger, M.M., Banker, G.S., (Eds.), Marcel Dekker Inc., New York.

van der Voort Maarschalk, K., Bolhuis, G.K., (1998),
Improving properties of materials for direct compression,
Pharm. Tech. Europe, **10**, 28-34.

Van der Zwan, J., Siskens, C.A.M., (1982),
The compaction and mechanical properties of agglomerated materials,
Powder Technol., **33**, 43-54.

Van Doorne, H., Leijen, J.B., (1994),
The preservation of some oral liquid preparations,
Pharm. World Sci., **16**, 18-21.

Vane, L.M., Zang, G.M., (1997),
Effect of aqueous phase properties on clay particle zeta potential and electro-osmotic permeability: implications for electro-kinetic soil remediation processes,
J. Hazard. Mater., **55**, 1-22.

Van Kamp, H.V., Bolhuis, G.K., de Boer, A.H., Lerk, C.F., Lie-A-Huen, L., (1986),
The role of water uptake on tablet disintegration. Design of an improved method for penetration measurements,
Pharm. Acta Helv., **61**, 22-29.

van Olphen, H., (1977),
An Introduction to Clay Colloid Chemistry, 2nd Edition, Wiley, New York.

Van Schuylenborgh, J., (1951),
The electrokinetic behaviour of freshly prepared γ-AlOOH, α- and γ-$Al(OH)_3$,
Rec. Trav. Chim., **70**, 985-988.

Verwey, E.J.W., Overbeek, J.T.G., (1948),
Theory of the Stability of Lyophobic Colloids: The Interaction of Sol Particles having an Electrical Double Layer, Elsevier, Amsterdam.

Vicente-Rodríguez, M.A., Suarez, M., Bañares-Munoz, M.A., Lopez-Gonzalez, J., (1996),
Comparative FT-IR study of the removal of octahedral cations and structural modifications during acid treatment of several silicates,
Spectrochim. Acta, **A52**, 1685-1694.

Vico, L.I., (2003),
Acid-base behaviour and Cu^{2+} and Zn^{2+} complexation properties of the sepiolite/water interface,
Chem. Geol., **198**, 213-222.

Viseras, C., Aguzzi, A., Cerezo, P., López-Galindo, A., (2006),
Uses of clay minerals in semisolid health care and therapeutic products,
Appl. Clay Sci., In Press, doi:10.1016/j.clay.2006.07.006.

Viseras, C., López-Galindo, A., (1999),
Pharmaceutical applications of some Spanish clays (sepiolite, palygorskite, bentonite): some preformulation studies,
Appl. Clay Sci., **14**, 69-82.

Viseras, C., Meeten, G.H., López-Galindo, A., (1999),
Pharmaceutical grade phyllosilicate dispersions: the influence of shear history on floc structure,
Int. J. Pharm., **217**, 201-213.

Vučelić, D., Simić, D., Kovačević, O., Dojčinović, M., Mitrović, M., (2002),
The effects of grinding on the physicochemical characteristics of white sepiolite from Golesh,
J. Serb. Chem. Soc., **67**, 197-211.

Wagner, J.C., Pooley, F.D., Gibbs, A., Lyons, J., Sheers, G., Moncrieff, C.B., (1986),
Inhalation of china stone and china clay dusts: relationship between the mineralogy of dust retained in the lungs and pathological changes,
Thorax, **41**, 190-196.

Wang, J., Li, W., Gao, L., (2000),
The role of dispersant in the formation of spherical ZrO_2 particles prepared by heating of alcohol aqueous salt solutions,
J. Mater. Sci. Lett., **19**, 159-161.

Watanabe, W., Banno, K., Sugiura, S., (2000),
Calcined sepiolite-supported Pt/Fe catalyst,
Appl. Clay Sci., **16**, 59-71.

Watano, S., Furukawa, J., Miyanami, K., Osako, Y., (2001),
Quantitative evaluation of kneading and extrusion processes by pressure transmission characteristics of wet kneaded masses,
Adv. Powder Technol., **12**, 427-441.

Washburn, E.W., (1921),
The dynamics of capillary flow,
Phys. Rev., **17**, 273-283.

Webb, P.A., (2001),
An introduction to the physical characterization of materials by mercury intrusion porosimetry with emphasis on reduction and presentation of experimental data,
Micromeritics® Instrument Corporation, Norcross, Georgia.

Webb, P.A., Orr, C., (1997),
Analytical Methods in Fine Particle Technology,
Micromeritics® Instrument Corporation, Norcross, Georgia.

Webelements, (2007a),
Compounds of Iron, [Online],
http://www.webelements.com/webelements/compounds/text/Fe/Fe2O3-1309371.html. Accessed: 10/01/2007.

Webelements, (2007b),
Compounds of Zinc, [Online],
http://www.webelements.com/webelements/compounds/text/Zn/O1Zn1-1314132.html. Accessed: 10/01/2007.

Weir, M.R., Rutinduka, E., Detellier, C., Feng, C.Y., Wang, Q., Matsuura, T., Le Van Mao, R., (2001),
Fabrication, characterization and preliminary testing of all-inorganic ultrafiltration membranes composed entirely of a naturally occurring sepiolite clay mineral,
J. Membr. Sci., **182**, 41-50.

Wells, J. I., (1988),
Pharmaceutical Preformulation: The Physicochemical Properties of Drug Substances, 1st Edition, Ellis Horwood, Chichester.

Westermarck, S., Juppo, A.M., Kervinen, L., Yliruusi, J., (1999),
Microcrystalline cellulose and its microstructure in pharmaceutical processing,
Eur. J. Pharm. Biopharm., **48**, 199-206.

Wilson, I., (2004),
Special clays from attapulgite to sepiolite,
Ind. Miner., **446**, November, 54-61.

Wissing, S., Craig, D.Q., Barker, S., Moore, W.D., (2000),
An investigation into the use of stepwise isothermal high sensitivity DSC as a means of detecting drug-excipient incompatibility,
Int. J. Pharm., **199**, 141-150.

Wu, J., Ho, H., Sheu, M., (2001),
Influence of wet granulation and lubrication on the powder and tabletting properties of co-dried product of microcrystalline cellulose with beta-cyclodextrin,
Eur. J. Pharm. Biopharm., **51**, 63-69.

Xiao, C., Lu, Y., Liu, H., Zhang, L., (2001),
Preparation and characterization of konjac glucomannan and sodium carboxymethylcellulose blend films,
J. Appl. Polym. Sci., **80**, 26-31.

Yalçin, H., Bozkaya, O., (2004),
Ultramafic-rock-hosted vein sepiolite occurrences in the Ankara ophiolitic mélange, Central Anatolia, Turkey,
Clays Clay Miner., **52**, 227-239.

Yalçm, T., Alemdar, A., Ece, Ö.I., Güngör, N., (2002),
The viscosity and zeta potential of bentonite dispersions in presence of anionic surfactants,
Mater. Letters, **57**, 420-424

Yebra-Rodríguez, A., Martín-Ramos, J.D., del Rey, F., Viseras, C., López-Galindo, A., (2003),
Effect of acid treatment on the structure of sepiolite,
Clay Miner., **38**, 353-360.

York, P., (1992),
Crystal engineering and particle design for the powder compaction process,
Drug Dev. Ind. Pharm., **18**, 677-721.

Yu, X., Atalla, R.H., (1998),
A staining technique for evaluating the pore structure variations of microcrystalline cellulose powders,
Powder Technol., **98**, 135-138.

Zatz, J.L., Berry, J.J., Alderman, D.A., (1996),
Viscosity-imparting agents in disperse systems,
pp. 287-314 in: *Pharmaceutical Dosage Forms: Disperse Systems, Volume 1*, 2nd Edition, Lieberman, H.A., Rieger, M.M., Banker, G.S., (Eds.), Marcel Dekker Inc., New York.

Zatz, J.L., Kushla, G.P., (1996),
Gels,
pp. 399-421 in: *Pharmaceutical Dosage Forms: Disperse Systems, Volume 2*, 2nd Edition, Lieberman, H.A., Rieger, M.M., Banker, G.S., (Eds.), Marcel Dekker Inc., New York.

Zhang, Y., Law, Y., Chakrabarti, S., (2003),
Physical properties and compact analysis of commonly direct compression binders,
AAPS Pharm. Sci. Technol., **4**, Article 62.

Zografi, G., Kontny, M.J., Yang, A.Y., Brenner, G.S., (1984),
Surface area and water vapor sorption of microcrystalline cellulose,
Int. J. Pharm., **18**, 99-116.

APPENDICES

APPENDIX 1: UV calibration curves used to determine the concentration of paracetamol in solution

(1) Paracetamol in deionised water

Analytical wavelength: 257 nm

Concentration (g /100 mL) = (Absorbance – 0.0072) / 0.4339

$r^2 = 0.9999$

(2) Paracetamol in phosphate buffer pH 6.8

Analytical wavelength: 257 nm

Concentration (g /100 mL) = (Absorbance – 0.0243) / 0.4309

$r^2 = 0.9994$

APPENDIX 2: Saturation solubility of paracetamol in water at 25 °C

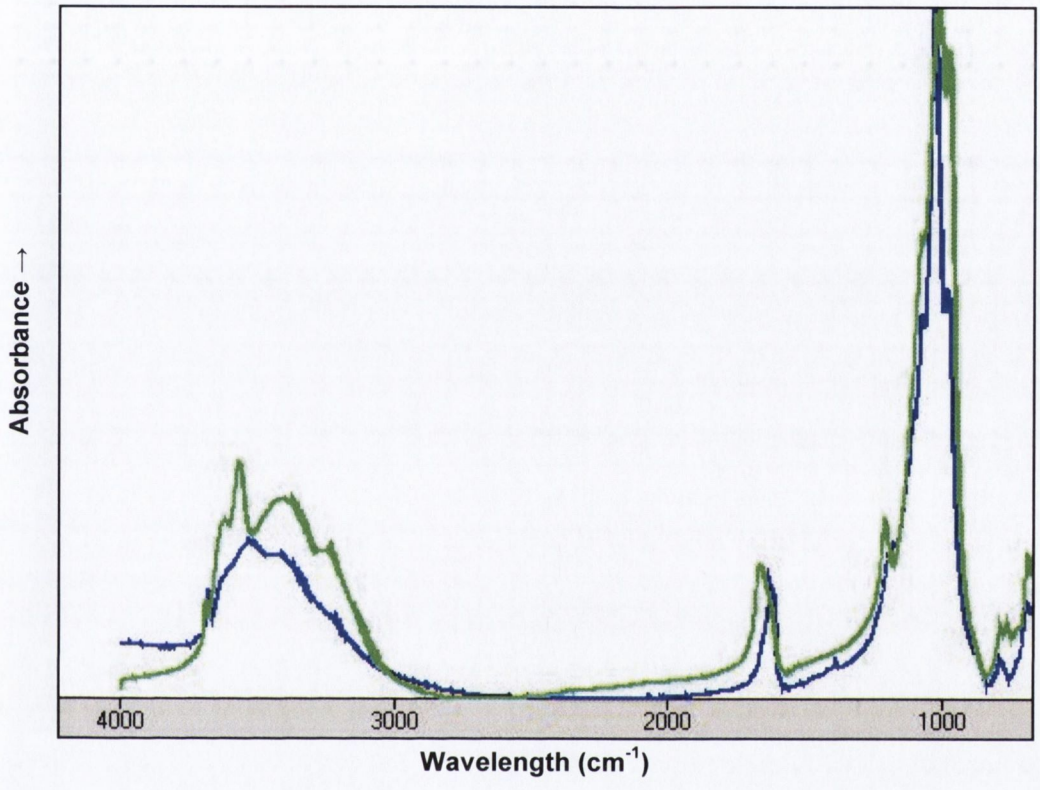
Mass dissolved after 24 h = 1.62 ± 0.13 g/ 100 mL

Mass dissolved after 48 h = 1.63 ± 0.11 g/ 100 mL

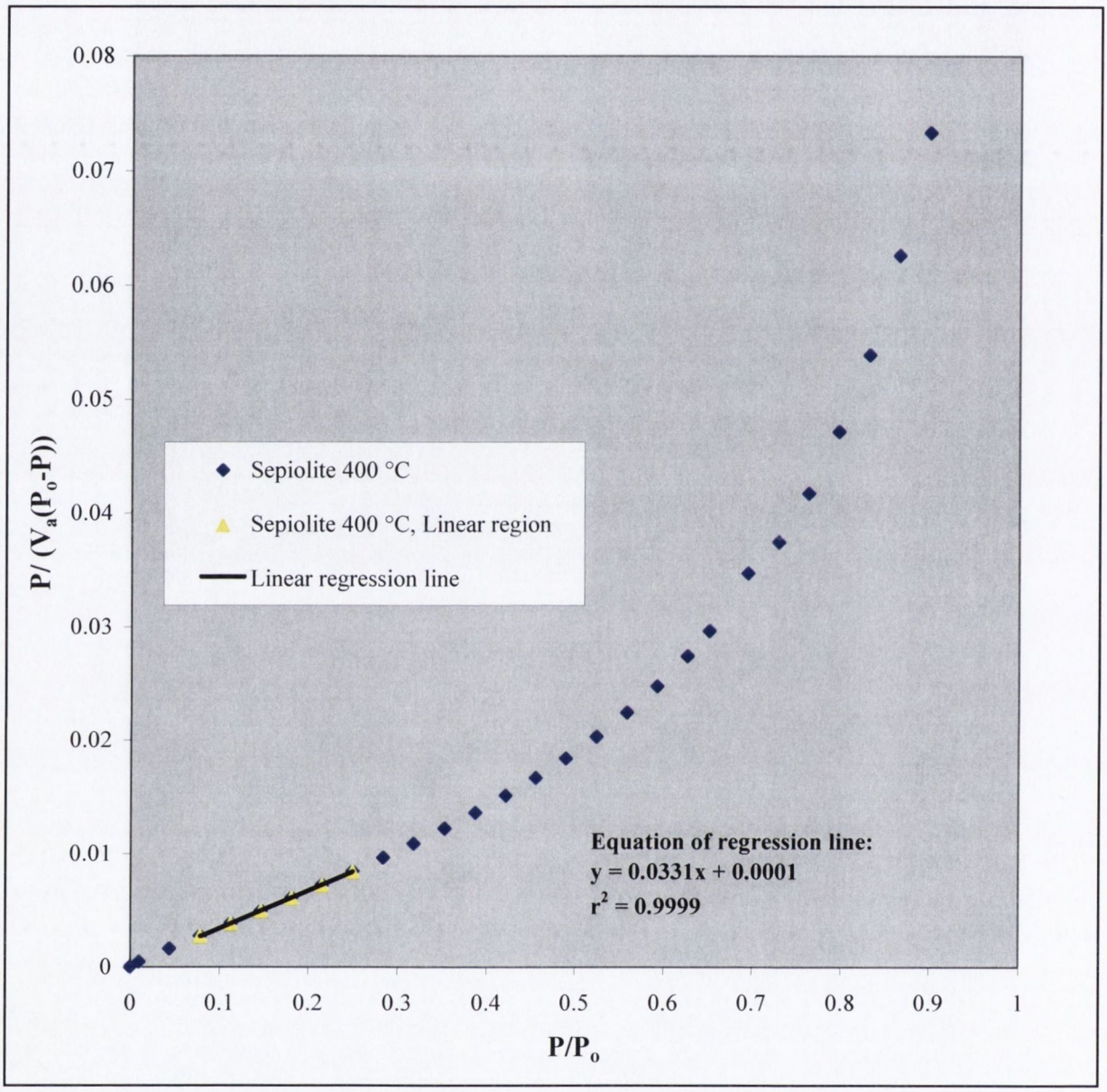
Average mass dissolved (i.e. saturation solubility) = 1.63 ± 0.17 g/ 100 mL

APPENDIX 3: FT-IR reference spectrum for sepiolite (FDM Reference Spectra)

- Reference spectrum: blue trace
- Untreated Pangel®-S9: green trace



APPENDIX 4: Sample BET transform plot (for sepiolite heated to 400 °C)



APPENDIX 5: DSC/ TGA traces used to establish sepiolite-excipient compatibility

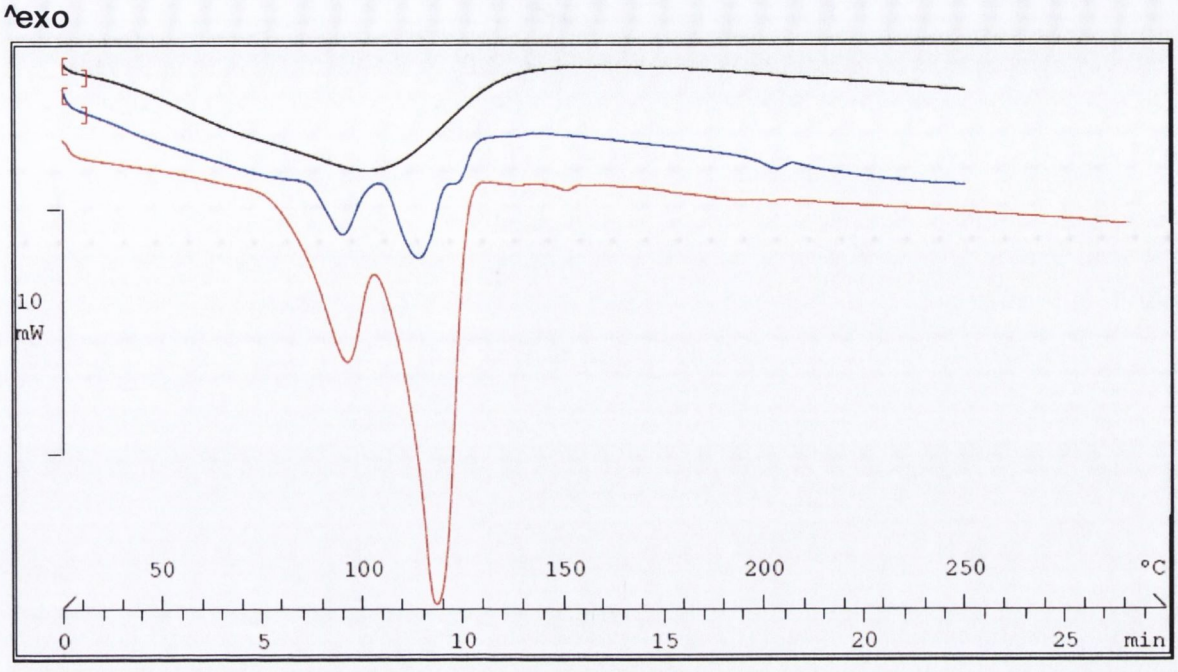


Figure A5a: DSC thermogram of sepiolite (black), magnesium stearate (red) and a 1:1 physical mixture of sepiolite and magnesium stearate (blue).

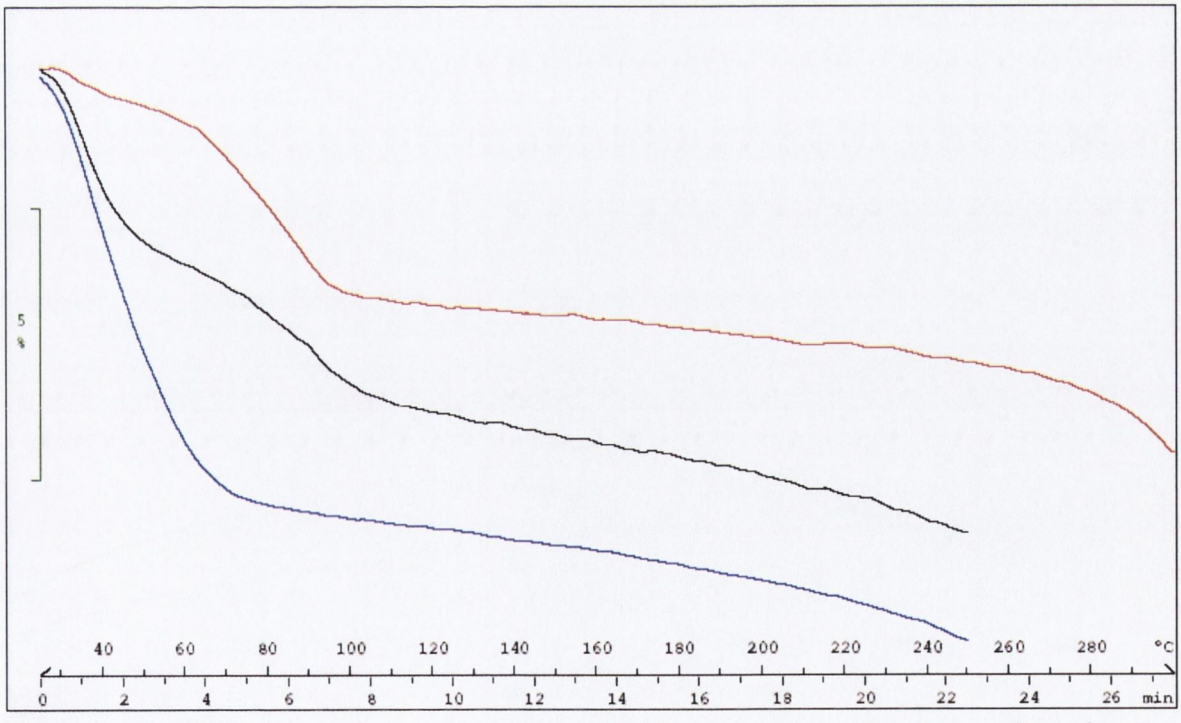


Figure A5b: TG thermogram of sepiolite (blue), magnesium stearate (red) and a 1:1 physical mixture of sepiolite and magnesium stearate (black).

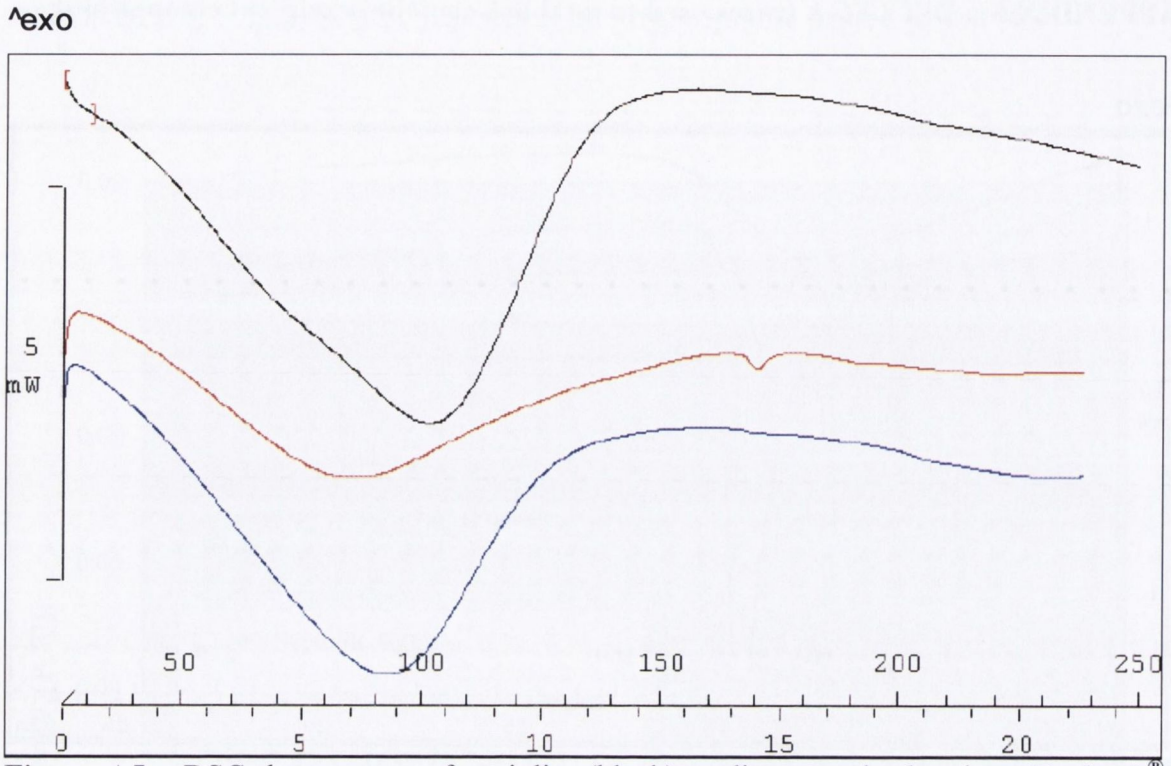


Figure A5c: DSC thermogram of sepiolite (black), sodium starch glycolate (Explotab®) (red) and a 1:1 physical mixture of sepiolite and sodium starch glycolate (blue).

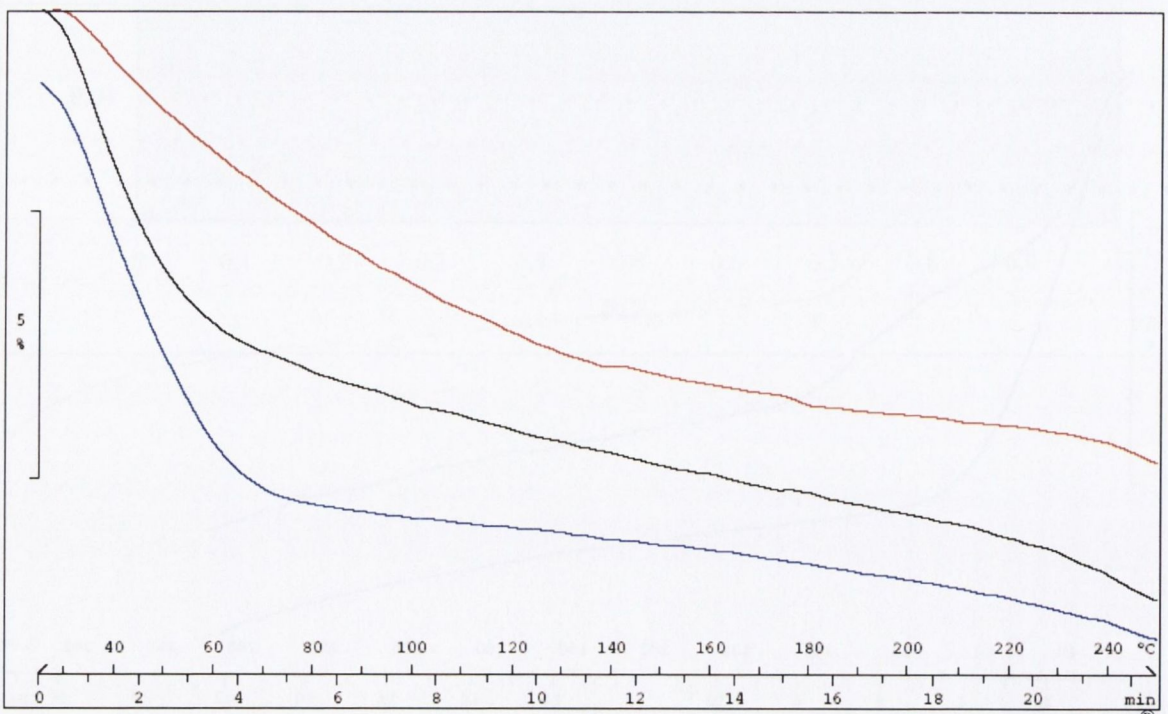


Figure A5d: TG thermogram of sepiolite (black), sodium starch glycolate (Explotab®) (red) and a 1:1 physical mixture of sepiolite and sodium starch glycolate (blue).

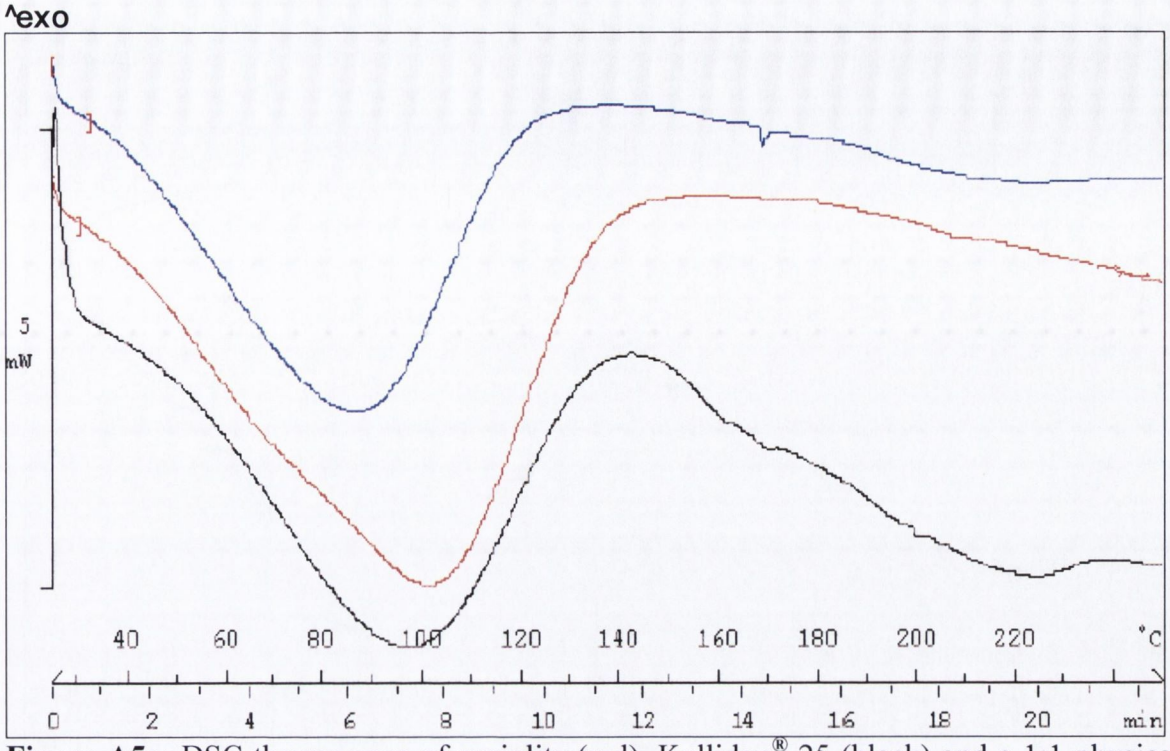


Figure A5e: DSC thermogram of sepiolite (red), Kollidon® 25 (black) and a 1:1 physical mixture of sepiolite and Kollidon® 25 (blue).

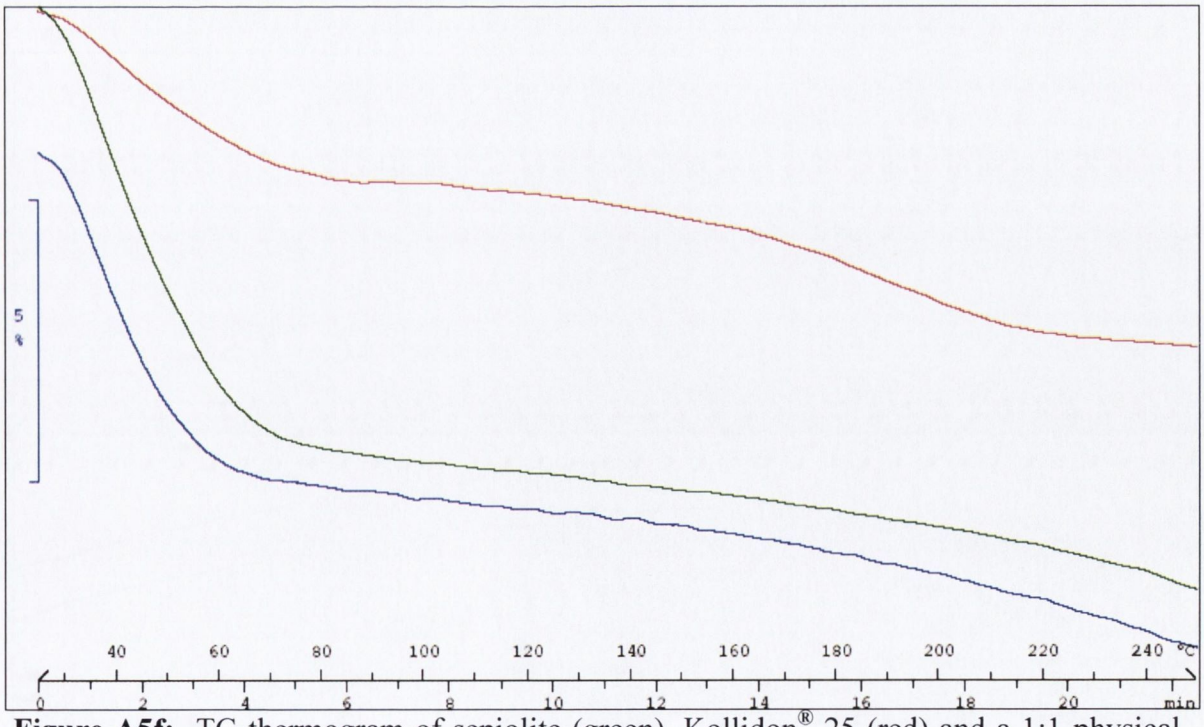


Figure A5f: TG thermogram of sepiolite (green), Kollidon® 25 (red) and a 1:1 physical mixture of sepiolite and Kollidon® 25 (blue).

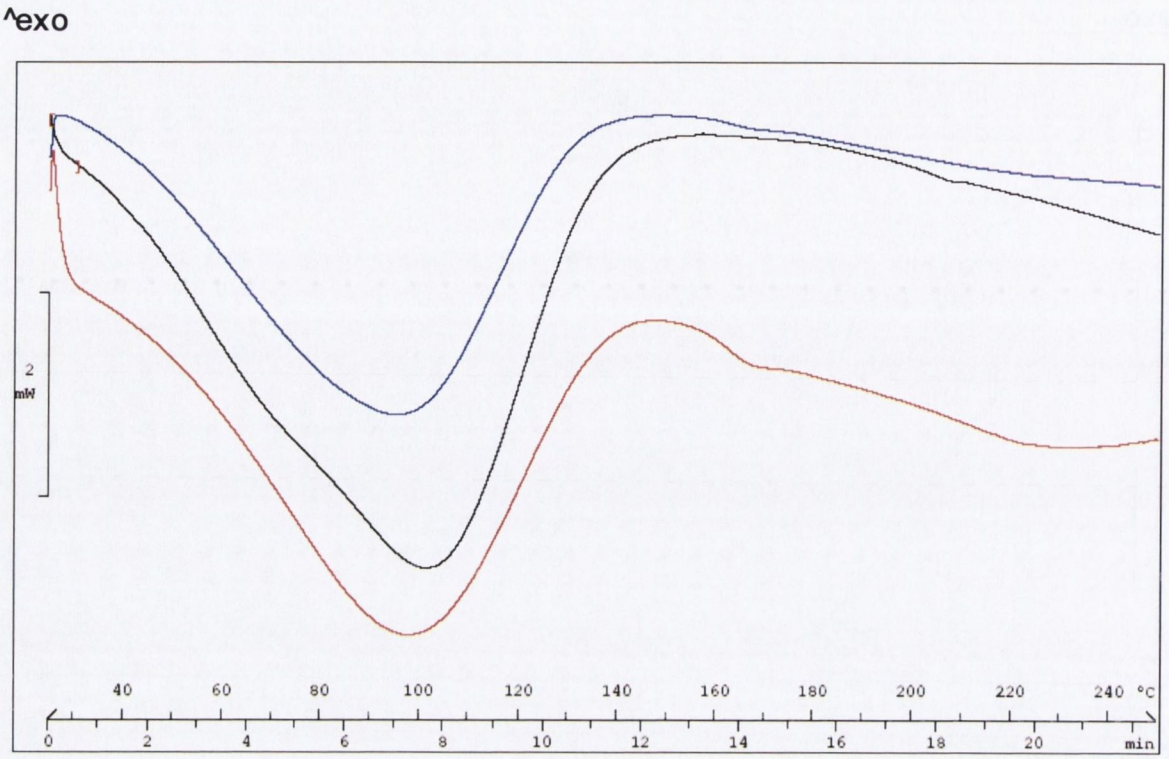


Figure A5g: DSC thermogram of sepiolite (black), Kollidon® 30 (red) and a 1:1 physical mixture of sepiolite and Kollidon® 30 (blue).

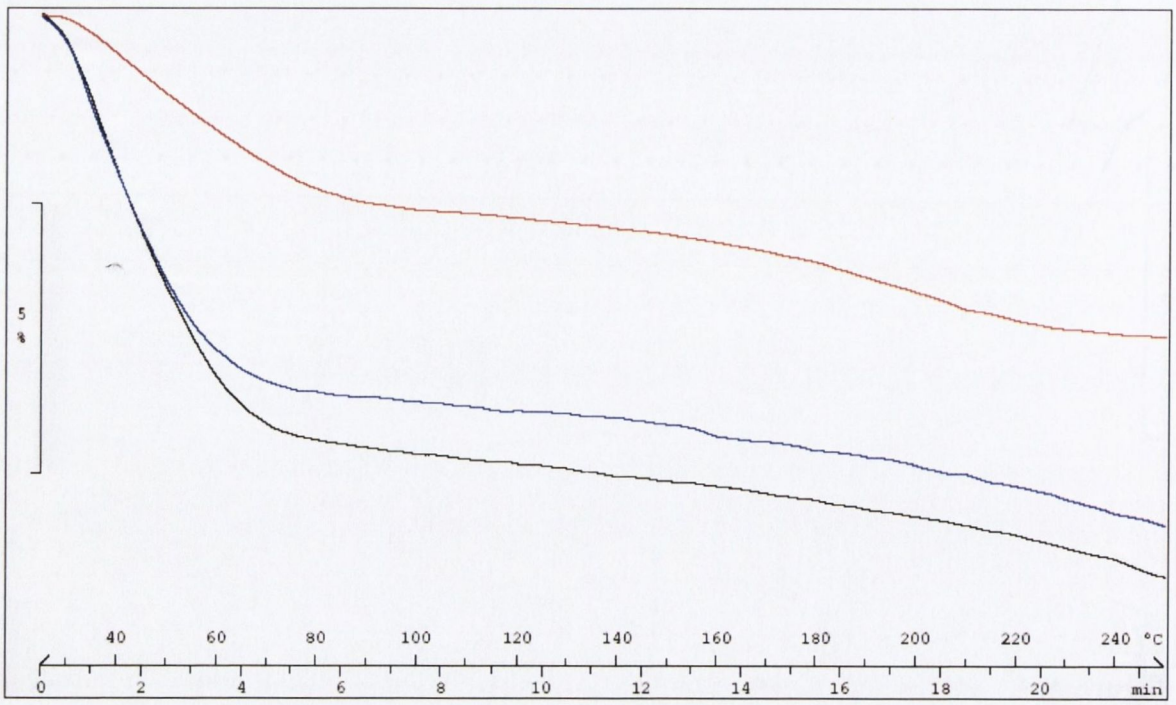


Figure A5h: TG thermogram of sepiolite (black), Kollidon® 30 (red) and a 1:1 physical mixture of sepiolite and Kollidon® 30 (blue).

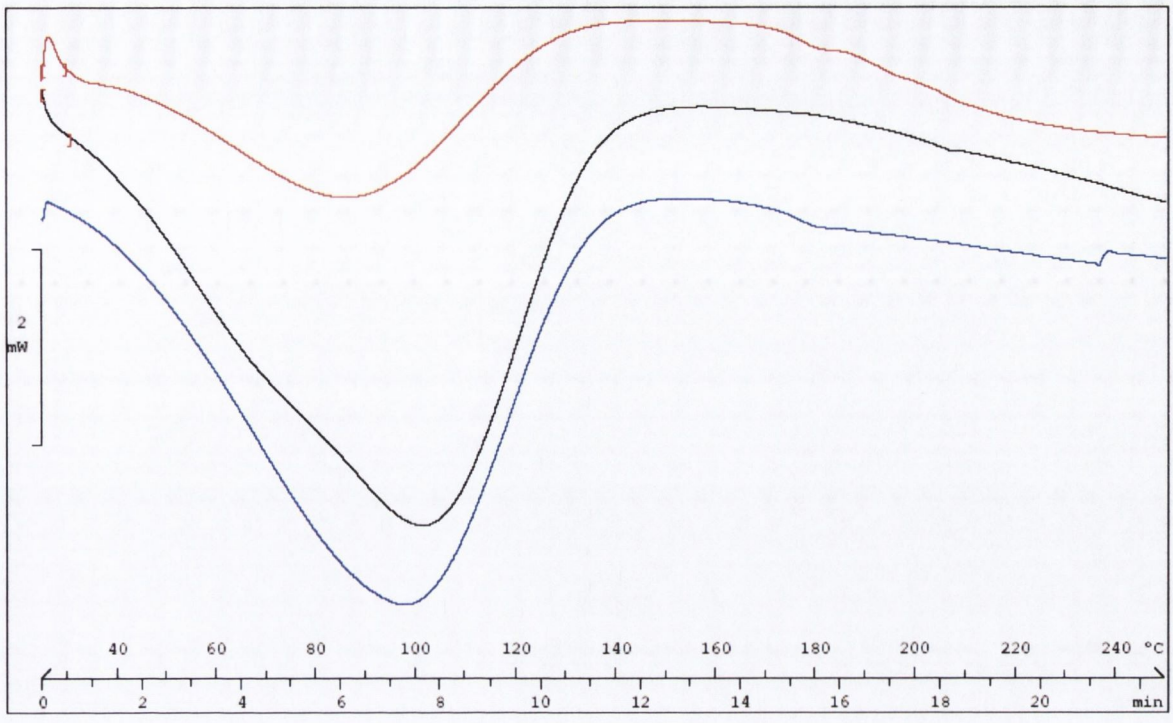


Figure A5i: DSC thermogram of sepiolite (black), Kollidon® 90F (red) and a 1:1 physical mixture of sepiolite and Kollidon® 90F (blue).

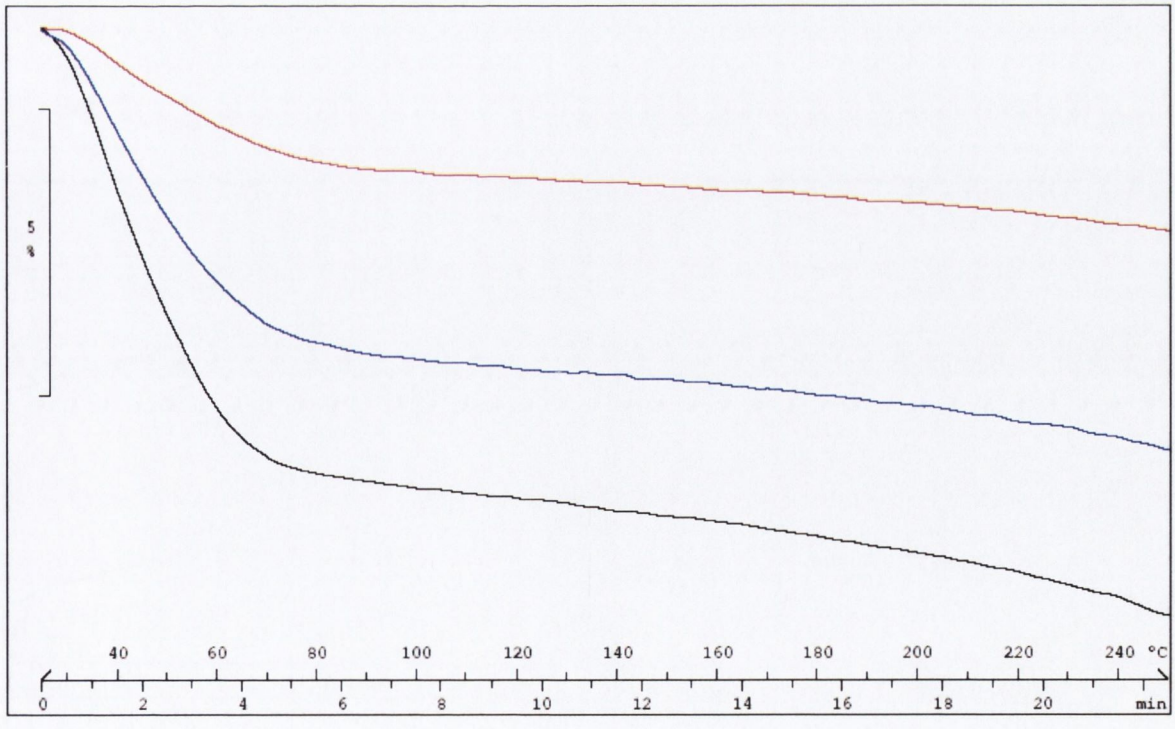


Figure A5j: TG thermogram of sepiolite (black), Kollidon® 90F (red) and a 1:1 physical mixture of sepiolite and Kollidon® 90F (blue).

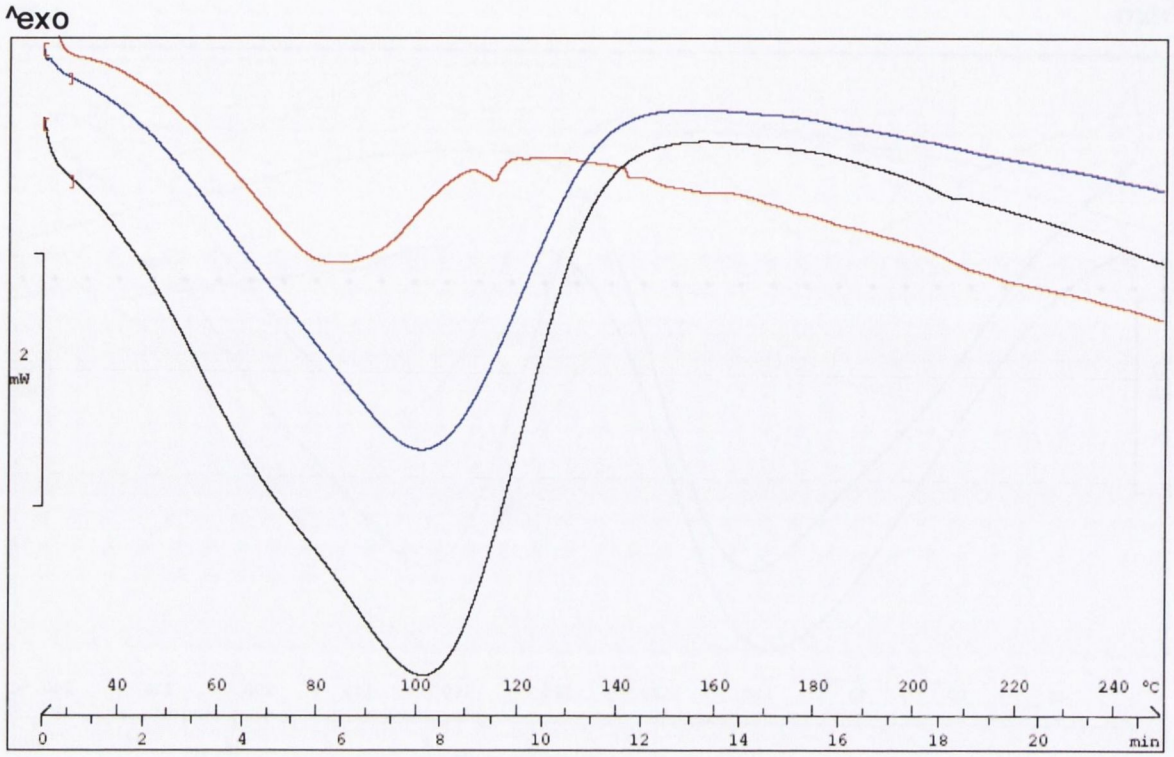


Figure A5k: DSC thermogram of sepiolite (black), Kollidon® VA 64 (red) and a 1:1 physical mixture of sepiolite and Kollidon® VA 64 (blue).

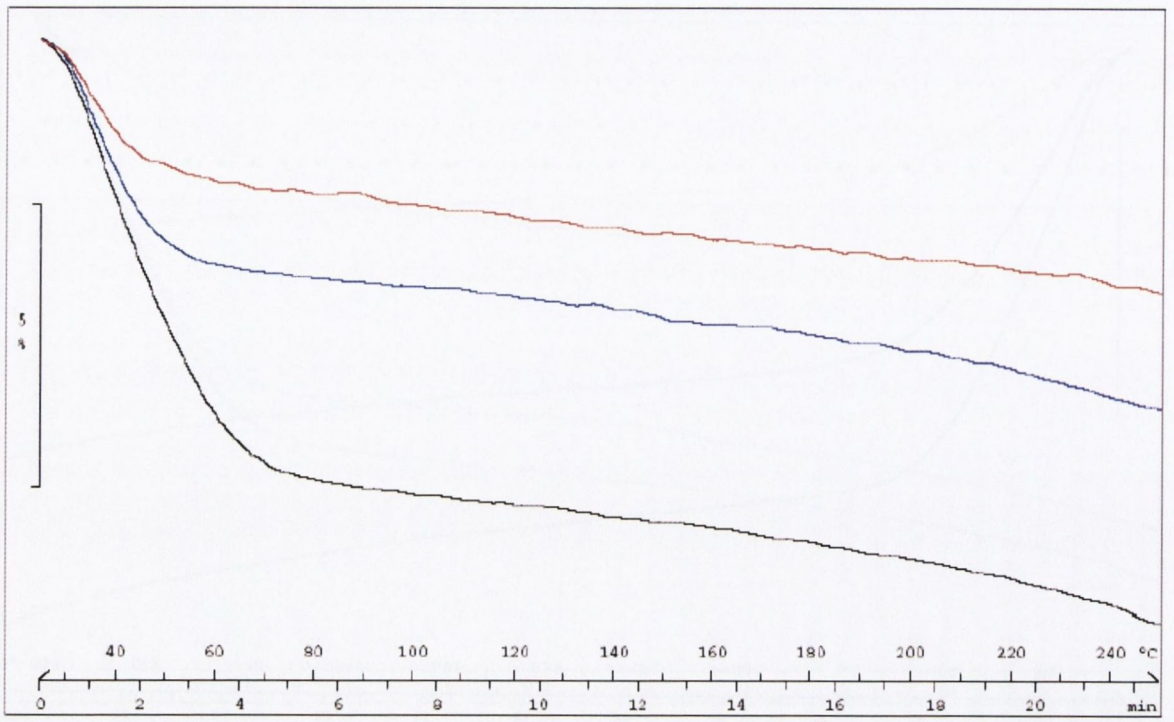


Figure A5l: TG thermogram of sepiolite (black), Kollidon® VA 64 (red) and a 1:1 physical mixture of sepiolite and Kollidon® VA 64 (blue).

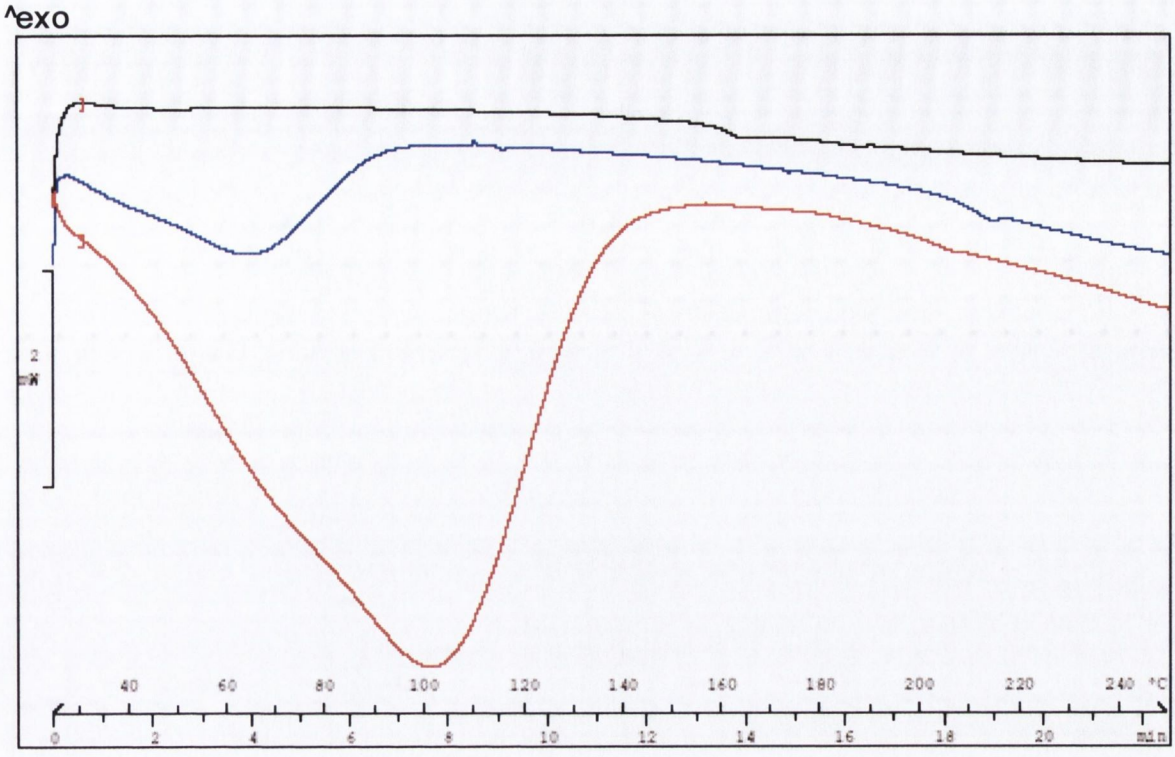


Figure A5m: DSC thermogram of sepiolite (red), Aerosil® 200 (black) and a 1:1 physical mixture of sepiolite and Aerosil® 200 (blue).

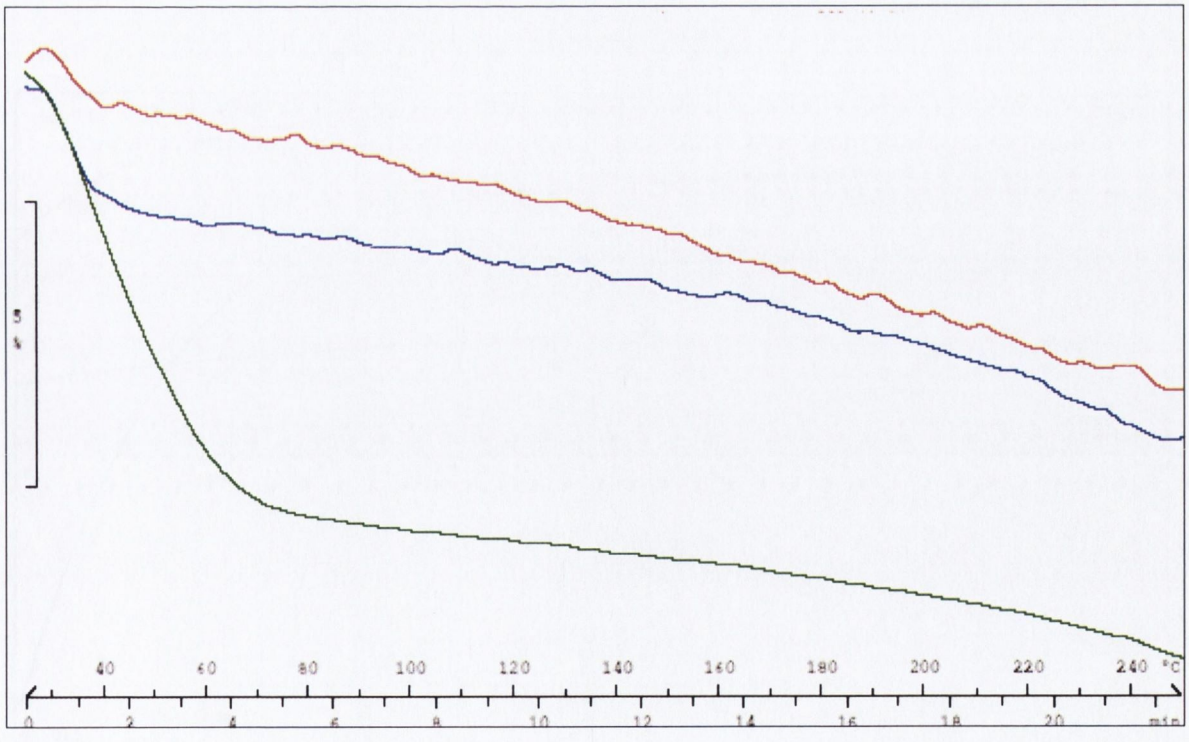


Figure A5n: TG thermogram of sepiolite (green), Aerosil® 200 (red) and a 1:1 physical mixture of sepiolite and Aerosil® 200 (blue).

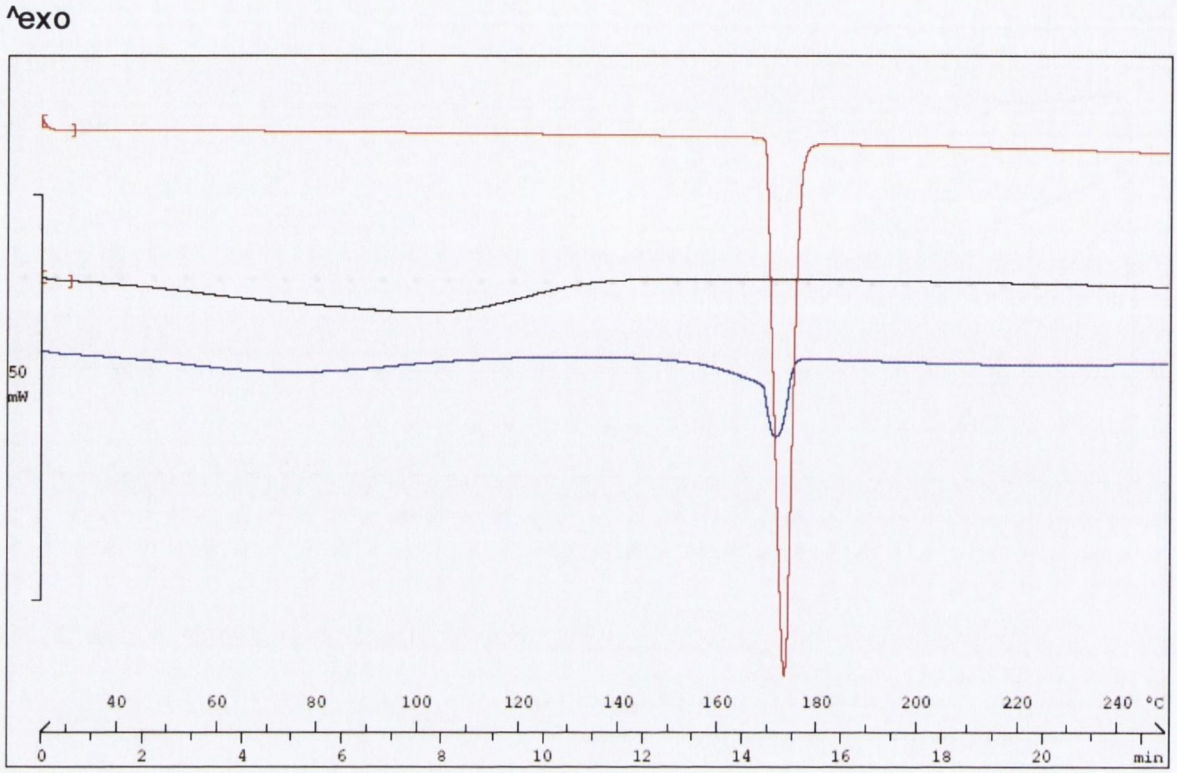


Figure A5o: DSC thermogram of sepiolite (black), paracetamol (red) and a 1:1 physical mixture of sepiolite and paracetamol (blue).

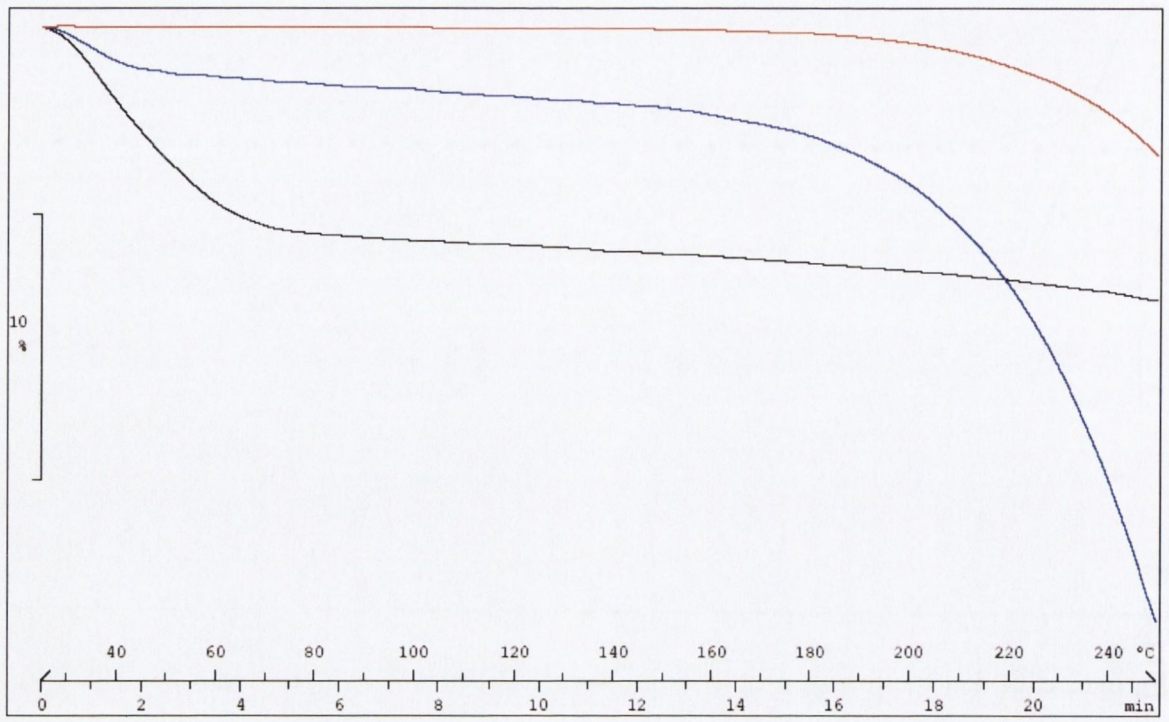


Figure A5p: TG thermogram of sepiolite (black), paracetamol (red) and a 1:1 physical mixture of sepiolite and paracetamol (blue).

APPENDIX 6: Rheological parameters for sepiolite suspensions treated with electrolytes

Table A6a. Rheological parameters for flow curves of NaCl-treated sepiolite suspensions.

Sodium Chloride concentration	5μM	50μM	0.5mM	5mM	50mM	0.5M	1M	1.5M
Herschel Bulkley Parameters								
Yield stress (Pa)	0.631±0.095	0.532±0.032	0.491±0.017	0.518±0.025	0.507±0.036	0.546±0.105	0.721±0.019	0.787±0.079
Consistency (Pa.s^n)	0.147±0.041	0.065±0.004	0.086±0.015	0.088±0.015	0.073±0.029	0.103±0.033	0.106±0.041	0.131±0.018
Rate index (-)	0.947±0.022	0.567±0.008	0.532±0.024	0.523±0.015	0.549±0.048	0.541±0.074	0.522±0.043	0.507±0.010
Correlation coefficient	0.92147	0.93194	0.93689	0.94053	0.91200	0.88278	0.90665	0.90873
Standard error	31.94	22.98	19.04	22.73	21.41	30.40	46.72	49.44
Bingham standard error	93.13	66.27	73.03	75.36	77.62	76.56	94.81	100.2
Newtonian standard error	275.0	229.7	236.3	233.9	233.1	255.2	294.4	323.0
Power law standard error	92.44	79.48	65.11	68.07	80.33	99.94	108.2	102.5
Casson standard error	45.21	25.17	30.88	32.15	32.94	33.12	46.35	56.65

Note: The lowest correlation coefficient of all replicates was quoted. The highest standard error of all replicates was quoted.

Table A6b. Rheological parameters for flow curves of $CaCl_2$-treated sepiolite suspensions.

Calcium Chloride concentration	**5μM**	**50μM**	**0.5mM**	**5mM**	**50mM**	**0.5M**	**1M**	**1.5M**
Herschel Bulkley Parameters								
Yield stress (Pa)	0.537±0.090	0.855±0.180	0.770±0.193	0.570±0.108	0.935±0.129	1.031±0.090	1.469±0.390	1.335±0.256
Consistency (Pa.s^n)	0.213±0.017	0.092±0.009	0.190±0.048	0.337±0.072	0.172±0.049	0.214±0.048	0.213±0.022	0.077±0.011
Rate index (-)	0.445±0.050	0.517±0.061	0.480±0.066	0.405±0.023	0.483±0.039	0.438±0.061	0.424±0.015	0.754±0.068
Correlation coefficient	0.94982	0.88315	0.89579	0.90561	0.89596	0.90137	0.72175	0.80053
Standard error	25.05	36.54	32.02	29.70	56.50	72.93	142.3	101.7
Bingham standard error	101.3	100.9	105.1	113.0	98.57	118.9	169.7	103.8
Newtonian standard error	301.1	335.3	325.8	317.0	338.8	376.1	531.7	384.4
Power law standard error	67.62	109.9	102.0	107.1	106.6	105.6	109.3	140.4
Casson standard error	51.99	52.88	53.90	61.63	60.70	83.27	157.6	105.7

Note: The lowest correlation coefficient of all replicates was quoted. The highest standard error of all replicates was quoted.

Table A6c. Rheological parameters for flow curves of cetrimide-treated sepiolite suspensions.

Cetrimide concentration	0.1µM	1µM	10µM	100µM	1mM	10mM	100mM	200mM
Herschel Bulkley Parameters								
Yield stress (Pa)	0.581±0.061	0.662±0.052	0.711±0.045	5.552±0.127	*	0±0	0.053±0.006	0.098±0.010
Consistency (Pa.s^n)	0.125±0.022	0.153±0.020	0.027±0.008	0.163±0.014	*	0.012±0.003	0.005±0.000	0.005±0.000
Rate index (-)	0.492±0.026	0.457±0.015	0.696±0.038	0.517±0.042	*	0.820±0.036	0.936±0.013	0.952±0.012
Correlation coefficient	0.97163	0.97845	0.97942	0.97556	*	0.92810	0.92902	0.91906
Standard error	23.25	19.21	26.63	108.6	*	13.59	13.39	12.71
Bingham standard error	86.54	88.25	50.15	186.4	*	27.46	14.93	14.01
Newtonian standard error	277.7	272.5	176.3	972.8	*	55.35	29.21	31.32
Power law standard error	76.0	72.41	64.62	160.5	*	13.59	14.34	15.29
Casson standard error	39.06	43.40	22.21	171.1	*	18.42	13.53	12.76

*Sample failed to move (i.e. measured shear rate was zero) over the applied shear stress range.

Note: The lowest correlation coefficient of all replicates was quoted. The highest standard error of all replicates was quoted.

Table A6d. Rheological parameters for flow curves of sodium citrate-treated sepiolite suspensions.

Sodium Citrate concentration	**0.1µM**	**1µM**	**10µM**	**100µM**	**1mM**	**10mM**	**100mM**	**200mM**
Herschel Bulkley Parameters								
Yield stress (Pa)	0.564±0.015	0.538±0.017	0.524±0.041	0.537±0.022	0.393±0.045	0.258±0.037	0.374±0.066	0.637±0.045
Consistency (Pa.s^n)	0.067±0.016	0.070±0.011	0.073±0.010	0.039±0.012	0.003±0.001	0.016±0.002	0.007±0.003	0.737±0.185
Rate index (-)	0.567±0.030	0.557±0.026	0.554±0.012	0.643±0.041	0.970±0.043	1.046±0.040	0.898±0.061	0.210±0.037
Correlation coefficient	0.92257	0.91989	0.93498	0.89898	0.94852	0.89668	0.92637	0.86851
Standard error	23.61	22.41	21.99	19.79	15.13	14.83	15.77	90.82
Bingham standard error	69.78	67.95	67.47	56.17	15.75	16.64	25.61	138.9
Newtonian standard error	230.7	236.4	231.3	212.2	99.93	51.40	128.2	385.9
Power law standard error	79.75	74.32	75.58	77.43	60.13	35.36	52.66	91.73
Casson standard error	27.75	26.43	25.25	19.90	35.12	26.94	21.85	114.1

Note: The lowest correlation coefficient of all replicates was quoted. The highest standard error of all replicates was quoted.

Table A6e. Rheological parameters for flow curves of NaPP-treated sepiolite suspensions.

Sodium Polyphosphate concentration	**0.1µM**	**1µM**	**10µM**	**100µM**	**1mM**	**10mM**	**100mM**	**200mM**
Herschel Bulkley Parameters								
Yield stress (Pa)	0.533±0.019	0.599±0.065	0.612±0.085	0.428±0.020	0.230±0.019	0.021±0.002	0±0	0±0
Consistency (Pa.s^n)	0.213±0.007	0.084±0.010	0.128±0.031	0.008±0.001	0.005±0.000	0.001±0.000	0.001±0.000	0.003±0.000
Rate index (-)	0.423±0.041	0.509±0.045	0.746±0.034	0.839±0.043	0.9365±0.016	1.116±0.025	1.126±0.044	0.984±0.008
Correlation coefficient	0.95110	0.92023	0.93953	0.96054	0.96061	0.97488	0.93634	0.97660
Standard error	28.11	28.99	25.76	17.82	15.74	13.52	13.46	14.21
Bingham standard error	97.04	86.94	87.68	29.52	27.51	16.86	16.36	17.73
Newtonian standard error	286.4	259.5	287.1	134.8	59.39	24.49	33.51	18.57
Power law standard error	69.15	94.04	92.70	51.04	32.26	13.90	13.65	17.21
Casson standard error	52.14	40.83	42.36	20.42	18.87	24.87	33.80	18.66

Note: The lowest correlation coefficient of all replicates was quoted. The highest standard error of all replicates was quoted.

APPENDIX 7: Rheological parameters for Calamine lotion variants

Table A7a. Standard error of fit of flow data for the calamine lotion variants to the different rheological models (refer to Table 8.4b).

Product	HB model standard error	Newtonian model standard error	Bingham model standard error	Power law standard error	Casson model standard error
	(-)	(-)	(-)	(-)	(-)
1	45.44	47.60	46.00	47.44	47.65
2	19.57	113.4	71.56	77.12	72.40
3	31.32	585.4	104.4	198.5	144.7
4	23.55	213.0	27.40	56.37	30.64
5	25.64	591.5	59.64	63.14	27.57
6	26.84	232.6	27.14	70.14	39.54
7	27.88	138.9	28.03	59.78	39.14
8	40.43	163.6	41.54	62.91	46.00
9	34.40	160.9	34.40	65.01	46.45
10	8.552	133.8	31.18	23.34	9.792
11	6.073	114.1	30.53	15.66	10.53
12	6.852	77.59	31.93	6.884	16.24
13	22.51	29.55	23.89	22.89	22.92

Note: The highest standard error of all replicates was quoted.

APPENDIX 8: Synopsis of preliminary results from image analysis of sepiolite pellets prepared by extrusion-spheronisation (ES) using water as a granulating agent

Sepiolite pellets were prepared with water using the ES method and equipment described by Barry (2005). The extrusion rate, spheronisation speed and time and quantity of granulating liquid (i.e. water) used are presented in Table A8a below, together with the resulting yield of pellets.

Table A8a. Extrusion-spheronisation parameters and resulting pellet yields.

Ratio of water to sepiolite	5 : 4 (by weight)
Extrusion rate	30 rpm
Spheronisation speed	1250 rpm
Spheronisation time	2.5 min
Drying temperature	40 °C
Yield of pellets in 850-1180 μm size range	42%
Yield of 'large' pellets (i.e. diameter > 1180 μm)	46%
Yield of 'fines' (i.e. diameter < 850 μm)	12%

The sphericity of pellets was determined using pellet parameters measured by an image analysis system (WinSEEDLE v5.1a, Regent Instruments, Inc., Canada) as described by Byrne (2003). An image of the sepiolite pellets in the desired size range (i.e. 850-1180 μm) is presented in Figure 8Aa below.

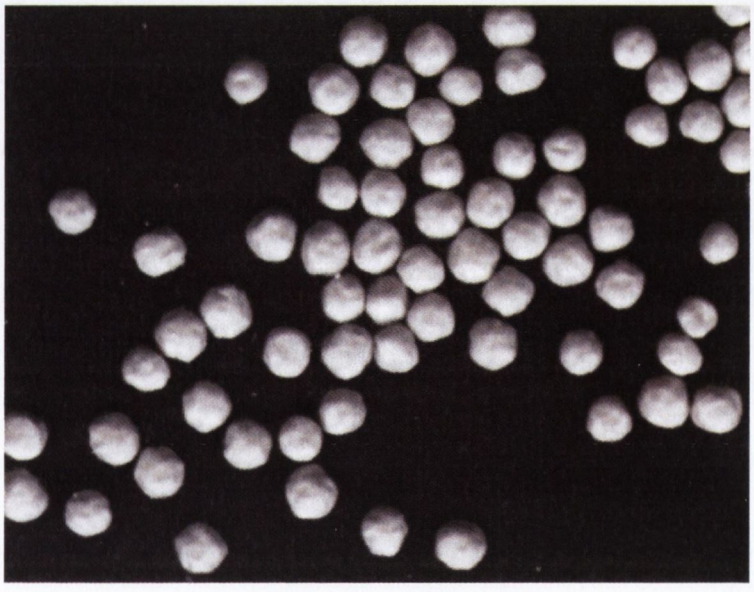


Figure A8a. Image of sepiolite pellets in the desired size range (850 – 1180 μm).

The sphericity of the pellets was calculated using two parameters, the projected perimeter length of the pellet, P_m, and the projected area, A. It was expressed in terms of Form PE where

$$\textbf{Form PE} = \frac{4\pi A}{P_m^2}$$

The Form PE of a perfect sphere is 1.00 while pellets with a Form PE of 0.833 or less have observable defects or distortions. Form PE is the inverse of a roundness parameter defined by Hileman *et al.* (1993).

Sphericity analysis was carried out on 650 pellets from the desired size range. Form PE was determined to be 0.922 ± 0.051; indicative of a very high degree of sphericity. The width-to-length ratio of the pellets was 0.945 ± 0.067; a result which further supported this conclusion.